AD-A001597

AFFDL-TR-74-47
Volume I
Final Report: June, 1972 — Sept., 1973

FRACTURE AND FATIGUE CRACK GROWTH BEHAVIOR OF SURFACE FLAWS AND FLAWS ORIGINATING AT FASTENER HOLES

Volume I - Results and Discussion

L. R. HALL
R. C. SHAH
W. L. ENGSTROM

THE BOEING AEROSPACE COMPANY
SEATTLE, WASHINGTON 98124

20071024040

MAY 1974

TECHNICAL REPORT AFFDL—TR—74—47
VOLUME I

Approved for public release; distribution unlimited.

AIR FORCE FLIGHT DYNAMICS LABORATORY
AIR FORCE SYSTEMS COMMAND
WRIGHT—PATTERSON AIR FORCE BASE, OHIO 45433

NOTICE

When Government drawings, specifications, or other data are used for any purpose other than in connection with a definitely related Government procurement operation, the United States Government thereby incurs no responsibility nor any obligation whatsoever; and the fact that the Government may have formulated, furnished, or in any way supplied the said drawings, specifications, or other data, is not to be regarded by implication or otherwise as in any manner licensing the holder or any other person or corporation, or conveying any rights or permission to manufacture, use, or sell any patented invention that may in any way be related thereto.

Copies of this report should not be returned unless return is required by security considerations, contractual obligations, or notice on a specific document.

AIR FORCE/56780/15 November 1974 — 600

ERRATA

Page	Item
NOTICE	The attached notice page should replace the previous one.
50	Q should be under the square root sign in equation (16).
170	The numerical values assigned to the ordinate axis of the central figure of Figure 68(a) should be omitted.
328	The specimen code for the bottom row of Table 37 should be FUTIA-1 rather than FUCTA-1.

NOTICE

When Government drawings, specifications, or other data are used for any purpose other than in connection with a definitely related Government procurement operation, the United States Government thereby incurs no responsibility nor any obligation whatsoever; and the fact that the Government may have formulated, furnished, or in any way supplied the said drawings, specifications, or other data, is not to be regarded by implication or otherwise as in any manner licensing the holder or any other person or corporation, or conveying any rights or permission to manufacture, use, or sell any patented invention that may in any way be related thereto.

Copies of this report should not be returned unless return is required by security considerations, contractural obligations, or notice on a specific document.

Dennis J. Golden

DENNIS J. GOLDEN, Major, USAF
Chief, Structural Integrity Branch
Structures Division
Air Force Flight Dynamics Laboratory

REPORT DOCUMENTATION PAGE

READ INSTRUCTIONS BEFORE COMPLETING FORM

1. REPORT NUMBER: AFFDL-TR-74-47	2. GOVT ACCESSION NO.
3. RECIPIENT'S CATALOG NUMBER	
4. TITLE (and Subtitle): FRACTURE AND FATIGUE CRACK GROWTH BEHAVIOR OF SURFACE FLAWS AND FLAWS ORIGINATING AT FASTENER HOLES, VOLUME I - RESULTS AND DISCUSSION	5. TYPE OF REPORT & PERIOD COVERED: FINAL TECHNICAL REPORT JUNE 1972 THRU SEPT. 1973
	6. PERFORMING ORG. REPORT NUMBER
7. AUTHOR(s): L. R. Hall, R. C. Shah, and W. L. Engstrom	8. CONTRACT OR GRANT NUMBER(s): F33615-72-C-1740
9. PERFORMING ORGANIZATION NAME AND ADDRESS: BOEING AEROSPACE COMPANY SEATTLE, WASHINGTON 98124	10. PROGRAM ELEMENT, PROJECT, TASK AREA & WORK UNIT NUMBERS
11. CONTROLLING OFFICE NAME AND ADDRESS: AIR FORCE FLIGHT DYNAMICS LABORATORY WRIGHT-PATTERSON AIR FORCE BASE OHIO 45433	12. REPORT DATE: MAY 1974
	13. NUMBER OF PAGES
14. MONITORING AGENCY NAME & ADDRESS (if different from Controlling Office): SAME	15. SECURITY CLASS. (of this report): UNCLASSIFIED
	15a. DECLASSIFICATION/DOWNGRADING SCHEDULE

16. DISTRIBUTION STATEMENT (of this Report)

APPROVED FOR PUBLIC RELEASE; DISTRIBUTION UNLIMITED

17. DISTRIBUTION STATEMENT (of the abstract entered in Block 20, if different from Report)

18. SUPPLEMENTARY NOTES

19. KEY WORDS (Continue on reverse side if necessary and identify by block number)

SUBCRITICAL CRACK GROWTH	OVERLOADS
STRESS INTENSITY FACTORS	SPECTRUM LOADS
FATIGUE	2219-T851 ALUMINUM
SURFACE FLAWS	9Ni-4Co-0.2C STEEL
FASTENER HOLE FLAWS	6Al-4V(ELI) TITANIUM

20. ABSTRACT (Continue on reverse side if necessary and identify by block number)

This combined experimental and analytical study was undertaken to investigate the fatigue crack growth behavior of surface flaws and part-thru and thru cracks originating at fastener holes. Three alloys (2219-T851 aluminum, 9Ni-4Co-0.2C steel, and 6Al-4V (ELI) beta annealed titanium) were tested under three different loading profiles (constant cyclic load, periodic overload, spectrum load). Surface flaw test variables included loading conditions (uniform tension, pure bending, combined bending and tension), stress ratio

(0.1, 0.3, 0.5), initial flaw shape ($0.15 < a/2c < 0.45$), and initial flaw depth ($0.2 < a/t < 0.8$). Fastener hole flaw variables included hole condition (conventional reamed and cold worked), fastener type (close tolerance and Taper-lok), and initial crack shape (uniform thru the thickness and quarter circular part-thru). All tests were conducted in air having a relative humidity of about 10 percent. Analytical work included derivation of stress intensity factors for cracked fastener holes. Solutions were developed for thru cracks originating at either loaded close tolerance fastener holes or Taper-lok fastener holes, and for part-thru cracks originating at either open holes or loaded and unloaded close tolerance fastener holes. Experimental results were compared to results derived from calculations based on modified linear elastic fracture mechanics procedures. Good agreement was obtained between experimental and calculated results for surface flaws subjected to constant cyclic loadings, and for close tolerance fastener holes subjected to constant cyclic and periodic overload loading programs. It was concluded that factors in addition to the crack growth retarding effects of overloads must be accounted for before adequate predictions of crack propagation lives under spectrum loads can be made for all loading spectra.

FOREWORD

This report describes an investigation of the fatigue crack growth characteristics of surface and fastener hole flaws performed by the Boeing Aerospace Company from 30 June 1972 through 31 December 1973 under Air Force Contract F33615-72-C-1740. The effort was conducted under project 486U, Air Force Flight Dynamics Laboratory (AFFDL), with Mr. Howard A. Wood acting as project engineer.

This program was conducted by the Research and Engineering Division of the Boeing Aerospace Company, Seattle, Washington, under the supervision of H. W. Klopfenstein, Structures Research and Development Manager. The Program Leader was J. N. Masters, Supervisor, Failure Mechanism Group. Technical Leader was L. R. Hall and program support was provided by R. C. Shah, analytical work; W. L. Engstrom, test coordination and data evaluation; A. A. Ottlyk, test engineering; and, D. G. Good and G. Buehler, technical illustrations and art work.

This report was submitted by the authors on 31 October 1973.

TABLE OF CONTENTS

		Page
1.0	INTRODUCTION	1
2.0	MATERIALS AND PROCEDURES	5
	2.1 Materials	5
	2.2 Procedures	7
	2.2.1 Specimen Preparation	7
	2.2.2 Experimental Procedures	9
	2.2.3 Experimental Approaches and Test Program	12
	2.2.4 Stress Intensity Factor Calculations	16
3.0	RESULTS AND DISCUSSION OF SURFACE FLAW TESTS	19
	3.1 Baseline Crack Growth Rate Tests	19
	3.1.1 Uniform Tension and DCB Tests	19
	3.1.2 Pure Bending Tests	21
	3.1.3 Summary	22
	3.2 Constant Cyclic Load Tests	23
	3.2.1 Uniform Tension Tests	23
	3.2.2 Combined Bending and Tension Tests	25
	3.2.3 Comparison of Predicted and Actual Results	26
	3.2.4 Flaw Interaction Effects	26
	3.3 Overload Tests	28
	3.3.1 Uniform Tension Overload Tests	28
	3.3.1.1 Crack Growth During Overloads	29
	3.3.1.2 Retardation Effects	31
	3.3.2 Combined Bending and Tension Tests	39
	3.4 Spectrum Load Tests	41
4.0	STRESS INTENSITY FACTORS FOR FLAWS AT FASTENER HOLES	45
	4.1 Summary	45
	4.2 Approach, Assumptions and Approximations	46

TABLE OF CONTENTS (Continued)

		Page
4.2.1	Cracks Originating at Open Holes	46
	4.2.1.1 Uniform Thru Cracks	46
	4.2.1.2 Semi-Elliptical Part-Thru Cracks	48
	4.2.1.3 Quarter-Elliptical Part-Thru Cracks	51
4.2.2	Cracks Originating at Unloaded Neat Filled Holes in a Plate	53
4.2.3	Cracks Originating at Loaded Neat Filled Holes in a Plate	54
	4.2.3.1 Two Symmetrical Thru Cracks Originating at a Loaded Neat Filled Hole	54
	4.2.3.2 One Thru Crack Originating at a Loaded Neat Filled Hole	55
	4.2.3.3 Two Semi-Elliptical Cracks Originating at a Loaded Neat Filled Hole in a Thick Plate	55
	4.2.3.4 Two Quarter-Elliptical Cracks Originating at a Loaded Neat Filled Hole in a Plate	56
	4.2.3.5 One Quarter-Elliptical Crack Originating at a Loaded Neat Filled Hole in a Plate	56
	4.2.3.6 Cracks at a Loaded Neat Filled Hole in a Plate Subjected to Tensile Loading	56
4.2.4	Thru Cracks at an Interference Fit Fastener	57
	4.2.4.1 Thru Cracks Subjected to Interference Stresses Alone	58
	4.2.4.2 Thru Cracks Subjected to Combined Applied and Interference Stresses	59

TABLE OF CONTENTS (Continued)

		Page
5.0	RESULTS AND DISCUSSION OF FASTENER HOLE FLAW TESTS	61
5.1	Static Fracture Tests of 4340 Steel Specimens	61
5.1.1	Fracture Toughness Tests	61
5.1.2	Open Hole and Loaded Close Tolerance Fastener Tests	61
5.1.3	Unloaded Interference Fit Fastener Tests	63
5.1.4	Loaded Interference Fit Fastener Tests	65
5.1.5	Summary	65
5.2	Constant Cyclic Load Tests	66
5.2.1	Conventional Open and Close Tolerance Fastener Filled Holes	67
5.2.2	Cold Worked Open and Fastener Filled Holes	69
5.2.3	Interference Fit Fastener Tests	71
5.2.4	Combined Bending and Tension Tests	74
5.2.5	Summary	75
5.3	Overload Tests	76
5.3.1	Conventional Open and Close Tolerance Fastener Filled Holes	76
5.3.1.1	Crack Growth During Overloads	77
5.3.1.2	Retardation Effects	78
5.3.2	Cold Worked Open and Fastener Filled Holes	80
5.3.3	Interference Fit Fastener Tests	81
5.3.4	Summary	85
5.4	Spectrum Load Tests	87
5.4.1	Conventional Open and Close Tolerance Fastener Filled Holes	87
5.4.2	Cold Worked Open Holes	88
5.4.3	Interference Fit Fastener Tests	90

TABLE OF CONTENTS (Continued)

	Page
6.0 OBSERVATIONS AND CONCLUSIONS	93
6.1 Surface Flaw Test Observations	93
6.2 Cracked Fastener Hole Test Observations	94
6.3 Conclusions	98
REFERENCES	99
APPENDIX A - TEST SPECIMENS	341

LIST OF SYMBOLS

a	Crack depth for surface flaws and part-thru fastener hole flaws
a_p	Value of $a + r_y$
b	Specimen width (thickness) for double cantilever beam specimens
b_n	Crack width for double cantilever beam specimens
c	Half crack width for surface flaws. Crack length for uniform through-the-thickness fastener hole flaws.
c_1	Crack length at specimen surface for part-thru fastener hole flaws
c_2	Crack length at back specimen face for initial part-thru fastener hole flaws that have grown through the specimen thickness.
C	Specimen compliance for double cantilever beam specimens, i.e., load line deflection divided by applied load.
d	Diameter of fastener or fastener hole
E	Young's modulus
F	Denotes "function of"
$\mathcal{J}$	Strain energy release rate
h	Half specimen height for double cantilever beam specimens
I	Moment of inertia of specimen arms for double cantilever beam specimens.

LIST OF SYMBOLS (Continued)

K_I	Opening mode stress intensity factor
K_{II}	Sliding mode stress intensity factor
K_{max}	Maximum cyclic stress intensity factor for any load cycle.
K_m	Same as K_{max}
K_{min}	Minimum cyclic stress intensity factor for any load cycle
K_{th}	Peak cyclic threshold stress intensity factor for fatigue crack growth
K_o	Peak opening mode stress intensity factor generated by an overload.
K_{cr}	Critical opening mode stress intensity factor at which crack instability occurs.
K_{Ih}	Opening mode stress intensity factor for a pair of symmetrical semi-elliptical cracks originating at a hole in an infinite plate
K_{Ic}	Opening mode stress intensity factor for an elliptical crack embedded in an infinite tension-loaded solid.
K_{Ieb}	Opening mode stress intensity factor for an elliptical crack embedded in an infinite solid subjected to a uniform tension stress equal to the average bearing stress for a loaded fastener.

K_{I2H}	Opening mode stress intensity factor for two symmetrical part-thru quarter-elliptical cracks originating at an open hole or a hole filled with an unloaded close tolerance fastener in a semi-infinite plate.
K_{IIP}	Opening mode stress intensity factor for one part-thru quarter-elliptical crack originating at an open hole or a hole containing an unloaded close tolerance fastener in a finite thickness plate.
K_{I2P}	Same as K_{IIP} except the one crack is replaced by two symmetrical part-thru quarter-elliptical cracks.
ΔK	$K_{max} - K_{min}$
ΔK_{th}	Threshold stress intensity range for fatigue crack growth
ΔK_{eff}	Effective range of stress intensity factor defined by crack closure theory.
L	Crack length for uniform through-the-thickness cracks originating from a circular hole in a plate (used in analytical work only)
M	Magnification factor
m,n	Exponents
N	Denotes number of loading cycles
N_d	Increase in cyclic life due to an overload
P	Load applied to a fastener

Q	Shape factor for surface flaws (Figure 18)
R	Stress ratio = $\sigma_{min}/\sigma_{max}$
r	Radius of circular hole
r_y	Length of crack tip plastic zone formed by a loading cycle
S	Value of K_o/K_{max} resulting in crack growth arrest
t	Specimen or plate thickness
W	Specimen width
β	Angle in parametric equations describing the periphery of an elliptical flaw, i.e., $x = c \sin \beta$ and $y = a \cos \beta$
δ	Measured crack surface displacements for semi-elliptical surface flaws or diametral interference for Taper-lok fasteners
υ	Poisson's ratio
ρ_o	Crack tip plastic zone size due to an overload
σ	Stress
σ_T	Tensile Stress
σ_B	Bending stress
σ_b	Average bearing stress for a loaded fastener
σ_{ys}	0.2% offset yield strength

SUBSCRIPTS

i	Denotes initial conditions of the outset of a test

SUMMARY

This program is one in a series of research and development programs undertaken by the United States Air Force to develop methods and data needed for design against fracture in military aircraft. This combined experimental and analytical study was directed to an investigation of the fatigue crack growth and fracture behavior of both surface flaws and fastener hole flaws under loadings pertinent to military aircraft.

The surface flaw test program contained two hundred tests involving several variables including alloy, flaw shape, initial flaw depth, stress ratio, and loading profile. Tests were conducted on three alloys; namely, 2219-T851 aluminum, 9Ni-4Co-0.2C (190-210 ksi) steel, and 6Al-4V standard ELI beta annealed titanium, all in plate form. At the outset of each test, flaw depth-to-width ratios varied between 0.15 and 0.45 and flaw depth-to-thickness ratios varied from 0.2 to 0.8. Three different loading profiles were tested including constant amplitude, periodic overload, and spectrum loadings. In the constant amplitude tests, three stress ratios (0.1, 0.3, 0.5) and three different loading conditions (uniform tension, pure bending, and combined bending/tension) were investigated. In the periodic overload tests, one stress ratio (0.1) and two loading conditions (uniform tension and combined bending/tension) were tested. In the spectrum load tests, two different spectra representative of either fighter or bomber operations were used. All tests were conducted in air having a relative humidity of about ten percent.

The cracked fastener hole program involved both analytical and experimental work. The analytical work was directed to estimating stress intensity factors for cracked fastener holes. Solutions were derived for both part-through and through-the-thickness cracks originating at open holes and holes containing either loaded or unloaded close tolerance fasteners, and for through-the-thickness cracks originating at holes containing interference fit fasteners. The experimental work included forty-two tests of precracked 4340 steel specimens and two hundred tests of precracked 2219-T851 aluminum, 9Ni-4Co-0.2C steel, and 6Al-4V (ELI) beta annealed titanium alloy specimens.

The 4340 steel tests were conducted to experimentally evaluate methods developed to predict fracture strength of cracked structure. Specimens contained part-through cracks originating at either open holes or holes containing loaded or unloaded close tolerance and interference fit fasteners. The remaining aluminum, steel, and titanium alloy tests involved two hole conditions (conventional reamed and cold worked), two fastener types (close tolerance and Taper-lok), two crack shapes (uniform through-the-thickness and quarter-circular part-through), one initial crack depth-to-thickness ratio (0.33), two types of loading (uniform tension and combined bending/tension), and three loading profiles (constant amplitude, periodic overload, and spectrum load). In the constant amplitude and periodic overload tests, through-the-thickness cracks originating at loaded and unloaded Taper-lok fastener holes, and part-through cracks originating at open and filled conventional holes, open and filled cold worked holes, and Taper-lok fastener holes were tested. In the spectrum load tests, only part-through cracks were tested using the same fastening systems as tested in the constant amplitude and periodic overload tests. All test results were compared to predictions based on linear elastic fracture mechanics procedures.

Results of the surface flaw tests showed that existing methods for calculating crack propagation life for surface flaws subjected to constant amplitude loadings are adequate. However, existing methods used in this study for estimating the effects of periodic overloads and spectrum loads on surface flaw fatigue crack growth behavior are not adequate. Crack growth rates during overloads were about two orders of magnitude greater than predictions based on baseline crack growth rates and crack closure theory. Retardation effects of periodic overloads were strongly affected by crack depth-to-thickness ratio and no method currently exists to quantitatively explain such effects. Finally, crack growth behavior of surface flaws under spectrum loadings could not be adequately correlated using calculation procedures based on either linear cumulative damage theory or simple methods of accounting for overload effects.

In the cracked fastener hole tests, the shortest crack propagation lives were obtained from tests of close tolerance fasteners in conventional reamed holes. Both cold working of fastener holes and installation of Taper-lok fasteners increased crack propagation lives. For the range of parameters used in this program, it was found that good estimates of crack propagation lives for open and close tolerance fastener filled holes subjected to constant amplitude and periodic overload loading profiles could be based on stress intensity factors derived in this program and baseline crack growth data obtained from constant cyclic load tests of surface flaw specimens. Methods developed to quantitatively evaluate the effects of fastener interference on crack propagation life for through-the-thickness cracked fastener holes underestimated interference effects for the aluminum and titanium alloys. In the steel alloy tests, interference had little or no effect on crack propagation lives and calculations were in good agreement with experimental results. Methods of calculating crack propagation lives for part-through cracks originating at interference fit and cold worked fastener holes were not available. Finally, crack growth behavior of fastener hole flaws subjected to spectrum loadings could not be adequately correlated using existing methods of calculating crack propagation behavior.

It was concluded that factors in addition to the crack growth retarding effect of overloads must be accounted for before adequate predictions of crack propagation lives under spectrum loads can be made for all loading spectra. More work is required to evaluate effects of fastener interference and cold working of fastener holes on crack propagation lives in the presence of smaller initial crack sizes and higher values of load transfer than were tested in this report.

1.0 INTRODUCTION

New design criteria (1)* are currently being developed for military aircraft to minimize the possibility that crack-like defects in airframe components will result in loss of aircraft during a specified period of time. These criteria reflect the knowledge that all airframe components can contain crack-like defects that are either inherent in the materials or are introduced during production or service. To comply with the new criteria, methods are required to: 1) determine the worst possible combinations of defect sizes and operating conditions that could exist at the outset of the specified period; 2) evaluate critical defect sizes, i.e., sizes that would result in component failures; and 3) calculate the number of aircraft missions that could grow the initial crack-like defects to critical sizes. Attempts to limit the maximum size of initial defects have been based on improvements of and increased emphasis on nondestructive inspection techniques. Improvements in critical flaw size calculation methods are resulting from improved analysis techniques (2,3), and fracture toughness data (4). Aircraft life calculation methods are being upgraded by studying the effects of operating environments and loadings on subcritical crack growth characteristics of airframe materials (5,6). In addition, fracture control design criteria are being applied to the development of new approaches to damage tolerant design in metallic structures (7,8,9), and to the evaluation of the impact of fracture control criteria on efficiency of aircraft structure.

This program is one in a series of research and development programs undertaken by the United States Air Force to develop methods and data needed for design against fracture in military aircraft (2-9). Since both surface flaws and part-through or through-the-thickness cracks at fastener holes are commonly found in airframe components, this program was undertaken to investigate the fracture and fatigue crack growth behavior of both surface and fastener hole flaws under loadings pertinent to military aircraft.

---

* Numbers in parentheses refer to references at end of report.

The surface flaw test program involved a number of variables including alloy, flaw shape, initial flaw depth, loading profile, and stress ratio. Tests were conducted using three alloys, namely, 2219-T851 aluminum, 9Ni-4Co-0.2C (190-210 ksi) steel, and 6Al-4V standard ELI beta annealed titanium, all in plate form. At the outset of each test, flaw depth-to-width (a/2c) ratios were set at 0.15, 0.30 or 0.45, and flaw depth-to-thickness (a/t) ratios ranged from less than to greater than 50% of the specimen thickness. Tests were conducted under three different loading profiles including constant amplitude, periodic overload, and spectrum loadings. Three stress ratios (0.1, 0.3, 0.5) and three different loading conditions (uniform tension, pure bending, and combined bending and tension) were investigated in the constant amplitude tests. One stress ratio (0.1) and two loading conditions (uniform tension and combined bending and tension) were investigated in the periodic overload tests. Two different spectra representative of either bomber or fighter operations were investigated in the spectrum load tests. All tests were conducted in air having a relative humidity of about 10 percent.

The cracked fastener hole program involved both analytical and experimental work. The analytical work was directed to estimating stress intensity factors for both part-through and through-the-thickness cracks originating at open holes, and holes containing either loaded or unloaded close tolerance and interference fit fasteners. Much of the experimental work was directed to fatigue crack growth testing of fastener hole flaws in 2219-T851 aluminum, 9Ni-4Co-0.2C (190-210 ksi) steel, and 6Al-4V standard ELI beta annealed titanium alloy plate. Tests were conducted on specimens containing either part-through or through-the-thickness cracks originating at holes containing both loaded and unloaded close tolerance and interference fit fasteners. Both standard and cold worked fastener holes were tested. Three different loading profiles (constant amplitude, periodic overload, and spectrum load) were used in the cyclic tests. Two different spectra representative of either bomber or fighter operations were investigated in the spectrum load tests. A series of static fracture tests were conducted on precracked 4340 (220-240 ksi) steel specimens to experimentally evaluate methods of predicting fracture strength of

structure. All specimens contained part-through cracks originating either at open holes or holes containing loaded or unloaded close tolerance and Taper-lok fasteners. Results of all fastener hole flaw tests were compared to predictions based on modified linear elastic fracture mechanics procedures.

2.0 MATERIALS AND PROCEDURES

Materials and experimental procedures are described in this section. Plate materials were characterized by conducting standard mechanical property tests and results are included in Section 2.1. Details of approaches to specimen preparation and testing are included in Section 2.2.

2.1 Materials

Four different plate alloys were tested in this program, including 2219-T851 aluminum, 6Al-4V standard ELI beta annealed titanium, 9Ni-4Co-0.2C (190-210 ksi) steel and 4340 (220-240 ksi) steel. The first three alloys are all candidates for use in fracture resistant components of high performance airframes. These alloys are being used in current programs, although the Ti-6Al-4V alloy is generally being used in the alpha-beta condition rather than the beta condition. Tests have indicated that for the Ti-6Al-4V alloy, beta annealing leads to superior stress corrosion cracking and corrosion fatigue crack growth resistance than does alpha-beta annealing (5). The 4340 alloy was used at the 220-240 ksi strength level for a series of stress intensity analysis verification tests because of its frangible and homogeneous nature.

The 2219-T851 aluminum alloy plates (1.0 x 36 x 72 inches) were purchased from Alcoa in the T851 condition per Boeing Material Specification BMS7-105C (equivalent to MIL-A-8920A). All plates came from the same heat and rolling batch. Specification limits on chemical composition are listed in Table 1 and mechanical properties measured by the Boeing Aerospace Company are included in Table 2.

The 6Al-4V standard ELI titanium alloy plates were obtained from excess material remaining after the cancellation of the Supersonic Transport Program. The plates, 0.60 x 55 x 129 inches, were produced by RMI per Boeing Material Specification XBMS7-174B. The B revision of this specification requires an extra low interstitial grade and annealing above the beta transus to provide high toughness and resistance to stress corrosion

cracking. Specification limits in chemical composition are listed in Table 1 and mechanical properties measured by the Boeing Aerospace Company are listed in Table 2.

The 9Ni-4Co-0.2C steel plate was purchased from Republic Steel in the form of annealed 0.50 x 27 x 36 inch plates per North American Rockwell Specification ST0160LB0001. The plates were produced from Vacuum Arc Remelt No. 3831679 and were hot rolled, annealed, blasted, and oiled prior to shipment. Chemical composition of the plates as determined by the supplier are listed in Table 1. The plates were heat treated to the 190-210 ksi strength level by the Boeing Aerospace Company using the following schedule:

(1) Normalize at 1650 $\pm$ 25°F for 30 minutes, air cool to room temperature.

(2) Austenitize at 1525 $\pm$ 25°F, hold at maximum temperature for 30 minutes then quench in oil at 60°F to 150°F.

(3) Cool within two hours to -100 $\pm$ 25°F and hold at temperature for one hour.

(4) Temper at 1025 $\pm$ 10°F for four hours then air cool to room temperature.

Mechanical properties of the heat treated plate are listed in Table 2.

The 4340 steel alloy plate was purchased in the form of an annealed hot rolled 0.625 x 30 x 60 inch plate per AMS 6359B, excepting paragraphs 5.2 and 8.1. Chemical composition of the plate as determined by the supplier is listed in Table 1. The material was heat treated to the 220-240 ksi strength level after specimen machining. Mechanical properties measured by the Boeing Aerospace Company are included in Table 2.

A summary of fasteners used in this program is included in Table 3. Both Taper-lok and close tolerance fasteners were used for each of the four plate alloys tested. Almost all tests involved the use of protruding head fasteners with the remaining tests making use of countersunk head fasteners. Fastener details including alloy, tensile strength, head configuration, finish, lubrication and supplier are summarized in Table 3.

2.2 Procedures

Procedures used for specimen preparation and testing are described in this section. Details of preflawing methods, installation of Taper-lok fasteners, and cold working of holes are described in the discussion of specimen preparation. Details of test environment, instrumentation, and loading profiles are described in the section covering test procedures.

2.2.1 Specimen Preparation

All specimen configurations used in this program are included in Appendix A. A summary of the specimen configurations used for each series of tests is presented in Table A1 in Appendix A. Specimen configurations are detailed in Figures A1 through A9.

Flaw Preparation

All flaws were prepared by growing fatigue cracks from crack starters. For surface and fastener hole flaws, crack starters were introduced using an electrical discharge machine, kerosene dialectric, and 0.06 inch thick circular electrodes. Electrode tips were machined to a radius of 0.003 inch and an included angle of less than 20 degrees. Fatigue cracks were grown from the periphery of the starter slots using loading cycles having a stress ratio of 0.06, cyclic frequency of 1800 cpm, and peak cyclic stresses of 10 ksi for the aluminum alloy and 25-30 ksi for the steel and titanium alloy specimens. The width of the precrack ranged from 0.02 to 0.05 inch. All 9Ni-4Co-0.2C steel surface flaw and fastener hole flaw specimens were baked at 400F for 4 hours to remove any hydrogen that may have been introduced by electrical discharge machining. Flaws at tapered holes were introduced prior to installation of the Taper-lok fasteners. Crack starters in double cantilever beam specimens consisted of 0.125

inch wide milled slots terminating in a chevron vee notch. Fatigue cracks were grown from the tips of the starter slots using cyclic loads having a stress ratio of 0.06 and frequency of 1800 cpm. The last 0.10 inch of precrack was grown using a peak cyclic stress intensity to Young's modulus ratio of less than 0.0012 $\sqrt{\text{inch}}$.

Taper-lok Drilling and Installation

Taper-lok drilling procedures were devised to minimize the number of different fasteners and drills required for this program. Since different drills are required for each of the six groups of Taper-lok fasteners (a group includes several lengths of bolts having the same head diameter) it was decided to limit the number of fastener groups used to one, namely Group II (manufacturer's designation). This was accomplished by drilling tapered holes as shown in Figure 1. Clamping bars were affixed to each specimen at the appropriate location and the tapered drill was inserted into the 0.50 inch diameter hole in the clamping bar. A tapered hole was drilled through the specimen with the clamping bar being used to control the maximum drill travel, i.e., the specimen was drilled as if the total stackup was equal to sum of the specimen and clamping bar thickness as shown in Figure 1b. Clamping bar thicknesses were approximately 0.5 inch for all alloys.

The method of installing Taper-lok fasteners is pictured in Figure 2. After the fastener was positioned in the hole thumb tight, a dial gage was clamped to the specimen with the plunger bearing against the head of the fastener. The bolt was drawn in a predetermined amount using a torque wrench. Bolt protrusion was controlled to within 0.001 inch. Installed fasteners protruded from the specimens as illustrated in Figure 1c. This condition is representative of installations where no pressure exists between the fastener head and joined part.

Cold Worked Holes

Methods developed by the Boeing Commercial Airplane Company were used to cold work fastener holes in this program. Two expansion levels were tested with the lower value 25% less than the higher value. For the aluminum and titanium alloy high expansion holes, a 0.355 inch diameter hole was drilled and the required initial crack was introduced. The hole was then

fitted with a lubricated split sleeve and a mandrel was drawn through the hole to cold expand it to a diameter of 0.374 inch. This was accomplished using the equipment shown in Figure 3. After removal of the mandrel, the hole diameter decreased to 0.366 inch and was reamed to the final size of 0.375 inch. For the 9Ni-4Co-0.2C steel alloy high expansion holes, the initial hole diameter was 0.333 inch. After the required crack was introduced, the hole was coated with a dry film lubricant (Fel Pro 300) and baked at 375°F for four hours. Cold working was accomplished by pushing a mandrel through the lubricated hole to cold expand it to a diameter of 0.358 inch. The holes were then reamed to 0.375 inch. The lower expansion levels were achieved by increasing initial hole diameter to 0.361 inch for the aluminum and titanium alloys and 0.339 inch for the steel alloy.

2.2.2 Experimental Procedures

Test Media

Tension loaded cyclic tests were conducted in desiccated air having a relative humidity of about 10 percent. This was accomplished by taping rectangular plexiglass containers containing a controlled amount of desiccant to the faces of all test specimens. Measurements of relative humidity in the containers varied from 5 to 15 percent. Test temperature was equal to ambient temperature which ranged from 69 to 75F. All bending/tension cyclic and static fracture tests were conducted in an air conditioned laboratory where the temperature is controlled to 72 $\pm$ 2F.

Fastener Loading

Fasteners were loaded using loading straps as shown in Figure 4. The position of the bearing block was adjusted by turning the cap screws until the block was snug against the fastener. The adjustable feature eliminated variations in loading from specimen to specimen due to small variations in the distance between the grip holes and loaded fastener hole. Furthermore, adjustments could be made throughout each test to keep the load transfer constant. Load transferred through the straps was measured using back-to-back pairs of uniaxial strain gages located as shown in Figure 4. The straps were precalibrated to determine relationships between strain output and load transfer. During each test, the strain

gages were connected to a strip chart recorder to produce continuous recordings of strap load versus cycles. A photograph of a specimen with loading straps is included in Figure 5.

Loading straps used for 4340 steel stress intensity verification tests did not have the adjustable feature shown in Figure 4. Consequently, the straps were pulled tight against the loaded bolt then clamped between two splice plates and the specimen grip as shown in Figure 6. The splice plates were bolted to a loading bar which was attached to the upper grip.

Five tests involving load transfer were conducted using the specimen configuration shown in Figure 7. Load transfer was effected by bolting a strap plate to the specimen. Load transfer was measured using back-to-back pairs of uniaxial strain gages attached to the strap plate. The strap plate was calibrated prior to being attached to the specimen and the strain gages were attached to a strip chart recorder throughout each test to obtain a continuous record of load transfer versus cycles. Teflon spacers were located between the specimen and strap plate to minimize load transfer due to friction.

Instrumentation

The following specialized instrumentation was used in this program:

(1) Clip gages to obtain records of crack displacements versus cycles for tension loaded surface-flawed specimens and crack displacement versus load for statically tested 4340 specimens.

(2) Strain gages on loading straps to measure load transfer for loaded fasteners.

For aluminum alloy specimens, clip gages were spring loaded against integrally machined knife edges. For titanium and steel specimens, knife edges were spot welded to the specimen as shown in Figure 8. For cyclic tests, clip gages were connected to strip chart recorders to obtain continuous recordings of crack displacement versus cycles. For static tests, both clip gage and load cell were connected to an X-Y plotter to obtain recordings of crack displacement versus applied load.

Tension/Bending

Combined bending and tension tests were conducted using a test machine that was modified to apply simultaneous longitudinal and lateral loads. The test setup is illustrated in Figures 9 and 10. Longitudinal loads were applied using an existing 150 kip vertical jack. Lateral loads were applied by a horizontally mounted 20 kip jack. The jack was supported by vertical posts bolted to the test frame. The lateral loads were reacted through supports located near each specimen grip. The supports were bolted to posts that transferred the lateral loads into the test frame. Lateral loads were transferred to and from the specimen using 3/4-inch diameter steel rods. Stresses at the center of each specimen were measured using four pairs of back-to-back uniaxial strain gages located on the crack plane. The strain gages also served as transducers in the feedback loop of a servo system used to control the applied loads.

Loading Profiles

Tests were conducted under constant, periodic overload, and spectrum loading profiles. Constant peak load and periodic overload tests were conducted at a cyclic frequency of 60 cpm. All loading cycles except the overloads were applied using a stress ratio of either 0.1, 0.3 or 0.5. Overloads had a stress ratio of zero. Two types of loading spectra were tested including one bomber and one fighter spectrum. Details of the bomber spectrum are included in Table 4 and Figure 11. Limit gross area stress levels were 33.6 ksi, 70 ksi, and 130 ksi for the aluminum, titanium, and steel alloys, respectively. Details of the fighter spectrum are included in Table 5. The fighter spectrum was obtained by randomizing the layers of an existing fighter spectrum using a book of random numbers and then adding two spike loads at the end of the spectrum to represent the six spike loads used in the original spectrum. The limit stress levels were 30.9 ksi, 61.8 ksi, and 91.0 ksi for the aluminum, titanium and steel alloys, respectively. The cycles within a given layer of each spectrum were applied at 240 cpm. The average cyclic rate for the spectra (total cycles in one spectrum divided by time to apply the spectrum) was 60 cpm.

2.2.3 Experimental Approaches and Test Program

Details and bases for the approaches used to generate data for each series of tests are described in the following paragraphs.

Baseline Tests

Tests were conducted to develop baseline crack growth rate data for use in evaluating subsequent test results. The program of baseline tests is summarized in Table 6.

Crack growth rates for the T-S direction (see Figure 12 for direction notation) were developed by testing surface-flawed specimens under cyclic tension loadings. Two specimens were tested for each stress ratio (R = 0.1, 0.3 and 0.5), for each alloy (2219-T851 aluminum, 6Al-4V (ELI) beta annealed titanium and 9Ni-4Co-0.2C (190-210 ksi) steel). One specimen contained two flaws and the second specimen contained only one flaw. Each specimen was tested under three different stress levels as follows: cycling was started at a low stress level and the crack depth was extended about 0.05 inch; the stress level was then increased to a higher value and the crack depth was grown an additional 0.05 inch; the final increment of crack growth was generated after a second increase in stress level. This procedure was selected to allow the generation of crack growth rate data over a wide range of K levels from a single specimen, and to provide data that could be used to evaluate stress level effects on crack growth rates.

Additional crack growth rates for the T-S direction were generated using pure bending stresses to see if K-rate correlations for tension and bending stresses coincided. This was accomplished by testing one surface flawed specimen under four point bending for each of two stress ratios (0.1 and 0.5) and three alloys (given in Table 6). Each specimen contained two flaws having different initial sizes.

Crack growth rates for the T-L direction were generated by testing double cantilever beam specimens under uniform cyclic loads. Cracks were grown over a series of predetermined increments of crack length. The first increment was induced using a peak cyclic load slightly greater than the load used to precrack the specimen. The peak cyclic load was then increased

by 100 lb for the aluminum alloy and 500 lbs for the steel and titanium alloys and a second increment of crack growth was generated. This procedure was repeated until data were generated for the required range of ΔK. Crack growth increments averaged about 0.3 inch in length.

Constant Cyclic Load Tests

Tests were conducted to evaluate crack growth characteristics of both surface and fastener hole flaws under uniform cyclic loads. These tests were intended to be a first step toward the understanding of crack growth behavior under spectrum loadings.

The uniform load test program for surface flaws is summarized in Table 7. One specimen was tested per alloy/test condition. For aluminum and steel alloy tension loaded tests, each specimen (Figure 13) contained three flaws having nominal initial a/2c values of 0.15, 0.30, and 0.45, and depths chosen to yield the same value of stress intensity factor at each flaw tip during the first loading cycle. Titanium alloy specimens contained only two flaws with initial a/2c values of 0.15 and 0.40. The initial depth of all flaws in a given specimen was either less than or greater than 50 percent of the specimen thickness. For all combined bending and tension tests, each specimen contained only one flaw at the center of the specimen.

The uniform load test program for cracked fastener holes is summarized in Table 8. Both part-through and uniform through-the-thickness cracks were tested for each of the three test alloys. Each specimen contained three initial defects as shown in Figure 14. A single specimen contained one of the following combinations of flaw origins: (1) one loaded and two unloaded interference fit fasteners; (2) one loaded close tolerance fastener, one unloaded close tolerance fastener, and one open hole with all holes close reamed; (3) one loaded close tolerance fastener, one unloaded close tolerance fastener and one open hole with all holes cold worked then close reamed.

The peak cyclic stress level was periodically lowered throughout each test and a number of lower stress fatigue cycles were applied to the test specimen. This procedure generated fine bands of fatigue crack growth around the periphery of the flaws that could be identified on the fracture faces of the specimens. An example of the marking bands in an aluminum alloy specimen is shown in Figure 15. The marking bands allowed a post-test evaluation of the change in flaw dimensions throughout each test.

Overload Tests

Overload tests were conducted by repeatedly subjecting specimens to one of the three loading profiles shown in Figure 16. Most tests were conducted using loading program A in which periodic tensile overloads were applied to the test specimen. A smaller number of tests were conducted using loading program B which included periodic small compressive overloads. A limited number of tests were conducted on titanium alloy specimens using loading program C in which each tensile overload was followed immediately by a small compressive load.

The periodic overload test program for surface flaws is summarized in Table 9. Specimen details were the same as previously described for the uniform load tests. For each specific ratio of peak overload to peak cyclic stress, the first test was conducted by growing each crack between overloads by an amount equal to or greater than Δa_1 where

$$\Delta a_1 = 0.5 \, (K_o/\sigma_{ys})^2 \qquad (1)$$

and K_o is the stress intensity factor generated at the crack tip by the peak overload stress. The above value of Δa_1 is about five times the commonly used plane strain plastic zone size of $1/3\pi \, (K/\sigma_{ys})^2$ (Ref. 10). Hence, it is believed that interactive effects between overloads were minimized by this procedure. In subsequent tests, the frequency of overloads was increased.

The periodic overload program for cracked fastener hole tests is summarized in Table 10. Specimen details are the same as previously described for the uniform load tests, except that one additional combination of

flaw origins was used, namely, one loaded interference fit fastener, one unloaded interference fit fastener, and one open cold worked hole. Equation 1 was used to estimate the amount of crack growth required between overloads to reduce interactive effects to negligibly small values. Values of stress intensity factor were estimated using an approximate procedure given in Reference 11. The initial tests for each value of peak overload stress were conducted using an overload period selected to minimize interaction effects between overloads.

Spectrum Load Tests

Tests were conducted to provide data with which to compare results of analytical predictions of crack propagation behavior. Specimen details for both surface flawed and cracked fastener hole specimens were the same as for the uniform load and periodic overload tests (Figures 13 and 14).

The spectrum load test program for surface flaws is summarized in Table 11. Two specimens were tested for each of the six alloy/spectrum combinations. In one specimen, all three flaws had initial flaw depths less than 50 percent of the specimen thickness. In the second specimen, all flaws had initial depths greater than 50 percent of the specimen thickness. Two different spectra were used including a bomber and a fighter spectrum. Details of the bomber spectrum are included in Table 4 and Figure 11. Details of the fighter spectrum are included in Table 5.

The spectrum load test program for cracked fastener hole tests is summarized in Table 12. The first twelve specimens listed in Table 12 included two specimens for each of the six alloy/spectrum combinations. Specimen configuration was the same as that used for uniform load and periodic overload tests. Each specimen contained three flaw origins. The first specimen contained one loaded interference fit fastener, one unloaded interference fit fastener and one open cold worked hole. The second specimen contained one loaded close tolerance fastener, one unloaded close tolerance fastener, and one open hole. The remaining six tests in Table 12 were all conducted under the bomber spectrum. Specimen configuration is shown in Figure 7. Two specimens were tested for each

alloy (except steel), including one specimen in which the strap plate was attached to the specimen using one interference fit fastener and one close tolerance fastener in a cold worked hole, and a second specimen using one plain and one countersunk close tolerance fastener. For the steel alloy, only the close tolerance fastener specimen was tested.

Static Fracture Tests of 4340 Steel Specimens

This series of static fracture tests was conducted to evaluate the accuracy of fracture strength predictions based on approximate stress intensity factor calculations accomplished in this program. The 4340 steel alloy was chosen because of its homogeneous and frangible nature when heat treated to high strength levels.

The test program for 4340 steel static fracture tests is summarized in Table 13. Tests were conducted for both single and double corner cracks originating at open holes, loaded interference fit fasteners, unloaded interference fit fasteners, and loaded close tolerance fasteners. Other test variables included hole diameter (0.25 and 0.375 inch), and flaw depth-to-thickness ratio (0.4, 0.6 and 0.8). All tests were conducted by loading the specimens to failure using a loading rate of 100 ksi per minute. All specimens were instrumented with clip gages spring loaded against knife edges spot welded to the specimen. The spot welds were located 0.06 $\pm$ 0.01 inch away from the edge of the hole and immediately above and below the mouth of the crack.

2.2.4 Stress Intensity Factor Calculations

Methods used for calculating stress intensity factors for both surface flawed and pin-loaded double cantilever beam specimens are described in this section. Methods for calculating stress intensity factors for cracked fastener hole specimens were developed during the course of this program and are described in Section 4.0.

Tension Loaded Surface Flaws

Stress intensity factors for tension loaded surface flawed specimens were calculated using solutions due to Shah and Kobayashi (12). Stress intensity factors at the points of maximum crack depth were calculated using the equation

$$K_I = F(a/c,\ a/t)\ \sigma_T\sqrt{\pi a/Q} \qquad (2)$$

where the function F(a/c, a/t) accounts for the effect of both front and back specimen face on stress intensity factor at the point of maximum depth. Values of F(a/c, a/t) are included in Figure 17. In addition, σ_T is applied stress, 'a' is crack depth, and Q is factor that accounts for the effect of crack shape and plasticity at the crack tip on stress intensity factor. Values of Q are included in Figure 18. Stress intensity factors at the end of the major axes of the flaws (at the specimen surfaces) were calculated using the equation

$$K_I = 1.1\ \sigma_T\sqrt{\pi a/Q}\ \cdot\ \sqrt{a/c} \qquad (3)$$

where 1.1 was taken as a best estimate of the effect of the front specimen face on stress intensity factor at the specimen surface. This estimate was based on solutions contained in Reference 13. The remainder of the equation is the Irwin (14) solution for stress intensity factor at the end of the semi-major axis of an embedded elliptical flaw in a body subjected to tensile stresses acting perpendicular to the flaw plane. Symbols 'a' and Q were previously defined.

Stress intensity factors for surface flaws subjected to pure bending stresses were calculated using solutions provided by Shah and Kobayashi (15) and Grandt (16). At the point of maximum depth, stress intensity factor was calculated using the equation

$$K_I = M_{BO}\ \sigma_B\sqrt{\pi a/Q} \qquad (4)$$

where values of M_{BO} were taken from Reference 15 and are plotted in Figure 19. At the specimen surfaces, stress intensity factors at the end of the major axes of the flaws were calculated using Equation 4 with M_{BO} replaced by a different set of factors (M_{B90}) which were taken from Reference 16 and are plotted in Figure 20.

Stress intensity factors for double cantilever beam specimens were calculated using the equation

$$K_I = \frac{2P}{b}\left[\frac{b}{b_n}\right]^{1/2}\left[\frac{3(a+0.6h)^2 + h^2}{(1-\mu^2)h^3}\right]^{1/2} \qquad (5)$$

where P is applied load
b is specimen width
b_n is crack width
h is one-half specimen height
E is Young's modulus
a is crack length
μ is Poisson's ratio

Equation 5 is based on the relationship between strain energy release rate ($\mathcal{G}$) and specimen compliance (C) (17)

$$\mathcal{G} = \frac{P^2}{2b_n} \cdot \frac{\partial C}{\partial a}$$

and the semi-empirical relationship between load and specimen compliance (18)

$$C = 2/3EI\ [(a+0.6h)^3 + h^2 a] \qquad (6)$$

Equation 6 has been found to be an accurate representation of specimen compliance for the specimen configurations used in this program (5). Stress intensity factor was obtained from $\mathcal{G}$ using the equation

$$K_1^2 = \frac{E\mathcal{G}}{1-\mu^2} \qquad (7)$$

which is applicable to conditions of generalized plane strain. There is some question as to whether the $1-\mu^2$ term in Equation 7 is applicable. However, its contribution to calculated stress intensity factors is small.

3.0 RESULTS AND DISCUSSION OF SURFACE FLAW TESTS

Results of each of the four series of surface flaw tests (baseline, constant cyclic load, overload, and spectrum load) are presented and discussed in the following subsections.

3.1 Baseline Crack Growth Rate Tests

Tests were conducted to determine baseline crack growth rate data under uniform tension, pure bending, and combined bending and tension loadings. These data were used as a baseline against which to compare data from the remaining series of tests.

3.1.1 Uniform Tension and DCB Tests

Crack growth rate data for the thickness (T-S) direction resulting from baseline tests of 2219-T851 aluminum, 9Ni-4Co-0.2C steel, and 6Al-4V standard ELI beta annealed titanium are plotted as a function of peak cyclic stress intensity factor in Figures 21, 22 and 23, respectively. Tabulated results are included in Tables 1 through 9 in Volume 2 of this report. Data were generated using three stress ratios (0.1, 0.3 and 0.5) and three different peak cyclic stress levels for each stress ratio. All data points having similar shading were generated using a single peak cyclic stress level.

The crack growth rate data were fitted using the equation:

$$da/dN = C(K_{max} - K_{th})^m (\Delta K)^n \qquad (8)$$

where da/dN = fatigue crack growth rate in inches/cycle
C = a constant
K_{max} = peak cyclic stress intensity factor
K_{th} = peak cyclic threshold stress intensity factor
ΔK = range in stress intensity factor
m,n = exponents

Values of C, m and n were determined by least square fitting the data in Figures 21 through 23 using the following assumed values of K_{th}: 1.5 ksi $\sqrt{in}$ for the aluminum, 10 ksi$\sqrt{in}$ for the steel, and 5 ksi$\sqrt{in}$ for the titanium. The following values of C, m and n resulted.

Alloy	C	m	n
Al-2219-T851	0.34×10^{-8}	0.84	2.40
Fe-9Ni-4Co-0.2C	0.40×10^{-8}	0.57	1.76
Ti-6Al-4V βA	0.33×10^{-10}	1.02	3.00

The solid lines in each of the Figures 21 through 23 are plots of Equation 8 using the appropriate values of C, m and n. It is evident that the equation provides a good representation of the combined effects of stress ratio and stress intensity factor on fatigue crack growth rates over most of the K ranges tested. For the aluminum and titanium alloys, crack growth rates for the highest K values are larger than given by Equation 8 since the equation does not account for the known behavior that crack growth rates tend to very large values as K_{max} approaches K_{cr}. The ranges of K_{max} over which Equation 8 did show good agreement with the data are $14 < K_{max} < 28$ ksi $\sqrt{in}$ for the aluminum alloy, $15 < K_{max} < 100$ ksi $\sqrt{in}$ for the steel alloy, and $20 < K_{max} < 60$ ksi $\sqrt{in}$ for the titanium alloy.

Multiple maximum cyclic stress levels were used in generating baseline data to determine whether peak cyclic stress level had any effect on crack growth rates over and above its contribution to stress intensity factor. Earlier investigations (19,20) led to the observation that crack growth rates for surface flaws at constant stress ratio and stress intensity factor appeared to be inversely proportional to the square of the peak cyclic stress level. Such stress level effects manifest themselves as a layering of crack growth rate data with respect to stress level on K versus da/dN plots. In this investigation, two or three data points were generated at each stress ratio and peak cyclic stress level. Each set of data points generated at a single stress level is joined by a short dashed line in Figures 21 through 23. The data showed no consistent tendency to be layered with respect to stress level, although some individual

sets of data did exhibit slopes less than the slope of the solid lines used to represent all the data. It was concluded that, for the ranges of stress intensity factors used in the baseline tests, the data for a given alloy and stress ratio were best correlated by a single crack growth rate curve rather than a family of curves including one curve for each peak cyclic stress level.

Crack growth rates for the lateral (T-L) direction were generated by testing double cantilever beam specimens having the configuration shown in Figure A2. Specimen thicknesses were 0.45 inch for the aluminum alloy, 0.50 inch for the steel alloy, and 0.375 inch for the titanium alloy. The resulting crack growth rate data are plotted in Figures 24 through 26 along with solid curves representing average crack growth rates for the T-S direction. Tabulated results are included in Tables 10 through 14 in Volume 2 of this report. For the aluminum and steel alloys, there is excellent agreement between crack growth rate data for the two directions. Only a limited amount of crack growth rate data were obtained for the T-L direction in the titanium alloy (Figure 26) due to experimental difficulties. Crack growth rate curves taken from Reference 5 are included in Figure 26 to aid in evaluation of the data. The agreement between the Reference 5 curves and the data generated herein is good as is the agreement between crack growth rates for the T-S and T-L directions. Hence, it was concluded that crack growth rates for both the T-S and T-L directions could be represented by a single crack growth rate expression, namely, Equation 8 fitted to the baseline data for the T-S direction.

3.1.2 Pure Bending Tests

Crack growth rates for both the depthwise (T-S) and lateral (T-L) directions were measured by growing surface cracks under pure bending stresses as described in Section 2.2.3. Raw data from these tests are listed in Tables 15 through 17 in Volume 2 of this report. Crack growth rate data are plotted on graphs of crack growth rate versus peak cyclic stress intensity factor in Figures 27 through 29. Rates for the T-S direction were obtained from periodic determinations of crack depth and rates for

the T-L direction were obtained from similar measurements of crack width. The solid curves in the figures are the average curves used to represent baseline crack growth rate data obtained from the uniform tension tests.

For the T-S direction, crack growth rates in the aluminum and steel alloys tend to be slower under pure bending stresses than under uniform tension stresses. Furthermore, the effects of stress ratio appear to be more pronounced for bending stresses than for tension stresses. On the other hand, agreement between crack growth rate data for bending and tension stresses in the titanium alloy is good. For the T-L direction, agreement between crack growth rates for bending and uniform tension stresses was good for all three alloys.

There does appear to be some differences between crack growth rates generated under pure bending and uniform tension stresses when correlated using the stress intensity factor formulations described in Section 2.2.4 of this report. It is not clear whether these differences arise from systematic errors in stress intensity factor calculations or from fundamental differences in crack growth behavior under bending and uniform tension stresses. Since the differences were not large (usually less than a factor of two), it was assumed in this report that K - da/dN correlations for bending and uniform tension stresses were equivalent.

3.1.3 Summary

Baseline crack growth rate data for both the T-S and T-L directions were in good agreement for all three test alloys, including 2219-T851 aluminum, 9Ni-4Co-0.2C steel, and 6Al-4V standard ELI beta annealed titanium. The combined effects of stress intensity factor and stress ratio on crack growth rate were well accounted for by fitting Equation 8 to the crack growth rate data. Equation 8 does not account for the known behavior that crack growth rates tend to large values as the peak cyclic stress intensity factor approaches the critical stress intensity factor. Attempts to determine whether peak cyclic stress level had any effect on crack growth rates over and above its contribution to stress intensity factor were inconclusive. It appeared that the crack growth rate data could be better correlated by ignoring possible stress level effects. Finally,

there did appear to be some differences between crack growth rate data generated under pure bending and uniform tension stresses. For constant peak cyclic stress intensity factor, crack depth growth rates under pure bending stresses tended to be moderately slower than rates under uniform tension stresses. This effect was more pronounced at R = 0.5 than at R = 0.1.

3.2 Constant Cyclic Load Tests

3.2.1 Uniform Tension Tests

Constant cyclic load tests were conducted by growing surface flaws under uniform cyclic loads until they penetrated the specimen thickness. Specimen configurations are detailed in Figure A5. Experimental procedures are included in Section 2.2.2 and experimental approach and test programs are outlined in Section 2.2.3. Raw data from all tests are tabulated in Tables 18 through 33 in Volume 2 of this report. Fatigue crack growth rates for the depthwise (T-S) direction are plotted as a function of peak cyclic stress intensity factors in Figures 30 through 32. Similar data for the lateral (T-L) direction are plotted in Figures 33 through 35.

There were two major differences between the constant cyclic load tests and the baseline tests: 1) tests were conducted for a much wider range of crack depth-to-width ratios and crack depth-to-thickness ratios; and 2) specimens were only about one-half as thick as the baseline specimens.

Crack depth growth rate data obtained from constant cyclic load tests are in good agreement with comparable data obtained from baseline tests for all three test alloys. This is illustrated in Figures 30 through 32 where the data points represent constant cyclic load data and the solid curves are average baseline crack growth rate curves. For the aluminum and steel alloys, there was a tendency for the constant cyclic load data for R = 0.1 to fall slightly to the right of the baseline curve. This result may have been due to systematic effects of change in specimen thickness. However, the differences are too small to be important. Accordingly, it was concluded that stress intensity factors calculated using Equation 2 can be

used to correlate crack depth growth rate data for a wide range of surface flaw geometries ($0.15 < a/2c < 0.50$ and $0.2 < a/t < 1.0$) in aluminum, steel, and titanium alloy components.

Crack width growth rate data obtained from constant cyclic load tests exhibited considerable scatter and were in poor agreement with comparable data obtained from baseline tests for all three test alloys. This is illustrated in Figures 33 through 35 where crack growth rate data from the two series of tests are compared. Crack width growth rates from the constant cyclic load tests tended to be significantly faster than crack growth rates from the baseline tests. This effect was more pronounced for deep, wide flaws than for shallow, short flaws. There are a number of factors that probably contributed to the poor agreement including: 1) inaccuracies in stress intensity factor formulas; 2) non-elliptical crack shapes; and 3) presence of the stress-free front specimen face. It is difficult to evaluate the relative effects of the foregoing factors. However, it is believed that Equation 3 underestimated the stress intensity factors at the ends of the semi-major axes of the flaws. Equation 3 was obtained by multiplying the stress intensity factor at the end of the major axis of a fully embedded elliptical crack by a constant factor of 1.1. Smith (21) and Thresher and Smith (13) have calculated stress intensity factors at the points where the peripheries of semi-circular surface flaws and part-circular cracks intersect the specimen surface and derived factors for Equation 3 ranging from 1.1 to 1.26. Recent unpublished work by Smith has led to even higher factors for Equation 3 for long deep surface cracks. Hence, it does appear that Equation 3 underestimated the stress intensity factors at the ends of the major axes of the surface flaws. On the basis of this work, a multiplying factor of 1.25 would be more appropriate for Equation 3 than the factor of 1.1 that was used in this program. The potential effects of the other factors that may have affected crack width growth rate correlations (crack shape and stress free specimen face) cannot be quantitatively evaluated. Nevertheless, it is believed that inaccuracies in stress intensity factor correlations were the major contributor to the poor crack width growth rate correlations shown in Figures 33 through 35.

3.2.2 Combined Bending and Tension Tests

Combined bending and tension tests were conducted by subjecting surface flawed specimens to combined axial and lateral loads as described in Section 2.2.3 of this report. Raw test data are tabulated in Tables 22 through 35 in Volume 2 of this report. Fatigue crack growth rate data for both the depthwise (T-S) and lateral (T-L) directions are plotted as a function of peak cyclic stress intensity factor in Figures 36, 37 and 38 for the aluminum, steel and titanium alloys, respectively.

For the depthwise (T-S) direction, crack growth rates measured under combined bending and tension stresses tend to be slower than the average baseline tension rates for the aluminum and titanium alloys. On the other hand, agreement is good for the steel alloy. In these tests, the uniform tension component of the stress fields contributed two-thirds or more of the stress intensity factor at the crack tip and so it is surprising that data for the different stress fields did not show more consistent agreement. At this time, it is not known why the agreement was not better.

For the lateral (T-L) direction, agreement between crack growth rate data measured under combined bending and tension and uniform tension stress fields are in reasonably good agreement. Previously described pure bending and uniform tension tests led to the result that crack growth rates for the lateral (T-L) direction were faster than baseline rates for uniform tension stresses, and equal to or slower than baseline rates for pure bending stresses. In the combined bending/tension tests, the bending stresses were responsible for a higher percentage of total stress intensity factor for the lateral direction than for the depthwise direction. Consequently, reasonable agreement was obtained between bending/tension and baseline crack growth rate data.

Some unresolved differences were noted between crack growth rate data obtained with and without the presence of bending stresses. However, since crack growth rates in the absence of bending stresses were always equal to or greater than rates obtained with bending stresses present, it was concluded that baseline uniform tension crack growth rate data could be safely used to predict crack propagation lives for structures subjected to combined bending and tension stresses.

3.2.3 Comparison of Predicted and Actual Results

For each of the surface flaws that were tested under uniform tension stresses, predictions were made of the number of loading cycles that would be required to grow the crack from its initial to final depth when growing under the actual test conditions. Predictions were made by simultaneous integration of Equation 8 for both the depthwise and lateral directions, i.e.,

$$\frac{da}{dN} = \frac{dc}{dN} = C(K_{max} - K_{th})^m (\Delta K)^n \qquad (8)$$

Values of K_{th}, C, m and n for each alloy were obtained from a least square fit of the baseline tension da/dN data as described in Section 3.1.1. Integration of crack depth growth was carried out between the limits of measured initial and final crack depth. Integration of crack width growth was carried out from a lower limit of measured initial crack width until the calculated crack depth reached the measured final crack depth. Hence, the predicted crack shape (a/2c) at the end of the test differed from the actual a/2c. Predicted lives are summarized and compared to actual lives in Tables 14, 15 and 16 for the aluminum, steel and titanium alloys, respectively. Predicted lives are plotted against test lives in Figure 39.

The agreement between predicted and actual test lives was very good. The ratio of actual to predicted life ranged from a minimum of 0.6 to a maximum of 1.3. The result shows that baseline crack propagation data can be used in conjunction with the stress intensity formulations described in Section 2.2.4 to predict crack propagation behavior of surface flaws in structures subjected to constant cyclic tension stresses. Predictions could be improved slightly by modifying Equation 3 for stress intensity factor at the ends of the major axes of surface flaws. This could be accomplished by increasing the multiplying factor from 1.1 to 1.25 as discussed in Section 3.2.1.

3.2.4 Flaw Interaction Effects

There was evidence that some test results from the aluminum alloy deep flaw specimens were affected by interaction between the three flaws in a given specimen. This is illustrated in Figure 40 where both experimental

and predicted flaw depth versus cycle curves are included for aluminum alloy deep flaw specimens SUTA1-2 and SUTA5-2. Predictions were made as described in Section 3.2.2, except that experimental and predicted values of cycles to breakthrough for Flaw No. 3 were forced to agree for each specimen. In specimen SUTA1-2, the relationship between experimental and predicted results is different for Flaw No. 2 than for the other two flaws. Crack depth growth for Flaw No. 2 proceeded more slowly than predicted and the discrepancy between predicted and experimental results increased as crack depth increased. This result could have been due to the load alleviating effect of the two outer flaws (#1 and #3) on the middle flaw (#2). On the other hand, relationships between experimental and predicted crack growth behavior were different in the second deep flaw specimen SUTA5-2. In SUTA5-2, Flaw No. 3 grew faster than predicted, whereas Flaw No. 2 grew as predicted. Since interaction effects would result in a slowing down of crack growth rates, the results of Specimen SUTA5-2 indicate that flaw interaction was not a significant factor unless the interactive effects were the same for all three flaws.

There are no theoretical solutions giving stress intensity factors for an array of parallel surface flaws. However, some insight can be gained from stress analyses for arrays of through-the-thickness cracks. The selection of crack spacing for the specimens in this program (3.5 inches for the aluminum alloy and 3.0 inches for the steel alloy) was based on an approximate solution (22) for stress intensity factors at the tips of arrays of parallel through-the-thickness cracks. This solution showed that load alleviation due to cracks having lengths equal to the maximum surface crack lengths tested in this program would influence the stress intensity factors by less than two percent. However, other similar solutions (23, 24) yield a greater influence of flaw interaction on stress intensity factor than the Reference 1 solution. For the aluminum alloy specimens in which crack length was limited to 1.8 inches by stop drilling, Reference 24 predicts that stress intensity factors would be reduced by 6% for the outer cracks and 14% for the middle cracks, assuming equal lengths for all three cracks. It is believed that these values are good estimates of the maximum effects of flaw interaction on stress intensity factors that

occurred in this test program. Since the maximum effects are not large and occurred only during the latter stages of some tests, it was concluded that flaw interaction was not a significant factor in the test program reported herein.

3.3 Overload Tests

Overload cyclic tests were conducted by repeatedly subjecting surface flaw specimens to one of the three loading programs shown in Figure 16. Most tests were conducted using loading program A, which contained an initial tensile overload followed by a block of uniform load cycles having a peak cyclic stress less than that of the overload. The remaining tests were conducted using loading programs B and C which contained either a compressive load cycle or a tensile/compressive loading cycle followed by a block of uniform load cycles. Experimental procedures are outlined in Section 2.2.2. Experimental approach and test program are described in Section 2.2.3. Forty-five specimens were equally divided between each of the three test alloys (2219-T851 aluminum 9Ni-4Co-0.2C steel, 6Al-4V beta annealed titanium) as summarized in Tables 17 through 19. Tests designated as single overload tests were subjected to only one loading program, or multiple loading programs in which the overloads (positive or negative) were believed to be separated by a sufficient number of cycles to minimize interactive effects. Tests designated as periodic overload tests were subjected to more frequent overloads to investigate interactive effects between overloads. Test results are tabulated in Tables 36 through 80 in Volume 2 of this report.

3.3.1 Uniform Tension Overload Tests

The most significant results of the uniform tension overload tests were: 1) tensile overloads resulted in subsequent transient reductions in crack growth rates relative to rates that would have existed in the absence of the overloads; 2) tensile overloads resulted in large amounts of apparent crack growth during the overload cycle; 3) small compressive loads applied immediately after tensile overloads reduced the crack growth retardation effects of the tensile overloads; and 4) small periodic negative loads had no detectable influence on subsequent crack growth rate behavior. These results are discussed in detail in the following sections.

3.3.1.1 Crack Growth During Overloads

It appeared that each tensile overload resulted in significantly more crack growth than would be predicted on the basis of uniform load crack growth rate data. This inference was based on the appearance of the fracture surfaces of the test specimens which contained regularly spaced dark bands around the initial flaw periphery, with the number of bands equal to the number of overloads. The dark bands are illustrated in Figure 41 where the fracture surfaces of the three flaws in Specimen SPOTA-2 are shown. Specimen SPOTA-2 was subjected to five tensile overloads having peak stress levels of 36 ksi, including one at the outset of the test and one every 13,000 cycles thereafter. Between overloads, the specimen was subjected to uniform cyclic loading having a peak cyclic stress of 18 ksi and stress ratio of 0.1. It was concluded that the dark bands most probably resulted from crack growth that occurred during the overload cycle and the light areas resulted from fatigue crack growth between overloads. Comparable fracture surfaces from steel alloy specimen SPOTS-1 and titanium alloy specimen SPOTT-3 are shown in Figures 42 and 43. For the titanium alloy, periodic bands of crack growth that occurred during overloads were readily observed only with the use of polarizing lenses.

Based on the assumption that the width of the dark bands on the fracture surfaces did represent crack growth during overloads, crack depth growth rates for the overload cycles were plotted against peak stress intensity factors due to the overloads in Figures 44 through 46. Baseline crack growth rate curves are included in each of the figures for comparison. The crack growth rates for the overload cycles are approximately two orders of magnitude greater than comparable baseline rates for all three alloys. Hence, it appears that tensile overloads result in considerably more crack growth than would be predicted on the basis of uniform cyclic load crack growth rates. Similar results have been previously reported in the literature for beta annealed Ti-6Al-4V(5) and 2024-T3 aluminum (25).

Crack closure theory predicts larger crack growth rates for single overloads than those predicted on the basis of uniform load crack growth rate data. Hence, an attempt was made to see if the discrepancies between

baseline and overload crack growth rates could be explained using crack closure theory. According to crack closure theory, residual displacements left in the wake of a propagating crack come in contact at low loads and prevent the crack from closing completely. Hence, the effective ΔK (ΔK_{eff}) is somewhat less than the applied ΔK calculated by substituting the applied load range (ΔP) into the applicable stress intensity factor equation. Elber (26) was the first to observe crack closure and proposed the following relationship between ΔK_{eff} and ΔK for uniform stress loading profiles

$$\Delta K_{eff} = (0.5 + 0.4R)\Delta K \qquad (9)$$

where R is the stress ratio. There is some doubt as to the validity of Equation 9 (27) but it will be used in the following analysis since it predicts the largest crack closure effects reported to date. When a crack is growing under a uniform cyclic loading profile having a stress ratio of 0.1, Equation 9 predicts that the crack faces do not completely separate until the stress level reaches 51 percent of the peak cyclic stress level. When the loading program is interrupted by a single overload, the opening stress during the overload remains the same but the peak stress level is increased, and $\Delta K_{eff}/\Delta K$ for the overload is larger than predicted by Equation 9. The crack growth rate data and curves in Figures 44 through 46 were replotted as a function of ΔK_{eff} in Figures 47 through 49, where it is seen that crack closure theory alone does not explain the large crack growth rates observed during tensile overloads.

In the foregoing analysis, it was assumed that the width of the periodic dark bands on the fracture faces was equal to the amount of crack growth that occurred during the overloads. This assumption needs to be substantiated before any definite conclusions can be drawn with respect to the effects of overloads on growth of surface flaws. It is possible that electron fractography would be able to establish a relationship between band width and crack growth during overloads. In the absence of such information, however, it is recommended that the detrimental effects of overloads on surface flaw growth be assumed to be as large as those indicated by the results in this program.

3.3.1.2 Retardation Effects

Single Overload Tests

The effects of single overloads on crack growth rate behavior were evaluated using continuous recordings of crack displacement versus loading cycles obtained from each test. The test record obtained from aluminum alloy specimen SOTA-1 (Figure 50) is typical of records obtained from specimens subjected to tensile and tensile/compressive overloads. Specimen SOTA-1 was subjected to two overloads having peak stress levels of 36 ksi followed by uniform cycling to peak cyclic stress of 18 ksi. The initial overload was applied at the outset of the test and the second overload was applied 20,700 cycles later. Figure 50 also includes a record of crack displacement versus cycles for Specimen SUTA-1 which was tested under a uniform cyclic loading profile having a peak stress of 18 ksi. The test record obtained from Specimen SOTA-3 (Figure 51) is typical of records obtained from specimens subjected to compressive loads (Program B in Figure 16). Specimen SOTA-3 was subjected to a compression cycle having a minimum stress of -1.8 ksi at the outset of the test followed by uniform cycling to a peak cyclic stress of 18 ksi. Figure 51 also includes a record of crack displacement versus cycles for Specimen SUTA-1 which was tested under a uniform cyclic loading profile having a peak stress of 18 ksi. The test records for the two specimens are in good agreement.

The characteristics of the test record for Specimen SOTA-1 shown in Figure 50 are typical of the records obtained from all aluminum alloy single overload specimens. The slope of each segment of the records between successive overloads appeared to be minimum immediately after the overload. The slope then gradually increased with increasing number of loading cycles and returned to values that would have been existent in the absence of the overload. The application of a second overload caused an abrupt decrease in the slope of the test record and a repeat of the above described behavior. The effect of plastic deformations on the slopes of the test records are believed to have been small since both plastic zone sizes and the rate of change of plastic zone size with increase in crack size were small. Hence, it is reasonable to

assume that changes in measured crack displacement resulted primarily from changes in crack dimensions and that crack growth rates were proportional to the slopes of the test records. Accordingly, it was inferred from the test records that tensile overloads resulted in an abrupt decrease in crack growth rates with minimum rates occurring immediately after the overload. Crack growth rates gradually increased from the minimum value until they returned to values that would have existed in the absence of the overload.

The effects of tensile overloads on crack growth rate behavior observed in this program are different from results reported in the literature (28, 29) which show that crack growth rates after a tensile overload rapidly decrease to a minimum value after traversing about one-quarter of the crack tip plastic zone formed by the overload, and then increase to values slightly less than would have been expected in the absence of the overloads. Since the previous results were obtained using one-eighth inch thick specimens and visual crack length measurements at the specimen surface, the possibility exists that surface effects could have influenced the results. It is also possible that the reaction of surface flaws to tensile overloads is different from that of thin through-cracked specimens. More work will be required to explain differences in observed crack growth rate behavior after tensile overloads.

The test records of crack displacement versus cycles were used to determine the increase in cyclic life or delay cycles (N_d), and the increment of crack length after each overload over which the crack growth rate behavior was influenced by the overload (Δa_d). This was accomplished as illustrated in Figure 50 where test records for uniform cyclic load Specimen SUTA-1 and single overload Specimen SOTA-1 are plotted. After the minimum level of crack displacement at which the slope of the test record for the overloaded specimen became equal to that for the uniform load specimens was determined, N_d and $\Delta\delta_d$ were read from the graph as shown in Figure 50. The value of Δa_d corresponding to $\Delta\delta_d$ was determined from graphs of a versus δ for each of the flaws. Some adjustments were made to the test records before values of N_d and Δa_p were determined. Adjustments were required because of small differences in initial crack

dimensions from specimen to specimen and because of data scatter. Data scatter was accounted for by shifting the uniform load test record up or down so that the ratio of crack displacement to crack depth at the outset of both uniform load and overload tests was the same. Variations in crack size were accounted for by shifting the uniform load curve either right or left until the test records for both uniform load and overload specimens intersected the ordinate at a common point.

Values of N_d and Δa_p for aluminum, steel, and titanium single overload specimens are summarized in Tables 20 through 25. There are two tables of data for each alloy, including one for shallow flaw specimens and one for deep flaw specimens. Tests conducted using an overload ratio of 2 yielded several thousand delay cycles, whereas tests conducted using an overload ratio of 1.5 yielded considerably fewer delay cycles (usually less than 1000). Negative loads had no detectable effect on subsequent crack growth rate behavior.

Only one test was conducted using tension/compression overload cycles. Titanium deep flaw specimen SOTT-6 was tested using overload cycles having peak tensile and compressive stresses equal to +2.0 and -0.2 times the subsequent peak cyclic stress of 27 ksi, respectively. The compressive stress was applied after the tensile stress. Specimen SOTT-4 was tested in an identical manner except that the compressive stress was eliminated from the overload cycle. A comparison of N_d values for the two specimens included in Table 25 shows that the compressive stresses applied to Specimen SOTT-6 reduced the number of delay cycles by about 50 percent.

Values of Δa_p listed in Tables 20 through 25 are generally greater than calculated plastic zone sizes due to the overloads $\rho_o = 1/3\ \pi\ (K_o/\sigma_{ys})^2$. The average value of the ratios of $\Delta a_p/\rho_o$ varied between alloys and between shallow and deep flaw tests for a given alloy. For example, the average values of $\Delta a_p/\rho_o$ for the aluminum, steel and titanium alloy shallow flaw tests were 1.3, 2.4 and 1.9, respectively. For the deep flaw tests, average $\Delta a_p/\rho_o$ values were 2.6, 4.0 and 1.3 for the aluminum, steel, and titanium alloys, respectively.

The effects of single overloads on subsequent crack growth rate behavior observed in this program are in qualitative agreement with overload effects predicted using methods suggested by Wheeler (30) and Willenborg (31). The Willenborg method presently predicts total retardation of crack growth after overloads equal to or greater than twice the subsequent peak cyclic stress level. In this program, overloads to twice the subsequent cyclic stress did not totally retard crack growth and so the Willenborg model was not used in evaluating test results.

In light of the prior experimental observations, Wheeler suggested that crack growth rates after an overload could be approximated using the equation

$$\left(\frac{da}{dN}\right)_r = \left(\frac{da}{dN}\right)_u \left(\frac{r_y}{a_p - a}\right)^m ; \; a + r_y < a_p \qquad (10)$$

where: $(da/dN)_r$ is retarded crack growth rate after an overload;

$(da/dN)_u$ is the corresponding uniform load crack growth rate;

$(a_p - a)$ is distance from crack tip to elastic-plastic interface formed by the overload;

r_y is the size of the plastic zone formed by a loading cycle applied after the overload;

m is an exponent.

Past use of Equation 10 led to the observation that the exponent m is not constant but has to be varied to fit different sets of experimentally determined crack propagation data. Approximate values of N_{d_2} were calculated using Equation 10 with $(a_p - a)$ equal to $1/3\ \pi\ (K_o/\sigma_{ys})^2$ where K_o is the peak stress intensity factor during the overload cycle, and r_y equal to $1/3\ \pi\ (K_m/\sigma_{ys})^2$ where K_m is the peak cyclic stress intensity factor. Calculations were made for various values of the exponent m. Two approximations were made to simplify the calculations: 1) the value of crack tip stress intensity factor was assumed to be constant as the crack tip traversed the plastic zone formed by the overload; 2) the

integration was performed block by block of cycles rather than cycle by cycle.

Results of the calculations are compared to actual test data in Figures 52 through 54 where the values of delay cycles are plotted as a function of peak cyclic stress intensity factors for the aluminum, steel, and titanium alloys, respectively. Each figure contains data for one alloy and two overload ratios. For the overload ratio of 2, data points for the aluminum alloy fell between curves corresponding to m = 1.0 and 1.5, whereas data points for the steel and titanium alloys fell between curves corressponding to m = 1.5 and 2.0. For the overload ratio of 1.5, most data points fall between curves corresponding to m = 1 and m = 2, although a few data points fall well outside of this range. The scatter factor was about two for the data obtained using the higher overload ratio. This amount of scatter is normal for crack propagation tests. For the overload ratio of 1.5, the values of delay cycles were smaller than for the overload ratio of 2, and were more sensitive to variations in crack growth rate behavior. Hence, the scatter factor increased with decrease in overload ratio.

In summary, single tensile overloads can have a strong influence on fatigue crack propagation behavior by inducing large amounts of crack growth during the overload and by retarding crack growth rates after the overload. Present methods of estimating crack growth due to single tensile overloads (K - rate correlations and crack closure theory) greatly underestimate such growth. Retardation effects were in qualitative agreement with crack growth rate models that predict minimum crack growth rate immediately after the overload followed by monotonically increasing crack growth rates. The Wheeler method (30) of computing crack growth rates after overloads was found to be in reasonable agreement with the test data as long as an appropriate value of the exponent m in the crack growth rate equation is used. The value of m was found to be influenced by alloy.

Periodic Overload Effects

The effects of periodic overloads on crack growth behavior are illustrated on graphs of crack depth versus loading cycles in Figures 55 through 66. Each figure contains two or three graphs including one for each of the flaws in a given specimen. Each graph contains data obtained from several specimens including the baseline specimen tested under a uniform stress loading profile, and comparable specimens tested under periodic overload programs having a single overload ratio. With few exceptions, cyclic life increased with increase in either overload frequency or overload ratio. One exception is shown in Figure 59 where a decrease in overload period from 11,000 to 7,500 cycles resulted in a decrease in cyclic life for 9Ni-4Co-0.2C steel alloy specimens. For reasons that could not be determined, overloads in the less frequently overloaded specimen appeared to result in greater crack growth retardation than did the overloads in the more frequently overloaded specimen. No experimental error could be detected nor was the additional crack growth caused by the more frequent overloads sufficient to explain the difference in crack propagation life.

The effects of periodic overloads were evaluated by fitting the Wheeler model (Equation 10) to the crack growth data between each successive overload. The values of the exponent m required to force agreement between the model and experimental results were calculated for each overload. The value of m is a measure of the retarding effect of overloads on subsequent crack growth rates, and the higher the value of m the greater the retardation. Values of m were plotted against crack depth-to-thickness ratio in Figures 67 through 71 for both shallow and deep flaw specimens and for each of the three test alloys. For the aluminum and titanium alloys, the exponent m increased rapidly with increase in a/t (and number of overloads). For the steel alloy shallow flaw specimens, the exponent m decreased in value before it started to increase as the flaw tip approached the back specimen face. For all tests except those for steel alloy shallow flaws, the overloads appeared to have a cumulative effect on crack growth behavior. Such cumulative effects could be due in part to crack closure effects. Residual deformations resulting from an overload could affect crack growth behavior after

subsequent overloads by increasing crack closure loads. Increases in crack closure loads could reduce effective stress intensity factors and lower crack growth rates relative to those that would have existed in the absence of the overload. For the steel alloy shallow flaws, reasons for the initial trend of decreasing m with increasing a/t are not known at this time.

It was observed that as the crack tips closely approached the back specimen faces, the rate of increase of m with increase in a/t underwent a marked increase. When overloads were applied to deep surface cracks, the additional plastic deformations allowed by the presence of the stress free back surface could have resulted in increased crack closure loads, crack tip blunting, or residual compressive stresses, all of which could have enhanced the effect of the overload on subsequent retardation of crack growth rates. The effects of crack depth-to-thickness ratio on crack growth retardation due to overloads led to situations where cyclic life was inversely proportional to initial crack depth as illustrated in the upper part of Figure 72.

An unplanned change in overload frequency during the testing of Specimen SPOTA-1 yielded an interesting result. The first five 36 ksi overloads were separated by 9000-18 ksi loading cycles. The fifth and sixth overloads were separated by only 4500-18 ksi loading cycles. The overload frequency was then increased to 9000 cycles for the remainder of the test. Values of the exponent m required to make the Wheeler equation (Equation 10) fit the data between each overload were calculated. The value of m for the 4500 cycle intervals were 2.0 or greater whereas the maximum m value for the adjacent 9000 cycle intervals was 1.6. This result indicates that the Wheeler method may underpredict initial retardation and overpredict later retardation of crack growth rate in arriving at the total number of delay cycles due to the overload.

Gray (32) recently proposed an expression for calculating the Wheeler exponent m as follows:

$$m = \frac{\frac{n}{2} \log (\Delta K_{th}/\Delta K)}{\log (1/S)} \qquad (11)$$

where ΔK_{th} = threshold stress intensity range

ΔK = applied stress intensity range

n = exponent where $da/dN = C(\Delta K)^n$

S = value of K_o/K_{max} resulting in subsequent crack growth arrest

Equation 11 yields m values that depend both on material and the value of ΔK subsequent to the overload.

Equation 11 was used to determine the range of m values that would be calculated for each block of uniform stress cycles between overloads applied in the periodic overload tests. Values of ΔK_{th} = 4, 8 and 9 ksi $\sqrt{in}$ and S = 2.3, 2.3 and 2.8 were used in the calculations for the aluminum, steel, and titanium alloys, respectively.

Values of Wheeler Exponent

Alloy	Calculated (Eqn 11)	From Data Fitting
Al-2219-T851	1.4 - 3.0	0.7 - 2.4
Fe-9Ni-4Co-0.2C	1.3 - 2.7	0.8 - 2.5
Ti-6Al-4V βA	2.0 - 2.6	1.7 - 2.5

The agreement between calculated and fitted values is quite good with the calculated values tending to be moderately higher than the fitted values. The best agreement was obtained for the titanium alloy and the worst for the aluminum alloy for which the calculated values were consistently higher than those obtained by data fitting.

3.3.2 Combined Bending and Tension Tests

Three specimens of each alloy were tested under combined bending and tension stresses as summarized in Table 26. Overloads for the aluminum alloy specimens were applied using axial loads only. Overloads for the steel and titanium alloy specimens were applied using both axial and lateral loads equal to the capacity of the test machine.

All overloads resulted in bands of apparent crack growth on the fracture surfaces of the specimens. The appearance of the bands was identical to similar bands observed in the uniform tension tests. The widths of most of the bands fell within the scatter zones of crack growth rates for the axially loaded specimens shown in Figures 44 through 46, a few bands on the steel alloy specimens were less than 10^{-3} inches wide and were smaller than comparable band widths in the axially loaded specimens. There did not appear to be any significant differences in crack growth behavior during overloads between axially loaded specimens and combined axial and laterally loaded specimens.

Results of the aluminum alloy tests are plotted on graphs of crack depth versus cycles in Figure 73. The effect of the periodic overloads on crack growth behavior was dependent on the peak stress levels applied during the overloads. Where the peak tensile overload stress was 27 ksi, the stress intensity factors at the crack periphery were smaller during the overload than during the subsequent uniform stress cycling and cyclic life was shorter for the overloaded specimen than for the comparable uniformly loaded specimen. When the peak tensile overload stress was 36 ksi, the peak overload stress intensity factor at maximum crack depth ranged from 1.25 to 1.50 times the subsequent peak cyclic stress intensity factor as the crack grew from its initial to final depth. The same ratios ranged from 1.06 to 1.40 at the end of the semi-major axes of the flaw. The crack growth behavior of Specimen SOBA-1 (which was overloaded only at the outset of the test and after 3700 loading cycles) was nearly identical to that for the uniformly loaded specimen except for the crack growth that occurred during the overload. Crack propagation life was

increased in Specimen SPOBA-1 by the application of 36 ksi overloads every 1650 cycles. However, the increase was small and the damage done by the overloads appeared to nearly offset the beneficial effect of the subsequent retardation of crack growth rates.

Results of the steel alloy tests are plotted on graphs of crack depth versus loading cycles in Figure 74. The ratios of peak overload stress intensity factor at maximum crack depth ranged from about 1.3 to 1.45 times the peak cyclic stress intensity factors applied immediately after the overloads as the crack grew from their initial to final depths. The effects of the overloads on crack depth growth rate behavior were fairly small and appeared to be maximum for deep cracks.

Results of the titanium alloy tests are plotted on graphs of crack depth versus loading cycles in Figure 75. The ratios of peak overload stress intensity factor at maximum crack depth ranged from about 1.3 to 1.4 times the peak cyclic stress intensity factors applied immediately after the overloads as the cracks grew from their initial to final depths. For crack depths near the initial values, the overloads had only a small effect on overall average crack growth rate. For intermediate crack depths, average crack growth rates in the overloaded specimens appeared to be consistently larger than in the uniformly loaded specimens. For deep cracks, the application of frequent overloads resulted in a marked decrease in crack growth rates as previously noted for the steel specimens.

The foregoing combined bending and tension tests did not yield sufficient information to determine whether stress state had any effect on the influence of periodic overloads on crack growth rate behavior. The overload ratios were not sufficiently large to yield changes in crack propagation life that were larger than possible changes due to data scatter. It did appear that when overload ratios were less than 1.4, the effect of periodic overloads on crack propagation behavior was small, except for

the case of very deep surface flaws when overloads resulted in a slowing down of crack propagation rates.

3.4 Spectrum Load Tests

Spectrum load tests were conducted by growing surface flaws under uniform tension loadings representative of either bomber or flight operations. Test procedures are described in Section 2.2.2 and experimental approach is outlined in Section 2.2.3. Raw test data are tabulated in Tables 81 through 92 in Volume 2 of this report. Results are illustrated on graphs of crack depth versus number of spectra in Figures 76 through 81 of this report. Two figures are presented for each of the three alloys including one figure for the bomber spectrum and one for the fighter spectrum. Two graphs are shown in each figure including one graph for a shallow flaw specimen and one for a deep flaw specimen. Each graph contains one curve for each of the flaws located within a given specimen.

The data were analyzed to determine if reasonable surface crack propagation life estimates for spectrum loadings could be based on crack propagation calculation methods containing simple models to account for crack growth retardation effects due to overloads. Initial calculations were conducted using linear cumulative damage assumptions and procedures described in Section 3.2.3. Each monotonic load increase between successive load reversals was counted as a load cycle. For analyses purposes, infrequently applied loads were assumed to be applied fractionally during each load spectrum, e.g., one-in-ten spectrum loads were applied as 0.10 cycle increments during each spectrum. Actual and calculated lives for each flaw are summarized in Table 27. Ratios of actual to calculated crack propagation life were plotted against initial crack depth to specimen thickness ratios, $(a/t)_i$. Envelopes encompassing data points for a given alloy and spectrum are shown in Figure 82. For the bomber spectrum, agreement between actual and calculated lives was good for all tests. Life ratios for all three alloys were insensitive to initial crack depth-to-thickness ratio. The envelope for the steel alloy tends to fall above those for the aluminum and titanium alloys.

However, the differences are not sufficiently large to be considered significant. For the fighter spectrum, agreement between actual and calculated lives was poor for most flaws. Furthermore, life ratios tended to decrease with increasing $(a/t)_i$ for the aluminum alloy and increased with increasing $(a/t)_i$ for the steel and titanium alloys. It was previously noted in Section 3.3.1.2 that the crack growth retarding effects of periodic overloads increased with increasing (a/t). The same effect is apparent in the steel/fighter and titanium/fighter spectrum load data but not in the aluminum/fighter spectrum load data.

If existing overload models had been used to acount for crack growth retardation effects in the bomber and fighter spectrum life calculations, all ratios of actual to calculated life would have decreased. Hence, agreement between actual and calculated lives would have improved for the steel/fighter, titanium/fighter, and possibly the aluminum/fighter and steel/bomber flaws. On the other hand, agreement would have degraded for the aluminum/bomber and titanium/bomber flaws. Furthermore, overload model calculations would not have changed the dependence of life ratio on initial crack depth-to-thickness ratio. Accordingly, it was concluded that commonly used overload models (30, 31) are not sufficiently sophisticated to provide accurate predictions of crack propagation life for spectrum loaded surface flaws.

There are many possible reasons for the failure of calculation procedures containing simple overload models to consistently predict crack growth behavior with an acceptable level of accuracy. Even in the absence of overloads, crack growth rate equations may not accurately represent crack growth behavior over the whole range of ΔK and R values encountered in loading spectra. Baseline crack growth rates are usually available for moderate to high ΔK values at R ratios less than 0.5. Spectrum loadings often generate very low ΔK values at R ratios greater than 0.5. It is usually assumed that the equation used to fit the baseline data is valid for ΔK and R values outside of the test range and such assumptions could result in errors in crack propagation estimates. In the present program, for example, baseline crack growth rates for the aluminum alloy were generated for $0.1 < R < 0.5$ and $12 < K < 25$ ksi $\sqrt{in}$.

The bomber spectrum generated ΔK values as low as 1.2 ksi $\sqrt{in}$ and stress ratios as high as 0.94. It was assumed that Equation 8 could be used to extrapolate the baseline data to the wider range of ΔK and R values generated by the bomber spectrum. However, this approach may have resulted in unknown systematic errors in linear cumulative damage life predictions. In addition to unknowns in baseline crack propagation behavior, there are still many unknowns in crack propagation under spectrum loads. For example, the effects of frequent changes in mean load usually encountered in spectrum loads is not understood. In this program, it was found that changes in mean load during overloads resulted in increases in crack size that were orders of magnitude greater than predictions based on baseline crack growth rate data. No method is currently available to account for this effect. Frequent load changes also lead to small numbers of loading cycles in a given load layer of a spectrum load. Hence, crack growth retardation effects during the first few cycles after an overload are of considerable importance to the understanding of crack growth behavior under spectrum loads. Test results from this program indicated that maximum crack growth rate retardation occurred immediately after the overload. Other investigators (28, 29) have reported that maximum retardation does not occur immediately after the overload. Hence, a better understanding of cycle by cycle crack growth rate behavior after changes on mean load would be useful. Other factors such as negative loads have measurable (33) but poorly understood, influences on crack growth rate behavior. In summary, there are many factors that affect crack propagation behavior under spectrum loads and it appears that the retardation effect due to overloads does not completely dominate spectrum load crack growth behavior.

Flaw Interaction Effects

It initially appeared that the middle flaw of the three flaws in each aluminum alloy deep flaw specimen was influenced by flaw interaction effects. This is illustrated in Figure 83 where the crack depth versus spectra curves for the middle flaws (Flaw #2) indicate a decrease in crack growth rate with increasing crack depth near the end of each test. This behavior may have resulted in part from load alleviating effects of the two outer flaws on the central flaw as the outer flaws

become large in size (this matter was previously discussed in Section 3.2.3). Test results are compared to calculated results obtained from modified linear cumulative damage calculations in Figure 83. The calculated results were obtained by modifying the baseline crack growth rate data to force good agreement between experimental and calculated results for Flaw #3. The calculations show that crack depth versus spectra curves for Flaws No. 2 and No. 3 in Specimen SSTA-3 could be expected to intersect as they did in the experiment. It also appears that flaw interaction effects were small since experimental and calculated crack propagation behaviors for the middle flaw were in good agreement over most of the range of flaw depths that were tested. It was concluded that flaw interaction effects influenced the crack propagation data only to a limited extent.

4.0 STRESS INTENSITY FACTORS FOR FLAWS AT FASTENER HOLES

Results of analytical work directed to the derivation of stress intensity factors for cracked fastener holes are described, discussed, and summarized in this section. The initial summary contains a listing of the resulting approximate stress intensity factor equations and the figures containing values of parameters and factors required for quantitative calculations. The subsequent material describes the approaches, assumptions and approximations used to derive each of the stress intensity factor equations.

4.1 Summary

Approximate stress intensity factors were derived for both thru cracks and part-thru cracks originating at loaded and unloaded close tolerance and interference fit fasteners.

Ten different cases involving thru cracks were solved as summarized in Table 28. New solutions were obtained for cracked holes containing loaded close tolerance fasteners (Cases 1b, 1c, 2b, 2c), unloaded interference fit fasteners in load-free plates (Cases 1d, 2d), and unloaded interference fit fasteners in plates subjected to remotely applied uniform tension stresses (Cases 1e and 2e). No general formula can be given for stress intensity factors at cracked interference fit fastener holes because of the non-linear nature of the problem and the large number of variables involved. It was concluded that stress intensity factors for cracked holes filled with unloaded close tolerance fasteners (Cases 1a and 2a) could be considered equal to stress intensity factors for open holes having the same geometry and loading conditions for $L/r > 0.1$.

Eight different cases involving part-thru cracks were solved as summarized in Table 29. Solutions were obtained for cracked open holes (Cases 3a and 4a), and holes containing unloaded or loaded close tolerance fasteners in plates subjected to uniform tension (Cases 3b-d and 4b-d).

4.2 Approach, Assumptions and Approximations

Stress analysis of a fastener joint in a plate, even in the absence of a flaw, is a complex nonlinear problem involving variable contact between the fastener and the plate. For loaded neat fit fasteners in a plate subjected to applied remote loading, the area of contact between the fastener and the plate varies with load and hence, the stress distribution also changes with load. For interference fit fasteners, plastic yielding generally occurs near the hole and further complicates the problem of determining the stress distribution near the fastener. When a flaw originates from the fastener hole, the analysis is further complicated since the crack reduces the rigidity of the structure surrounding the hole and changes the contact condition. At this time, it is not possible to obtain exact or numerical solutions for the stress intensity factors of three-dimensional crack problems such as part-thru cracks originating at an unfilled or a filled hole. Stress intensity factors for such problems have to be obtained using simplifying assumptions, approximations, and judicious estimates. In this study, assumptions and approximations were verified, wherever possible, with known two-dimensional and three-dimensional crack problems prior to using them to obtain stress intensity factors for the part-thru cracks at a hole.

4.2.1 Cracks Originating at Open Holes

4.2.1.1 Uniform Thru Cracks

It was reasoned that stress intensity factors for two symmetrical thru cracks of length L originating from an open hole in a plate (Figure 84b) could be obtained by solving an equivalent problem consisting of a pressurized center crack of length 2L in a plate (Figure 84c). Each half of the symmetrical pressure distribution is identical to the stress distribution along the x axis adjacent to an open hole in a plate subjected to uniform tension (Figure 84a). This belief was based on the following reasoning. It is known that for infinitely wide plates, stress intensity factors for a single edge crack length L are approximately 10 percent higher than those for a center crack of length 2L. This is due to the introduction of the stress free surface in the edge-cracked plate. In

the problem at hand, the hole periphery is a stress free surface, but its effect should be offset by the curvature of the hole periphery. Hence, symmetrical cracks originating at holes should be equivalent to central through cracks rather than edge cracks.

Stress intensity factors for thru cracks pressurized by σ_{zz} (X,o) are given by the following equations (35).

$$K = \frac{1}{\sqrt{\pi L}} \int_{-L}^{L} \sigma_{zz}(X,o) \sqrt{\frac{L+X}{L-X}}\, dx \qquad (12)$$

where the stresses $\sigma_{zz}(X,o)$ are given in Figure 84c. Stress intensity factor, K, can be represented in nondimensional form, F(L/r), as follows:

$$F_1(L/r) = K/(\sigma\sqrt{\pi L})$$

Results of the foregoing approximate solution for cracked open holes are compared to results of Bowie's numerical solution (36) in Figure 85. The dotted curve represents results of the approximate solution and the solid curve represents results from Bowie's solution. The discrepancy between the two solutions is less than 7 percent for $0.05 \leq L/r \leq \infty$. Hence, it was concluded that the foregoing approximate technique could be used to obtain stress intensity factors for all thru-cracked fastener hole geometries investigated in this program. The approximate technique consisted of two steps including: 1) determining the stress distribution adjacent to the fastener hole in question; and 2), solving the equivalent problem of a pressurized central thru crack in a plate.

Stress intensity factors for fastener holes cracked on only one side were obtained by multiplying the solution for symmetrically cracked holes by the factor shown in the following equation:

$$K\Big|_{\substack{\text{one}\\\text{crack}}} = \sqrt{\frac{2r+L}{2r+2L}}\; K\Big|_{\substack{\text{two}\\\text{cracks}}} \qquad (13)$$

This approach resulted from the knowledge that, when crack length is very large with respect to hole diameter, the effect of the hole on stress intensity factor is negligible and stress intensity factors can be calculated using equations for central thru cracks of length 2r+2L (two cracks) and 2r+L (one crack). Since stress intensity factors (K) vary with the square root of crack length, the relationship between K for two symmetrical long cracks at a hole and one long crack at a hole is given by Equation 13. As an approximation, Equation 13 was used for all L/r values (short and long cracks) to compute stress intensity factors for open holes with cracks originating from one side only with results shown in Figure 86. The results were compared to those from Bowie's numerical solution for the same problem and the two solutions agree within 2 percent for $0.05 \leq L/r \leq \infty$. In view of the good agreement between the two solutions, Equation 13 was used to calculate stress intensity factors for all single thru crack fastener hole problems investigated in this program.

4.2.1.2 Semi-Elliptical Part-Thru Cracks

It was desired to use the thru crack approximate technique to compute stress intensity factors for two semi-elliptical cracks originating at a hole in a thick plate (Figure 87). This technique required solutions for stress intensity factors generated by embedded elliptical cracks subjected to non-uniform internal pressure distributions. Available solutions for pressurized elliptical cracks in infinite solids are limited to pressure distributions (p) in the form of a polynominal of x and y defined as follows (37).

$$p(x,y) = \sum_{i=o}^{3} \sum_{j=o}^{3} A_{ij}\, x^i y^i \qquad (i+j) \leq 3 \qquad (14)$$

It is not possible to exactly fit pressure distributions adjacent to fastener holes using Equation 14. This is illustrated in Figure 88 where the prescribed stress distribution is the actual stress distribution adjacent to a hole in a plate and the fitted stress distribution was obtained by least square fitting the expression $A_{oo}+A_{20}X^2$ to the prescribed stresses. There are considerable differences between the two

stress distributions. For thru cracks, however, it was believed that as long as the area under the fitted stress curve (A_f) was approximately the same as the area under the prescribed stress curve (A_p), the stress intensity factors calculated using the two different stress distributions would not differ greatly. This assumption was examined using the problem of two symmetrical thru cracks originating at an open hole. The actual stresses were least square fitted by the equation $A_{00}+A_{20}X^2$ for various ratios of crack length to radius of hole, L/r. The error between the fitted stress and the prescribed stress was defined as follows:

$$\text{Percent error} = \frac{\text{Prescribed stress - fitted stress}}{\text{Prescribed stress}}$$

The error between the prescribed and fitted stresses increased as L/r increased. For L/r = 0.2, the error was smaller than ± 7 percent; for L/r = 6.0, the range of error was +49.3 to -34.2 percent of depending upon the value of X. However, the areas under the curves of the fitted stress and prescribed stress (A_f and A_p) compared remarkably well for all L/r ratios and values of A_f/A_p ranged from 1.01 to 1.09 as L/r ranged from 0.1 to 6.0. The stress intensity factors calculated using fitted stresses are plotted as open circles in Figure 85 and agreed within one percent with the previously calculated stress intensity factors. The stress intensity factors calculated from the fitted stress agreed within 8 percent with Bowie's solution over the range of L/r from 0.05 to 6.0. In view of the good agreement, fitted stresses were used in an initial attempt to solve the part-thru crack problem illustrated in Figure 87.

Initial estimates of stress intensity factors for two semi-elliptical cracks originating at a hole in a thick plate were made by solving the equivalent problem of a pressurized fully embedded elliptical crack using methods described in Reference 34. Pressure distribution was obtained by least square fitting the actual stress distribution adjacent to the hole using the expression $A_{00} + A_{20}X^2$. The resultant stress intensity factors (K_{Ih}) were normalized with respect to the stress intensity factor K_{Ie} for an elliptical crack having the same crack

depth-to-length ratio in an infinite solid subjected to the applied tension, σ. The non-dimensionalized factor $F_5(a/c, c/r, \beta)$ is defined as follows:

$$F_5(a/c, c/r, \beta) = \frac{K_{Ih}}{K_{Ie}} \tag{15}$$

where

$$K_{Ie} = \sigma \frac{\sqrt{\pi a}}{Q} \left[\cos^2\beta + \frac{a^2}{c^2} \sin^2\beta\right]^{1/4} \quad \text{if } a/c \leq 1.0$$

$$K_{Ie} = \sigma \frac{\sqrt{\pi c}}{Q} \left[\sin^2\beta + \frac{c^2}{a^2} \cos^2\beta\right]^{1/4} \quad \text{if } a/c > 1.0 \tag{16}$$

The non-dimensionalized factor $F_5(a/c, c/r, \beta)$ was determined for (a/c) values ranging from 0.1 to 1.0, and c/r values ranging from 0.1 to 10.0. Figure 89 shows values of the factor F as a function of a/c and β for three values of c/r, namely $c/r = 0.2$, 1.0 and 3.0. Values of F were quite insensitive to a/c for all c/r values. The maximum variations of F occurred for $\beta = 90°$ and $c/r = 1.0$ where the variation was less than 13%. In view of this result, it was concluded that F_5 could be assumed to be independent of a/c.

Stress intensity factors for two semi-circular cracks originating at a hole in a thick plate (Figure 87 with $a = c$) were calculated by solving the equivalent problem of a pressurized penny shaped crack. The penny shaped crack was pressurized by the exact two dimensional stress distribution adjacent to a hole in a plate (see Figure 84a) and stress intensity factors were calculated by numerical-analytical integration of the Green's function for stress intensity factor for a penny shaped crack given by Smith (38). Details of the Green's function and numerical-analytical integration are given in Reference 34. Results of the Green's function approach are included in Figure 90 and are compared to results obtained using the fitted stress approach in Figure 89. There are significant differences both in magnitude and distribution of stress intensity factors between the two solutions, particularly for large c/r ratios. The

maximum differences occur for very small values of β, i.e., at points on the crack periphery near the hole.

In view of the foregoing results, stress intensity factors for semi-elliptical cracks originating at fastener holes were obtained using the Green's function approach to calculate values of F_5 (it was previously concluded that F_5 could be considered to be independent of a/c), Equation 16 to calculate K_{Ie}, and Equation 15 to calculate K_{Ih}.

There is no stress intensity factor solution available with which to compare the results of the foregoing approximate solution. However, the approximate solution can be reduced to a two-dimensional crack problem by letting $a/c \to \infty$. The problem then reduces to the two-dimensional problem of two symmetrical thru cracks, each of length c, originating at a hole in a thick plate. The stress intensity factor K_{Ie} from Equation 16 is given by $\sigma\sqrt{\pi c}$ at $\beta = 90°$. Stress intensity factor K_{Ih} is then given by the equation $F(c/r, 90)\sigma\sqrt{\pi c}$. Values of $F(c/r, 90)$ agree within four percent with F(L/r) values from Bowie's solution for the range of $0.1 \leq c/r \leq 10.0$. Since the foregoing agreement was not a built-in condition to the approximate solution, such agreement gives confidence in the accuracy of the solution.

4.2.1.3 Quarter-Elliptical Part-Thru Cracks

The above solution of stress intensity factor for two semi-elliptical cracks in a thick plate (Figure 91a) was used to estimate the stress intensity factors for one or two quarter-elliptical cracks at a hole in a finite thickness plate (Figure 91c and 91d). As an intermediate step, stress intensity factors (K_{I2H}) for two quarter elliptical cracks at a hole in a semi-infinite solid (Figure 91b) were estimated by introducing a correction factor to account for the stress free front surface M_F (a/c, β), i.e.,

$$K_{I2H} = M_F\ (a/c,\ \beta)\ K_{Ih} \qquad (17)$$

M_F values were assumed to be independent of β for $0 \leq \beta < 90°$, and to be given by the equation developed for the point of maximum depth ($\beta = 0°$) on the periphery of a surface flaw in a uniform tension stress field, namely (39):

$$M_F\ (a/c,\ \beta) = 1.0 + 0.12\ (1 - a/2c)^2 \qquad (18)$$

At $\beta = 90°$, stress intensity solutions for part-circular cracks (40) show that values of M_F (a/c, 90) vary from 1.1 to 1.23. In this study, M_F (a/c, 90) was assumed to be 1.11.

The stress intensity factor, K_{I2P}, for two quarter elliptical cracks at a hole in a finite thickness plate (Figure 91c) can be estimated by introducing a second correction factor M_B (a/c, a/t, β) to account for the effects of the stress free back surface, i.e.,

$$K_{I2P} = M_F\ (a/c,\ \beta) \cdot M_B\ (a/c,\ a/t,\ \beta) \cdot K_{Ih} \qquad (19)$$

Back surface correction factors M_B are presently available only for an elliptical crack in a semi-infinite solid subjected to uniform tension (41, 42) and these factors were used to estimate K_{I2P} in the above equation. Values of M_B for a/c = 1.0 are plotted in Figure 92. M_B values for other a/c ratios can be obtained from Reference 41. Stress intensity factors, K_{I1P}, for one quarter elliptical crack in a finite thickness plate (Figure 91d), can be estimated from K_{I2P} by introducing a factor similar to that given by Equation 13. A quarter-elliptical crack having a depth 'a' and length 'c' has an area equal to that of a thru crack of length $\frac{\pi\ ac}{4t}$. Thus, the stress intensity factor for one quarter elliptical crack, K_{I1P}, was approximated by the following equation.

$$K_{I1P} = M_F(a/c,\ \beta) \cdot M_B(a/c,\ a/t,\ \beta) \cdot \sqrt{\frac{2r + \pi\ ac/4t}{2r + 2\pi ac/4t}} \cdot K_{Ih} \qquad (20)$$

4.2.2 Cracks Originating at Unloaded Neat Filled Holes in a Plate

Neat filled holes are holes filled with an insert having precisely the same diameter as the hole. The probability of occurrence of a true neat filled hole in real structure is remote. However, close tolerance fastener filled holes could exhibit behaviors approximating those of a neat filled hole in some instances. Accordingly, the neat filled hole problem was investigated to evaluate potential effects of close tolerance fasteners on stress intensity factors for cracked fastener holes.

Both magnitude and distribution of stresses adjacent to a hole containing an unloaded neat fit insert are different from those for stresses adjacent to an open hole as illustrated in Figure 93. The results shown in Figure 93 were obtained from exact solutions of the contact problem, namely, an infinite plate with a smooth circular insert (43, 44, 45). As seen from Figure 93, the effect of contact conditions and fastener material on the stress σ_{zz} along x axis is less than 3 percent for x/r greater than 1.3 for two extreme problems: 1) a plate containing a rigid fastener; and 2) a plate containing a highly flexible fastener (open hole). For real materials, the effect on σ_{zz} along z = 0 of contact conditions and plate/fastener materials for a neat filled hole in a plate subjected to uniform remote stress is equal to or smaller than the above noted effects. For $1.0 \leq x/r \leq 1.3$ (i.e., crack lengths smaller than 0.3r), the difference in stress σ_{zz} at $\theta = 0°$ between the previously considered two extreme cases ranges from 3 to 22 percent. Hence, the stress intensity factor solution for cracks at open holes would over-estimate the stress intensity factor for small cracks at neat filled holes. It is conceivable that for very rigid fasteners and extremely small cracks ($L/r \ll 0.1$), stress intensity factors for neat filled holes could be over-estimated by as much as 20 percent using the open hole solution. For most practical situations, however, it is believed that the over-estimate would be less than 10 percent. Hence, it was concluded that the solution derived for stress intensity factors at cracks originating from an open hole in a plate can also be used for the corresponding case of a neat filled hole.

It is of interest to note that the maximum tensile stress on the hole-fastener periphery generally occurs at the point of contact separation, i.e., $\theta \simeq 20°$. Figure 94 shows the distribution of circumferential stress $\sigma_{\theta\theta}$ around the hole periphery for four different combinations of plate/fastener materials. The difference between maximum stresses for the filled hole and the open hole is less than 8 percent, as shown in Figure 94. In the case of fatigue of a filled hole with no cracks, crack initiation does not have to occur at $\theta = 0°$. In the absence of the influence of other factors, the crack probably would initiate at the point of maximum stress ($\theta \simeq 20°$) and grow towards $\theta = 0°$.

4.2.3 Cracks Originating at Loaded Neat Filled Holes in a Plate

Using the Green's function approach described in Section 4.2.1.2 and stress distributions obtained from Reference 34, stress intensity factors for cracks originating at loaded neat filled holes were calculated with results described below. One additional approximation was used in these calculations, namely, shear stresses existing along the crack plane were ignored since they are small.

4.2.3.1 Two Symmetrical Thru Cracks Originating at a Loaded Neat Filled Hole

Stress intensity factor (K_I) for two thru cracks, each of length L, originating at a neat filled hole loaded by a force P, is represented by the following equation (34):

$$K_I = \sigma_b \sqrt{\pi L} \cdot F_3(L/r) \qquad (21)$$

where σ_b = bearing stress = $\frac{P}{2rt}$

$2r$ = diameter of hole

t = thickness of plate

F_3 (L/r) is the non-dimensional factor which is given as a function of the ratio of crack length to hole radius, L/r, in Figure 95.

4.2.3.2 One Thru Crack Originating at a Loaded Neat Filled Hole

Stress intensity factor (K_I) for one thru crack of length L originating at a neat filled hole, loaded by a force P, is given by the following equation (34):

$$K_I = \sigma_b \sqrt{\pi L} \cdot F_4 \ (L/r) \qquad (22)$$

where σ_b is bearing stress, and $F_4(L/r)$ is a non-dimensional factor which is given as a function of the ratio of crack length to hole radius (L/r) in Figure 96.

4.2.3.3 Two Semi-Elliptical Cracks Originating at a Loaded Neat Filled Hole in a Thick Plate

Stress intensity factor (K_{Ih}) for two semi-elliptical cracks originating at a neat filled hole loaded by a force P in a thick plate (Figure 87), is represented by the following equation (34). It is assumed that plate thickness t is significantly larger than 2a or 2c, i.e., $t \geq 6a$ or $t \geq 6c$.

$$K_{Ih} = F_6(c/r,\beta)\ K_{Ieb} \qquad (23)$$

$$K_{Ieb} = \sigma_b(\pi a/Q)^{1/2}[\cos^2\beta + (a^2/c^2)\sin^2\beta]^{1/4};\ a/c \leq 1.0 \qquad (24)$$

$$K_{Ieb} = \sigma_b(\pi c/Q)^{1/2}[\sin^2\beta + (c^2/a^2)\cos^2\beta]^{1/4};\ a/c > 1.0$$

where a, c, r, β, and σ are defined in Figure 87. $F_6(c/r, \beta)$ is plotted against the parametric angle β for various values of c/r varying from 0.1 to 7.50 in Figure 97. Using Equations 23 and 24 and Figure 97, stress intensity factors can be calculated for any point on the semi-elliptical crack periphery for the case of two semi-elliptical cracks emanating from a loaded neat filled hole in a thick plate.

4.2.3.4 Two Quarter Elliptical Cracks Originating at a Loaded Neat Filled Hole in a Plate

Stress intensity factors for two quarter ellipical cracks originating at a loaded neat filled hole in a finite thickness plate can be obtained by multiplying stress intensity values for two semi-elliptical cracks in a semi-infinite solid (Section 4.2.3.3) by factors to account for the effect of the stress free front surface (M_F) and the stress free back surface (M_B), i.e.,

$$K_I = F_6 \cdot K_{Ieb} \cdot M_F \cdot M_B \qquad (25)$$

Values of M_F and M_B are given by Equation 18 and Figure 92, respectively.

4.2.3.5 One Quarter Elliptical Crack Originating at a Loaded Neat Filled Hole in a Plate

Stress intensity factors for one quarter elliptical crack at a loaded neat filled hole in a plate can be obtained by multiplying stress intensity values for two quarter elliptical cracks in a plate (Section 4.2.3.4) by a factor to account for the change in number of crack locations as follows:

$$K_I = F_6 \cdot K_{Ieb} \cdot M_F \cdot M_B \sqrt{\frac{2r + \pi ac/4t}{2r + 2\pi ac/4t}} \qquad (26)$$

The basis for the additional factor was discussed in Section 4.2.1.2.

4.2.3.6 Cracks at a Loaded Neat Filled Hole in a Plate Subjected to Tensile Loading

Consider: 1) the case of a plate containing a loaded neat filled hole subjected to a remote tensile loading (Figure 98a); 2) the case of a plate containing a neat filled hole and subjected to a remote tensile load Q (Figure 98b); and 3) the case of a plate containing a loaded neat filled hole (Figure 98c). Since the contact area changes between the load cases of Figures 98a, 98b, and 98c, the stress distribution for the case of Figure 98a cannot be obtained just by linearly superposing the stress distributions for load cases of Figures 98b and 98c. Knowing

that the contact problem is nonlinear and still applying the linear superposition principle, it is shown in Reference 34 that the stress distribution σ_{zz} along x-axis (z = 0) for the load case of Figure 98a can be represented within 5 percent error by the superposition of σ_{zz} along the x-axis for the loading cases shown in Figures 98b and 98c. Since stress intensity factors (K_I) for cracks lying along the x-axis depend only on the stress σ_{zz} along the x-axis in an uncracked plate, it appears that good estimates of stress intensity factors for cracks emanating from a loaded neat filled hole in a plate subjected to remote loading (Figure 98a) can be obtained by linearly superposing stress intensity factors for cracks at a neat filled hole in a plate subjected to remote loading (Figure 98b), and for cracks at a loaded neat filled hole (Figure 98c). Stress intensity factors for the latter two cases are discussed in Section 4.2.3.

4.2.4 Thru Cracks at an Interference Fit Fastener

Substantial plastic yielding can occur around a hole filled with an interference fit fastener with the extent of plastic yielding governed by the level of interference and the remotely applied loading on the plate. An exact elastic-plastic solution to this problem is not presently available. However, a numerical elastic-plastic analysis for stresses near an interference fit fastener hole in an uncracked plate is available for one specific condition, i.e., one interference level, one fastener-plate material combination, and one uniform applied stress (46). The Reference 46 numerical elastic-plastic solution was used to check an approximate elastic-plastic solution derived for the stress σ_{zz} across the x-axis (z = 0) for an uncracked plate containing an interference fit fastener and subjected to either no applied loading, or a uniform unixial tensile stress (34). The advantage of the approximate solution over the numerical elastic-plastic solution (46) is that it can be used for any interference level, any fastener-plate combination, and any applied remote tensile stress.

A comparison of stress distributions σ_{zz} along the x-axis between the approximate (34) and numerical (46) solutions is given in Figure 99 for an aluminum plate of uniaxial tensile yield strength of 70 ksi which contains a 0.25 inch diameter steel fastener installed using a diametral interference of 0.004 inch. Figure 99 gives comparisons for three conditions: 1) stress distribution σ_{zz} due to interference alone; 2) stress distribution σ_{zz} due to interference and an applied remote stress of σ = 25 ksi; and 3), stress distribution σ_{zz} due to interference and unloading of the applied stress of σ = 25 ksi. Both stress distribution and location of elastic-plastic boundary given by the approximate solution agree quite well with those given by the numerical analysis. The stresses given by approximate solution are up to 15 percent higher than those given by numerical analysis except for the small stresses near the fastener. Thus, stress intensity factors which are derived using stress distributions given by approximate analysis will be slightly higher than those derived from the stress distribution given by numerical analysis.

From Figure 99, it can be seen that the stress distribution in an uncracked plate with interference fastener is dependent upon prior load history when the material around the fastener goes into yielding. Stress distribution σ_{zz} along the x-axis near the fastener is dependent upon uniaxial tensile yield strength of the material, both Young's modulus and Poisson's ratio for the plate and fastener materials, interference level (δ/d), and the applied uniaxial stress (σ). Hence, the stress intensity factors given in the subsequent figures are applicable only to specific conditions listed in each figure which are the conditions used in the experimental portion of this program.

4.2.4.1 Thru Cracks Subjected to Interference Stresses Alone

Stresses derived from the approximate elastic-plastic analysis for an uncracked 2219-T851 aluminum plate (σ_{ys} = 51.3 ksi) containing a steel interference fastener with no applied loading (34) were used along with the procedure described in Section 4.2.1 to obtain the stress intensity factors for two thru cracks at an interference fastener. It was assumed that the plate was not subjected to any remote loading after installation

of the fastener and that the material around the hole had not yielded prior to installation of the fastener. Stress intensity factor (K_I) for two thru cracks originating from an interference fastener was represented by the following equation (34):

$$K_I = F_I(L/r, \delta/d)\ \sigma_{ys}\sqrt{\pi L} \qquad (27)$$

where σ_{ys} is the uniaxial tensile yield strength of the plate material, L is the crack length of each of the two through cracks, and the stress intensity factor K_I is due to interference alone. $F_I(L/r, \delta/d)$ is given as a function of crack length to hole radius ratio (L/r) for various values of interference levels (δ/d) of 0.005, 0.0075, 0.010, 0.012, 0.014, and 0.016 in Figure 100. Values of $F_I(L/r, \delta/d)$ were derived for a 2219-T851 aluminum plate containing a steel fastener. Material properties taken for aluminum plate are σ_{ys} = 51.3 ksi, E = 10,000 ksi, ν = 0.3. For the steel fastener, E = 30,000 ksi and ν = 0.3. Reference 34 gives a values of $F_I(L/r, \delta/d)$ for various other material combinations, for various values of δ/d, and L/r values up to 10.0.

4.2.4.2 Thru Cracks Subjected to Combined Applied and Interference Stresses

Stress distribution, derived from the approximate elastic-plastic solution for a loaded uncracked plate containing an interference fit fastener (34), was used along with the procedure described in Section 4.2.1 to calculate the stress intensity factors for two cracks at an interference fastener in a plate subjected to uniaxial stress σ_{max}. Stress intensity factor (K_I) for two thru cracks originating from an interference fastener hole in a plate subjected to applied unixial tensile stress σ_{max} (Figure 101) is represented by the following equation (34)

$$K_I = F_{I\sigma}\ (L/r, \delta/d, \sigma_{max})\ \sigma_{ys}\ \sqrt{\pi L}$$

The function $F_{I\sigma}$ in Equation 28 is dependent upon the ratios of crack length to hole radius and diametral interference to diameter of fastener (or hole), and the applied stress σ_{max}. It also is dependent upon the plate/fastener material combination and the yield strength of the plate material. Values of $F_{I\sigma}(L/r, \delta/d, \sigma_{max})$ are given in Figures 101, 102 and 103 for the aluminum, steel and titanium alloys, respectively. The values of δ/d and σ_{max} for which $F_{I\sigma}$ values are given coincide with the test conditions used in this program.

As seen from Figure 99, the unloading process is elastic. If the cracked specimen is cycled from σ_{max} to σ_{min}, the stress intensity factor at σ_{min} (denoted by K_{min}) is given by the following equation:

$$K_{min} = K_I - (\sigma_{max} - \sigma_{min}) \sqrt{\pi L} \qquad (29)$$

where K_I is given by Equation 28 for the applied maximum stress σ_{max}. If the value of K_{min} is less than zero, K_{min} is taken as zero.

If the specimen is subjected to an overload cycle such as $\sigma_{ol} = \sigma_{max}$, then cycled at a lower stress range such as $\sigma_{umax} - \sigma_{umin}$, stress intensity factors for σ_{umax} and σ_{umin} can be calculated by the following equations (similar to Equation 29):

$$\begin{aligned} K_I|\sigma_{umax} &= K_I|\sigma_{ol} - (\sigma_{ol} - \sigma_{umax})\sqrt{\pi L} \\ K_I|\sigma_{umin} &= K_I|\sigma_{ol} - (\sigma_{ol} - \sigma_{umin})\sqrt{\pi L} \end{aligned} \qquad (30)$$

$K_I|\sigma_{ol}$ is given by Equation 28. If $K_I|\sigma_{umax}$ and $K_I|\sigma_{umin}$ given by the above equations are less than zero, they are assumed to be equal to zero.

Stress intensity factor for only one crack at the fastener may be estimated from that of two cracks by using the factor described in Section 4.2.1 by Equation 18.

5.0 RESULTS AND DISCUSSION OF FASTENER HOLE FLAW TESTS

Results of cracked fastener hole tests are described, analyzed, and discussed using the following breakdown: 1) static fracture tests of 4340 steel alloy specimens; 2) constant cyclic load tests, overload tests, and spectrum load tests of 2219-T851 aluminum, 9Ni-4Co-0.2C steel, and 6Al-4V beta-annealed titanium alloy specimens.

5.1 Static Fracture Tests of 4340 Steel Specimens

Forty-two 4340 (220-240 ksi) steel alloy specimens were statically fractured to evaluate the applicability of engineering estimates of stress intensity factors to the prediction of fracture strength of metallic structures containing cracked fastener holes. The program of fracture toughness, open hole, loaded close tolerance fastener, unloaded interference fit fastener, and loaded interference fit fastener tests is summarized in Table 13 and described in Section 2.2.3. The tests yielded the following results.

5.1.1 Fracture Toughness Tests

Two surface flaw specimens and two center cracked specimens (Figure A9b) were tested to measure fracture toughness for the T-S and T-L directions of the 4340 plate. Since the cracked fastener hole specimens had to be heat treated in two groups, one surface flaw and one center-cracked specimen were included in each of the heat-treat groups. Results of the static fracture tests are summarized in Tables 30 and 31. There were small differences in fracture toughness values for each heat treat group and each test direction. However, all values were within $\pm$5% of the median value of 72 ksi $\sqrt{in}$.

5.1.2 Open Hole and Loaded Close Tolerance Fastener Tests

Twelve specimens containing part-through cracks at open holes were tested. Six specimens contained cracks originating from both sides of the hole. Cracks were nominally quarter-circular in shape and had targeted depth-to-thickness ratios of 0.4, 0.6 and 0.8. Two hole diameters (0.25 and 0.375 inch) were used in the presence of both single and double sided cracks. The results are summarized in Table 32 and failure

stress for each of the specimens is plotted against crack depth-to-thickness ratio in Figure 104. Results were very consistent except for one specimen having a hole diameter of 0.375 inch and crack depth-to-thickness ratio of 0.75. No reason for the one seemingly spurious result could be determined.

Six specimens containing corner cracks at holes containing loaded close tolerance fasteners were tested. Three specimens contained a single crack originating from one side of the hole and three specimens contained two cracks including one originating from each side of the fastener hole. Cracks were nominally quarter-circular in shape and had targeted depth-to-thickness ratios of 0.4, 0.6 and 0.8. Test results are summarized in Table 33 and failure stress for each specimen is plotted against crack depth to thickness ratio in Figure 105. Double sided cracks resulted in consistently lower failure stresses than did the single sided cracks and failure stresses decreased with increasing crack size for both single and double crack specimens.

Results were analyzed to determine the locations on the flaw peripheries at which calculated stress intensity factors equaled the fracture toughness at maximum load. This was accomplished as shown in Figures 106 and 107 where variations in stress intensity factor around the periphery of each flaw are shown. Horizontal lines were drawn to represent average and average $\pm$10% values of fracture toughness for the T-S direction as determined from surface flaw tests. Calculated stress intensity factors appeared to be in best agreement with fracture toughness values when α = 25 degrees (α is defined in Figure 106) where ratios of calculated to measured fracture toughness ranged from 0.83 to 1.19. Even though the calculated stress intensity factors are higher at the edge of the hole (α = 0°) then at α = 25°, it would not be expected that fracture would initiate at the edge of the hole due to the release of constraint to crack tip deformations resulting from the stress free hole surface. Rather, fracture would be expected to initiate some distance away from the hole surface after constraint to crack tip deformations builds up to a level equivalent to plane strain conditions. Hence, the conclusions that fractures in these tests originated at a point about 25 degrees away from the hole surface appears to be reasonable.

On the basis of the foregoing results, it was concluded that effective stress intensity factors at maximum crack depth for all part-through fastener hole flaws in this program should be set equal to calculated stress intensity factors for points on the crack peripheries 25 degrees away from the hole surface. This procedure is applicable to quarter-circular or near quarter circular cracks originating at open holes, or holes filled with close tolerance fasteners subjected to low load transfer. For elliptical cracks and/or high load transfer, this procedure may not be applicable and should not be used unless verified by test.

5.1.3 Unloaded Interference Fit Fastener Tests

Eighteen specimens containing corner cracks originating at holes containing unloaded interference fit fasteners were tested. Using 0.25 inch diameter fasteners, three specimens were tested for two interference levels (0.0018 and 0.0042 inch) and two crack geometries (single and double sided quarter-circular part-through cracks). The interference levels are the maximum and minimum values allowed for standard interference installations. Using 0.375 inch diameter fasteners, three specimens were tested for each of the single and double sided crack geometries. Interference level was 0.0054 inch which was the maximum value allowed for standard interference installations. Each set of three specimens contained flaws having targeted depth-to-thickness ratios of 0.4, 0.6 and 0.8. Test results are summarized in Tables 34 and 35. Failure stresses are plotted against crack depth-to-thickness ratios in Figures 104 and 105. Results for the 0.25 inch diameter holes indicate that interference level had very little effect on fracture stress for all flaw sizes tested. For both single and double cracks, failure stresses for cracked fastener holes filled with interference fit fasteners installed using both maximum and minimum interference levels were in good agreement with failure stresses for cracked open holes. Results for the 0.375 inch diameter holes were less consistent than were results for the smaller diameter holes. For the smallest flaw sizes tested, cracked holes containing interference fit fasteners yielded higher failure stresses than did open holes. For intermediate flaw sizes, interference fit fasteners again increased failure stress but to

a smaller extent than for the smallest flaw sizes. For the largest flaw sizes, interference fit fasteners increased failure stress for the single side cracks but had no effect on failure stress for the double side cracks.

Results for the unloaded interference fit fastener tests could not be quantitively evaluated since methods for calculating fracture stress in the presence of part-thru cracks were not available. However, some insight into the effect of interference fit fasteners on fracture strength can be gained by comparing stress fields adjacent to open holes and holes containing unloaded interference fit fasteners as shown in Figure 108. Near the hole, stresses are lower in the presence of the interference fit fastener. However, the combined applied and interference forces cause the material to go into general yielding adjacent to the fastener whereas, in this particular example, the material near the open hole remains in the elastic state. Hence, if the beneficial effects on crack stability of the lower stresses more than offset possible detrimental effects due to yielding, fracture stresses for cracks having small size-to-hole diameter ratios could be elevated by the presence of inteference fit fasteners. Apparently, such was the case for the smallest crack sizes tested in the presence of 0.375 inch diameter interference fit fasteners in this program. Further away from the hole, strains are in the elastic range for both open and filled holes and stresses become larger in the presence of interference fit fasteners than near open holes. Hence, stress intensity factors at locations on crack peripheries away from the holes could be larger in the presence of interference fit fasteners and result in lower failure stresses. For intermediate crack size-to-hole diameter ratios, fracture strength in the presence of cracks originating at open and interference fit fastener holes could be nearly equal. The latter situation appeared to be existent in most of the tests described in this section, particularly the tests involving 0.25 inch diameter holes.

It is not possible to generalize concerning the effects of interference fit fasteners on fracture strength of cracked fastener holes. There are innumerable possible combinations of fastener material, plate material, applied stress, interference level, hole diameter, crack size, and crack shape, many of which yield different effects of interference fit

fasteners on fracture strength. A more fundamental understanding of the effects of interference fit fasteners on stability of cracks originating at fastener holes is required before any general conclusions can be drawn about fracture strength of cracked interference fit fastener filled holes.

5.1.4 Loaded Interference Fit Fastener Tests

Six specimens containing flaws originating at holes filled with loaded interference fit fasteners were statically fractured. Two groups of three specimens were tested. One group contained single flaws originating from only one side of the fastener hole, and the other group contained two flaws including one flaw originating from each side of the fastener hole. All flaws were approximately quarter-circular in shape and had nominal depth-to-thickness ratios of either 0.4, 0.6 or 0.8. Test results are tabulated in Table 36. Failure stress for each specimen is plotted against the corresponding flaw depth-to-thickness ratio in Figure 105. Load transfer was small and failure stresses were only slightly lower for the loaded fastener tests than for the unloaded fastener or open hole tests. In most cases, there was very little difference between failure stresses for close tolerance and interference fit fastener tests. The most significant effects were those of crack size and number of cracks. There was a distinct decrease in failure stress with increase in either crack size or number of cracks. Results for the loaded fastener tests could not be quantitatively evaluated due to the lack of applicable stress intensity factor solutions. The loaded fastener tests were similar to the previously described unloaded fastener tests and the discussion for the unloaded tests is equally applicable to the loaded fastener tests.

5.1.5 Summary

Static fracture tests of 4340 steel (220-240 ksi) alloy specimens containing part-thru cracks originating at open or close tolerance fastener holes yielded straight forward results. Failure stress was found to decrease with increasing crack size, hole diameter, faster load, and number of cracks (one or two). An analysis of the results led to the conclusion that fractures initiated some distance away from the hole at

a location on the crack boundary where constraint to crack tip deformations had increased to plane strain constraint conditions. This location appeared to lie at an average angle of about 25 degrees away from the wall of the hole. In the remainder of this program, effective intensity factors for all part-through fastener hole flaws originating at close tolerance filled and open holes will be computed at a point on the crack periphery 25 degrees away from the wall of the hole.

Results of static fracture tests of 4340 steel (220-240 ksi) alloy steel specimens containing part thru cracks originating at interference fit fastener filled holes were less straight forward than were those for specimens containing precracked close tolerance fastener holes. Failure stress was found to decrease with increasing crack size, fastener load, and number of cracks. The effect of hole diameter on failure stress was dependent on both crack size and number of cracks; both increases and decreases in fracture stress with increasing hole diameter were observed. Finally, interference level was found to have little or no effect on fracture stress for the conditions tested in this program. It was concluded, however, that a fundamental understanding of the effects of fastener interference level on stability of cracks originating at fastener holes is required before any general conclusions can be drawn concerning fracture strength of cracked interference fit fastener filled holes.

5.2 Constant Cyclic Load Tests

Constant cyclic load tests were conducted on specimens containing cracks originating at open holes, close tolerance fastener holes, and interference fit fastener holes. Both open and close tolerance fastener holes were tested in the conventional and cold worked conditions. Specimen configuration for 2219-T851 aluminum alloy specimens containing close tolerance fasteners is shown in Figure 109. Each specimen contained one loaded fastener, one open hole and one surface flaw. Specimen configuration for 9Ni-4Co-0.2C steel and Ti-6Al-4V βA alloy specimens was similar to that shown in Figure 109 except the open hole was filled with a finger tight close tolerance fastener, and the surface flaw was replaced by an open hole. Specimen configuration for all interference fit fastener

specimens is shown in Figure 110. Each specimen contained one loaded and one unloaded interference fit fastener installed using average interference values for standard installations. The third hole was filled with either a second unloaded interference fit fastener, or was cold worked and left unfilled.

5.2.1 Conventional Open and Close Tolerance Fastener Filled Holes Three specimens containing part-thru cracks originating at open and close tolerance fastener filled holes were tested. One specimen was tested for each alloy including 2219-T851 aluminum alloy specimen FUCTA-1, 9Ni-4Co-0.2C steel specimen FUCTS-1, and 6Al-4V βA titanium specimen FUCTT-1. Test details for each of the three specimens are listed in the uppermost lines of Tables 37 through 39. Raw test data are tabulated in Tables 93, 99 and 104 in Volume 2 of this report. Test data are plotted on graphs of crack size versus cycles in Figures 111 through 113. In the upper graphs, crack depth (a) is plotted against cycles until the flaw depth equals the specimen thickness; thereafter, values of the sum of specimen thickness and crack length at the back specimen face ($a+c_2$) are plotted against cycles. In the lower graphs, crack length at the front specimen face (c_1) is plotted against cycles. In all cases, cracks originating at loaded holes grew faster than cracks originating at open or filled holes and there was essentially no difference between crack growth behavior of open and filled holes. In the aluminum alloy specimen, the fastener hole flaws grew considerably faster than a surface flaw having approximately the same initial depth and length dimensions.

Crack shape underwent only moderate changes as the cracks grew through the specimen thickness. This result is illustrated in Figure 114 where crack width at the front specimen face (c_2) is plotted against crack depth. Crack depth increased at a slightly faster rate than crack width.

A comparison was made between experimental and calculated cyclic lives for each flaw to evaluate the usefulness of the previously described engineering estimates of stress intensity factors in predicting cyclic

life for cracked fastener holes. Calculated lives were obtained by integrating crack growth rates over each increment of growth generated in the tests. Crack growth rates were obtained using the appropriate baseline crack growth rate data and stress intensity factors were calculated using the methods described in Section 4.0. In the depthwise direction, stress intensity factors were calculated at points on the crack periphery located at a 25 degree angle away from the wall of the hole. This procedure was based on results of the 4340 static fracture tests as described in Section 5.1.2. In the lateral direction, stress intensity factors were calculated at the surface of each specimen. The transition from a part-thru crack to a thru crack was made by assuming that a part-thru crack having a depth equal to the specimen thickness was equivalent to an equal area uniform thru crack. Thru cracks having unequal crack lengths at each side of the specimen were assumed to be equivalent to uniform thru cracks having a length equal to the average of the unequal surface lengths of the non-uniform crack.

Two different calculations were made for each flaw. In one calculation, stress intensity factors and crack growth data for the depthwise direction were used to estimate the number of cycles required to grow the crack through the specimen thickness. In the second calculation, stress intensity factors and crack growth data for the lateral direction were used to estimate the number of cycles required to grow the crack through the specimen thickness. In both calculations, the transition from a part-thru to thru crack was made as described above and life calculations were continued until the calculated crack length reached the maximum crack length measured in the tests.

Comparisons between calculated and experimental lives are illustrated in Figure 115. Agreement between calculations and experiment is good in all cases. Ratios of actual to calculated life ranged from a low of 0.75 for the aluminum alloy to a high of 1.63 for the titanium alloy. For the aluminum and steel alloys, there was very little difference between results of the calculations made for the depthwise and lateral directions. This result indicates that stress intensity factors for both the depthwise and lateral directions were equally accurate. For

the titanium alloy, the discrepancy between results of depthwise and lateral calculations was greater than for the other two alloys. This result may have been due to the fact that crack growth rates were more sensitive to stress intensity factors for the titanium alloy than for the aluminum and steel alloys. Hence, small increases in stress intensity factor resulted in reasonably large changes in calculated life for the titanium alloy specimens. Finally, ratios of calculated to actual life tended to be smaller for the loaded holes than for both open and filled holes.

For the range of parameters used in these tests, it was found that accurate calculations of crack propagation life for cracked fastener holes could be made using stress intensity factors calculated as described in Section 4.0 of this report, and baseline crack growth rate data obtained from surface flaw specimens. However, these tests were limited to simple loading profiles, part-circular cracks, one initial crack depth to hole diameter ratio, and either no load transfer or low load transfer. Hence, even though the results obtained herein are encouraging, further work is needed to investigate crack propagation behavior for cracks having smaller initial size to hole diameter ratios and subjected to greater load transfer though the fastener.

5.2.2 Cold Worked Open and Fastener Filled Holes

Three specimens containing part-thru cracks originating at cold worked fastener holes were tested. One specimen was tested for each alloy including FUCCA-1 for the aluminum alloy, FUCCS-1 for the steel alloy, and FUCCT-1 for the titanium alloy. Each specimen contained one high expansion hole containing a loaded close tolerance fastener, one high expansion filled with an unloaded close tolerance fastener, and one open hole for which the amount of cold expansion was reduced by 25 percent. Test details for each of the three specimens are listed in Tables 37 through 39. Raw data are listed in Tables 94, 100 and 105 in Volume 2 of this report.

Growth characteristics for cracks originating at cold worked holes were different from those for cracks originating at conventional holes. For the cold worked holes, crack depth growth was accentuated along the face

of the hole as illustrated in Figure 116 where the fracture surfaces of two aluminum alloy cold worked hole specimens are drawn to scale. Specimen TCA-1 was subjected to 1000 loading cycles having a peak cyclic stress of 28 ksi. It is evident that crack depth increased considerably more than crack width. Specimen TCA-2 was subjected to 36,400 loading cycles having a peak cyclic stress of 28 ksi. Again, crack depth growth was accentuated along the face of the hole. These results indicate that the cold working process probably produces residual stresses that are greater at the edge of the hole than at small distances away from the hole.

Crack depth growth rates for cold worked holes were considerably slower than rates for conventional holes even though cold working resulted in accentuated crack growth along the face of the hole. This result is illustrated in Figure 117 where crack length is plotted as a function of loading cycles for both conventional and cold worked open holes. There appears to be an initial period of very slow crack growth rate for the cold work holes similar to the crack growth behavior observed after tensile overloads.

Crack propagation lives for cold worked hole specimens were compared to calculated lives for cracked conventional fastener holes having the same initial crack geometry as the cold worked holes. Calculated lives were equal to the number of cycles that would have been required to grow the initial crack depth to the final crack depth observed in the cold worked hole specimens if the crack had originated at a conventional hole. Hence, the calculated final crack widths were larger than the actual crack widths in the cold worked hole specimens. This procedure was selected to yield lower bound values of increase in crack propagation life due to cold working. Results of the calculations are summarized in Figure 118. Cold working resulted in about a tenfold increase in crack propagation life except for the low expansion open hole in the steel alloy specimen. In these tests, the titanium alloy responded most favorably to the cold working process but it is not obvious whether this result would be generally applicable. The effect of the amount of cold expansion was stronger in the steel alloy than in the titanium

alloy. A twenty-five percent reduction in cold expansion resulted in decreases in crack propagation life of about 70 percent for the steel alloy and about 20 percent for the titanium alloy. The effect of expansion level was not determined for the aluminum alloy.

Stress intensity factors applicable to cold worked holes were not available and, hence, it was not possible to apply the results of this program to conditions that differ from those used in these tests. The effect of cold working on crack propagation life should depend on initial crack shape, initial crack size, crack size to hole diameters ratio, and interference level. Additional analyses and test data will be required to better characterize the effects of cold working of fastener holes on crack propagation life.

5.2.3 Interference Fit Fastener Tests

Test parameters for each of eleven test specimens containing interference fit fasteners are listed in Tables 37 through 39. One specimen containing uniform thru cracks was tested for each alloy including specimen FUTIA-1 for the aluminum alloy, Specimen FUTIS-1 for the steel alloy, and Specimen FUTIT-1 for the titanium alloy. The remaining specimens were fabricated with part-thru cracks originating from the fastener holes as illustrated in the first column of each table. Specimens having codes beginning with the letter "T" were exploratory specimens and were tested to determine practical stress levels at which to conduct the main body of tests. Specimens having codes beginning with the letter "F" were part of the main body of tests. In all but one specimen (FUCIA-1) in the main body of tests, holes No. 1 and No. 2 contained interference fit fasteners installed using an interference value midway between the maximum and minimum interference levels for standard interference installations. Interference level for hole No. 3 was set at the minimum level for standard installations in the aluminum alloy specimens, and midway between the average and maximum values for standard installations in the steel and titanium alloy specimens. In aluminum alloy Specimen FUCIA-1, interference values were set at either the maximum value allowed by specifications for the Boeing 747 airframe, or the minimum allowable value for standard installations. Test results for

thru-cracked and part-thru cracked specimens are presented and discussed in the following two subsections.

Results for Thru-Cracked Specimens

Results of thru-cracked specimen tests are plotted on graphs of crack dimensions versus cycles in Figures 119 through 121. Raw test data are included in Tables 95, 101 and 106 in Volume 2 of this report.

Results were evaluated by comparing experimentally determined lives to calculated lives. Two different life calculations were made including one which accounted for and one which ignored the effect of interference fit fasteners on crack growth behavior. The former calculation was based on methods of calculating stress intensity factors for cracked interference fit fastener holes described in Section 4.0 of this report. The latter calculation was made assuming that the holes were filled with close tolerance fasteners and stress intensity factors were determined using the Bowie solution (31) for the unloaded holes, and both Bowie's and Shah's solution (Figure 96) for loaded holes. Methods of accounting for the effect of interference on crack propagation at loaded holes were not available so calculations accounting for interference effects were confined to unloaded holes. Experimental and calculated lives are summarized in Figure 122. For the aluminum alloy, calculations that ignored interference effects greatly underestimated crack propagation life whereas calculations that accounted for interference effects were in reasonable good agreement with test results. For the steel alloy, interference fit fasteners did not have a strong influence on crack propagation life and both calculations were in good agreement with experimental results. For the titanium alloy, both methods of calculation greatly underestimated experimental life.

In summary, interference fit fasteners resulted in substantial improvements in crack propagation life for the aluminum and titanium alloys, but had only a small influence on crack propagation lives for the steel alloy. Methods developed to estimate the effect of interference on crack propagation life indicate that effects should be quite sensitive to initial crack length to hole diameter (c/r) ratios. For very small

c/r values, substantial improvements in crack propagation life should result from the use of interference fit fasteners. For large c/r values, interference fit fasteners would be expected to reduce crack propagation life. For some intermediate range of c/r values, interference fasteners should have little or no effect on crack propagation life. In this program, both calculations and experiment showed that initial c/r ratios for the steel specimens were in the range where interference fit fasteners would not be expected to have a strong influence on crack propagation life. For the titanium alloy, calculations indicated that interference fit fasteners would not be expected to have a strong influence on crack propagation life whereas they resulted in a marked increase in life. For the aluminum alloy, both calculations and experiment showed an increase in crack propagation life due to the interference fit fasteners. Although the results in this program indicate that methods developed to estimate crack propagation lives for cracked fastener holes tend to yield conservative results, more investigation is needed to evaluate this trend for a wide range of test conditions.

Results for Part-Thru Cracked Specimens

Results of part-thru cracked specimen tests are plotted on graphs of crack dimensions versus cycles in Figures 123 through 139. Raw test data are included in Tables 96 and 97 (aluminum alloy), 102 (steel alloy) and 107 (titanium alloy) in Volume 2 of this report.

Crack shape change characteristics of part-thru cracks growing from interference fit fastener filled holes were different from those for close tolerance fastener filled holes for the aluminum and titanium alloys. This is illustrated in Figure 114 where it is evident that ratios of crack width growth rate to crack depth growth were maximum for cracked interference fit fastener holes. This reflects the ability of interference fit fasteners to retard crack depth growth more than crack width growth. For the steel alloy, crack shape change behavior was insensitive to all test variables including fastener type and condition of hole.

The effect of interference level on fatigue crack growth of part-thru fastener hole flaws in the 2219-T851 aluminum alloy is illustrated in Figure 140. The interference level of 0.0024 inch is the minimum

permissible value for standard installations of 0.375 inch diameter bolts. The interference level of 0.006 is slightly greater than the maximum specified value of 0.0054 inch for standard installations. Crack propagation life increased by a factor of about 2.5 when interference level was increased from minimum to maximum values. Crack propagation lives for Taper-lok fastener filled holes ranged from 2 to 5 times comparable lives for open holes as interference level was increased from minimum to maximum values. The above results are not applicable to all interference fit fastener installations since variables such as crack size, crack shape, and hole diameter will influence results. In general, it is believed that increase in crack propagation life due to interference fit fasteners will increase with decreasing crack size to hole diameter ratios when interference to hole diameter ratio is kept constant.

Methods were not available for computing stress intensity factors for part-thru cracks originating at interference fastener filled holes. Hence, experimentally determined crack propagation lives were compared to calculated lives based on stress intensity factors computed for close tolerance fastener filled holes. Results are summarized in Figure 141 where ratios of actual to calculated life are shown for specimen FUCIA-2, FUCIS-1, and FUCIT-1. For the aluminum and titanium alloy specimens, the cracked interference fit fastener holes yielded cyclic lives ranging from three to five times the lives that would have been anticipated for comparable cracked close tolerance fastener holes. For the steel alloy specimens, interference fit fasteners had very little effect on crack propagation life. These results are similar to those obtained from the thru-cracked specimen tests where all but the steel alloy specimens yielded beneficial effects of interference fit fasteners on crack propagation life. At the present time, it is not clear why the interference fit fasteners in the steel alloy specimens did not retard crack depth growth rate more than observed in these tests.

5.2.4 Combined Bending and Tension Tests

Three specimens containing part-thru cracks originating at Taper-lok filled fastener holes were tested under combined bending and tension

stresses. One specimen was tested for each alloy including FBCIA-1 for the aluminum alloy, FBCIS-1 for the steel alloy, and FBCIT-1 for the titanium alloy. Test details for all three specimens are listed in Table 40. Raw test data are included in Tables 98, 103 and 108 in Volume 2 of this report.

Results are plotted on graphs of crack depth versus crack width in Figure 142 along with similar results for specimens tested under uniform tension stresses. The bending stresses resulted in larger ratios of crack width growth to crack depth growth than did the tensile stresses. Hence, bending stresses do have a significant effect on fatigue crack growth behavior of part-thru fastener hole flaws.

Methods for calculating stress intensity factors for the test specimens were not available and it was not possible to quantitatively evaluate the results. In view of the limited number of tests, no attempt was made to derive any "rules of thumbs" for accounting for the effect of bending stresses on crack growth behavior of fastener hole flaws. Quantitative evaluation of bending stress effects will be possible only after considerable additional analysis and testing.

5.2.5 Summary

For the 2219-T851 aluminum and 6Al-4V βA titanium alloys, crack propagation lives for open or close tolerance fastener filled conventional holes were increased by the use of either cold working procedures or Taper-lok fasteners as shown in Figure 113. For the 9Ni-4Co-0.2C steel alloy, crack propagation lives were increased by cold working of fastener holes whereas Taper-lok fasteners had little or no effect.

Methods developed for calculating crack propagation lives for close tolerance fastener filled holes yielded calculated lives that were in good agreement with experimental results for all three test alloys. Methods developed for computing crack propagation lives for thru-cracks originating at interference fastener filled holes yielded calculated lives that were in good agreement with experimental results for the aluminum and steel alloys, but underestimated experimentally measured lives for the titanium alloy.

5.3 Overload Tests

Overload tests were conducted by repeatedly subjecting specimens containing cracked fastener holes to either of the loading programs A or C shown in Figure 16. The number of cycles between overloads was varied from specimen to specimen to study effects of overload frequency. Tests were conducted on both open and close tolerance fastener holes in either the conventional or cold worked conditions, and on Taper-lok fastener holes. Both loaded and unloaded fasteners were tested. Specimen configurations were identical to those used for the constant cyclic load tests as described in Section 5.2.

5.3.1 Conventional Open and Close Tolerance Fastener Filled Holes

Thirteen specimens containing open and close tolerance fastener filled holes were tested including five 2219-T851 aluminum alloy specimens, four 9Ni-4Co-0.2C steel alloy specimens and four 6Al-4V βA titanium alloy specimens. Test details are listed in the topmost lines of Tables 41 through 43. Aluminum alloy specimens contained one loaded fastener, one open hole, and one surface flaw. Steel and titanium alloy specimens contained one loaded close tolerance fastener, one unloaded close tolerance fastener, and one open hole. Each hole contained a part-thru quarter-circular crack located in a plane lying perpendicular to the applied load as illustrated in the first column of each of the tables. Loading details, flaw dimensions, and hole diameters are listed in the tables. Raw data for all specimens are listed in Tables 109 through 114 (aluminum alloy), 124 through 127 (steel alloy) and 140 through 143 (titanium alloy) in Volume 2 of this report. Results are plotted on graphs of crack dimensions versus cycles in Figures 143 through 158 of this report.

The most significant results of the overload tests can be summarized as follows: 1) the application of periodic tensile overloads resulted in increased crack propagation life for all types of cracked fastener holes; 2) crack propagation life increased with increasing frequency of overloads for the range of variables studied in these tests; 3) tensile overloads resulted in large amounts of apparent crack growth during each overload cycle; 4) small compressive loads applied immediately after

tensile overloads reduced the effectiveness of tensile overloads in increasing crack propagation life.

5.3.1.1 Crack Growth During Overloads

It appeared that each tensile overload resulted in significantly more crack growth than would be predicted on the basis of uniform load crack growth rate data. The fracture surfaces of each specimen contained a number of regularly spaced bands separated by regions of fatigue crack growth. This is illustrated by photographs of the fracture surfaces for the loaded and open holes in aluminum alloy Specimen FPOCTA-2 shown in Figure 159. Specimen FPOCTA-2 was subjected to five overloads including one at the outset of the test and one every 4600 cycles thereafter. Since the light colored shiny bands resulted from fatigue crack growth that occurred between overloads, it was concluded that the width of the intermediate dark bands represented crack growth that occurred during the overloads. Fracture surfaces from steel alloy specimen FPOCTS-1 and titanium alloy specimen FPOCIT-1 are shown in Figures 160 and 161, respectively. Bands of apparent crack growth during overload were readily observable on the steel alloy specimens. Similar bands on the titanium alloy fracture surfaces could be seen only when viewed through polarizing lenses.

Apparent crack depth and crack width growth rates during overloads were plotted against peak cyclic stresses intensity factors in Figures 162 through 164. Baseline crack growth rates are plotted in each of the figures for comparison. Crack growth rates during overloads lie one to two orders of magnitude to the right of the baseline crack growth rates for all alloys. However, peak overload stress intensity factors were large precentages of the fracture toughness values for all alloys and many of the overload stress intensity factors were greater than values used to generate baseline crack growth rates. Both of these situations may have contributed to the differences between baseline and overload crack growth rate data. Nevertheless, these tests provided strong evidence that crack growth rates during overloads can be significantly greater than indicated by baseline crack growth rate data.

The only available crack growth theory that predicts accelerated crack growth rates during overloads is crack closure theory. As discussed in Section 3.3.1.1 of this report, crack closure theory alone cannot explain the large overload crack growth rates observed in these tests.

5.3.1.2 Retardation Effects

Since no instrumentation was used, results of overload tests of cracked fastener hole specimens could not be subjected to as detailed an evaluation as was possible for the instrumented surface flaw overload tests. However, results for cracked fastener hole tests were qualitatively similar to those for the surface flaw overload tests in that, for constant peak cyclic stress between overloads, crack propagation life increased with increase in both peak overload stress and overload frequency. Effects of peak overload stress are illustrated in Figure 165 where crack depth is plotted against loading cycles for part-thru cracks originating at loaded close tolerance fastener holes. Results for filled and open holes were similar to those illustrated in Figure 165. Effect of overload frequency are illustrated in Figures 143 through 158. Regardless of test conditions, crack propagation life increased with increase in overload frequency.

Two tests were conducted in which each tensile overload was followed immediately by a small negative load prior to initiation of constant load cycling. Results from aluminum alloy Specimen FPOCTA-2 and titanium alloy Specimen FPOCTT-3 are illustrated in Figures 143, 144, 153, 154 and 155. These figures also contain data for specimens tested without negative overloads. The effect of the negative loads was to decrease crack propagation life. The decrease was small for the loaded and open holes in the aluminum alloy specimen and for the filled and open holes in the titanium alloy specimen. The decrease was substantial for the loaded fastener hole in the titanium alloy specimen. It was not possible to quantitatively evaluate the effects of negative loads on the fatigue crack propagation behavior of cracked fastener holes since there are no existing methods for calculating crack propagation lives that account for negative load effects. Since the effects of negative loads on crack propagation life are detrimental, more effort should be directed to the understanding of such effects.

Crack propagation lives were compared to calculated lives obtained using stress intensity factors from Section 4.0 of this report, Wheeler's procedure for estimating effects of overloads on crack growth rates (see Section 3.3.1.2), and baseline crack growth rate data. No calculations were made for specimens subjected to negative loads.

The calculations showed that when an exponent of m=2 was used in Equation 10, very good agreement was obtained between experimental and calculated lives for all three alloys. This is illustrated in Figure 166 where ratios of calculated to experimental life are plotted for each of the fastener holes in all test specimens. The ratios range from a low of 0.6 to a high of 1.25. For the aluminum and titanium alloys, calculations tend to underestimate lives for loaded fastener and overestimate lives for open holes. This result is similar to that obtained for constant cyclic load specimens. It appears that the analyses presented in Section 4.0 slightly overestimated stress intensity factors for the loaded fasteners in the aluminum and titanium alloy specimens. For the steel alloy, agreement between calculated and experimental lives was excellent for all specimens.

The tendency for increasing values of Wheeler's exponent m with increasing crack depth to thickness ratios noted in the surface flaw tests could not be detected in the fastener hole flaw tests. Moreover, the value of m=2 that led to good agreement between calculated and experimental fastener hole flaw results was significantly greater than most of the m values resulting from surface flaw tests. Values of m=2 were obtained only from tests of deep surface flaws when the ligament between flaw tip and back specimen face was entirely yielded. The fastener hole flaws existed in regions of very high stress adjacent to the fastener holes and some yielding very likely took place in most tests. This situation may explain, in part, why fastener hole flaws reacted to overloads in a manner similar to that for deep surface flaws.

Finally, one situation that led to crack growth retardation in the program was the application of torque while installing the unloaded close tolerance fastener in titanium alloy specimen FOCTT-1. Rather than being installed

finger tight, the bolt was torqued to 150 in-lb. As a result, both crack depth and crack width growth were more than an order of magnitude slower than values observed for cracked holes containing finger tight bolts.

5.3.2 Cold Worked Open and Fastener Filled Holes

Three specimens containing part-thru cracks originating at cold worked fastener holes were tested. One specimen was tested for each alloy including aluminum alloy specimen FOCCA-1, steel alloy specimen FOCCS-1, and titanium alloy specimen FOCCT-1. Each specimen contained one high expansion hole containing a loaded close tolerance fastener, one high expansion hole filled with an unloaded close tolerance fastener, and one open hole for which the amount of cold expansion was reduced by 25 percent. Test details for each of the three specimens are listed in Tables 41 through 43. Raw data are included in Tables 114, 128 and 144 in Volume 2 of this report.

Crack growth characteristics of overloaded cold worked hole specimens were the same as previously noted for the constant load cold worked hole specimens. Crack depth growth proceeded at a considerably faster rate than did crack width growth and crack depth growth was accentuated along the wall of the hole as illustrated in Figure 116.

Crack propagation life for each crack in the overloaded cold worked hole specimens was compared to calculated life for a geometrically identical cracked conventional fastener hole. The conventional hole was assumed to be subjected to only the constant cyclic load portion of the overload test program, i.e., overload effects were ignored. A similar comparison was previously made for the constant cyclic load cold worked hole specimens. Results of both sets of calculations are summarized in Figure 118. In five of the eight tests for which direct comparison can be made, overloads reduced the beneficial effects of cold working on crack propagation life. In two tests, crack propagation life was increased by the overloads. In one test, the overload had no effect whatsoever on crack propagation life. For the loaded fastener in the aluminum alloy overload specimen, crack propagation was almost totally retarded and the overload appeared to have a strong beneficial effect on crack propagation life. A twenty-five

percent reduction in cold expansion resulted in decreases in crack propagation life of about 20 and 50 percent for the steel and titanium alloys, but appeared to increase crack propagation life for the aluminum alloy.

The overload ratios of 1.4 for the aluminum and 1.5 for the steel and titanium alloy specimens were not very large. Previous results for overload tests of cracked conventional fastener holes indicated that overloads to less than 1.5 times the subsequent peak cyclic stress do not have a very large effect on crack propagation life. Hence, the tendency for the overloads to decrease crack propagation life for cracked cold worked fastener holes may not be very significant. Nevertheless, more investigation is required for higher overload ratios to determine whether or not overloads can be detrimental to crack propagation lives for cold worked fastener holes. Since methods of calculating stress intensity factors for cracks originating at cold worked fastener holes are not available, it is not possible to predict effects of overloads on crack propagation lives for cold worked holes under conditions other than those tested in this program.

5.3.3 Interference Fit Fastener Tests

Test parameters for each of twenty-two test specimens containing interference fit fasteners are listed in Tables 41, 42, and 43 for the aluminum, steel, and titanium alloys, respectively. Two specimens containing uniform thru cracks were tested for each alloy. Test details are listed at the bottom of the first page of each table. The remaining specimens were fabricated with part-thru cracks originating from the fastener holes as illustrated in the first column of each table. Test details are summarized in the upper parts of the second page of each table. Holes 1 and 2 in each specimen contained Taper-lok fasteners installed using interference levels midway between the maximum and minimum values for standard installations. Hole No. 3 was either filled with a Taper-lok bolt installed using a second interference level, or was cold worked, reamed, and left unfilled.

Results for Thru-Cracked Specimens

Results of thru-cracked specimen tests are plotted on graphs of crack length versus cycles in Figures 119, 120, and 121 for the aluminum, steel, and titanium alloy specimens, respectively. Results for the loaded and unloaded fasteners are plotted separately in the upper and lower graphs of each figure. Raw test data are listed in Tables 117 and 118 (aluminum alloy), 132 and 133 (steel alloy), and 147 and 148 (titanium alloy) in Volume 2 of this report.

Overloads resulted in considerably more crack growth than would be predicted on the basis of uniform load crack growth rate data. Results were similar to those for close tolerance fastener filled holes where crack growth during overloads was about two orders of magnitude greater than the baseline crack growth rates corresponding to the overload cycles.

Ratios of experimental to calculated life were determined and plotted in Figure 167. For the aluminum alloy, two different methods of calculation were used. One method accounted for the effects of both interference and overloads on crack propagation behavior. This was accomplished by using stress intensity factors for interference fit fastener filled holes and the Wheeler method to account for overload effects. An exponent of m=2 was used in the Wheeler formula (Equation 10). The second method ignored interference effects but accounted for overload effects. This was done by using stress intensity factors for close tolerance fastener filled holes and the Wheeler method to account for overloads. For the steel and titanium alloys, only the latter method of calculation was used. Figure 167 shows that, for the aluminum and titanium alloys, calculations that did not account for the effects of interference yielded lives that ranged from 1/5 to 1/30 of the experimental lives. This result means that the Taper-lok fasteners increased lives by factors ranging from 5 to 30. For the steel alloy specimens, Taper-lok fasteners increased lives by factors ranging from 1.4 to 2.3. Hence, Taper-lok fasteners were not as effective in the steel alloy as in the aluminum and titanium alloys. It is not clear at this time whether or not this result might be peculiar to the particular conditions tested in this program. Calculation methods that did account for effects of interference in the aluminum alloy specimens

yielded calculated lives that ranged from 50 to 90% of the experimental lives. Hence, methods developed to account for interference effects or crack propagation from interference fit fastener holes were very effective for the limited situations in which they were evaluated.

Results for Part-Thru Cracked Specimens

Results of part-thru cracked specimen tests are plotted on graphs of crack dimensions versus cycles in Figures 123 through 139.

Crack growth results for part-thru cracks originating at Taper-lok fastener holes are not evaluated quantitatively since methods for estimating crack propagation life for such situations are not available. Qualitatively, test results are similar to those for part-thru cracks originating at close tolerance fastener filled holes as described below:

(1) Overloads resulted in bands of apparent crack growth that were visible to the naked eye.. It was not possible to compare baseline and overload crack growth rates since stress intensity factors for the cracked interference fit fastener holes were not available.

(2) Cyclic lives increased with increase in peak overload stress for constant peak cyclic stress. This is illustrated in Figure 168 where the effect of overload magnitude on cyclic life is illustrated for loaded fastener tests in each of the three alloys. The effect of peak overload stress in the titanium alloy tests was very pronounced. Overloads to 1.5 times the subsequent peak cyclic stress had only a small retarding effect on crack growth rates whereas overload to 1.75 times the peak cyclic stress had a very strong retarding effect. For the aluminum and steel alloys, the increase in cyclic life with increase in peak overload was more gradual than for the titanium alloy.

(3) With some exceptions, cyclic life increased with increase in overload frequency over the range of frequencies used in these tests. This result is illustrated in Figures 123 through 139 where each figure contains crack growth data for a single peak overload stress and several overload frequencies. One exception to this result occurred in each of the aluminum, steel and titanium alloy tests. For the aluminum alloy, a decrease in period of 1.5X overloads from 21,480 to 8,000 cycles resulted in a decrease in cyclic life as shown in Figure 127. For the steel alloy, a decrease in period of 1.75X overloads from 8850 to 5450 cycles resulted in a small decrease in crack propagation life as shown in Figure 130. Several factors probably contributed to these exceptions from the general trend of results including small differences in initial crack size, and data scatter. For the titanium alloy, a decrease in period of 1.5X overloads from 15,000 to 7,500 cycles resulted in a small decrease in crack propagation life as shown in Figure 137. Since 1.5X overloads had only small retarding effects on titanium alloy crack growth rates, moderate changes in overload period would not be expected to result in large differences in crack propagation life. Changes in life due to data scatter may have dominated the 1.5X overload titanium alloy results in this program.

(4) Small negative loads applied immediately after tensile overloads tended to reduce the retarding effect of the overload on subsequent crack growth rates in the aluminum and steel alloys. This result is illustrated in Figures 126 and 130 where it is evident that crack propagation lives were reduced by the negative loads. The reduction appears large in the aluminum alloy tests because of substantial differences in initial crack sizes in the test specimens. If the effect of initial crack size is accounted for, the effect of the negative loads is small as was the case for the steel alloy specimens. For the titanium alloy tests (Figure 137) negative loads appeared to increase crack propagation life. However, the crack growth

retarding effects of the 1.5X overloads were so small that this result cannot be considered meaningful.

Test results for part-thru cracks originating at Taper-lok fastener holes were not quantitatively evaluated due to the lack of applicable stress intensity factors. It was previously shown in Figure 122 that Taper-lok fasteners increased crack propagation lives under constant cyclic load conditions by factors ranging from 3 to 5 for the aluminum and titanium alloys but had very little effect on crack propagation life for steel alloy. The effects of overloads on both close tolerance and Taper-lok fastener filled holes seemed to be approximately equivalent and so it appears that the effects of Taper-lok fasteners on crack propagation life were about the same as noted above for the constant load tests.

Only one static fracture resulted in all of the Taper-lok fastener cyclic tests conducted in this program. Aluminum alloy specimen FPOCIA-1 failed during the application of the eighth overload at a peak stress level of 39.5 ksi. At the time of failure, the part-thru crack had grown to a depth of 0.317 inch and length of 0.456 inch and a 0.114 inch uniform thru crack had originated and grown from the opposite side of the hole. If the fastener hole had been filled with a close tolerance fastener and the thru crack had not originated at the opposite side of the hole, the calculated stress intensity factor at the time of failure would have been 48 ksi$\sqrt{\text{in}}$. Since this is a reasonable value of fracture toughness for the 2219-T851 plate, it appears that the Taper-lok fastener did not have a large effect on fracture strength in the cited test.

5.3.4 Summary

Overload tests were conducted on 2219-T851 aluminum, 9Ni-4Co-0.2C steel, and 6Al-4V βA titanium alloy specimens containing quarter-circular part-thru fastener hole flaws originating at close tolerance fasteners, Taper-lok fasteners, and cold worked holes. In addition, specimens containing uniform thru cracks originating at Taper-lok fastener filled holes were tested. In all specimens, overloads resulted in large amounts of apparent crack growth. For the close tolerance and thru-cracked Taper-lok

fastener holes, apparent crack growth rates during overloads were about two orders of magnitude greater than corresponding baseline crack growth rates. Results for the cold worked and part-thru cracked Taper-lok fastener holes could not be quantitatively evaluated but appeared similar to those for the close tolerance fastener hole tests.

Periodic tensile overloads having peak stresses greater than about 1.5 times the intermediate peak cyclic stress resulted in increased crack propagation life for all but the cold worked fastener holes. For cold worked fastener holes, peak overload stresses ranging from 1.4 to 1.5 times the subsequent peak cyclic stress appeared to have a slight tendency to decrease crack propagation life. Crack propagation life tended to increase with increasing overload frequency for the close tolerance and Taper-lok fastener holes. Overload frequency effects were not evaluated for cold worked holes. There were some exceptions to the above observation for low overload ratios. It was also observed that small negative loads applied immediately after the tensile overloads had a tendency to reduce crack propagation life.

Good agreement between experimental and calculated crack propagation lives for close tolerance fastener and thru-cracked Taper-lok fastener filled holes was obtained. For aluminum and titanium part-thru fastener hole flaw specimens, Taper-lok fasteners resulted in crack propagation lives that ranged from 3 to 5 times calculated lives for comparable close tolerance fastener holes. Similar ratios ranged from 6 to 19 for cold worked fastener holes. For aluminum and titanium thru cracked specimens, Taper-lok fasteners resulted in crack propagation lives ranging from 5 to 30 times calculated lives for comparable close tolerance fastener holes. For steel alloy part-thru crack specimens, crack propagation lives for Taper-lok fastener holes ranged from 0.9 to 1.2 times calculated lives for comparable close tolerance fastener holes. Similar ratios ranged from 5 to 10 for cold worked holes and from 1.4 to 2.3 for thru-cracked Taper-lok fastener holes. It was evident that Taper-lok fasteners were more effective in increasing crack propagation life in aluminum and titanium alloy specimens than in steel alloy specimens. It is not known whether or not this result is peculiar to the particular combinations of variables used in these tests.

5.4 Spectrum Load Tests

Spectrum load tests were conducted by subjecting specimens containing precracked fastener holes to spectrum loadings representative of either bomber or fighter loadings. Precracks consisted of part-thru quarter-circular cracks having initial depths of about one-third the specimen thickness. Some tests were conducted on conventional reamed holes that were either open or filled with loaded and unloaded close tolerance fasteners. Other tests were conducted on taper reamed holes filled with either loaded or unloaded Taper-lok fasteners. A few tests were conducted on open cold worked holes. Specimen configurations for all specimens except those having codes beginning with the letters "FV" were the same as previously described for constant cyclic load tests in Section 5.2. Specimen configuration for the specimens having codes beginning with the letters "FV" is shown in Figure 7.

5.4.1 Conventional Open and Close Tolerance Fastener Filled Holes

Nine specimens containing open and close tolerance fastener filled holes were tested including three specimens for each of the aluminum, steel, and titanium alloys. Test details for each of the specimens are listed in the upper rows of Tables 44, 45, and 46. Raw crack propagation data for each flaw are listed in Tables 155 through 157 (aluminum alloy), 164 through 166 (steel alloy), and 171 through 173 (titanium alloy) in Volume 2 of this report. Results are plotted on graphs of crack dimension versus number of spectra in Figure 169 through 177.

Test results were very consistent from alloy to alloy with few exceptions. In all but one specimen, crack growth rates increased monotonically with increase in crack size. Cracks originating at loaded fastener holes grew faster than did cracks originating at unloaded fastener holes, and there was essentially no difference in crack propagation behavior between open and unloaded filled holes.

Exceptions to the above trends were noted in aluminum alloy specimen FSCTA-2 tested under the fighter spectrum. As shown in Figure 170, crack propagation rates in FSCTA-2 decreased with increasing crack size.

This result was more pronounced for the loaded fastener hole than for the open hole and is similar to that previously noted in the surface flaw tests where crack growth retardation effects of overloads increased with increasing crack depth. This behavior could reflect an increase in crack growth retardation effects due to overloads with increase in local yielding in the vicinity of the crack. This possibility is speculative at this time and applicable only to the aluminum alloy. It was also observed that differences in crack propagation lives between the bomber and fighter spectrum were more pronounced for the steel alloy than for either of the aluminum or titanium alloys. This result indicates that crack growth behavior under spectrum loading may be alloy dependent.

An analysis was undertaken to determine if reasonable estimates of crack propagation life for part-thru cracks originating at fastener holes could be based on stress intensity factors derived in Section 4.0 of this report, baseline crack growth rates, and a simple model to account for crack growth retardation effects due to overloads. Initial calculations were based on linear cumulative damage theory. Stress intensity factors were calculated as described in Sections 4.2.1 and 4.2.2 of this report. Ratios of experimental to calculated life are plotted for each flaw in Figure 178. For the bomber spectrum, life ratios ranged between 0.6 and 1.1 with an average value of 0.8. For the fighter spectrum, life ratios ranged from 1.5 to 5.2 and averaged 3.8. Incorporation of simple overload models in the calculations would have increased calculated life for all flaws and lowered all ratios of experimental to calculated life. Hence, the agreement between experiment and calculation would have been improved for the fighter spectrum tests and degraded for the bomber spectrum tests. Apparently, factors other than first order retardation effects must be accounted for in crack propagation calculations to improve overall agreement between actual and calculated lives for the spectra tested in this program.

5.4.2 Cold Worked Open Holes

Nine specimens each containing one precracked high expansion cold worked hole were tested including three aluminum alloy specimens, two steel alloy specimens, and four titanium alloy specimens. Test details for each cold

worked hole are listed in Tables 44, 45, and 46 for the aluminum, steel, and titanium alloys, respectively. Specimens having codes beginning with the letters "FS" were configured as shown in Figure 110 and each contained one open cold worked hole. Specimens having codes beginning with the letters "FV" were configured as shown in Figure 7 and contained one loaded close tolerance fastener in a cold worked hole. Raw crack propagation data are contained in Tables 158 through 160 (aluminum alloy), Tables 167 and 168 (steel alloy), and Tables 174 through 177 (titanium alloy) in Volume 2 of this report. Results are plotted on graphs of crack dimensions versus number of spectra in Figures 179 through 187.

Spectrum load crack growth characteristics for cold worked holes were similar to those for constant cyclic load tests. Crack growth rates were considerably slower than were rates for cracked conventional holes, and crack depth growth was accentuated along the face of the hole as illustrated in Figure 116.

Crack depth growth rates for cold worked holes were roughly equivalent to crack depth growth rates for unloaded Taper-lok fasteners. The Taper-lok fasteners were installed using interference levels midway between the maximum and minimum values for standard installations. In the aluminum alloy, crack depth growth rates for the cold worked holes tended to be moderately faster than rates for the average interference Taper-lok fastener holes as seen in Figures 179 and 180. In the steel alloy specimens, crack depth growth rates for the cold worked holes were slightly slower under the bomber spectrum and considerably slower under the fighter spectrum than were comparable rates for the Taper-lok fastener holes. In the titanium alloy specimens, agreement between crack depth growth rates for cold worked and unloaded Taper-lok fastener holes were good in all specimens. Crack width growth rates for cold worked holes were consistently slower than were crack width growth rates for the Taper-lok bolt holes.

Comparisons of crack growth behavior for open cold worked holes, loaded Taper-lok fasteners, and loaded close tolerance fasteners under the bomber spectrum are shown in Figures 188, 189 and 190. Quantitative comparisons

between crack propagation life for cold worked holes and loaded fastener holes could not be made since only small amounts of crack growth had occurred at the cold worked holes by the time the crack propagation life of the loaded Taper-lok hole in the same specimen had been exhausted. It was evident that cold working of fastener holes was considerably more effective in increasing crack propagation lives of cracked fastener holes than were Taper-lok fasteners installed to an average interference level for standard installations.

5.4.3 Interference Fit Fastener Tests

Nine specimens containing loaded and unloaded precracked Taper-lok fastener holes were tested including three aluminum alloy specimens, two steel alloy specimens, and four titanium alloy specimens. Test details for each Taper-lok fastener hole are listed in Tables 44, 45 and 46 for the aluminum, steel and titanium alloys, respectively. Specimens having codes beginning with the letters "FS" were configured as shown in Figure 110 and each contained one loaded and one unloaded fastener. Specimens having codes beginning with the letters "FV" were configured as shown in Figure 7 and each contained one loaded Taper-lok fastener. Raw crack propagation data are contained in Tables 161 through 163 (aluminum alloy), Tables 169 and 170 (steel alloy) and Tables 178 through 181 (titanium alloy) in Volume 2 of this report. Results are plotted on graphs of crack dimensions versus number of spectra in Figures 179 through 187.

The effect of load transfer on crack propagation behavior was variable. In the aluminum alloy, ratios of unloaded to loaded fastener crack propagation lives were 2:1 for the bomber spectrum and 4:1 for the fighter spectrum in the presence of peak cyclic bolt loads equal to about 20% of the ultimate bolt load. In the steel alloy, ratios of unloaded to loaded fastener hole lives were 4:1 for both the bomber and fighter spectrum in the presence of peak cyclic bolt loads equal to about 30% of the ultimate bolt load. For the titanium alloy, the ratio of unloaded to loaded fastener lives were about 0.7 and 1.4 for the bomber spectrum and peak cyclic bolt loads equal to about 40% of the ultimate bolt load, and 1.0 for the fighter spectrum and peak cyclic bolt loads equal to 50% of the

ultimate bolt load. Reasons for the life ratio less than 1.0 for the titanium bomber spectrum tests could not be determined. In summary, these tests indicate that load transfer can have a significant effect on crack propagation life for Taper-lok filled fastener holes. In the aluminum alloy, the effect of load transfer on crack propagation life varied with loading spectrum. In the titanium alloy, considerable variations in load transfer effects were obtained. Reasons for these variations could not be determined.

Comparisons of crack growth behavior for loaded Taper-lok fasteners, loaded close tolerance fasteners, and open cold worked holes under the bomber spectrum are shown in Figures 188, 189, and 190 for the aluminum, steel, and titanium alloys, respectively. For the loaded fastener holes, ratios of crack propagation life for Taper-lok fastener holes to life for close tolerance fastener holes were 2.7 and 1.9 for the aluminum alloy bomber and fighter spectrum tests, 1.2 and 1.4 for the steel alloy bomber and fighter spectrum tests, and 1.3 and 1.1 for the titanium alloy bomber and fighter spectrum tests. The ratios were fairly insensitive to loading spectrum and were considerably lower for the steel and titanium alloys than for the aluminum alloy. These ratios are less than comparable constant cyclic load test ratios of 5.2, 1.4 and 4.7 for the aluminum, steel and titanium alloys, respectively. Hence, Taper-lok fasteners were less effective in retarding crack growth rates under spectrum loadings than under constant cyclic loadings, particularly for the aluminum and titanium alloys. As mentioned previously, Taper-lok fasteners were also less effective in retarding growth rates of fastener hole flaws than was cold working of fastener holes.

6.0 OBSERVATIONS AND CONCLUSIONS

6.1 Surface Flaw Test Observations

Baseline Tests

1) Peak cyclic stress level did not have a strong influence on the crack growth rate versus stress intensity factor correlations developed in this program.

2) Crack depth growth rates for surface flaws tended to be faster under pure tension stress than under pure bending stresses for constant stress intensity factors.

Constant Cyclic Load Tests

1) Methods used to correlate and/or calculate crack depth growth behavior under constant cyclic load conditions were adequate for the entire range of surface flaw geometries tested in this program ($0.15 < a/2c < 0.50$ and $0.2 < a/t < 1.0$).

2) More scatter was observed in crack width growth rate data than in crack depth growth rate data. However, crack propagation life for surface flaws is fairly insensitive to variations in crack width growth behavior.

Overload Tests

1) Tensile overloads resulted in subsequent transient reductions in crack growth rate relative to rates that would have existed in the absence of overloads.

2) Crack growth rate behavior after overloads was in qualitative agreement with results of crack retardation models due to Wheeler (30) and Willenborg (31). Crack growth rate reduction was maximum immediately after the overload and gradually diminished with increasing crack propagation.

3) Values of the exponent m in the Wheeler model required to force agreement between the model and experimental data varied with alloy and crack depth-to-thickness ratio.

4) Crack growth rate retarding effects of overloads underwent a marked increase as the crack tip closely approached the back specimen face.

5) Tensile overloads resulted in large amounts of apparent crack growth during the overload cycle. The amount of growth was about two orders of magnitude greater than would be predicted using crack closure theory and baseline crack growth rates.

6) Small compressive loads applied immediately after tensile overloads reduced the crack growth retardation effects of the tensile overloads.

7) Small periodic compressive loads in the absence of tensile overloads had no detectable effect on crack growth behavior of surface flaws.

Spectrum Load Tests

1) Crack growth behavior of surface flaws under uniform tension spectrum loadings representative of bomber and fighter operations could not be adequately correlated using calculation procedures both with and without simple methods of accounting for the crack growth retardation effects of overloads.

6.2 Cracked Fastener Hole Test Observations

General

1) Of the fastening systems tested (close tolerance fasteners in conventional reamed holes, close tolerance fasteners in cold worked holes, and Taper-lok fasteners in taper-reamed holes), close tolerance fasteners in conventional reamed holes yielded the shortest crack propagation lives.

2) In the 2219-T851 aluminum and 6Al-4VβA titanium alloys, both cold working of fastener holes and installation of Taper-lok fasteners increased crack propagation lives. Most Taper-lok fasteners were installed using average interference levels for standard installations. Fastener holes were cold worked using the Boeing Commercial Airplane Company's high interference split sleeve process.

3) In the 9Ni-4Co-0.2C steel alloy tests, Taper-lok fasteners had only small effects on crack propagation lives. This result is apparently peculiar to combinations of test variables similar to those tested in this program. Cold working of fastener holes resulted in substantial increases in crack propagation life in all steel alloy tests.

4) There was no difference in crack propagation behavior between open holes and holes filled with unloaded close tolerance fasteners in all materials.

Constant Cyclic Load Tests

1) In the aluminum and titanium alloy tests, Taper-lok fasteners installed using average interference values for standard installations yielded crack propagation lives ranging from 3 to 5 times comparable lives for conventional reamed close tolerance fastener holes. Fastener holes that were cold worked using the Boeing Airplane Company's high interference split sleeve process yielded crack propagation lives that ranged from 9 to 23 times comparable lives for conventional reamed fastener holes.

2) Cold working resulted in increases in crack propagation life that were greater for filled holes than for open holes.

3) For the range of parameters used in this program, it was found that good estimates of crack propagation life for close tolerance fastener and open holes could be made using stress intensity factors described in Section 4.0 of this report, and baseline

crack growth rate data obtained from surface flaw specimens as described in Section 3.1 of this report. Tests were limited to circular part-thru cracks, one crack depth to hole diameter ratio ($\simeq$ 1.0), and either low or no load transfer. Ratios of calculated to experimental lives were lower for loaded holes than for either filled or open holes.

4) Methods developed to quantitatively evaluate the effects of fastener interference on crack propagation life for thru-cracked fastener holes underestimated interference effects for the aluminum and titanium alloys. Calculated and experimental results were in good agreement for the steel alloy tests in which interference had little or no effect on crack propagation life. Methods for evaluating effects of fastener interference on crack propagation life for part-thru cracked fastener holes were not available.

Overload Tests

1) The application of periodic overloads to stress levels greater than about 1.5 times the subsequent peak cyclic stress level (the minimum overload ratio tested in this program) resulted in increases in crack propagation life.

2) Tensile overloads resulted in wide bands of apparent crack growth on each fracture surface. The band widths were about two orders of magnitude larger than the corresponding baseline crack growth rates for all three alloys.

3) Small compressive loads applied immediately after tensile overloads reduced the crack growth retardation effects of the overloads in all alloys.

4) For close tolerance fasteners and open holes, very good agreement was obtained between calculated and experimental lives when calculations were based on stress intensity factors described in Section 4.0 of this report, baseline crack growth rate data from surface

flaw specimens included in Section 3.1, and Wheeler's method (with an exponent of m = 2) to account for crack growth retardation due to overloads.

5) For the aluminum and titanium alloys, part-thru cracked Taper-lok fastener holes yielded crack propagation lives ranging from 3 to 5 times calculated lives for comparable close tolerance fastener holes; similar ratios ranged from 6 to 19 for cold worked open and filled holes. For the steel alloy, experimental lives for Taper-lok fastener holes ranged from 0.9 to 1.2 times calculated lives for comparable close tolerance fastener holes; similar ratios ranged from 5 to 10 for cold worked holes.

6) For the aluminum alloy thru-cracked specimens, Taper-lok fasteners yielded crack propagation test lives ranging from 5 to 18 times calculated lives for comparable close tolerance fastener holes and from 1 to 2 times calculated lives for Taper-lok fastener holes. Ratios of experimental crack propagation lives for interference fit fasteners to calculated lives for comparable close tolerance fastener holes ranged from 9 to 30 for the titanium alloy and from 1.4 to 2.3 for the steel alloy. No calculations accounting for interference effects were undertaken for the titanium and steel alloys.

Spectrum Load Tests

1) Interference fit fasteners resulted in smaller increases in crack propagation lives under spectrum loadings than under constant cyclic loadings.

2) When crack growth calculations were based on linear cumulative damage theory, stress intensity factors described in Section 4.0 of this report, and baseline crack growth rate data from surface flaw specimens from Section 3.1, ratios of experimental to calculated crack propagation lives for open and close tolerance fastener holes ranged from 0.6 to 1.1 (average of 0.8) for the bomber spectrum tests, and from 1.5 to 5.2 (average of 3.8) for the fighter spectrum tests.

6.3 Conclusions

1) Fatigue crack propagation lives of cracked fastener holes can be increased through the proper use of either interference fit fasteners or cold working procedures.

2) Reasonable estimates of crack propagation lives for cracks originating at conventional close tolerance fastener holes can be made for situations involving circular part-thru cracks having initial depth-to-hole-diameter ratios of about unity, simple loadings, and low load transfer. More work is required to expand the applicability of methods for calculating crack propagation lives for ranges of variables outside the scope of this program.

3) Current methods of calculating crack propagation lives are not sufficiently refined to provide adequate estimates of crack propagation lives under spectrum loadings.

4) The data generated in this program identified several potential contributors to discrepancies between experimental and calculated spectrum load crack propagation lives and, because of its consistency and level of detail, will serve as a basis for evaluating future refinements to crack propagation calculation methods.

REFERENCES

1. Military Specification MIL-A-XXXX (USAF), "Airplane Damage Tolerance Design Requirements," October 1973.

2. Improved Finite Element Methods for Fracture Analyses, USAF Contract F33615-72-C-1739, Bell Aerospace Company, Buffalo, N. Y., 1972.

3. Development and Evaluation of Methods of Plane Stress Fracture Analysis, USAF Contract F33615-72-C-1796, Northrop Corporation, Aircraft Division, Hawthorne, Calif., 1972.

4. Damage Tolerant Design Handbook - A Compilation of Fracture and Crack Growth Data for High Strength Alloys, Metals and Ceramics Information Center (Battelle Columbus) Report No. MCIC-HB-01, September 1973.

5. Hall, L. R., Finger, R. W., and Spurr, W. F., "Corrosion Fatigue Crack Growth in Aircraft Structural Materials," Air Force Materials Laboratory Report AFML-TR-73-204, September 1973.

6. Crack Growth Analysis for Arbitrary Spectrum Loading, USAF Contract F33615-72-C-1744, Grumman Aerospace Corp., Bethpage, N. Y., 1972.

7. Advanced Air Superiority Fighter Wing and Carrythrough Structure, USAF Contract F33615-72-C-1891, General Dynamics/Fort Worth Division, Fort Worth, Texas, 1972.

8. Advanced Air Superiority Fighter Wing Structures, USAF Contract F33615-72-C-1891, Northrop Corporation, Aircraft Division, Hawthorne, Calif., 1972.

9. Advanced Cargo/Tanker Structures, USAF Contract F33615-72-C-2165, The Boeing Commercial Airplane Company, Renton, Washington, 1972.

10. Irwin, G. R., "Plastic Zone Near a Crack and Fracture Toughness," Proceedings of Seventh Sagamore Ordinance Material Research Conference, Report No. MeTE 661-611/F, Syracuse University Research Inst., Aug. 1960.

11. Hall, L. R. and Finger, R. W., "Fracture and Fatigue Growth of Partially Embedded Flaws," Proceedings of the Air Force Conference on Fatigue and Fracture of Aircraft Structural Materials, Air Force Flight Dynamics Report AFFDL-TR-70-144, September 1970.

12. Shah, R. C. and Kobayashi, A. S., "On the Surface Flaw Problem," Proceeding of ComCam Symposium on the Surface Crack: Physical Problems and Computational Solutions, ASME, 1972.

13. Thresher, R. W. and Smith, F. W., "Stress Intensity Factors for a Surface Crack in a Finite Solid," Journal of Applied Mechanics, Vol. 39, Trans. of ASME, Vol. 95, March 1972.

14. Irwin, G. R., "Crack Extension Force for a Part-Through Crack in a Plate," Journal of Applied Mechanics, Vol. 29, Trans. ASME, Vol. 84, December 1962.

15. Shah, R. C. and Kobayashi, A. S., "Stress Intensity Factor for an Elliptical Crack Approaching the Surface of a Plate in Bending," ASTM Special Tech. Publication No. 513, September 1972.

16. Grandt, A. F. and Swedlow, G. M., "Stress Intensity Factors for Surface Cracks in Bending," ASTM Special Tech. Publication No. 513, September 1972.

17. Irwin, G. R., "A Continum-Mechanics View of Crack Propagation," Metallurgical Reviews, Vol. 10, No. 35, 1965.

18. Mostovoy, S., Crosley, P. B. and Ripling, E. J., "Use of Crack-Line-Loaded Specimens for Measuring Plane Strain Fracture Toughness," Journal of Materials, Vol. 2, No. 3, September 1967.

19. Tiffany, C. F., Lorenz, P. M. and Hall, L. R., "Investigation of Plane Strain Flaw Growth in Thick-Walled Tanks," National Aeronautics and Space Administration Report No. NASA CR-54837, February 1966.

20. Masters, J. N. and White, J. L., "Development of Fracture Toughness Properties of D6-AC Steel for F-111 Applications," Air Force Materials Laboratory Report AFML-TR-70-310.

21. Smith, F. W., Emery, A. F. and Kobayashi, A. S., "Stress Intensity Factors for Semi-Circular Cracks, Part 2 - Semi-Infinite Solid," Journal of Applied Mechanics, Vol. 34, Trans. ASME, Vol. 89, 1967.

22. Kobayashi, A. S., "Stress Intensity Factors for Multiple-Notched Specimens," Structural Development Research Memorandum No. 18, The Boeing Aerospace Company, Seattle, Washington, December 1967.

23. Isida, M., "Methods of Laurent Series Expansion for Internal Crack Problems," Methods of Analysis and Solution of Crack Problems, edited by G. C. Sih, Nordhoff, 1972.

24. Benthem, J. P., and Koiter, W. T., "Asymptotic Approximations to Crack Problems," Methods of Analysis and Solutions of Crack Problems, edited by G. C. Sih, Nordhoff, 1972.

25. McMillan, J. C. and Pelloux, R. N. M., "Fatigue Crack Propagation Under Program and Random Loads," ASTM Special Tech. Publication No. 415, 1966.

26. Elber, W., "The Significance of Fatigue Crack Closure," ASTM Special Tech. Publication No. 486, 1971.

27. Wei, R. P., "Load Interactions on Fatigue Crack Growth in Ti-6Al-4V Alloy," National Aeronautics and Space Administration Report No. NASA CR-2239, April 1973.

28. Von Euw, F. F. J., Hertzberg, R. W. and Roberts, R., "Delay Effects in Fatigue Crack Propagation," ASTM Special Tech. Publication No. 513, September 1972.

29. Trebules, V. W., Roberts, Jr., R., and Hertzberg, R. W., "Effect of Multiple Overloads in Fatigue Crack Propagation in 2024-T3 Aluminum Alloy," ASTM Special Tech. Publication No. 536, July 1973.

30. Wheeler, O. E., "Crack Growth Under Spectrum Loading," Report No. FZM-5602, General Dynamics Corporation/Fort Worth Division, Fort Worth, Texas, June 1970.

31. Willenborg, J., Engle, R. M., and Wood, H. A., "A Crack Growth Retardation Model Using an Effective Stress Concept," Tech. Memorandum 71-1FBR, Air Force Flight Dynamics Laboratory, WPAFB, January 1971.

32. Gray, T. D., "Fatigue Crack Retardation Following a Single Overload," Air Force Flight Dynamics Laboratory Tech. Memorandum AFFDL-TM-73-137-FBR, October 1973.

33. Wood, H. A. and Haglage, T. L., "Crack Propagation Test Results for Variable Amplitude Spectrum Loading in Surface Flawed D6 AC Steel," Report No. FBR-TM-71-2, Air Force Flight Dynamics Laboratory, WPAFB, February 1971.

34. Shah, R. C., "Stress Intensity Factors for Through and Part-Through Cracks at Unloaded and Loaded Open, Filled and Interference Fit Fastener Holes," The Boeing Aerospace Company Document D180-17951-1, 1974.

35. Paris, P. C., and Sih, G. C., "Stress Analysis of Cracks," Fracture Toughness Testing and Its Applications, ASTM-STP 381, 1965.

36. Bowie, O. L., "Analysis of an Infinite Plate Containing Radial Cracks Originating from the Boundary of an Internal Circular Hole," Journal of Mathematics and Physics, Vol. 35, 1956.

37. Shah, R. C., and Kobayashi, A. S., "Stress Intensity Factor for an Elliptical Crack Under Arbitrary Normal Loading," International Journal of Engineering Fracture Mechanics, Vol. **3**, No. 1, 1971.

38. Smith, F. W., Kobayashi, A. S., and Emery, A. F., "Stress Intensity Factors for Penny-Shaped Cracks, Part 1 - Infinite Solid," Journal of Applied Mechanics, Vol. 34, Transactions of ASME, 1967.

39. Kobayashi, A. S., and Moss, W. L., "Stress Intensity Magnification Factors for Surface-Flawed Tension Plate and Notched Round Tension Bar," Proceeding of the Second International Conference on Fracture, Brighton, England, 1969.

40. Thresher, R. W., and Smith, F. W., "Stress Intensity Factors for a Surface Crack in a Finite Solid," Journal of Applied Mechanics, Vol. 39, Transactions of ASME, 1972.

41. Shah, R. C., and Kobayashi, A. S., "Stress Intensity Factors for an Elliptical Crack Approaching the Surface of a Semi-Infinite Solid," International Journal of Fracture, Vol. 9, No. 2, 1973.

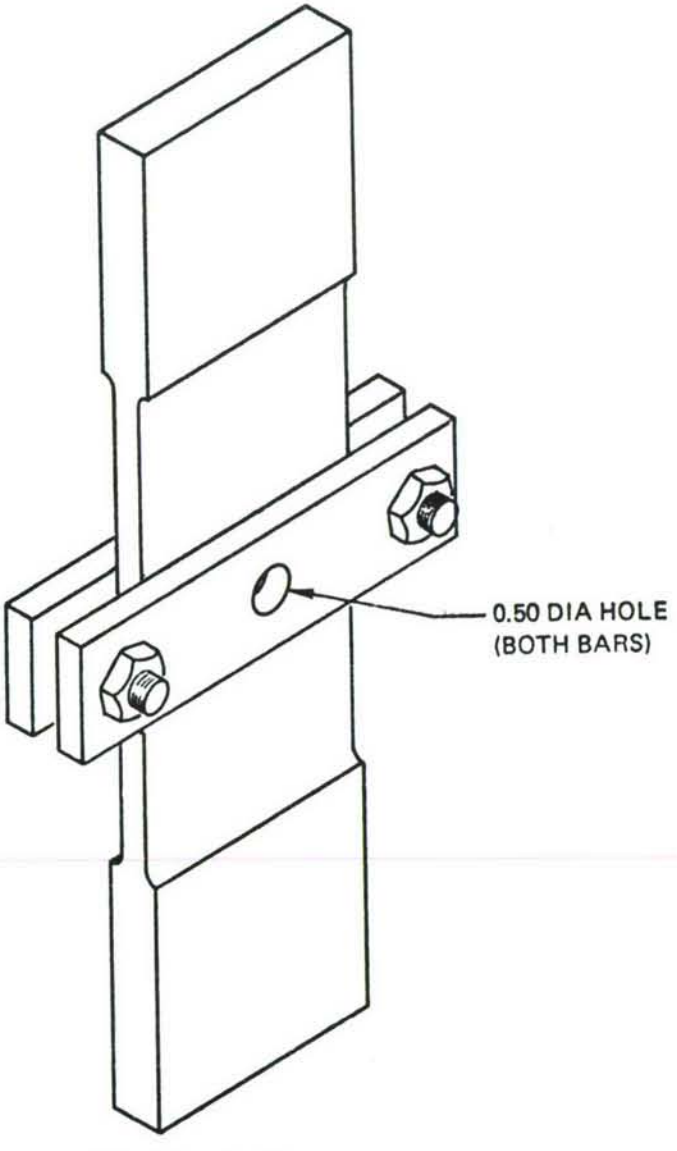
42. Shah, R. C., and Kobayashi, A. S., "On the Surface Flaw Problem," Proceedings of the Symposium on thy Surface Crack: Physical Problems and Computational Solutions, ASME, 1972.

43. Timoshenko, S., and Goodier, J. N., Theory of Elasticity, McGraw-Hill, Second Edition, 1951.

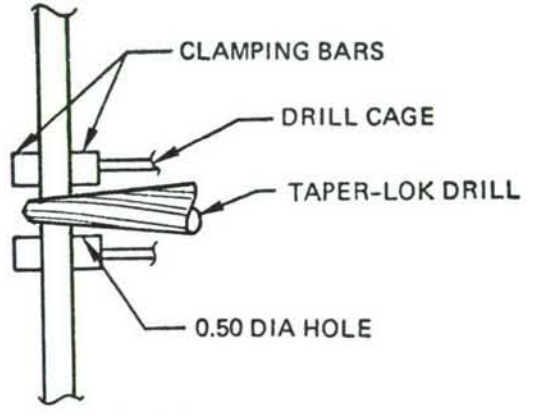
44. Mohaghegh, M., "Biaxial Stress Analysis of a Plate with a Fastener," Boeing Company Document D6-24-757 TN, 1971.

45. Wilson, Jr., H. B., "Approximate Determination of Contact Stresses in an Infinite Plate with a Smooth Circular Insert," Developments in Theoretical and Applied Mechanics, Vol. 2, Pergamon Press, 1963.

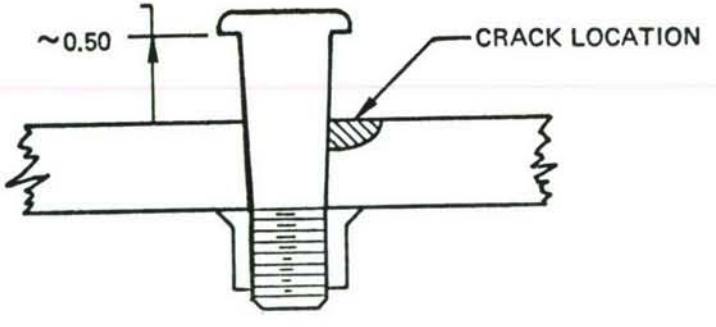
46. Brombolich, L. J., "Elastic-Plastic Analysis of Stresses Near Fastener Holes," AIAA Paper No. 73-252.



(a) Clamping Bars



(b) Drilling Technique



(c) Installed Fastener

Figure 1: Drilling Technique For Taper-Lok Fastener Holes



Figure 2: Installation of Taperlok Fasteners

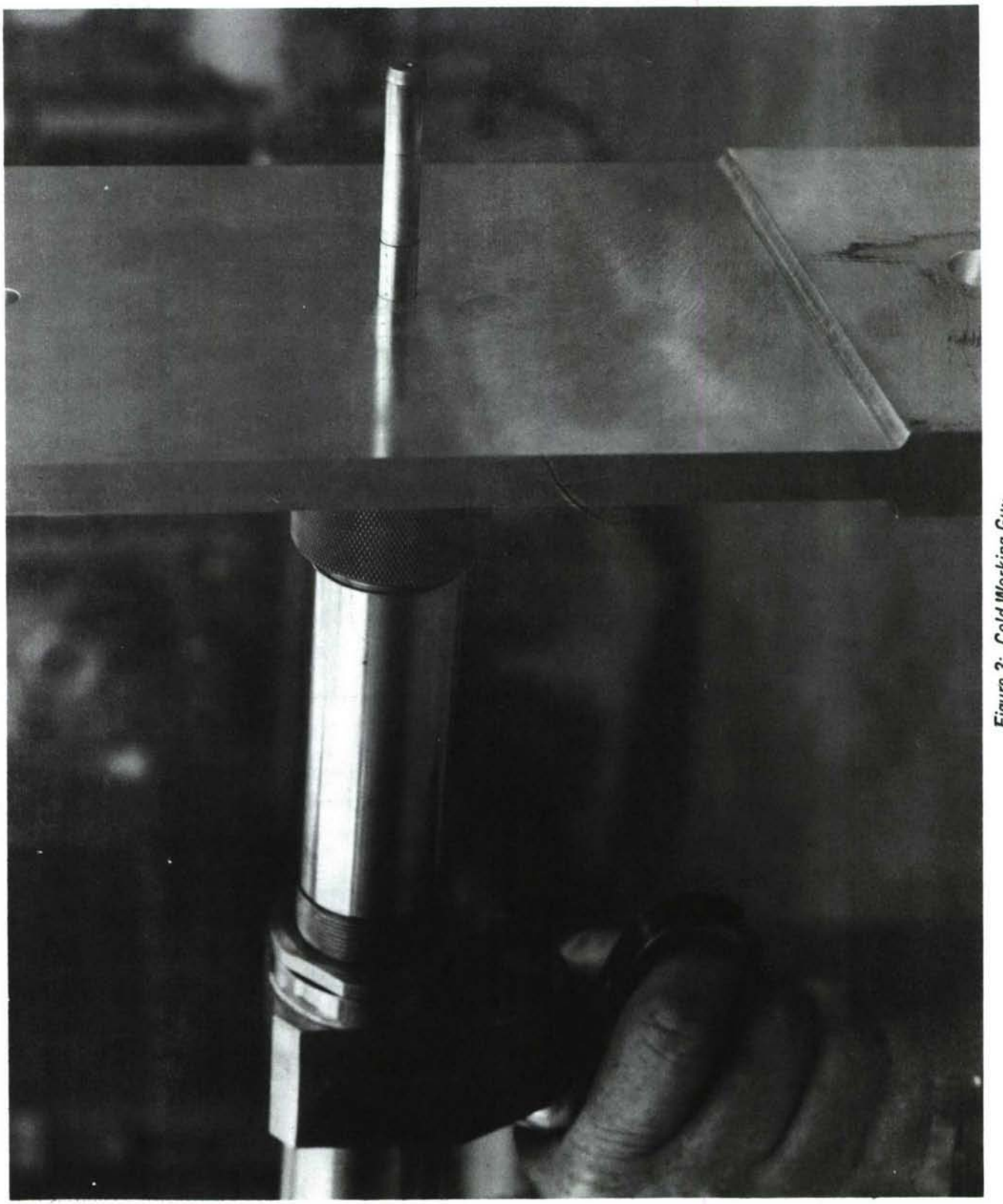


Figure 3: Cold Working Gun

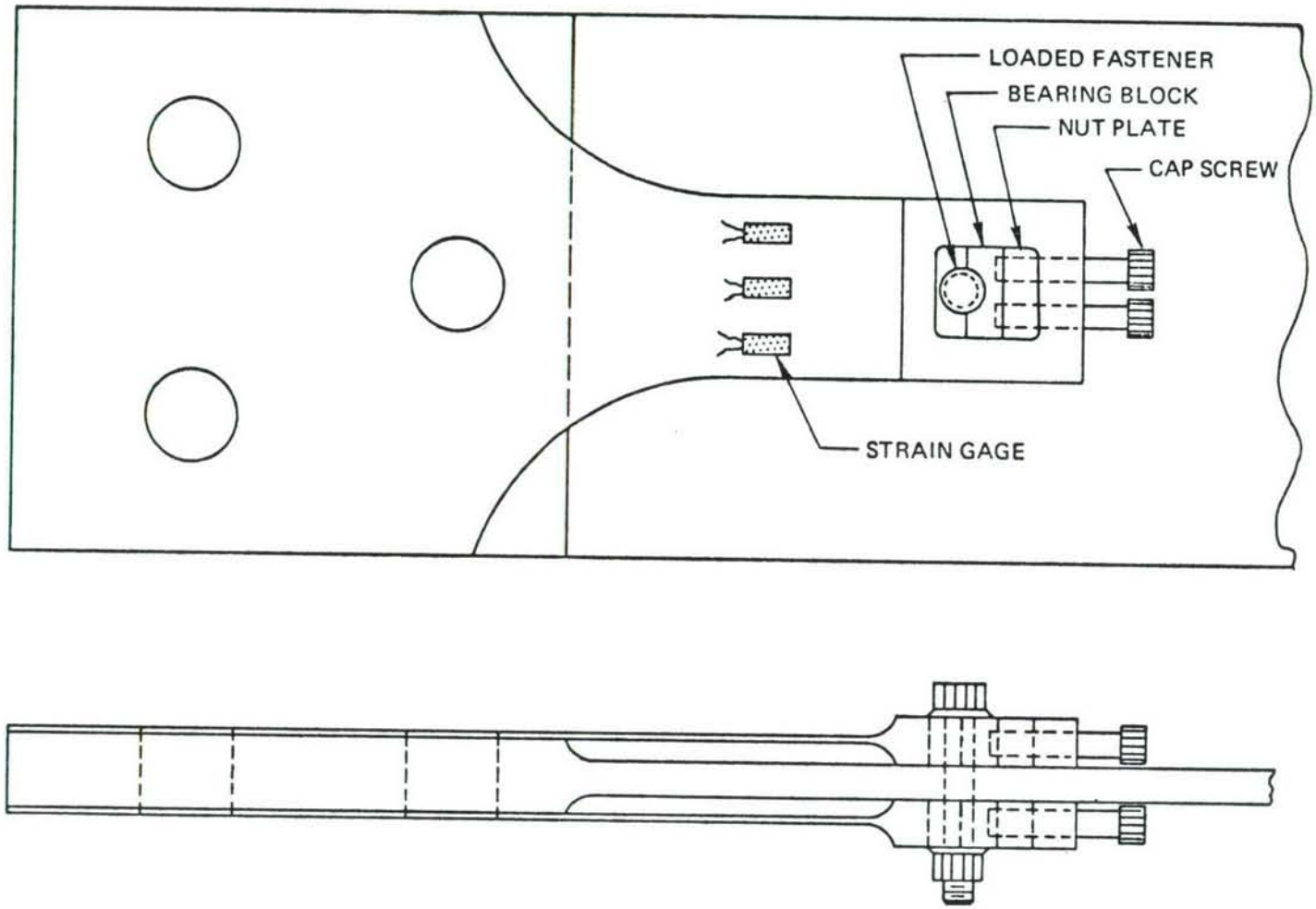


Figure 4: Test Set-Up For Loaded Fasteners

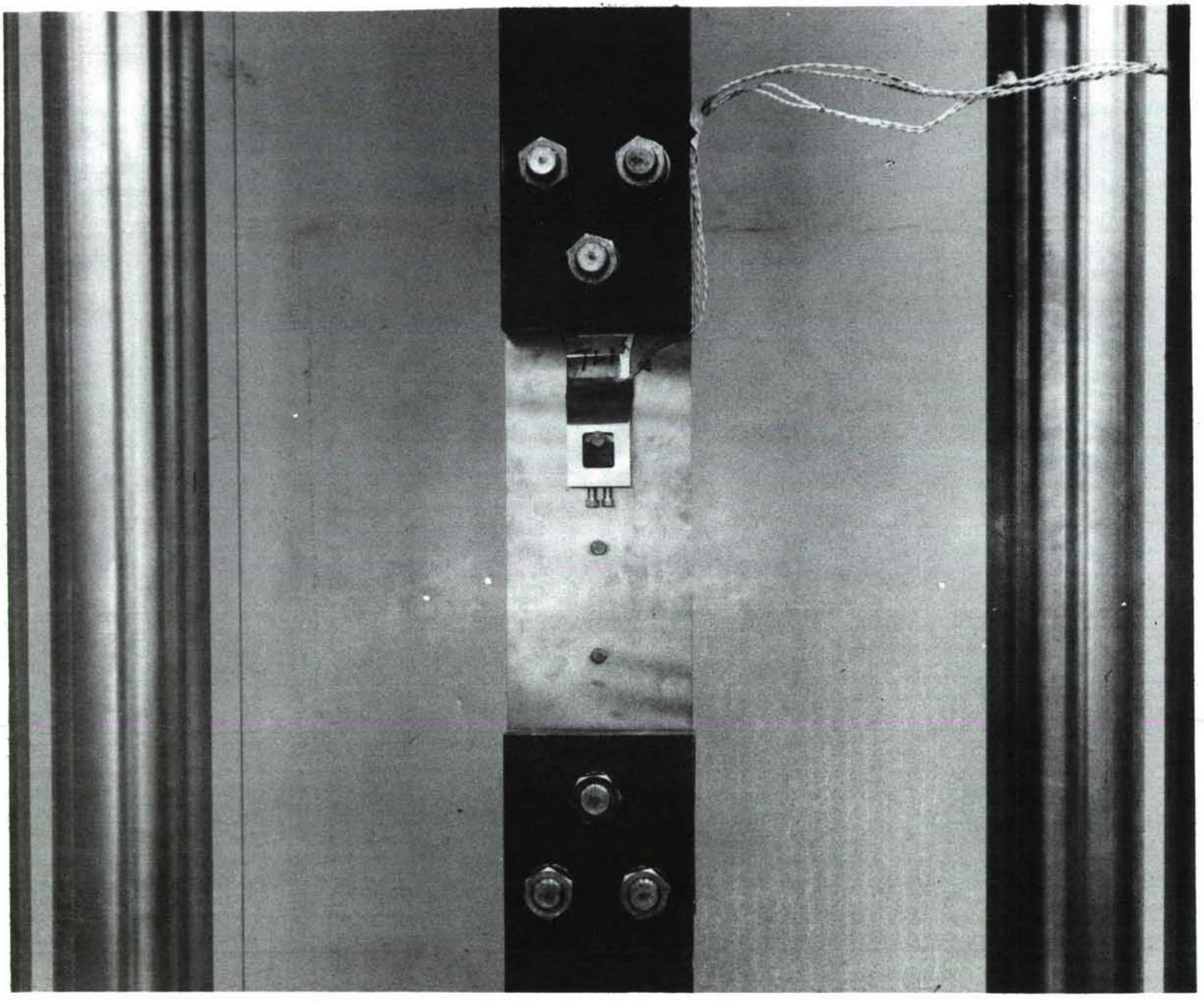


Figure 5: Test Specimen With Loading Straps

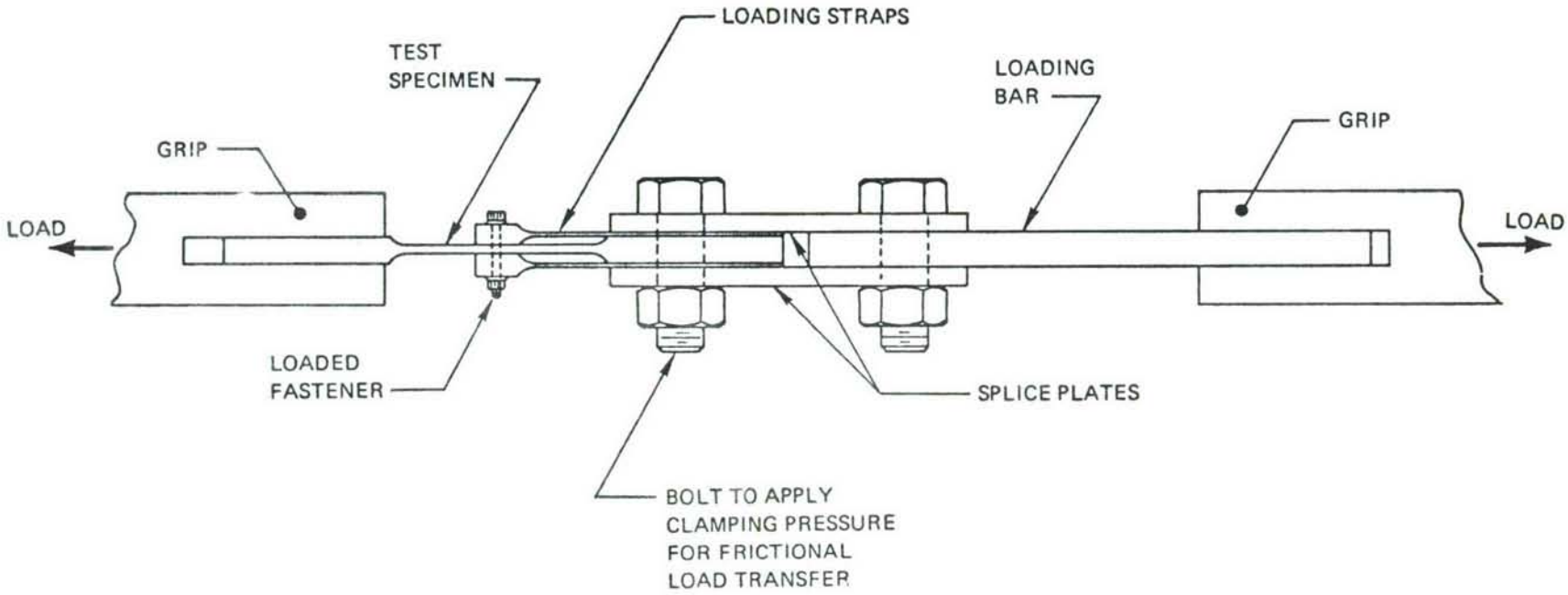


Figure 6: Setup For 4340 Steel Loaded Fastener Tests

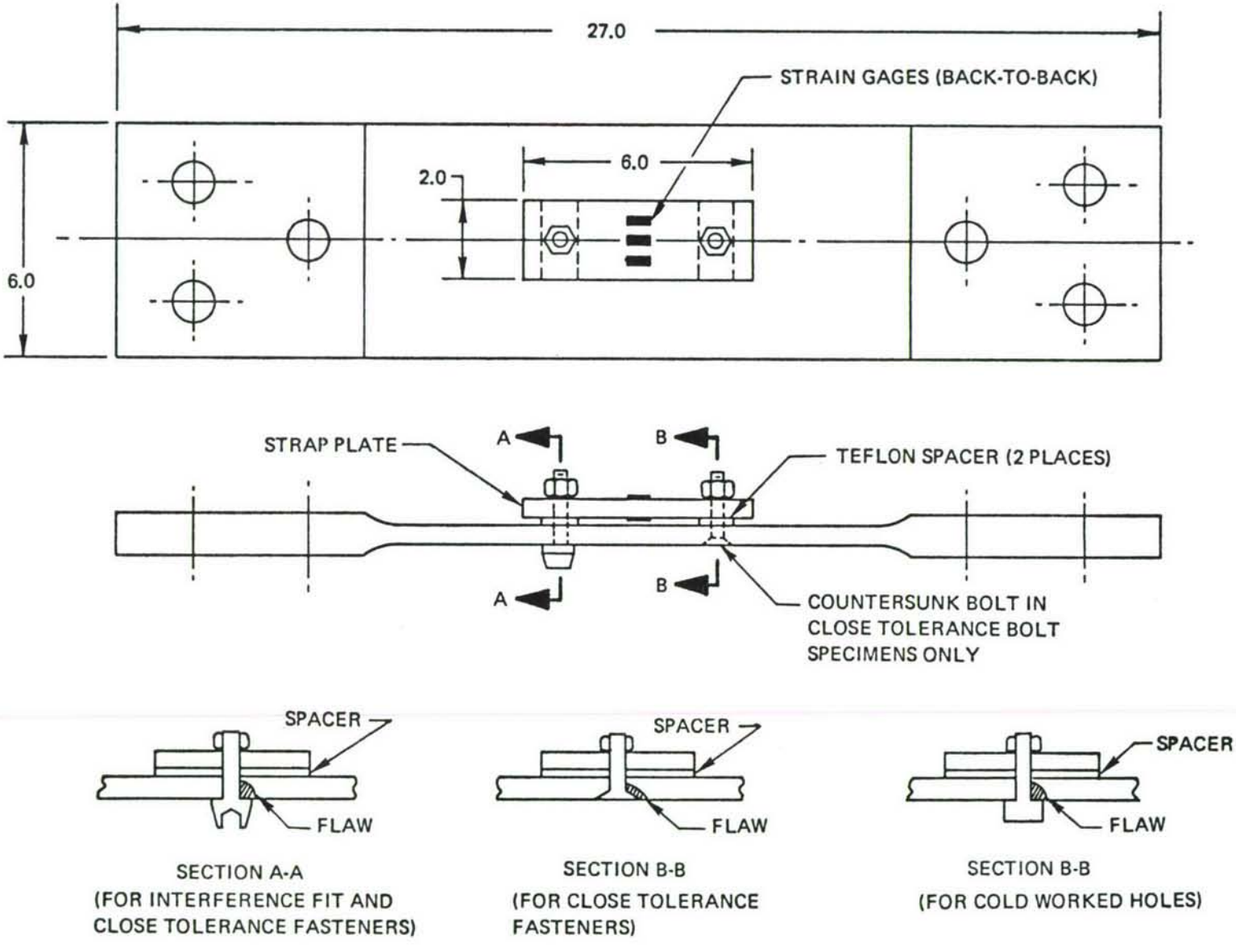


Figure 7: Specimen Configuration For Spectrum Loaded Verification Tests

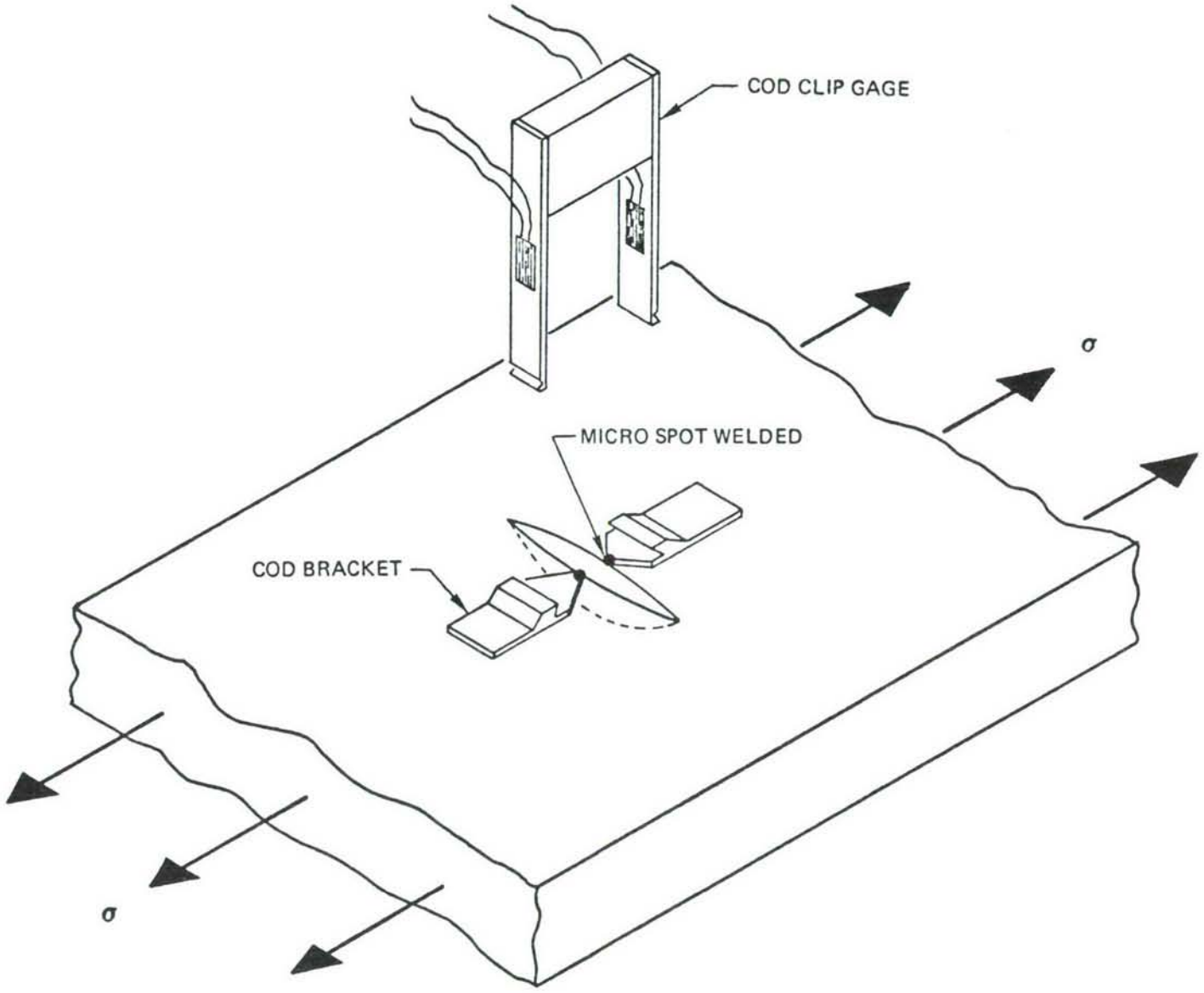


Figure 8: Instrumentation For Measuring Surface Flaw Displacements

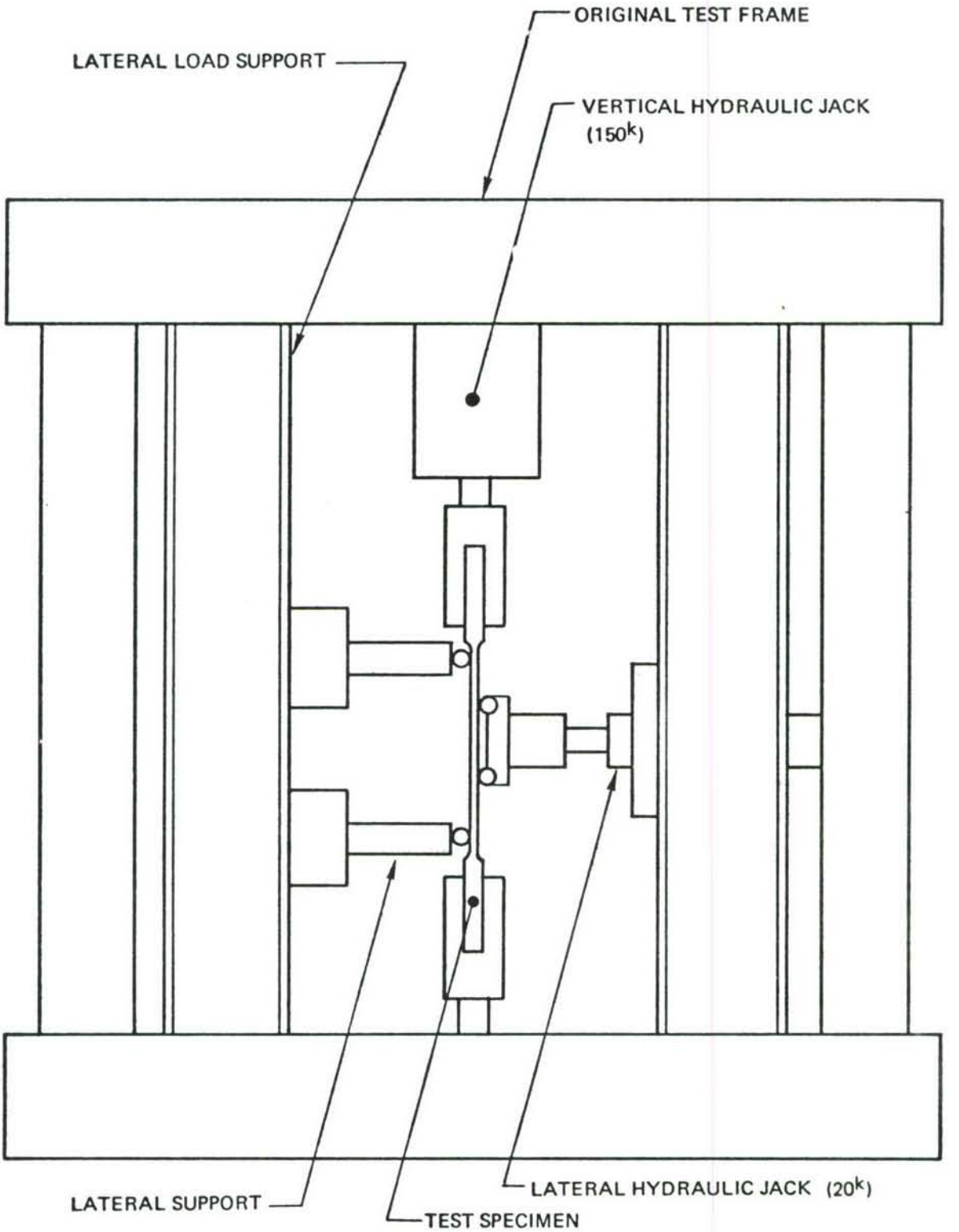


Figure 9: Test Setup For Combined Bending/Tension Tests

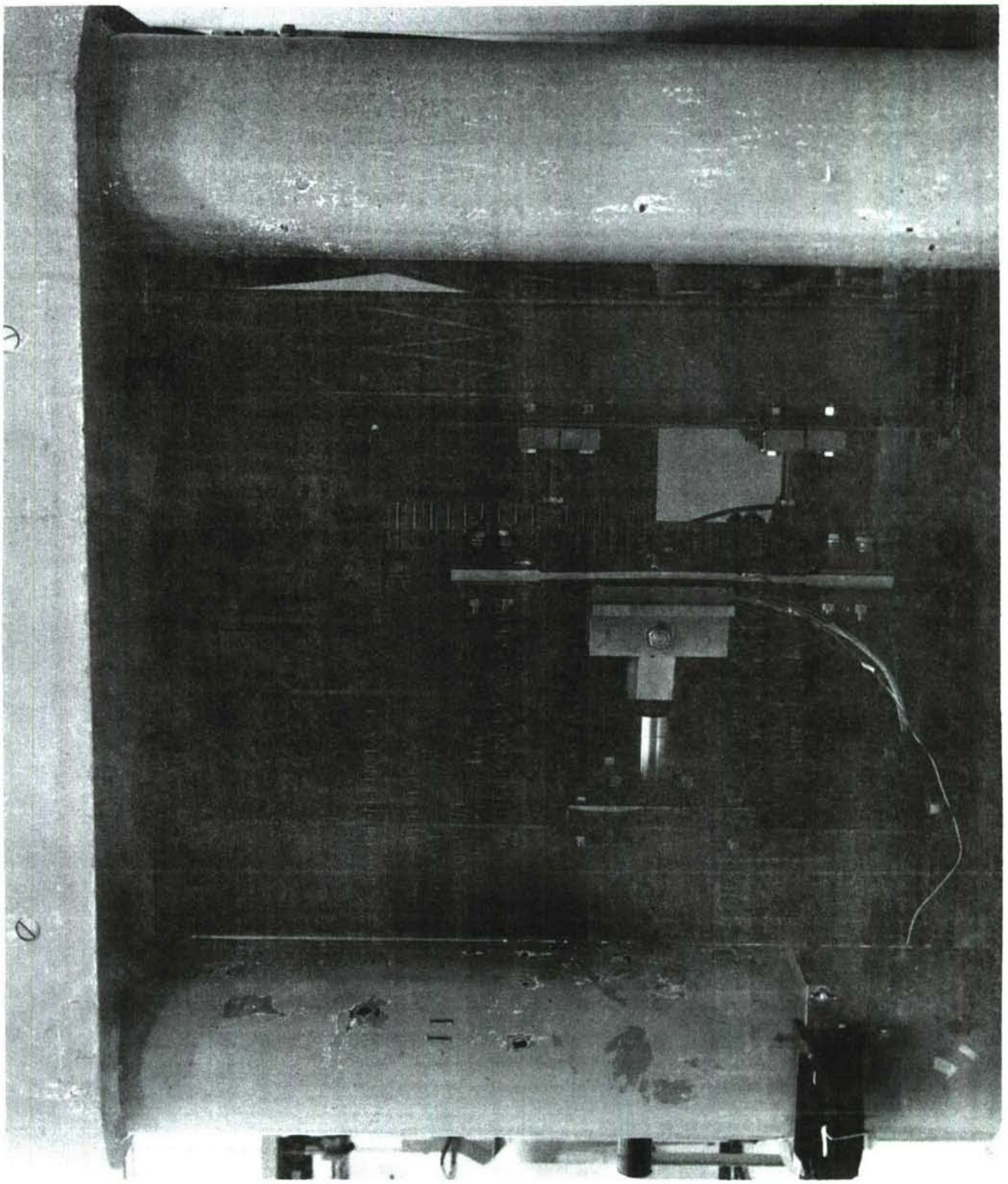
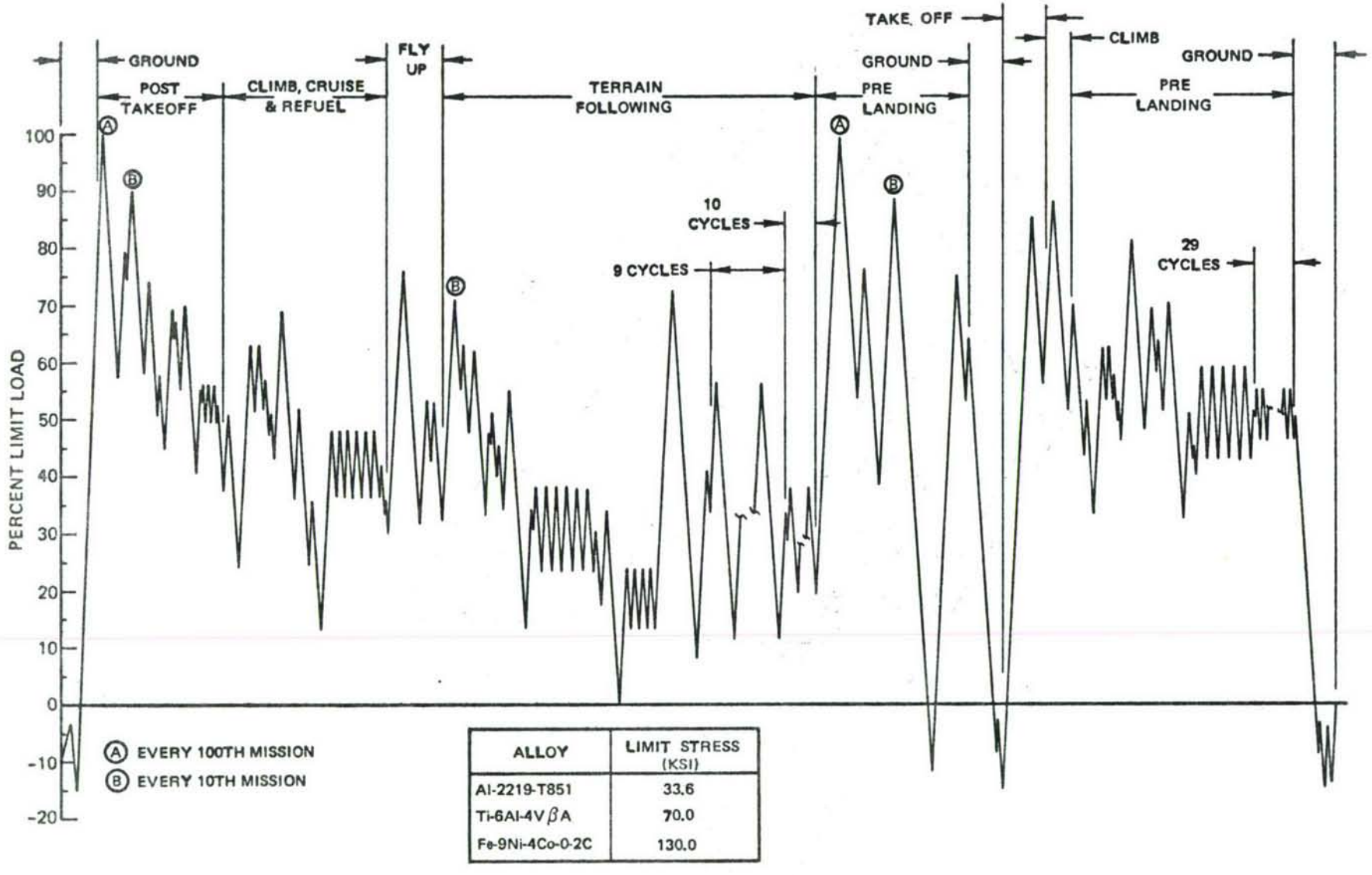


Figure 10: Combined Bending/Tension Test



ALLOY	LIMIT STRESS (KSI)
Al-2219-T851	33.6
Ti-6Al-4V βA	70.0
Fe-9Ni-4Co-0-2C	130.0

Figure 11: Bomber Spectrum

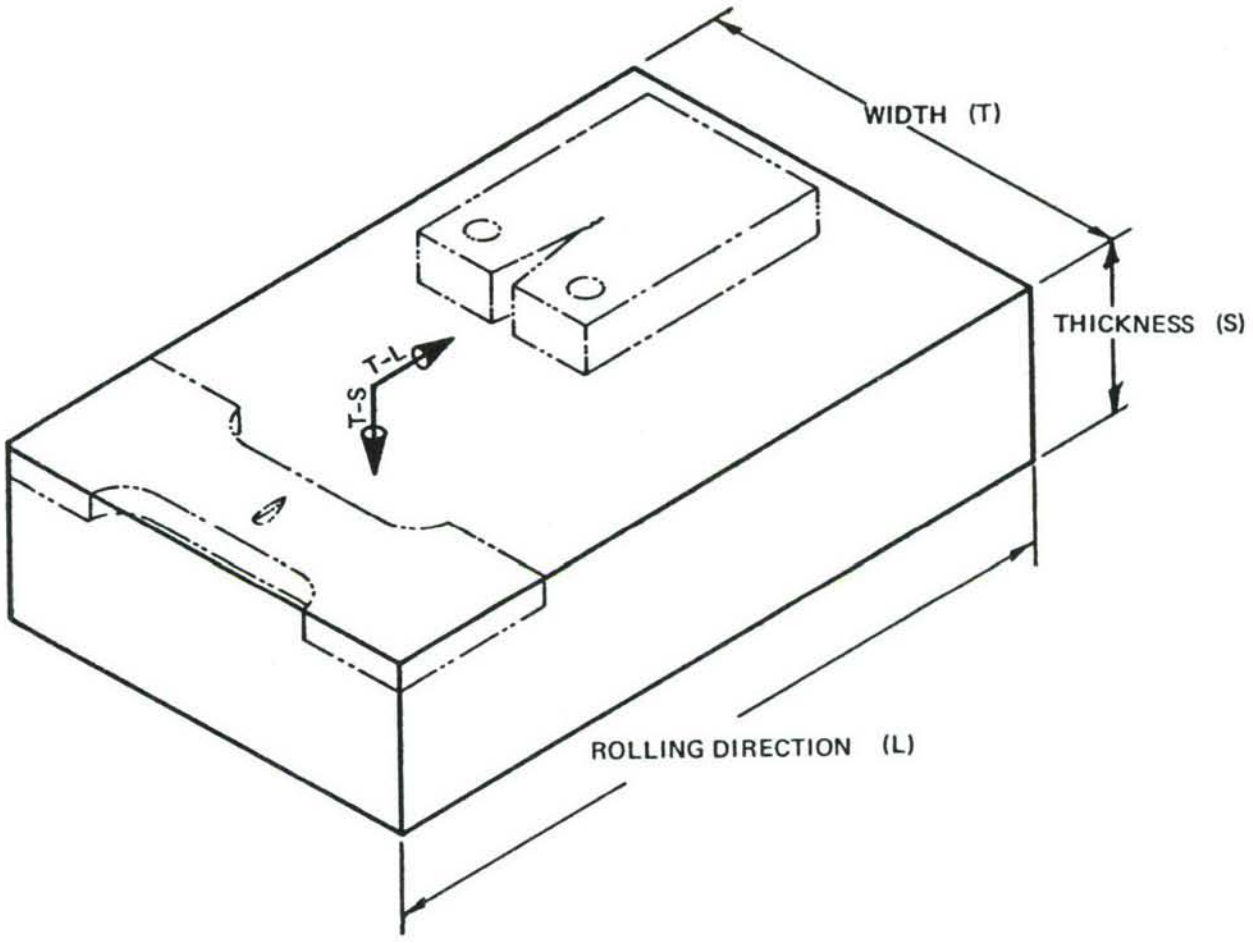
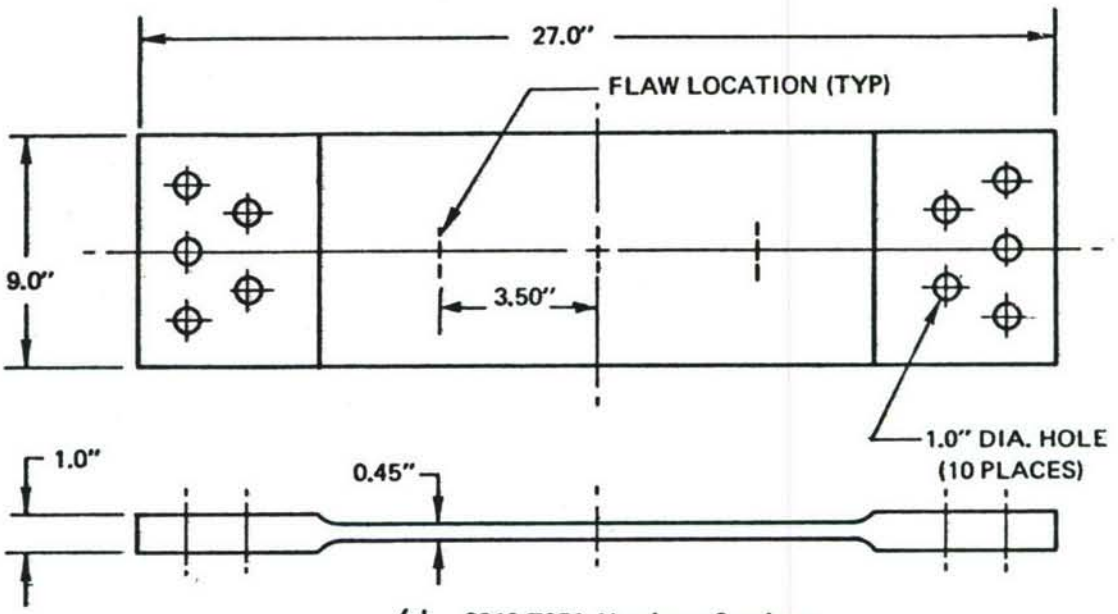
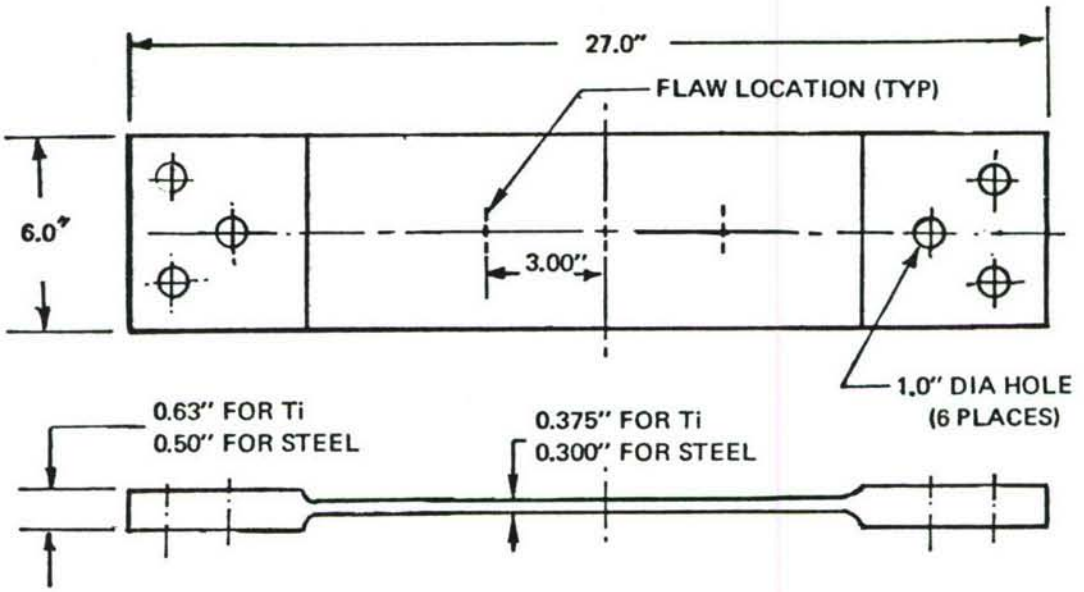


Figure 12: Crack Propagation Direction Nomenclature

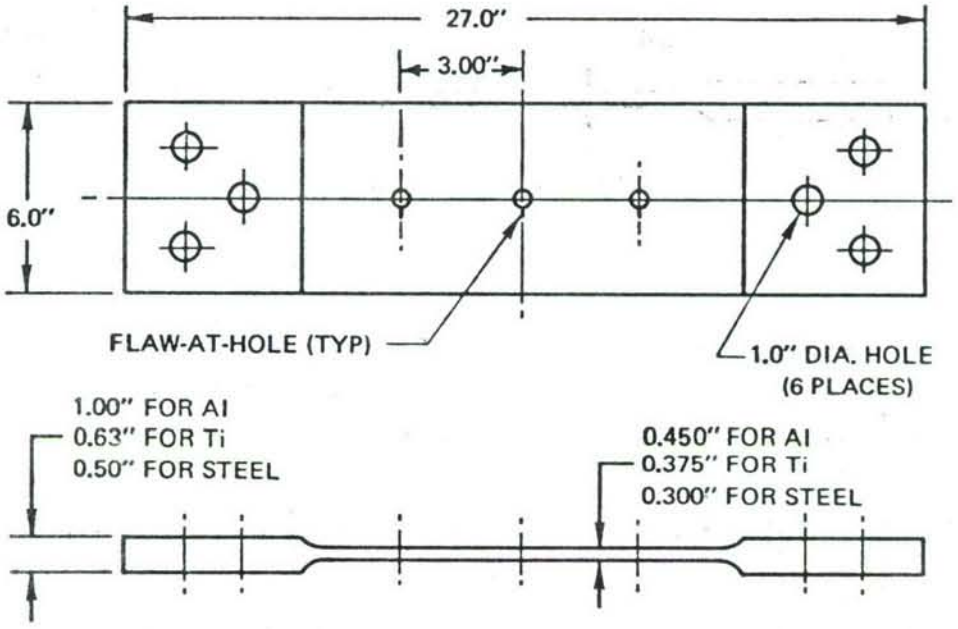


(a) 2219-T851 Aluminum Specimen



(b) 6Al-4V Titanium and 9Ni-4Co-0.2C Steel Specimens

Figure 13: Surface Flaw Cyclic Tension Specimens

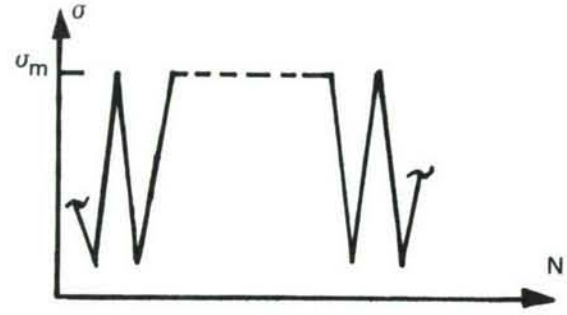


2219-T851 Aluminum ,
6Al-4V Titanium and
9Ni-4Co-0.2C Steel Specimens

Figure 14: *Flaw-At-Hole Tension Specimens*

SPECIMEN FUCTA–1

σ_m = 21 KSI
R = 0.1
f = 60 CPM
DESICCATED AIR
CLOSE TOLERANCE FASTENERS



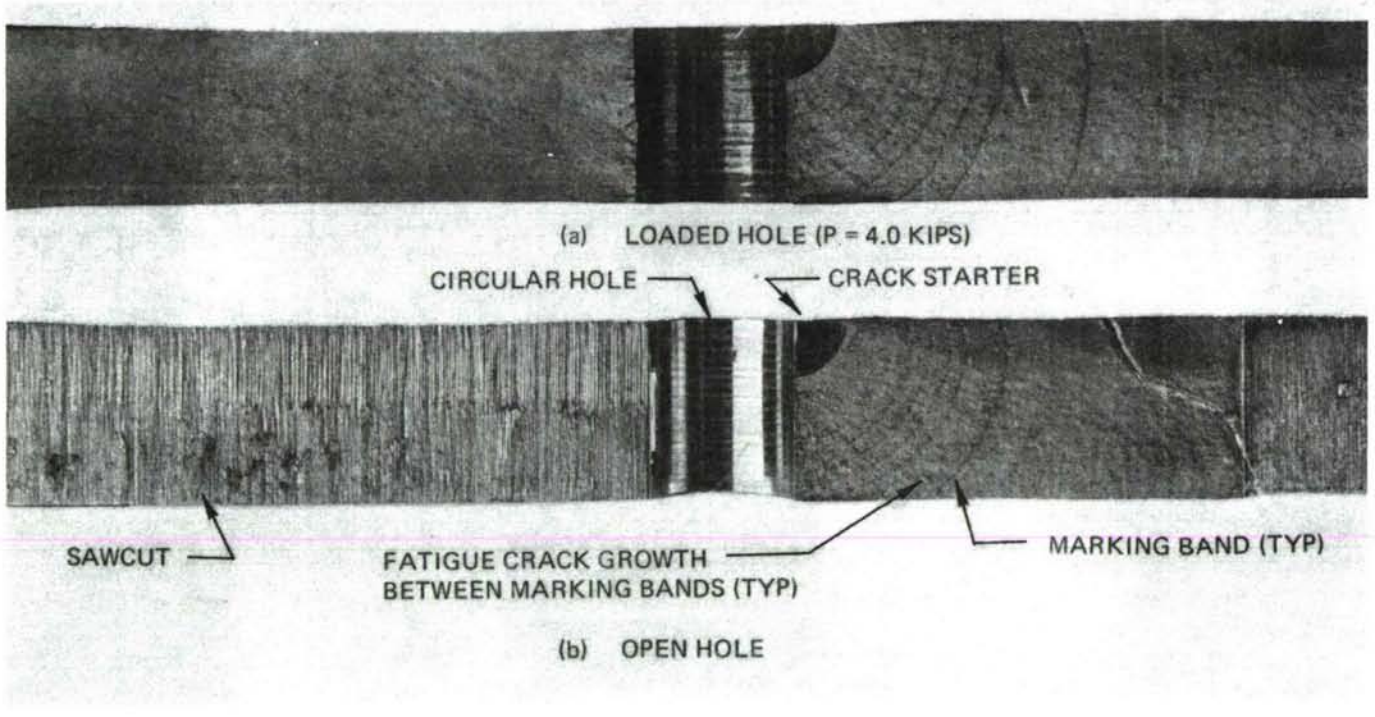


Figure 15: Fracture Faces For Aluminum Uniform Load Fastener Hole Flaw Specimens Illustrating Periodic Marker Bands Used To Track Crack Growth

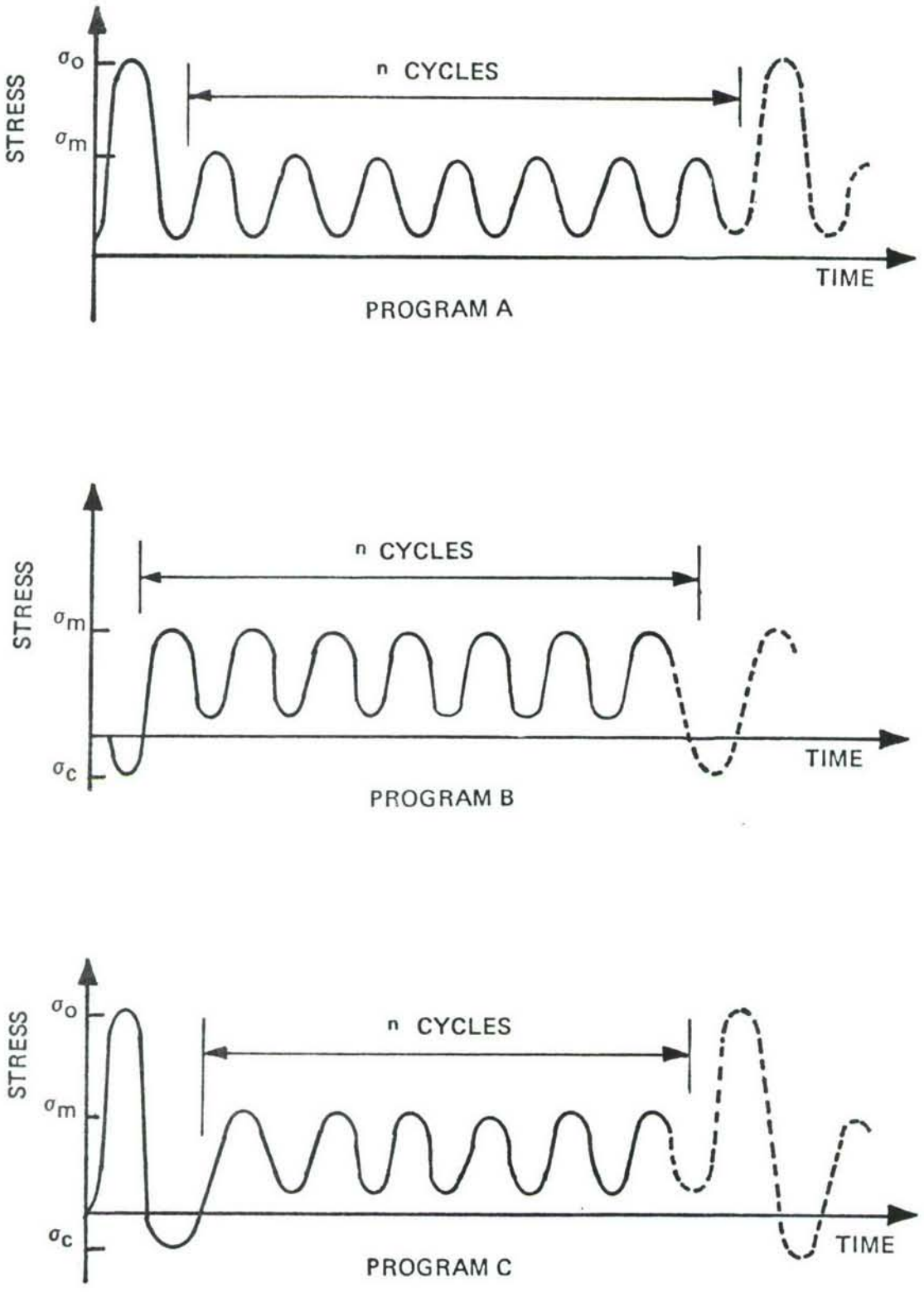


Figure 16: *Loading Programs For Overload Tests*

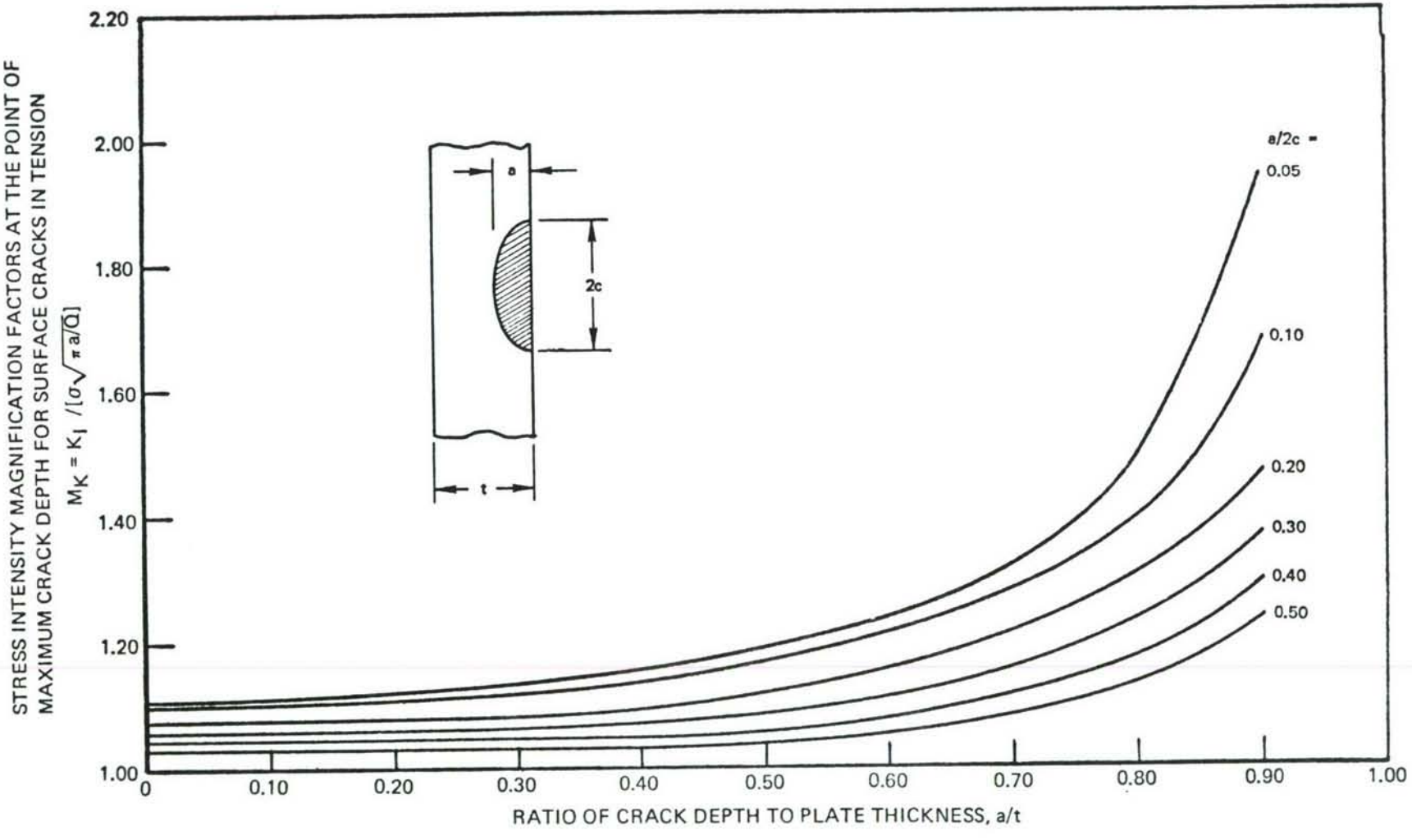


Figure 17: Stress Intensity Factors for Surface Flaws Subjected to Uniform Tension Loadings (Reference 42)

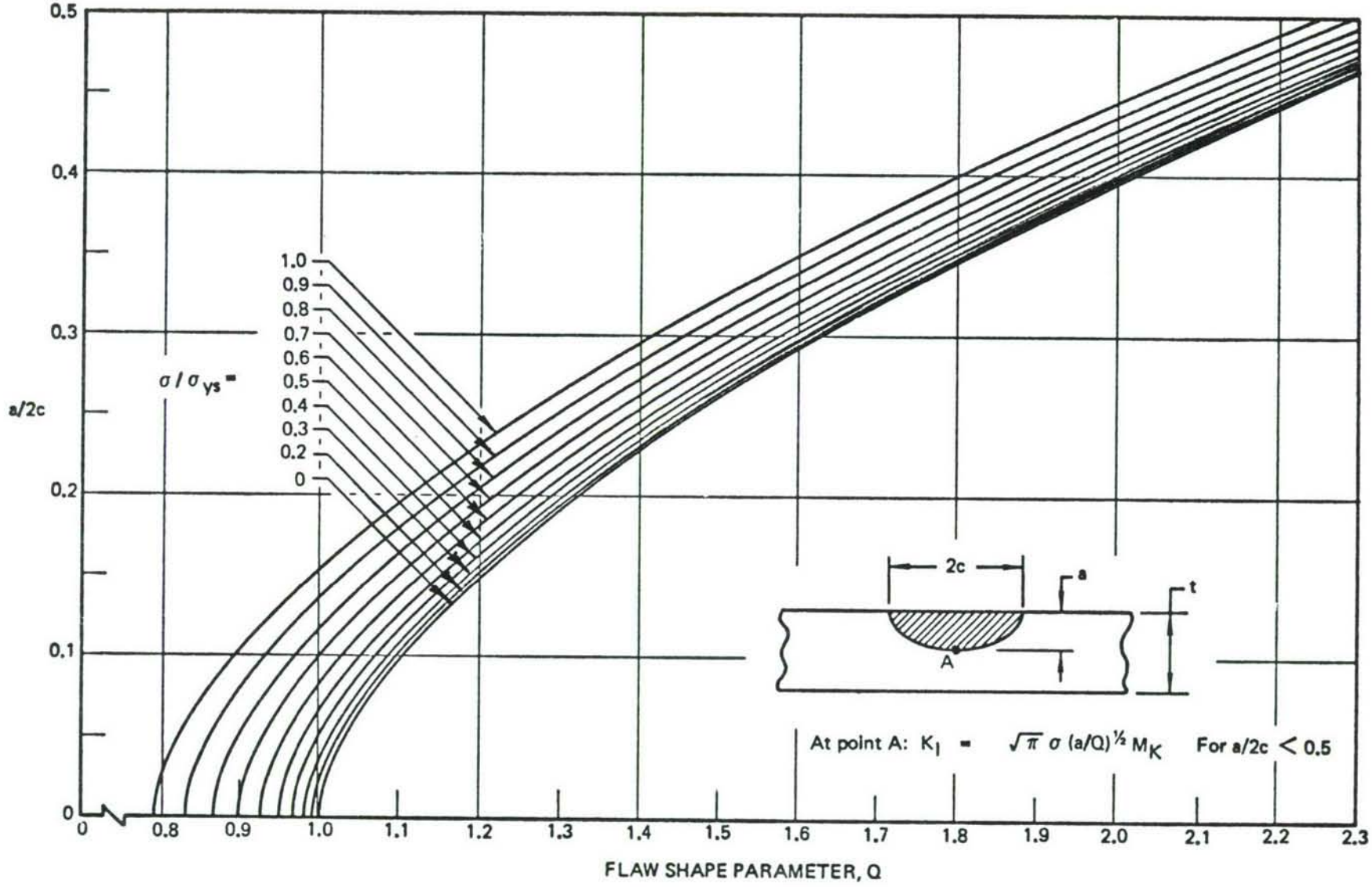


Figure 18: Shape Parameter Curves for Surface and Internal Flaws

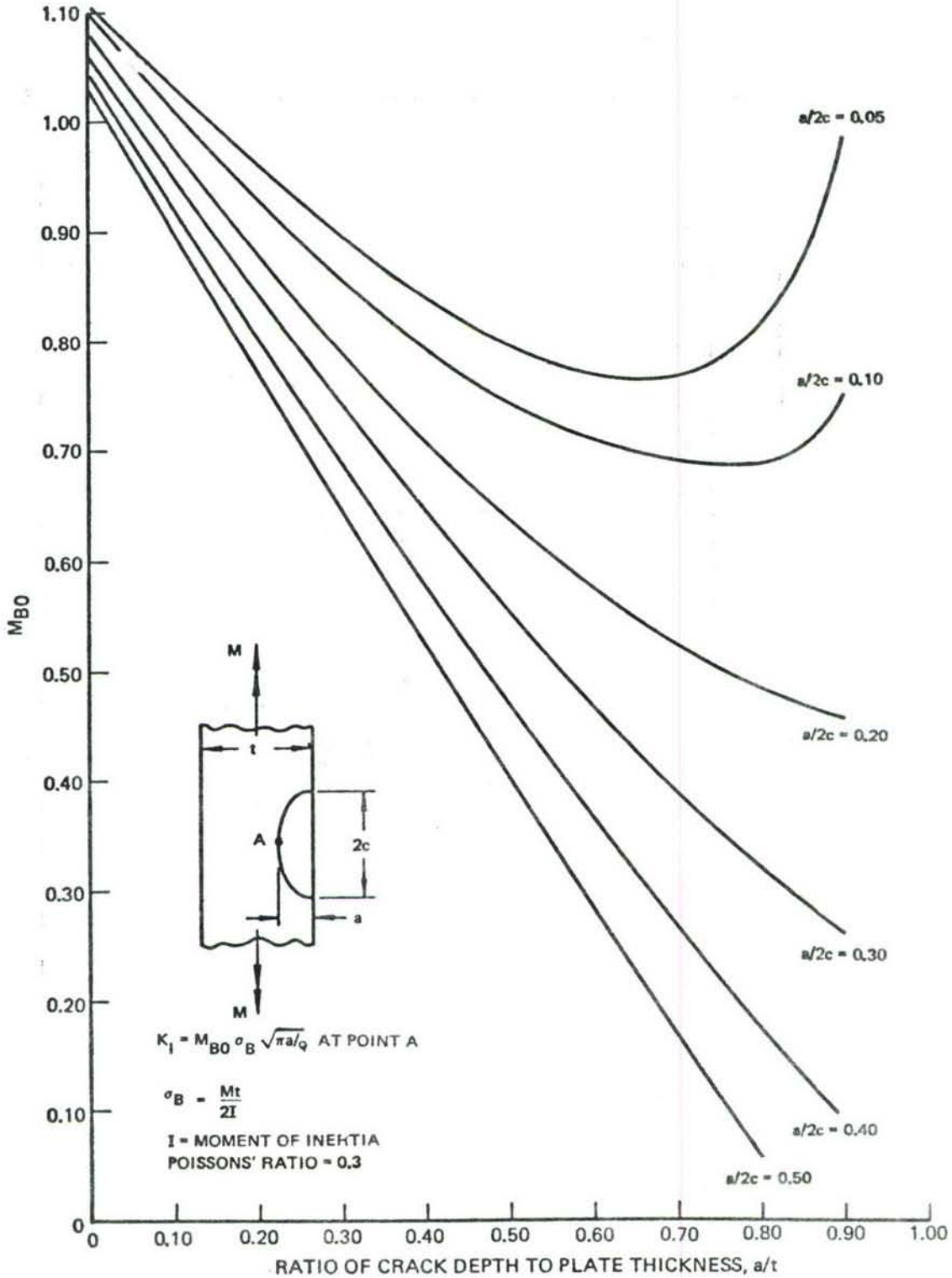


Figure 19: Stress Intensity Factors at the Point of Maximum Crack Depth for Surface Flaws Subjected to Bending Stresses

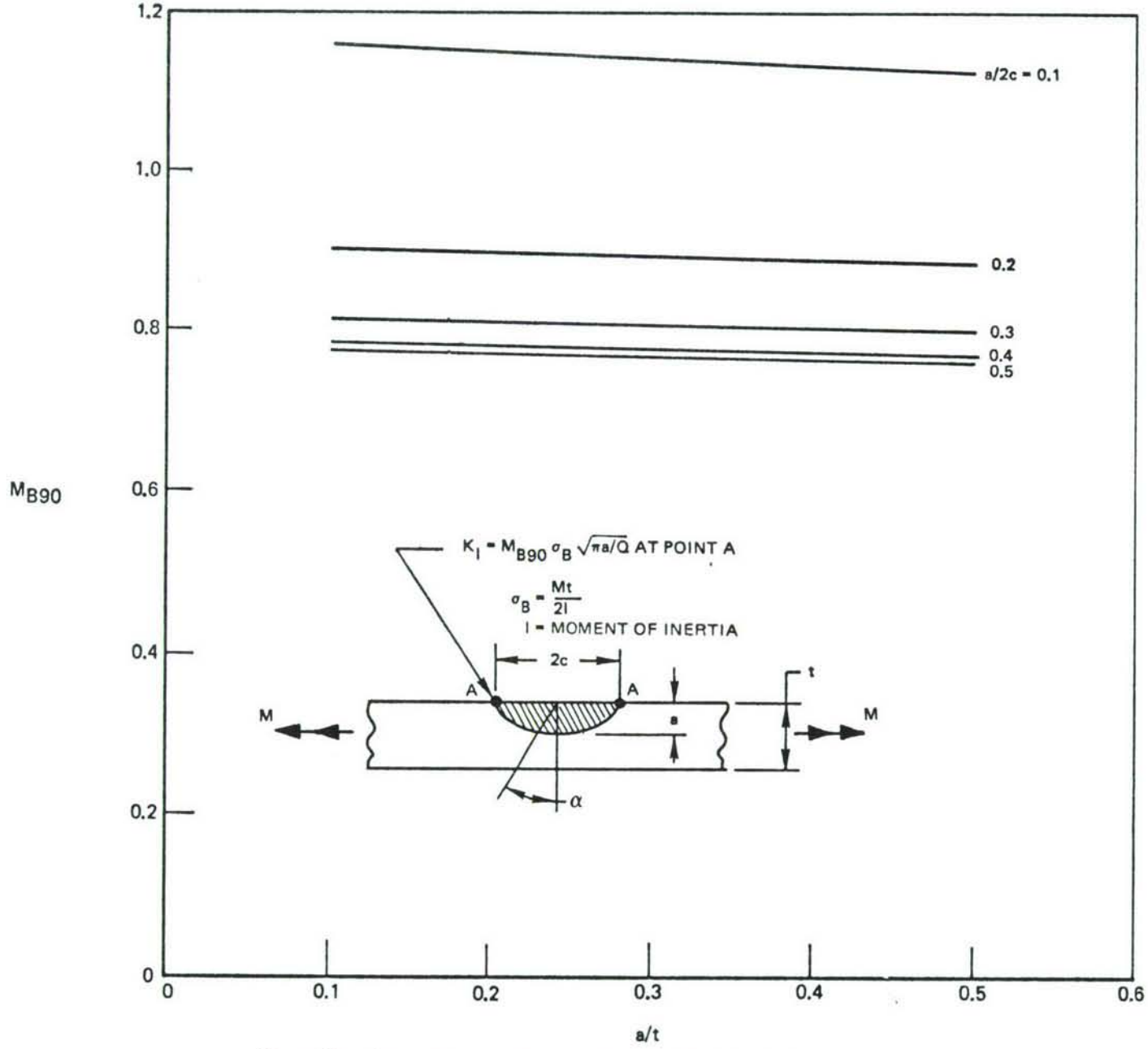


Figure 20: Stress Intensity Factors at Plate Surface for Surface Flaws Subjected to Bending Stresses

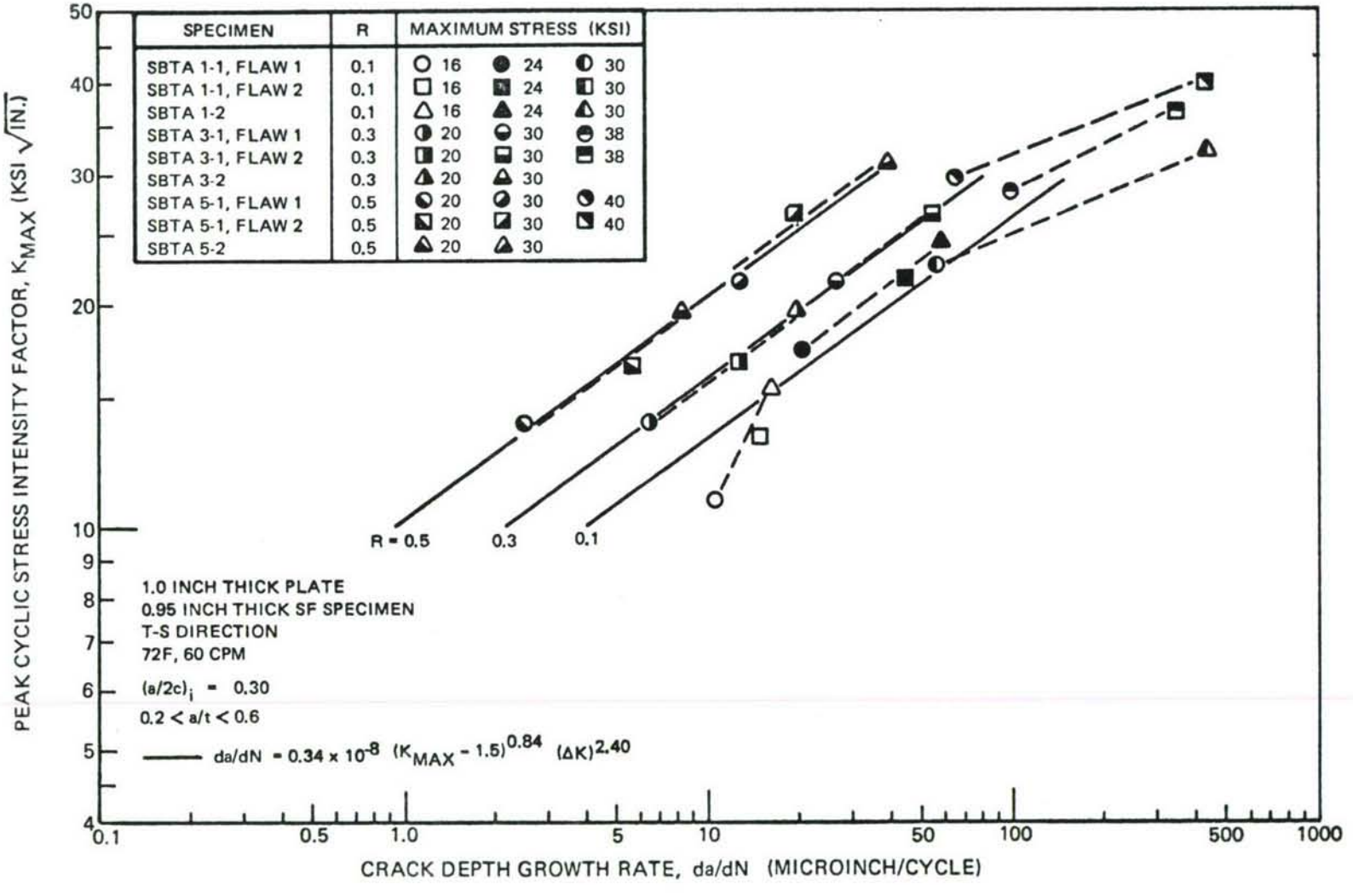


Figure 21: Stress Intensity Factor Vs. Crack Depth Growth Rate–Baseline Tension Cyclic Tests of 0.95 Inch 2219-T851 Aluminum Surface Flaw Specimens in Room Temperature Desiccated Air

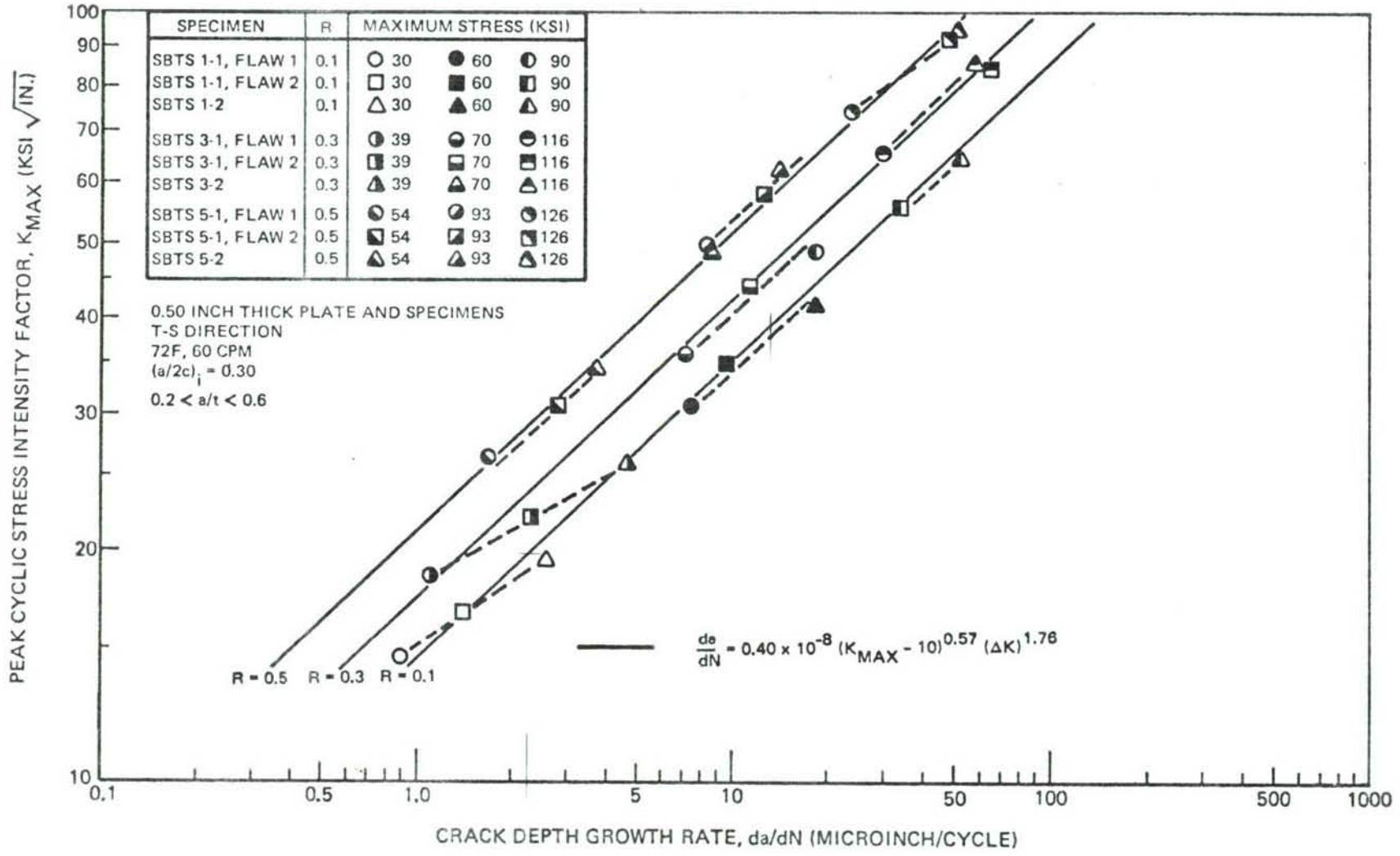


Figure 22: Stress Intensity Factor Vs. Crack Depth Growth Rate–Baseline Tension Cyclic Tests of Surface Flawed 9Ni-4Co-0.2C Steel Surface Flaw Specimens in Room Temperature Desiccated Air

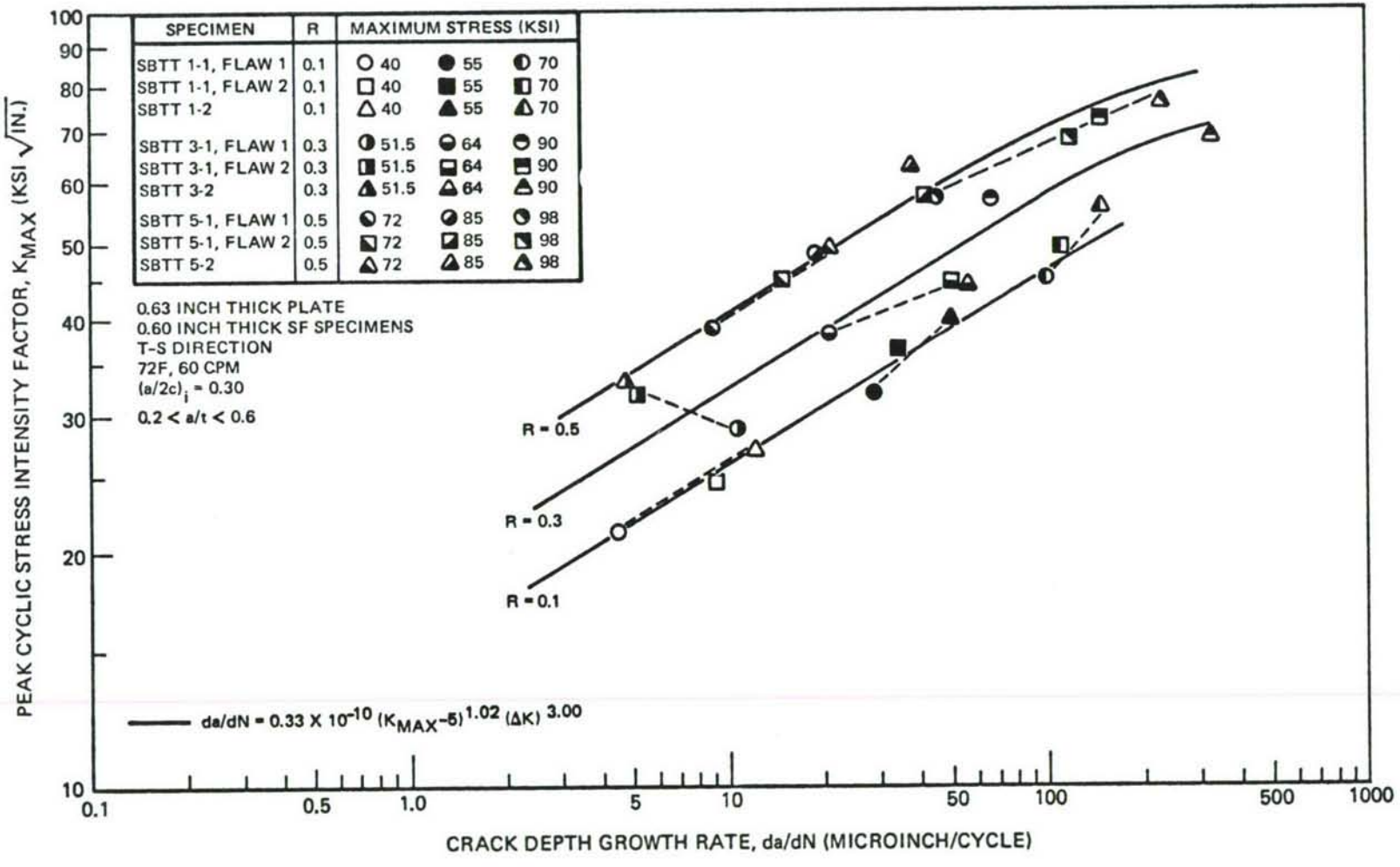


Figure 23: Stress Intensity Factor Vs. Crack Depth Growth Rate–Baseline Tension Cyclic Tests of 0.60 Inch 6Al-4V β-Annealed Titanium Surface Flaw Specimens in Room Temperature Desiccated Air

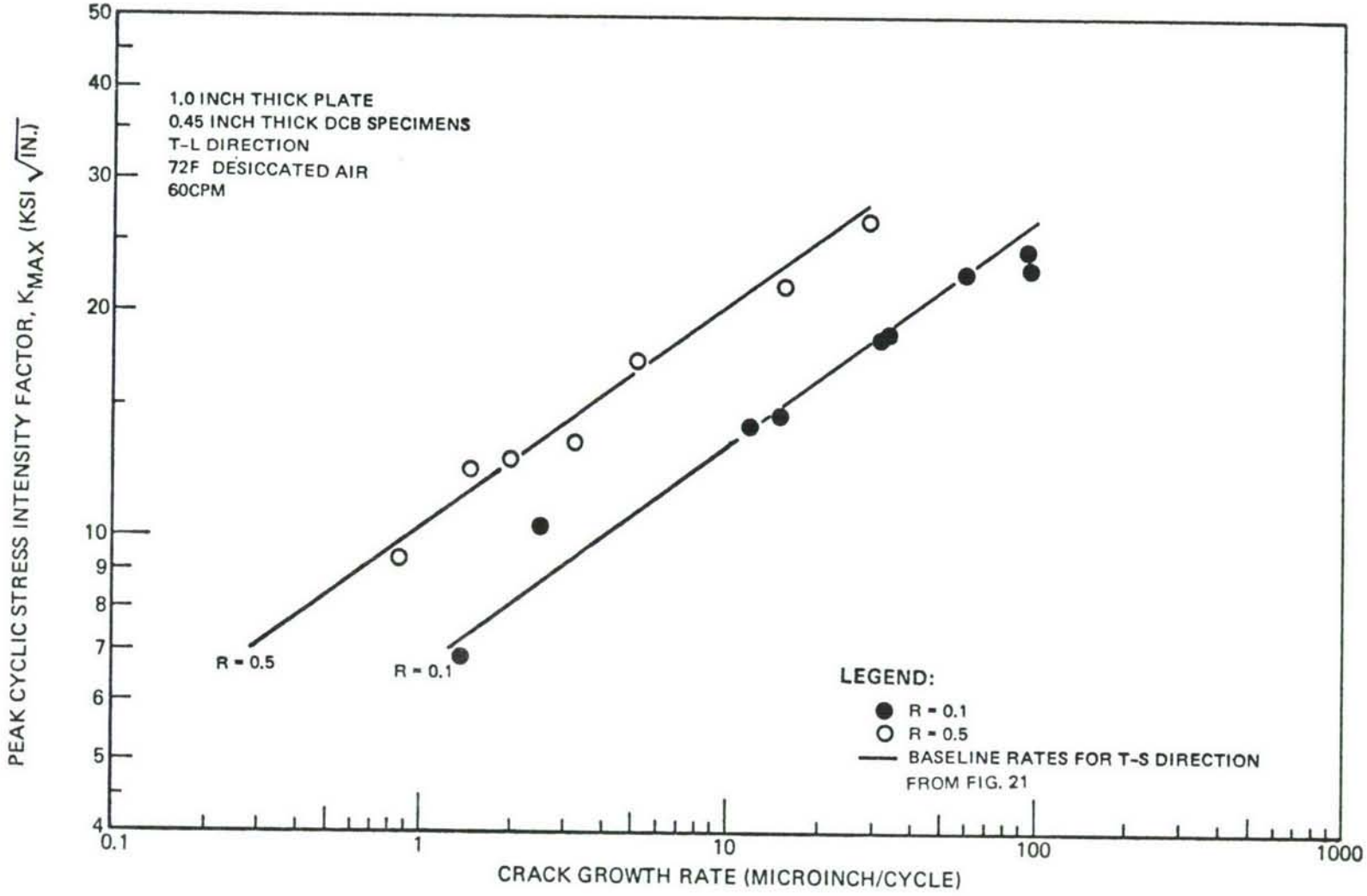


Figure 24: *Stress Intensity Factor Vs. Crack Growth Rate–Load Controlled Cyclic Tests of 2219-T851 Aluminum Alloy DCB Specimens*

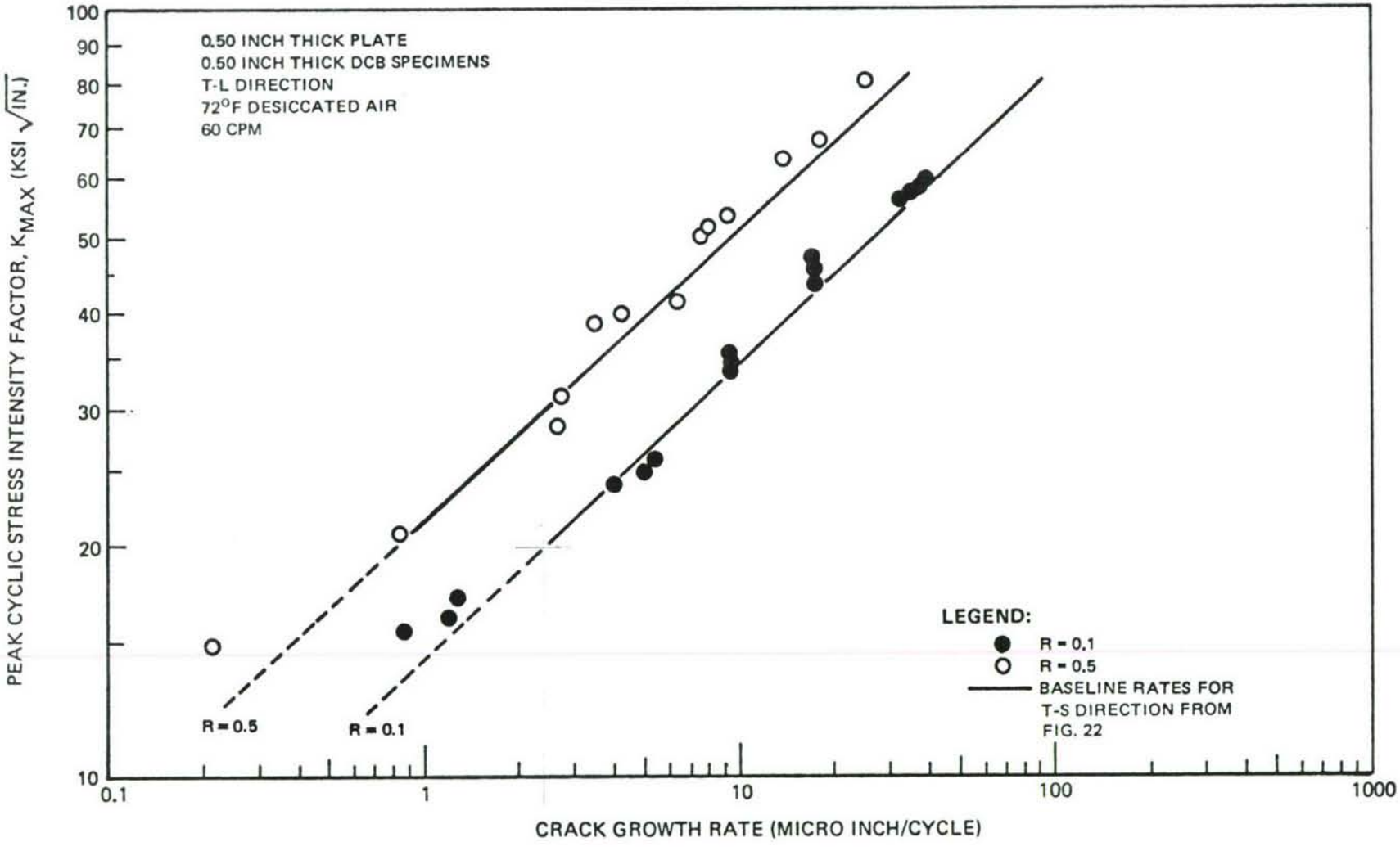


Figure 25: Stress Intensity Factor Vs. Crack Growth Rate—Load Controlled Cyclic Tests of 9Ni-4Co-0.2C Steel Alloy DCB Specimens

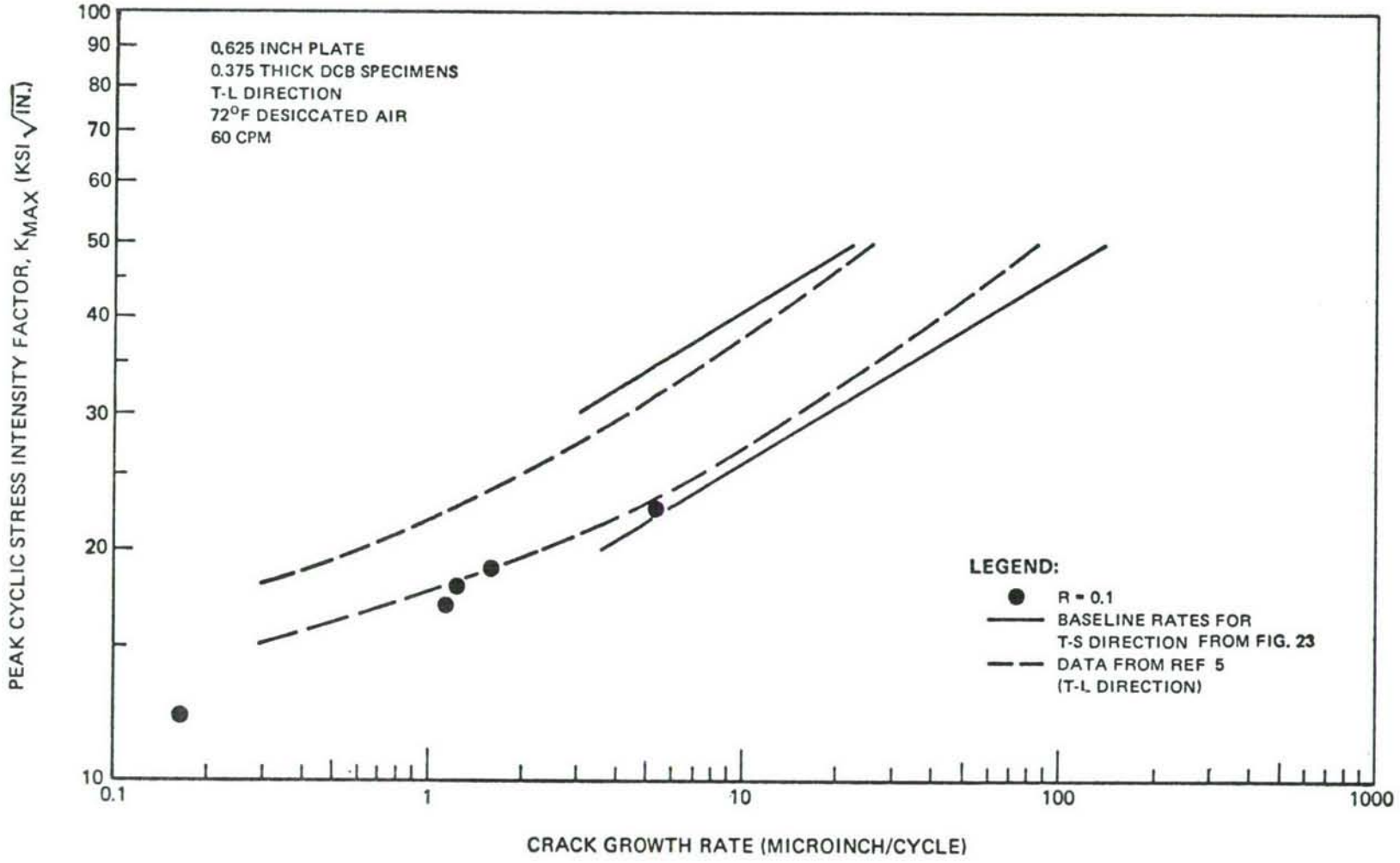


Figure 26: Stress Intensity Factor Vs. Crack Growth Rate—Load Controlled Cyclic Tests of 6Al-4V (Beta Annealed) Titanium Alloy DCB Specimens

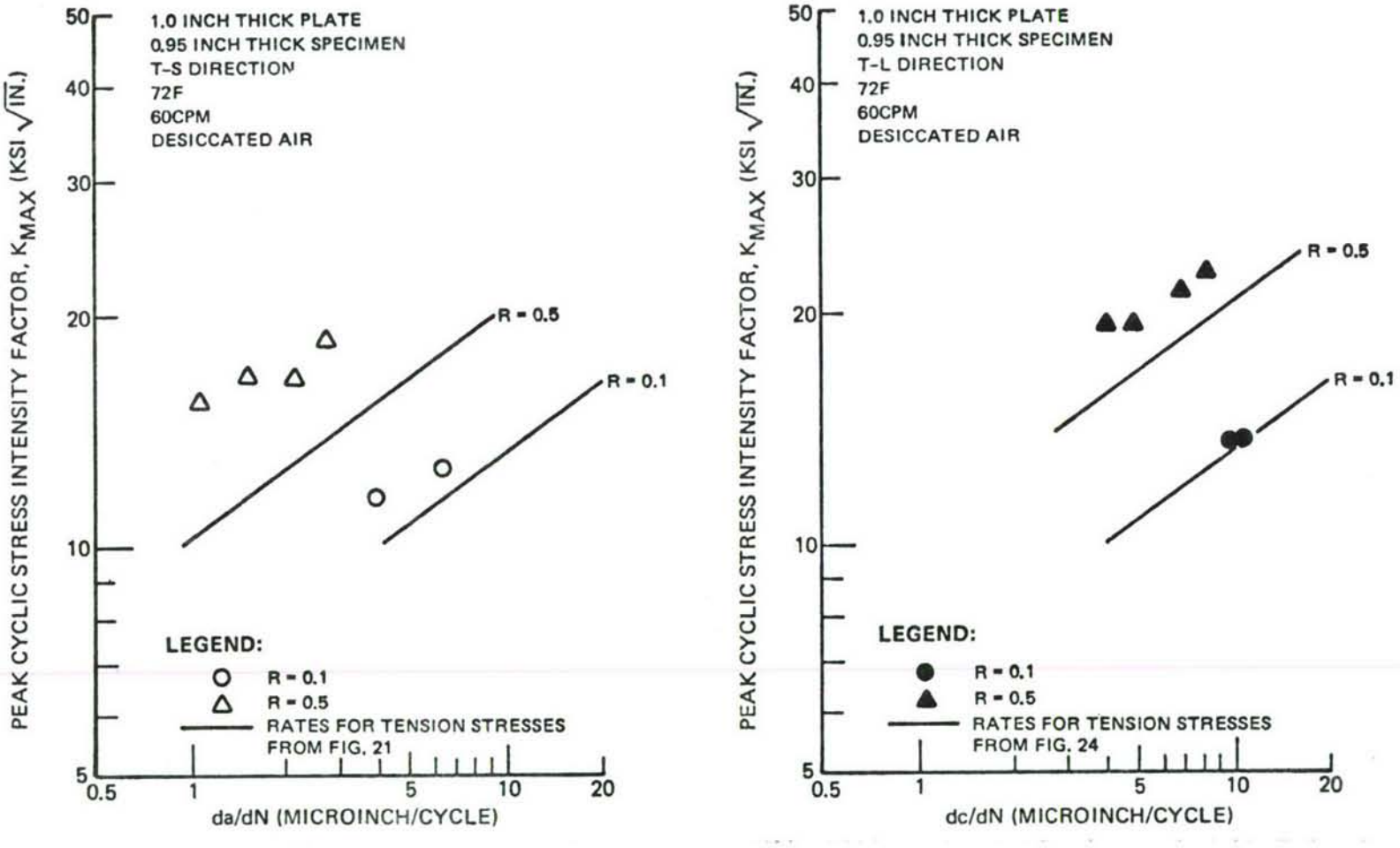


Figure 27: Stress Intensity Factor Vs. Crack Growth Rate—Pure Bending Cyclic Tests of 2219-T851 Aluminum Alloy Surface-Flawed Specimens

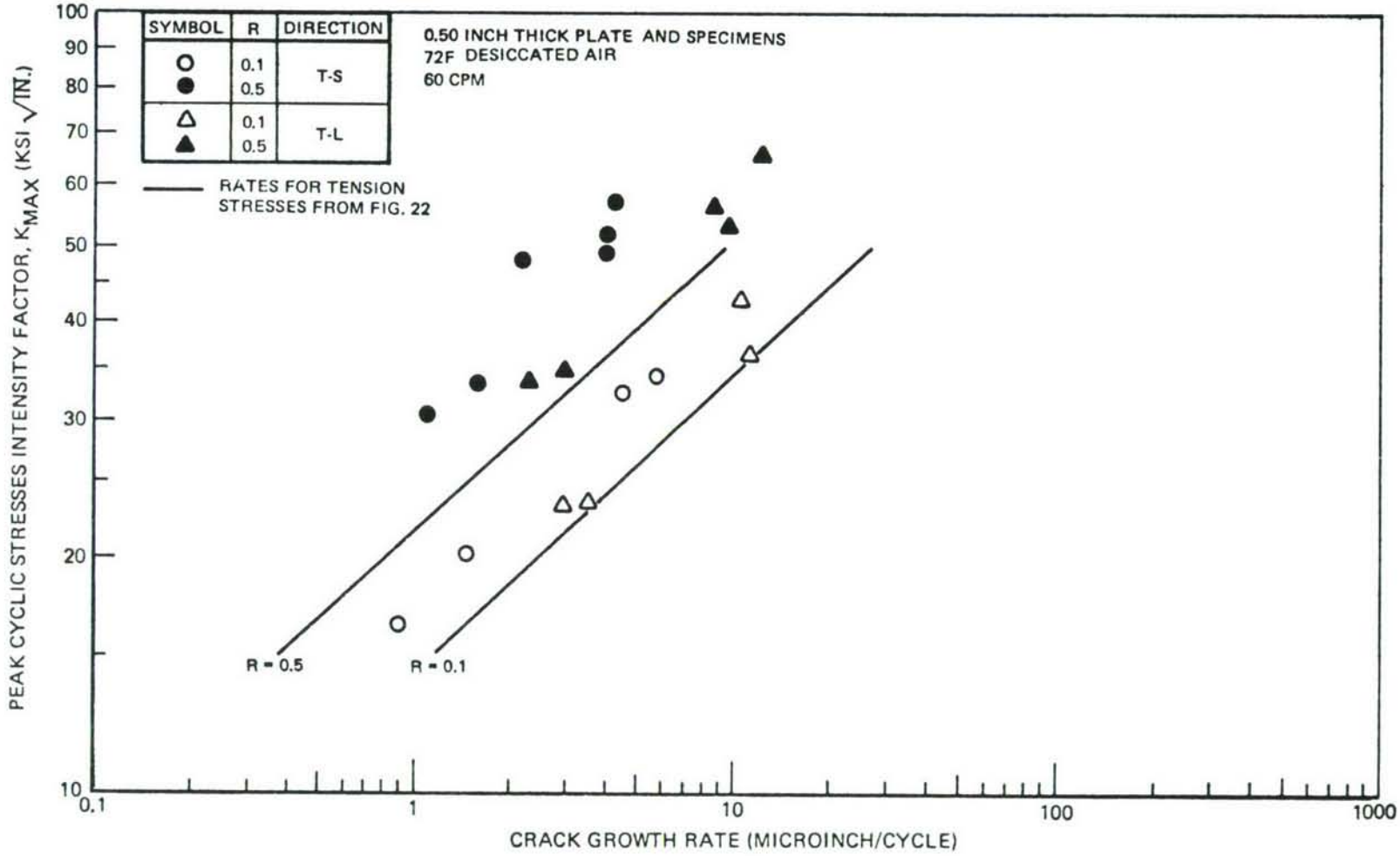


Figure 28: Stress Intensity Factor Vs. Crack Growth Rate–Pure Bending Cyclic Tests of 9Ni-4Co-0.2C Steel Alloy Surface Flawed Specimens

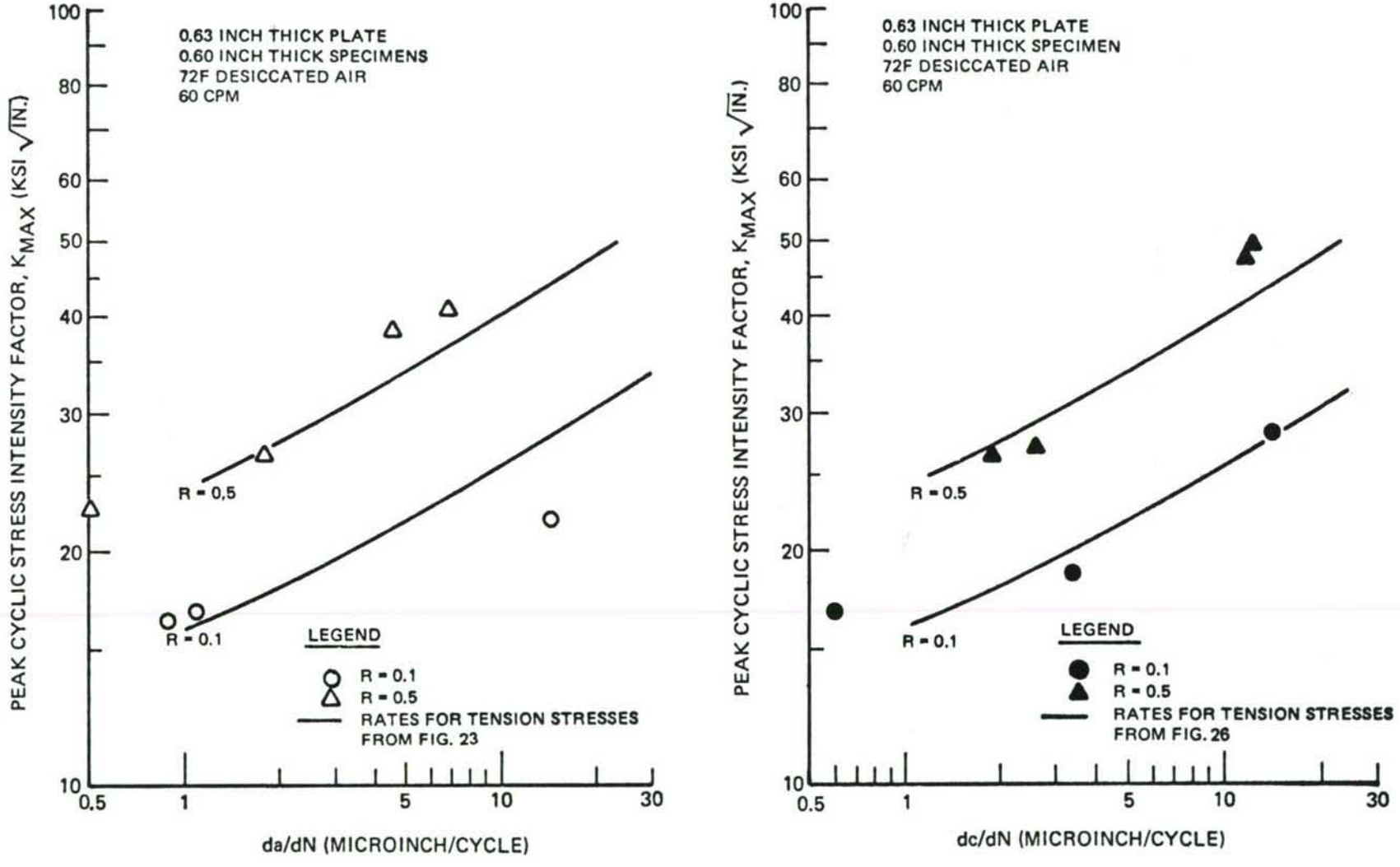


Figure 29: Stress Intensity Factor Vs. Crack Growth Rate–Pure Bending Cyclic Tests of 6Al-4V (β-Annealed) Titanium Alloy Surface Flawed Specimens

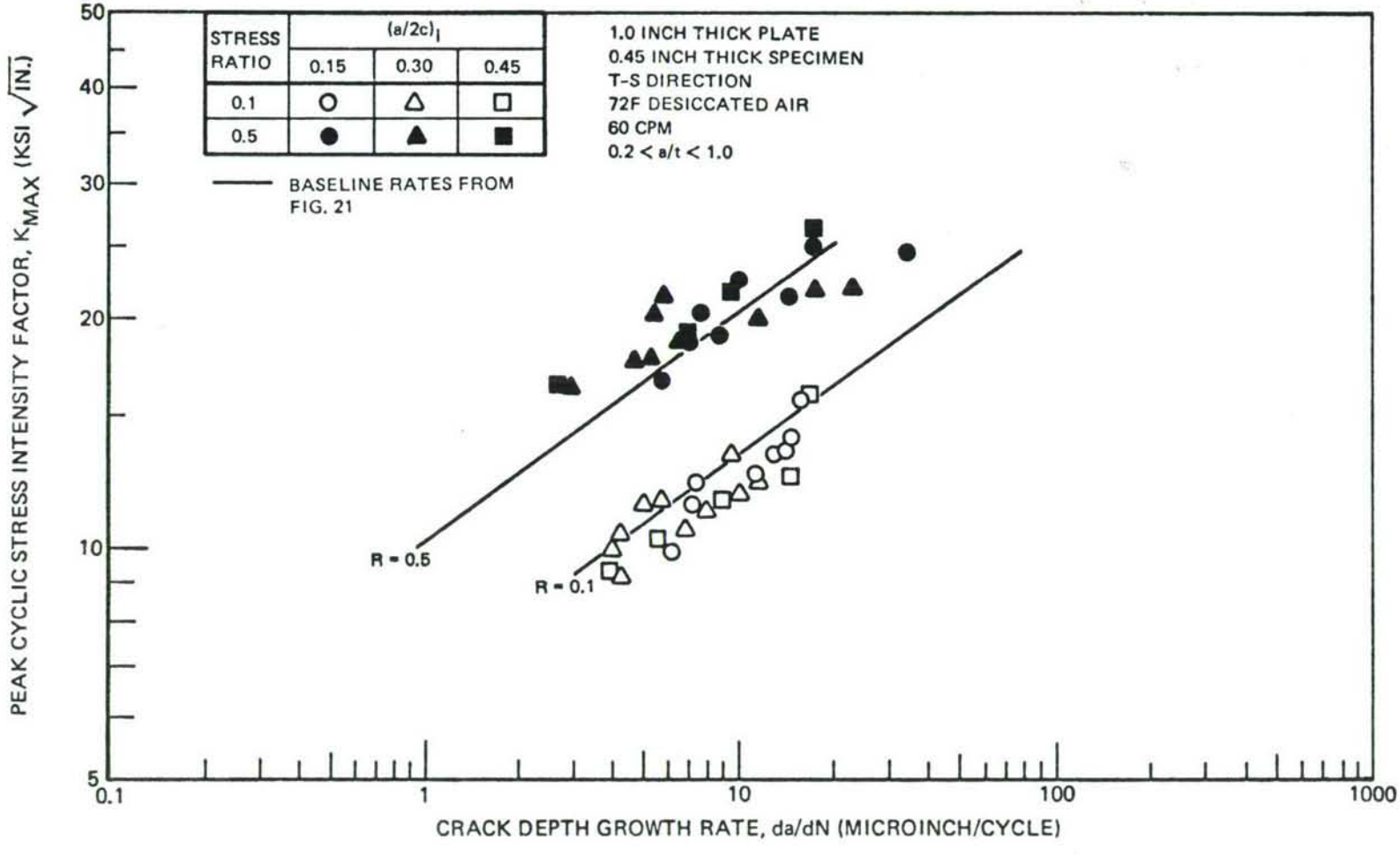


Figure 30: Stress Intensity Factor Vs. Crack Depth Growth Rate—Uniform Load Tension Tests of Surface Flawed 2219-T851 Aluminum Alloy Plate

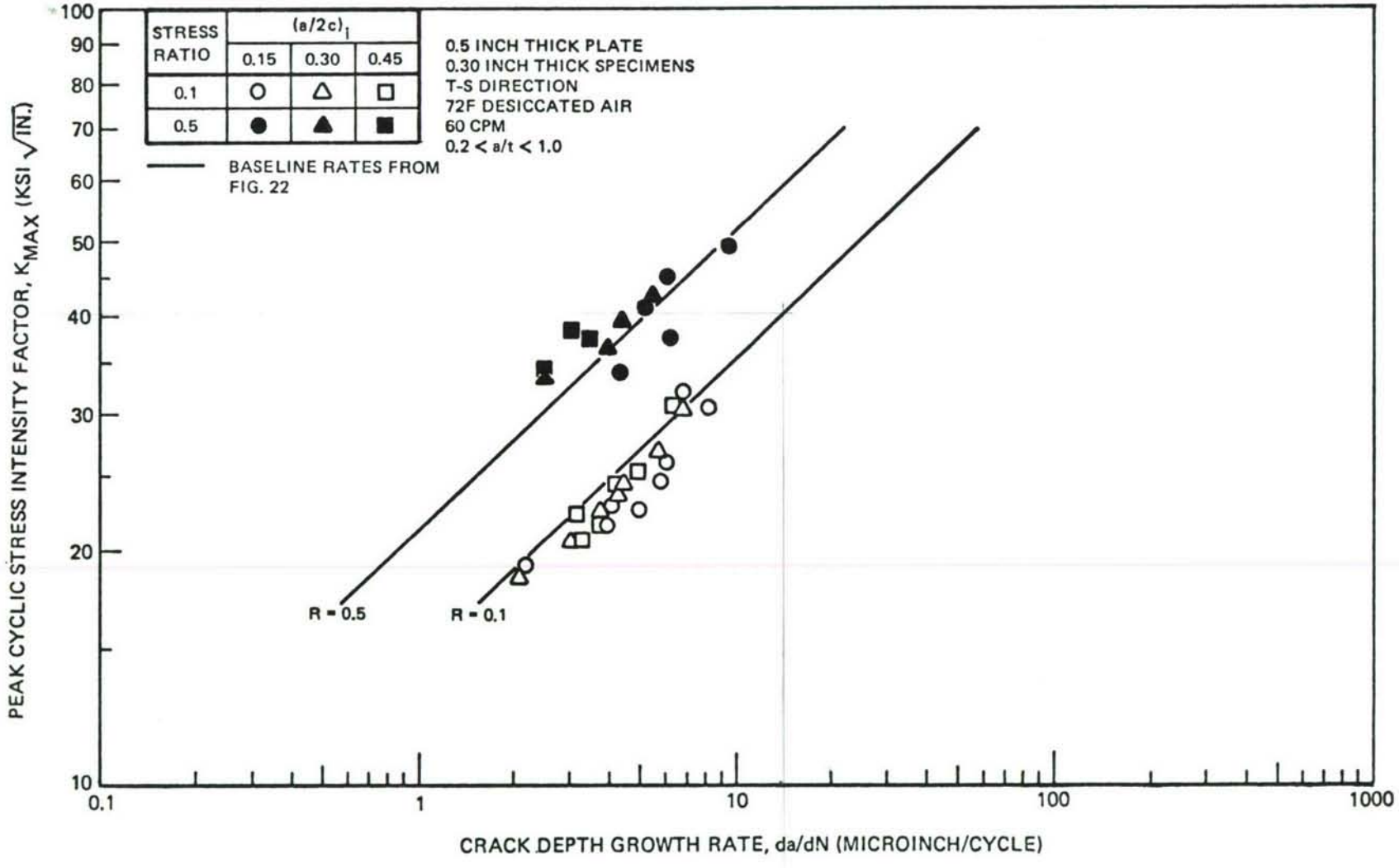


Figure 31: Stress Intensity Factor Vs. Crack Depth Growth Rate–Uniform Load Tension Tests of Surface Flawed 9Ni-4Co-0.2C Steel Alloy Plate

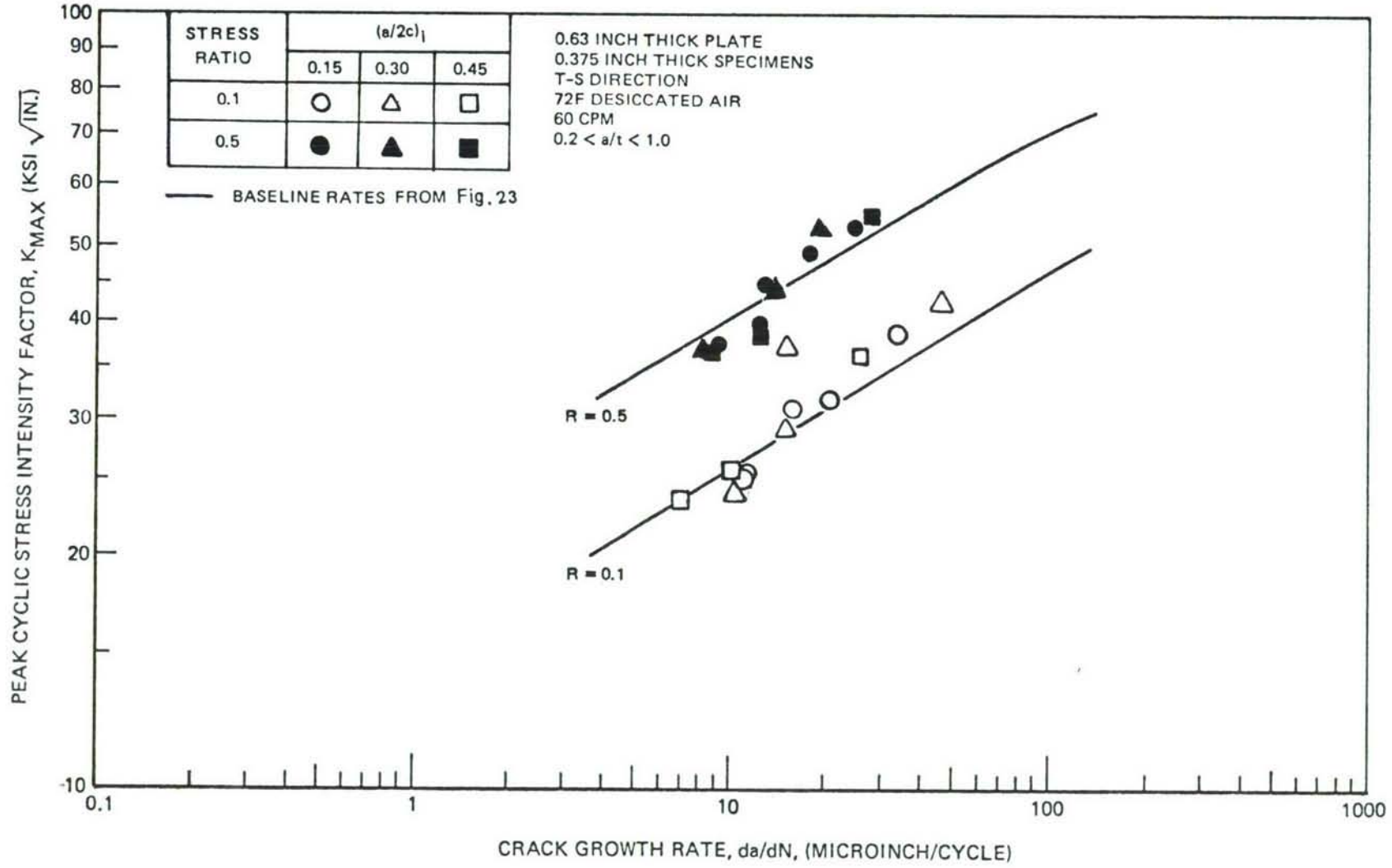


Figure 32: Stress Intensity Factor Vs. Crack Depth Growth Rate–Uniform Load Tension Tests of Surface Flawed 6Al-4V (β-Annealed) Titanium Alloy Plate

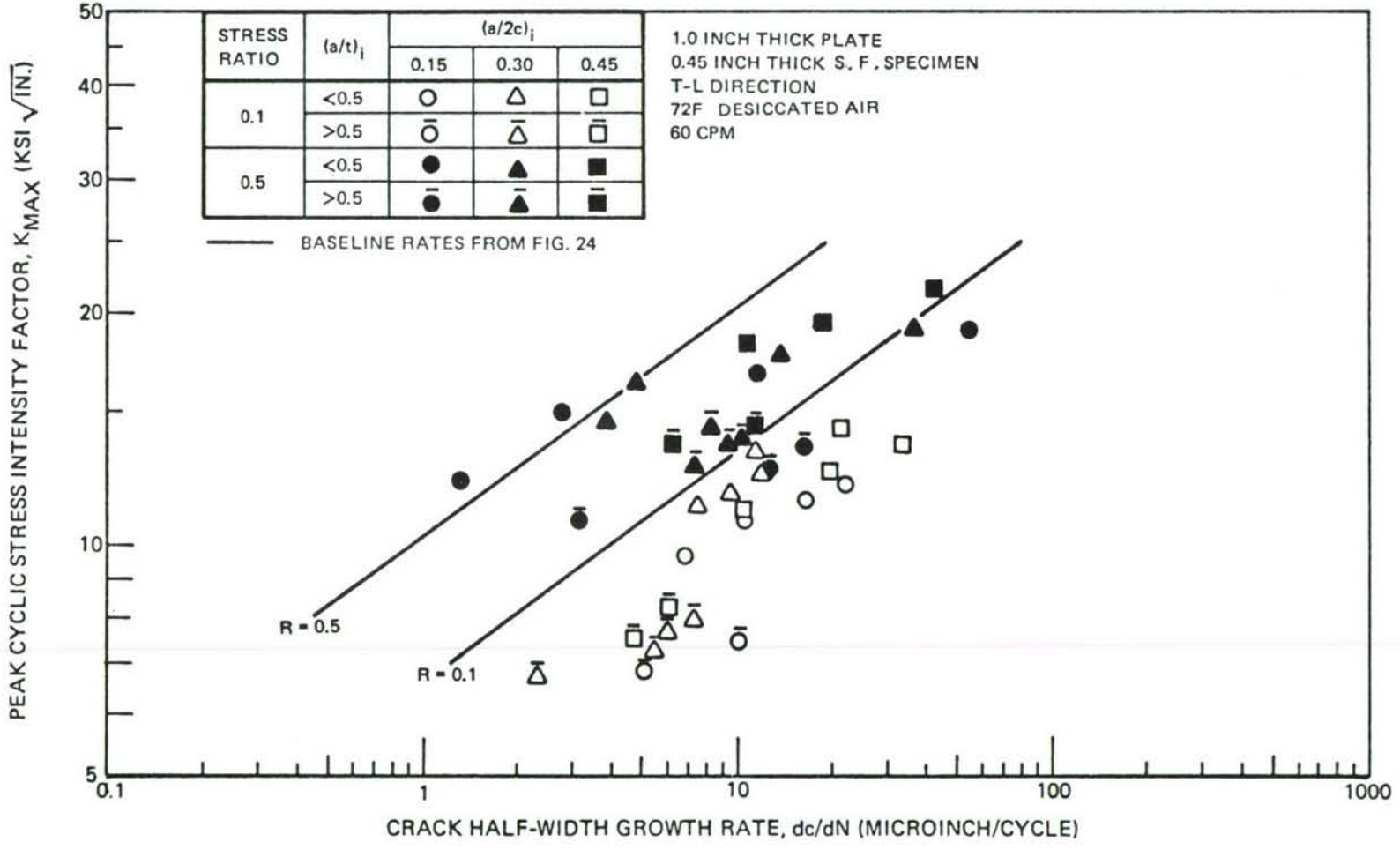


Figure 33: Stress Intensity Factor Vs. Crack Half-Width Growth Rate–Uniform Load Tension Tests of Surface Flawed 2219-T851 Aluminum Alloy Plate

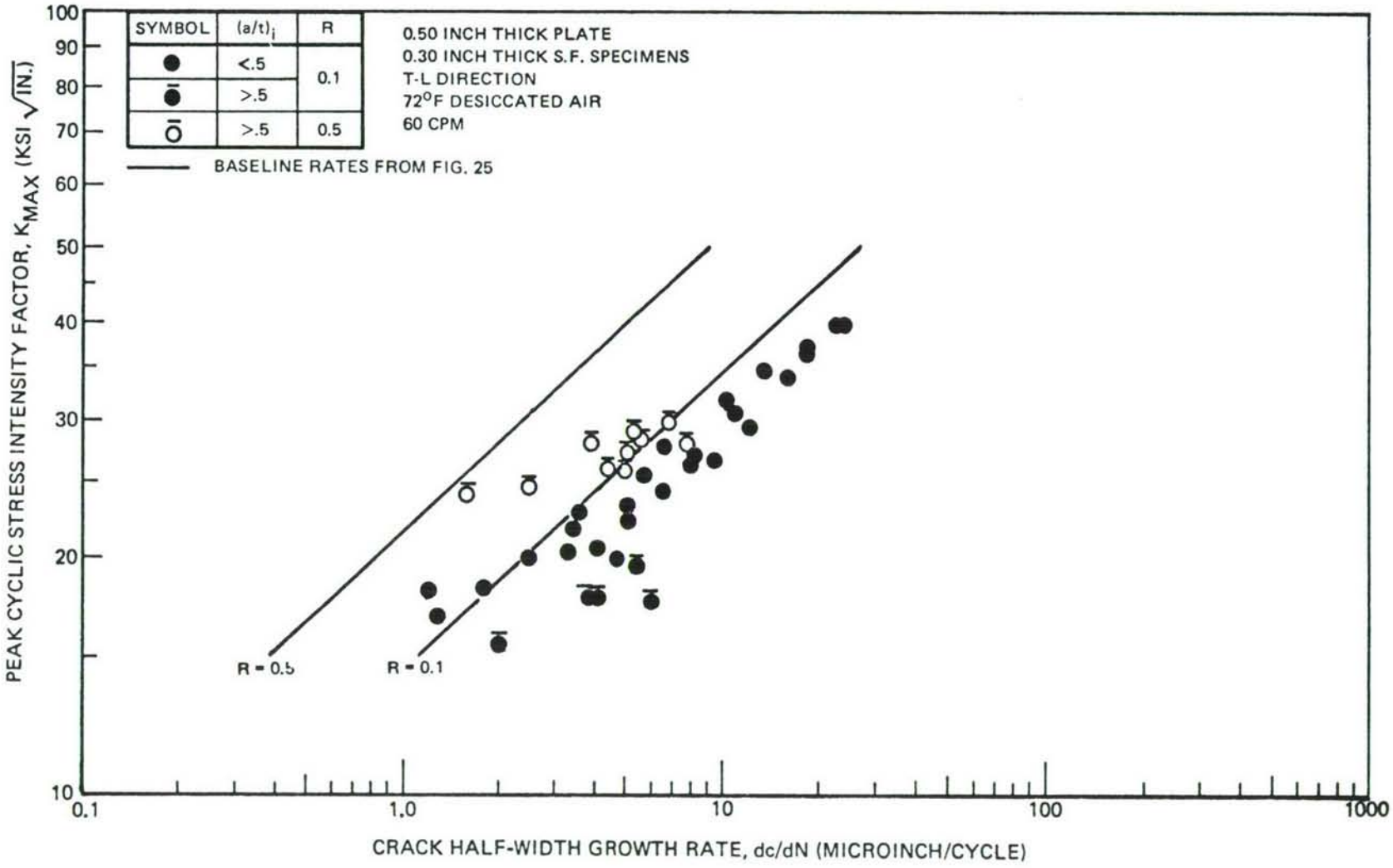


Figure 34: Stress Intensity Factor Vs. Crack Half-Width Growth Rate–Uniform Load Tension Tests of Surface Flawed 9Ni-4Co-0.2C Steel Alloy Plate

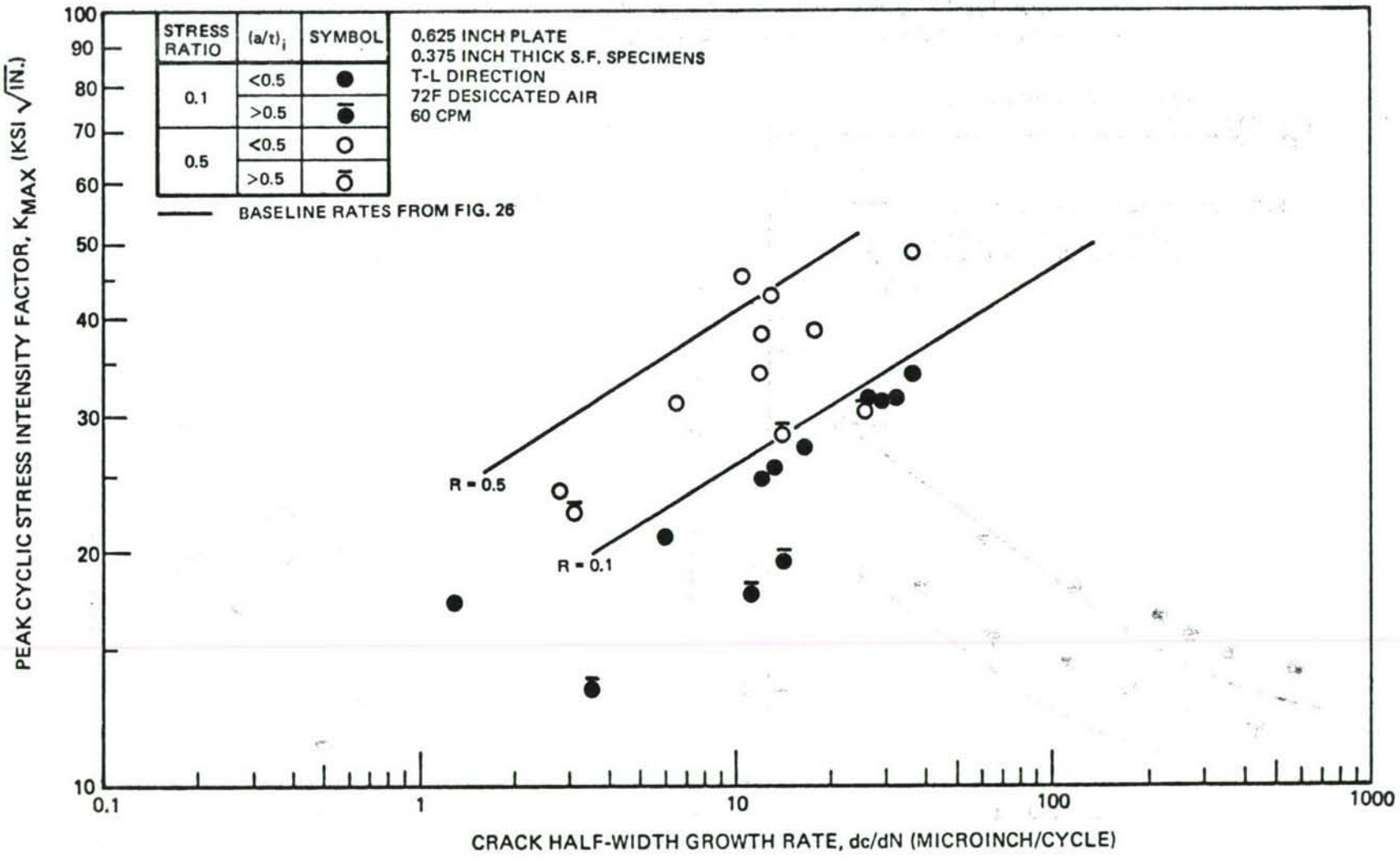


Figure 35: Stress Intensity Factor Vs. Crack Half-Width Growth Rate–Uniform Load Tension Tests of Surface Flawed Ti-6Al-4V (Beta Annealed) Plate

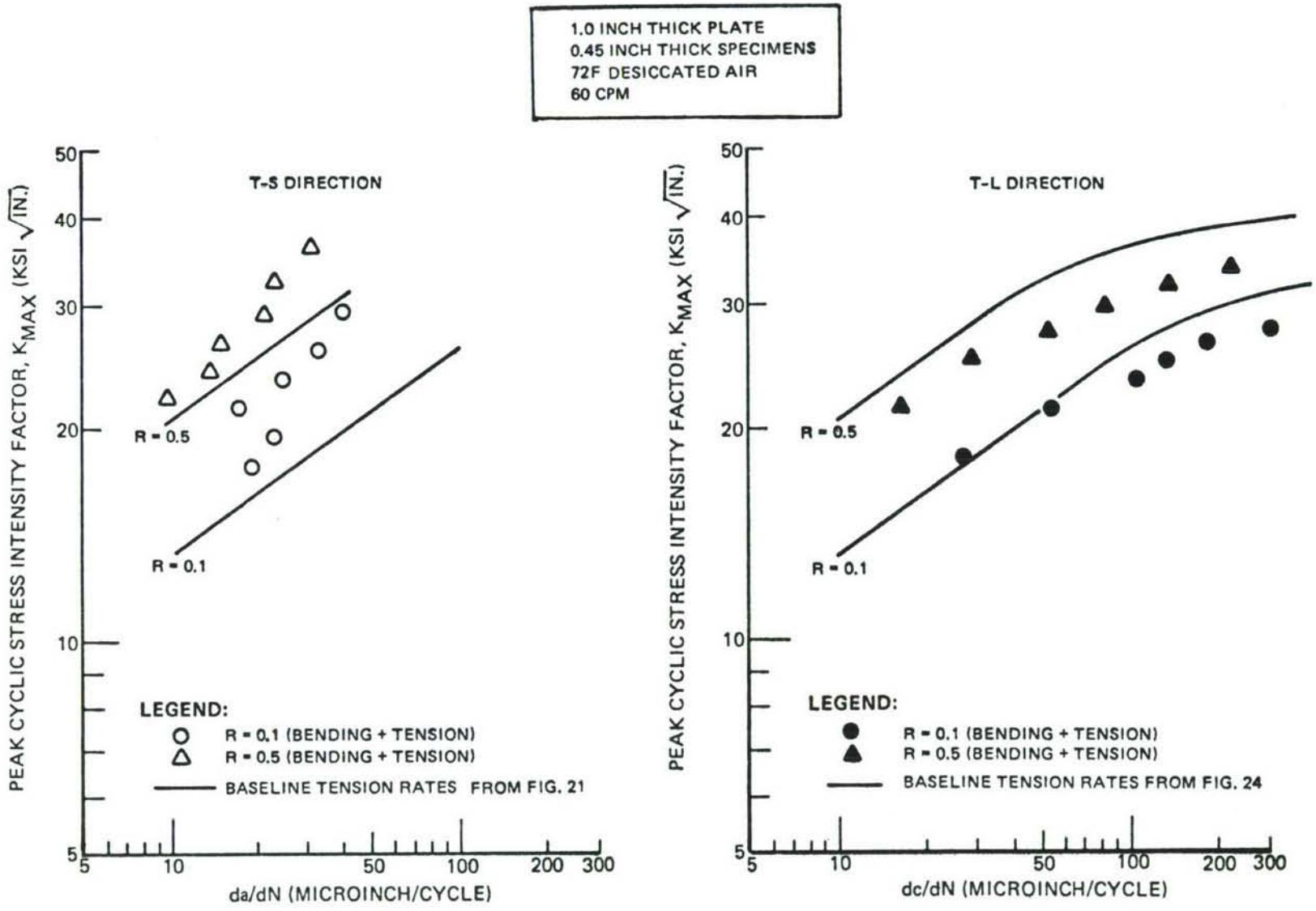


Figure 36: Stress Intensity Factor Vs. Crack Growth Rate - Combined Bending and Tension Tests of 2219-T851 Aluminum Alloy Surface Flawed Plate

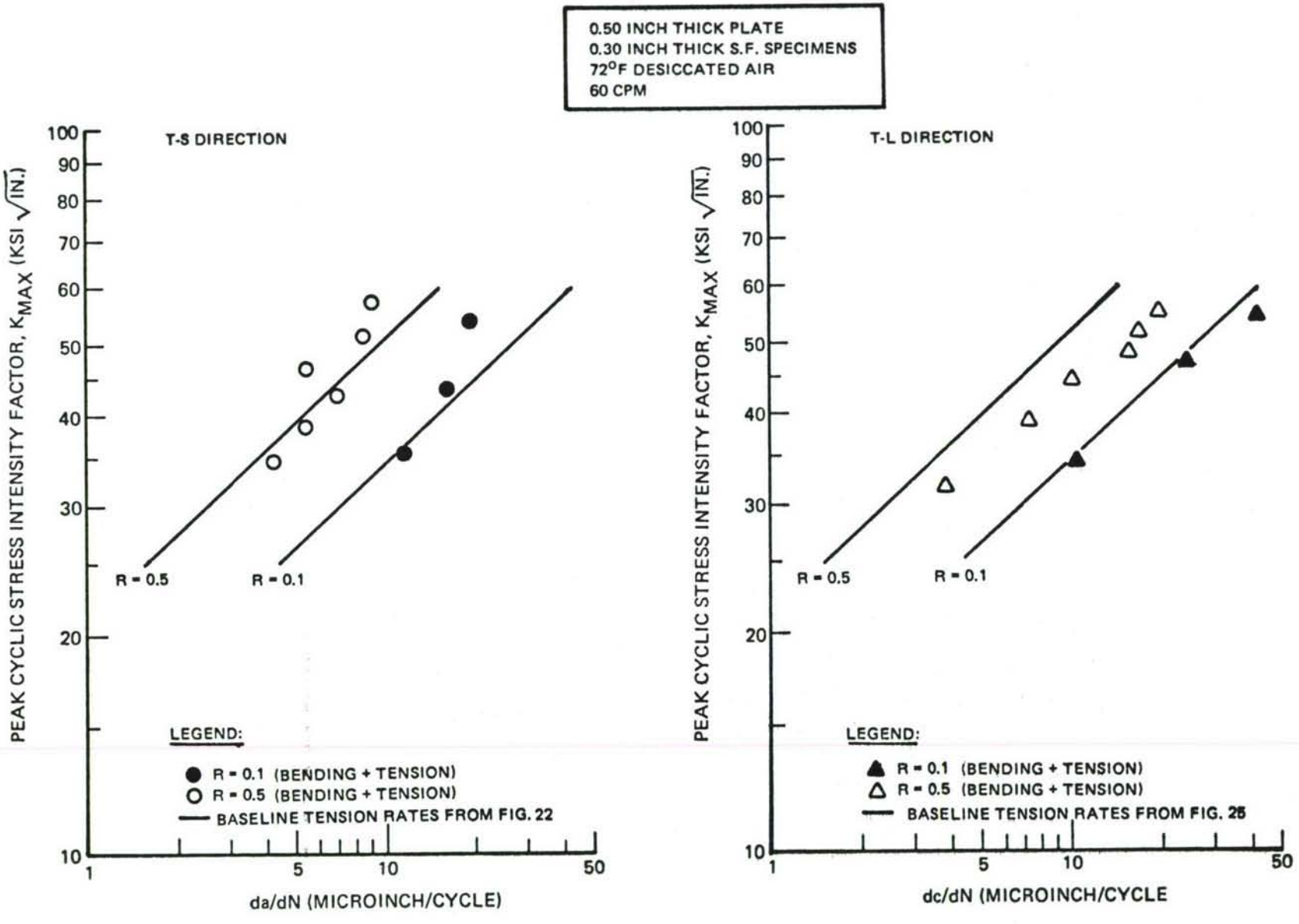


Figure 37: Stress Intensity Factor Vs. Crack Growth Rate—Combined Bending and Tension Tests of 9 Ni-4 Co-0.2C Steel Alloy Surface Flawed Plate

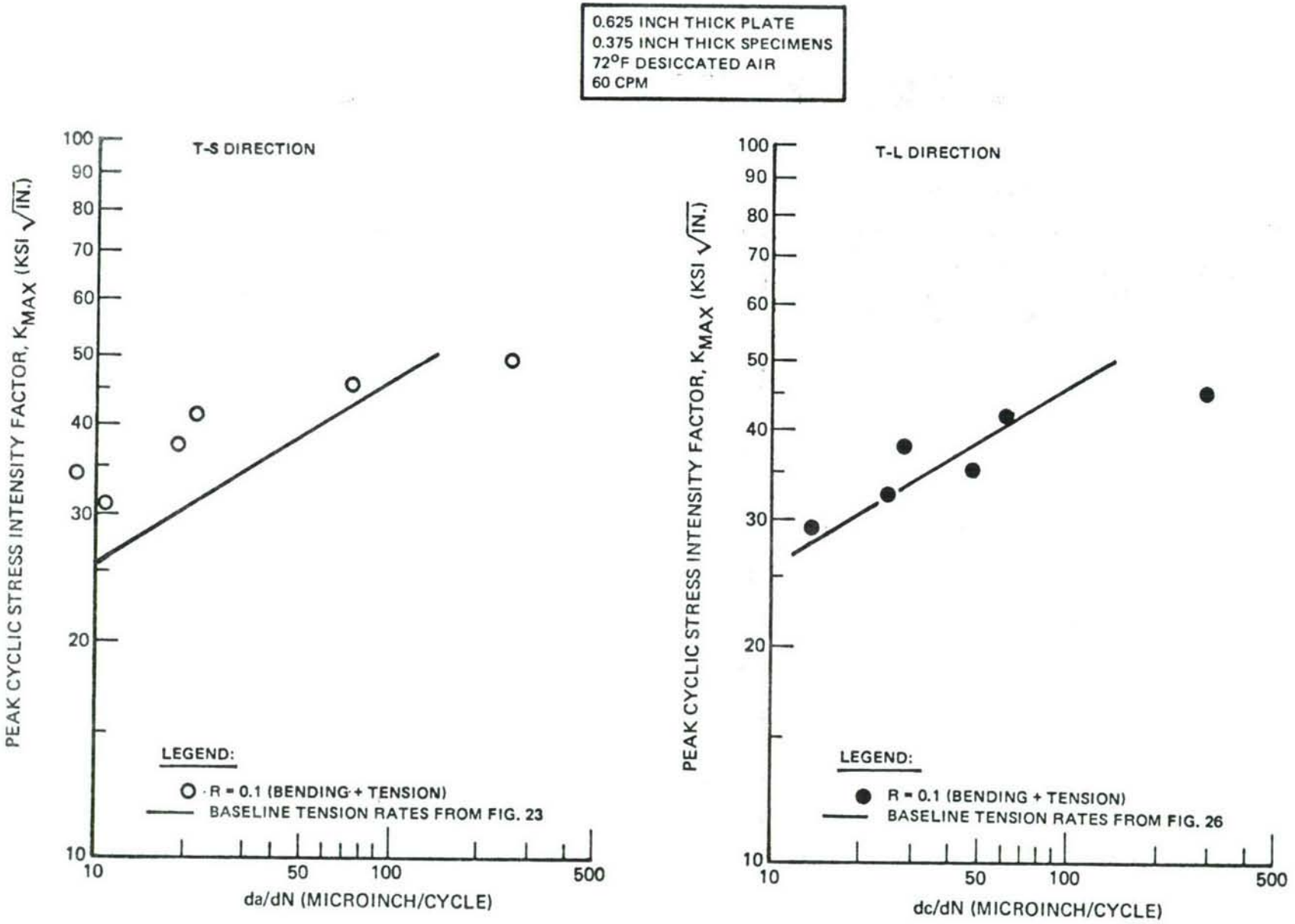


Figure 38: Stress Intensity Factor Vs. Crack Growth Rate—Combined Bending and Tension Tests of 6Al-4V (β-Annealed) Titanium Alloy Surface Flawed Plate

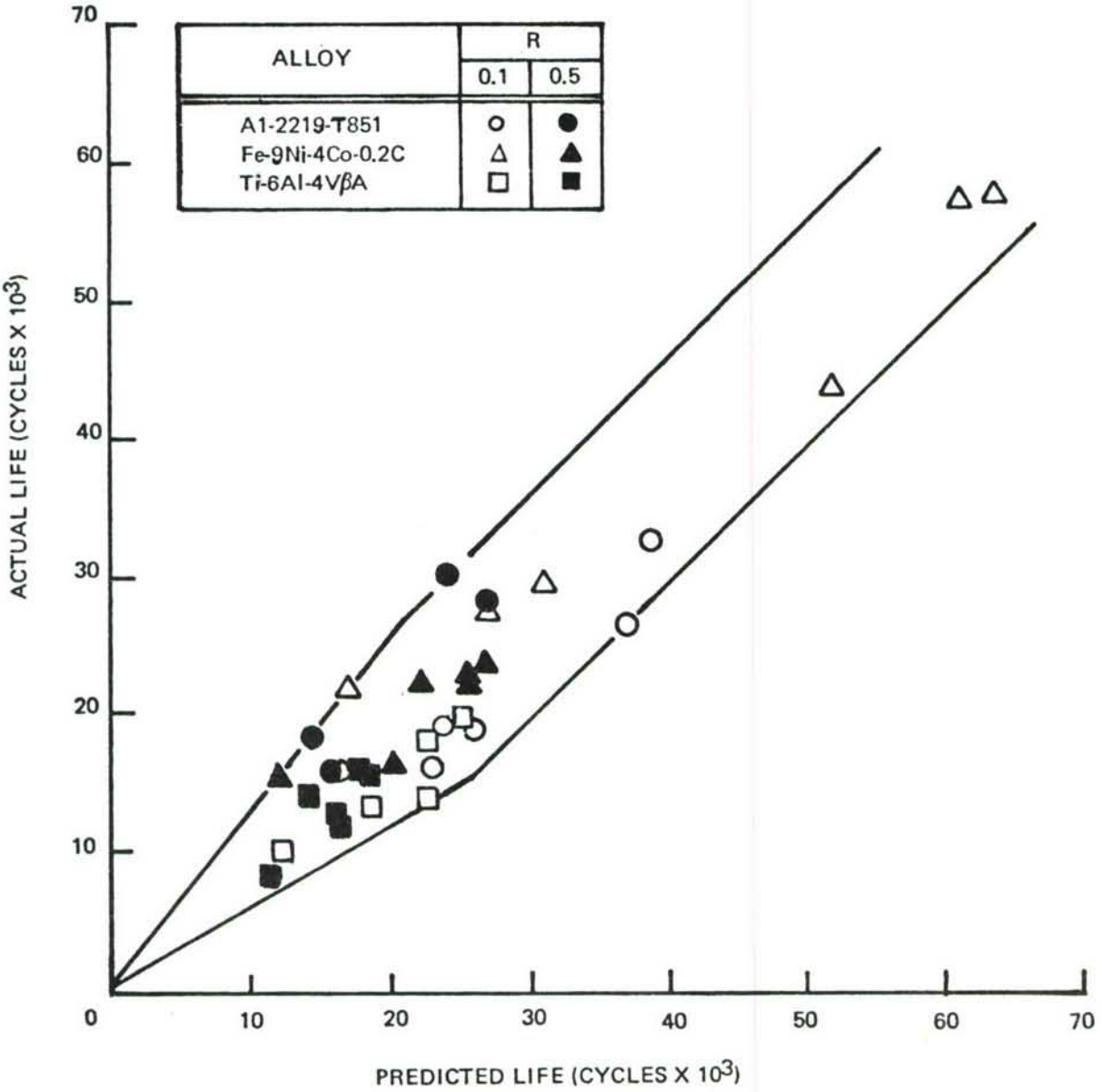


Figure 39: Comparison of Actual and Predicted Lives for Uniform Tension Loaded Surface Flaw Specimens

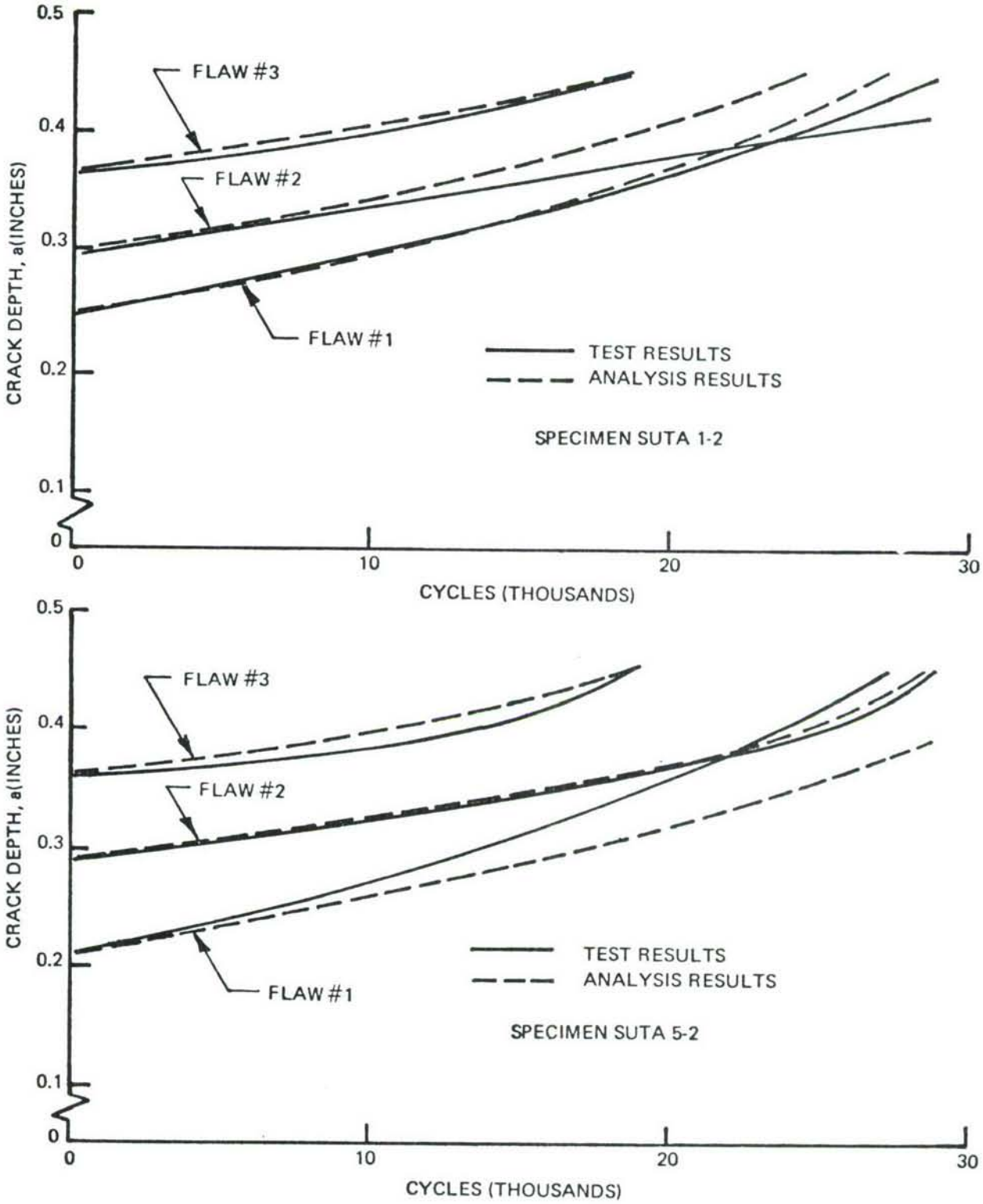
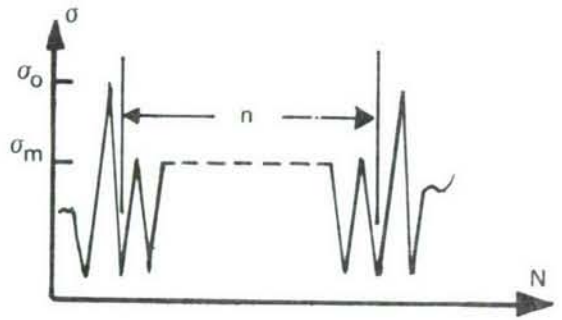


Figure 40: *Crack Depth Growth Vs. Cycles For 2219 – T851 Aluminum Alloy Constant Load Deep Flaw Specimens*

SPECIMEN SPOTA–2

σ_o = 36 KSI
σ_m = 18 KSI
n = 13,000 ~
R = 0.1
f = 60 CPM
DESICCATED AIR



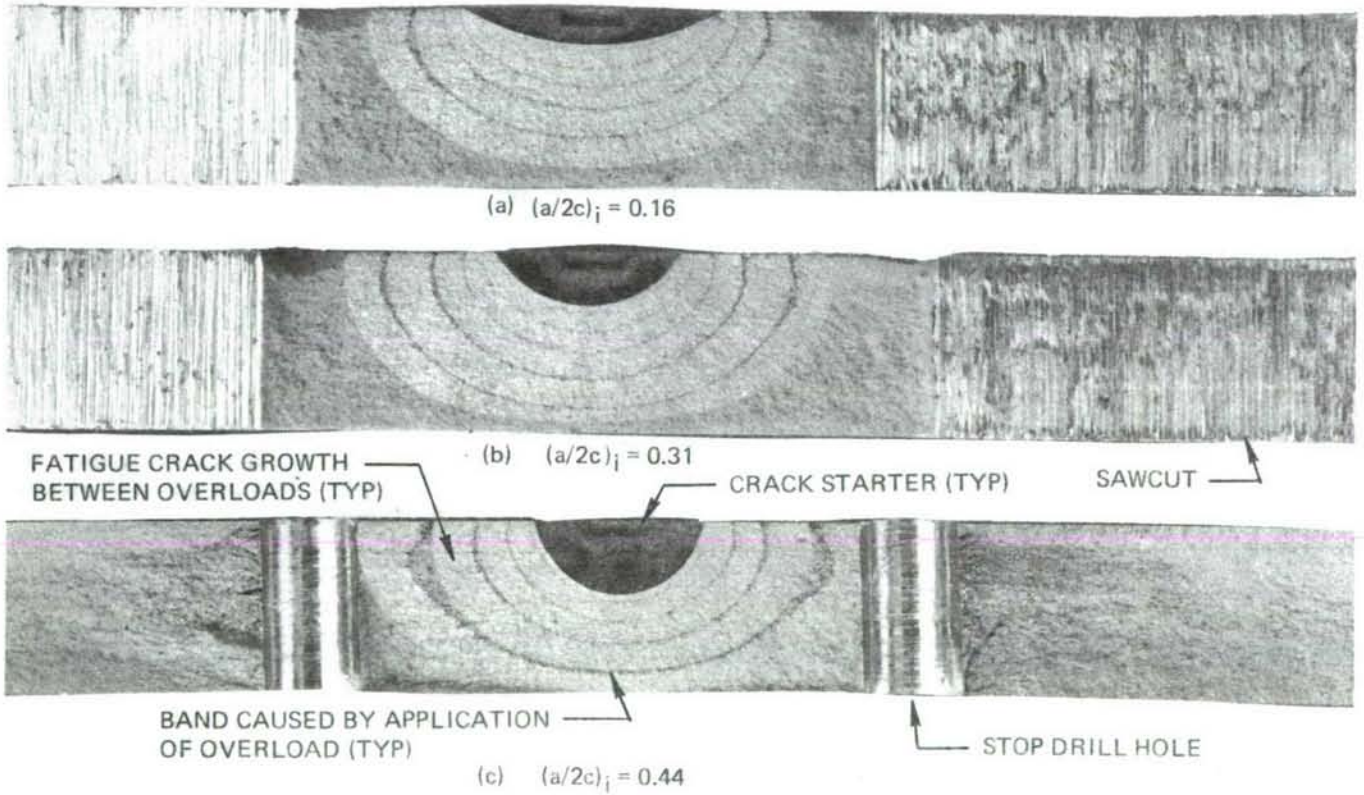


Figure 41. Typical Fracture Surfaces For 2219-T851 Aluminum Alloy Periodic Overload Surface Flaw Specimens

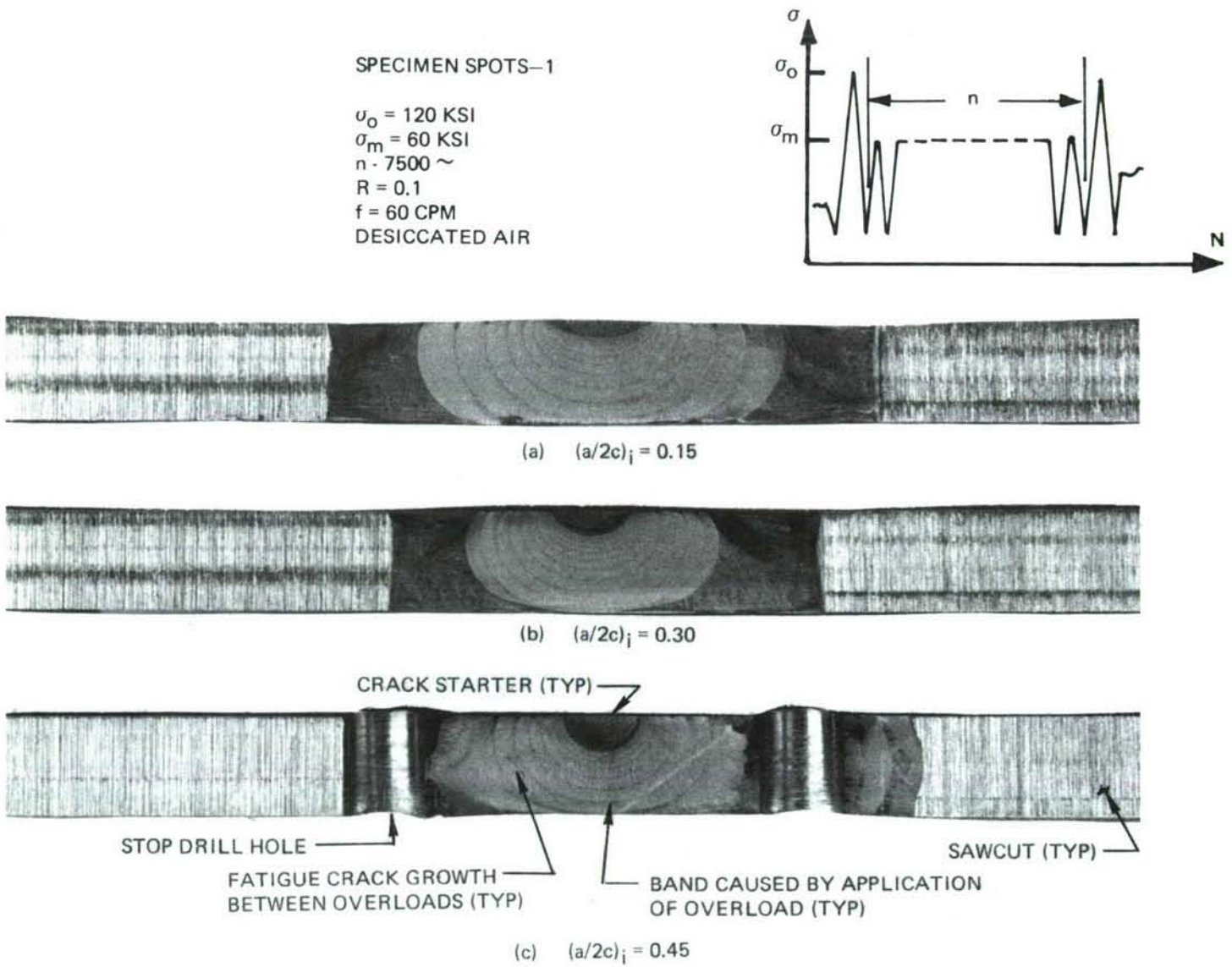
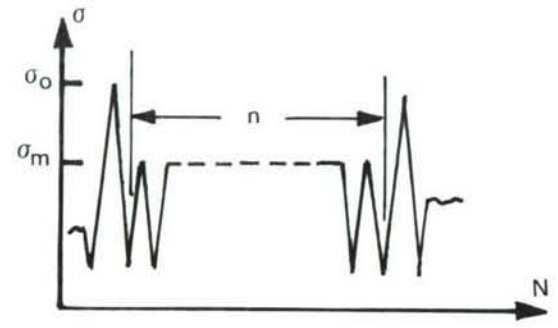


Figure 42: Typical Fracture Surfaces For $9N_j - 4C_o - 0.2C$ Steel Alloy Periodic Overload Surface Flaw Specimens

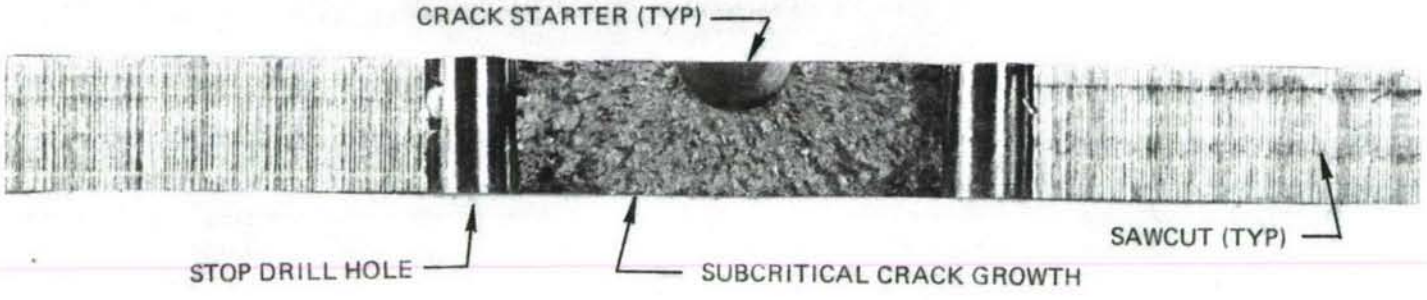
SPECIMEN SPOTT–3

σ_o = 67.5 KSI
σ_m = 45 KSI
n = 5000 ~
R = 0.1
f = 60 CPM
DESICCATED AIR





(a) $(a/2c)_i$ = 0.16



(b) $(a/2c)_i$ = 0.45

Figure 43: Typical Fracture Surfaces For 6A1–4V (Beta–Annealed) Titanium Alloy Periodic Overload Surface Flaw Specimens

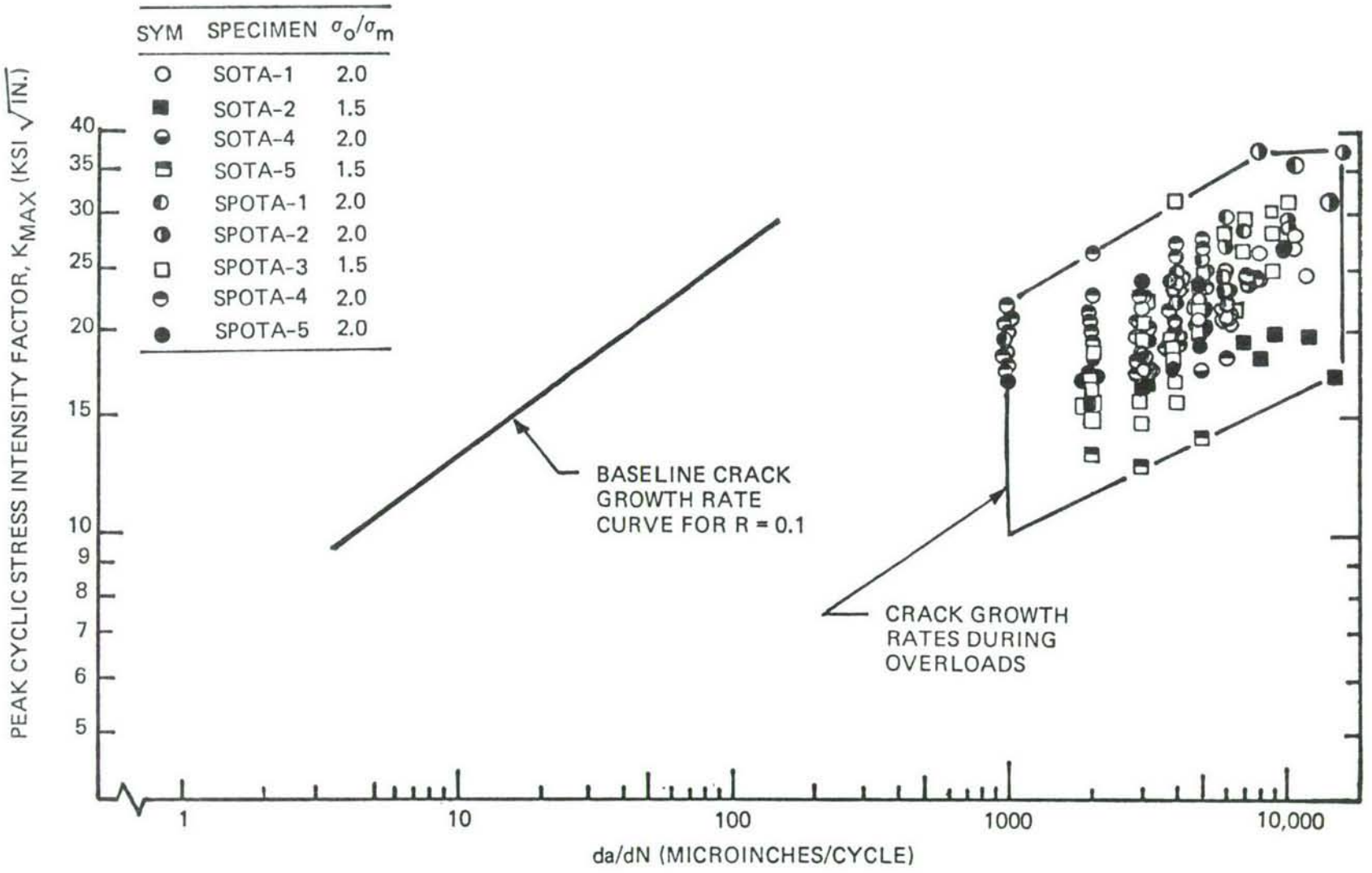


Figure 44: Comparison Between Crack Growth Rates During Overloads and Baseline Crack Growth Rates for Overloaded Aluminum Alloy Surface Flaw Specimens (Based on K_{MAX})

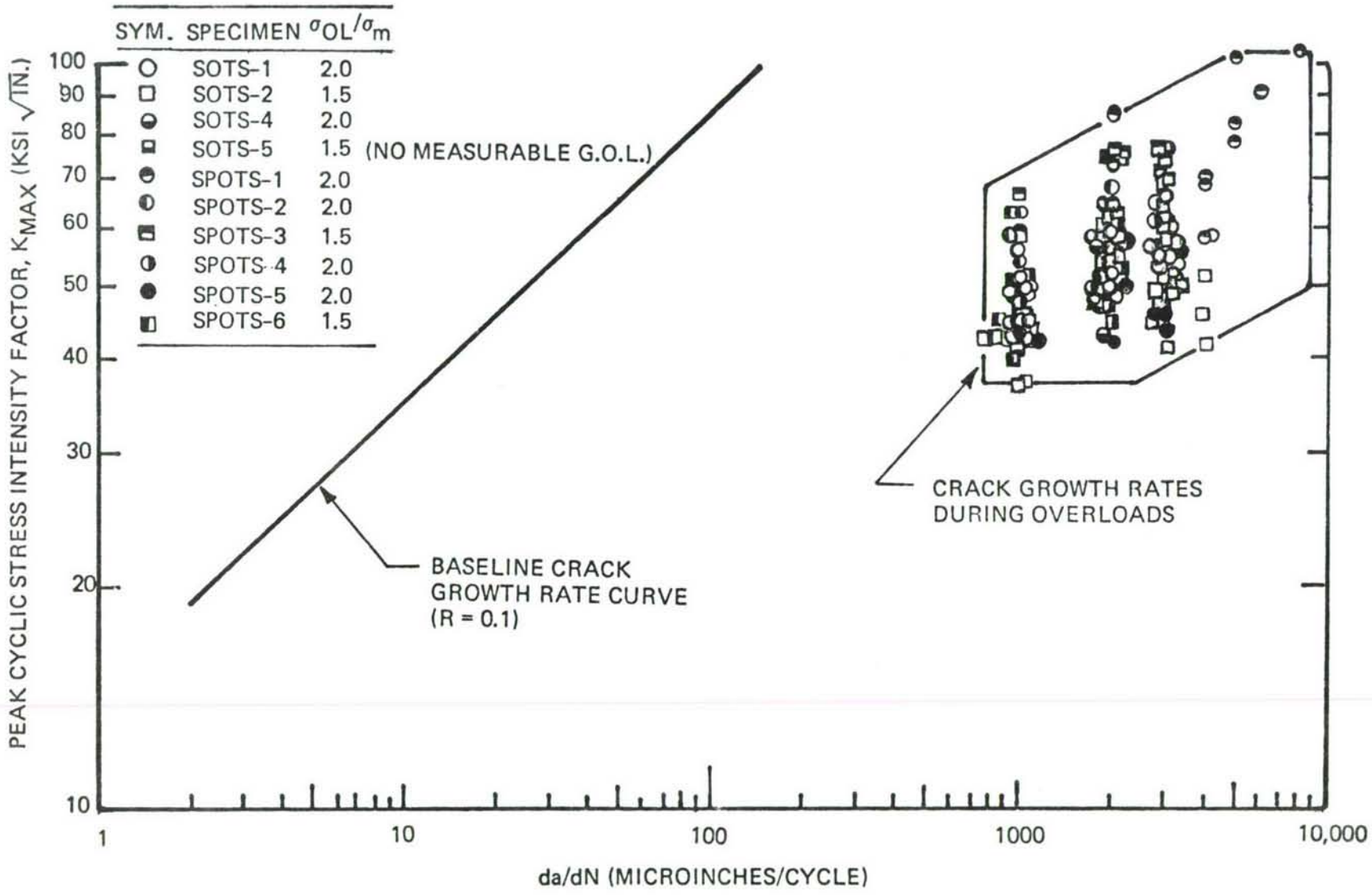


Figure 45: Comparison Between Crack Growth Rates During Overloads and Baseline Crack Growth Rates for Overloaded Steel Alloy Surface Flaw Specimens (Based on K_{MAX})

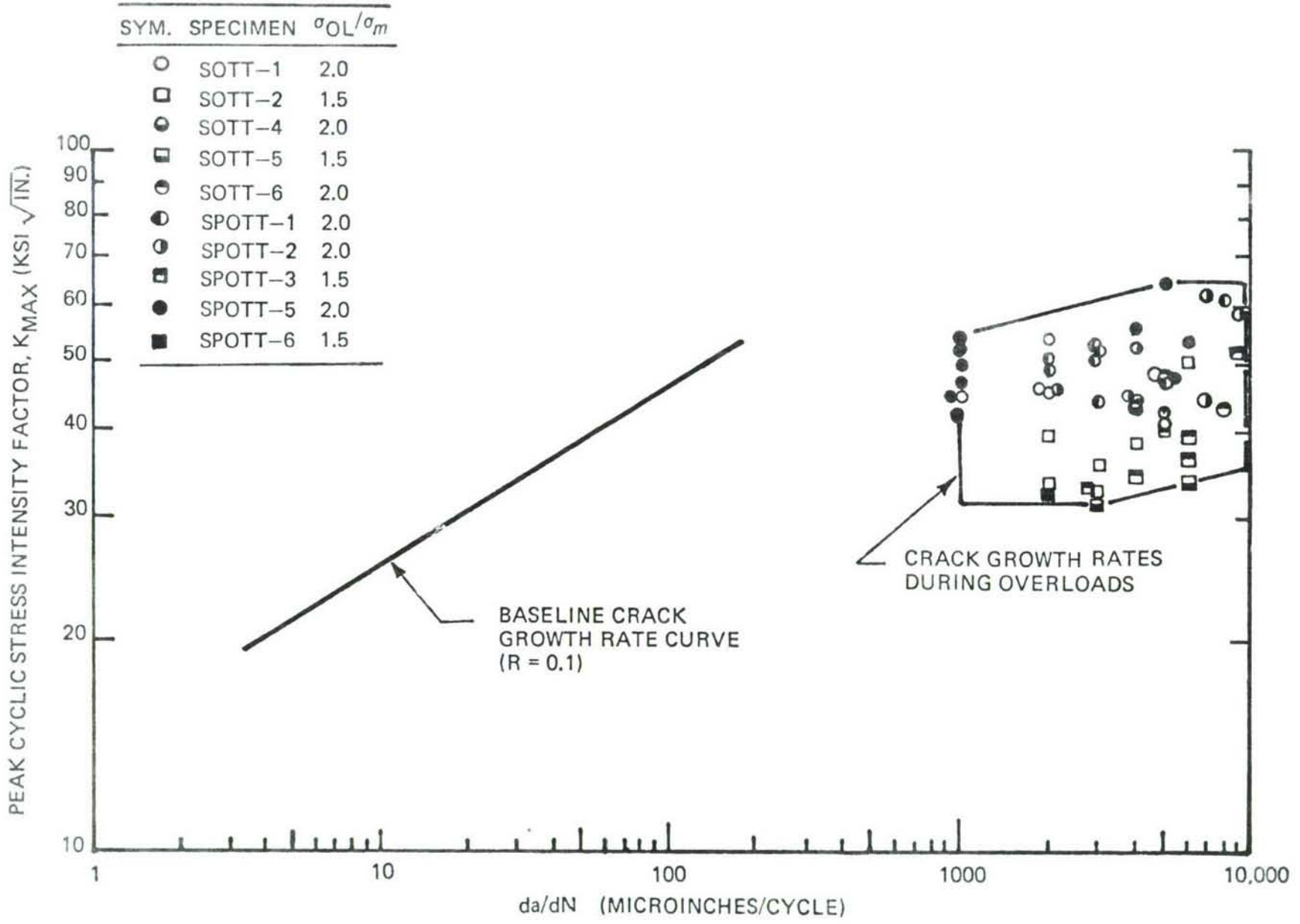


Figure 46: Comparison Between Crack Growth Rates During Overloads and Baseline Crack Growth Rates for Overloaded Titanium Alloy Surface Flaw Specimens (Based on K_{MAX})

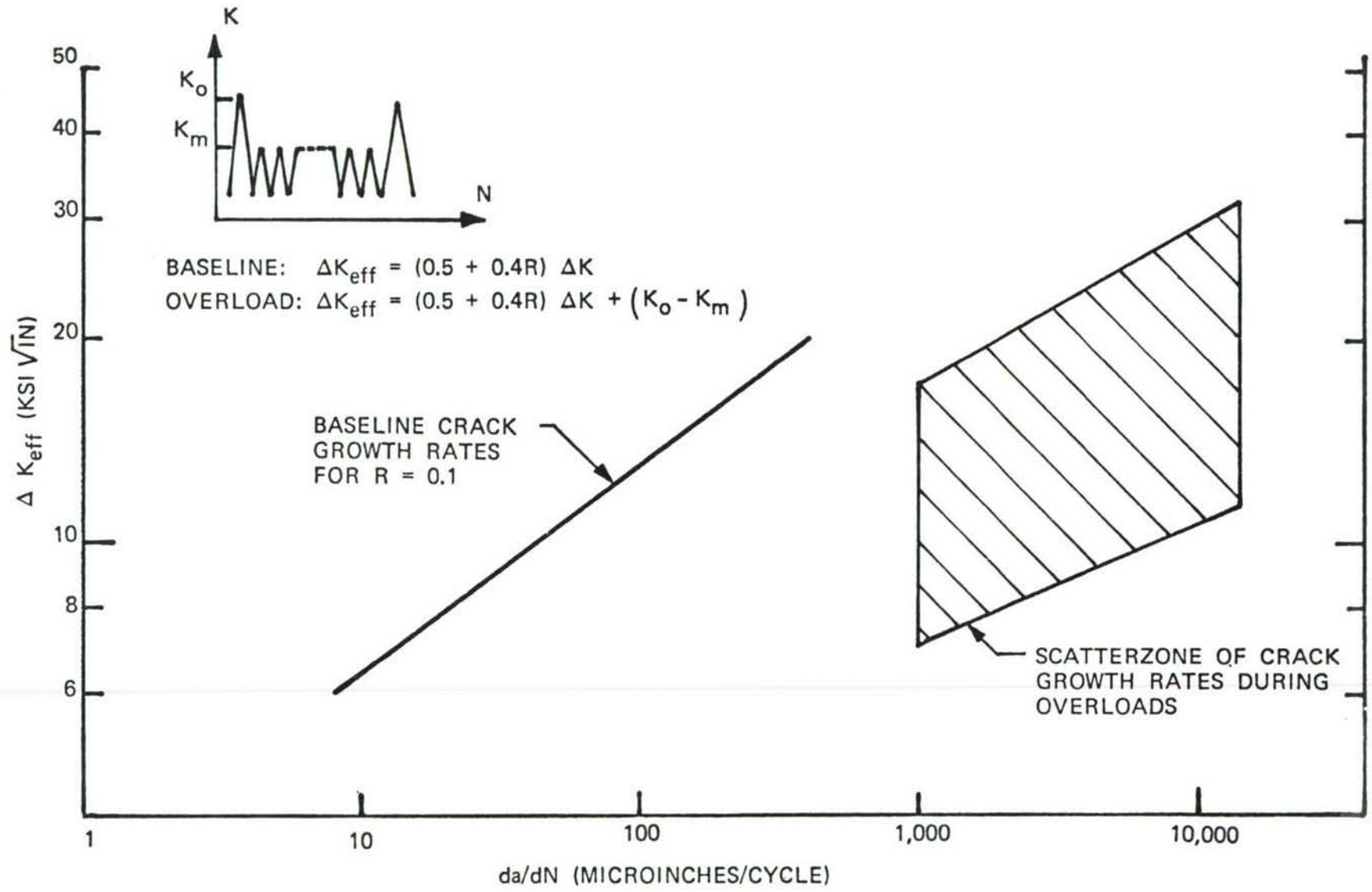


Figure 47: Comparison Between Crack Growth Rates During Overloads and Baseline Crack Growth Rates For Overloaded Aluminum Alloy Surface Flaw Specimens (Based on ΔK_{eff})

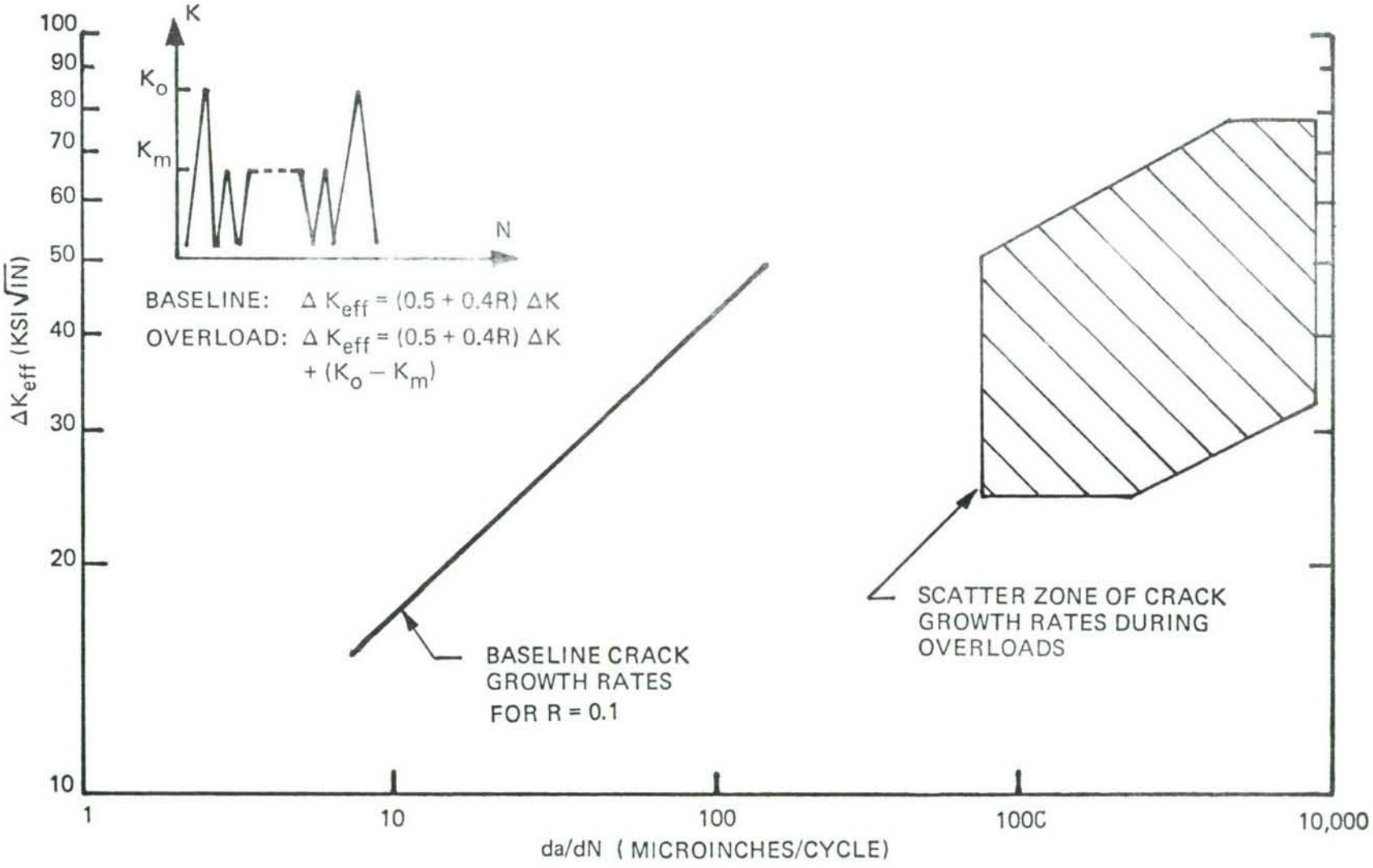


Figure 48: Comparison Between Crack Growth Rates During Overloads and Baseline Crack Growth Rates for Overloaded Steel Alloy Surface Flaw Specimens (Based on ΔK_{eff})

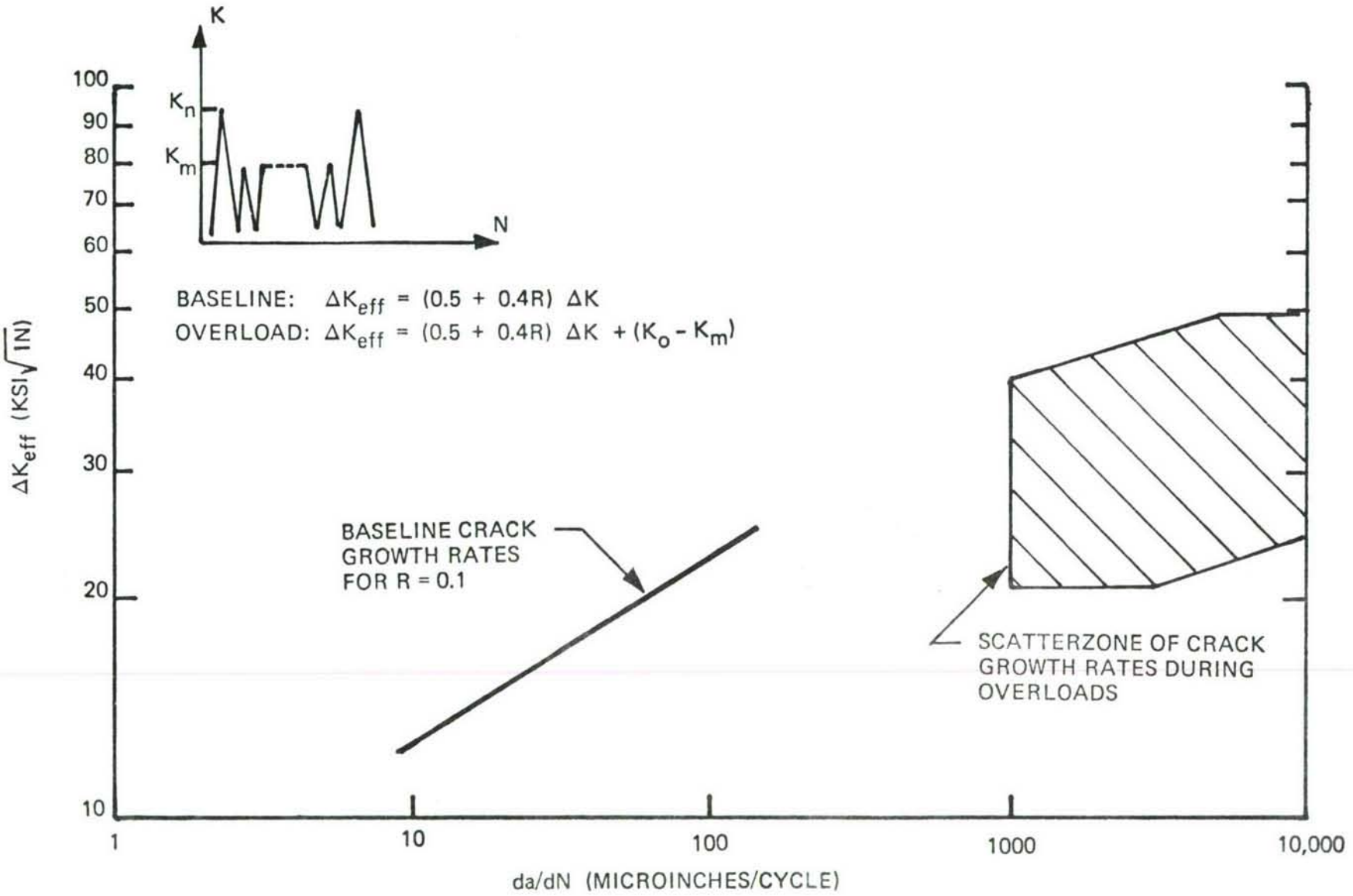


Figure 49: Comparison Between Crack Growth Rates During Overloads and Baseline Crack Growth Rates For Overloaded Titanium Alloy Surface Flaw Specimens (Based on ΔK_{eff})

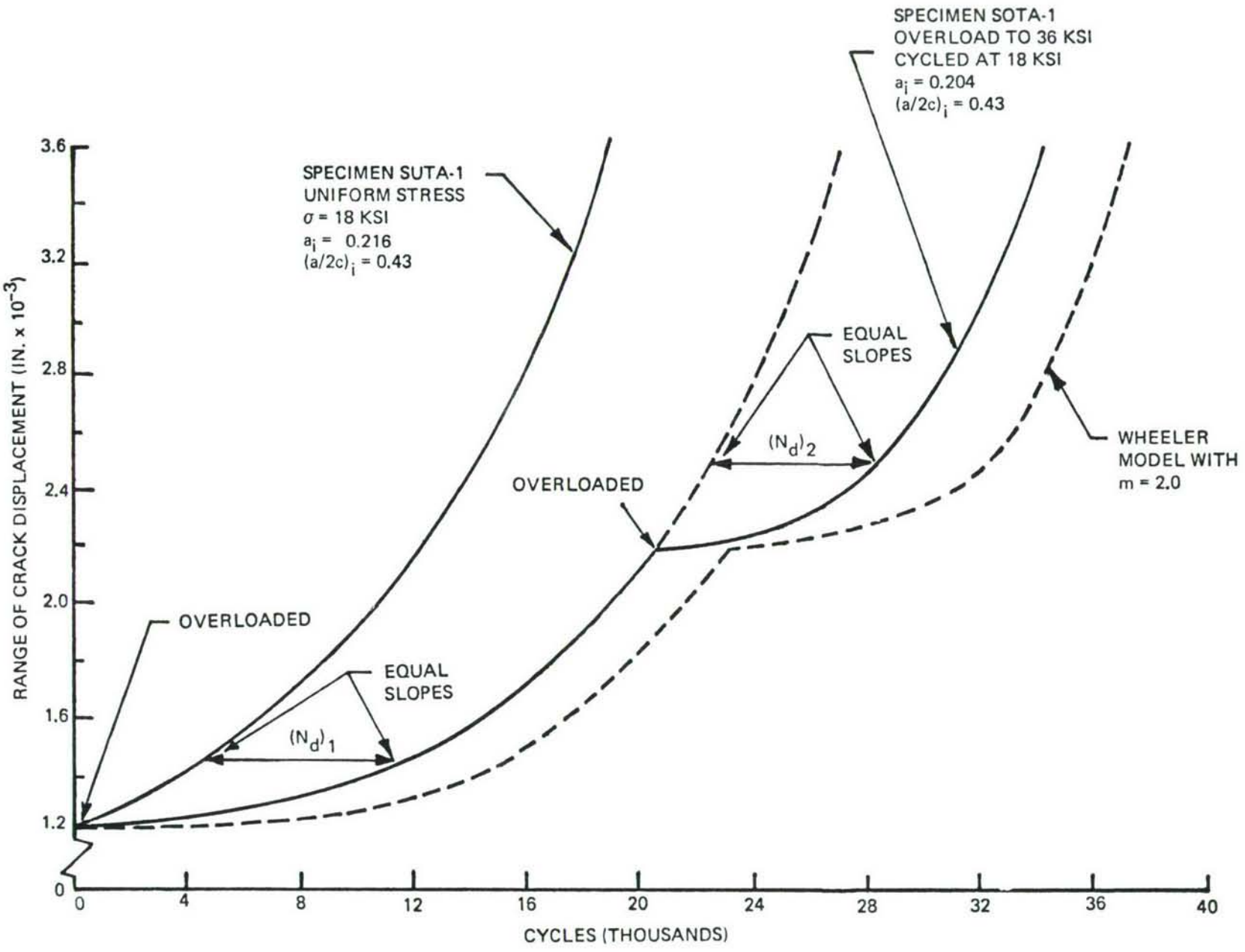


Figure 50: Method of Using Crack Displacement Versus Cycles Test Records to Determine Delay Cycles

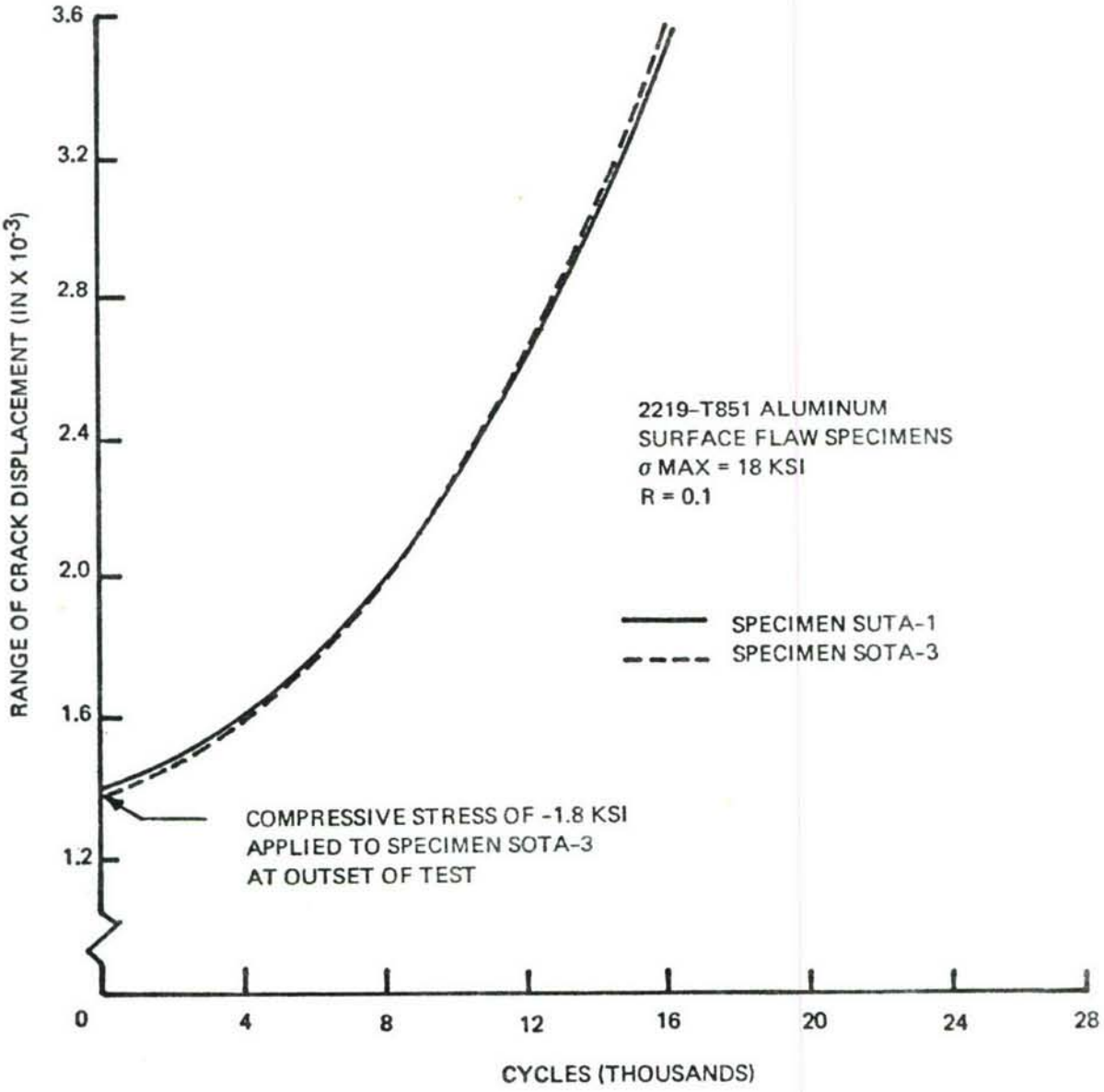


Figure 51: Test Records Illustrating Negligibly Small Effects of Initial Small Compressive Loads on Crack Growth Rate Behavior of Surface Flaws

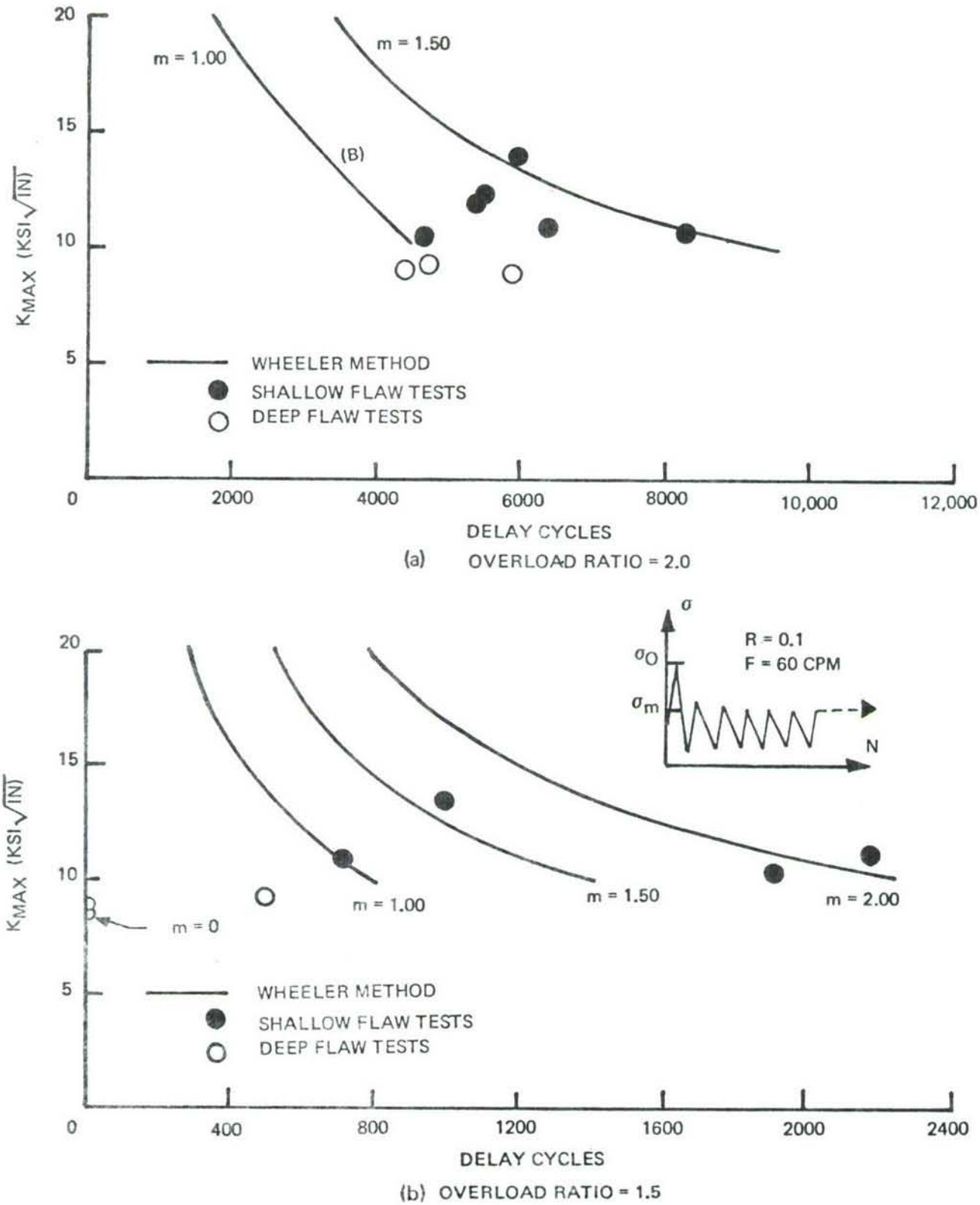


Figure 52: Experimental and Calculated Delay Cycles Resulting From Aluminum Alloy Single Overload Tests

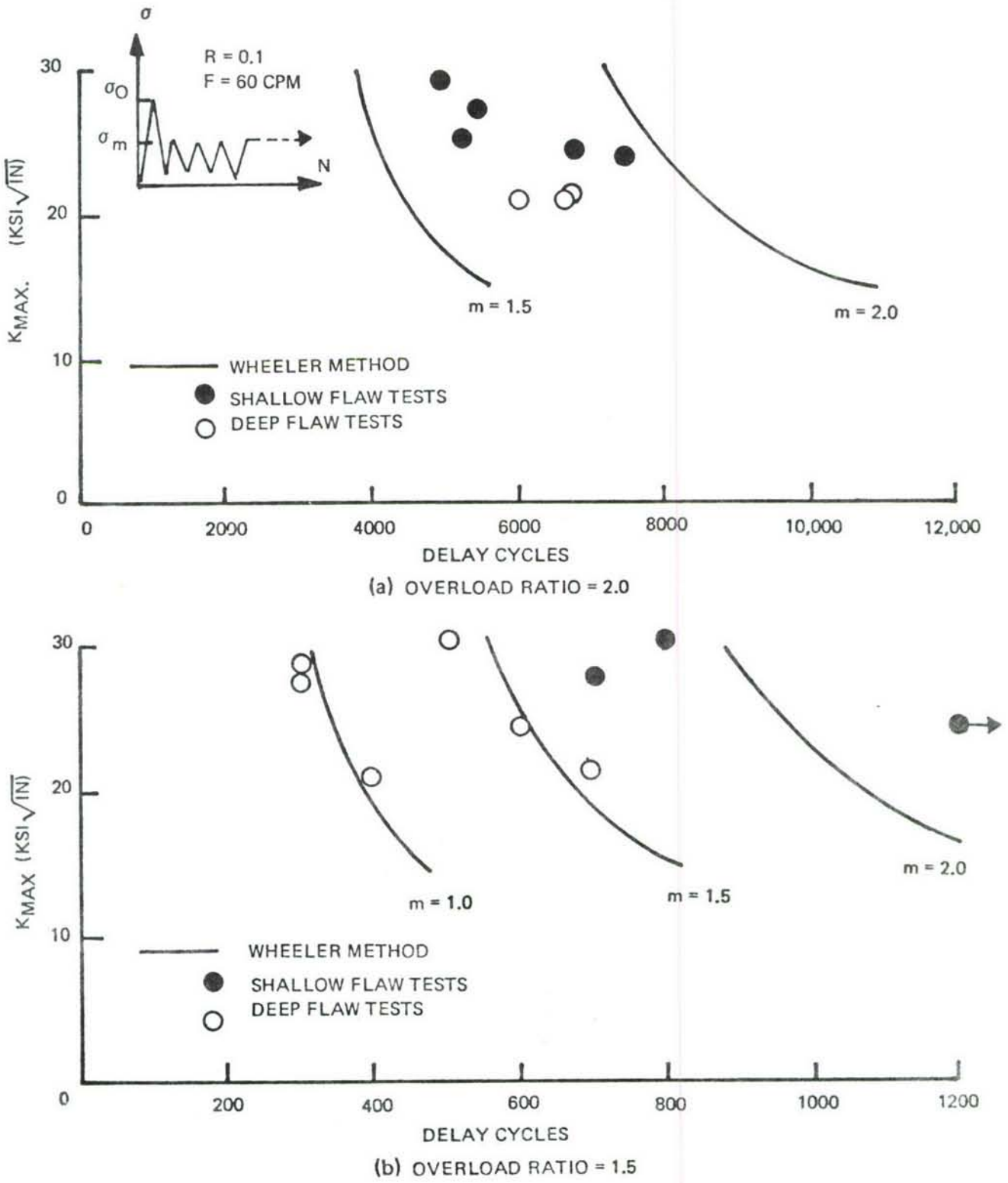
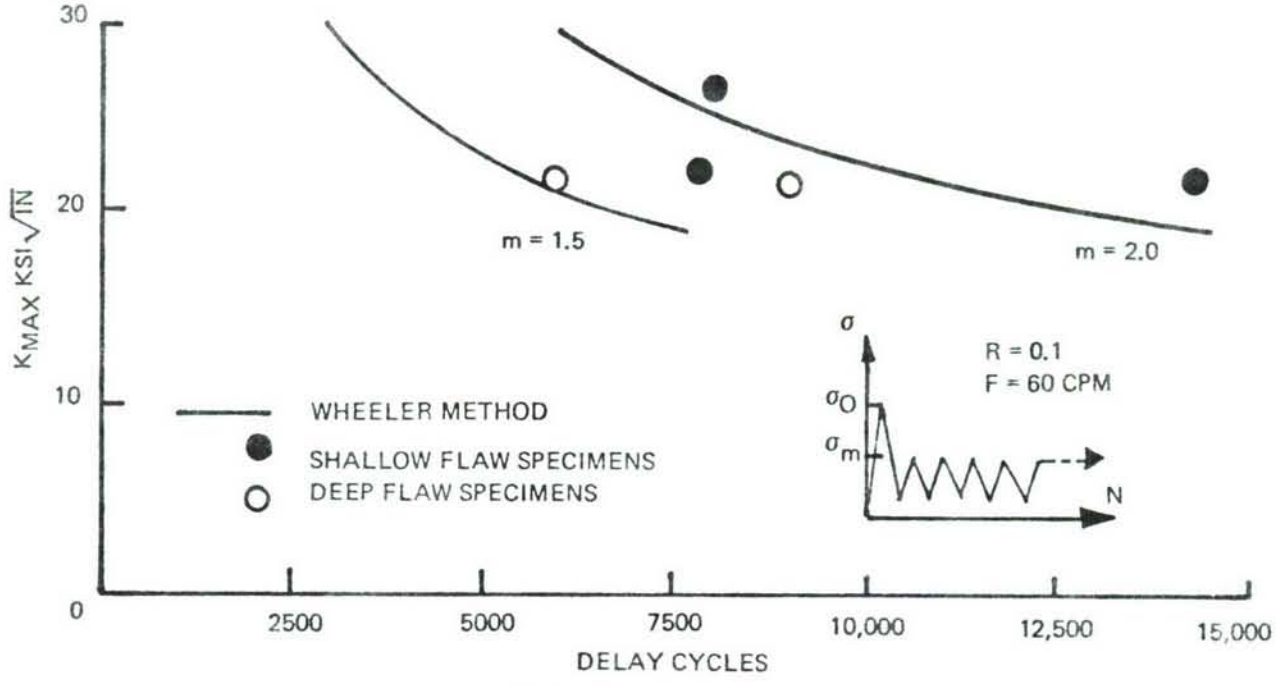
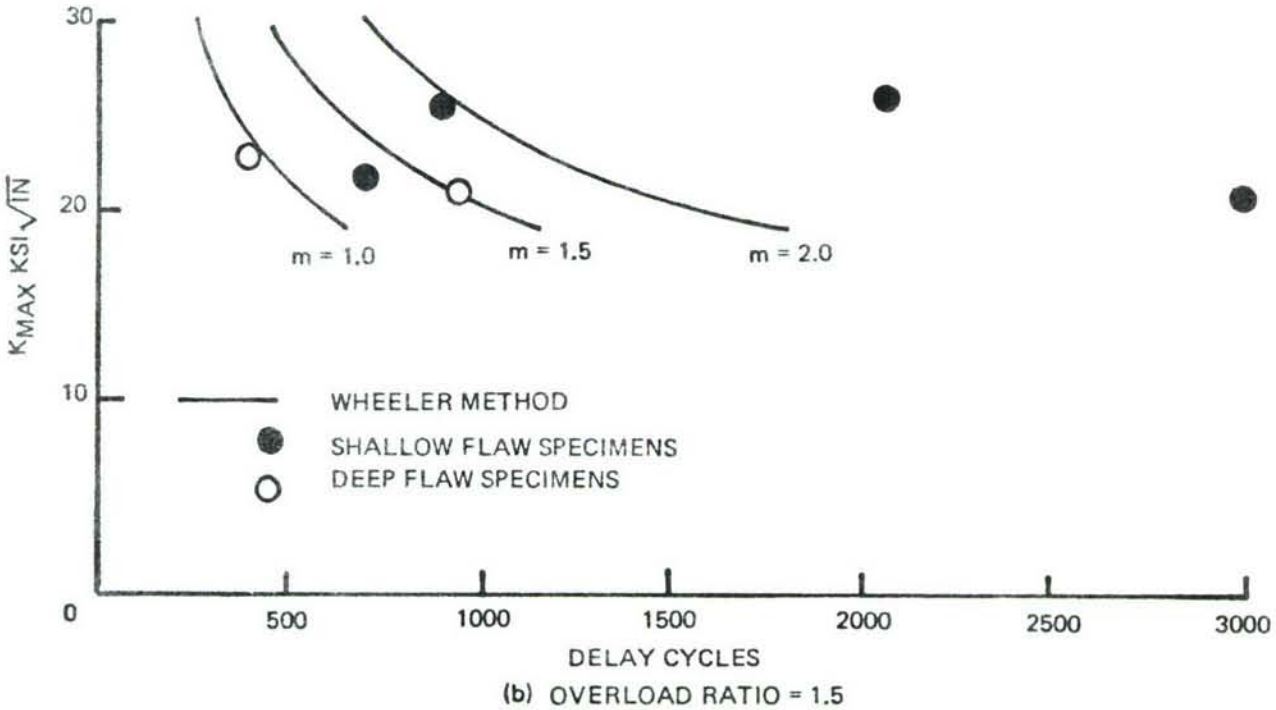


Figure 53: Experimental and Calculated Delay Cycles Resulting From Steel Alloy Single Overload Tests



(a) OVERLOAD RATIO = 2.0



(b) OVERLOAD RATIO = 1.5

Figure 54: Experimental and Calculated Delay Cycles Resulting From Titanium Alloy Single Overload Tests

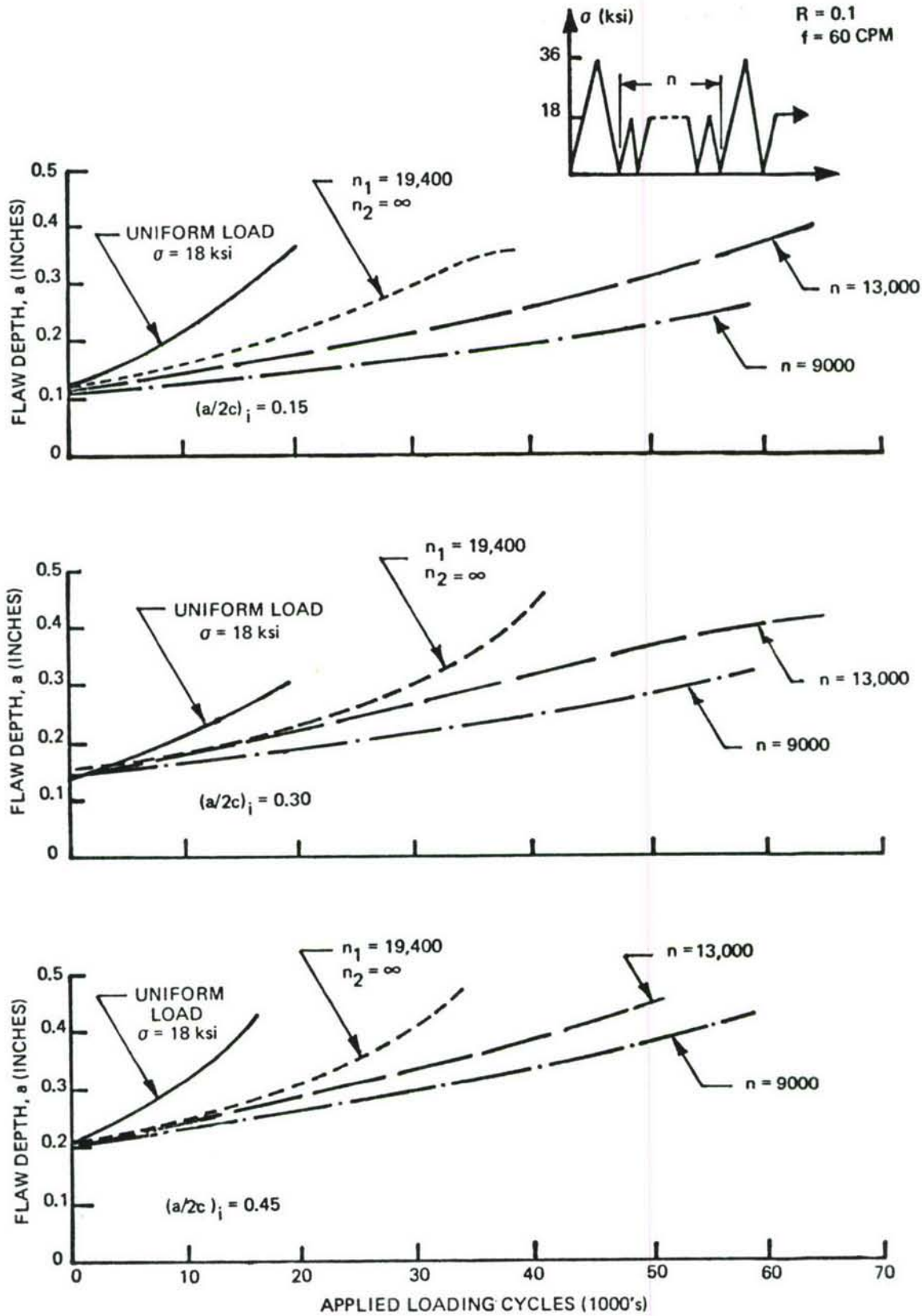


Figure 55: Effect of Periodic Overloads on Fatigue Crack Propagation of Surface Flaws in 2219-T851 Aluminum Alloy Plate, $(a/t)_i < 0.5$ $(\sigma_{OL}/\sigma_{MAX} = 2.0)$

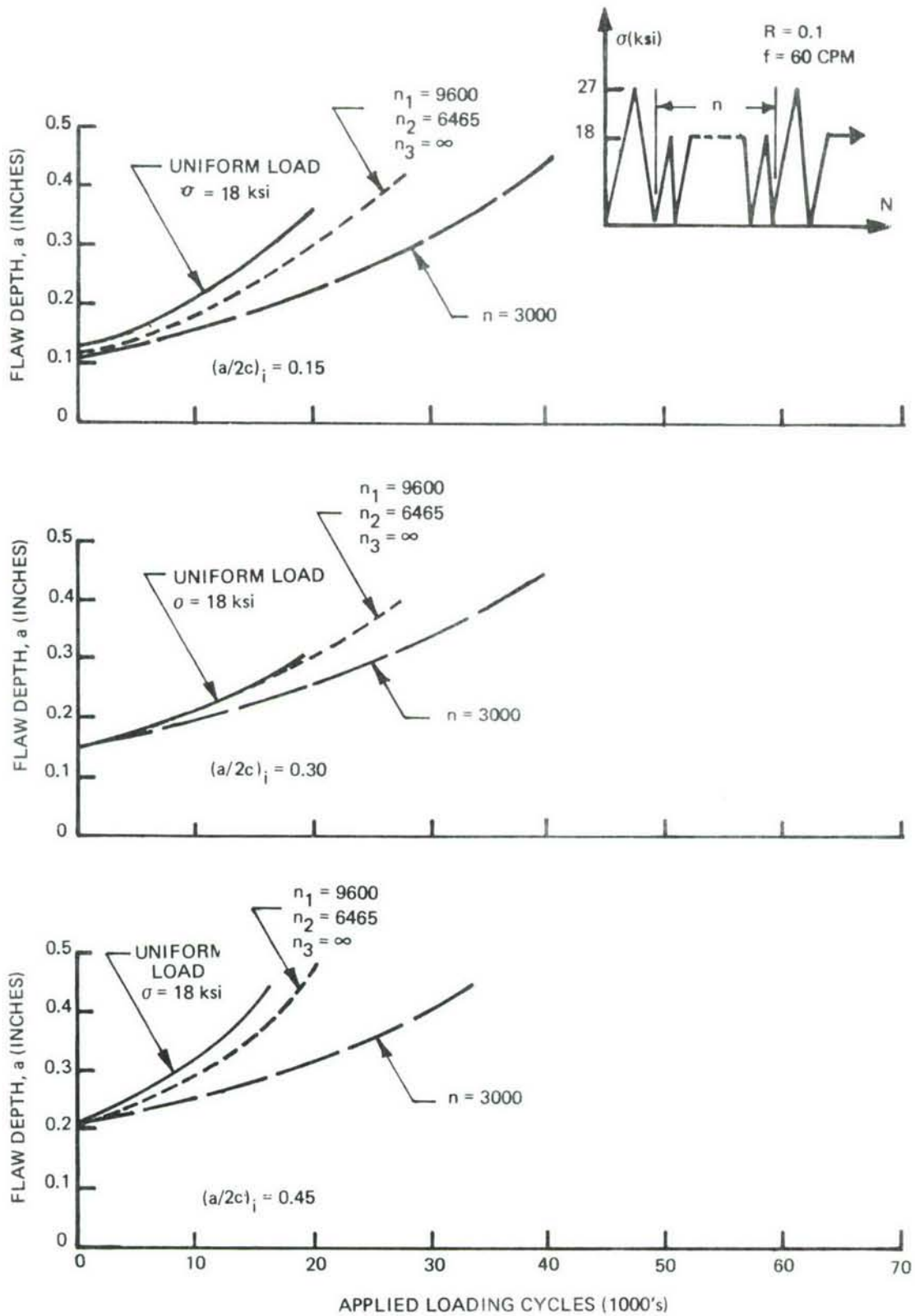


Figure 56: Effect of Periodic Overloads on Fatigue Crack Propagation of Surface Flaws in 2219-T851 Aluminum Alloy Plate, $(a/t)_i < 0.5$ $(\sigma_{OL}/\sigma_{MAX} = 1.5)$

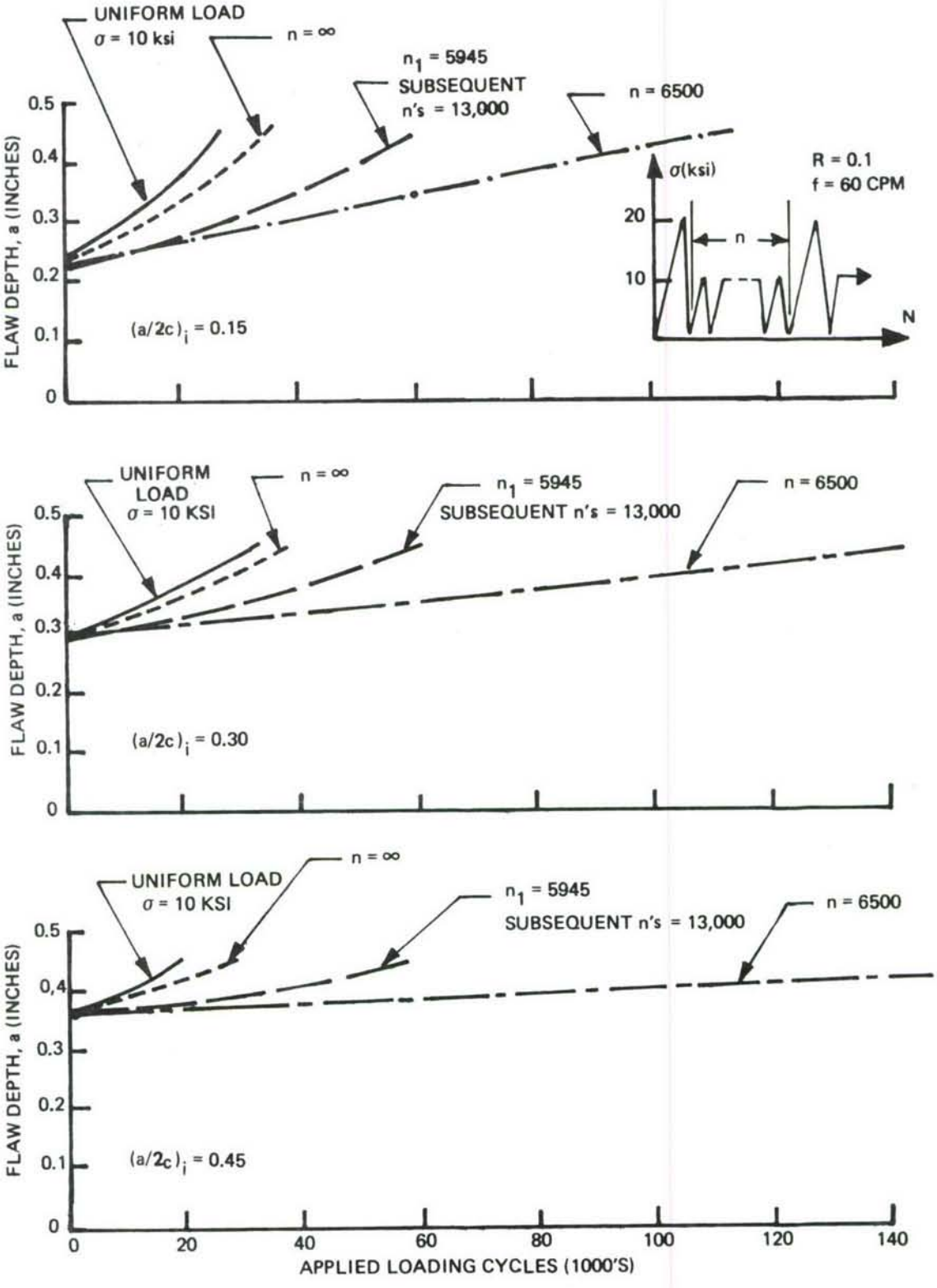


Figure 57: Effect of Periodic Overloads on Fatigue Crack Propagation of Surface Flaws in 2219-T851 Aluminum Alloy Plate, $(a/t)_i > 0.5$ $(\sigma_{OL}/\sigma_{MAX} = 2.0)$

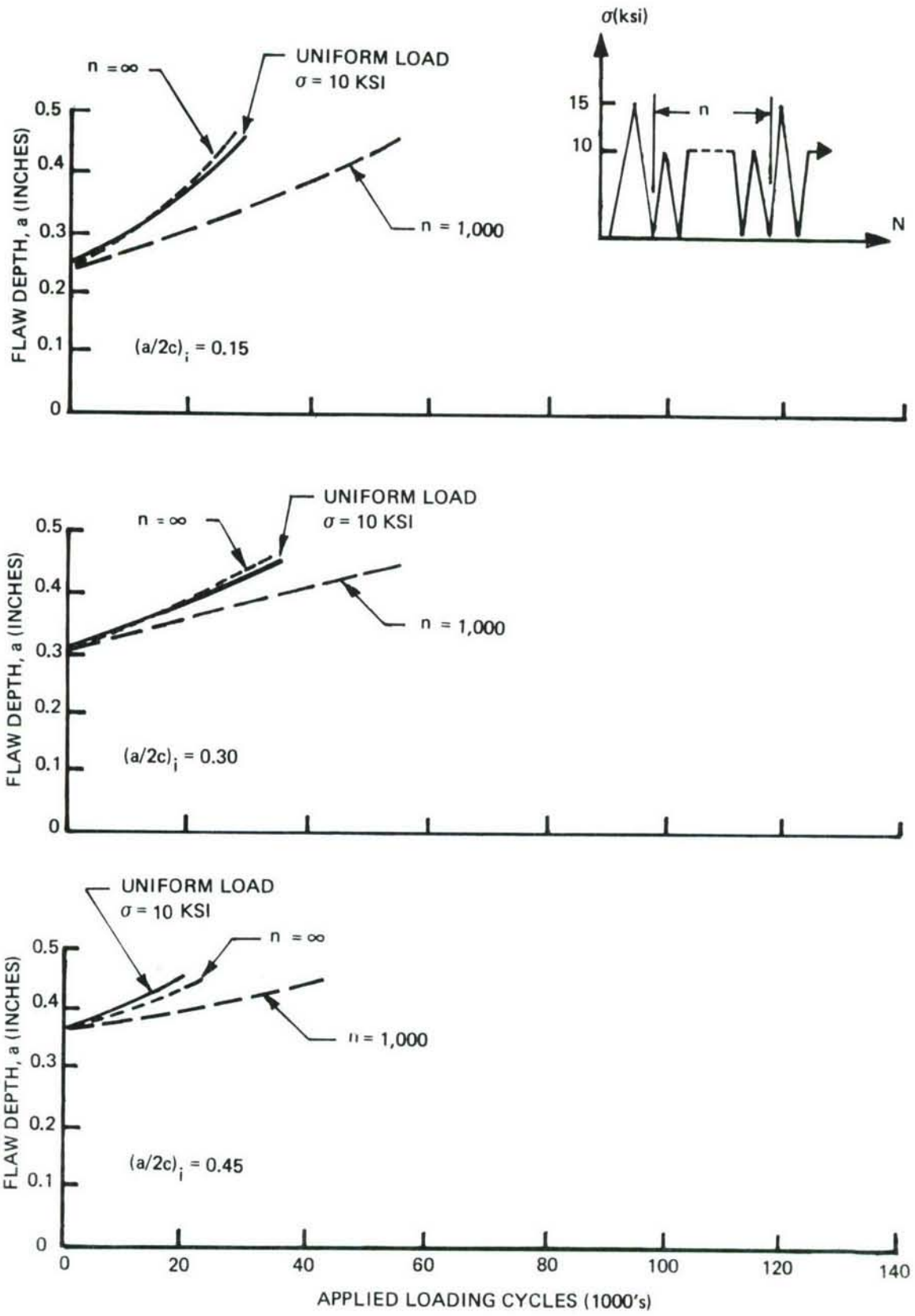


Figure 58: Effect of Periodic Overloads on Fatigue Crack Propagation of Surface Flaws in 2219-T851 Aluminum Alloy Plate $(a/t)_i > 0.5$ $(\sigma_{OL}/\sigma_{MAX} = 1.5)$

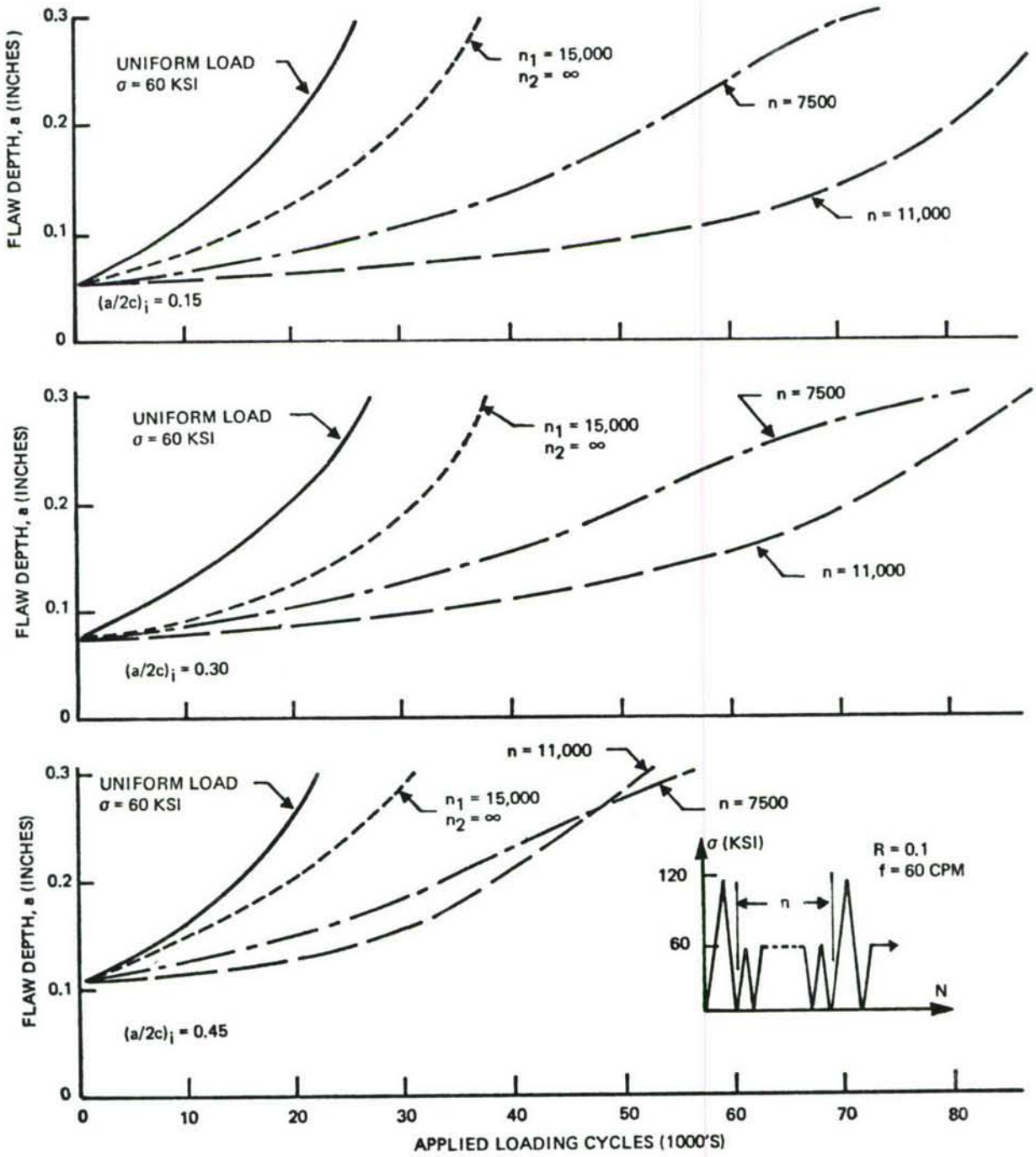


Figure 59: Effect of Periodic Overloads on Fatigue Crack Propagation of Surface Flaws in 9Ni-4Co-0.2C Steel Alloy Plate, $(a/t)_i < 0.5$ ($\sigma_{OL}/\sigma_{MAX} = 2.0$)

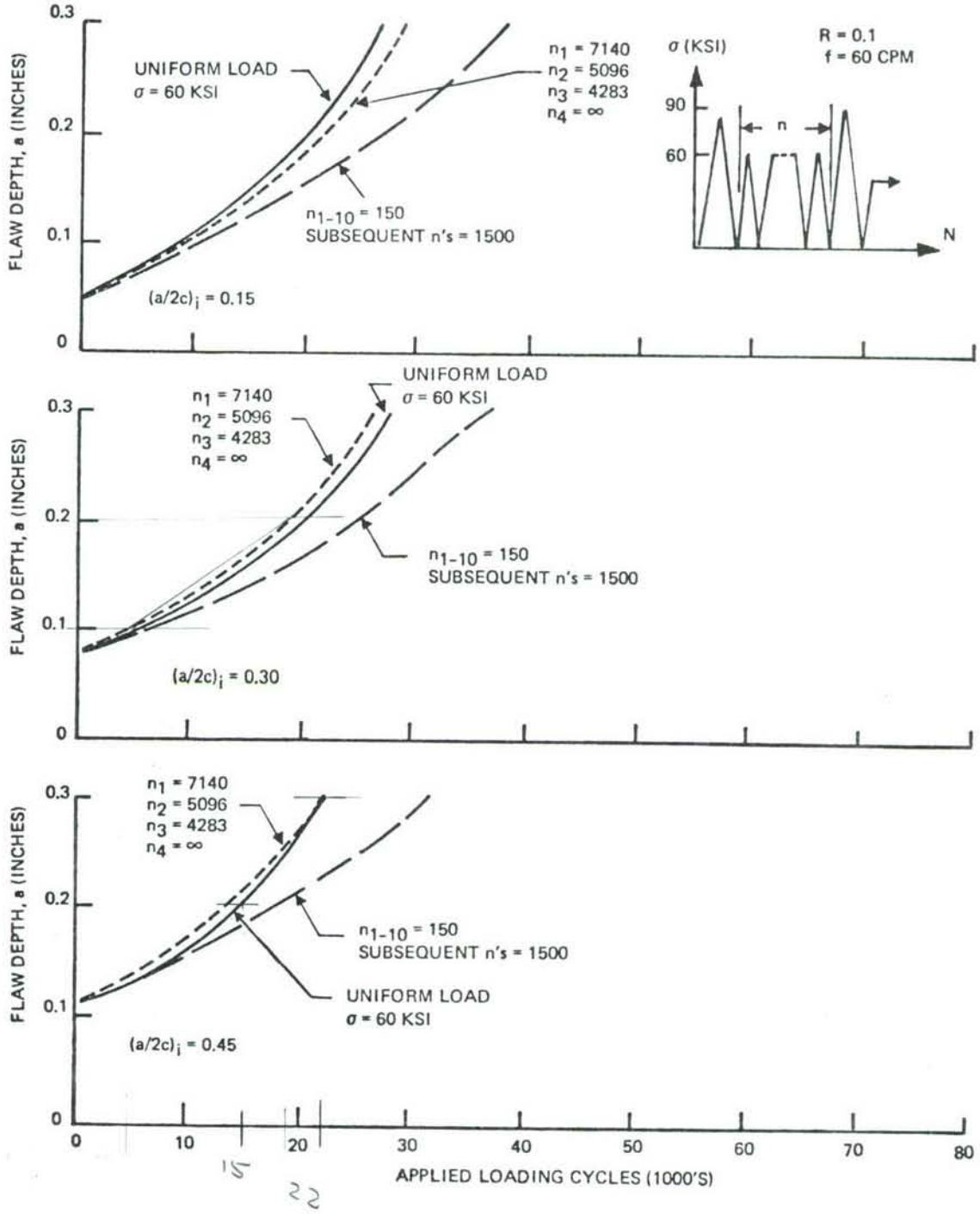


Figure 60: Effect of Periodic Overloads on Fatigue Crack Propagation of Surface Flaws in 9Ni-4Co-0.2C Steel Alloy Plate $(a/t)_i < 0.5$ ($\sigma_{OL}/\sigma_{MAX} = 1.5$)

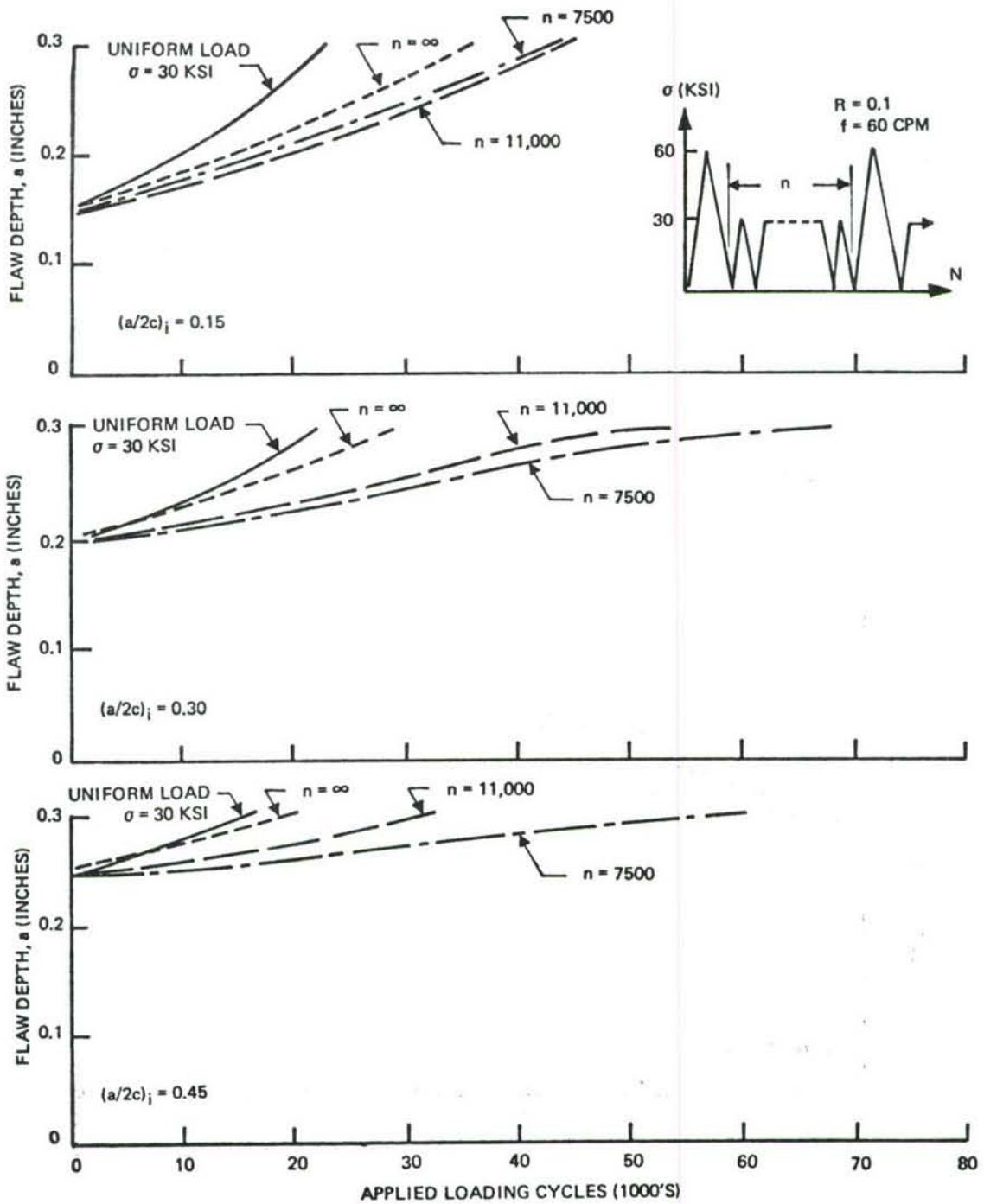


Figure 61: Effect of Periodic Overloads on Fatigue Crack Propagation of Surface Flaws in 9Ni-4Co-0.2C Steel Alloy Plate, $(a/t)_i > 0.5$ ($\sigma_{OL}/\sigma_{MAX} = 2.0$)

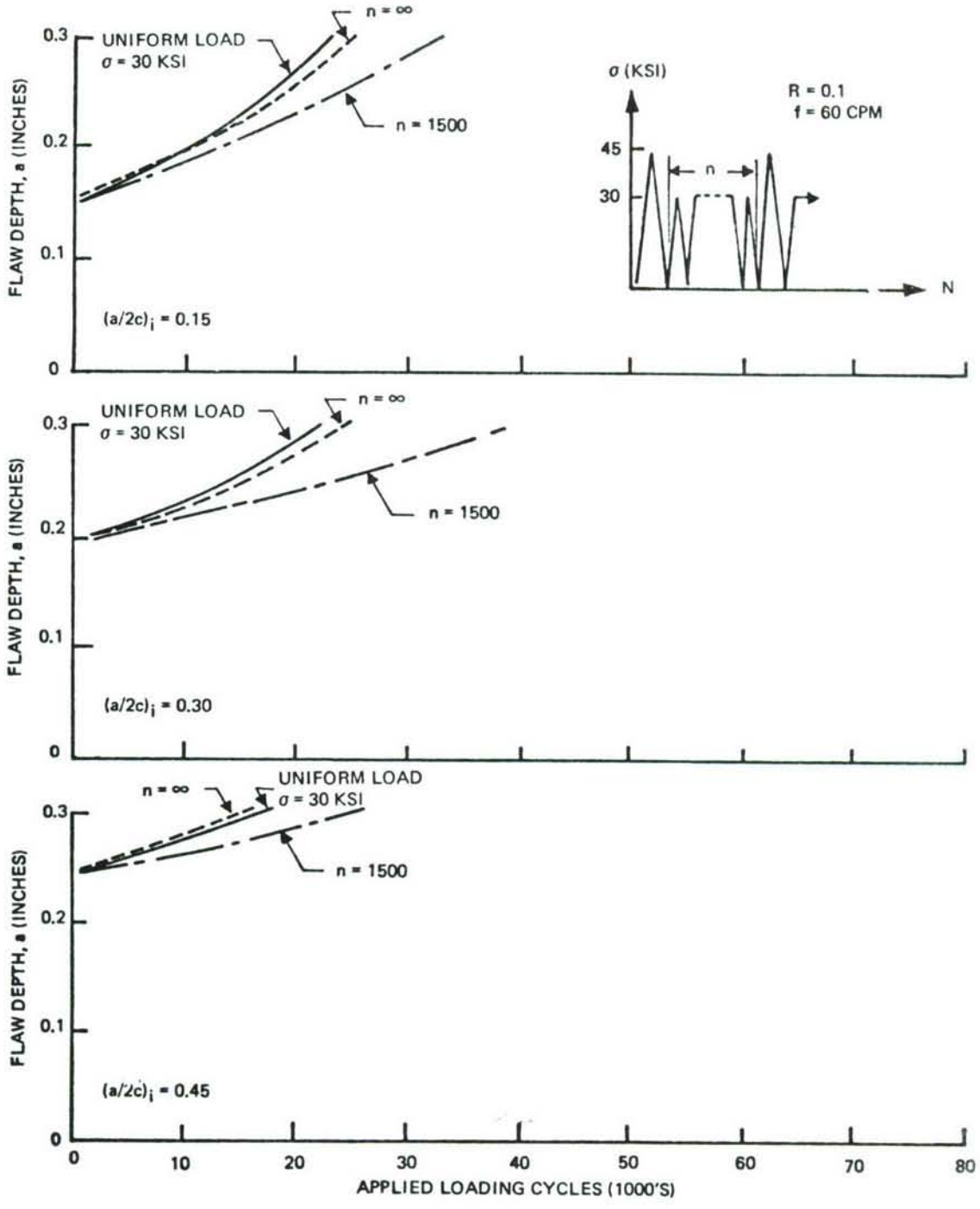


Figure 62: *Effect of Periodic Overloads on Fatigue Crack Propagation of Surface Flaws in 9Ni-4Co-0.2C Steel Alloy Plate $(a/t)_i > 0.5$ ($\sigma_{OL}/\sigma_{MAX} = 1.5$)*

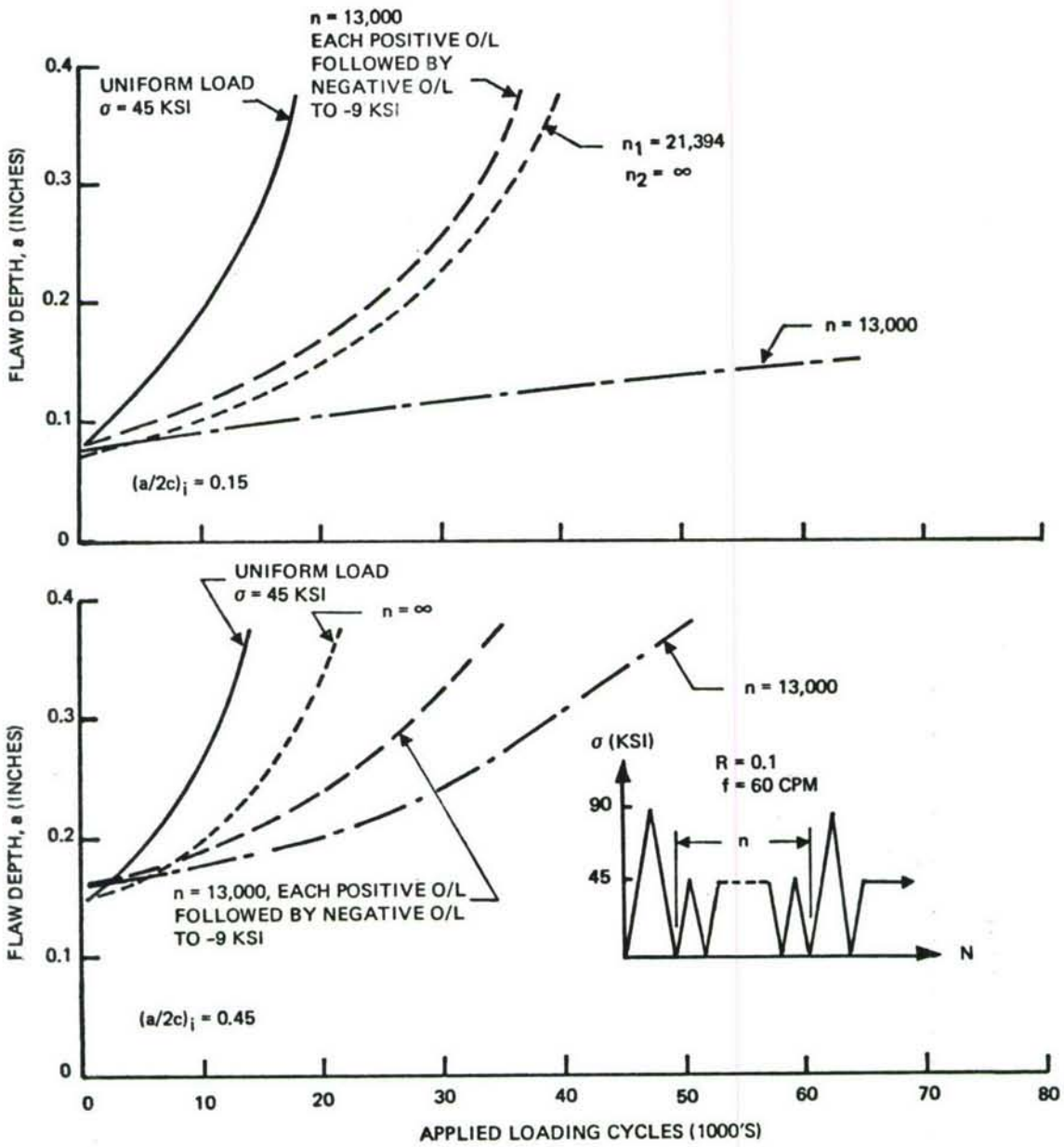


Figure 63: Effect of Periodic Overloads on Fatigue Crack Propagation of Surface Flaws in 6Al-4V (Beta Annealed) Titanium Alloy Plate, $(a/t)_i < 0.5$ ($\sigma_{OL}/\sigma_{MAX} = 2.0$)

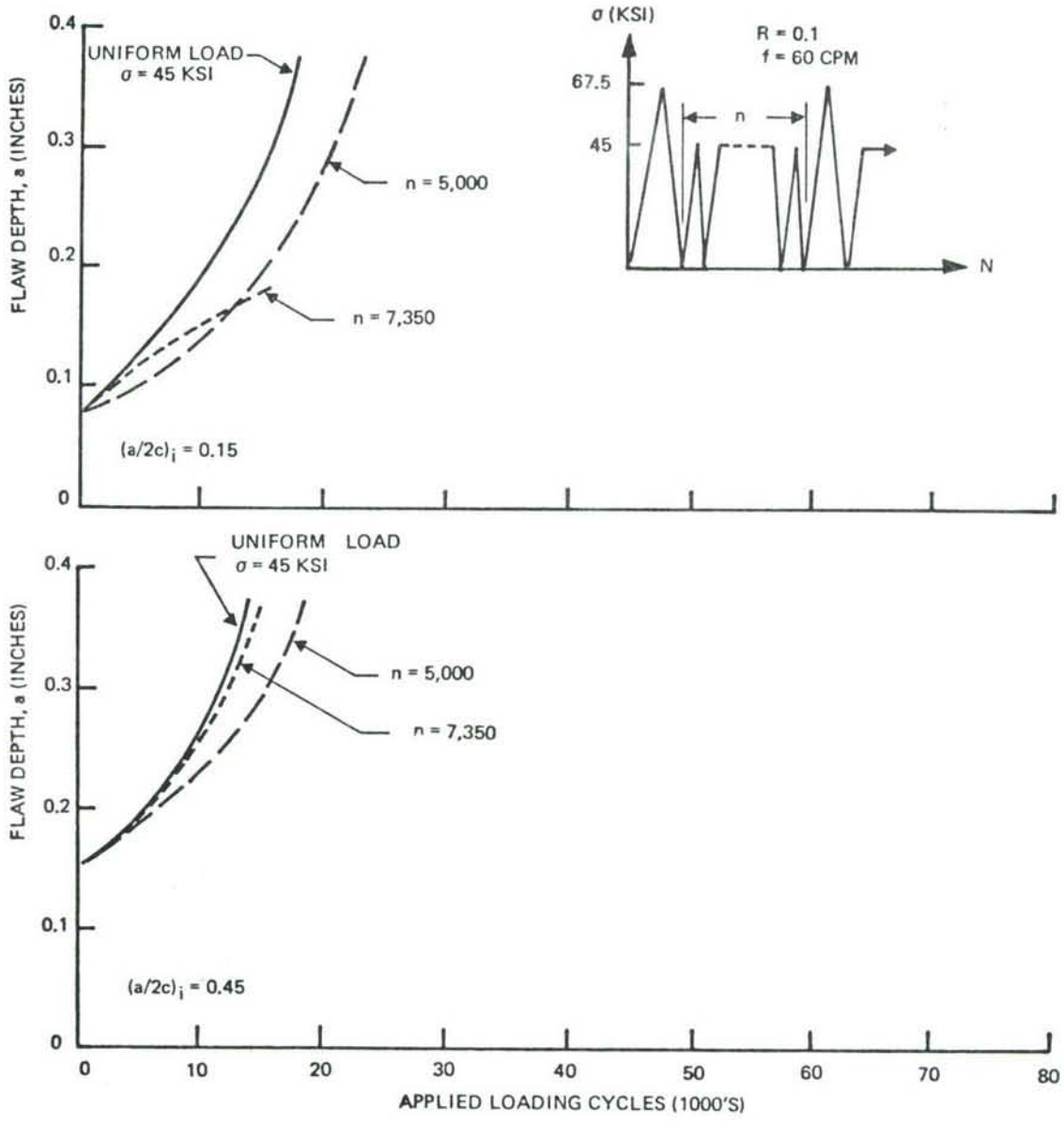


Figure 64: Effect of Periodic Overloads on Fatigue Crack Propagation of Surface Flaws in 6Al-4V (Beta Annealed) Titanium Alloy Plate, $(a/t)_i < 0.5$ ($\sigma_{OL}/\sigma_{MAX} = 1.5$)

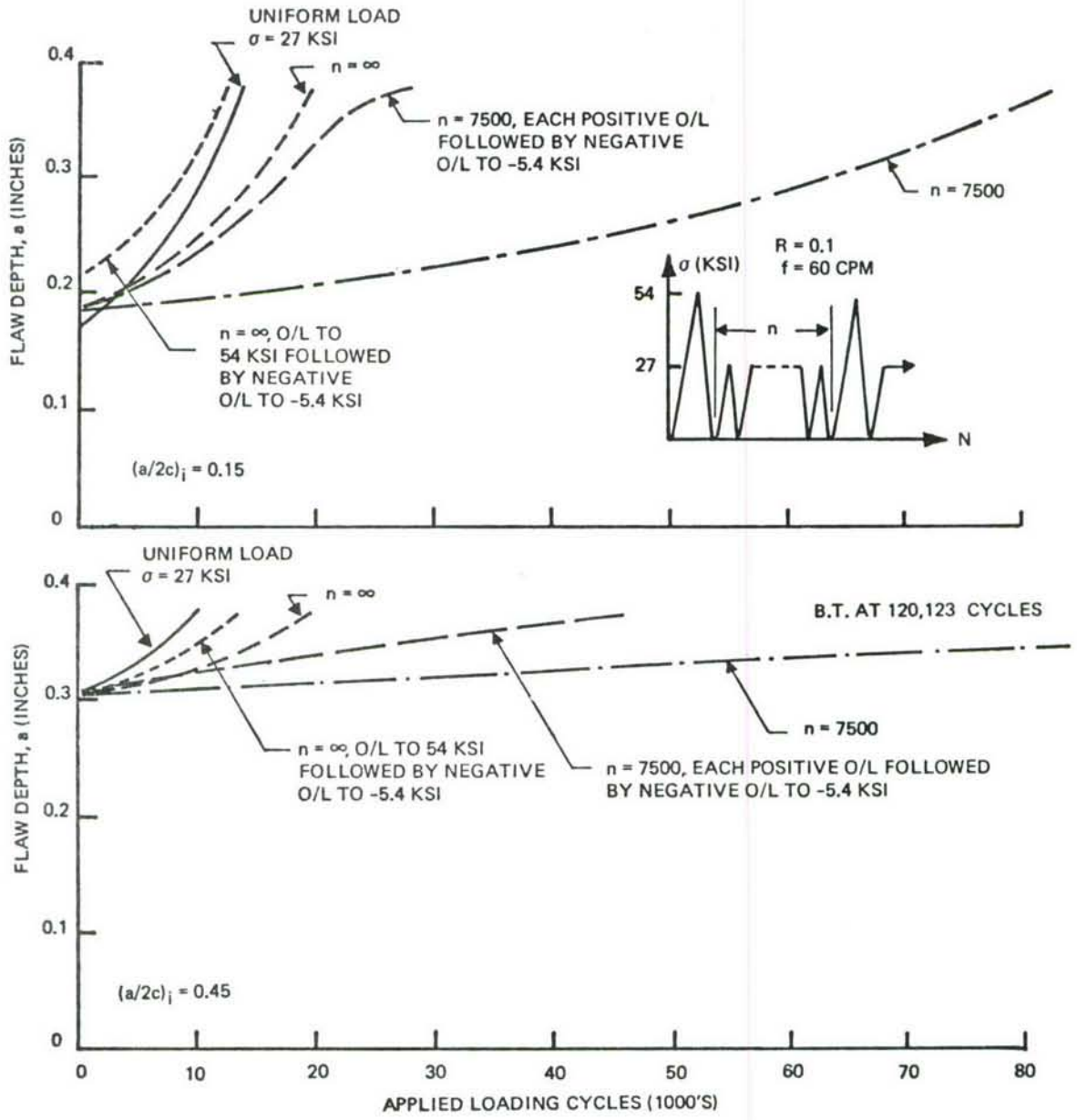


Figure 65: Effect of Periodic Overloads on Fatigue Crack Propagation of Surface Flaws in 6Al-4V (Beta Annealed) Titanium Alloy Plate, $(a/t)_i > 0.5$ ($\sigma_{OL}/\sigma_{MAX} = 2.0$)

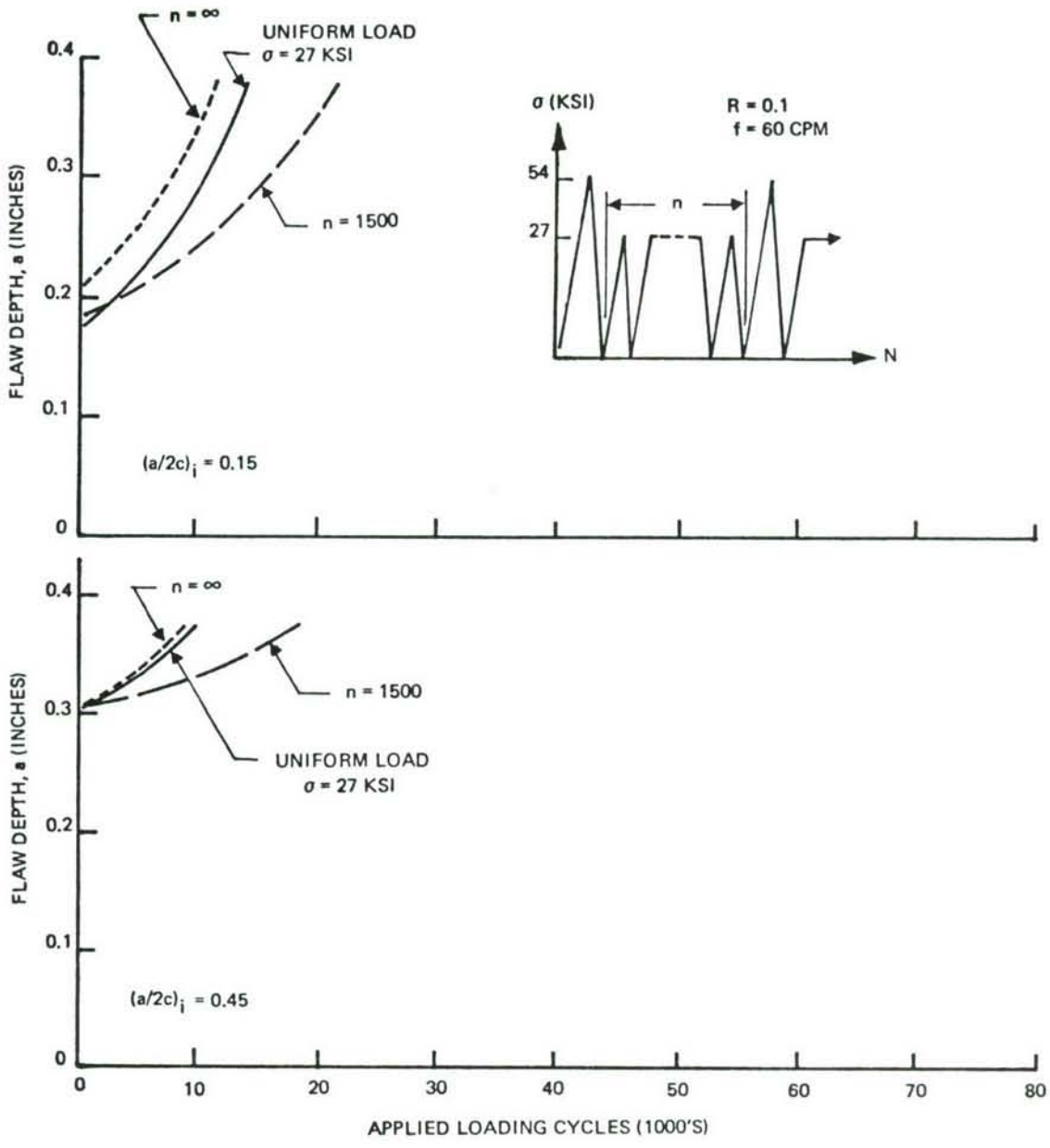


Figure 66: Effect of Periodic Overloads on Fatigue Crack Propagation of Surface Flaws in 6Al-4V (Beta Annealed) Titanium Alloy Plate, $(a/t)_i > 0.5$ ($\sigma_{OL}/\sigma_{MAX} = 1.5$)

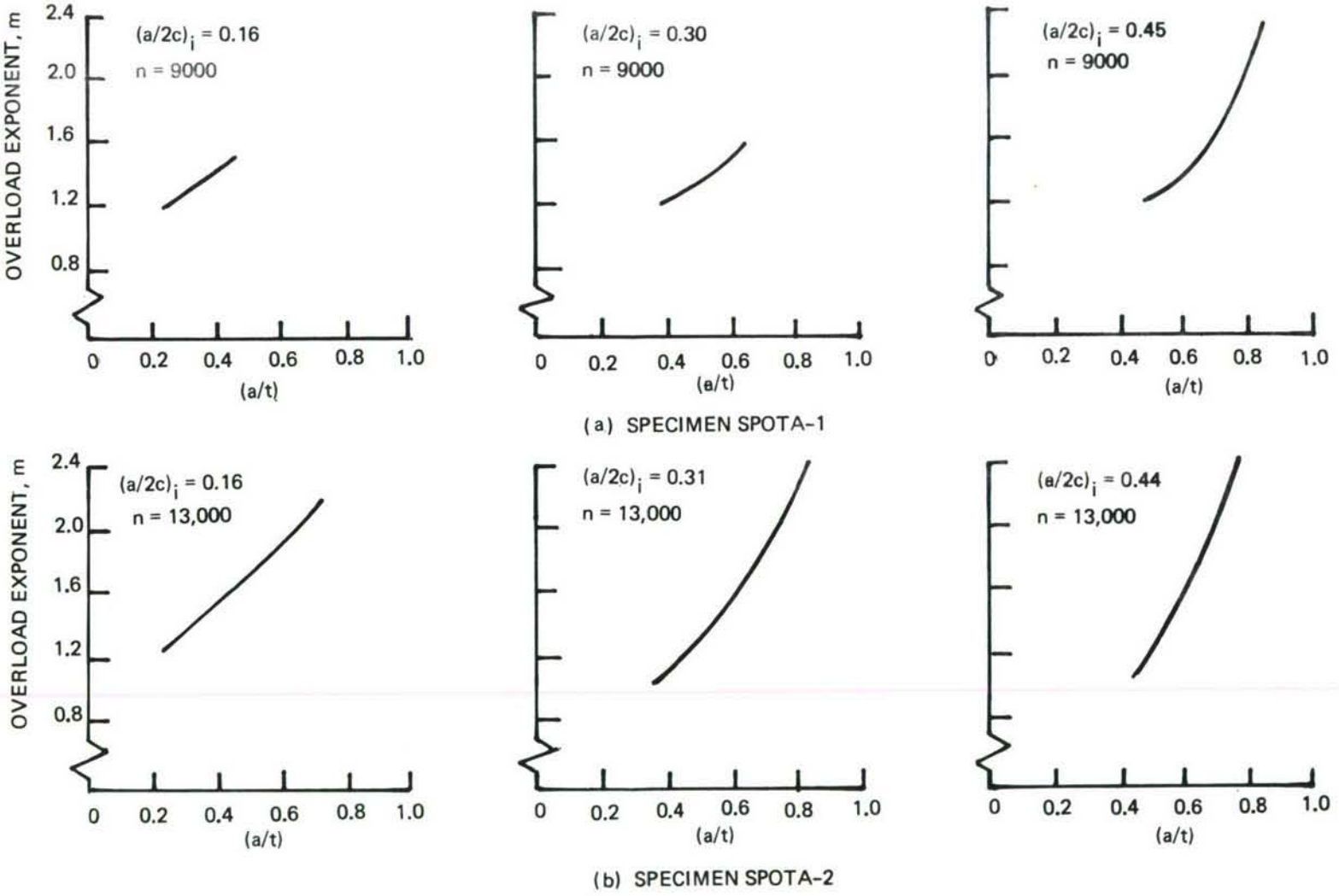


Figure 67: Variations in Overload Exponent (m) in 2219-T851 Aluminum Alloy Periodic Overload Specimens with $(a/t)_i < 0.5$ and Overload Ratio = 2.0

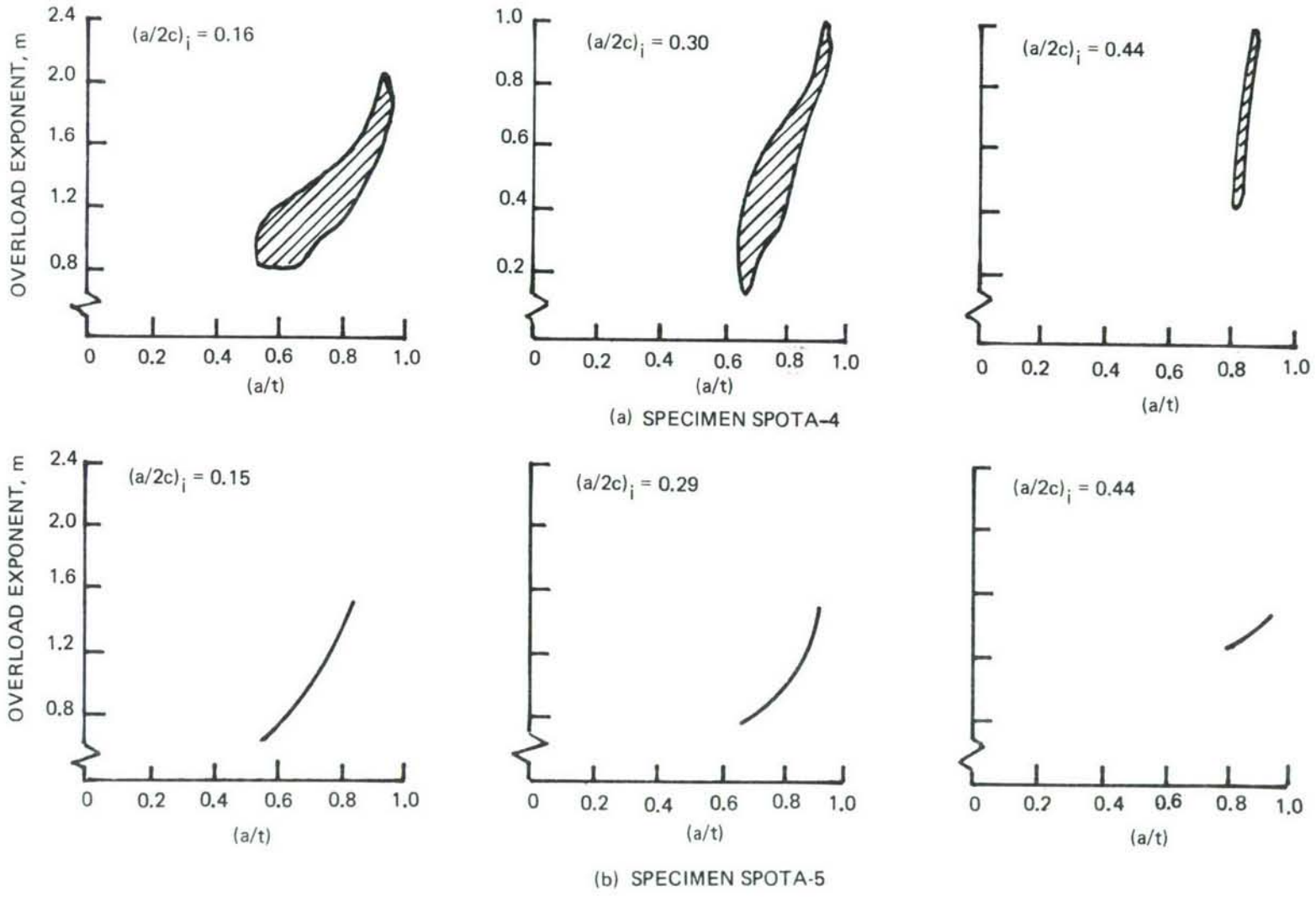


Figure 68: Variations in Overload Exponent (m) in 2219-T851 Aluminum Alloy Periodic Overload Specimens with $(a/t)_i > 0.5$ and Overload Ratio = 2.0

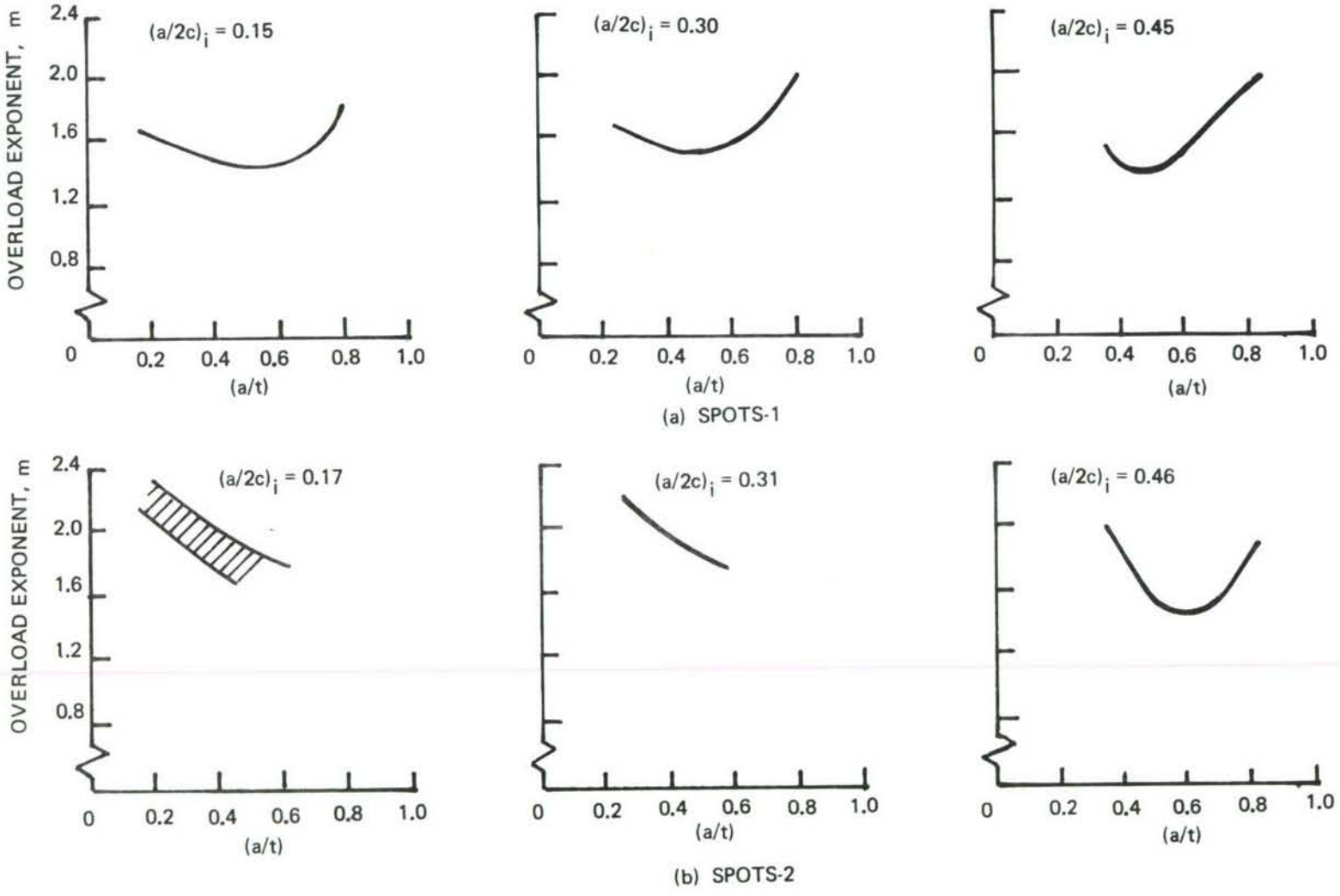


Figure 69: Variations in Overload Exponent (m) in 9Ni-4Co-0.2C Steel Alloy Periodic Overload Specimens with $(a/t)_i < 0.5$ and Overload Ratio = 2.0

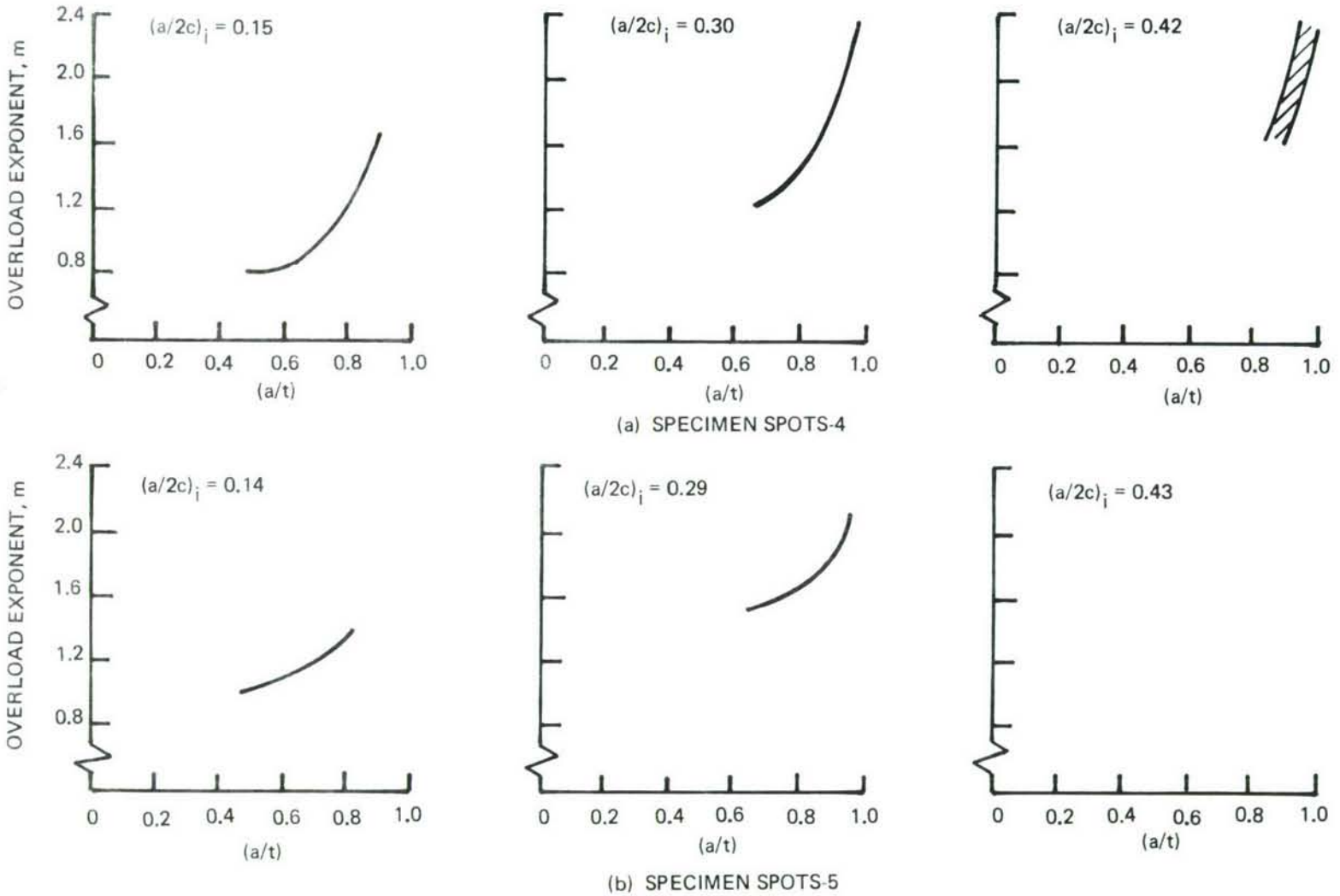


Figure 70: Variations in Overload Exponent (m) in 9Ni-4Co-0.2C Steel Alloy Periodic Overload Specimens with $(a/t)_i > 0.5$ and Overload Ratio = 2.0

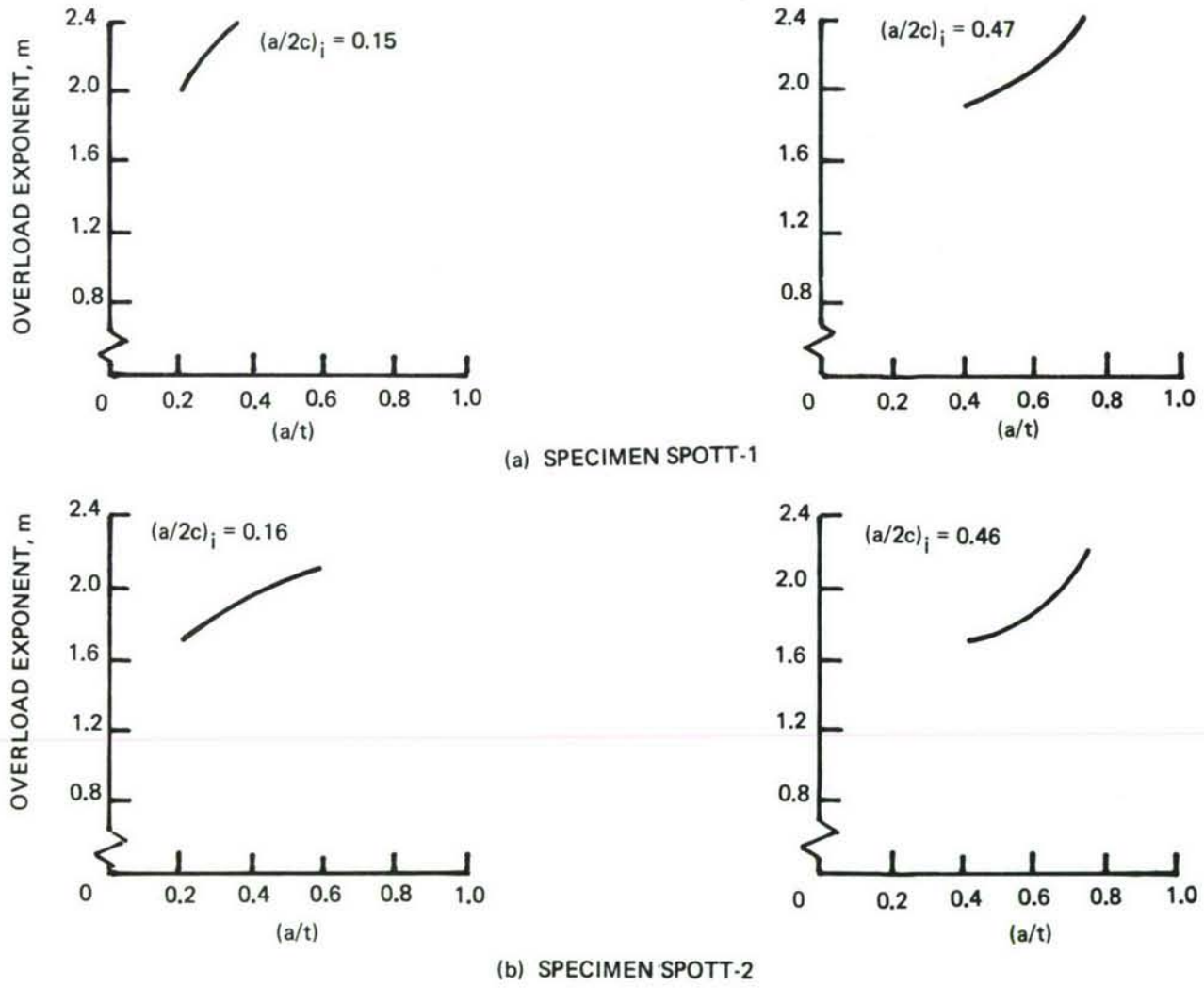


Figure 71: Variations in Overload Exponent (m) in Ti-6Al-4V (Beta Annealed) Alloy Periodic Overload Specimens with $(a/t)_i < 0.5$ and Overload Ratio = 2.0

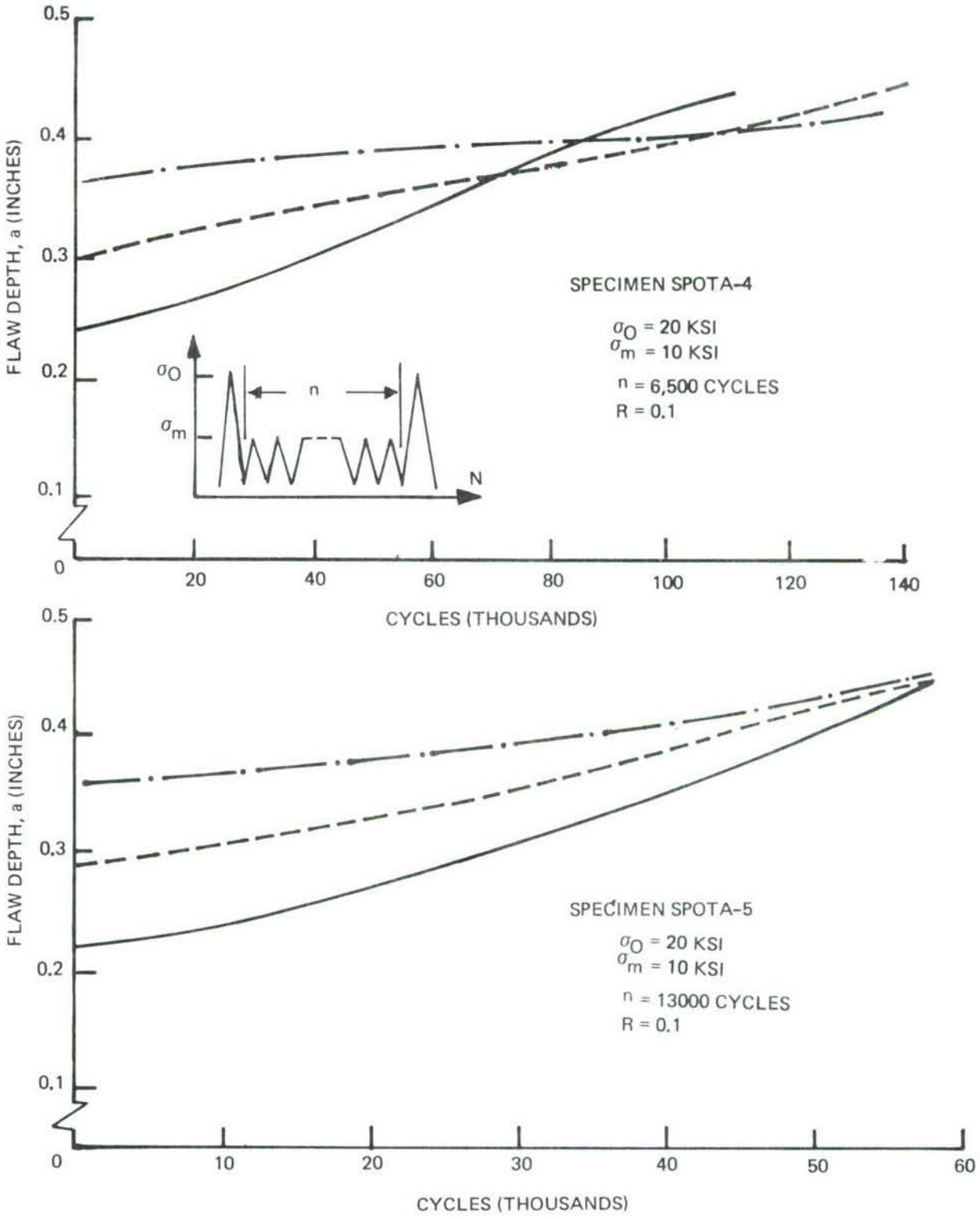


Figure 72: Crack Depth Versus Cycles for 2219-T851 Aluminum Alloy Periodic Overload Surface Flaw Specimens

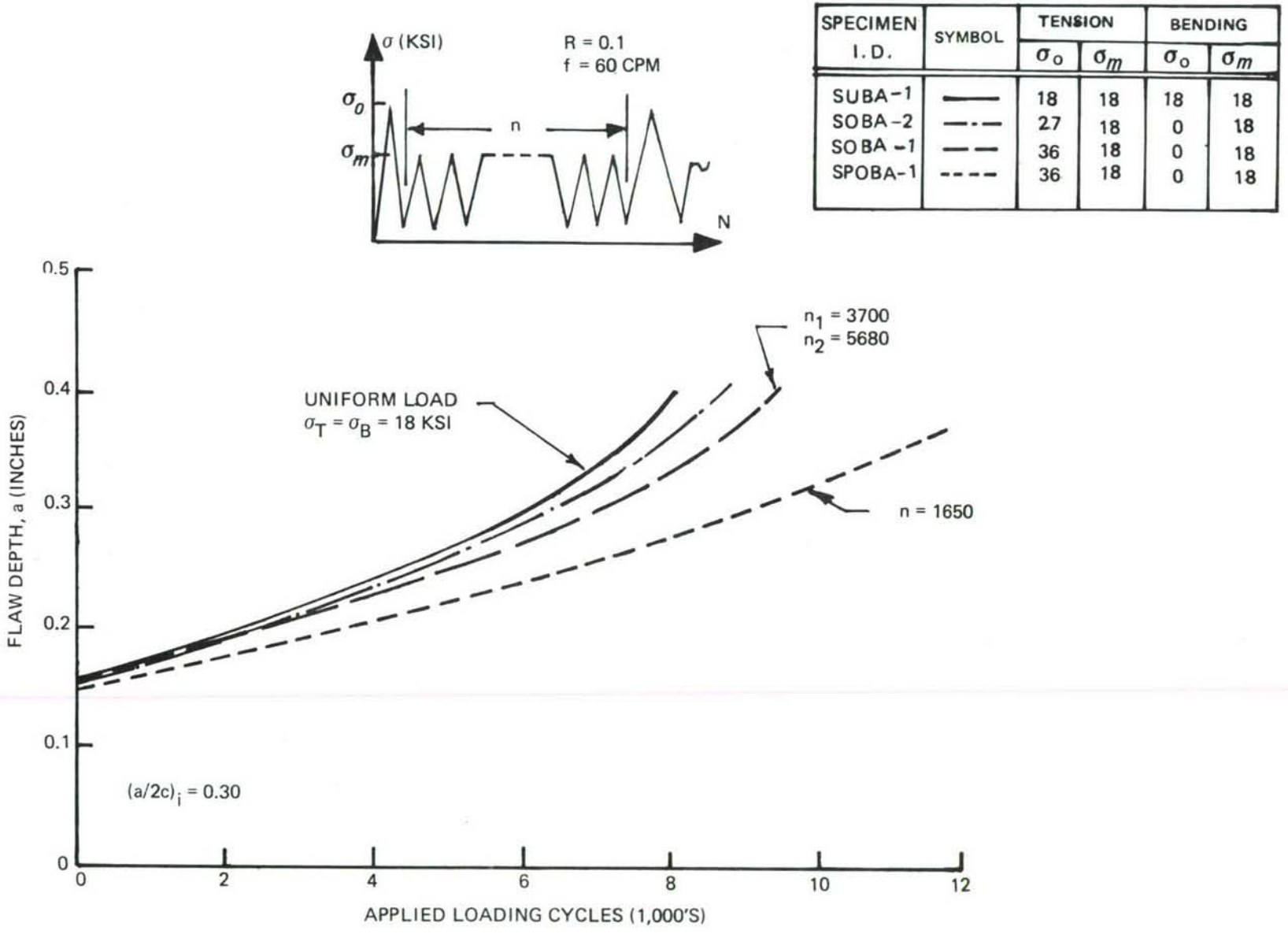


Figure 73: Effect of Periodic Overloads on Fatigue Crack Propagation of Surface Flaws in 2219-T851 Aluminum Alloy Plate Subjected to Combined Bending and Tension Loading

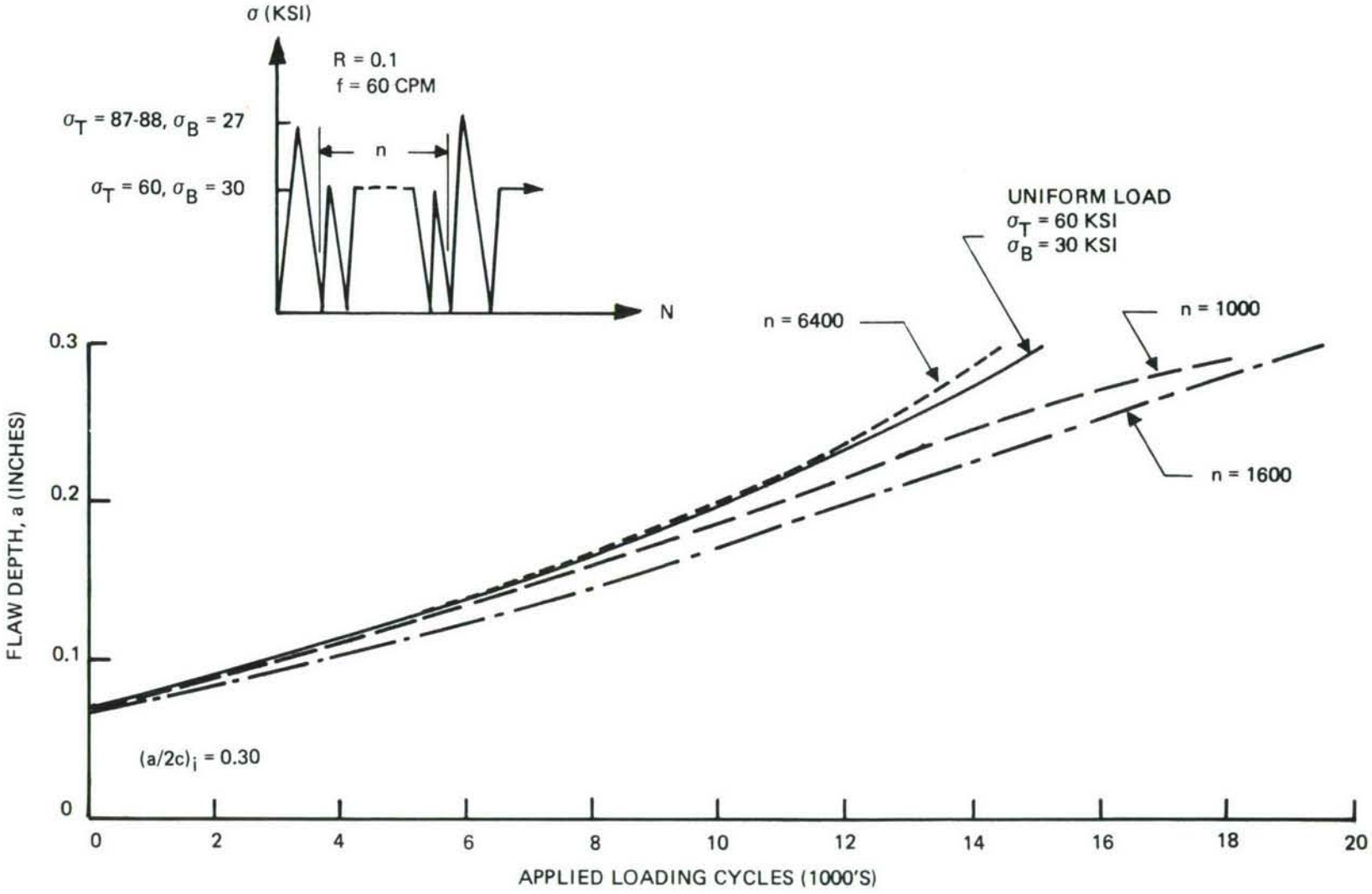


Figure 74: Effect of Periodic Overloads on Fatigue Crack Propagation of Surface Flaws in 9Ni-4Co-0.2C Steel Plate Subjected to Combined Bending and Tension Loading

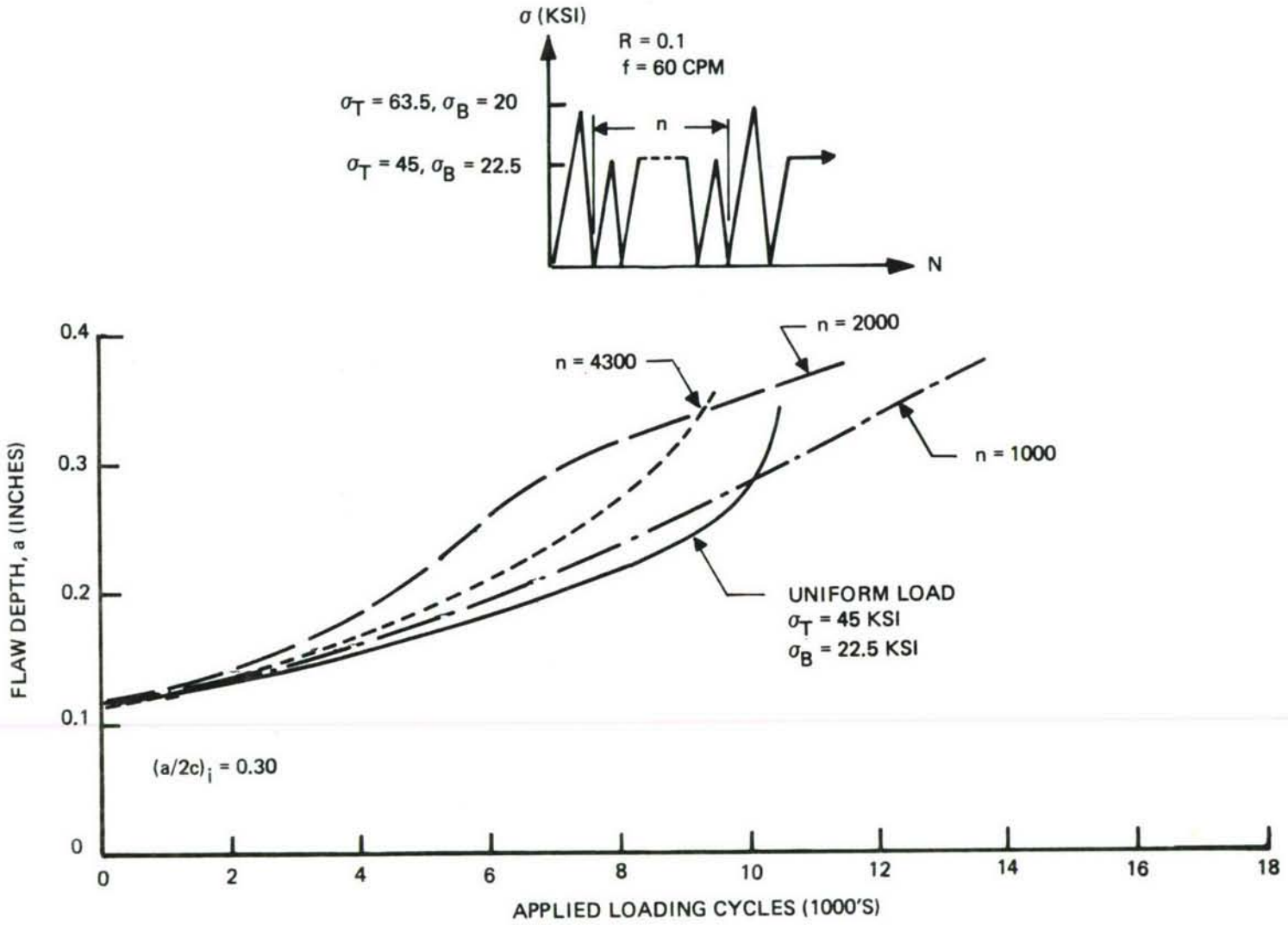


Figure 75: Effect of Periodic Overloads on Fatigue Crack Propagation of Surface Flaws in 6Al-4V (Beta-Annealed) Titanium Plate Subjected to Combined Bending and Tension Loading

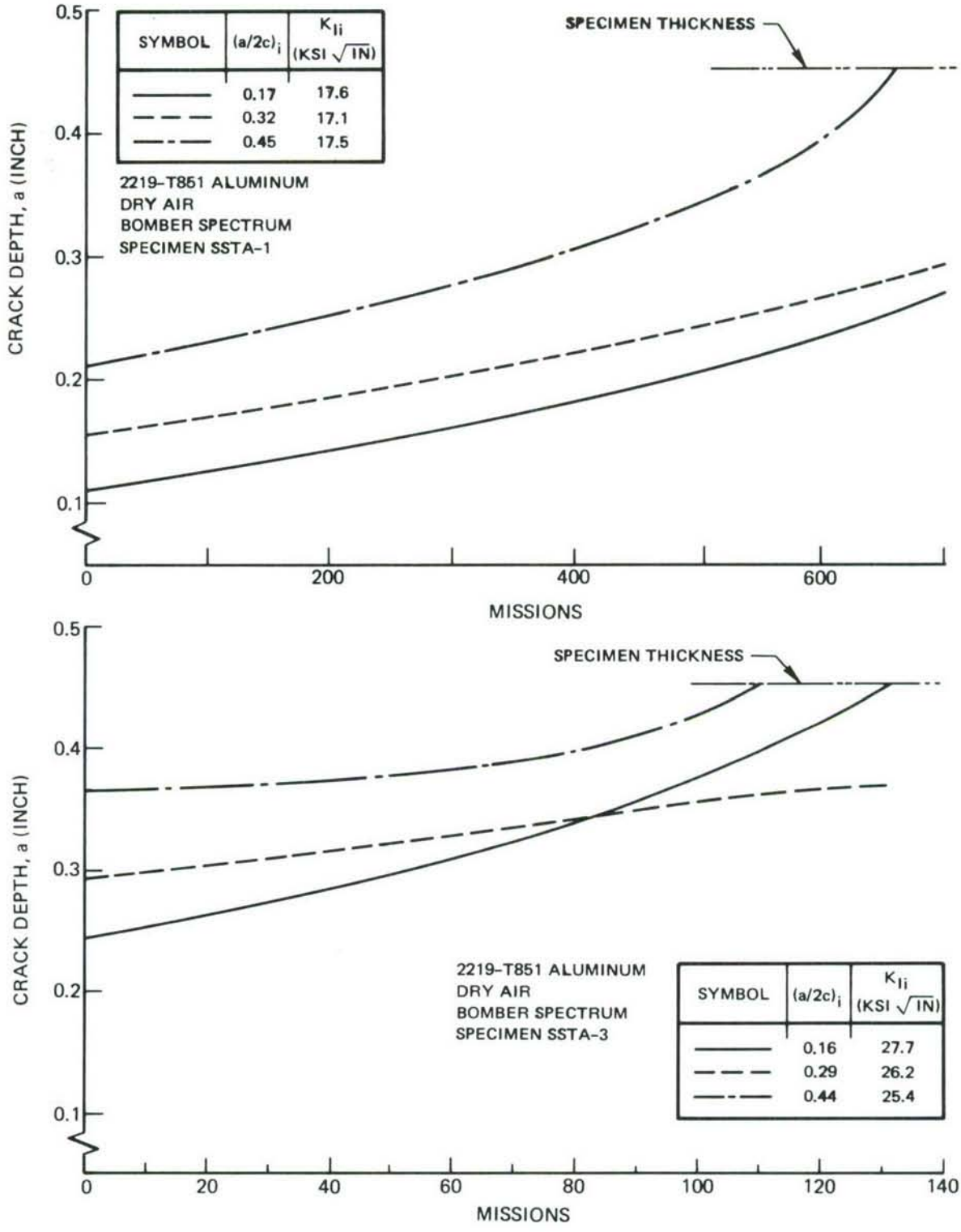


Figure 76: Crack Depth Growth Vs. Missions for Surface Flaws in 2219-T851 Aluminum Alloy Subjected to Bomber Spectrum

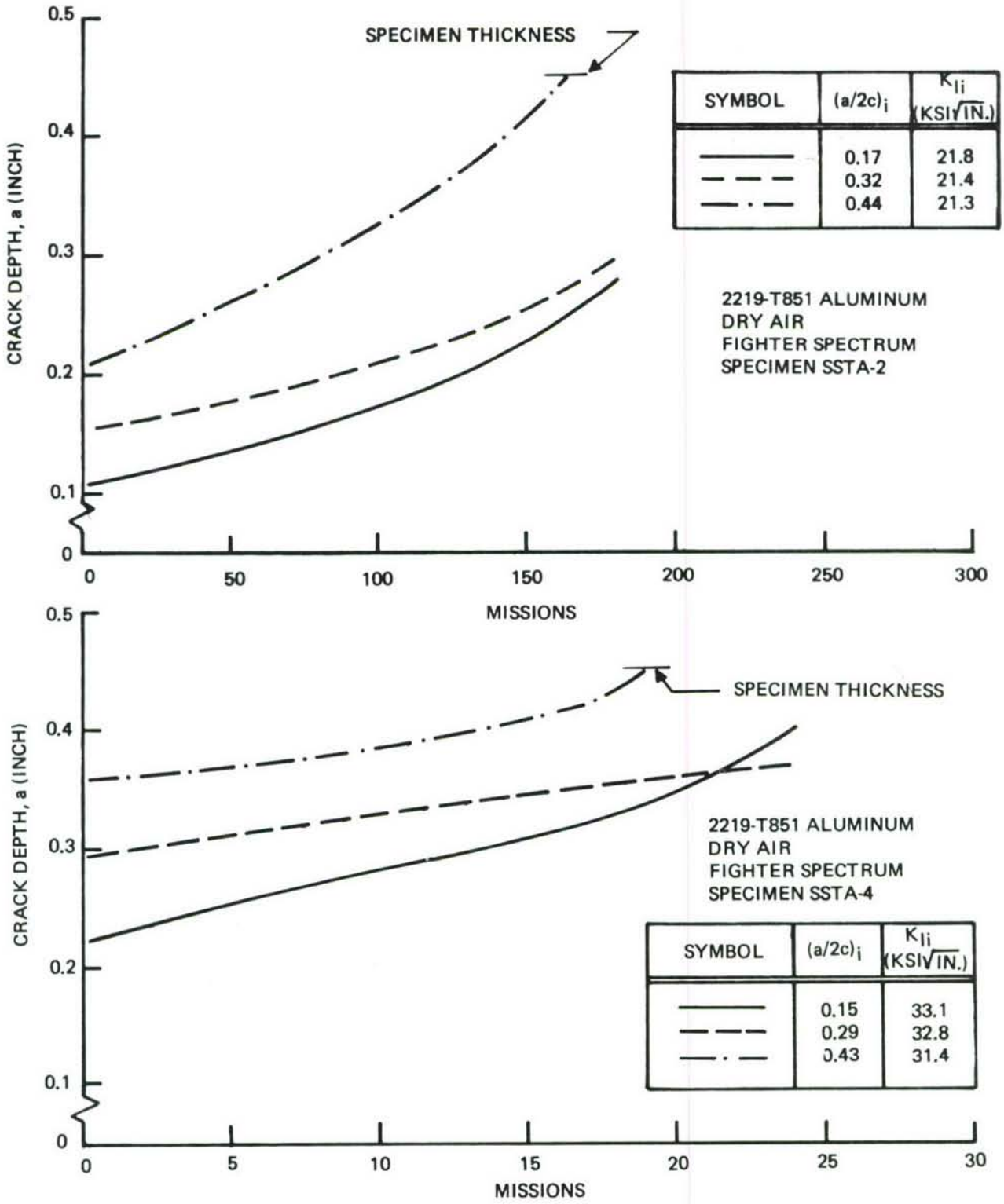


Figure 77: Crack Depth Growth Vs. Missions for Surface Flaws in 2219-T851 Aluminum Alloy Subjected to Fighter Spectrum

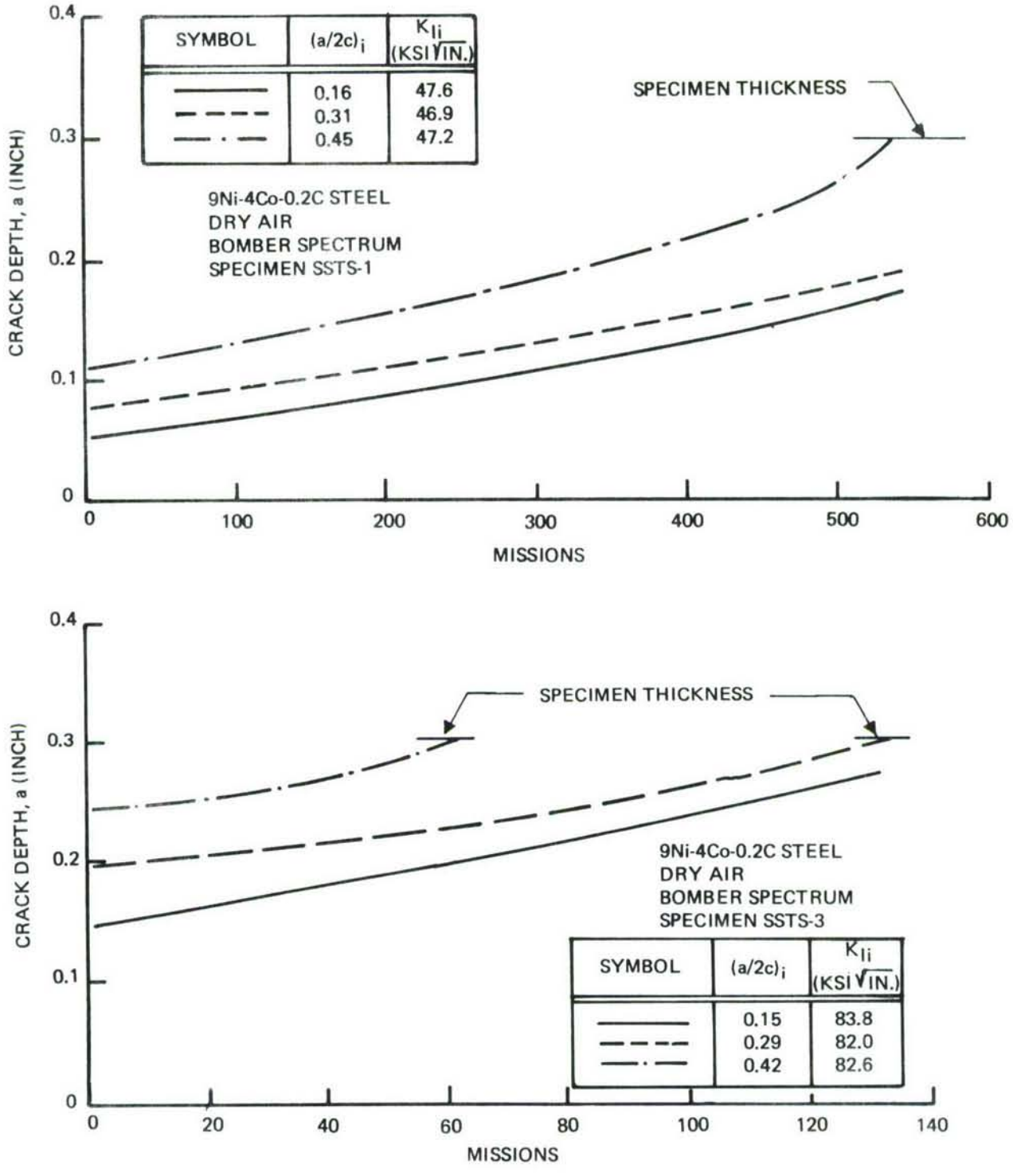


Figure 78: Crack Depth Growth Vs. Missions for Surface Flaws in 9Ni-4Co-0.2C Steel Alloy Subjected to Bomber Spectrum

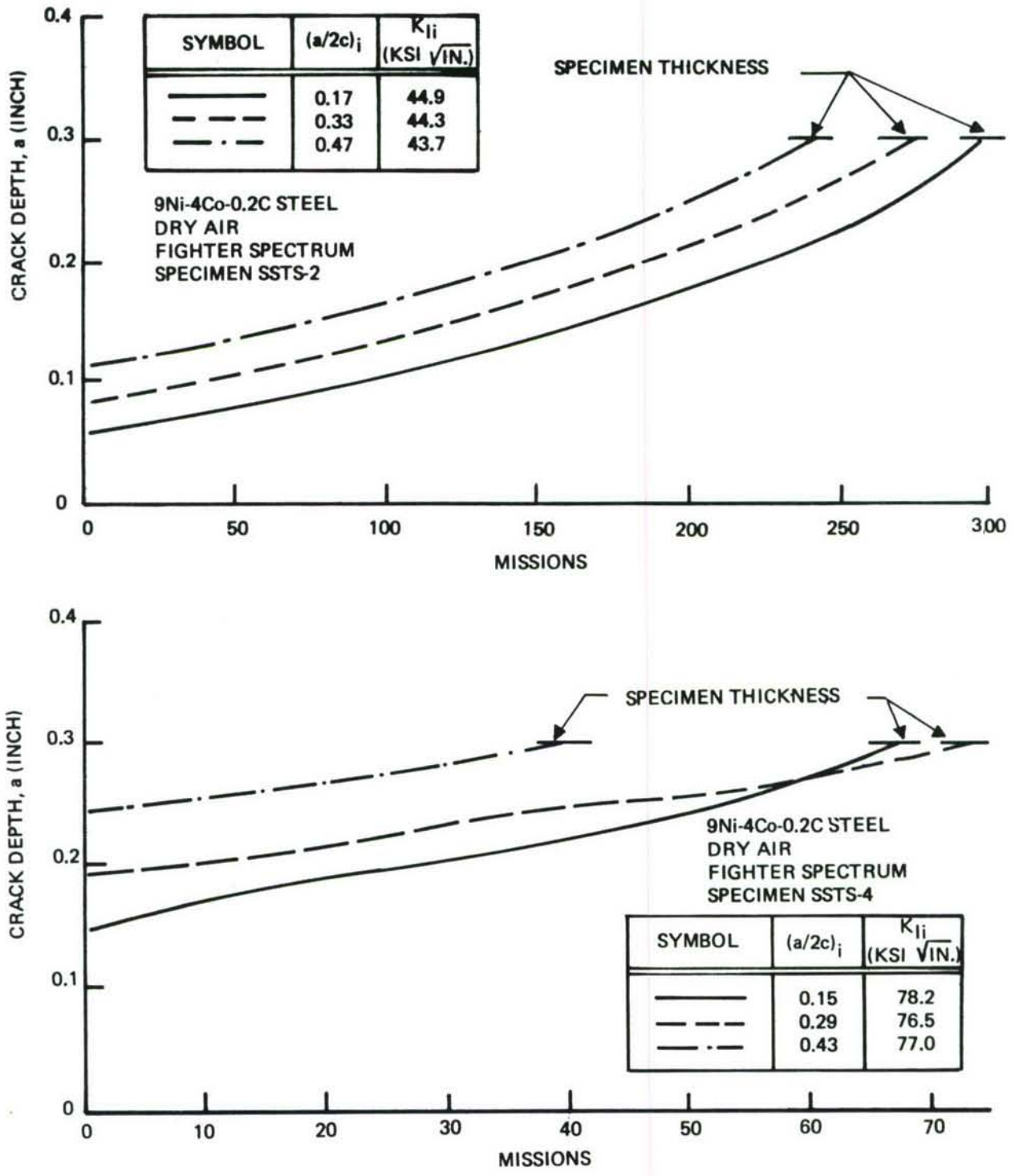


Figure 79: Crack Depth Growth Vs. Missions for Surface Flaws in 9Ni-4Co-0.2C Steel Alloy Subjected to Fighter Spectrum

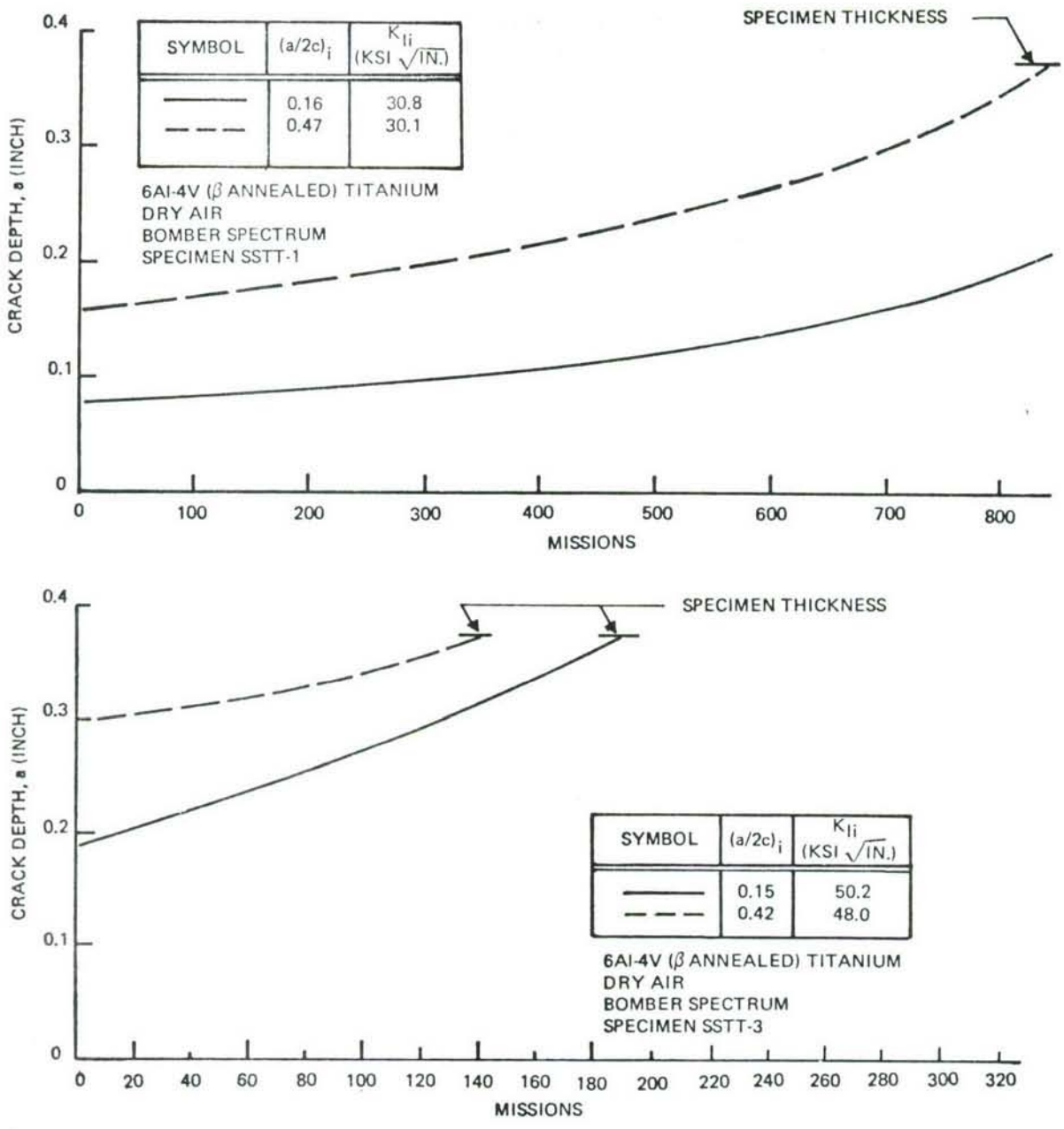


Figure 80: Crack Depth Growth Vs. Missions for Surface Flaws in 6AI-4V (Beta-Annealed) Titanium Alloy Subjected to Bomber Spectrum

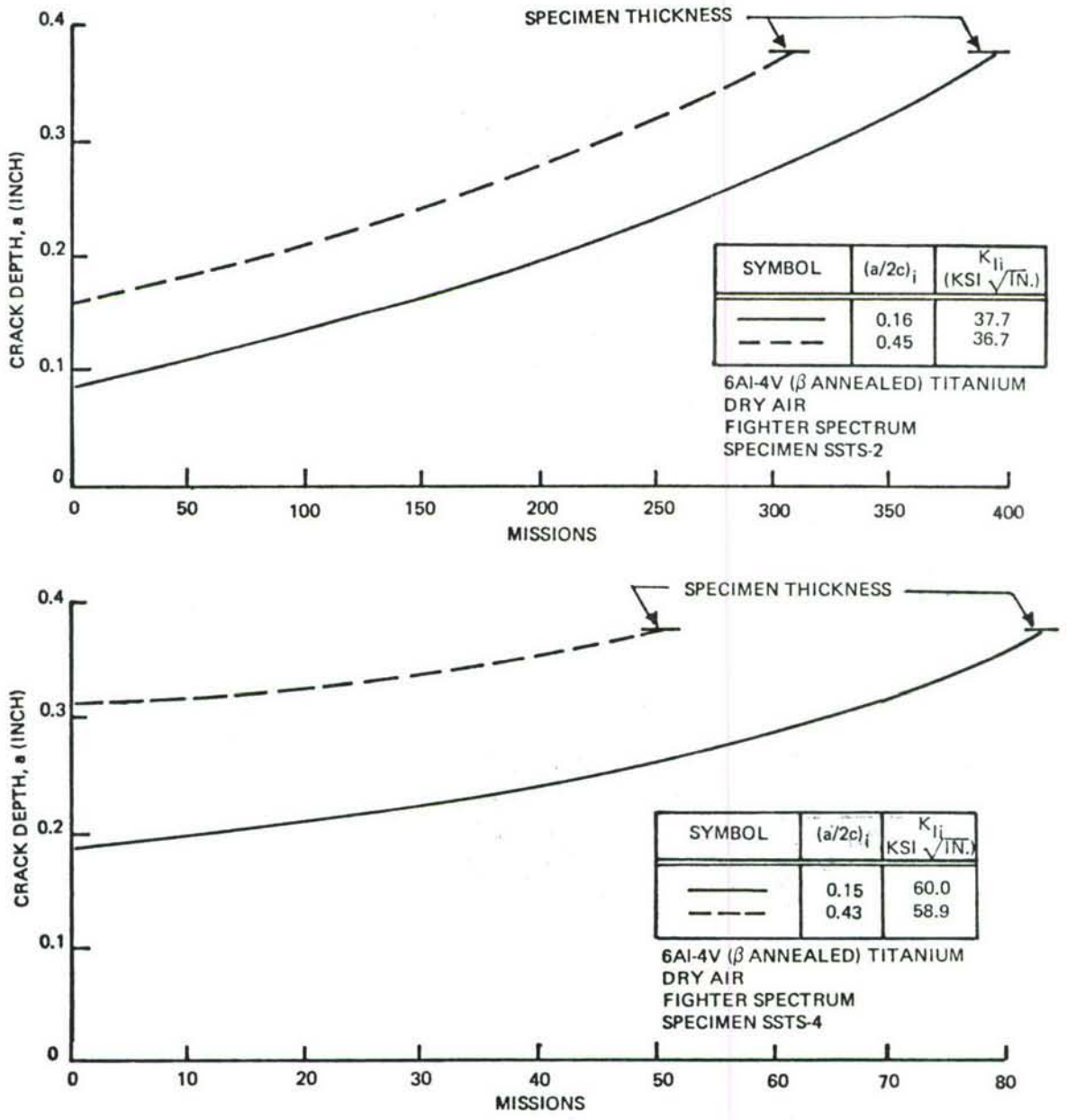


Figure 81: Crack Depth Growth Vs. Missions for Surface Flaws in 6Al-4V (Beta-Annealed) Titanium Alloy Subjected to Fighter Spectrum

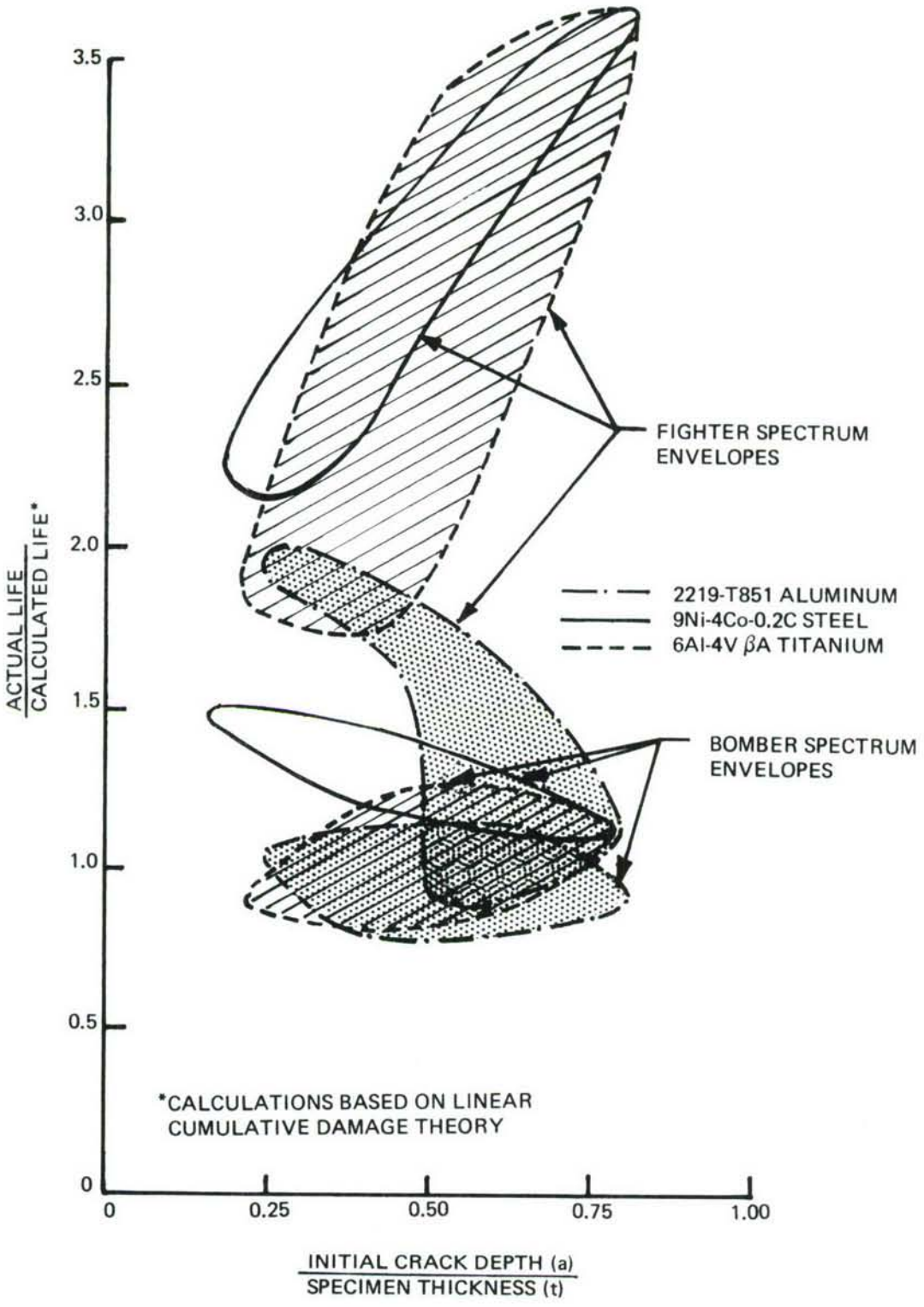
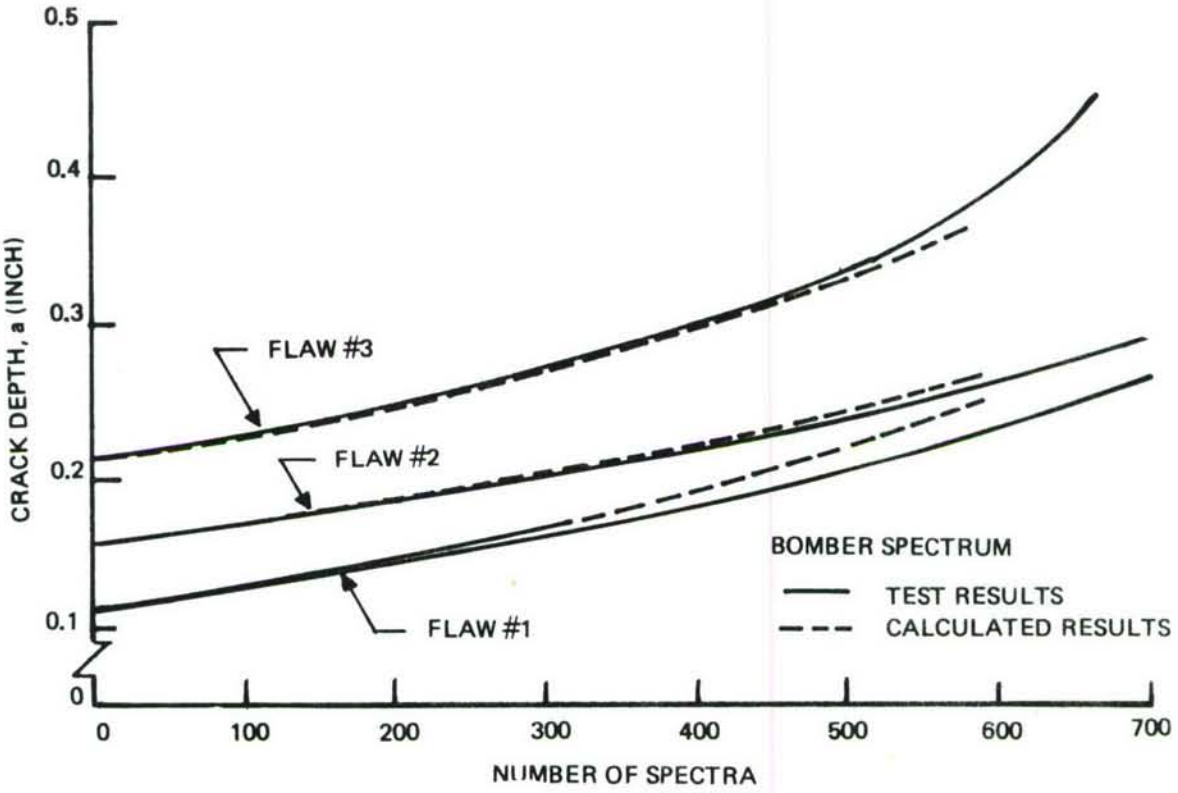
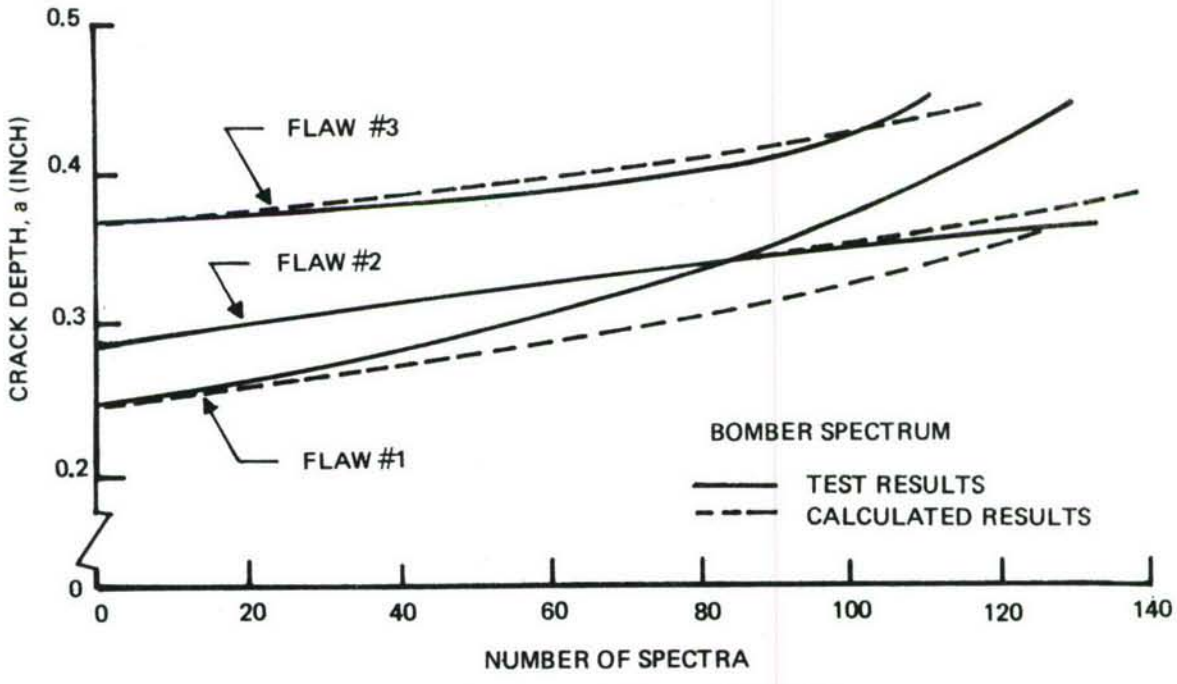


Figure 82: Comparison of Actual and Predicted Life for Spectrum Loaded Surface Flaw Specimens

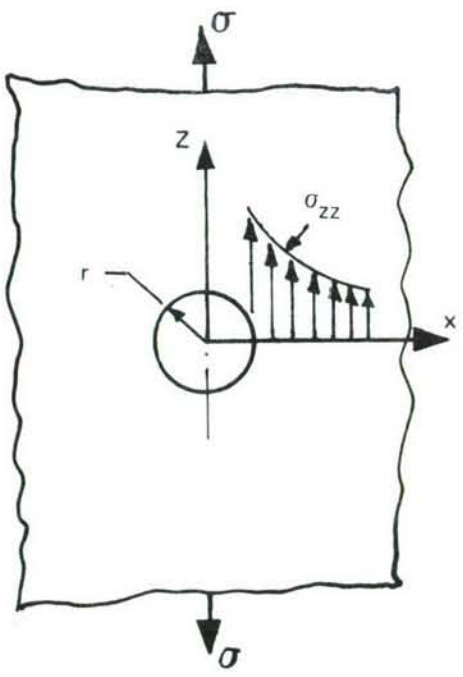


(a) SHALLOW FLAW SPECIMEN SSTA-1



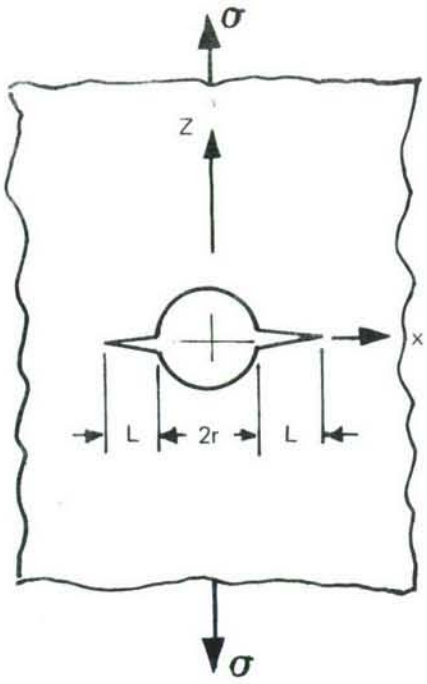
(b) DEEP FLAW SPECIMEN SSTA-3

Figure 83: Comparison of Experimental and Calculated Results for 2219-T851 Aluminum Alloy Spectrum Loaded Surface Flaw Specimens

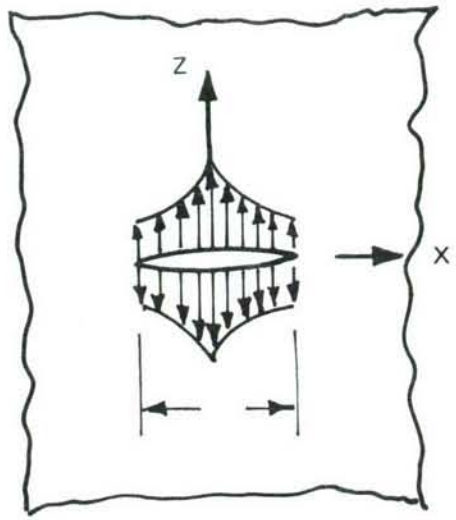


$$\sigma_{zz} = \frac{\sigma}{2}\left[2 + \frac{r^2}{x^2} + 3\frac{r^4}{x^4}\right]$$

(a) STRESS DISTRIBUTION NEAR AN OPEN HOLE IN A PLATE



(b) SYMMETRICAL THRU CRACKS ORIGINATING AT A HOLE IN A PLATE



$$\sigma_{zz}(X, 0) = \frac{\sigma}{2}\left[2 + \left(\frac{r}{r+X}\right)^2 + 3\left(\frac{r}{r+X}\right)^4\right] 0 \leq X \leq L$$

$$\sigma_{zz}(X, 0) = \frac{\sigma}{2}\left[2 + \left(\frac{r}{r-X}\right)^2 + 3\left(\frac{r}{r-X}\right)^4\right] - L \leq X \leq 0$$

$X = (x - r)$

(c) EQUIVALENT PROBLEM FOR b

Figure 84: Equivalent Problem for Determining Stress Intensity Factors for Two Symmetrical Thru Cracks Originating at an Open Hole

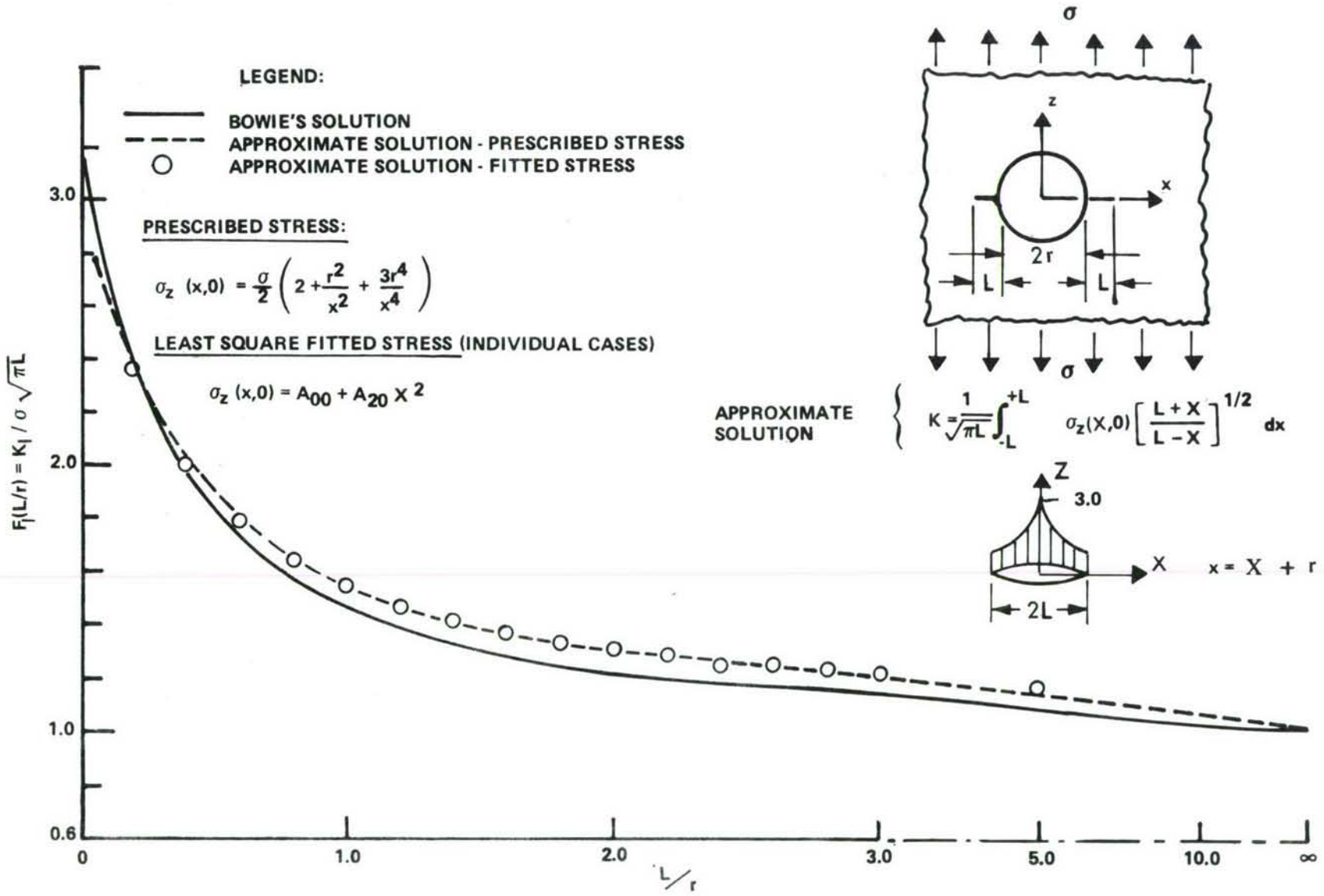


Figure 85: Stress Intensity Factors for Two Through-the-Thickness Symmetrical Cracks Originating at a Hole in a Plate Subjected to Tension

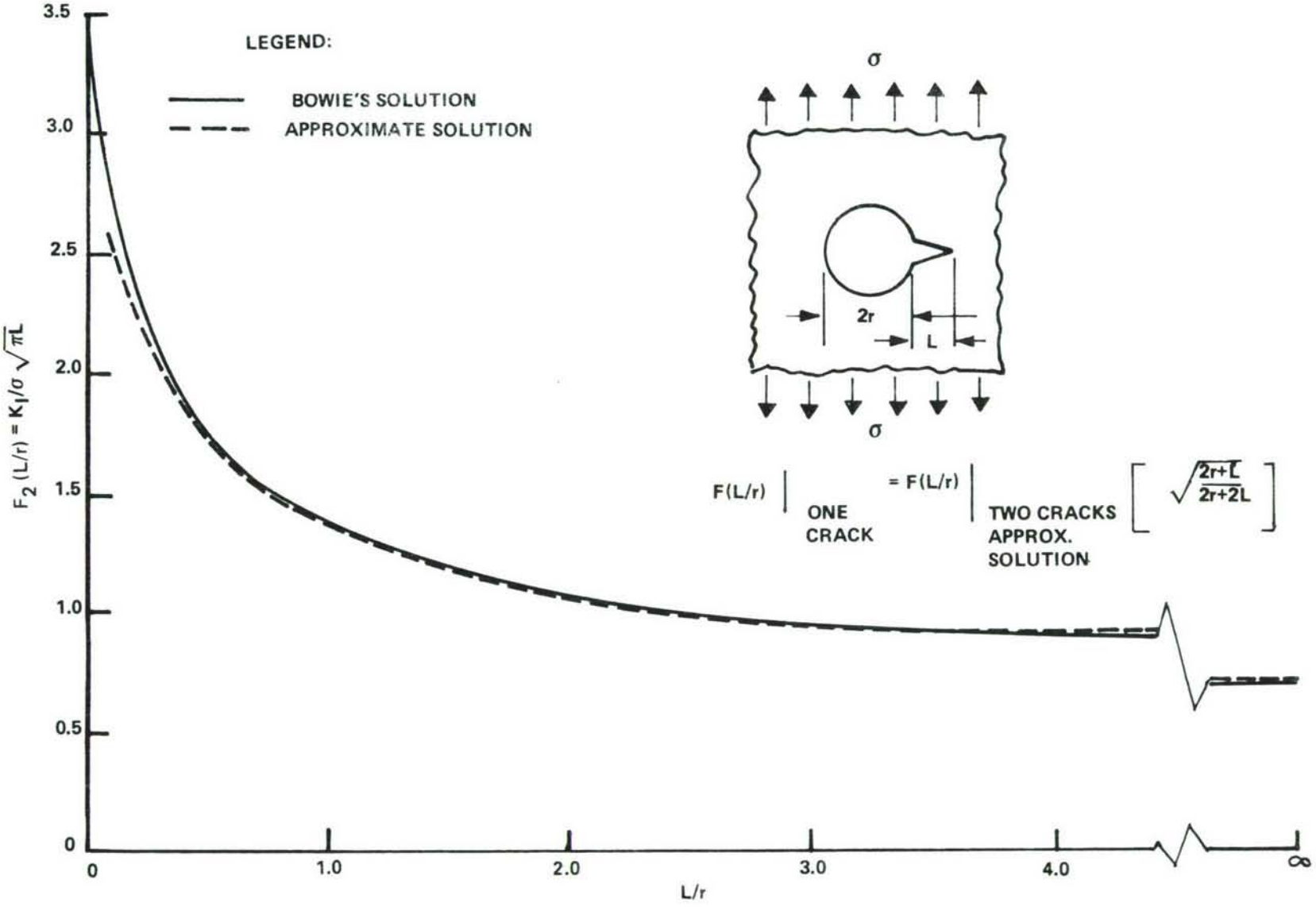


Figure 86: Stress Intensity Factors for One Through-the-Thickness Crack Originating at a Hole in a Plate Subjected to Tension

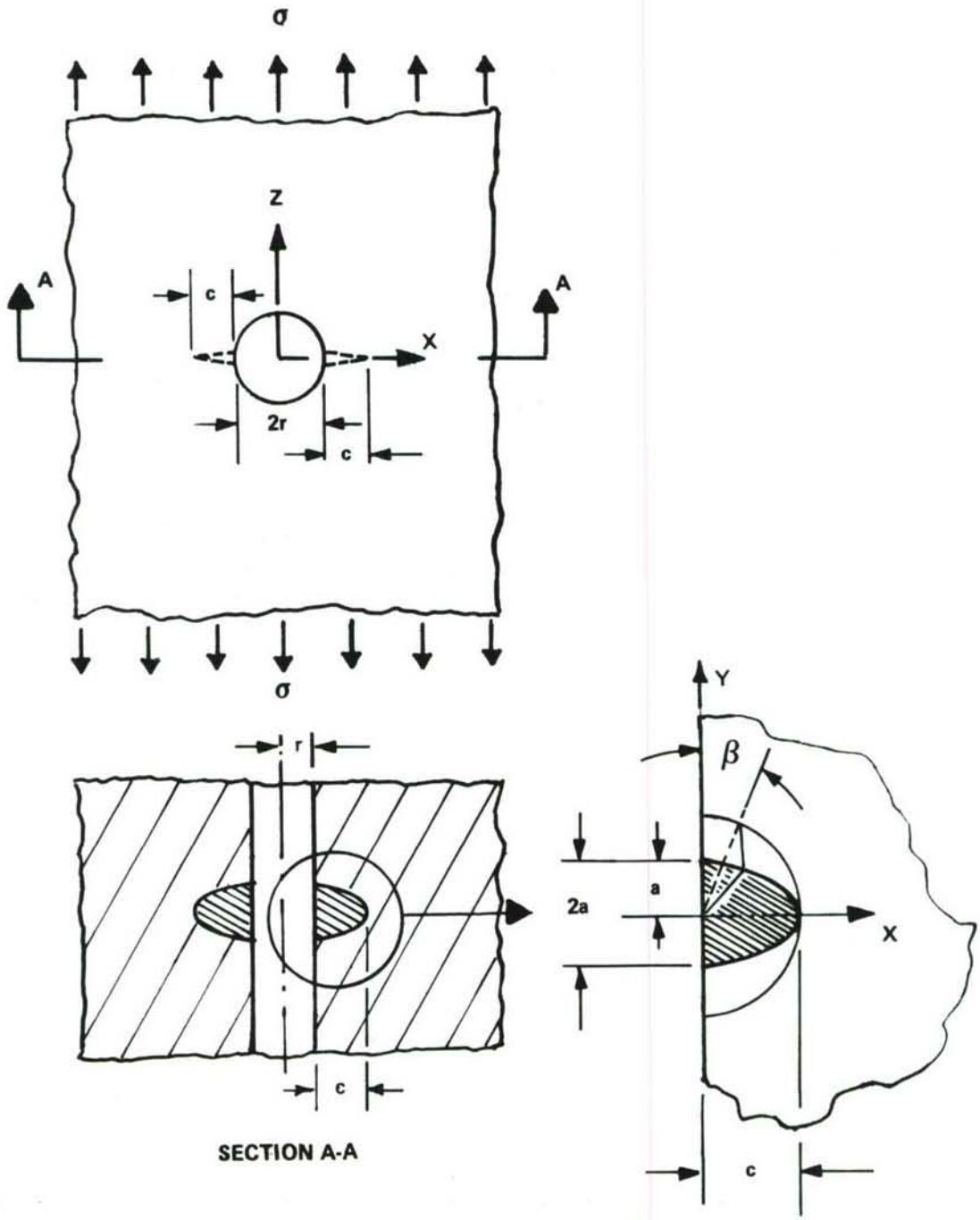


Figure 87: *Two Semi-elliptical Cracks Originating at a Hole in a Thick Plate*

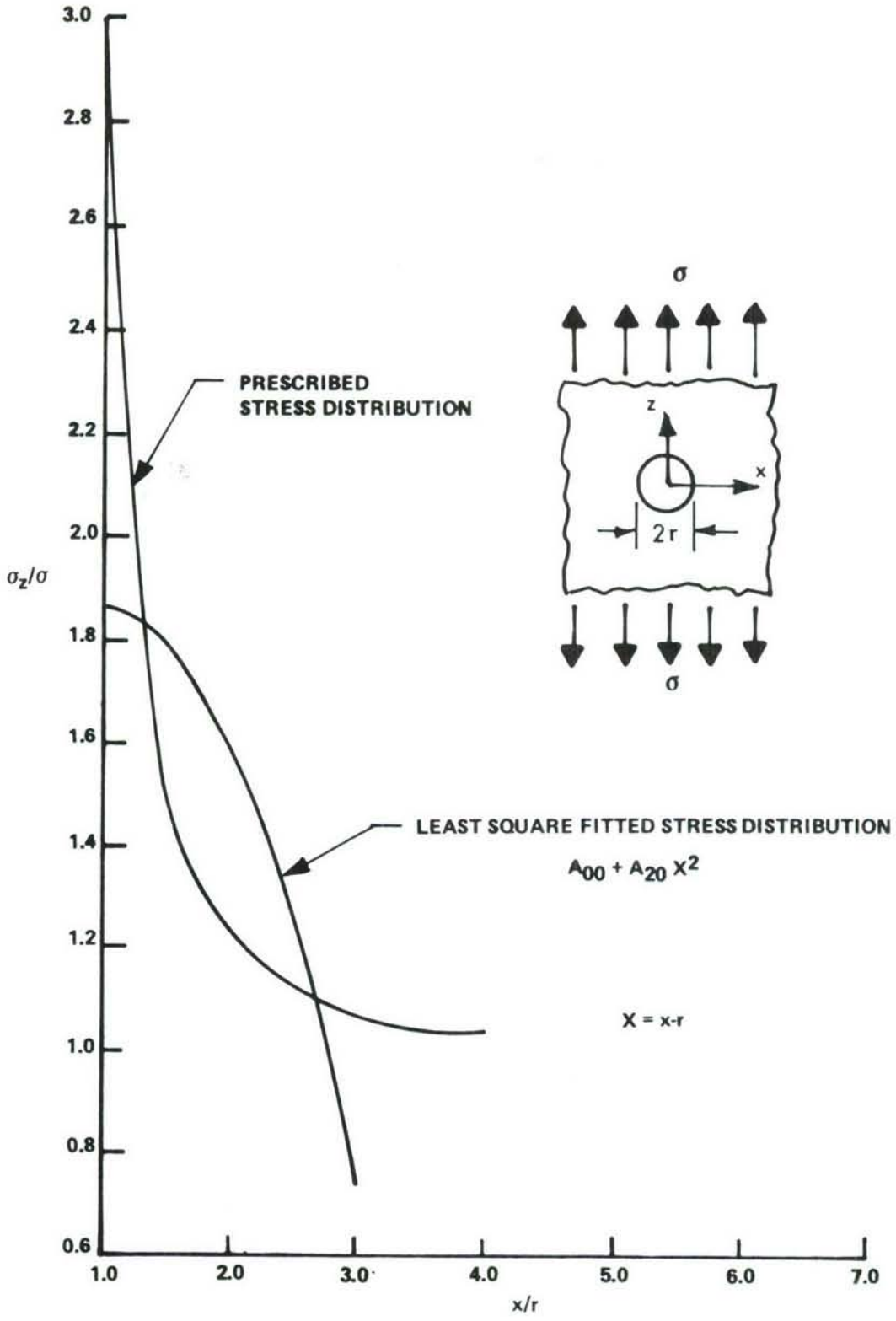


Figure 88: *Stress Distribution Due to a Hole in a Plate in Tension*

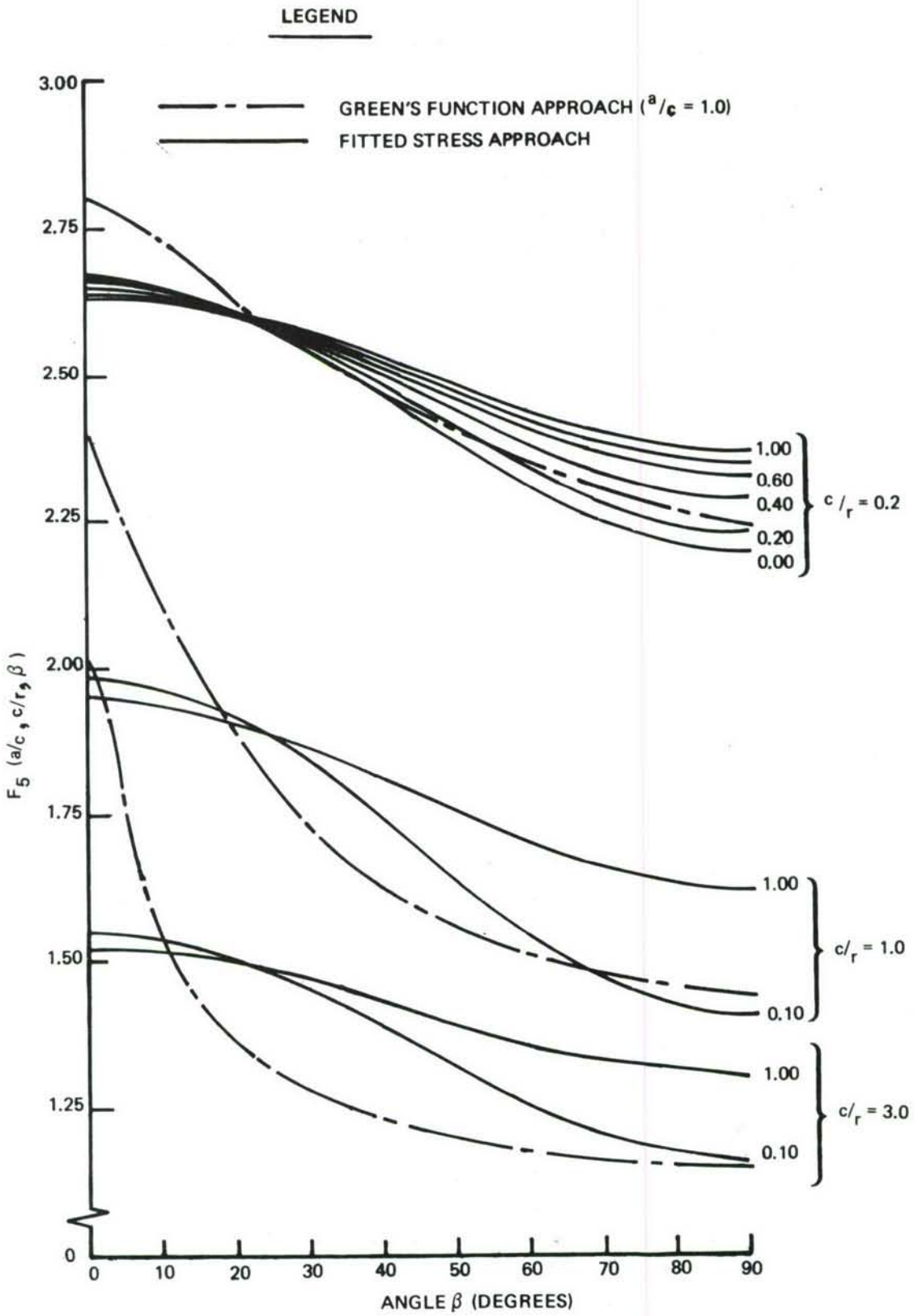


Figure 89: Comparison of Nondimensionalized Stress Intensity Factors Obtained from Green's Function and Fitted Stress Approaches

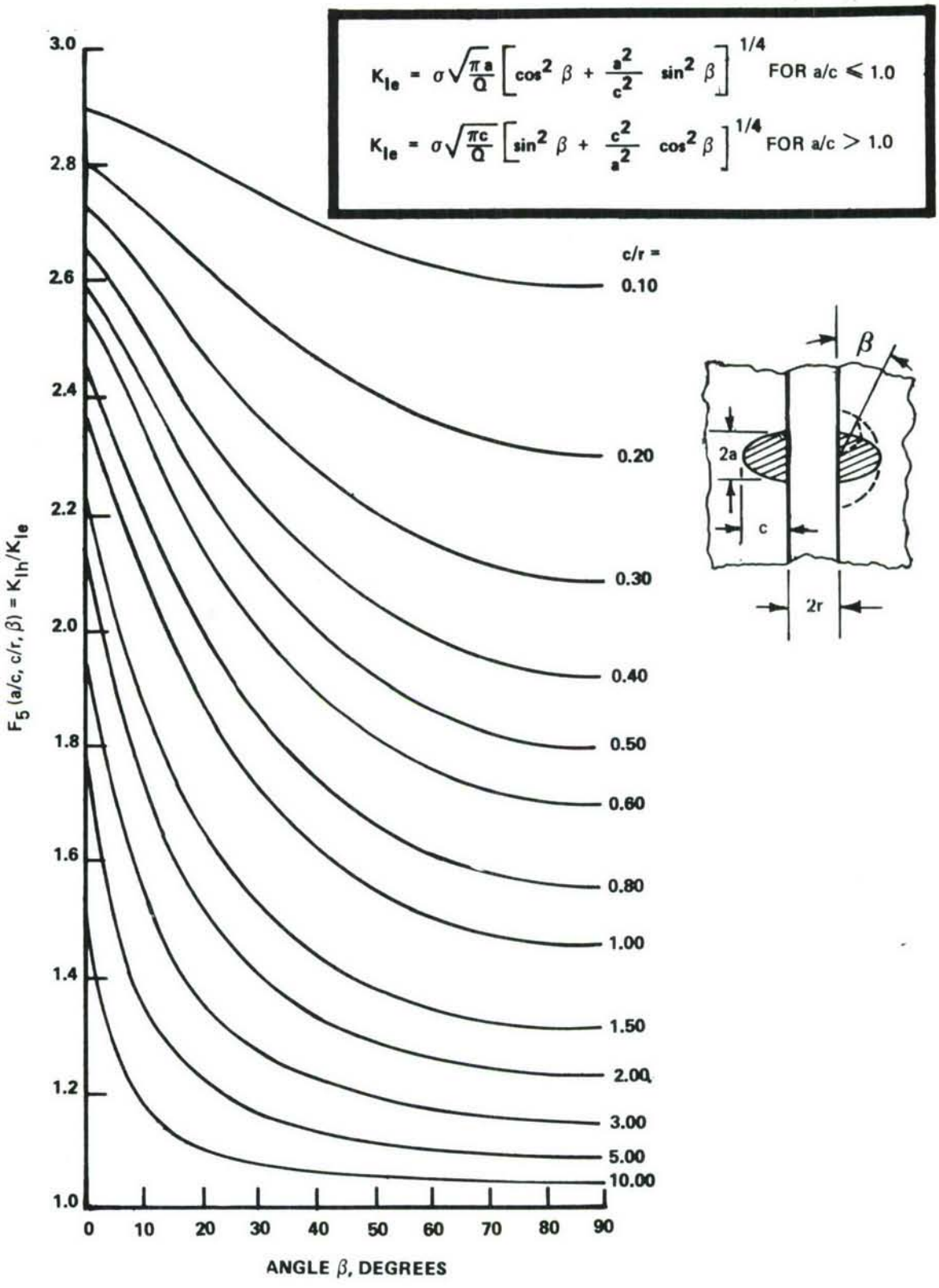


Figure 90: Nondimensionalized Stress Intensity Factors for Two Semi-Elliptical Cracks at a Hole in a Thick Plate (Figure 87)

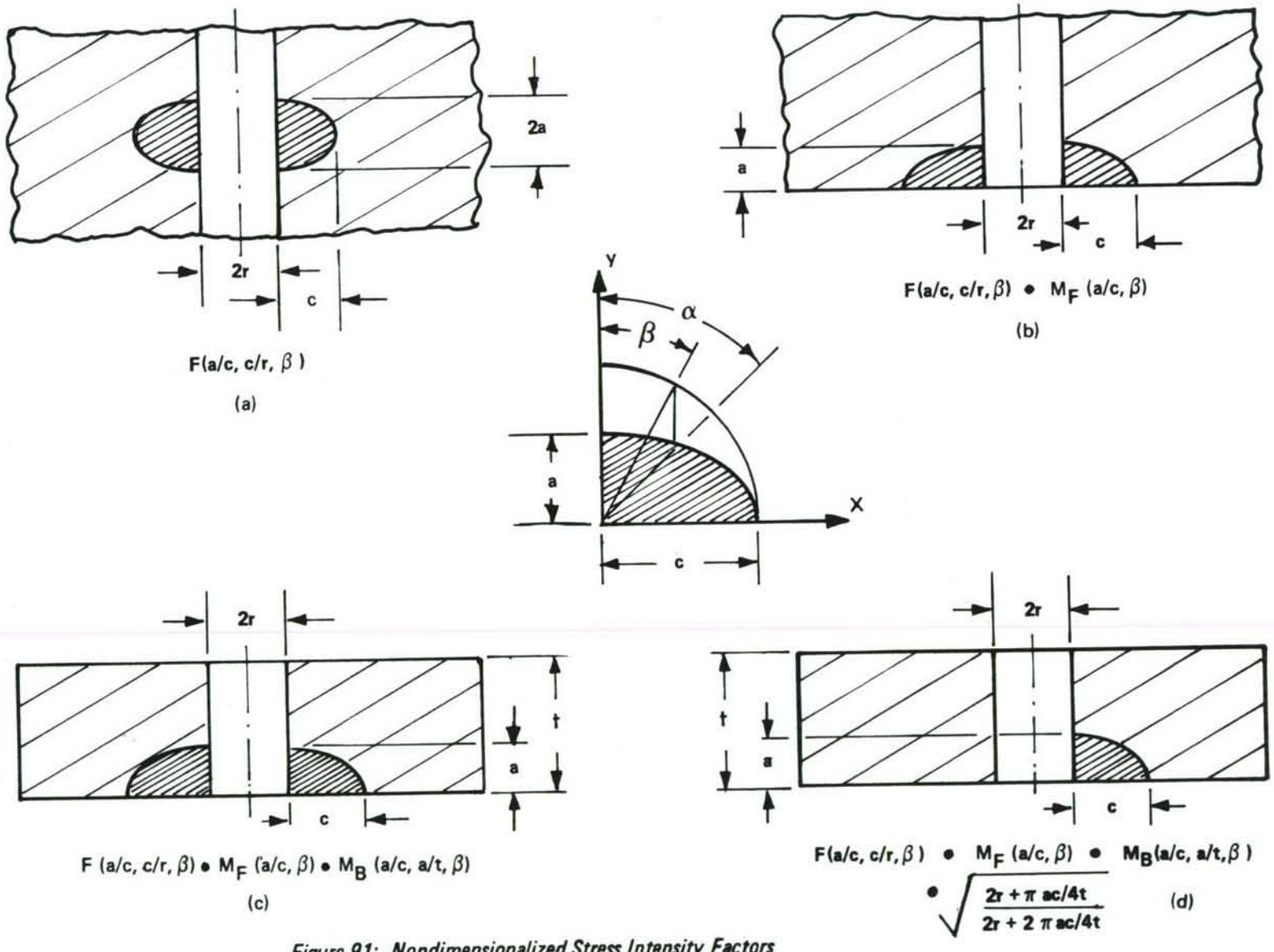


Figure 91: Nondimensionalized Stress Intensity Factors

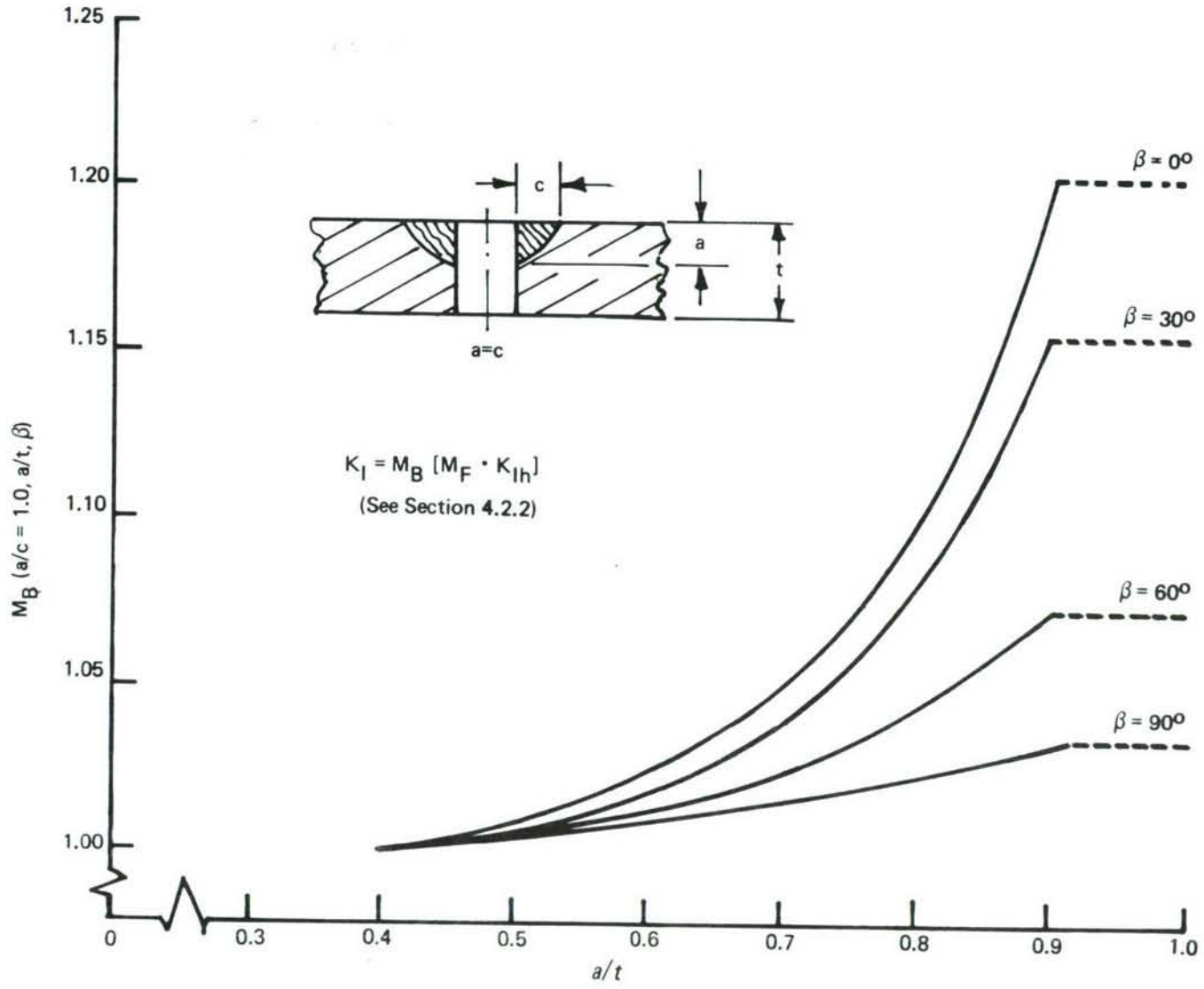


Figure 92: Assumed Back Surface Stress Intensity Magnification Factor for Quarter-Circular Part- Thru Fastener Hole Flaws

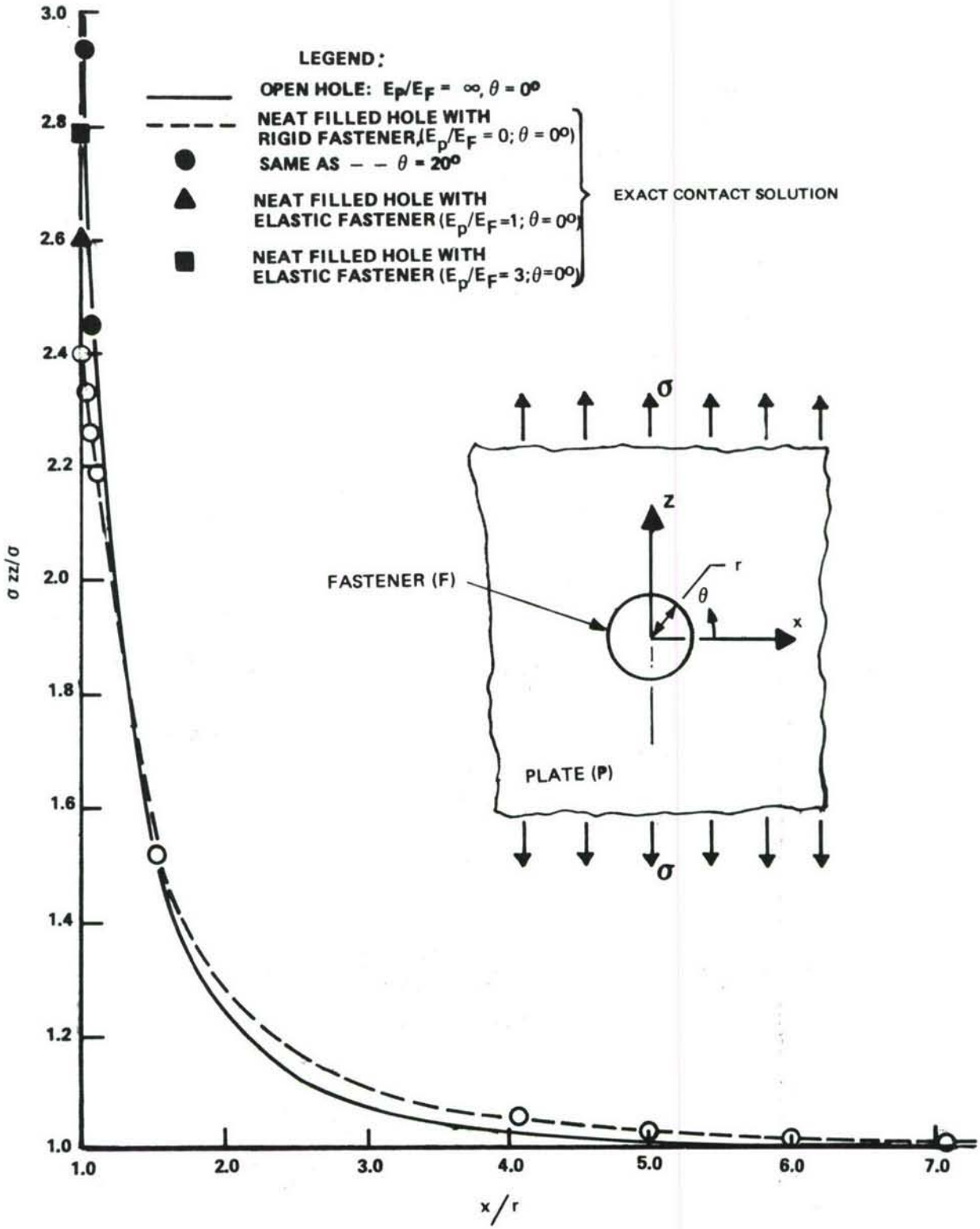


Figure 93: Stress Variation of σ_{ZZ}/σ along X-axis for a Plate Containing a Hole Filled with a Neat Fit Fastener

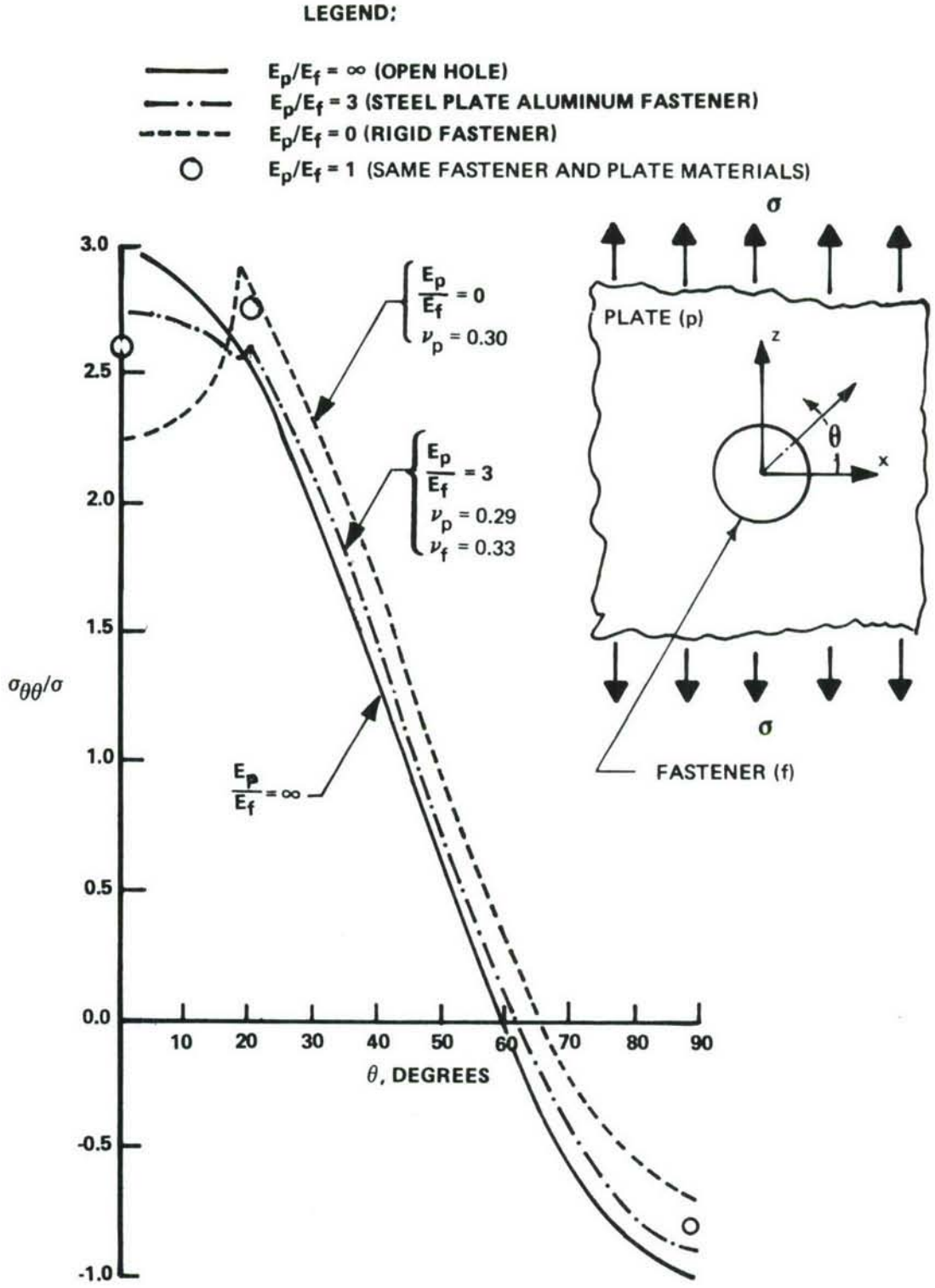


Figure 94: Variation of Circumferential Stress ($\sigma_{\theta\theta}/\sigma$) Around Periphery of a Hole Filled with a Neat Fit Fastener

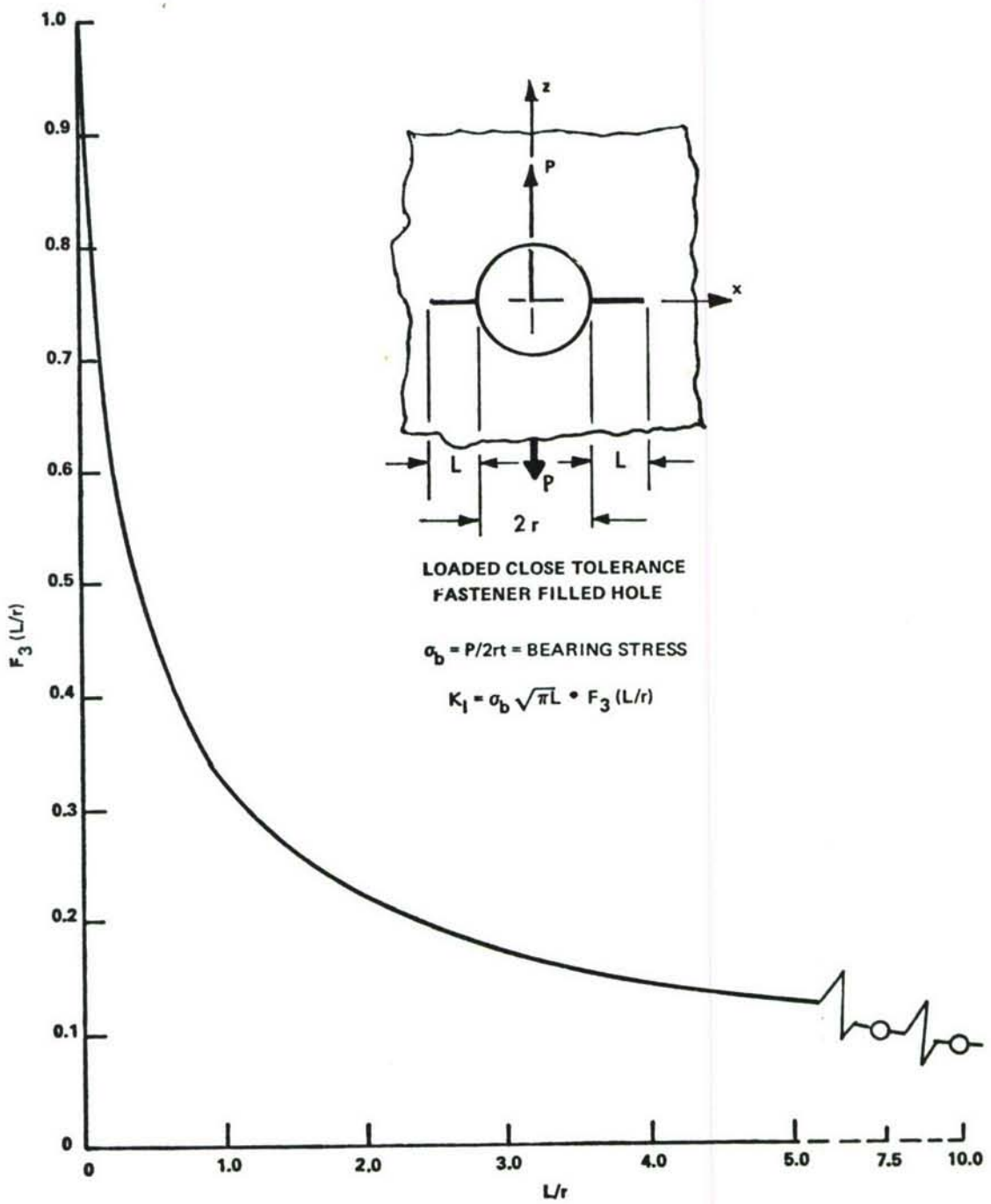


Figure 95: Nondimensionalized Stress Intensity Factors for Two Through Cracks Originating From a Loaded Close Tolerance Fastener

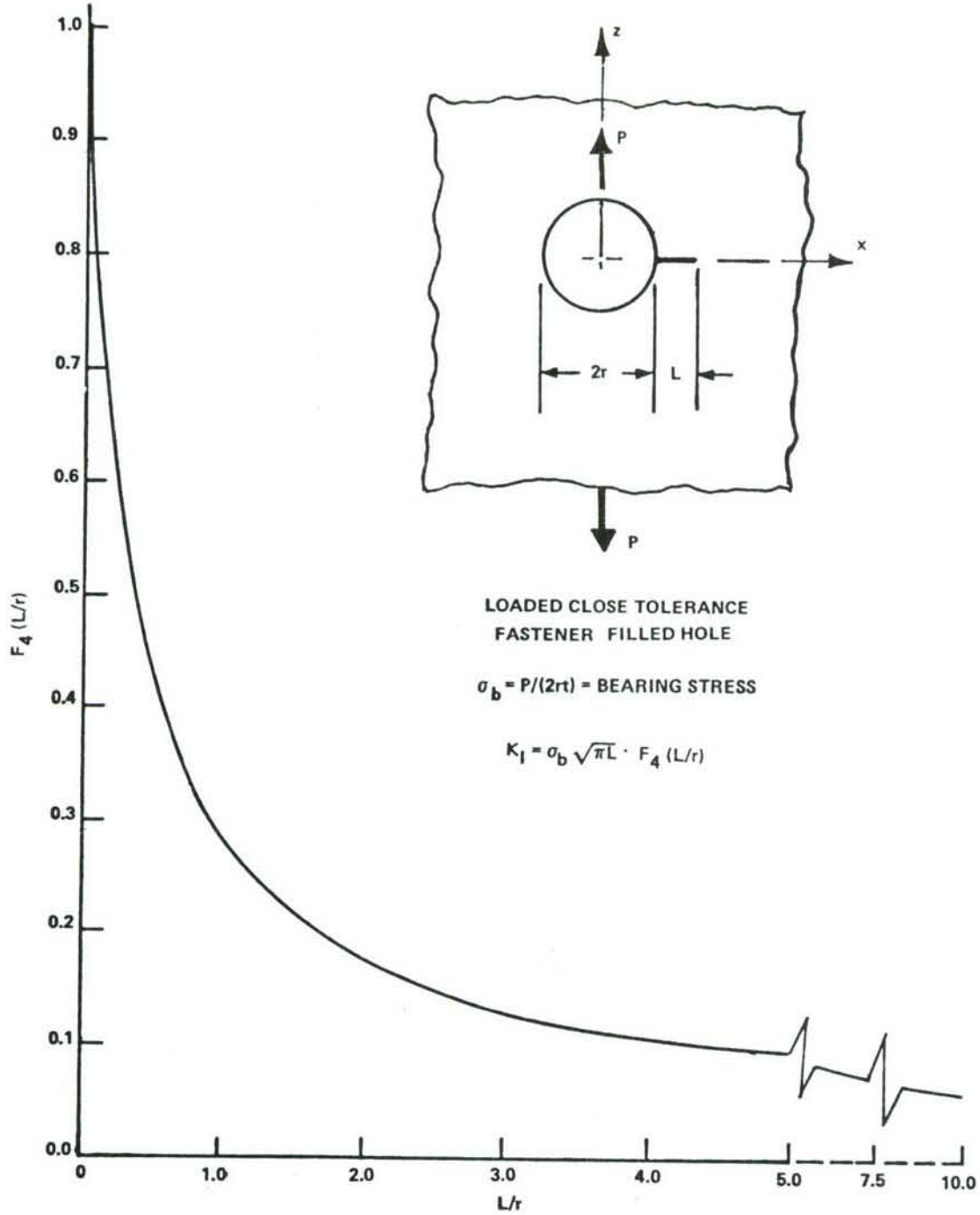


Figure 96: Nondimensionalized Stress Intensity Factors for One Through Crack Originating from a Loaded Close Tolerance Fastener

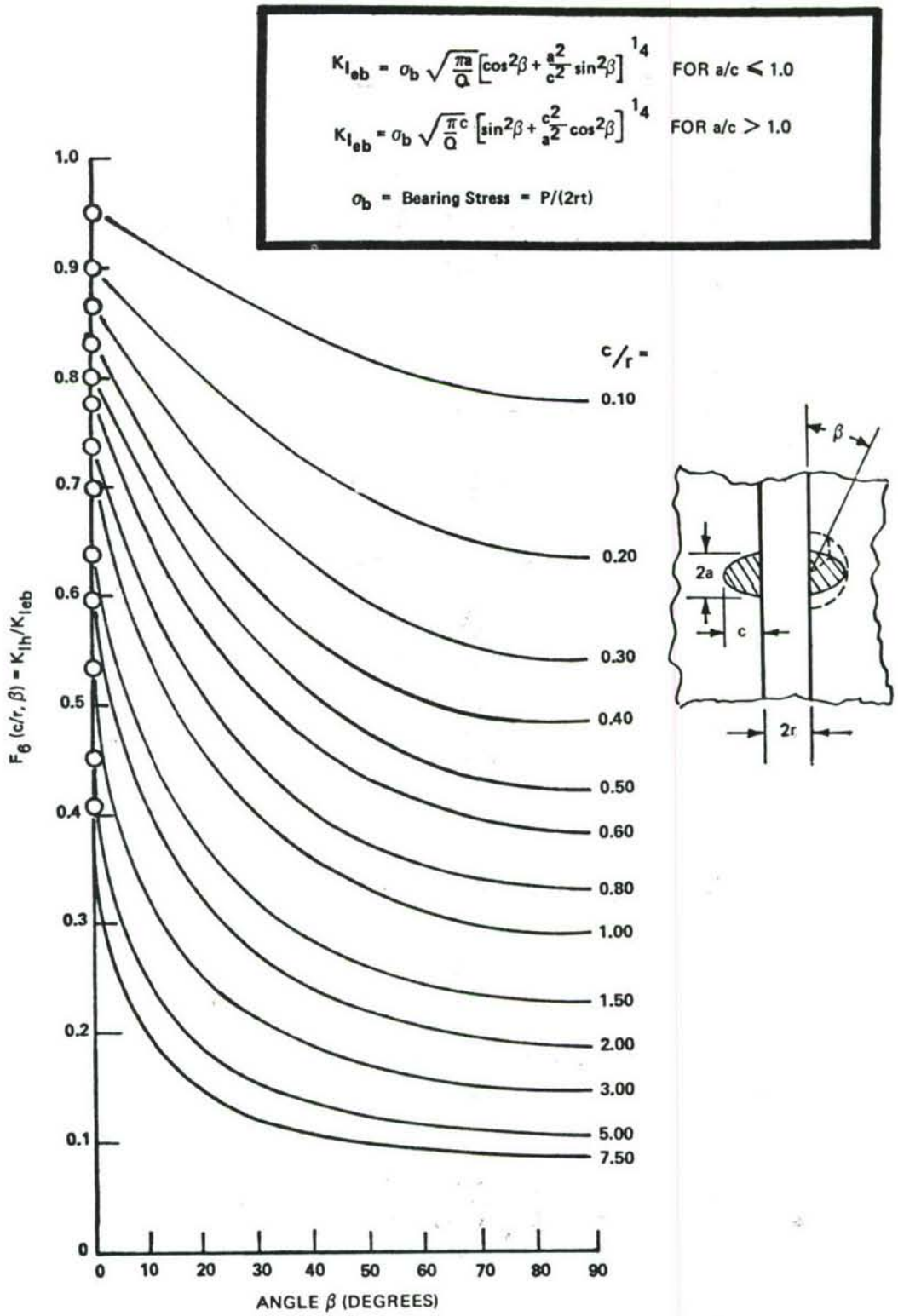


Figure 97: Nondimensionalized Stress Intensity Factors for Two Semi-Elliptical Cracks Originating from a Loaded Close Tolerance Fastener in a Thick Plate

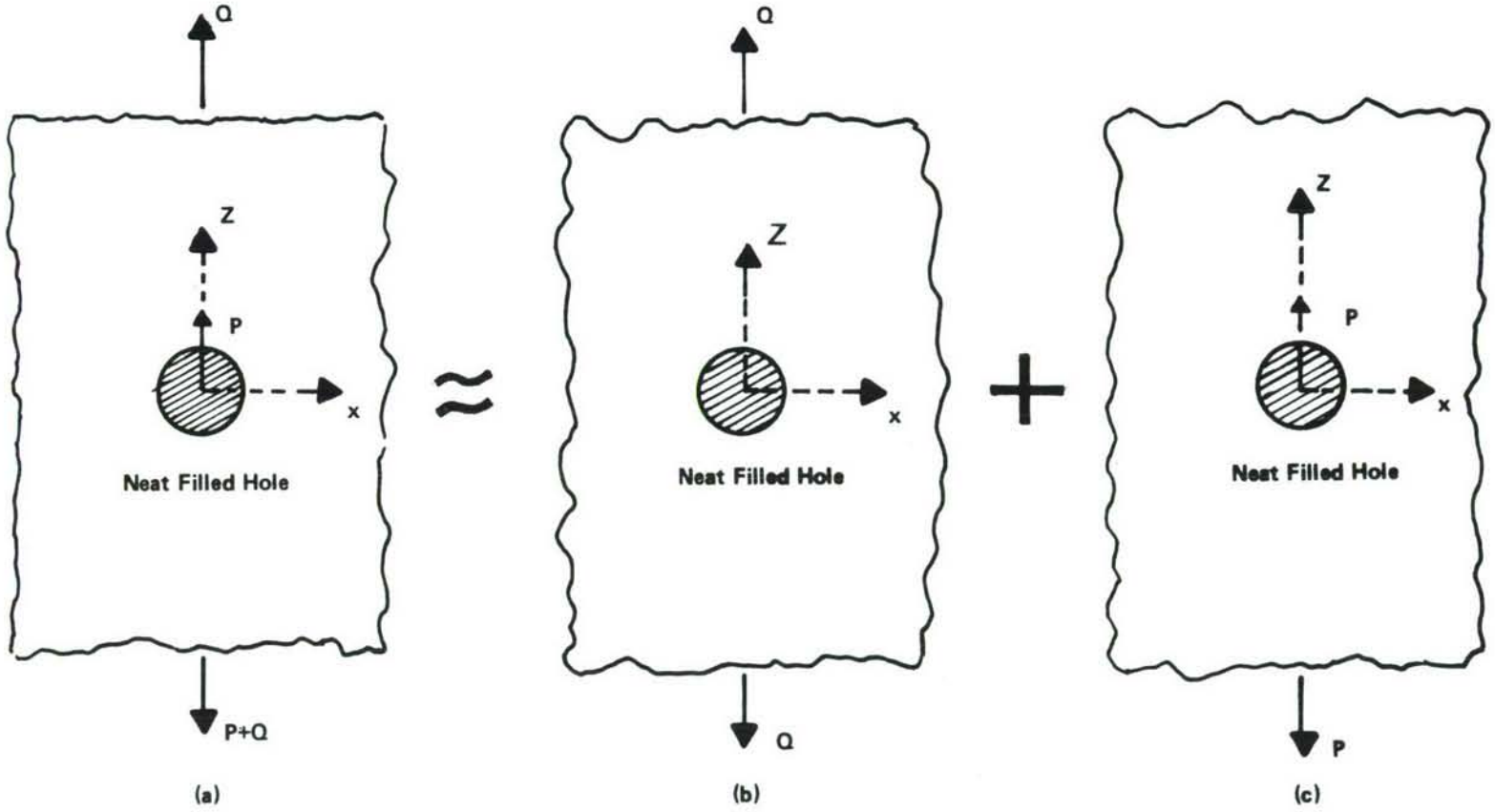


Figure 98: *Plate with Neat Filled Hole Subjected to Remote Loading and Load Transfer at Fastener*

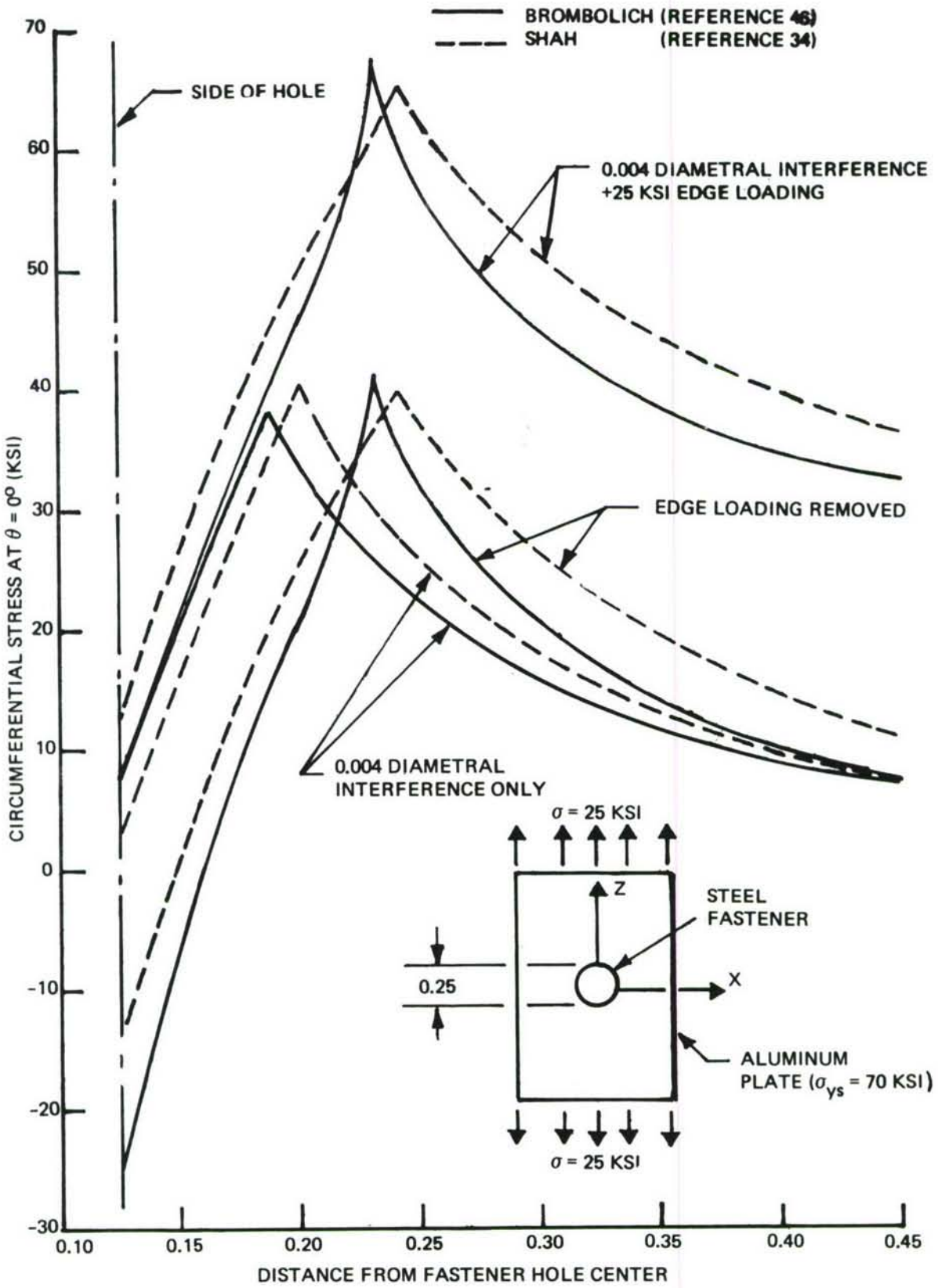


Figure 99: Stress σ_{zz} Along X-axis in an Aluminum Plate (σ_{ys} = 70 ksi) with a Steel Interference Fit Fastener Caused by Interference, Edge Loading, and Unloading

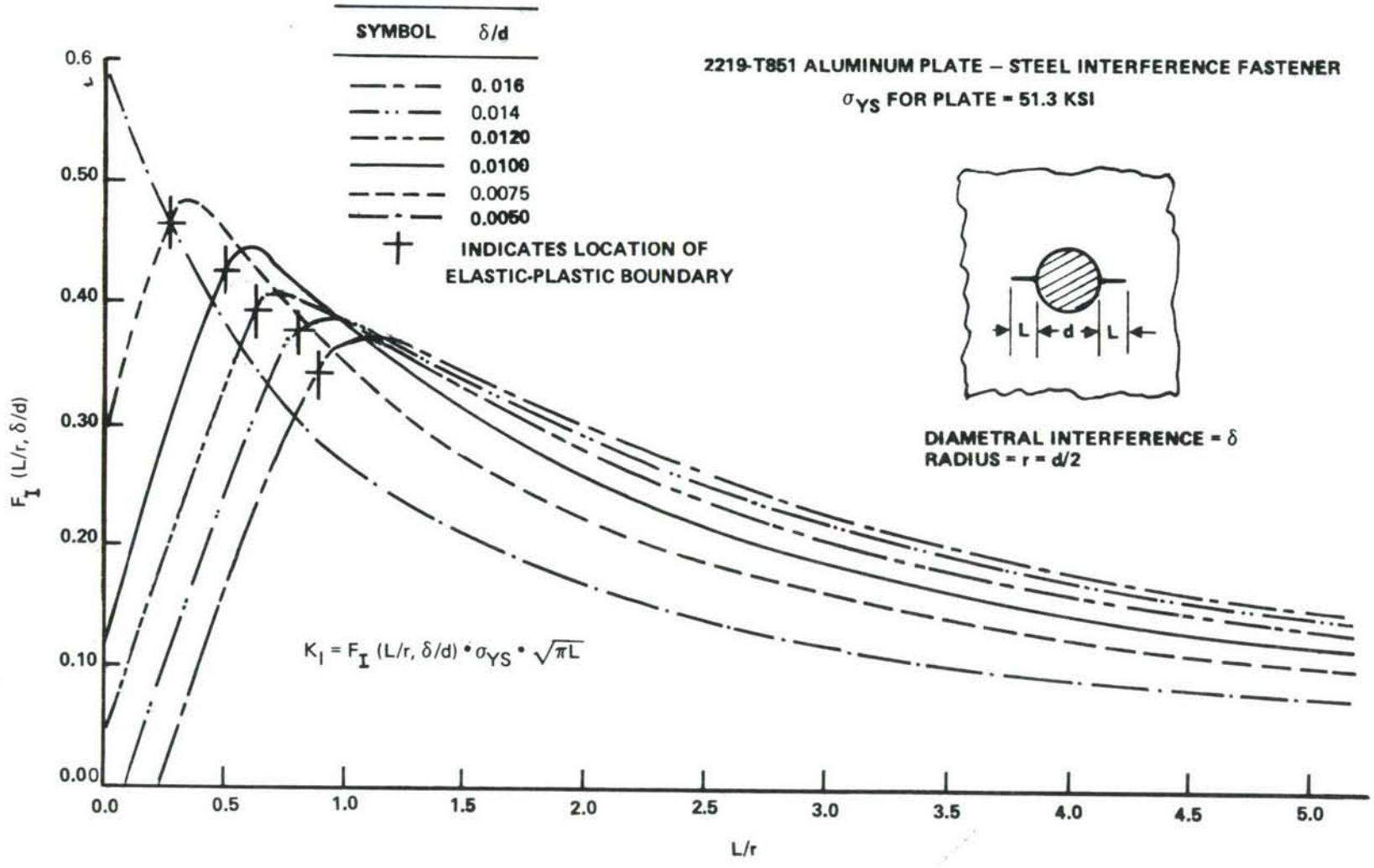


Figure 100: *Stress Intensity Factors for Two Through Cracks Originating at an Interference Fit Fastener Due to Interference Alone. (Plate Material = 2219-T851 Aluminum, Fastener Material = Steel)*

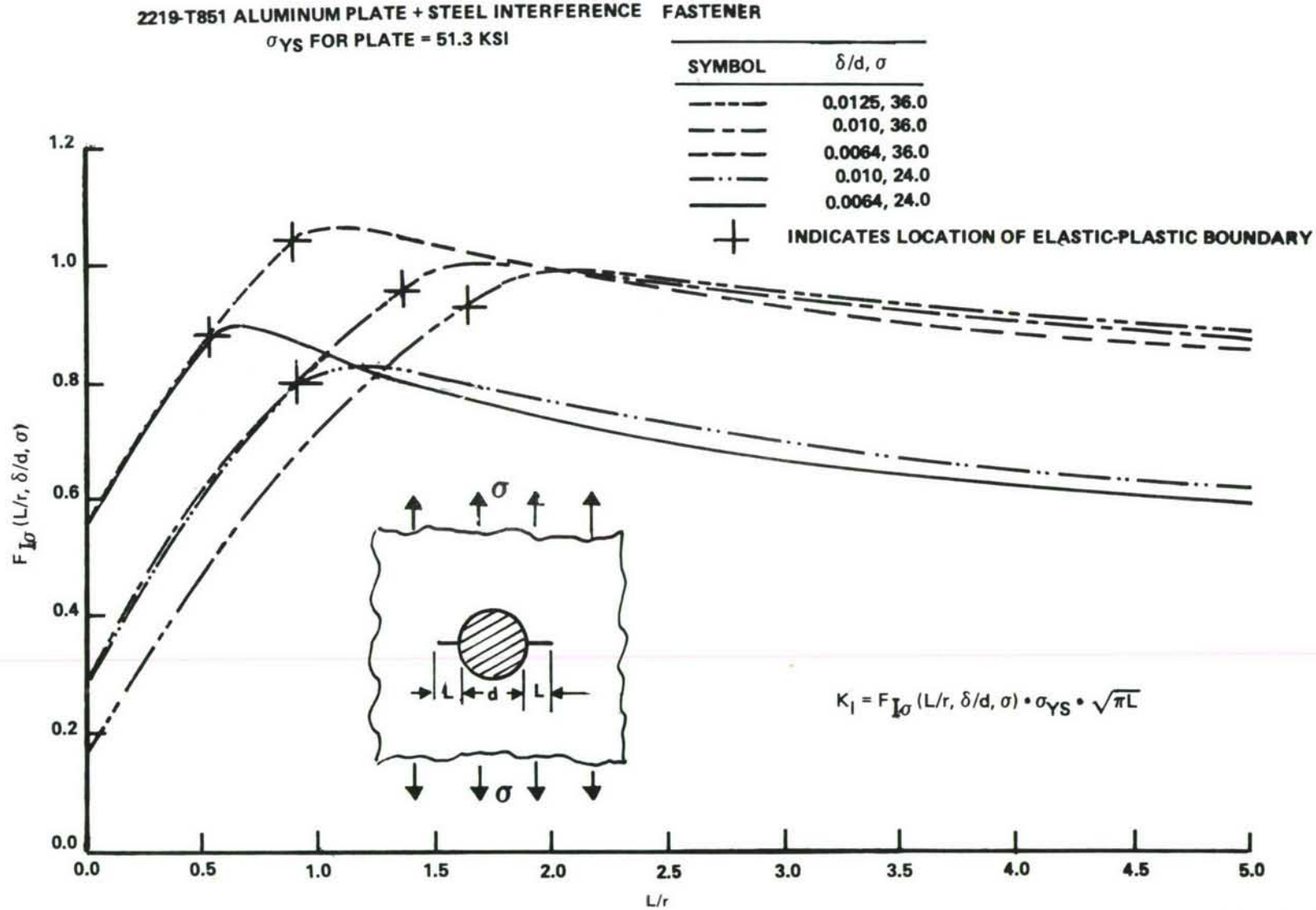


Figure 101: Stress Intensity Factors for Two Through Cracks Originating at an Interference Fit Fastener in a Plate Subjected to Uniaxial Tension (Plate Material = 2219-T851 Aluminum, Fastener Material = Steel)

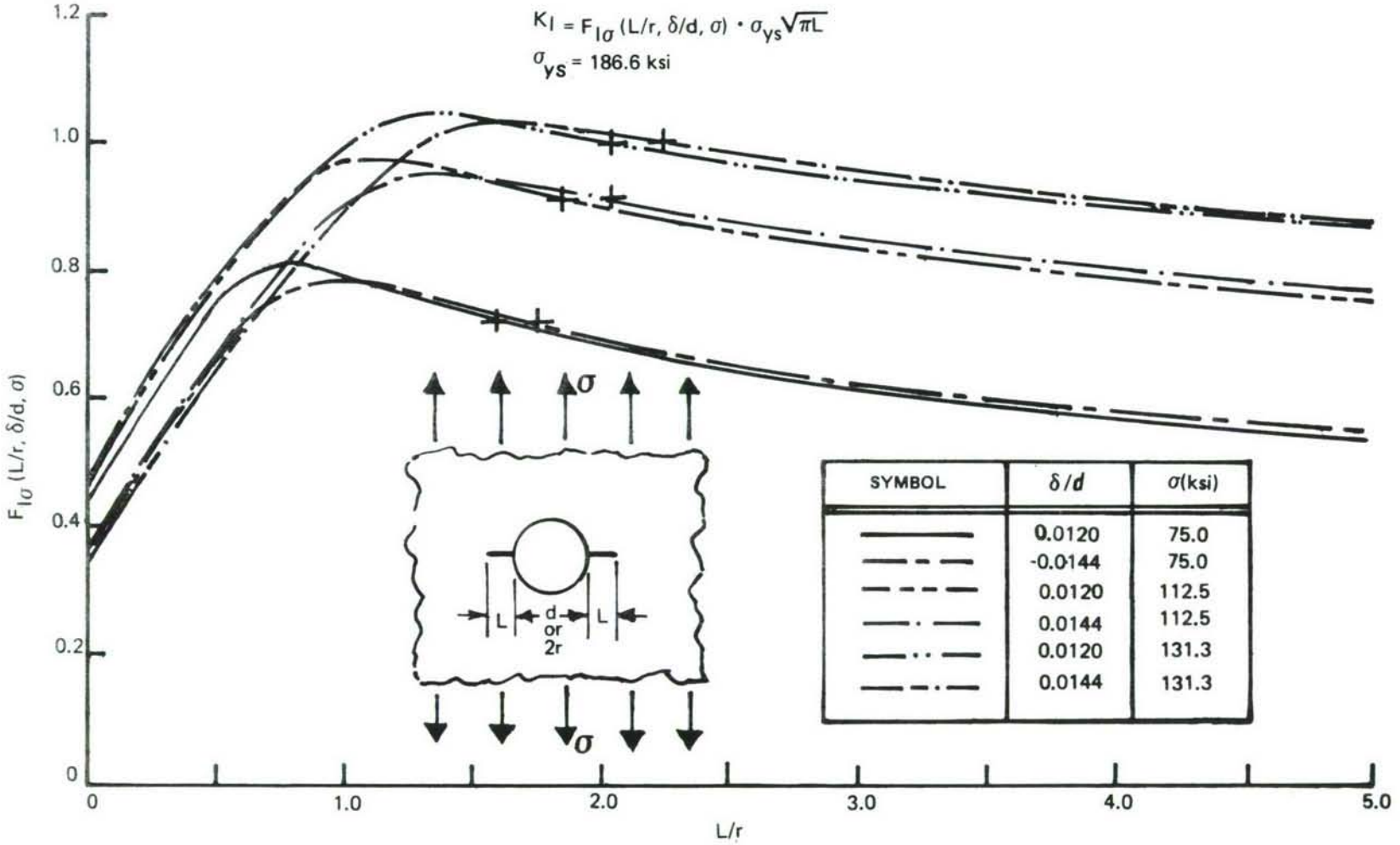


Figure 102: Stress Intensity Factors for Two Thru Cracks Originating at an Interference Fit Fastener in a Plate Subjected to Uniaxial Tension (Plate Material = 9Ni-4Co-0.2C Steel and Fastener Material = H-11 Steel)

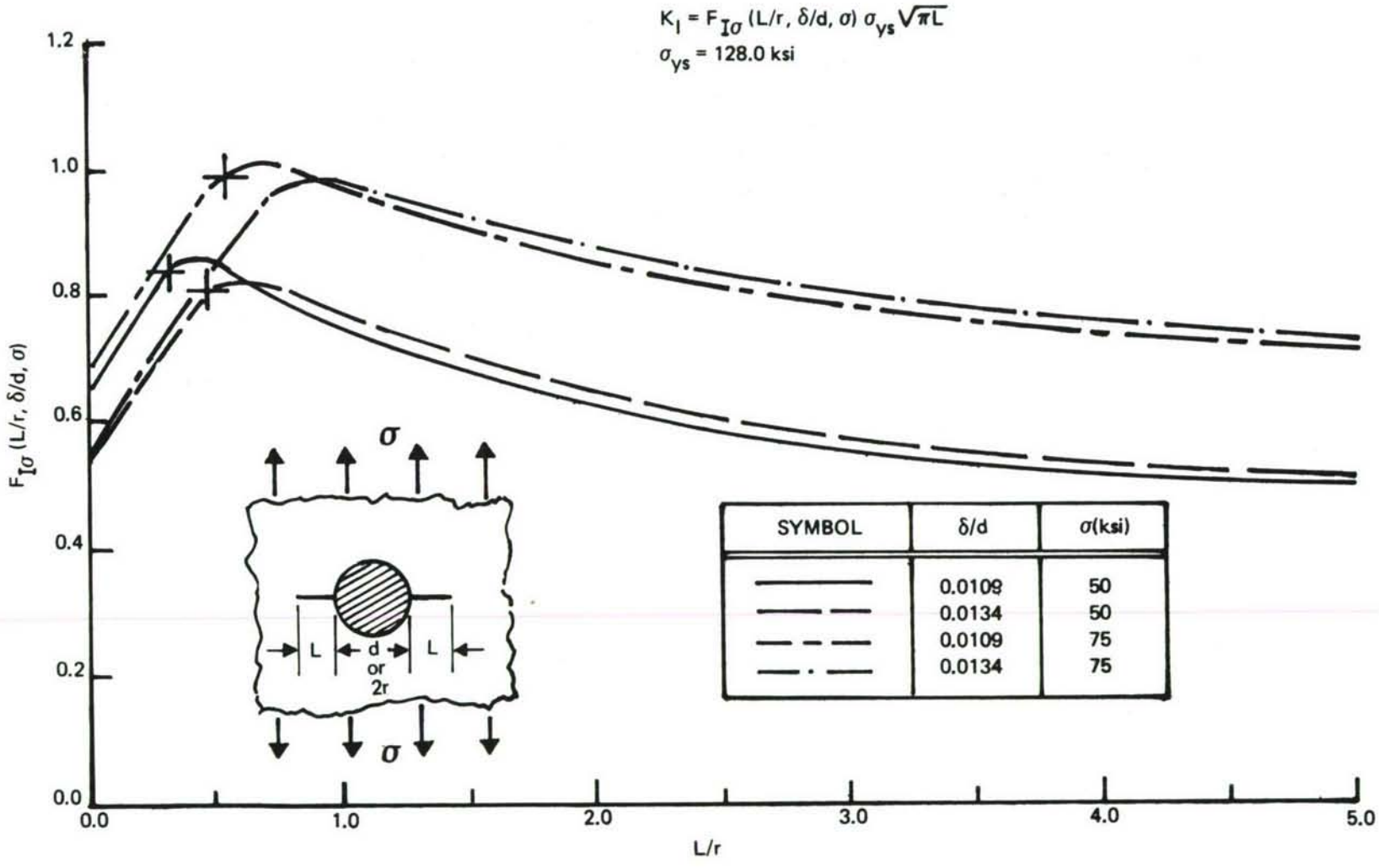


Figure 103: Stress Intensity Factors for Two Thru Cracks Originating at an Interference Fit Fastener in a Plate Subjected to Uniaxial Tension (Plate Material = 6Al-4V Titanium, Fastener Material = Titanium)

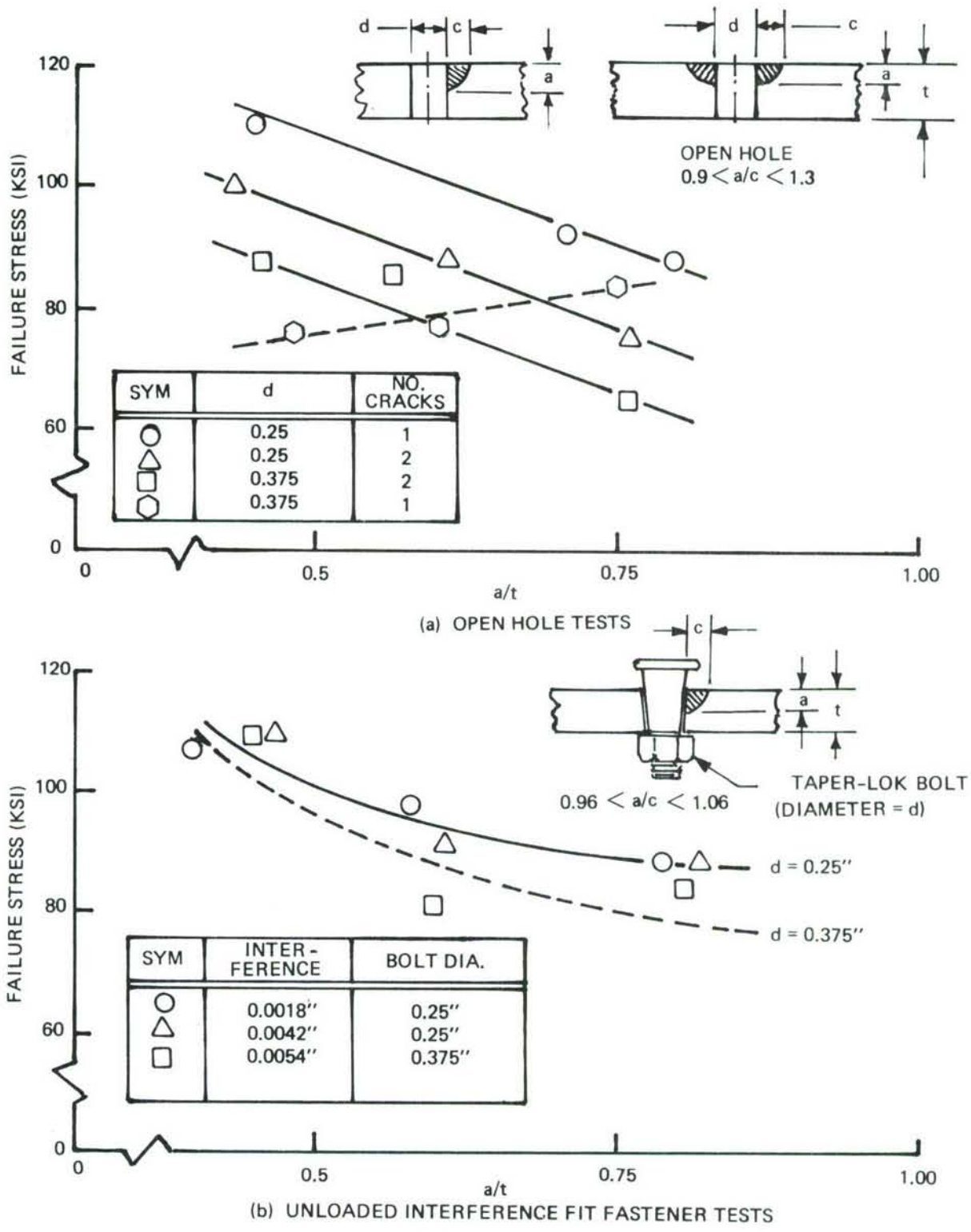


Figure 104: Static Fracture Test Results For 4340 Steel Fastener Hole Flaw Tests (Open Hole and Unloaded Interference Fit Fastener Tests)

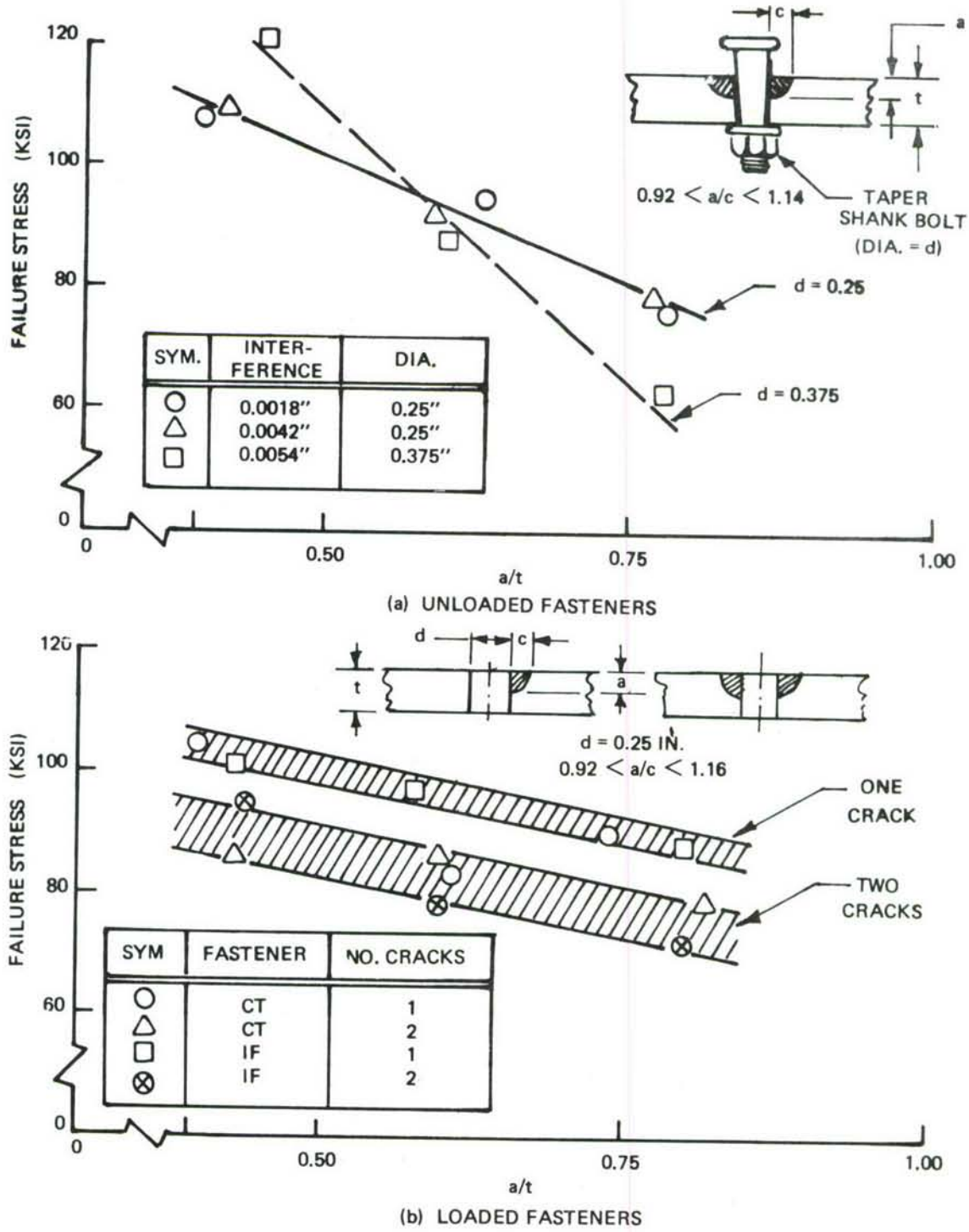


Figure 105: Static Fracture Test Results For 4340 Steel Fastener Hole Flaw Tests (Unloaded Interference Fit Fastener and Loaded Fastener Tests)

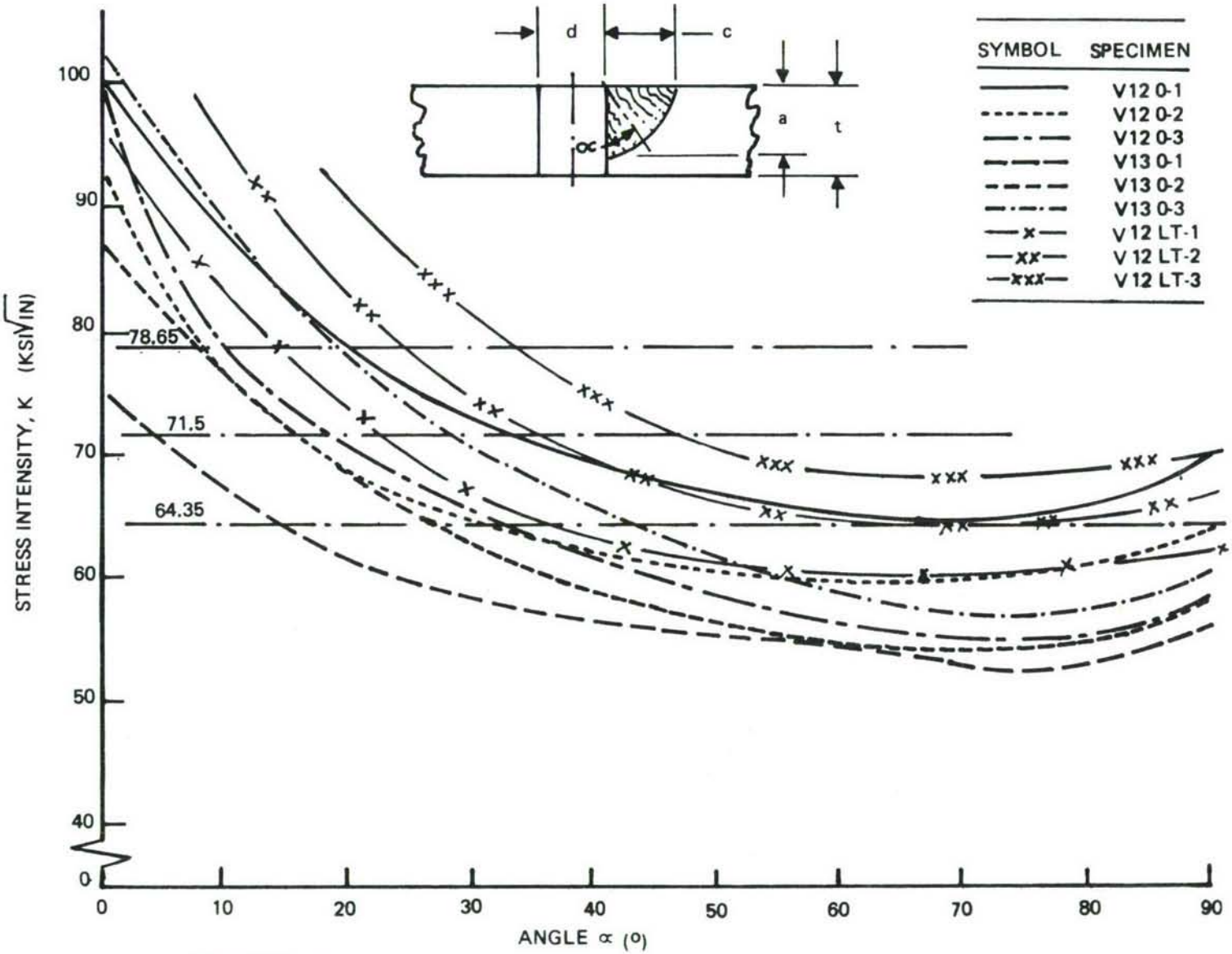


Figure 106 : Variation of Stress Intensity Factor Around Crack Periphery for 4340 Steel Fastener Hole Flaw Specimens (Single Crack Specimens)

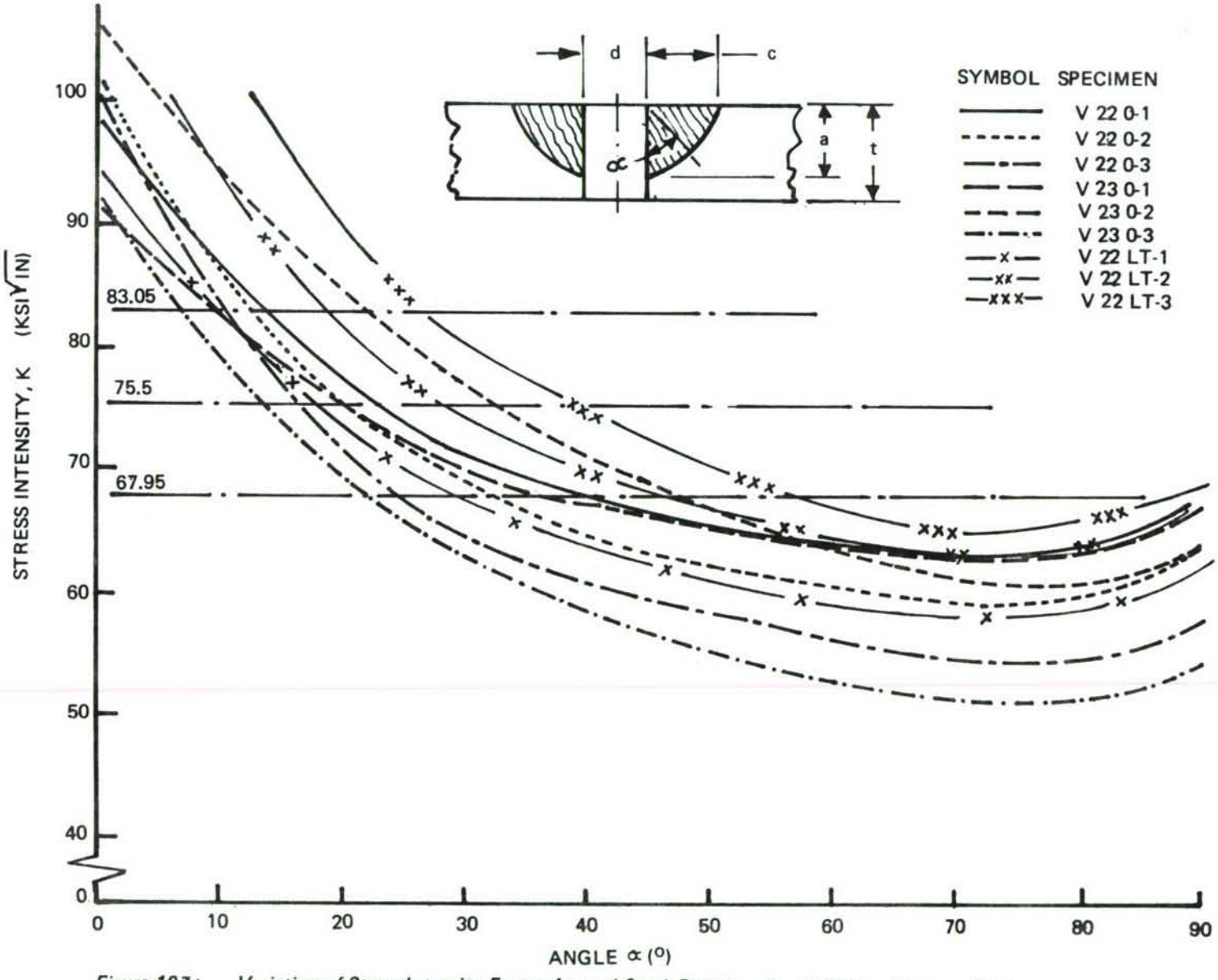


Figure 107: Variation of Stress Intensity Factor Around Crack Periphery for 4340 Steel Fastener Hole Flaw Specimens (Double Crack Specimens)

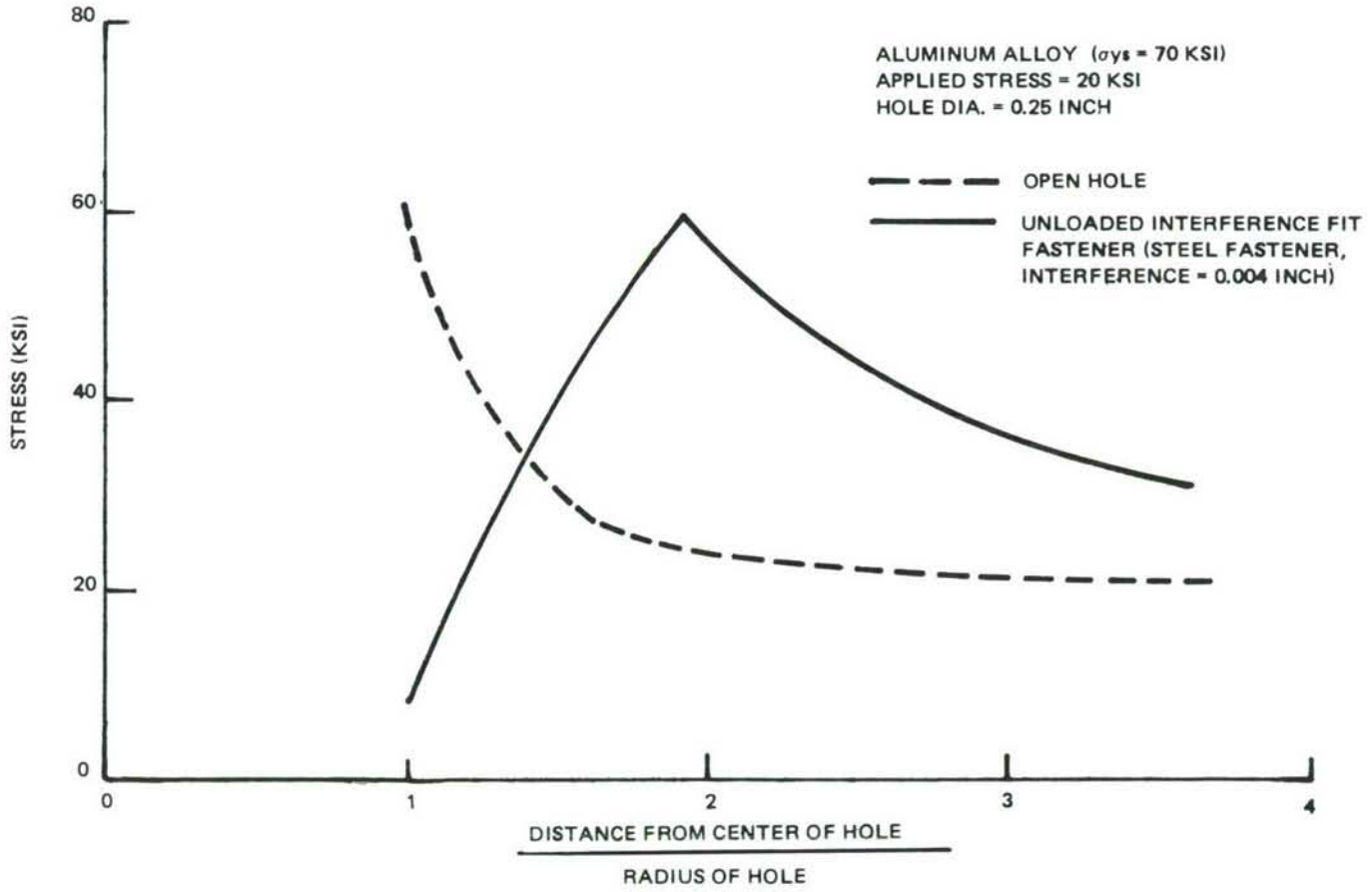


Figure 108: Stress Distributions Near an Open and Interference Fastener Filled Hole in Aluminum Alloy Plate

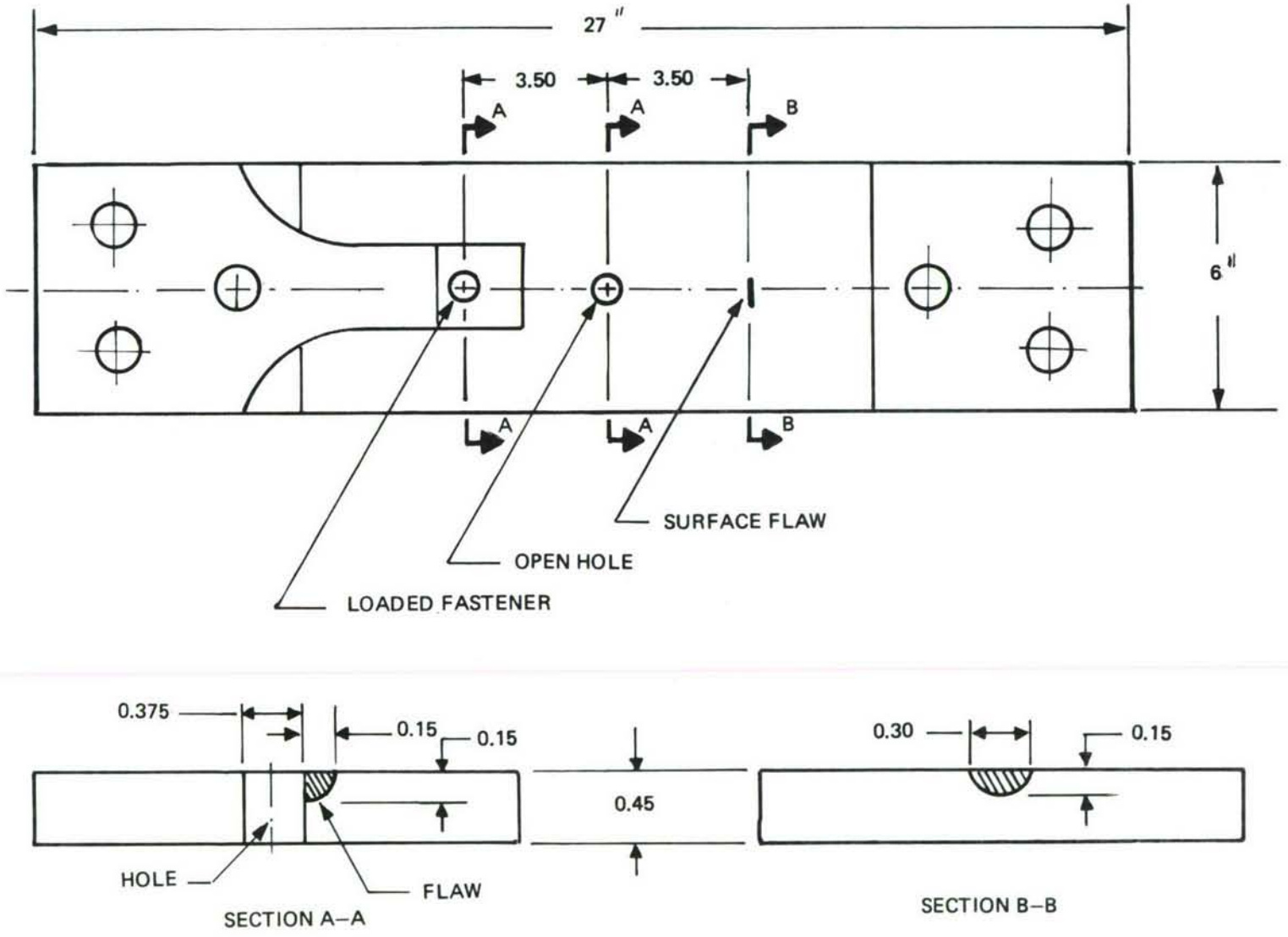
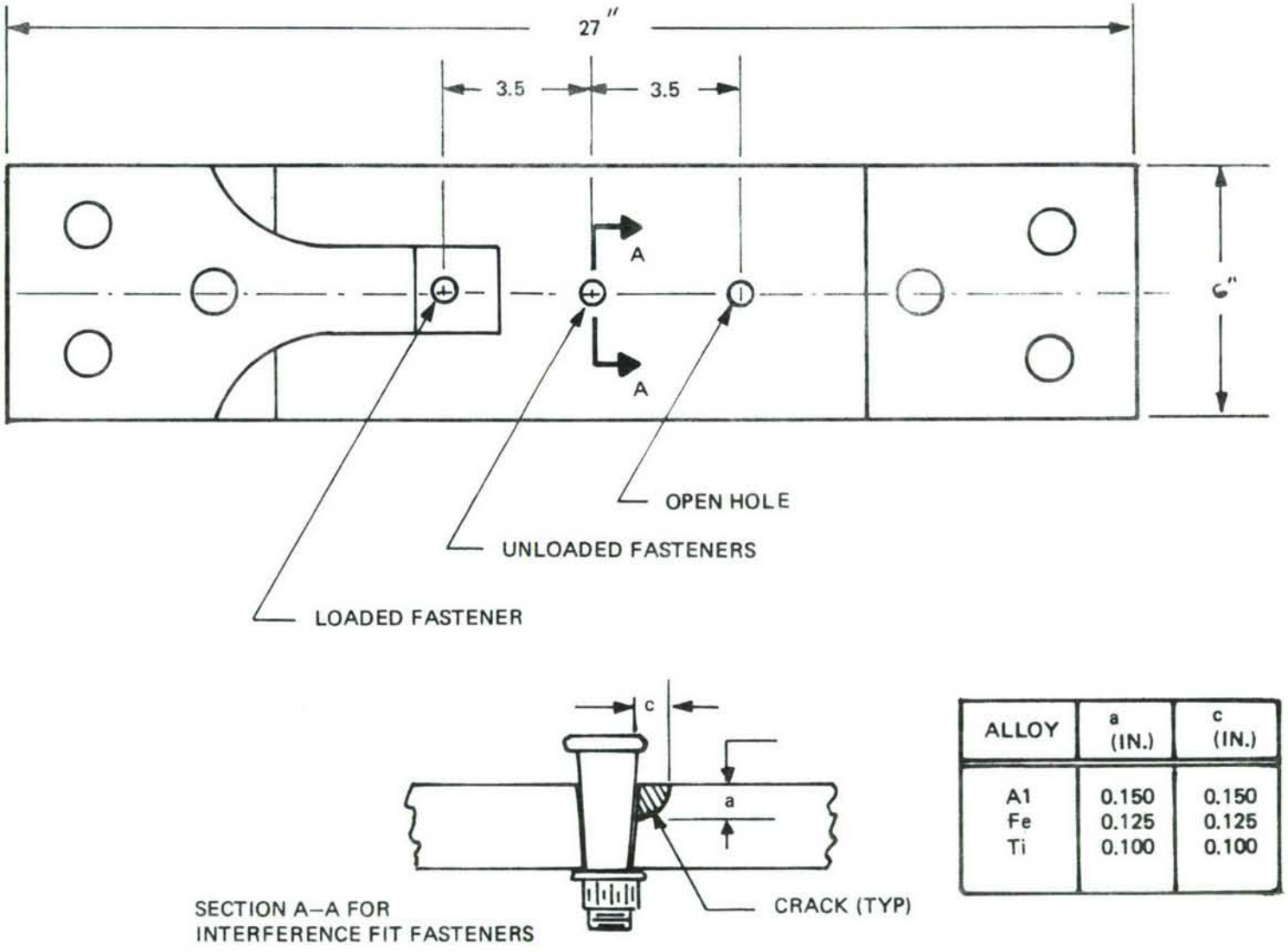


Figure 109: Specimen Configuration for Aluminum Alloy Close Tolerance Fastener Tests



ALLOY	a (IN.)	c (IN.)
A1	0.150	0.150
Fe	0.125	0.125
Ti	0.100	0.100

Figure 110: Specimen Configuration for Cracked Fastener Hole Tests

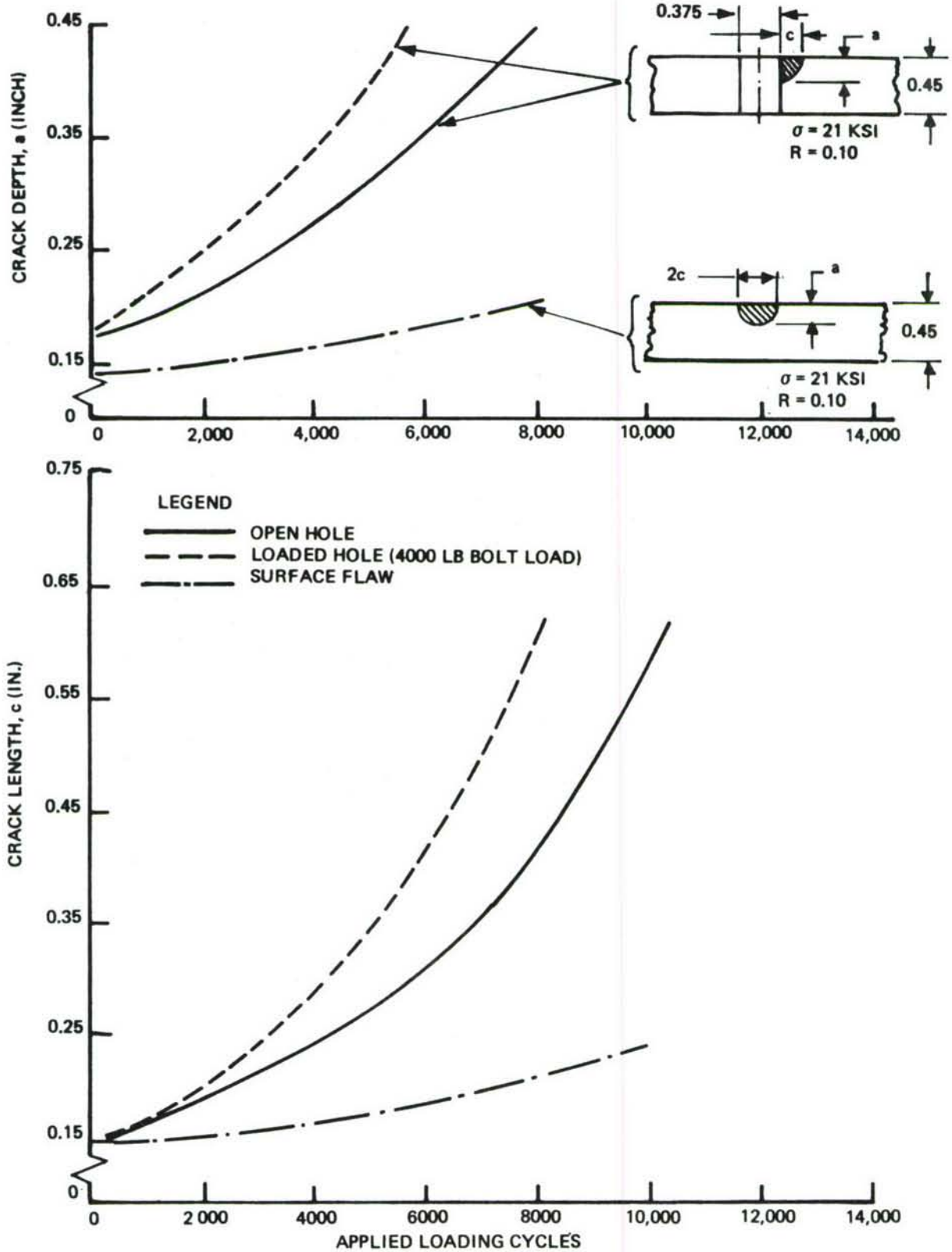


Figure 111: Crack Size Vs. Cycles for Part-Through Cracks Originating at Open and Close Tolerance Fastener Filled Holes, and Surface Flaws in 2219-T851 Aluminum Alloy

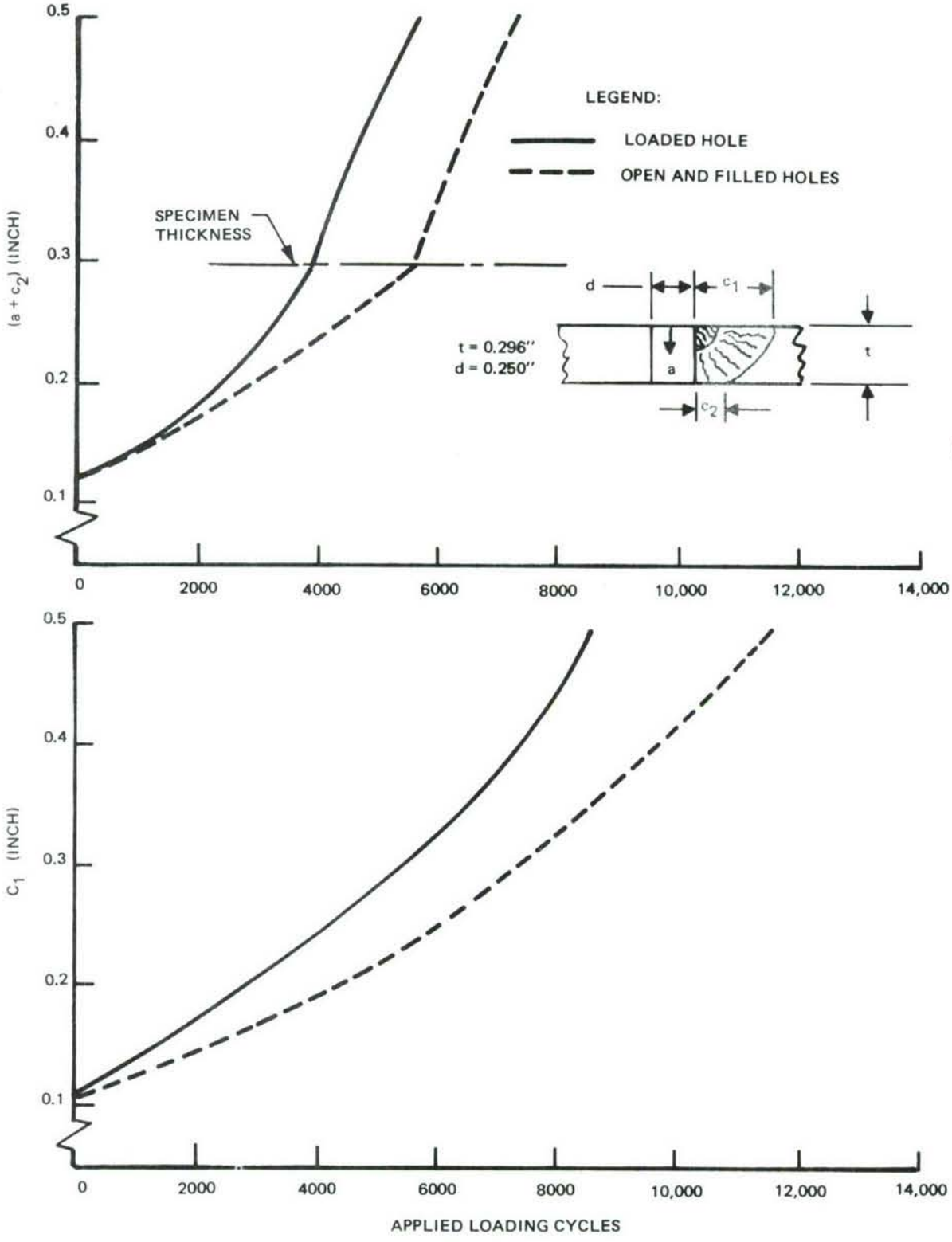


Figure 112: Crack Size Vs. Cycles for Part-Through Cracks Originating at Open and Close Tolerance Fastener Filled Holes in 9Ni-4Co-0.2C Steel Alloy

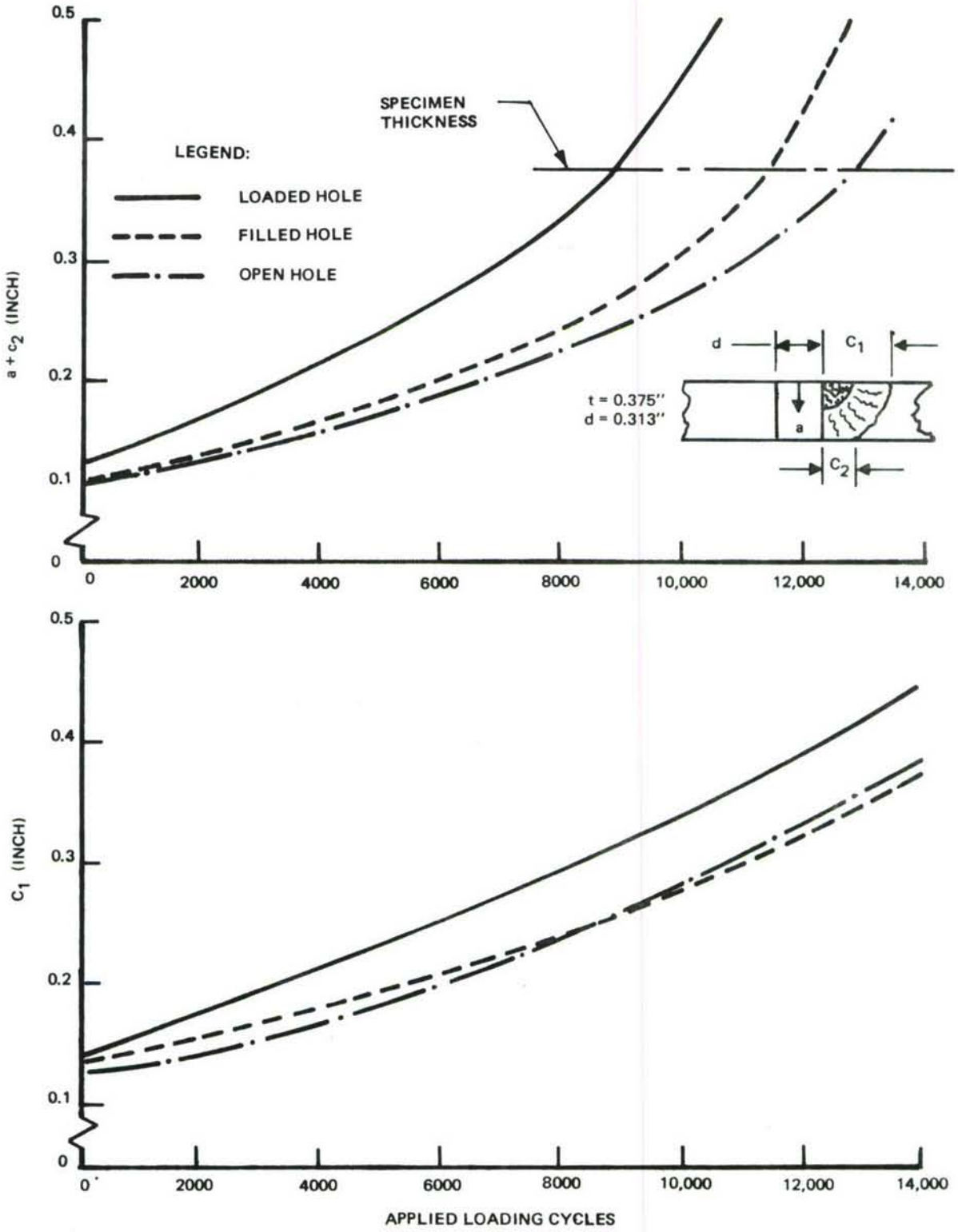


Figure 113: Crack Size Vs. Cycles for Part-Through Cracks Originating at Open and Close Tolerance Fastener Filled Holes in 6Al-4V βA Titanium Alloy

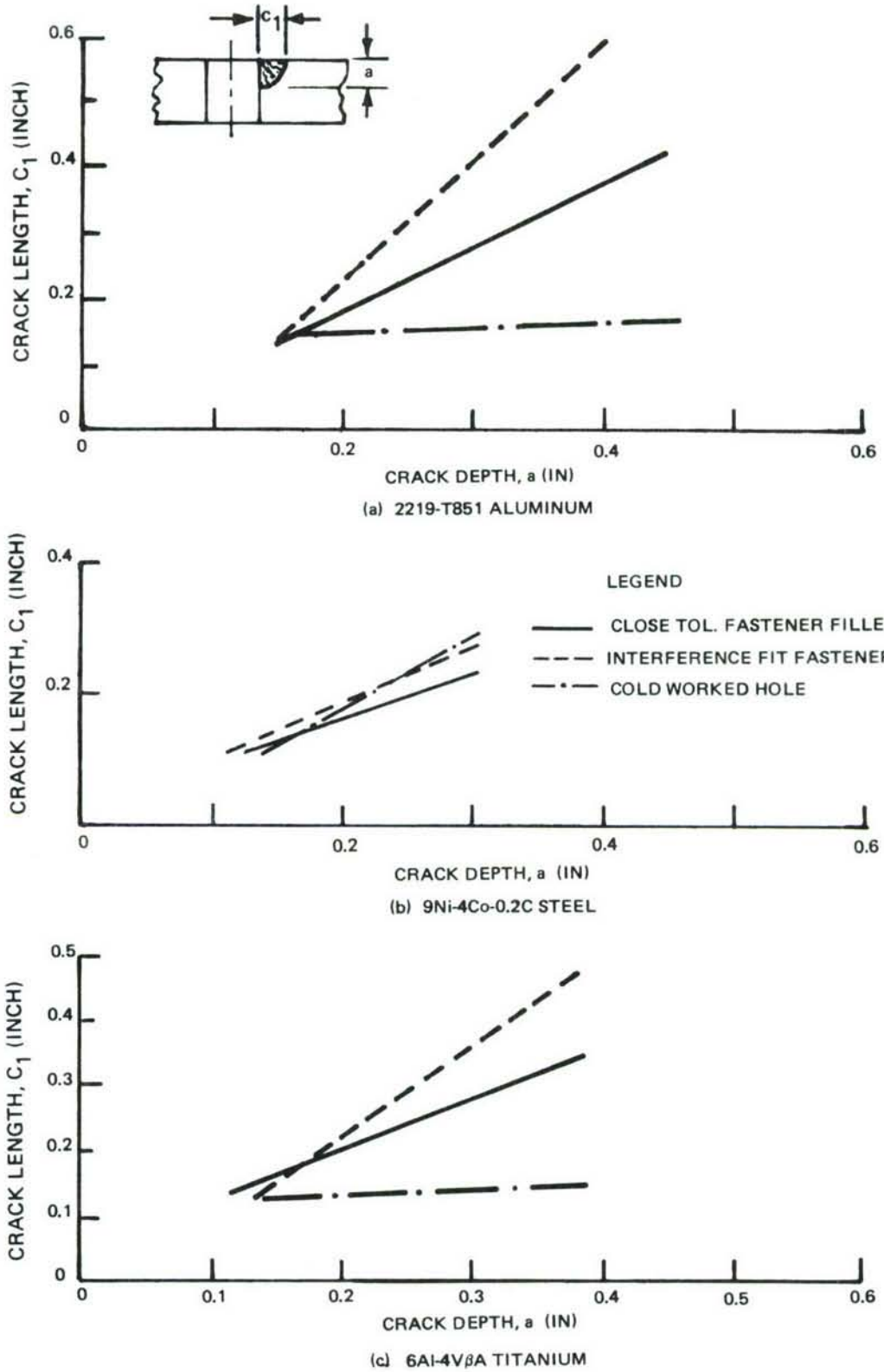


Figure 114: Comparison of Growth Characteristics for Constant Cyclic Load Tests of Part-Through Cracks Originating at Fastener Holes

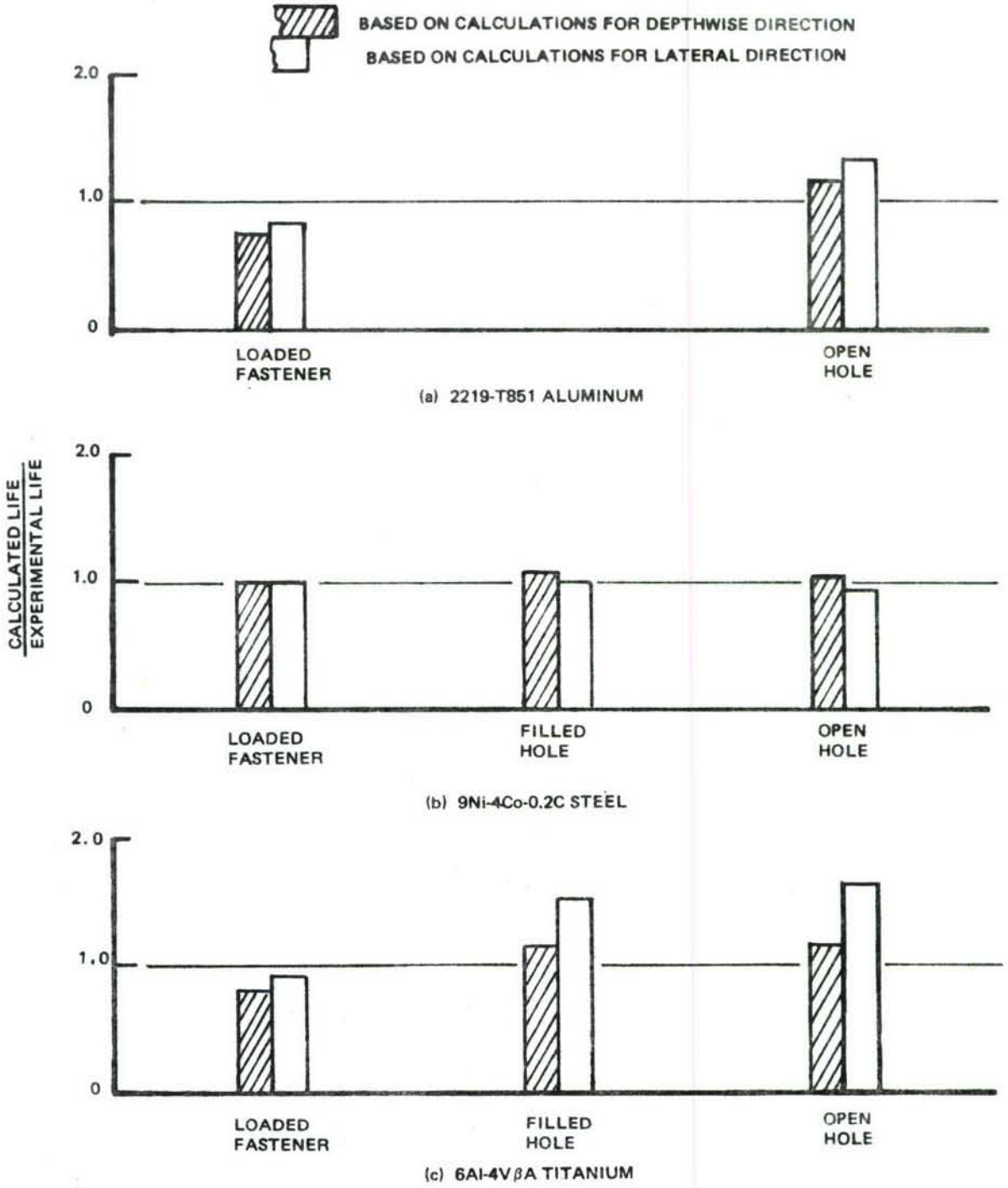


Figure 115: Comparison of Calculated and Experimental Lives for Part-Through Cracks Originating at Open and Close Tolerance Fastener Filled Holes

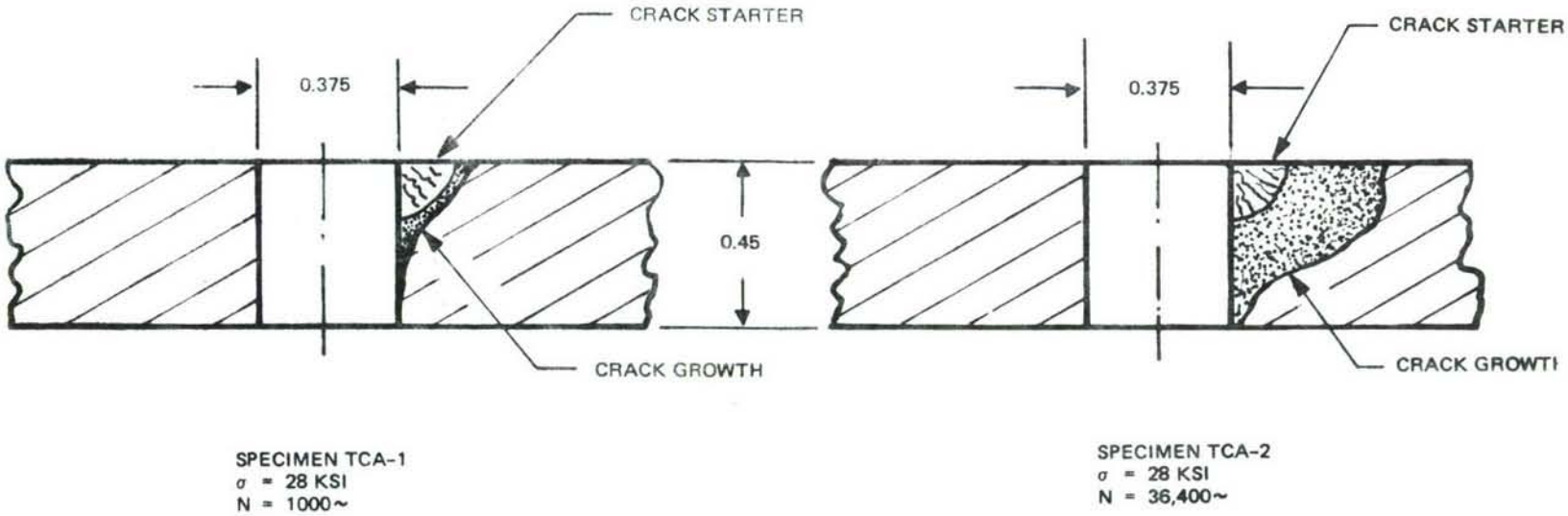


Figure 116: Crack Growth Observed in 2219-T851 Aluminum Alloy Cold Worked Hole Specimens

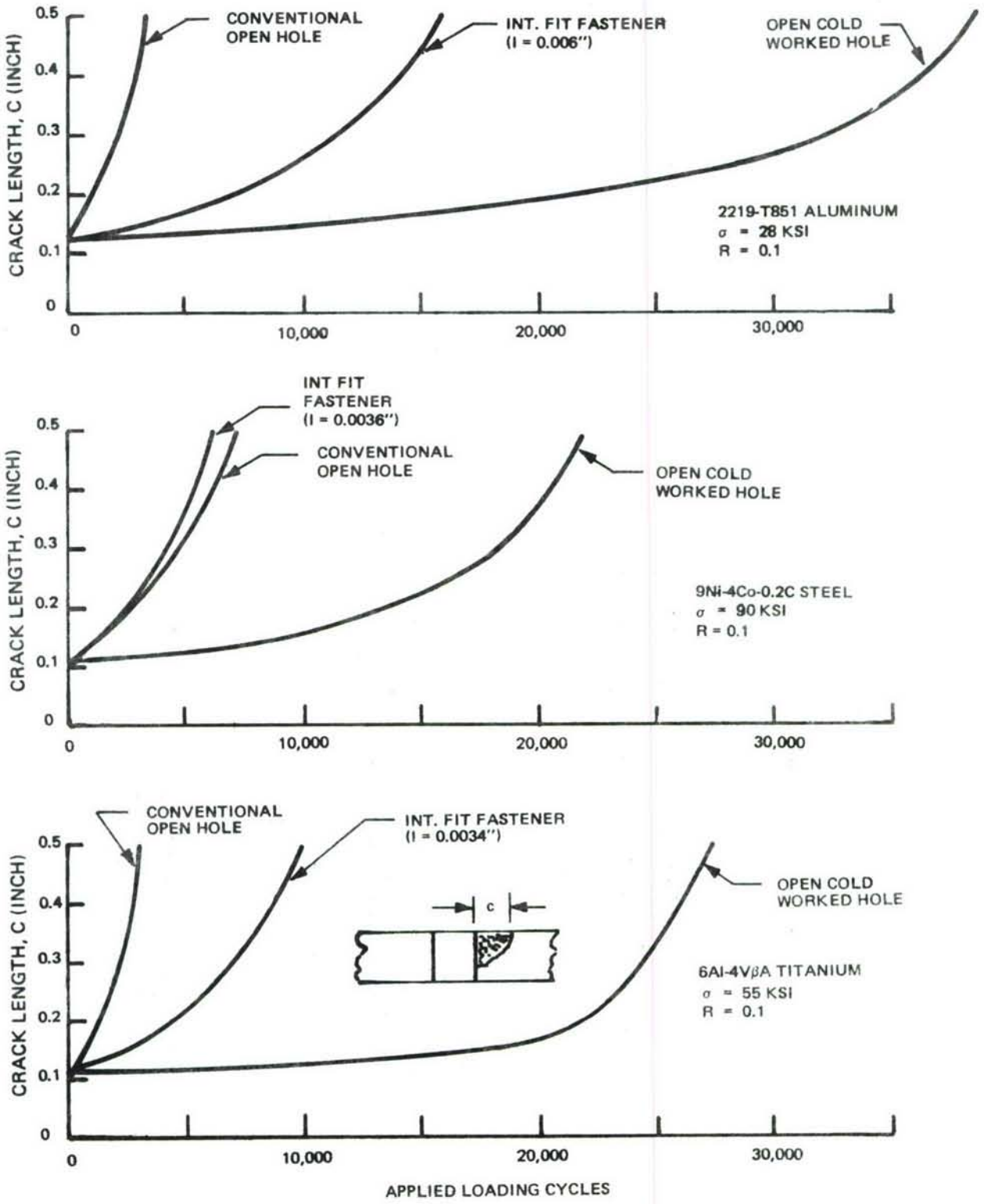


Figure 117: Crack Length Vs. Cycles for Part-Through Cracks Originating at Open Conventional, Open Cold Worked, and Interference Fit Fastener Filled Holes

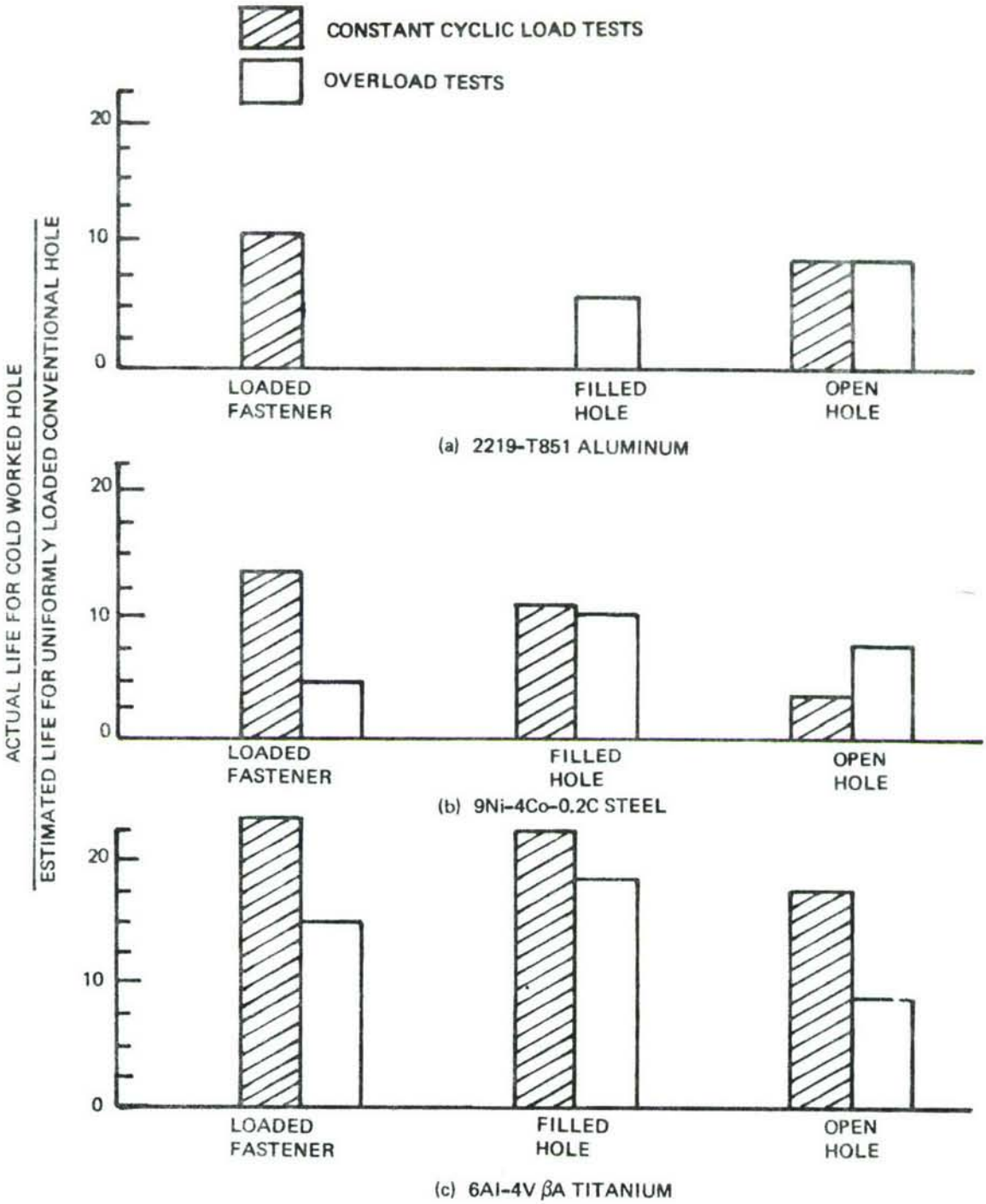


Figure 118: Comparison Between Crack Propagation Lives for Part-Through Cracks Originating at Cold Worked and Conventional Fastener Holes

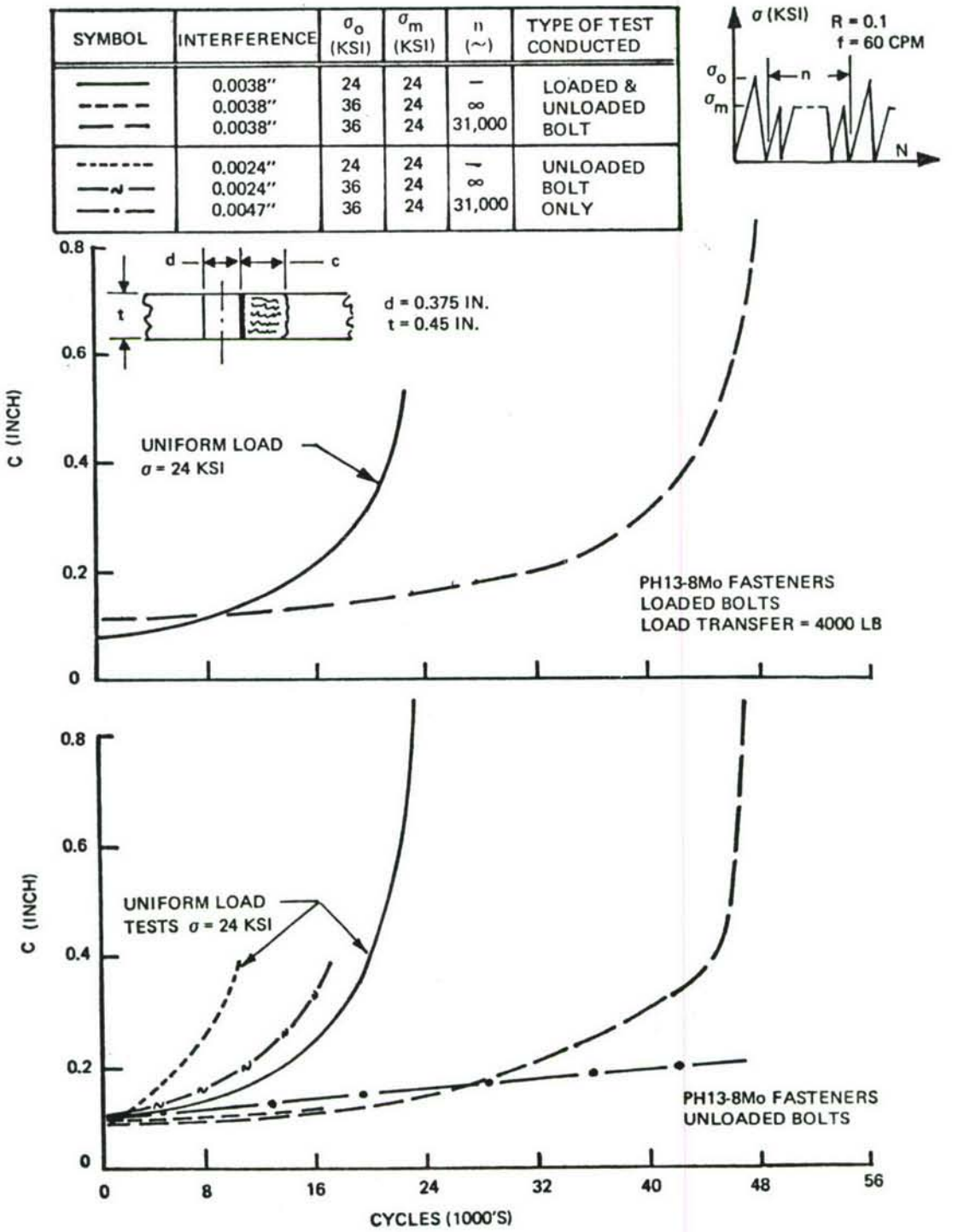


Figure 119: Effect of Periodic Overloads on Crack Growth Behavior of Thru Cracks Originating at Holes Containing Taper-Lok Fasteners in 2219-T851 Aluminum ($\sigma_o/\sigma_m = 1.5$)

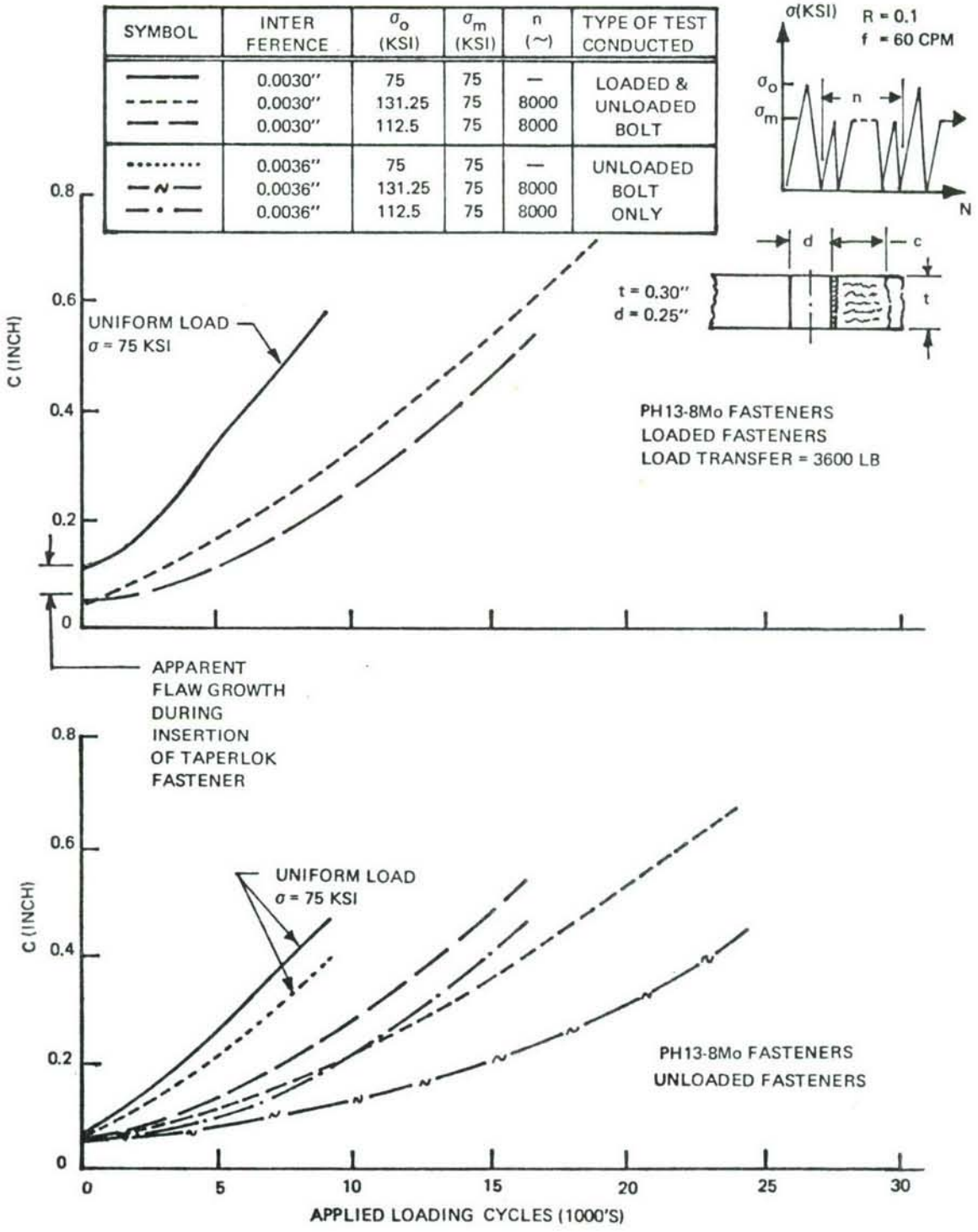


Figure 120: Effect of Periodic Overloads on Crack Growth Behavior of Thru Cracks Originating at Holes Containing Taper-Lok Fasteners in 9Ni-4Co-0.2C Steel (σ_o/σ_m = 1.75 and 1.5)

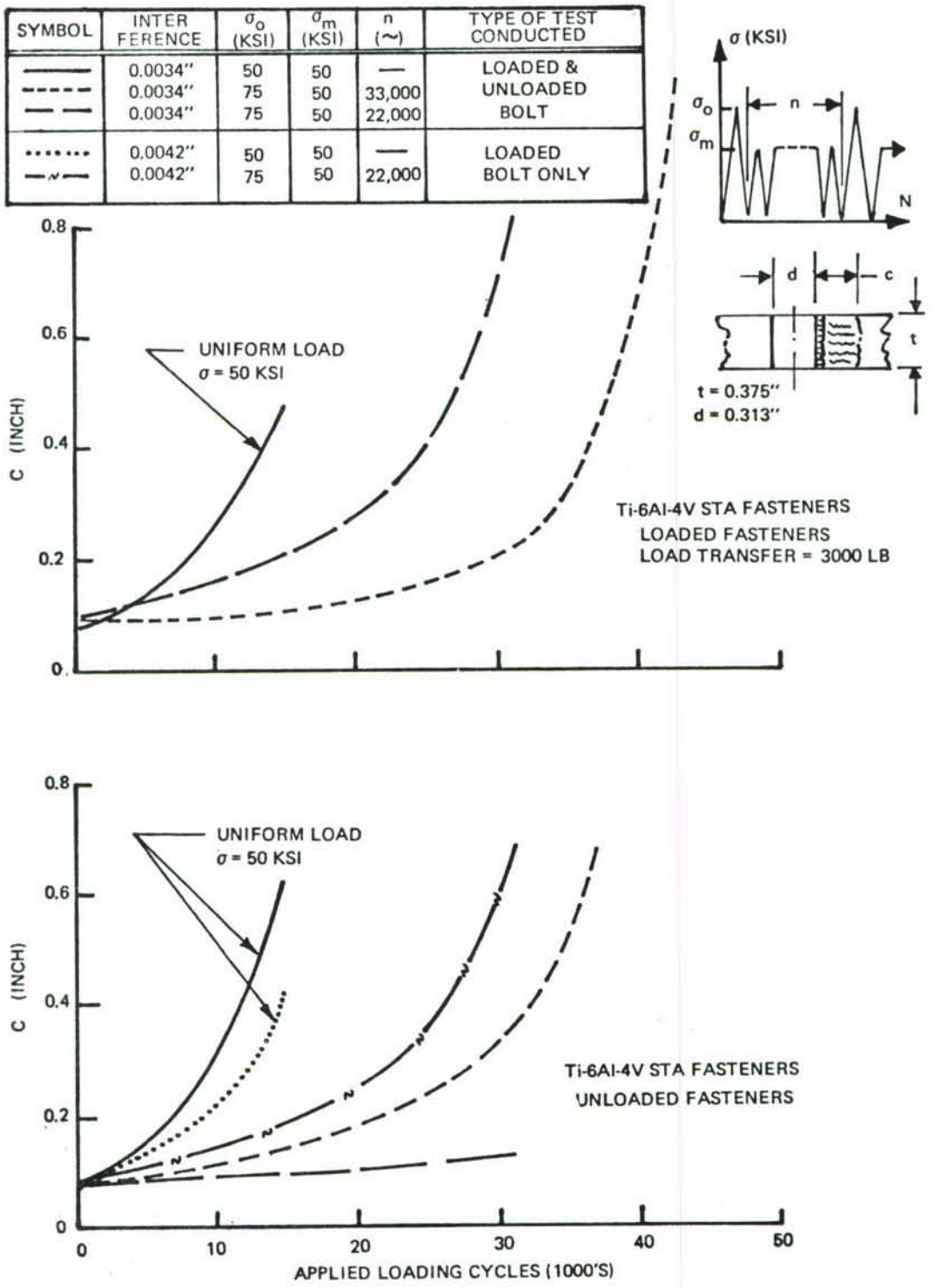


Figure 121: Effect of Periodic Overloads on Crack Growth Behavior of Thru Cracks Originating at Holes Containing Taper-Lok Fasteners in 6Al-4V βA Titanium (σ_o/σ_m = 1.5)

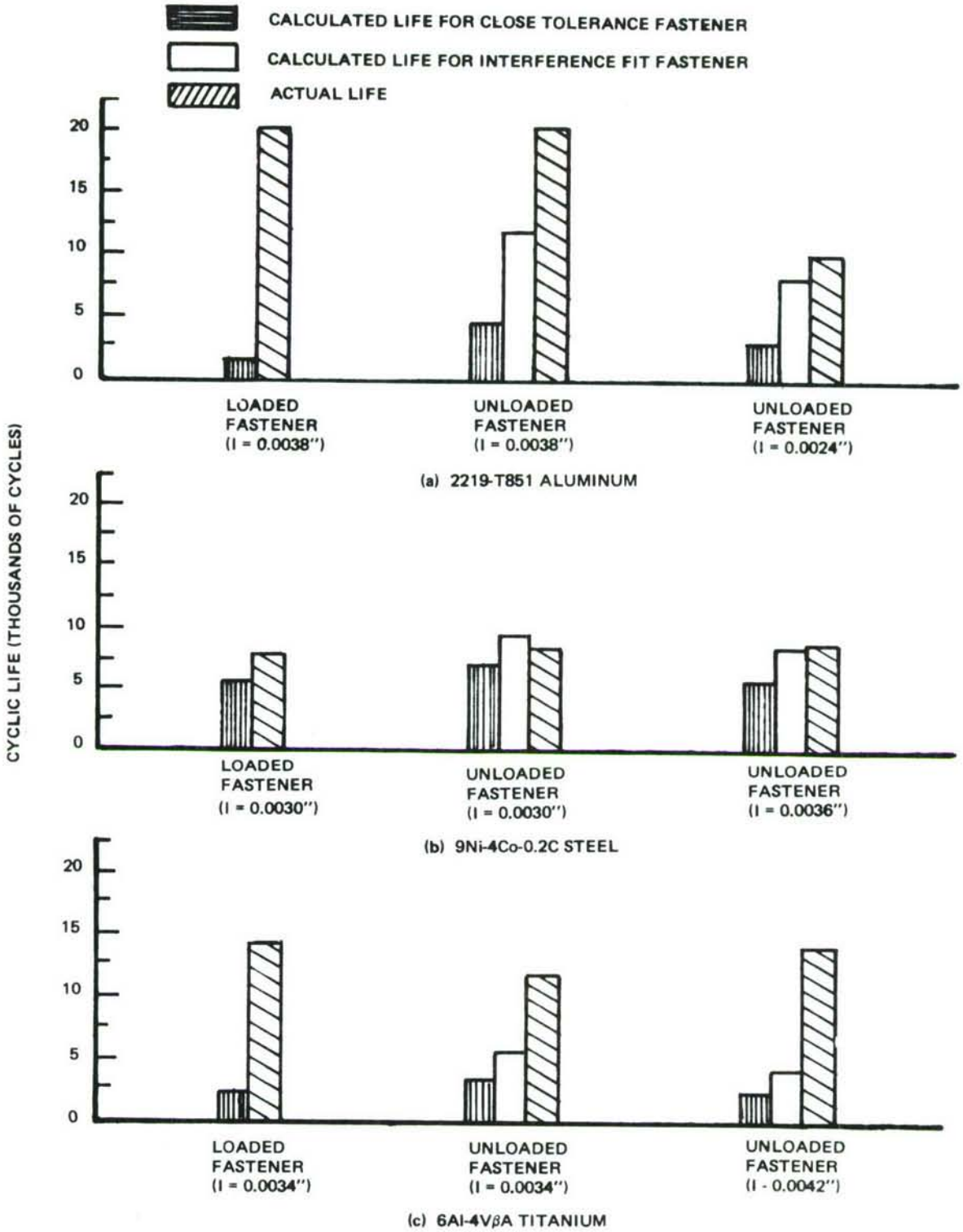


Figure 122 : Comparison of Experimental and Calculated Lives for Uniform Thru Cracks Originating at Interference Fit Fastener Holes

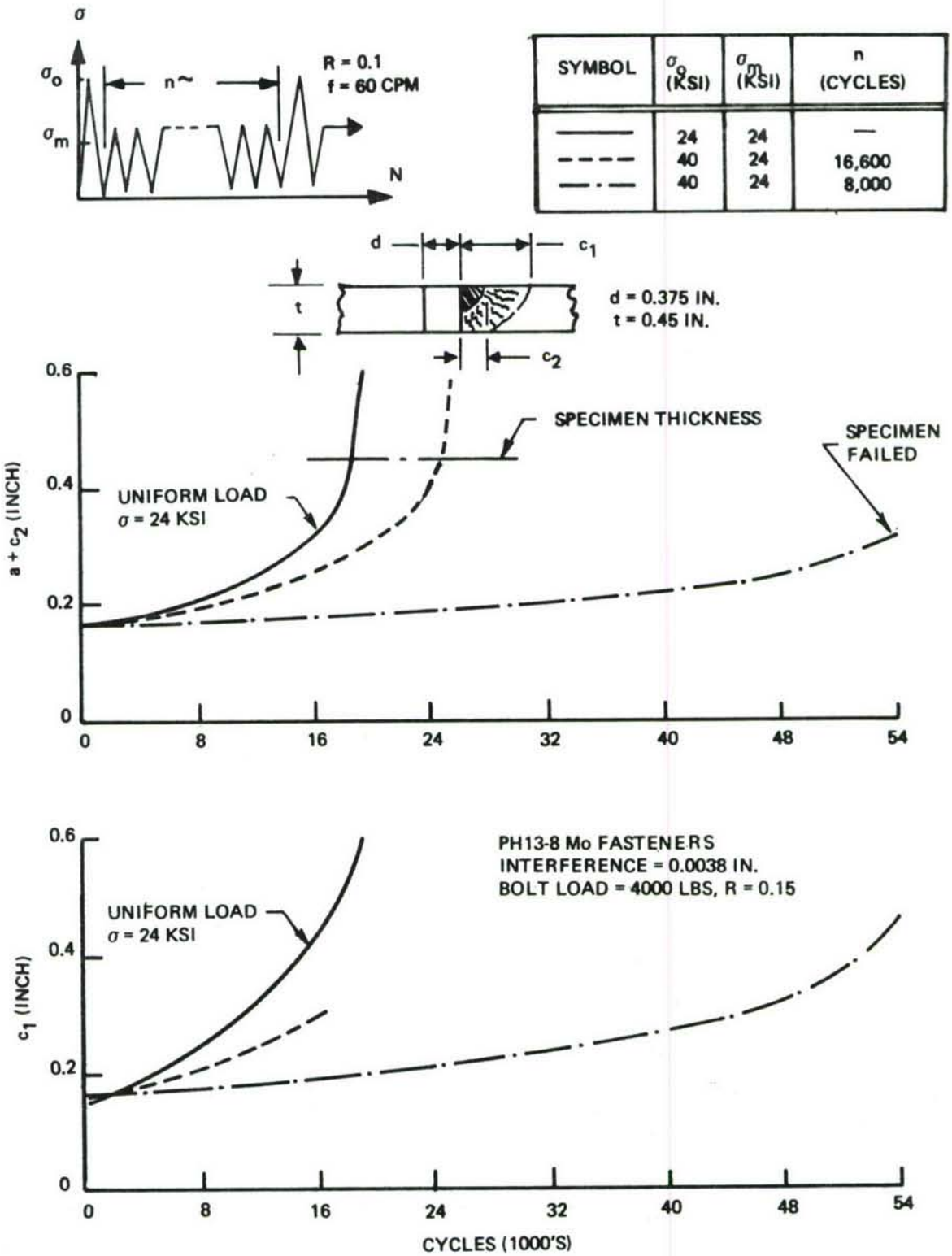


Figure 123: Effect of Periodic Overloads on Fatigue Crack Propagation of Part-Thru Cracks Originating Loaded Taper-Lok Fasteners in 2219-T851 Aluminum Alloy ($\sigma_0/\sigma_m = 1.67$)

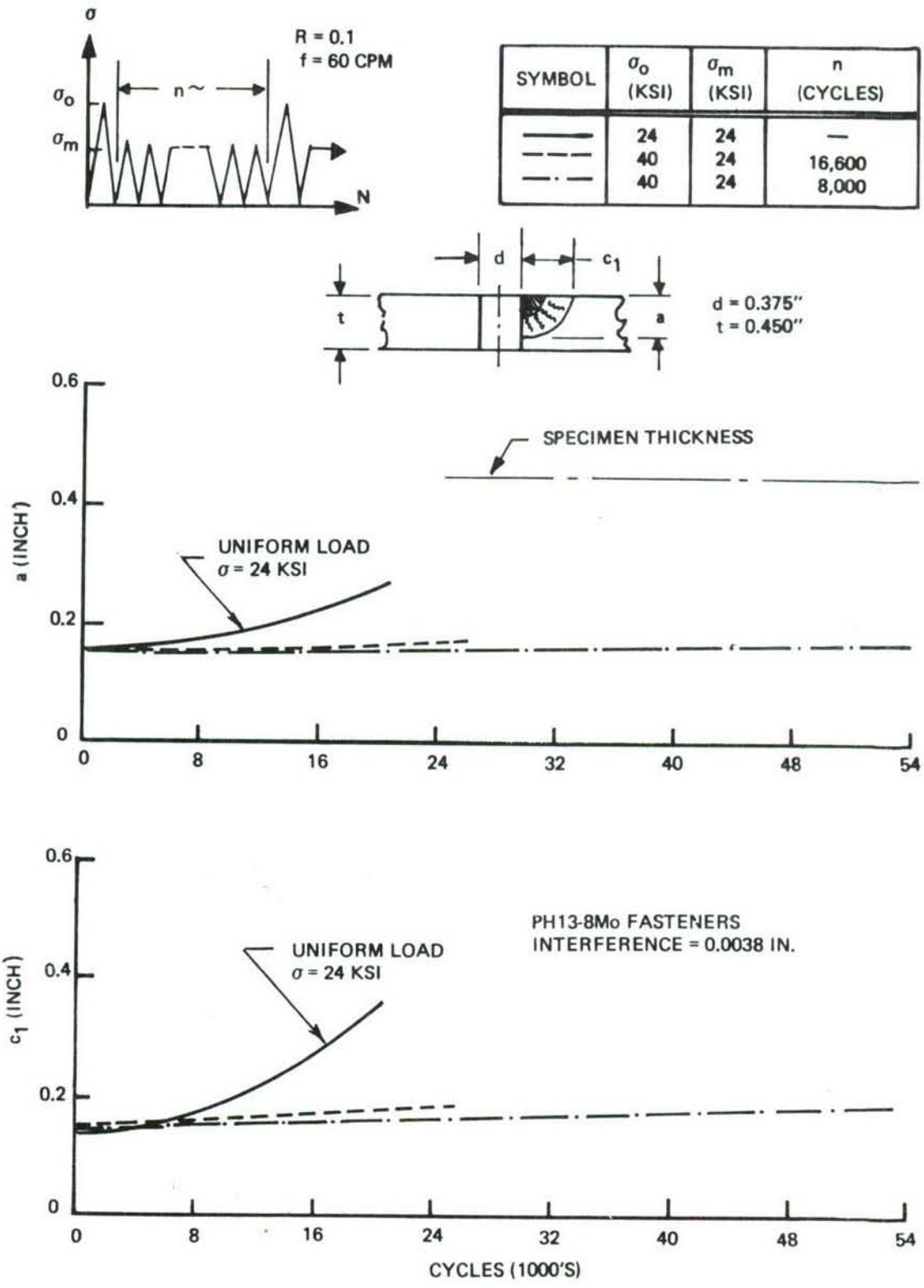


Figure 124: Effect of Periodic Overloads on Fatigue Propagation of Part-Thru Cracks Originating at Unloaded Taper-Lok Fasteners in 2219-T851 Aluminum Alloy (σ_0/σ_m = 1.67)

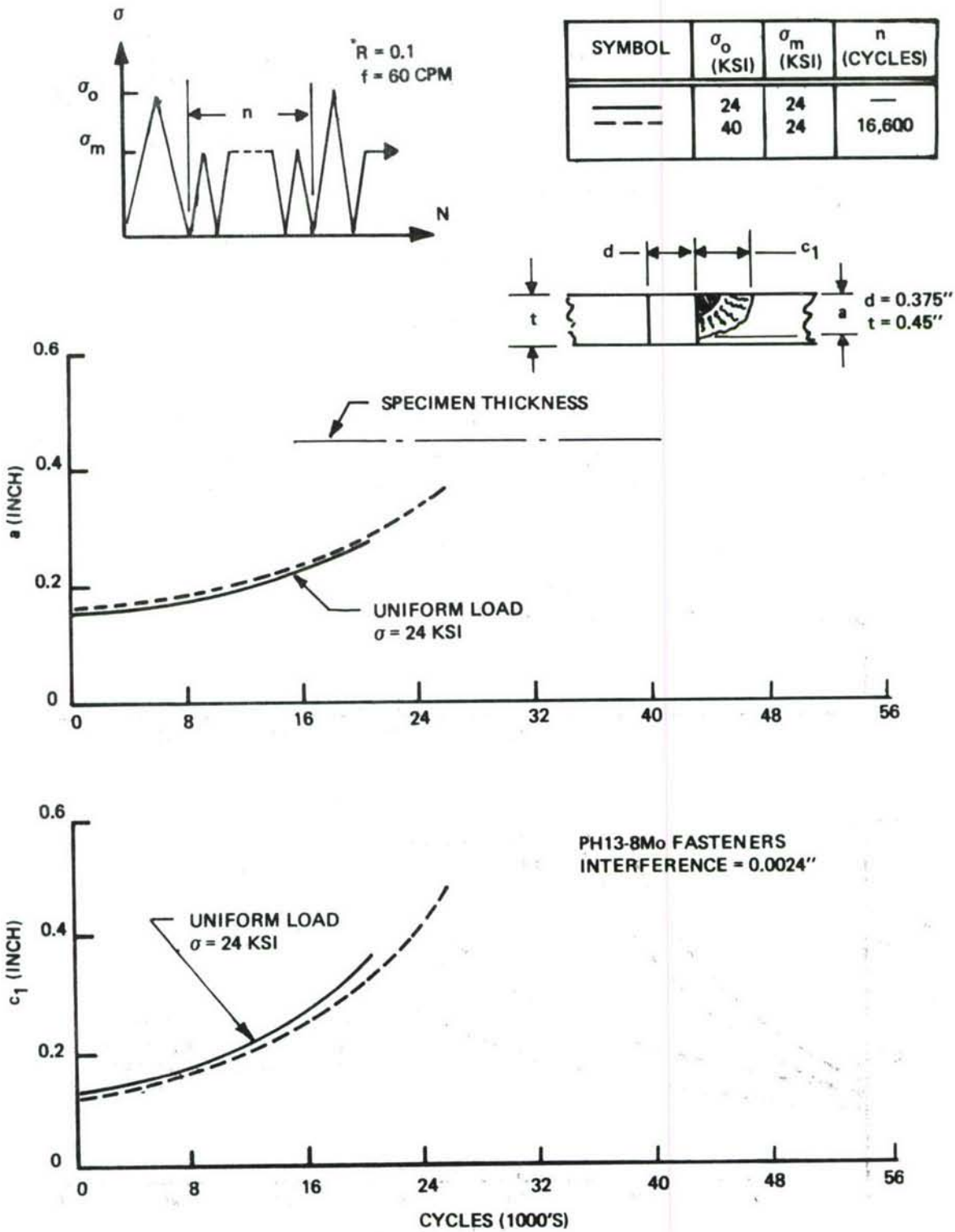


Figure 125: Effect of Periodic Overloads on Fatigue Crack Propagation of Part-Thru Cracks Originating at Unloaded Taper-Lok Fasteners in 2219-T851 Aluminum Alloy (σ_o/σ_m =1.67)

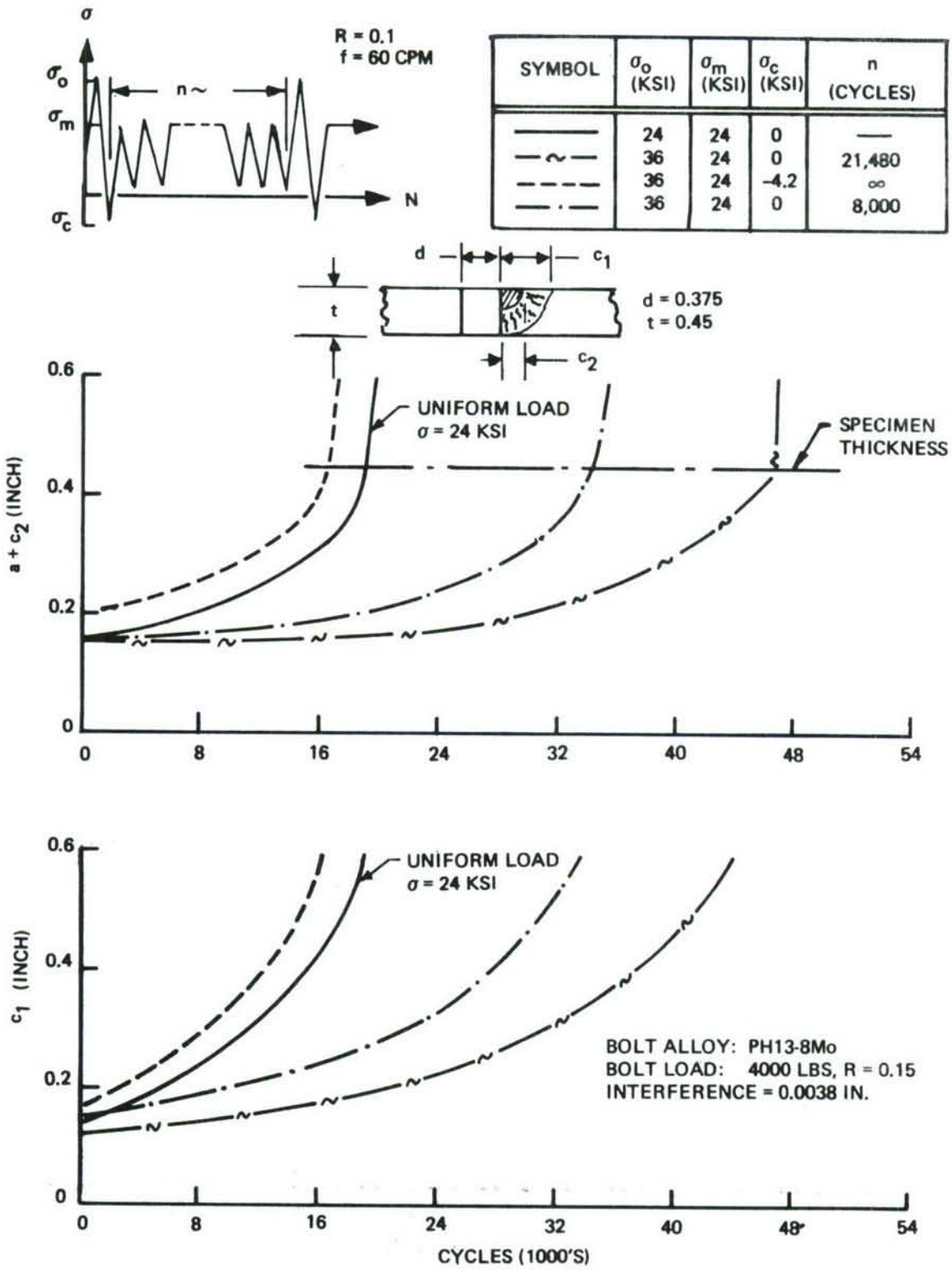


Figure 126: Effect of Periodic Overloads on Fatigue Crack Propagation of Part-Thru Cracks Originating at Loaded Taper-Lok Fasteners in 2219-T851 Aluminum Alloy ($\sigma_o/\sigma_m = 1.50$)

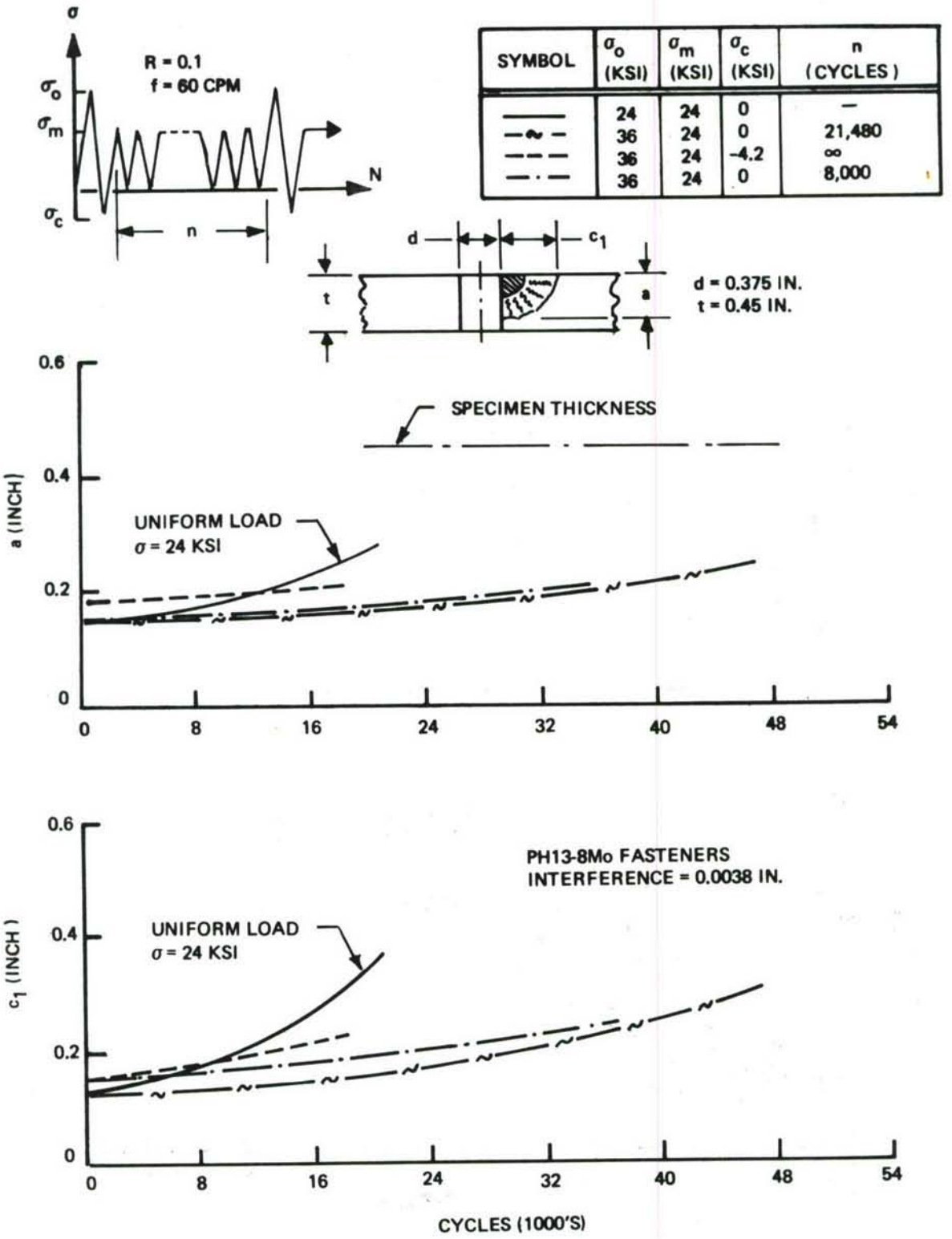


Figure 127: Effect of Periodic Overloads on Fatigue Crack Propagation of Part-Thru Cracks Originating at Unloaded Taper-Lok Fasteners in 2219-T851 Aluminum Alloy ($\sigma_o/\sigma_m = 1.50$)

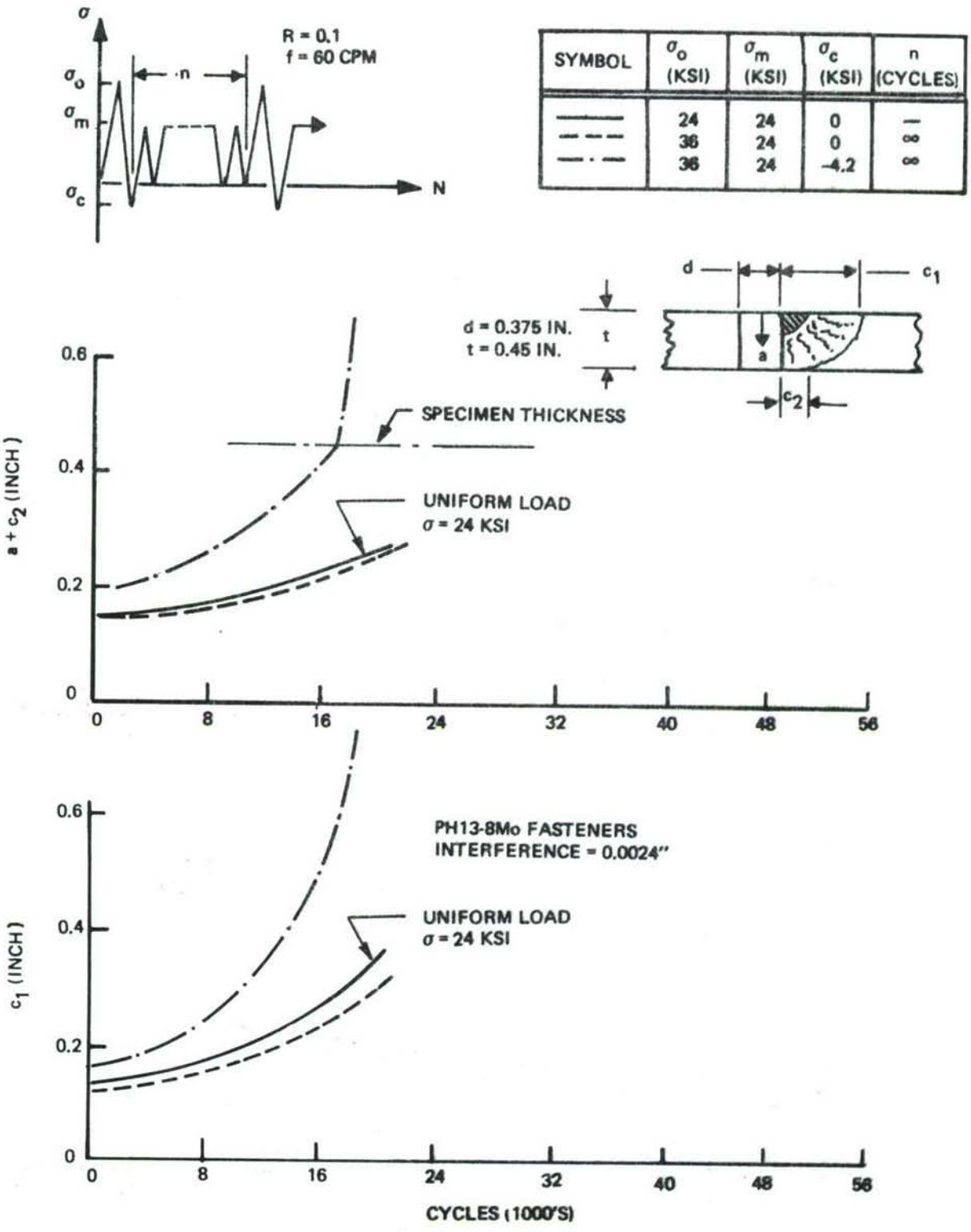


Figure 128: Effect of Periodic Overloads on Fatigue Crack Propagation of Part-Thru Cracks Originating at Unloaded Taper-Lok Fasteners in 2219-T851 Aluminum Alloy ($\sigma_o/\sigma_m = 1.50$)

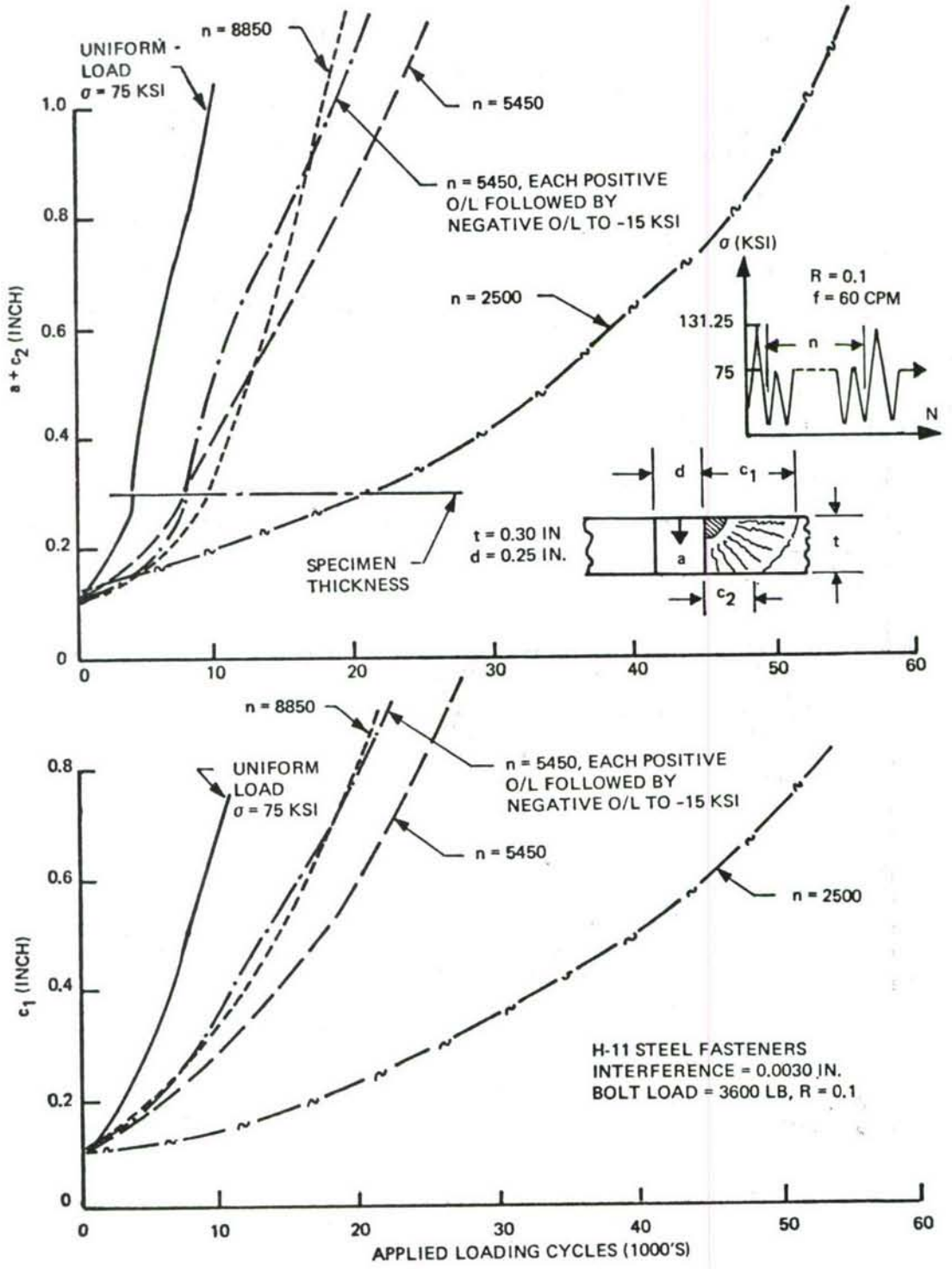


Figure 129: *Effect of Periodic Overloads on Fatigue Crack Propagation of Part-Thru Cracks Originating at Loaded Taper-Lok Fasteners in 9Ni-4Co-0.2C Steel Alloy ($\sigma_o/\sigma_m = 1.75$)*

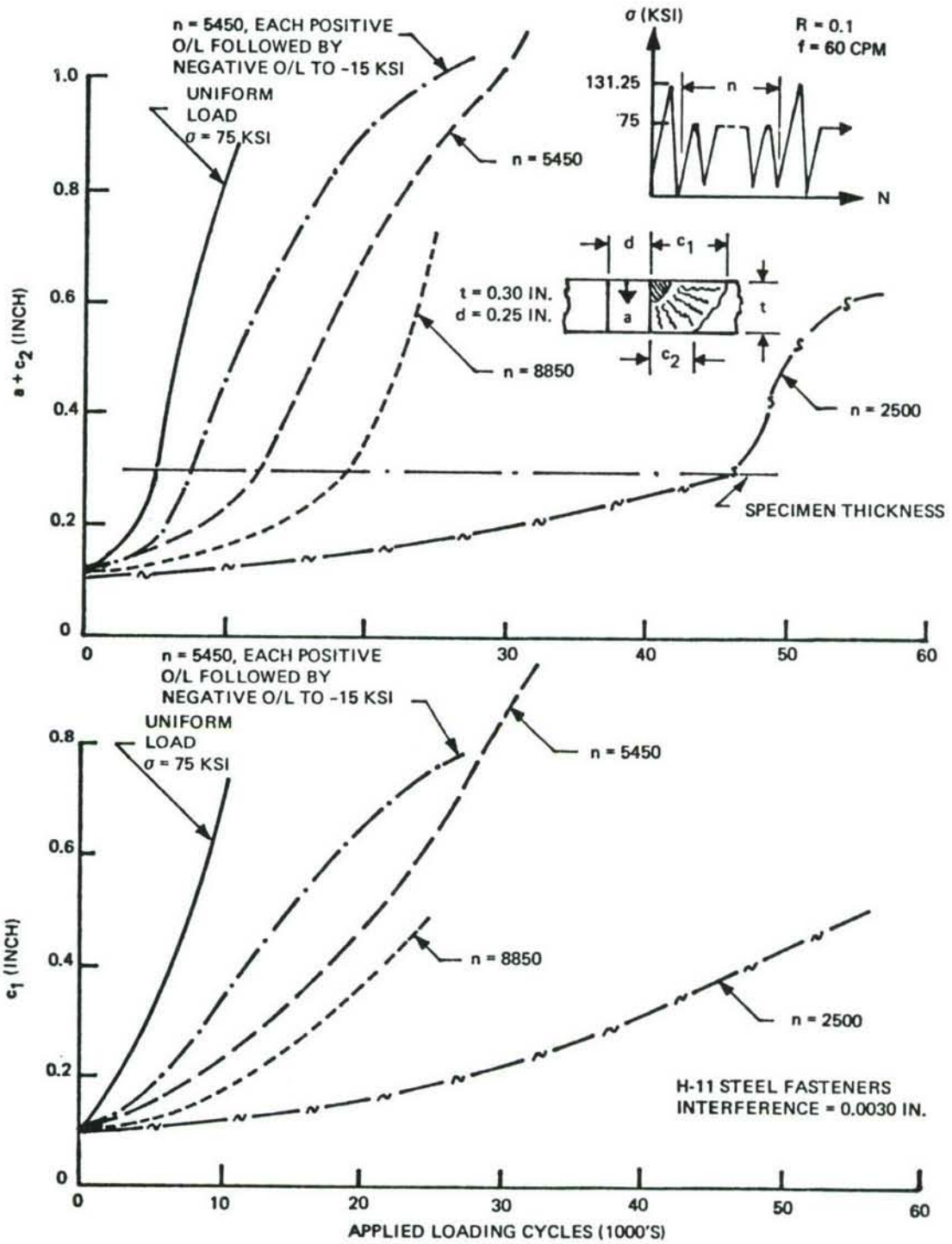


Figure 130: Effect of Periodic Overloads on Fatigue Crack Propagation of Part-Thru Cracks Originating at Unloaded Taper-Lok Fasteners in 9Ni-4Co-0.2C Steel Alloy (σ_o/σ_m = 1.75)

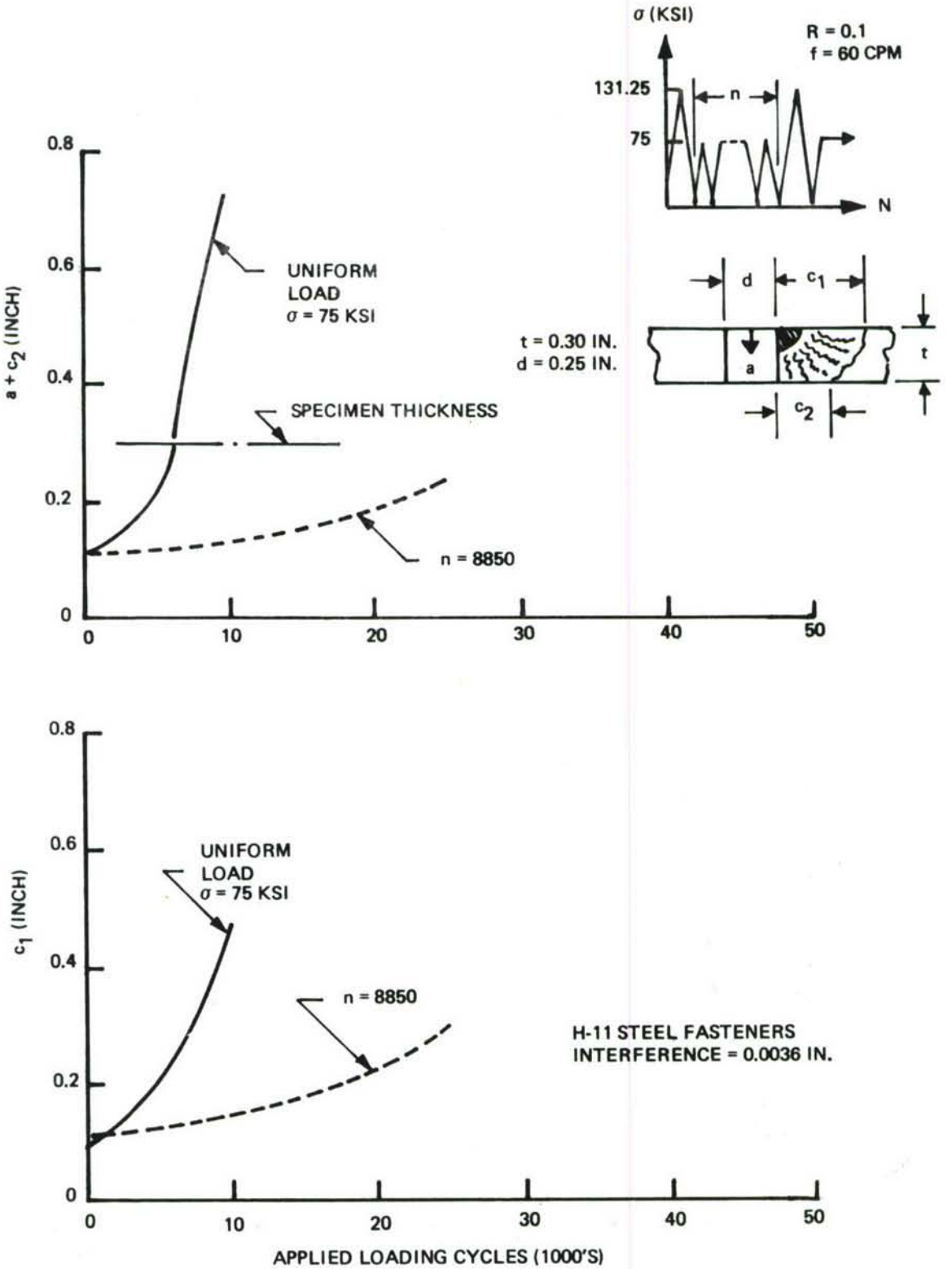


Figure 131: Effect of Periodic Overloads on Fatigue Crack Propagation of Part-Thru Cracks Originating at Unloaded Taper-Lok Fasteners in 9Ni-4Co-0.2C Steel Alloy (σ_o/σ_m = 1.75)

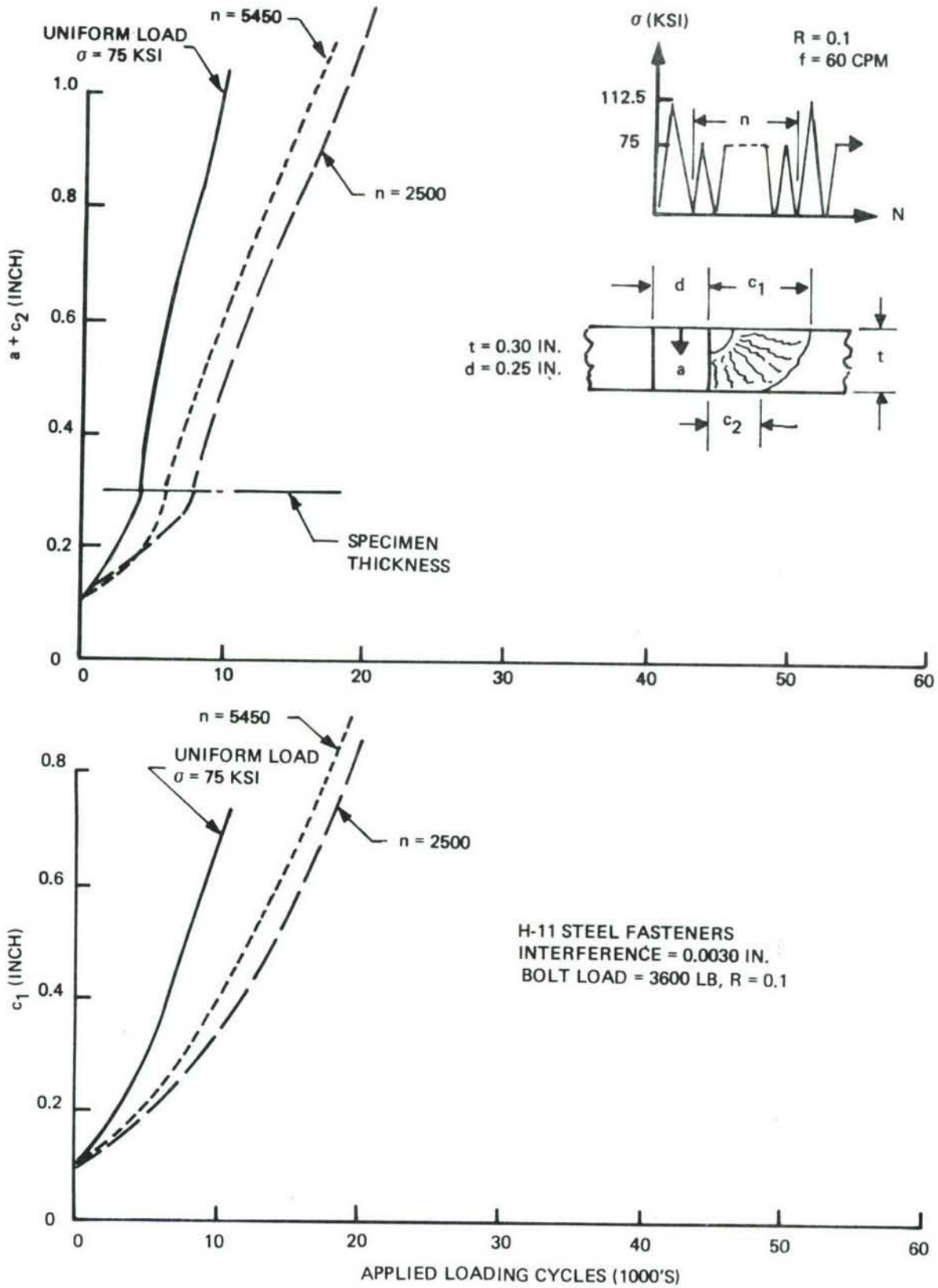


Figure 132: Effect of Periodic Overloads on Fatigue Crack Propagation of Part-Thru Cracks Originating at Taper-Lok Fasteners in 9Ni-4Co-0.2C Steel Alloy (σ_o/σ_m = 1.50)

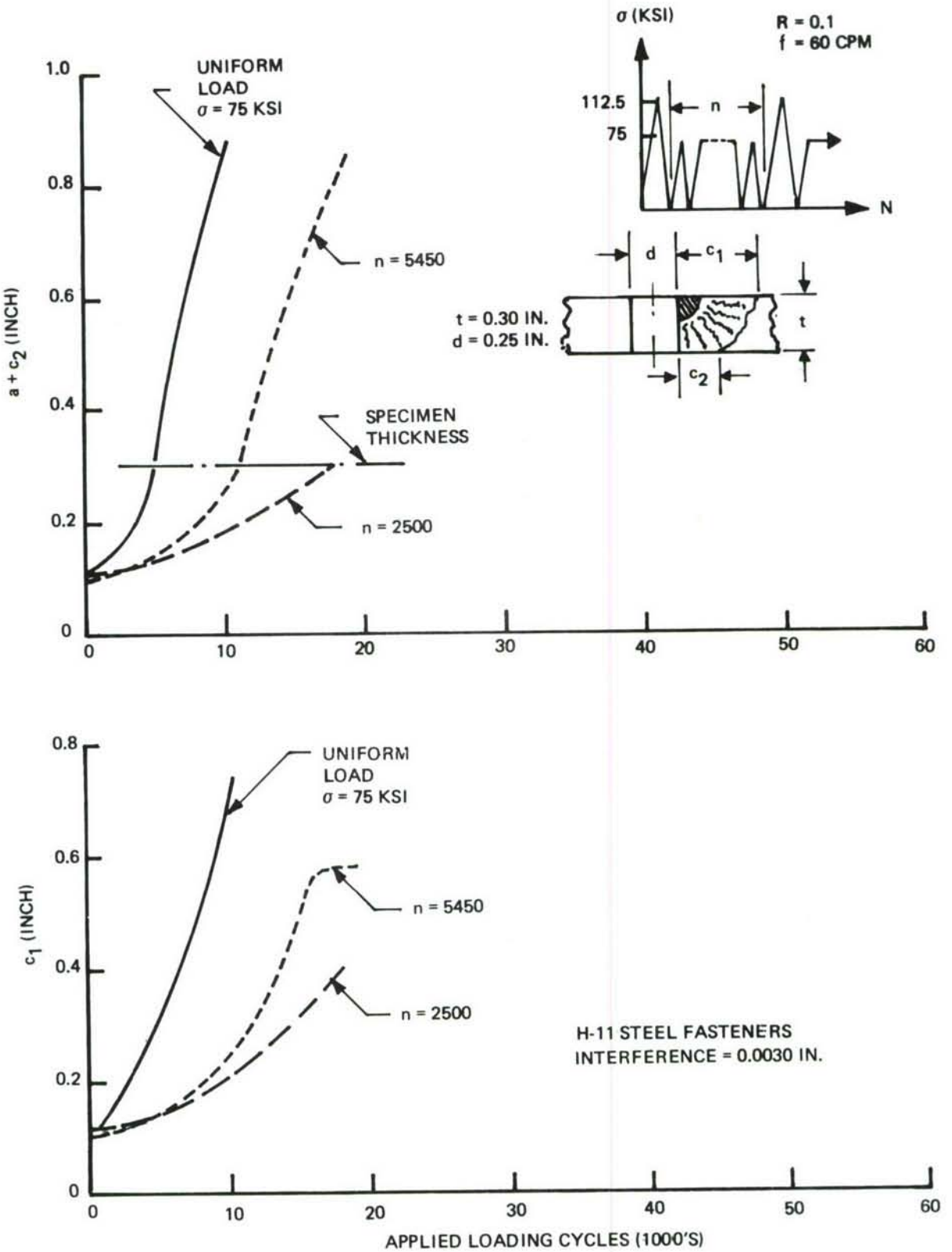


Figure 133: Effect of Periodic Overloads on Fatigue Crack Propagation of Part-Thru Cracks Originating at Unloaded Taper-Lok Fasteners in 9Ni-4Co-0.2C Steel Alloy (σ_0/σ_m = 1.50)

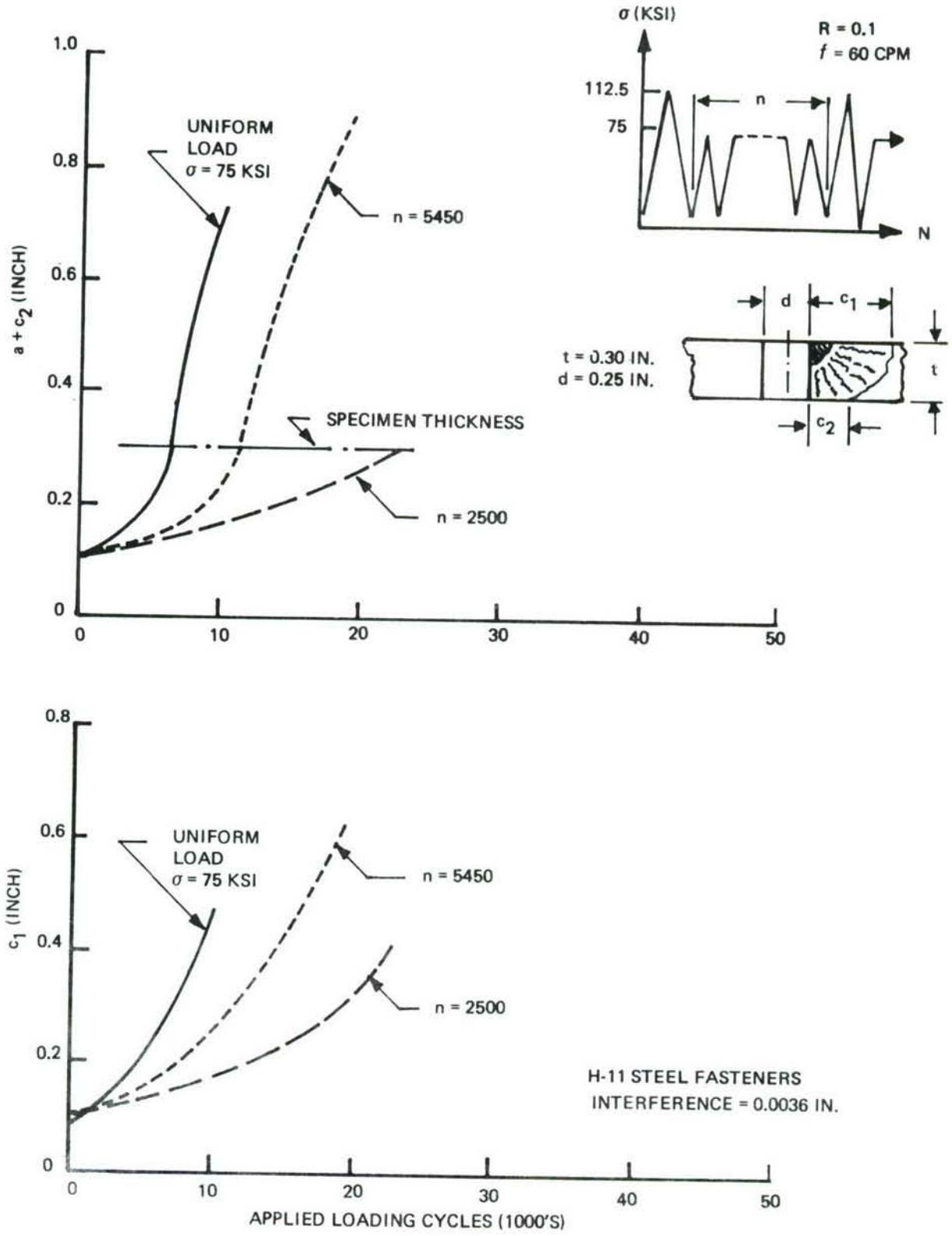


Figure 134: Effect of Periodic Overloads on Fatigue Crack Propagation of Part-Thru Cracks Originating at Unloaded Taper-Lok Fasteners in 9Ni–4Co–0.2C Steel Alloy ($\sigma_0 / \sigma_m = 1.50$)

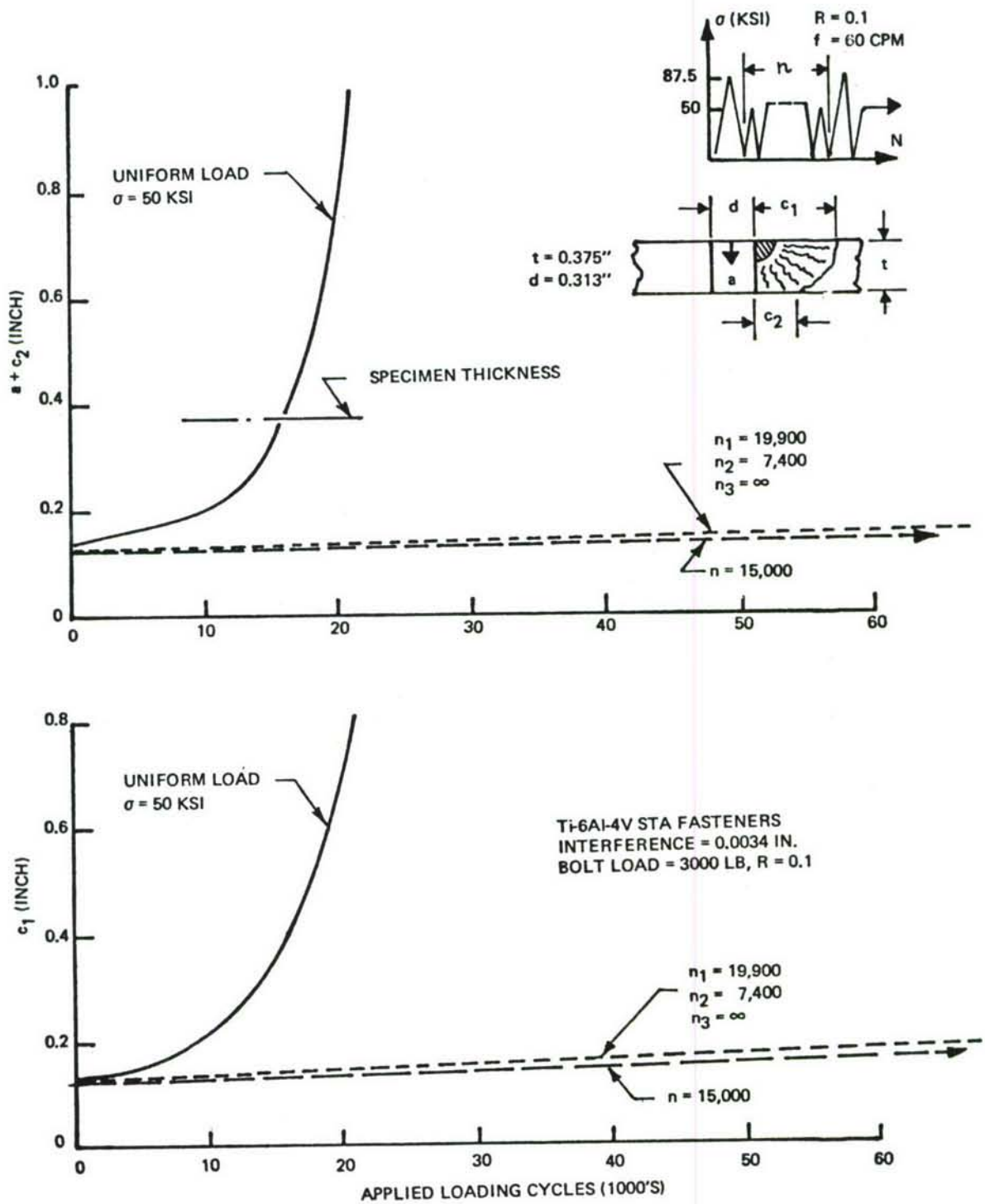


Figure 135: Effect of Periodic Overloads on Fatigue Crack Propagation of Part-Thru Cracks Originating at Loaded Taper-Lok Fasteners in 6Al-4V βA Titanium Alloy (σ_0/σ_m = 1.75)

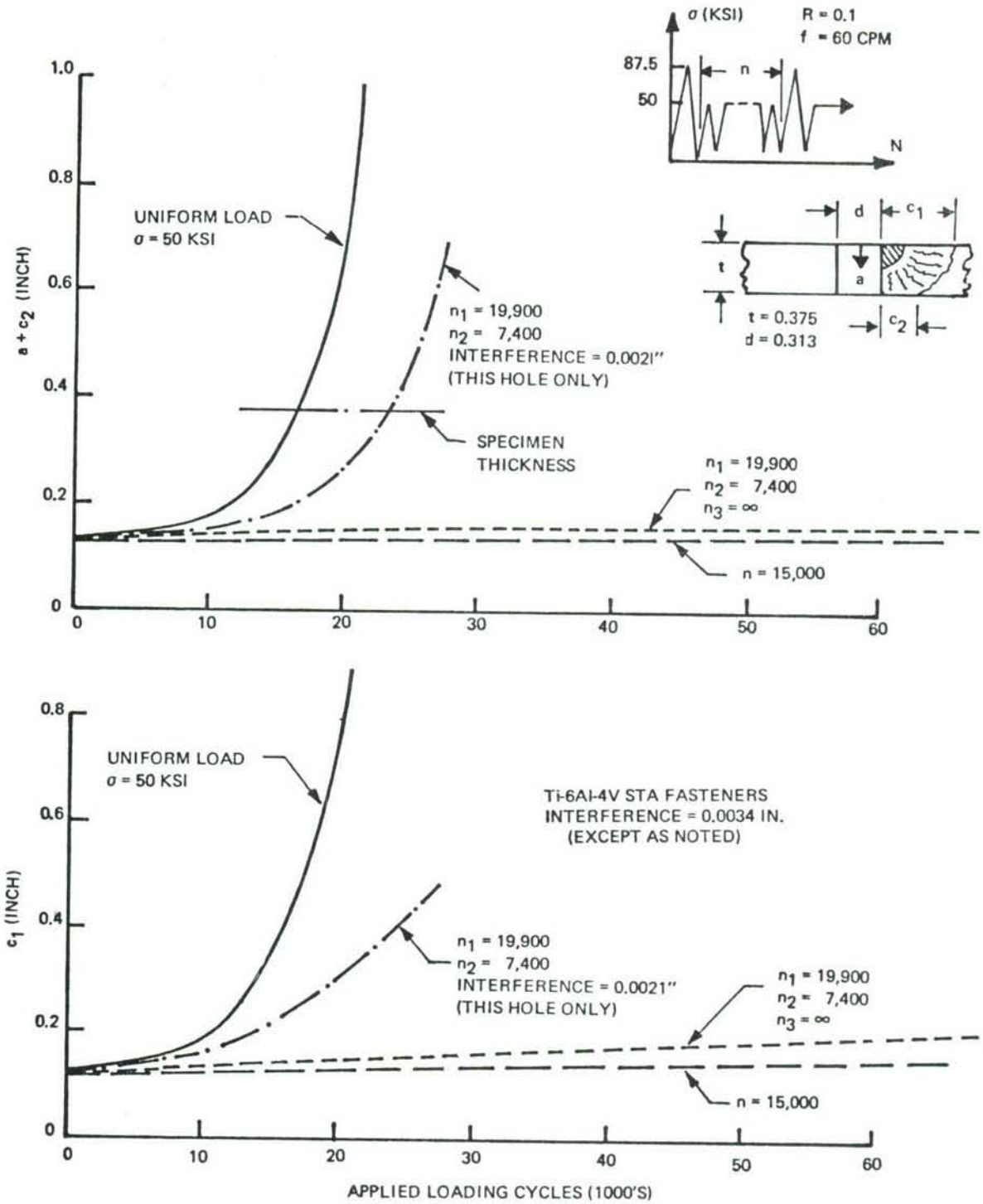


Figure 136: Effect of Periodic Overloads on Fatigue Crack Propagation of Part-Thru Cracks Originating at Unloaded Taper-Lok Fasteners in 6Al-4V βA Titanium Alloy (σ_0/σ_m = 1.75)

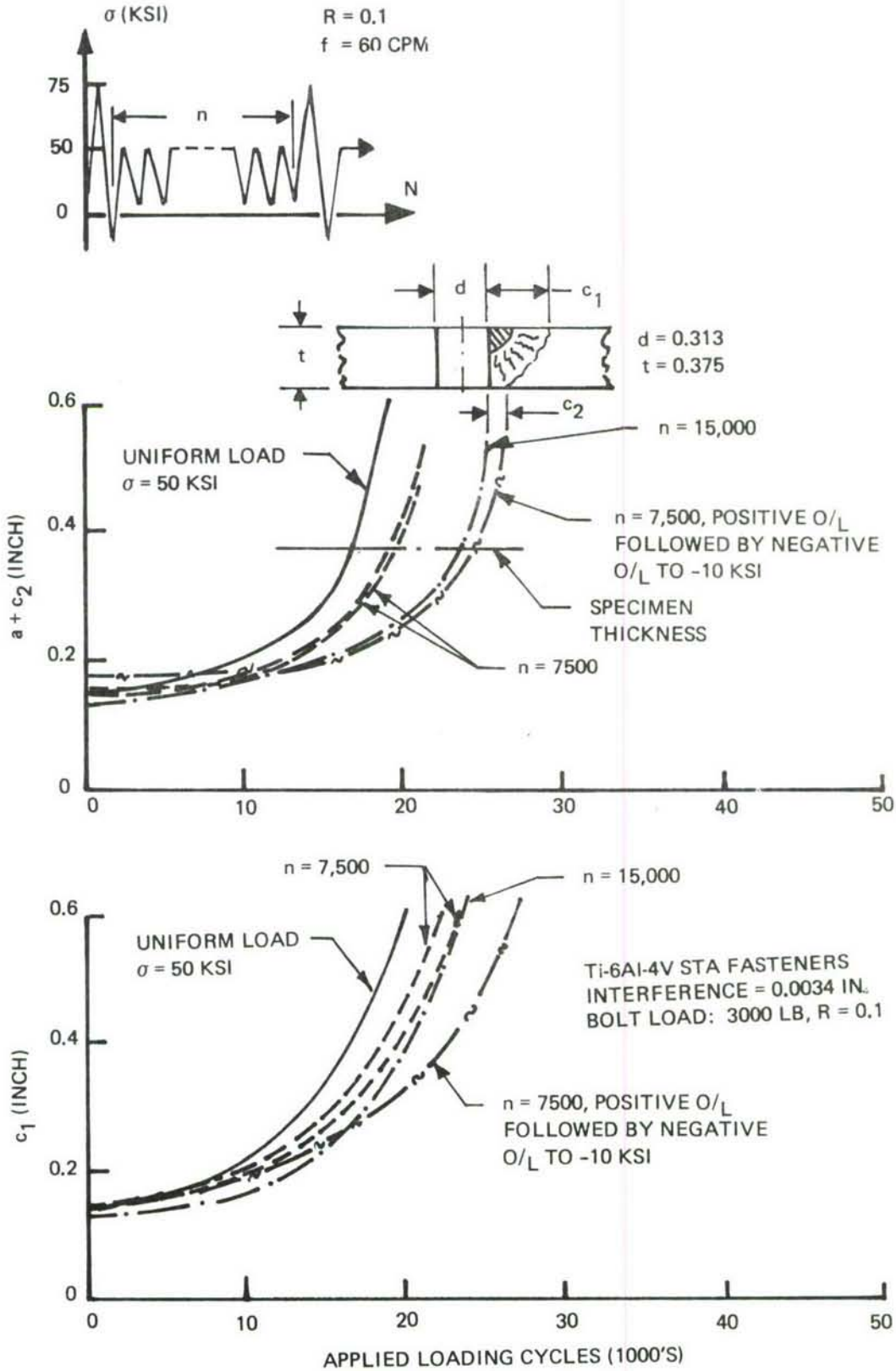


Figure 137: Effect of Periodic Overloads on Fatigue Crack Propagation of Part-Thru Cracks Originating at Loaded Taper-Lok Fasteners in 6Al-4V βA Titanium Alloy (σ_0/σ_m = 1.50)

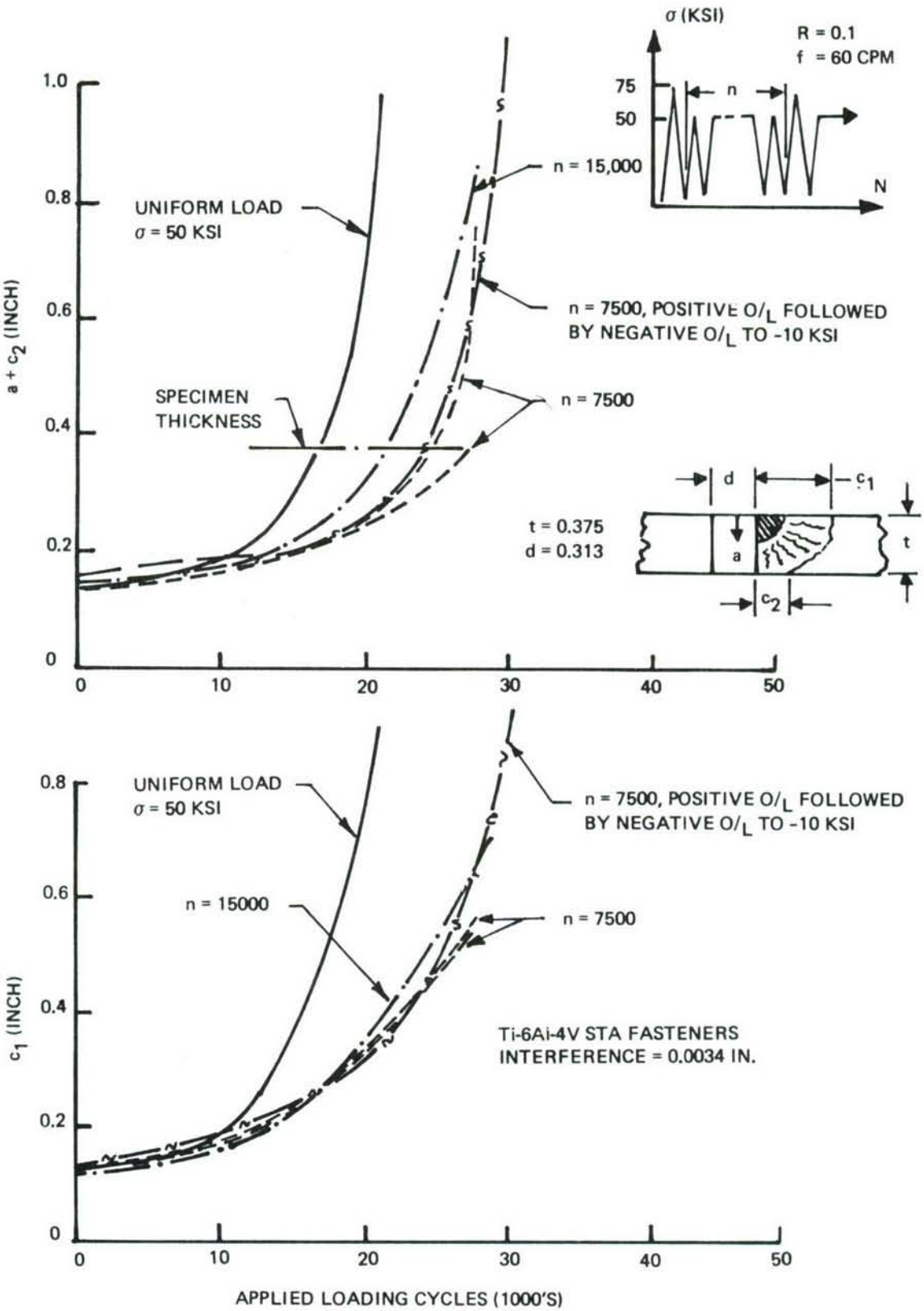


Figure 138: Effect of Periodic Overloads on Fatigue Crack Propagation of Part-Thru Cracks Originating at Unloaded Taper-Lok Fasteners in 6Al-4V βA Titanium Alloy (σ_o/σ_m = 1.50)

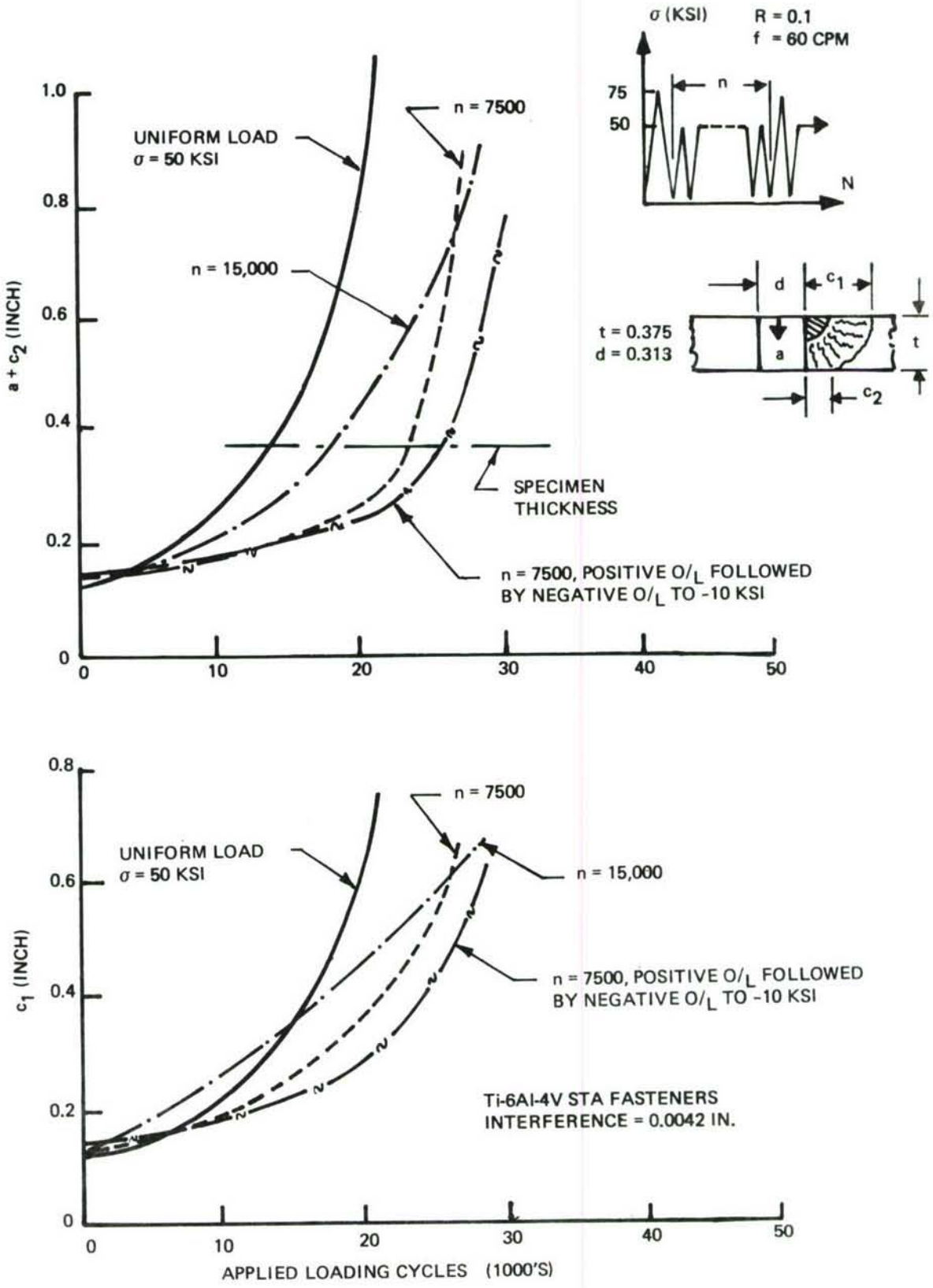


Figure 139: Effect of Periodic Overloads on Fatigue Crack Propagation of Part-Thru Cracks Originating at Unloaded Taper-Lok Fasteners in 6Al-4V βA Titanium Alloy (σ_0/σ_m = 1.50)

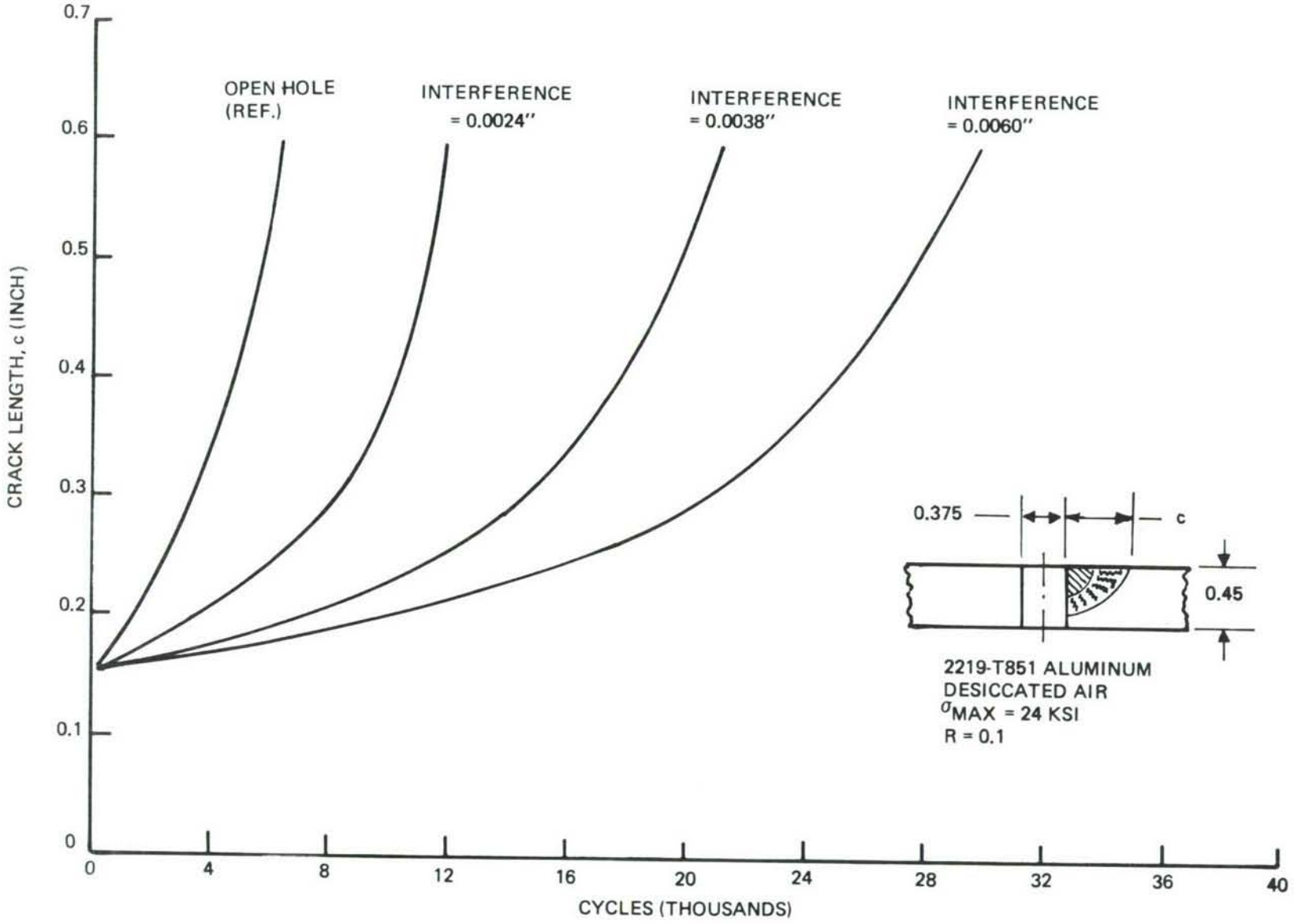


Figure 140: Effect of Taper-Lok Bolt Interference on Fatigue Crack Growth of Part-Thru Cracks in 2219-T851 Aluminum Alloy

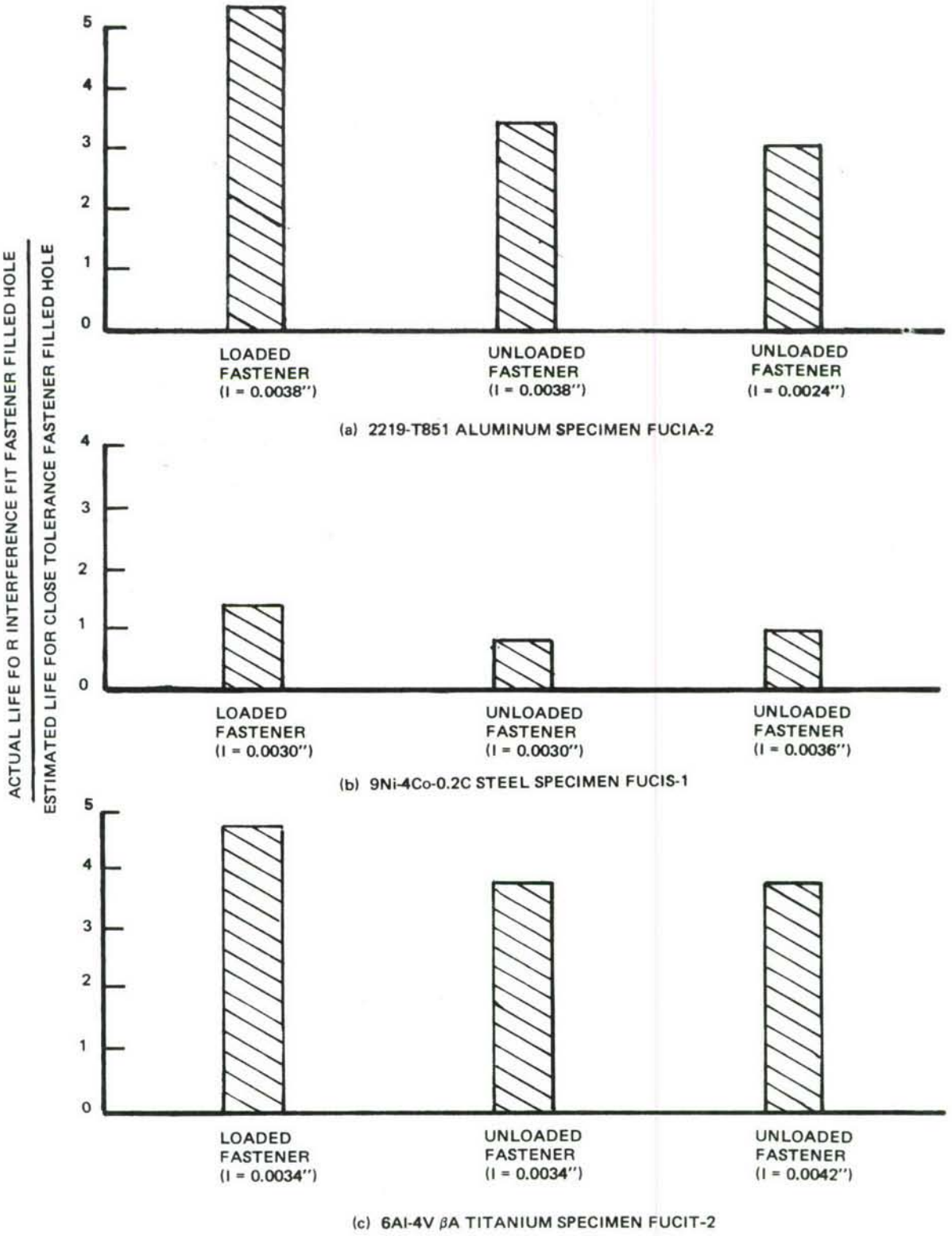
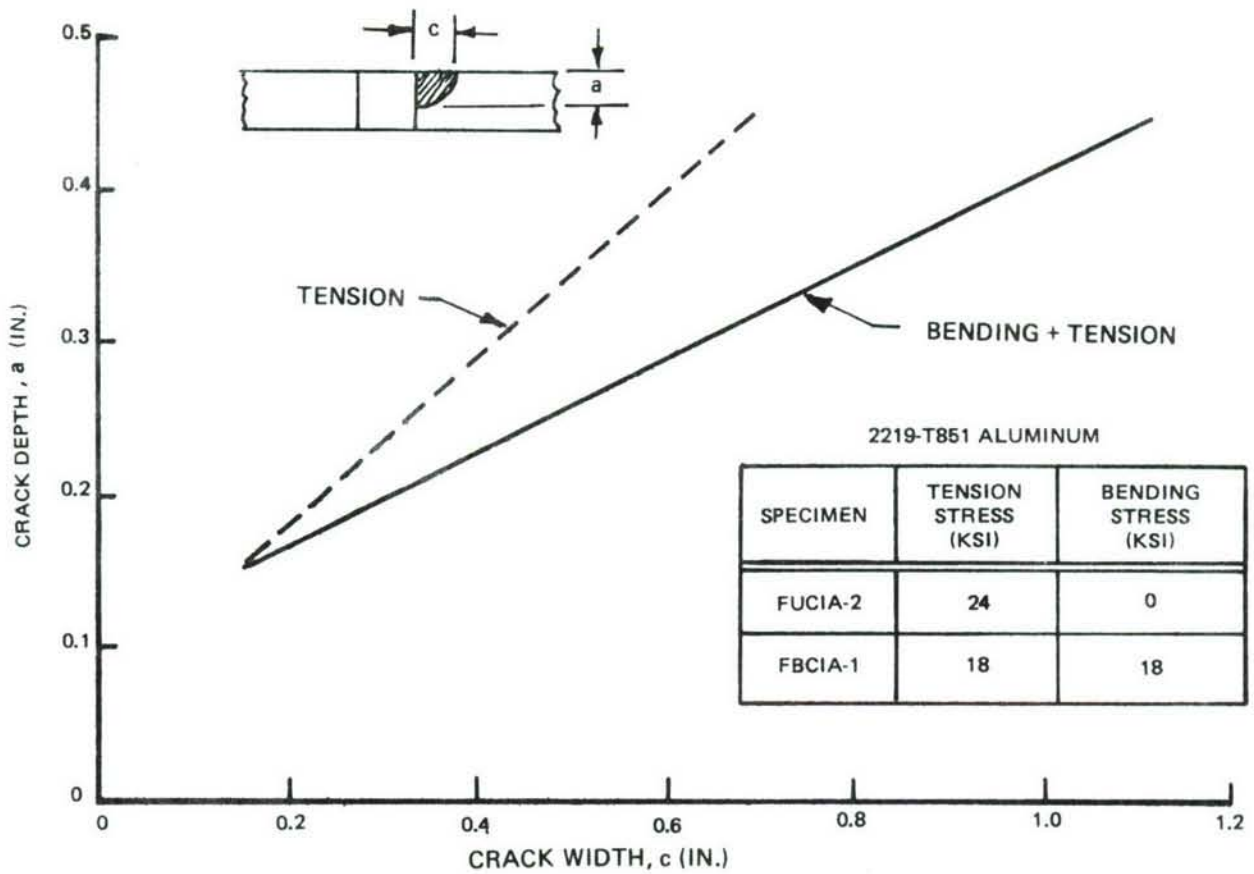
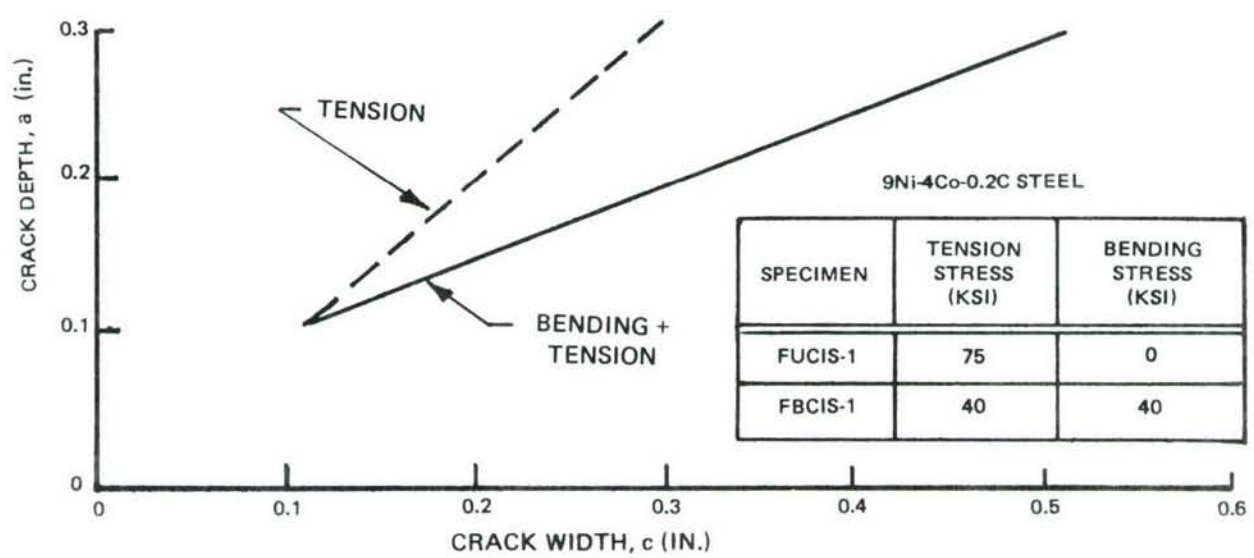


Figure 141: Comparison Between Crack Propagation Lives for Part-Thru Cracks Originating at Interference Fit and Close Tolerance Fastener Filled Holes



2219-T851 ALUMINUM

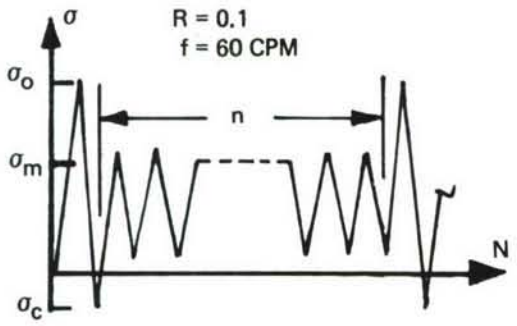
SPECIMEN	TENSION STRESS (KSI)	BENDING STRESS (KSI)
FUCIA-2	24	0
FBCIA-1	18	18



9Ni-4Co-0.2C STEEL

SPECIMEN	TENSION STRESS (KSI)	BENDING STRESS (KSI)
FUCIS-1	75	0
FBCIS-1	40	40

Figure 142: Comparison of Crack Growth Data for Part–Thru Cracks Originating at Taper-Lok Filled Holes Subjected to Tension or Combined Bending and Tension Stresses



SYMBOL	σ_o (KSI)	σ_m (KSI)	σ_c (KSI)	n (CYCLES)
———	21.0	21.0	2.1	—
— — —	36.8	21.0	2.1	9200
- - - -	36.8	21.0	2.1	4600
—·—	36.8	21.0	−4.2	4600

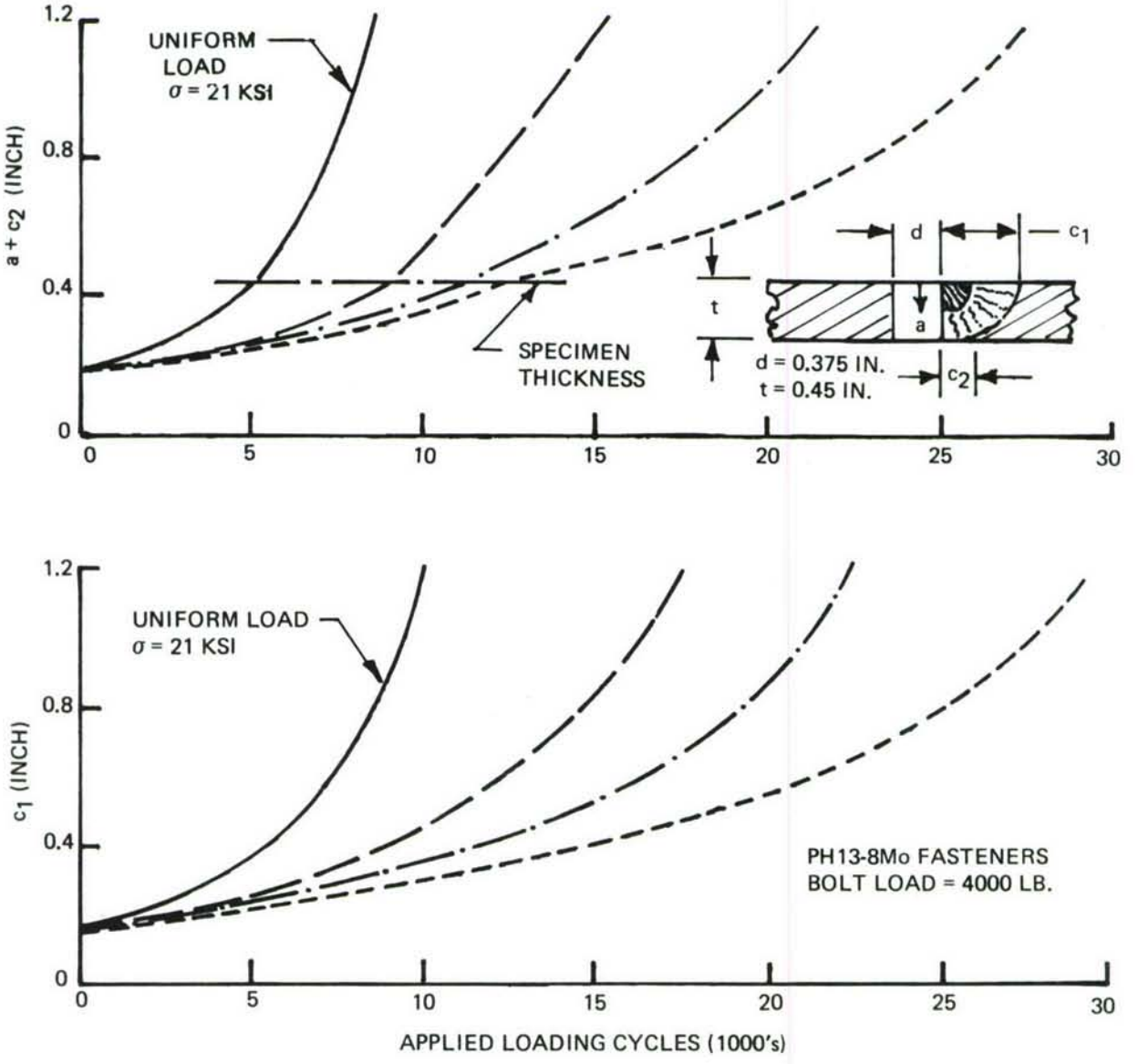
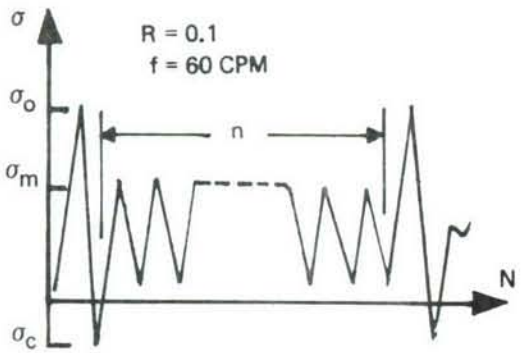


Figure 143: Effect of Periodic Overloads on Fatigue Crack Propagation of Part–Thru Cracks Originating At Loaded Close Tolerance Fasteners in 2219–T851 Aluminum Alloy ($\sigma_o/\sigma_m = 1.75$)



SYMBOL	σ_o (KSI)	σ_m (KSI)	σ_c (KSI)	n (CYCLES)
———	21.0	21.0	2.1	—
— — —	36.8	21.0	2.1	9200
- - - -	36.8	21.0	2.1	4600
—·—	36.8	21.0	−4.2	4600

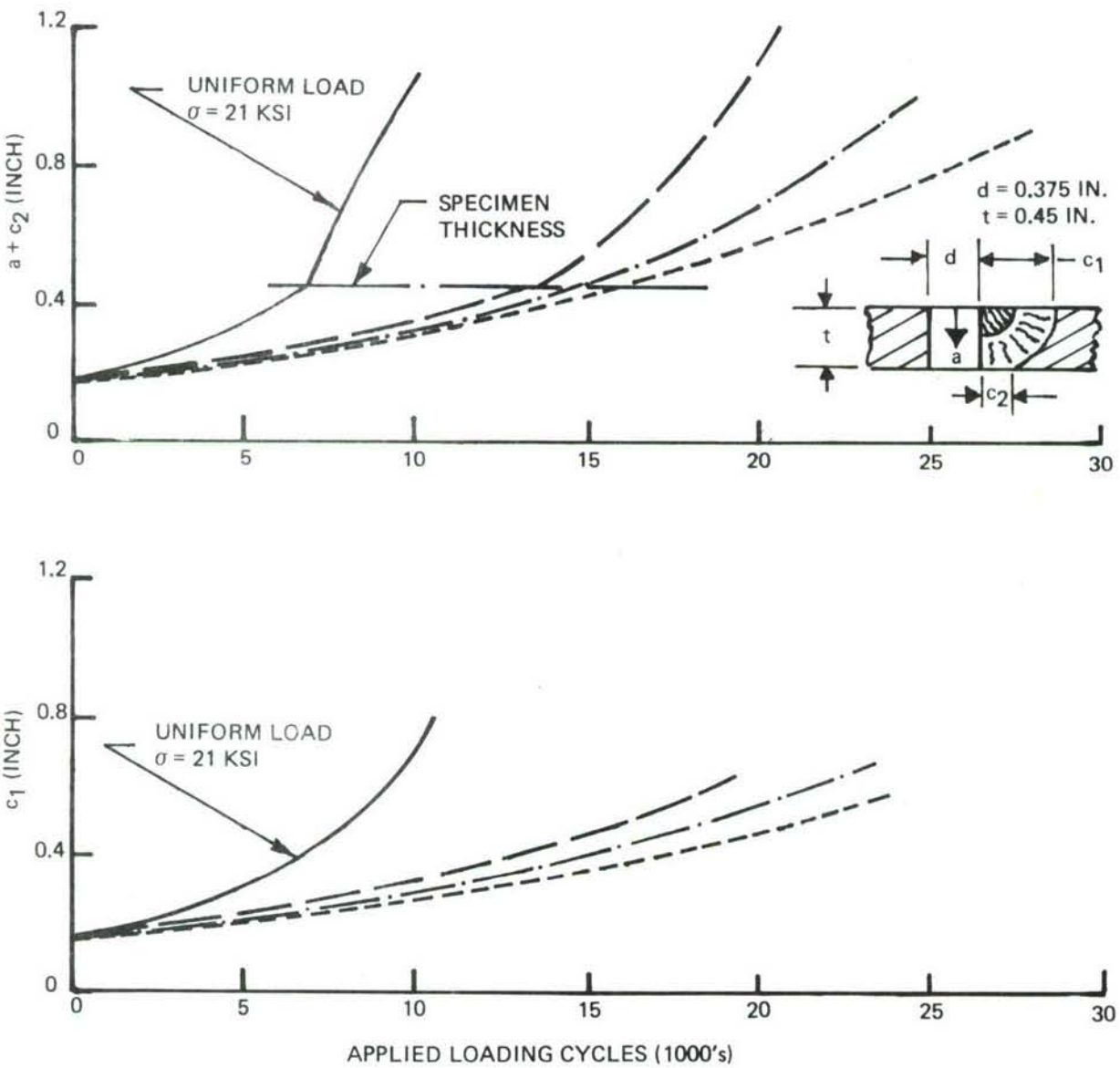


Figure 144: Effect of Periodic Overloads on Fatigue Crack Propagation of Part – Thru Cracks Originating at Open Holes in 2219–T851 Aluminum Alloy ($\sigma_o/\sigma_m = 1.75$)

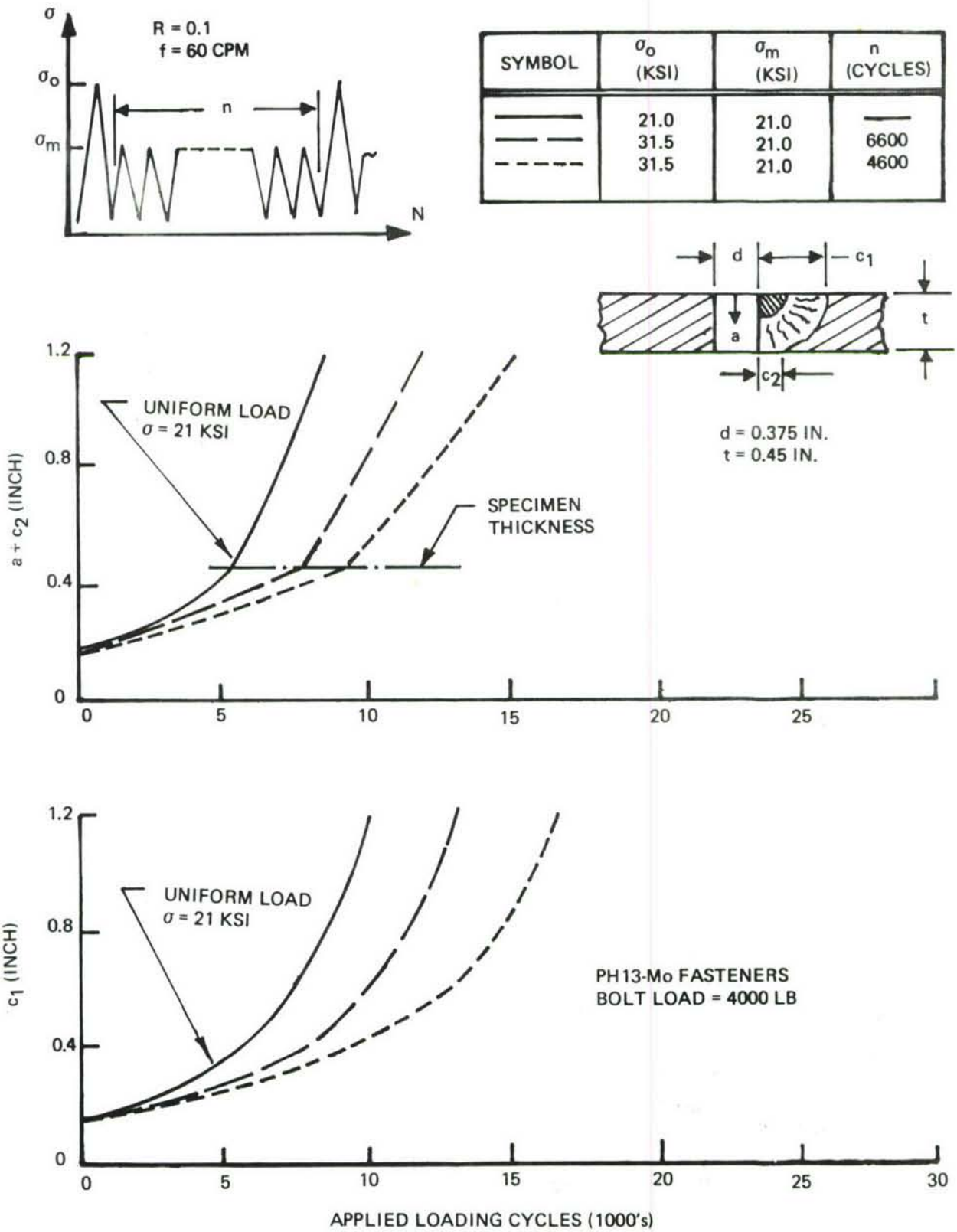


Figure 145: Effect of Periodic Overloads on Fatigue Crack Propagation of Part–Thru Cracks Originating at Loaded Close Tolerance Fasteners in 2219–T851 Aluminum Alloy (σ_o/σ_m = 1.50)

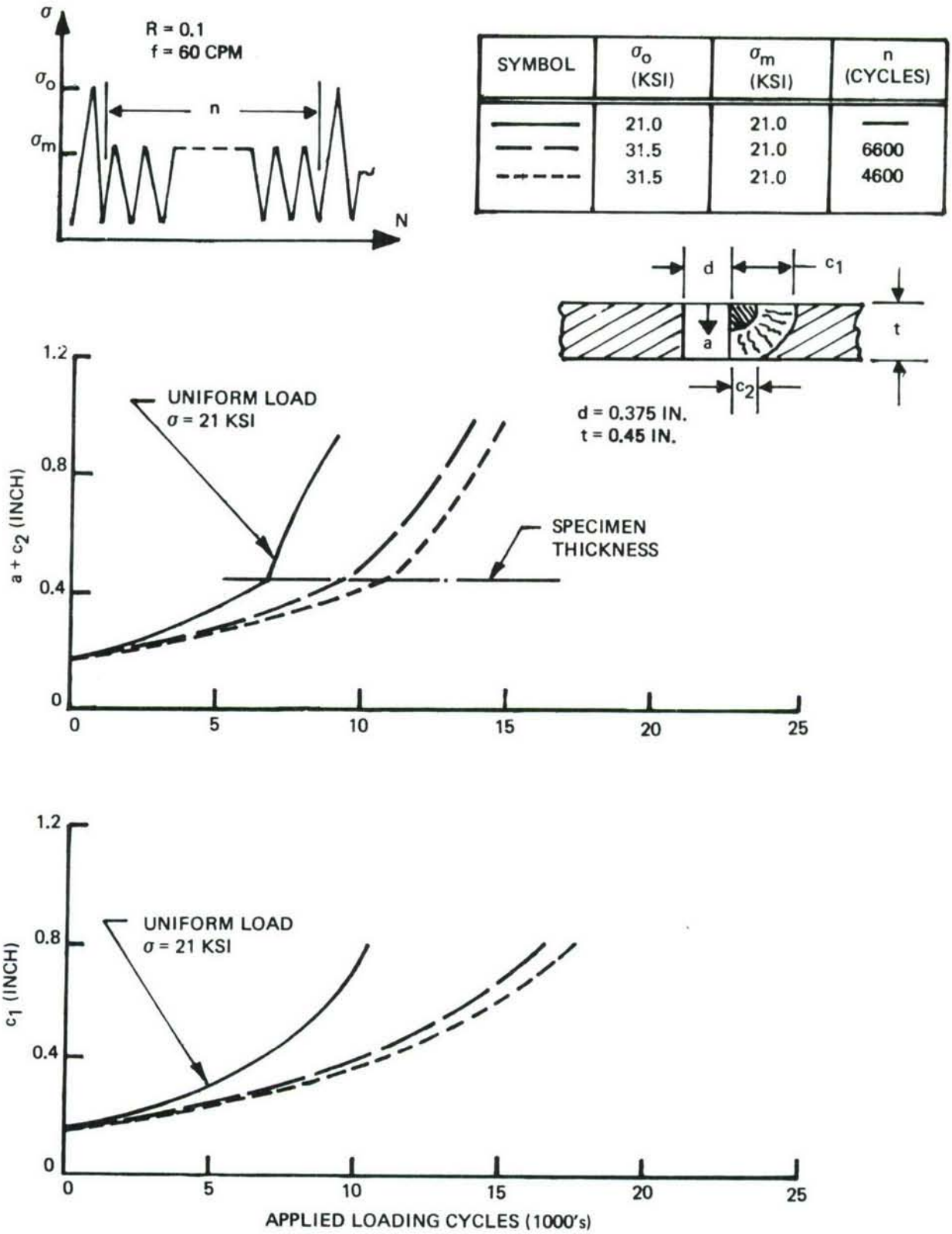


Figure 146: Effect of Periodic Overloads on Fatigue Crack Propogation of Part – Thru Cracks Originating at Open Holes in 2219–T851 Aluminum Alloy (σ_o/σ_m = 1.50)

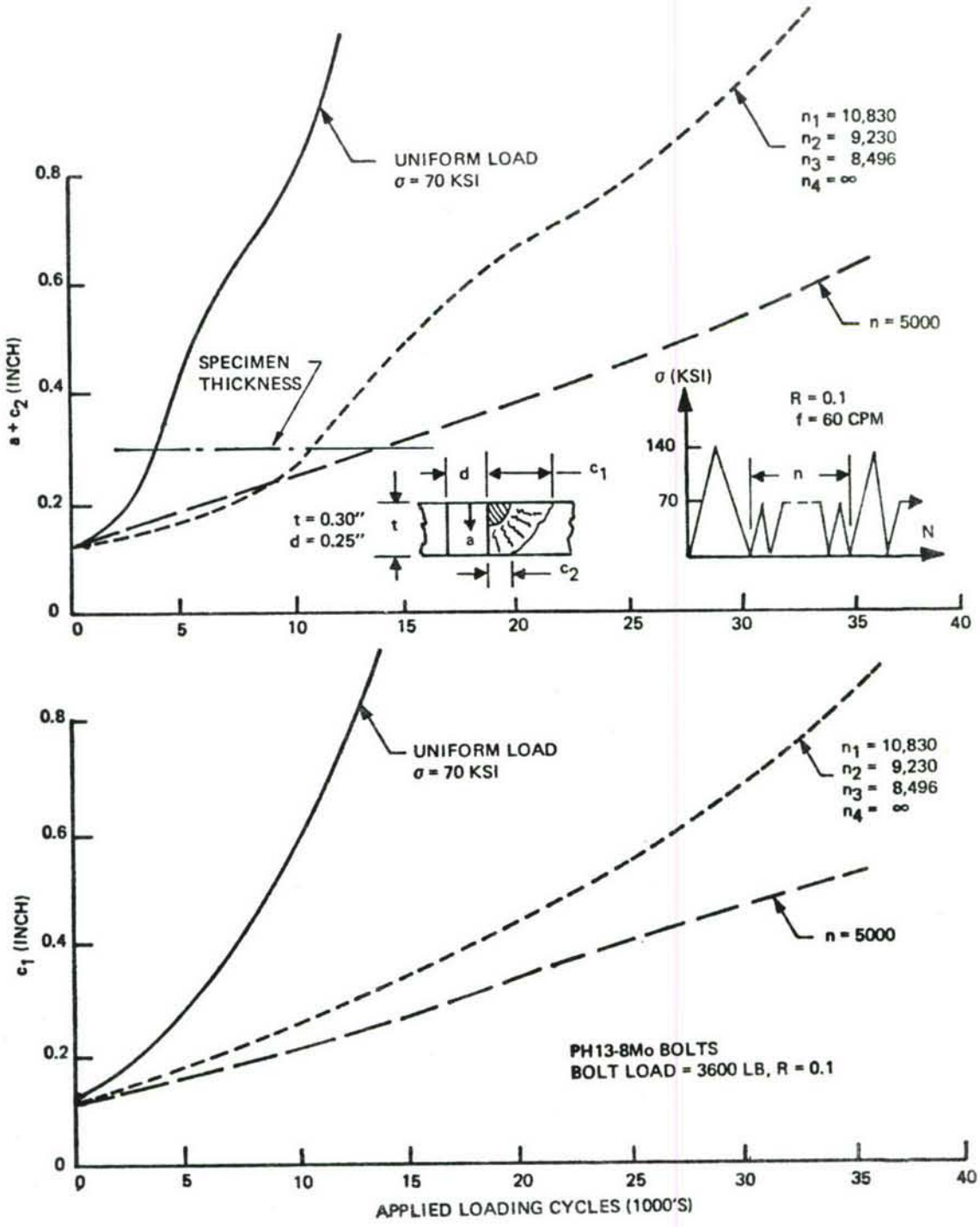


Figure 147: Effect of Periodic Overloads on Fatigue Crack Propagation of Part-Thru Cracks Originating at Loaded Close Tolerance Fasteners in 9Ni-4Co-0.2C Steel Alloy (σ_o/σ_m = 2.00)

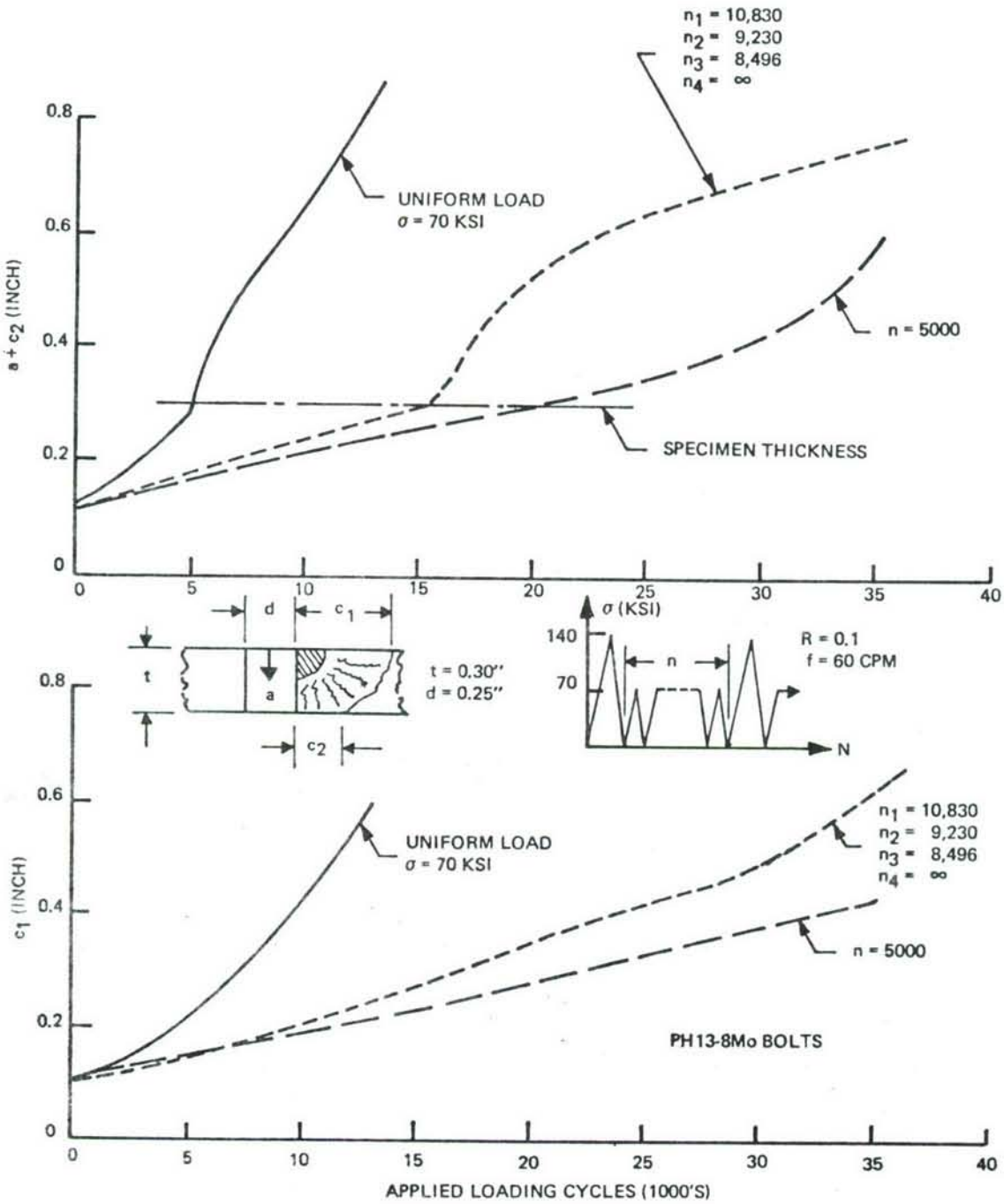


Figure 148: Effect of Periodic Overloads on Fatigue Crack Propagation of Part-Thru Cracks Originating at an Unloaded Close Tolerance Fastener in 9Ni-4Co-0.2C Steel Alloy (σ_o/σ_m = 2.00)

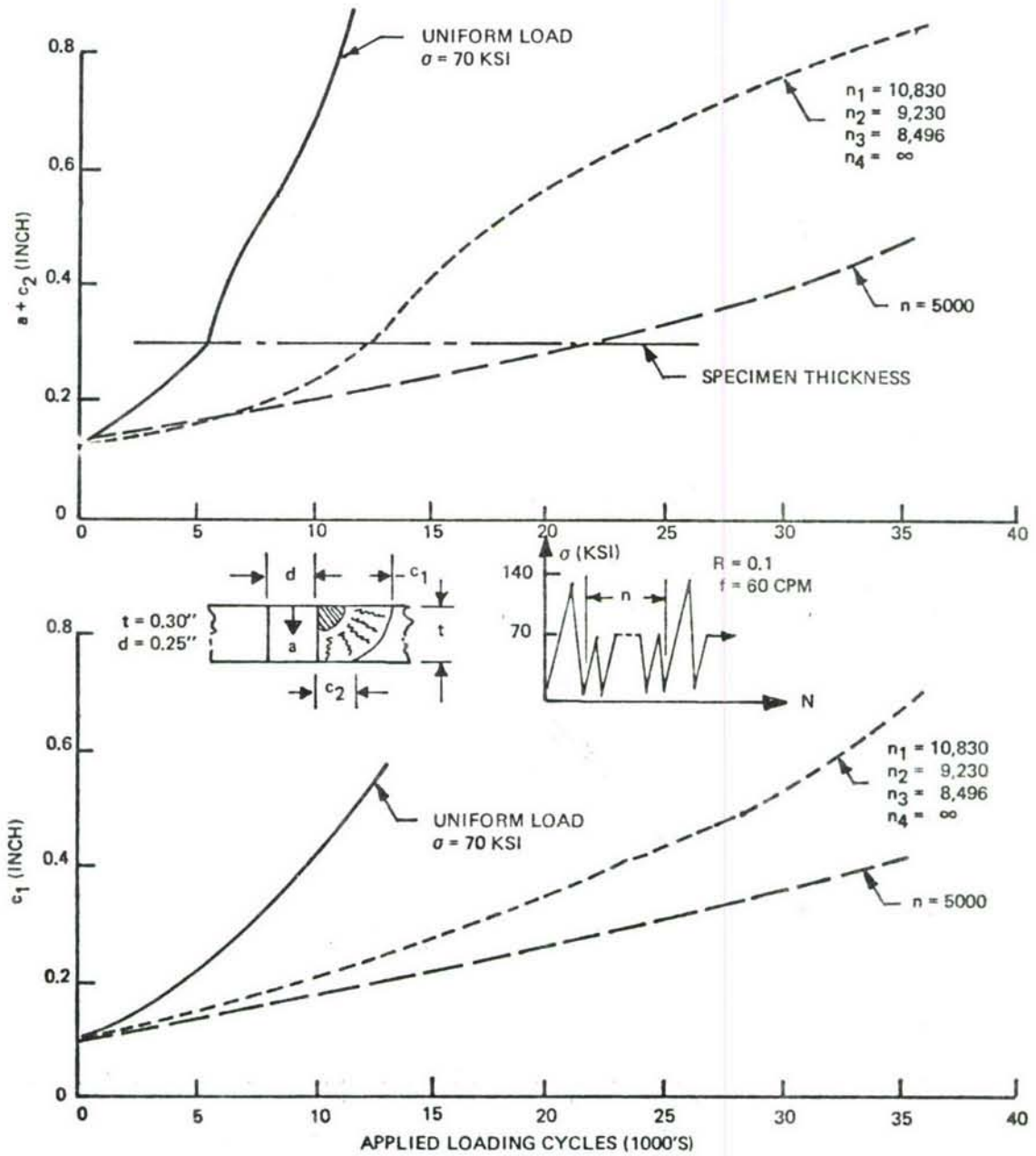


Figure 149: Effect of Periodic Overloads on Fatigue Crack Propagation of Part-Thru Cracks Originating at Open Holes in 9Ni-4Co-0.2C Steel Alloy (σ_o/σ_m = 2.00)

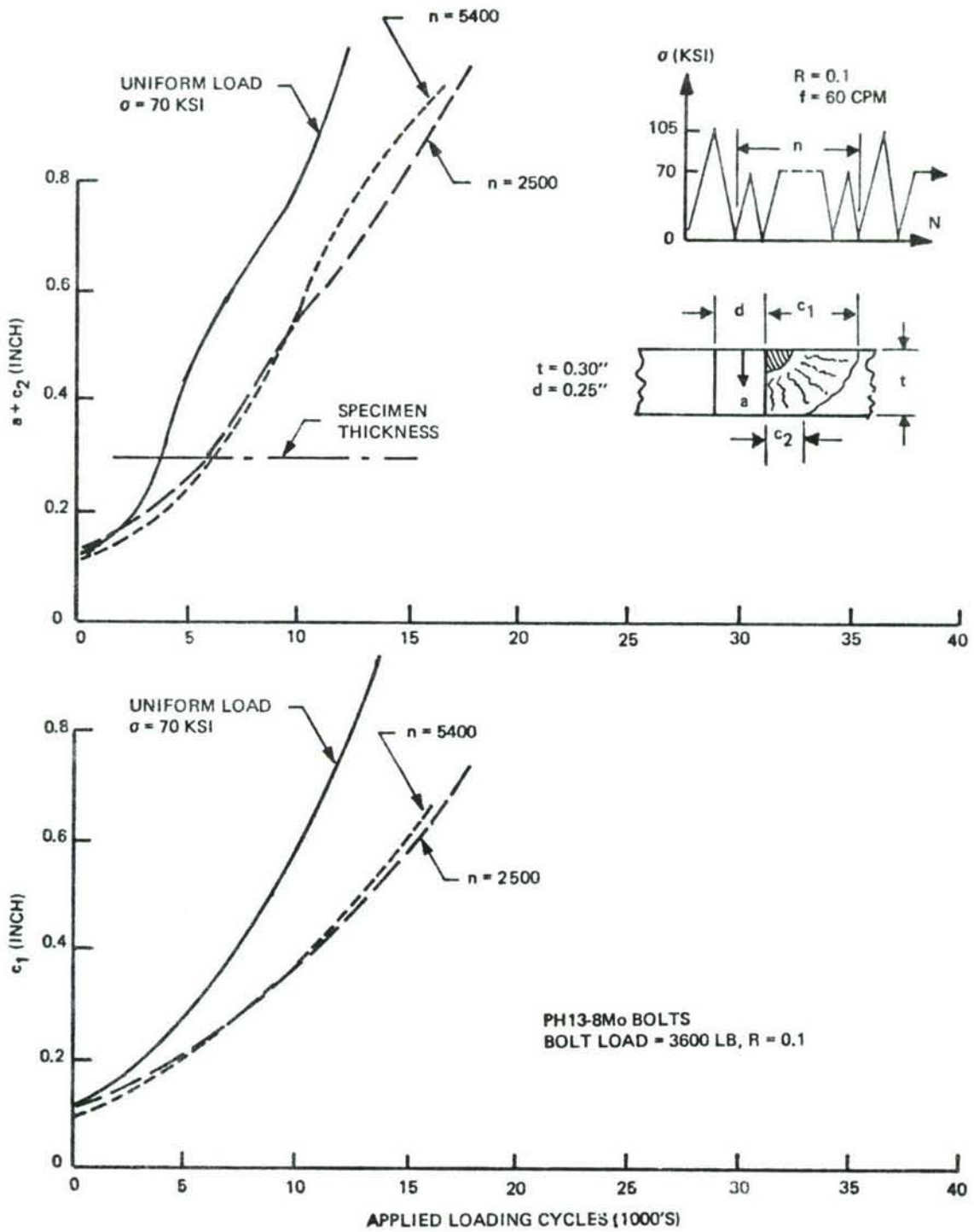


Figure 150: Effect of Periodic Overloads on Fatigue Crack Propagation of Part-Thru Cracks Originating at Loaded Close Tolerance Fasteners in 9Ni-4Co-0.2C Steel Alloy (σ_0/σ_m = 1.50)

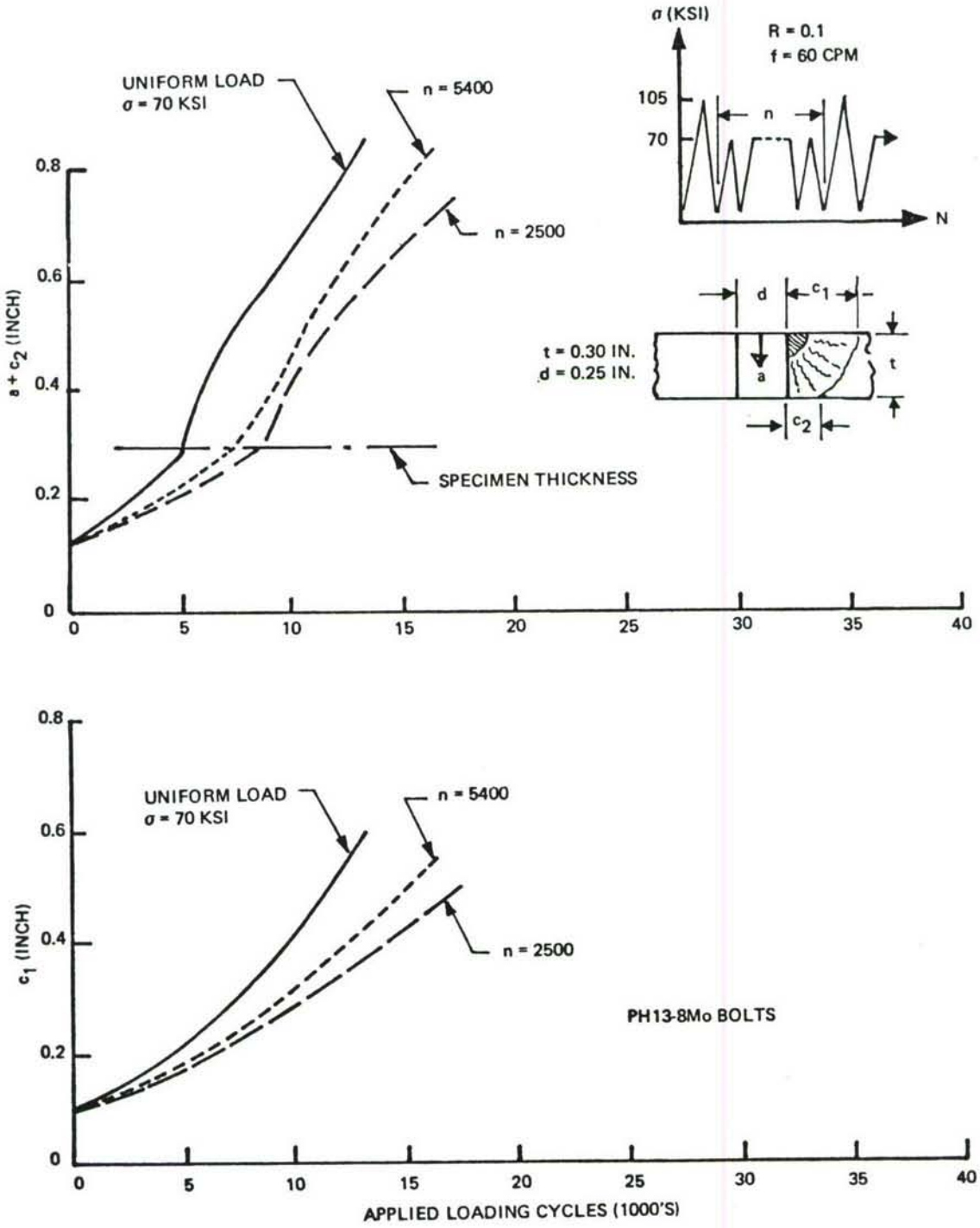


Figure 151: Effect of Periodic Overloads on Fatigue Crack Propagation of Part-Thru Cracks Originating at Unloaded Close Tolerance Fasteners in 9Ni-4Co-0.2C Steel Alloy (σ_o/σ_m = 1.50)

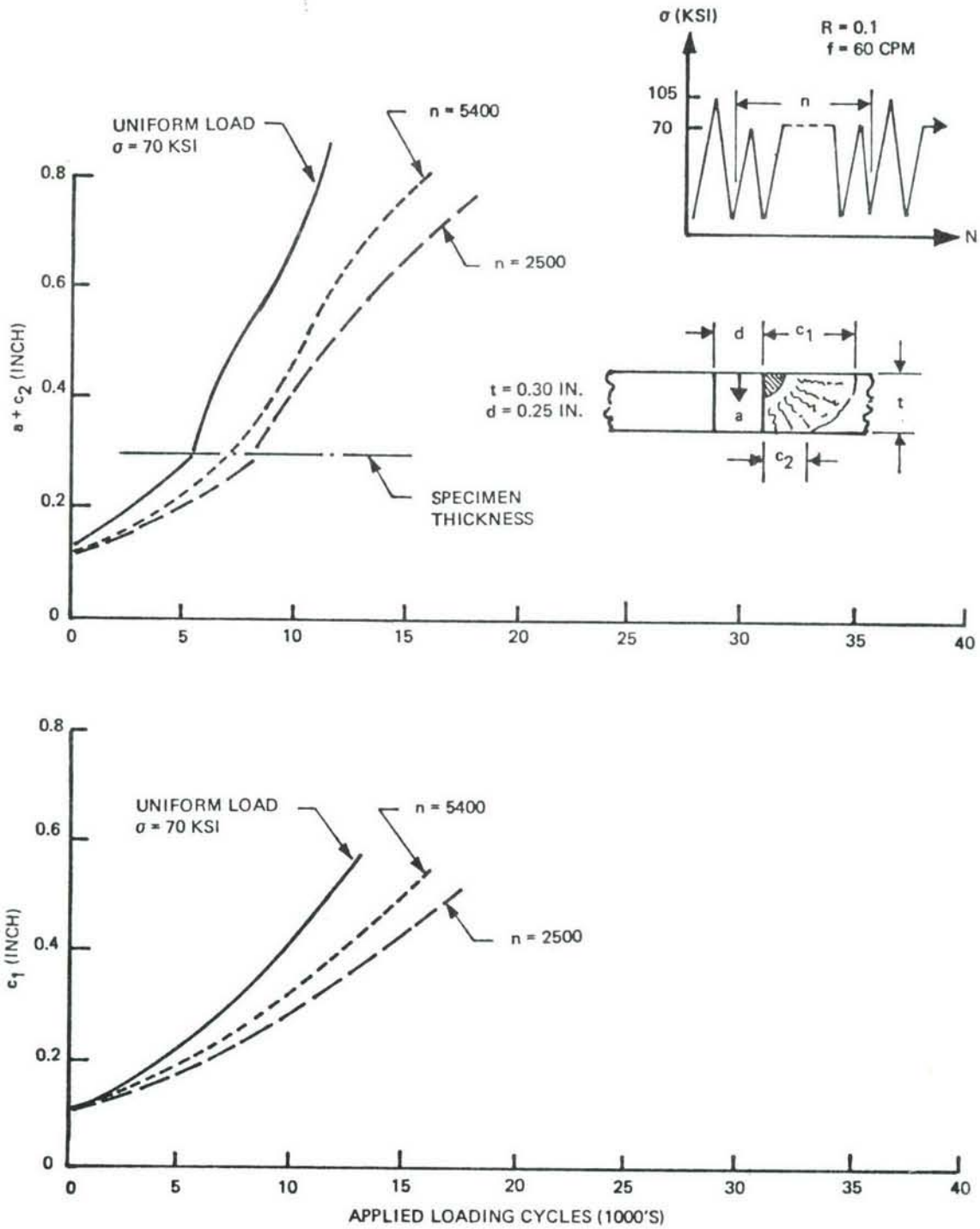


Figure 152: Effect of Periodic Overloads on Fatigue Crack Propagation of Part-Thru Cracks Originating at Open Holes in 9Ni-4Co-0.2C Steel Alloy (σ_0/σ_m = 1.50)

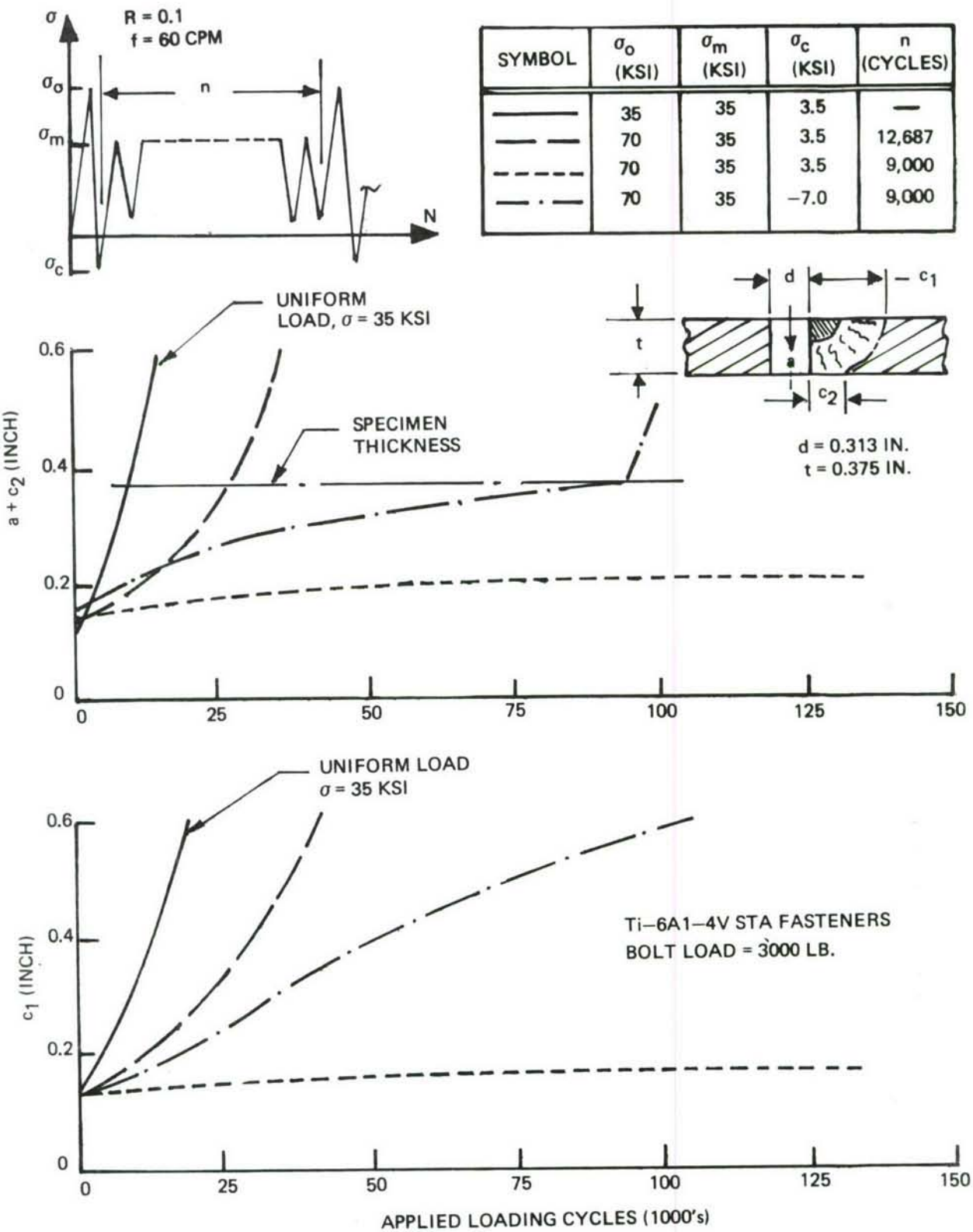


Figure 153: Effect of Periodic Overloads on Fatigue Crack Propagation of Part–Thru Cracks Originating at Loaded Close Tolerance Fasteners in 6A1–4V βA Titanium Alloy (σ_o/σ_m = 2.00)

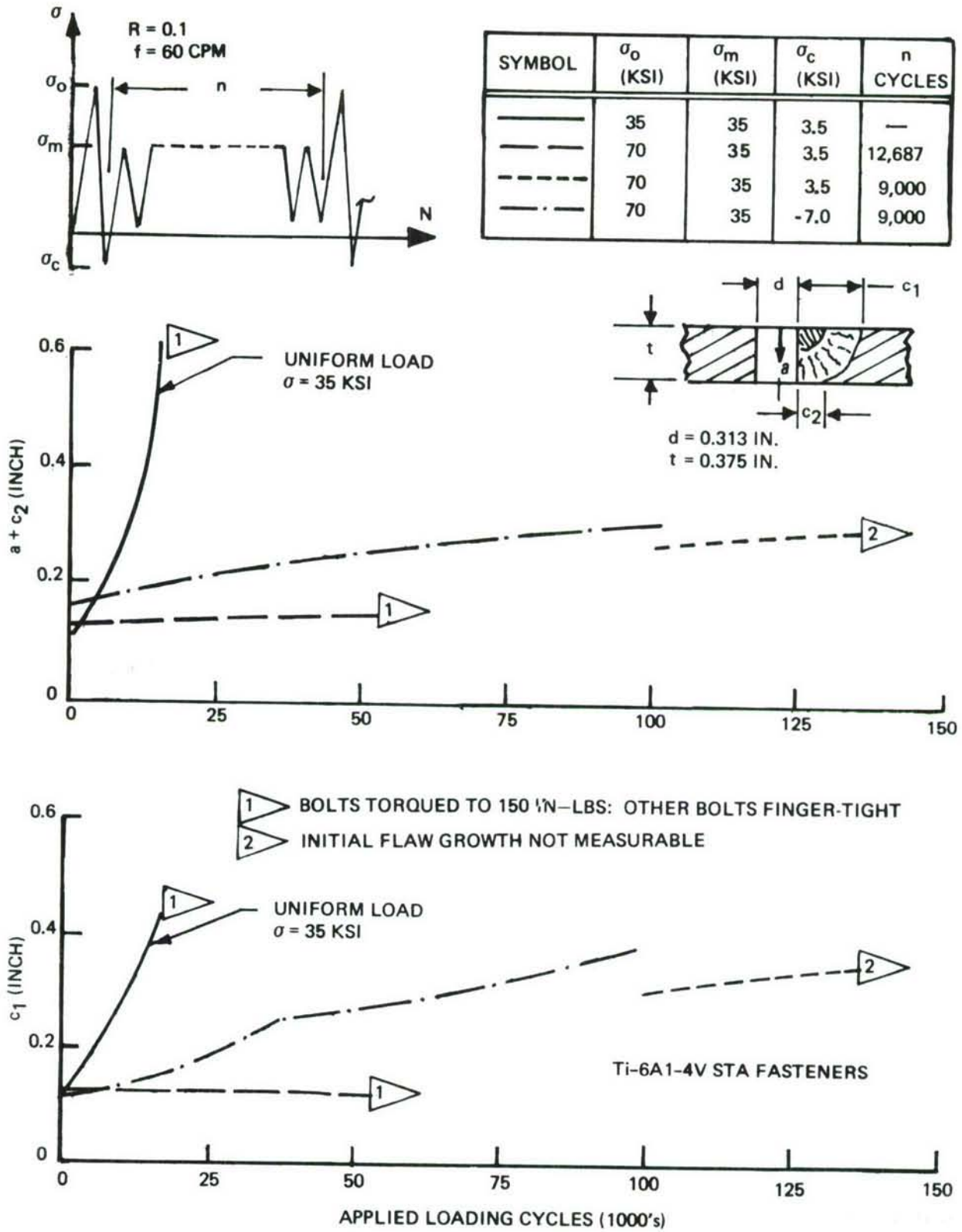


Figure 154: Effect of Periodic Overloads on Fatigue Crack Propagation of Part–Thru Cracks Originating at Unloaded Close Tolerance Fasteners in 6A1-4VβA Titanium Alloy (σ_o/σ_m = 2.00)

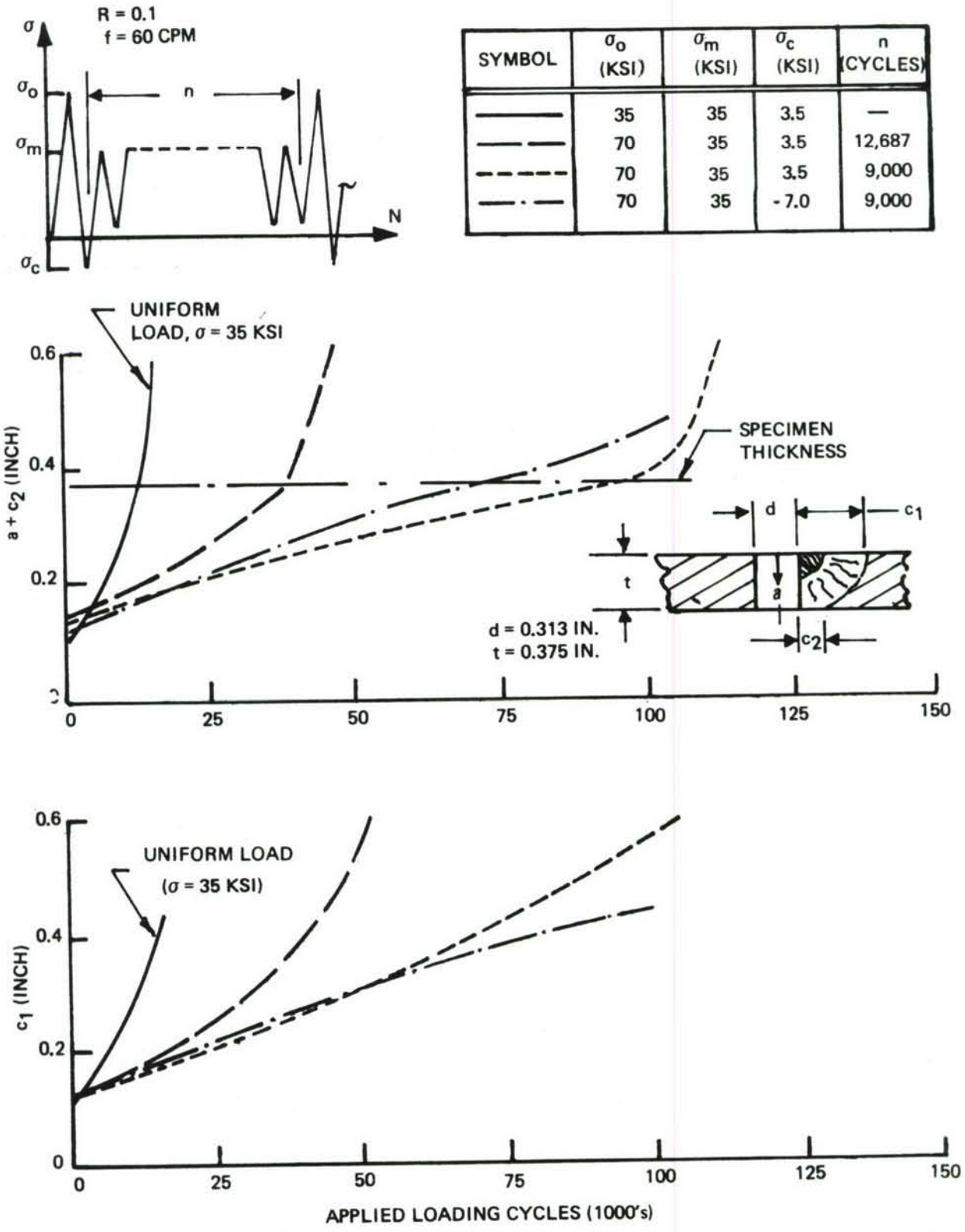
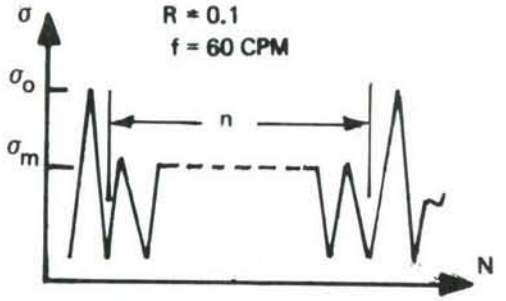
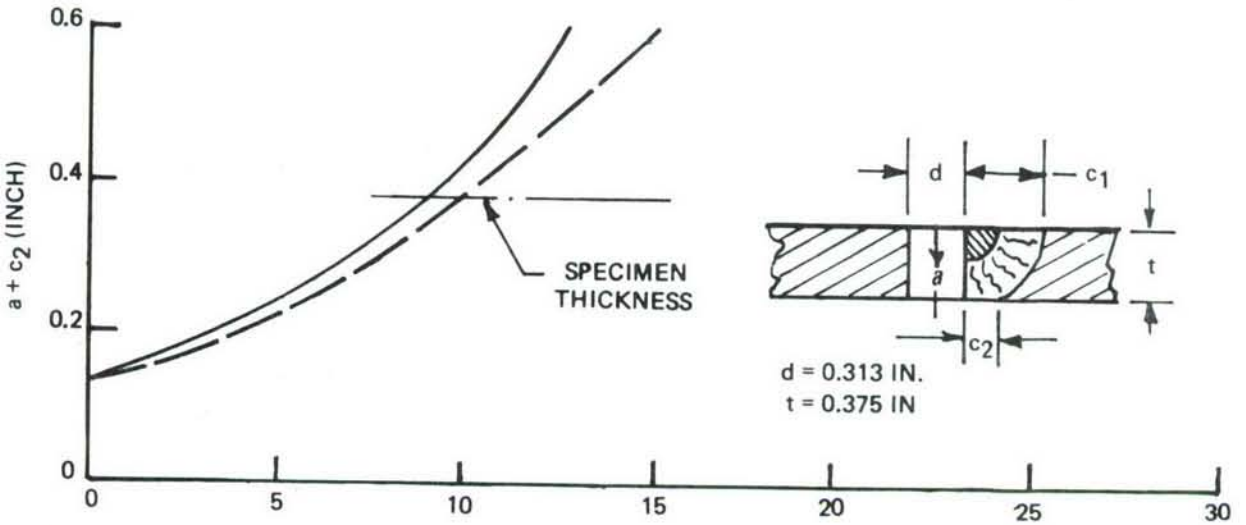


Figure 155: Effect of Periodic Overloads on Fatige Crack Propagation of Part-Thru Cracks Originating at Open Holes in 6A1-4VβA Titanium Alloy (σ_o/σ_m = 2.0)



SYMBOL	σ_o (KSI)	σ_m (KSI)	n (CYCLES)
———	35	35	—
— — —	52.5	35	9,000



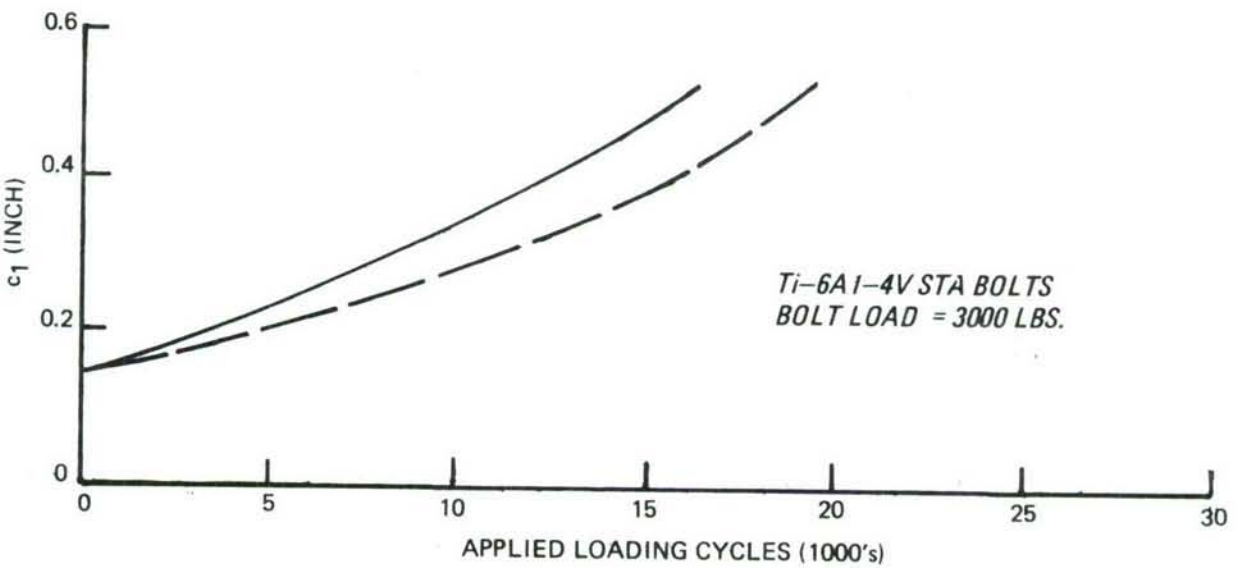


Figure 156: Effect of Periodic Overloads on Fatigue Crack Propagation of Part–Thru Cracks Originating at Loaded Close Tolerance Fasteners in 6Al–4VβA Titanium Alloy (σ_o/σ_m = 1.5)

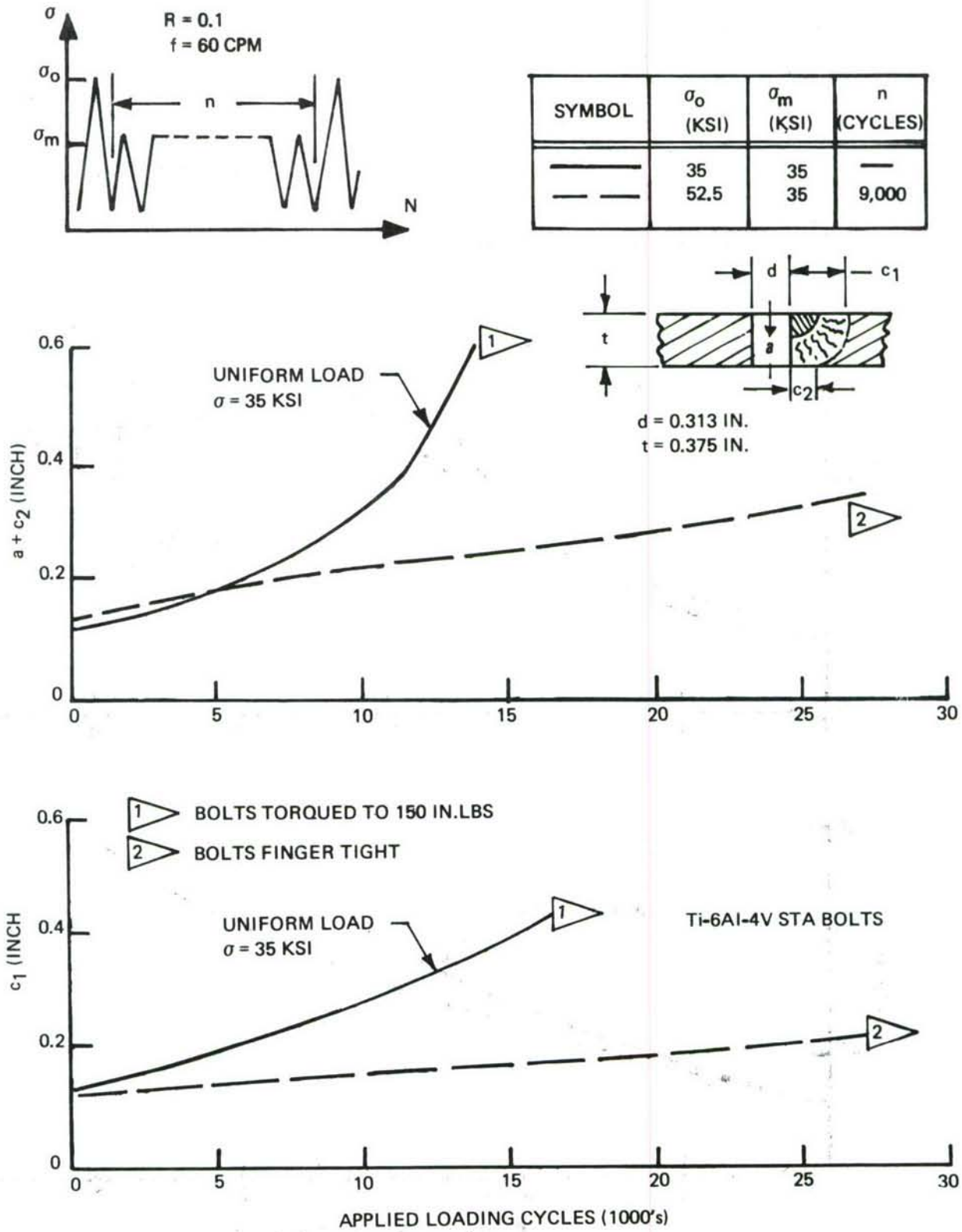


Figure 157: Effect of Overloads on Fatigue Crack Propagation of Part–Thru Cracks Originating at Unloaded Close Tolerance Fasteners in 6Al-4VβA Titanium Alloy (σ_o/σ_m = 1.50)

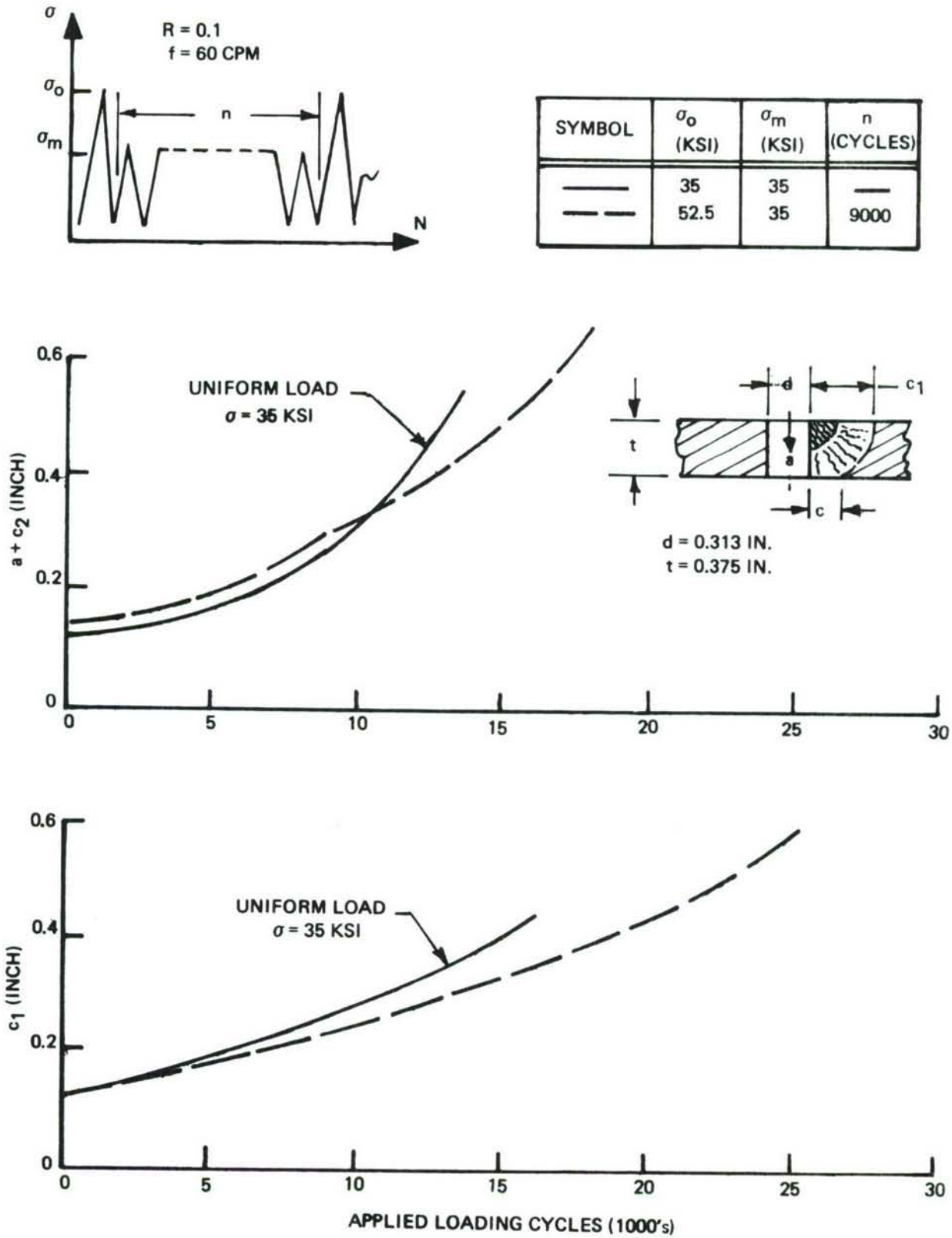
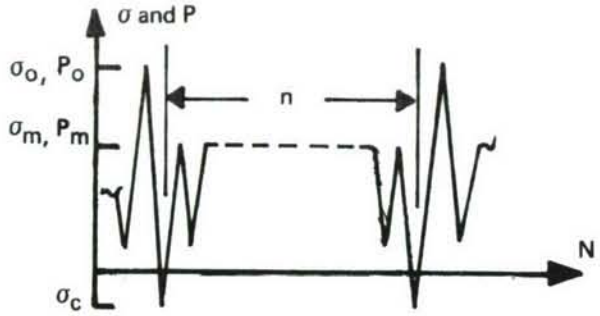


Figure 158: Effect of Periodic Overloads on Fatigue Crack Propagation of Part–Thru Cracks Originating at Open Holes in 6Al–4VβA Titanium Alloy ($\sigma_o/\sigma_m = 1.5$)

SPECIMEN FPOCTA–2

σ_o = 36.75 KSI
σ_m = 21.0 KSI
σ_c = – 4.2 KSI
n = 4600 ~
R = 0.1
f = 60 CPM
CLOSE TOLERANCE BOLTS
DESICCATED AIR



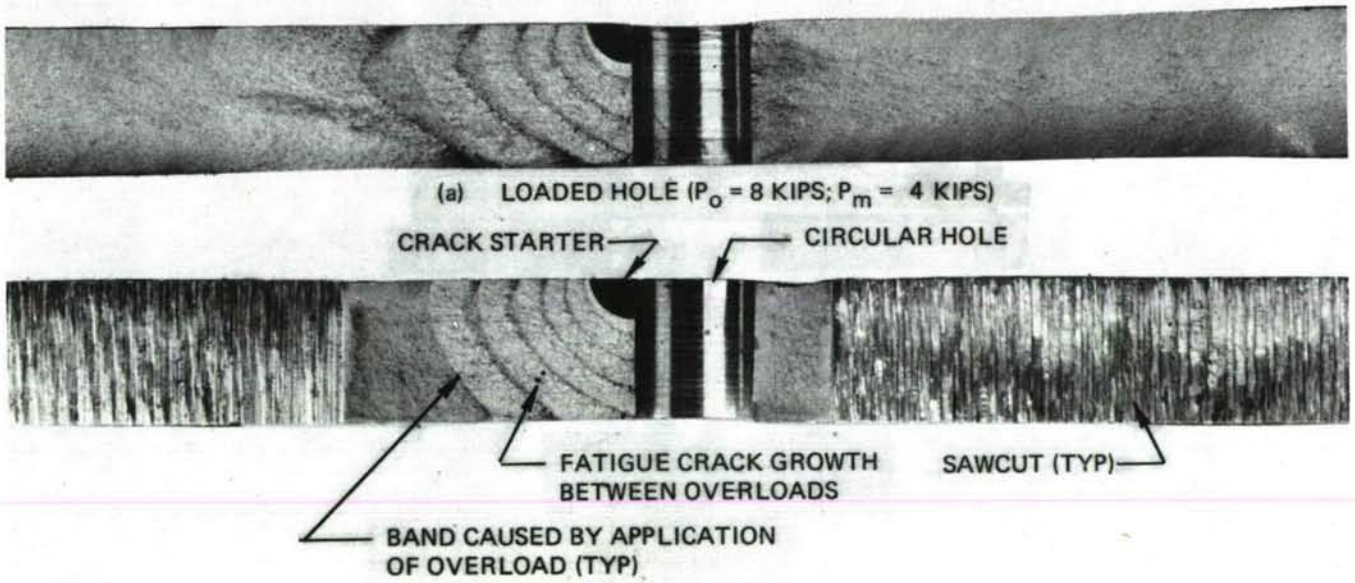
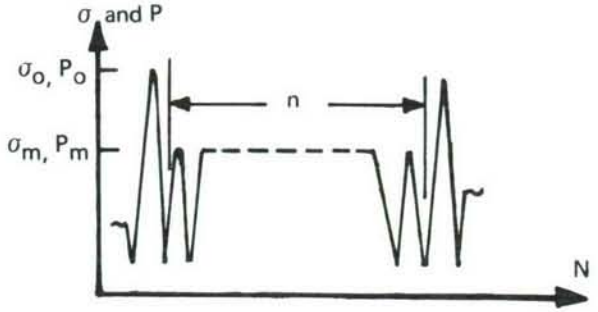


Figure 159: Typical Fracture Surfaces For 2219–T851 Aluminum Alloy Close Tolerance Fastener Specimens Tested Under Periodic Overloading Profiles

SPECIMEN FPOCTS-1

σ_o = 140 KSI
σ_m = 70 KSI
n = 5000 ~
R = 0.1
f = 60 CPM
CLOSE TOLERANCE BOLTS
DESICCATED AIR



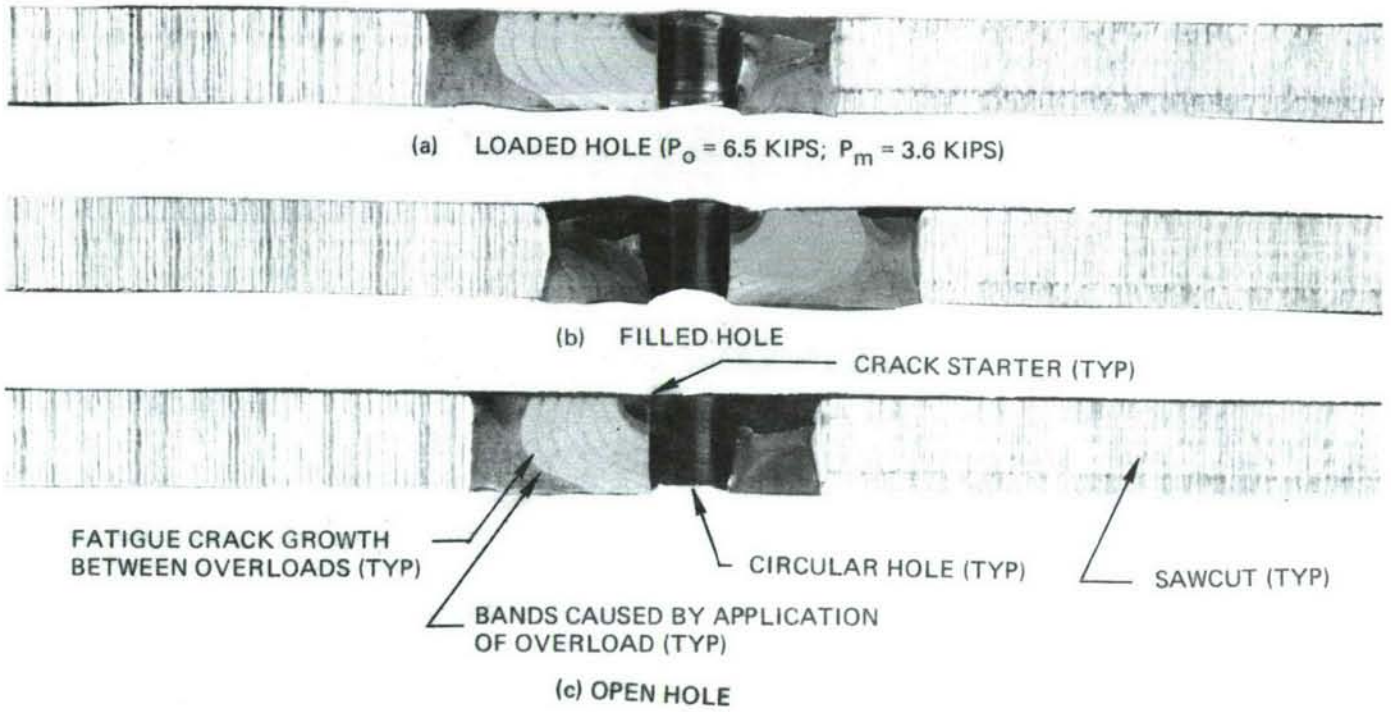
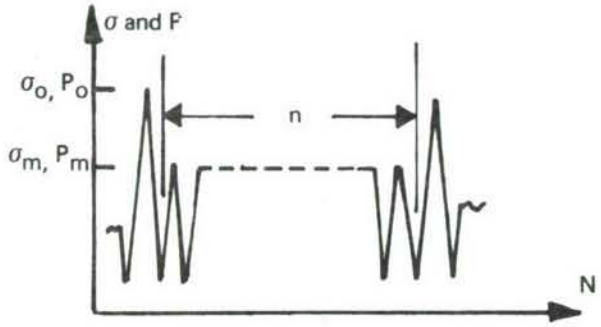


Figure 160: Typical Fracture Surfaces for $9N_i - 4C - 0.2C$ Steel Alloy Close Tolerance Fastener Specimens Tested Under Periodic Overload Loading Profiles

SPECIMEN FPOCIT–1

σ_o = 75 KSI
σ_m = 50 KSI
n = 7500 ~
R = 0.1
f = 60 CPM
DESICCATED AIR
TAPER-LOK FASTENERS
FASTENER INTERFERENCE = 0.0034"



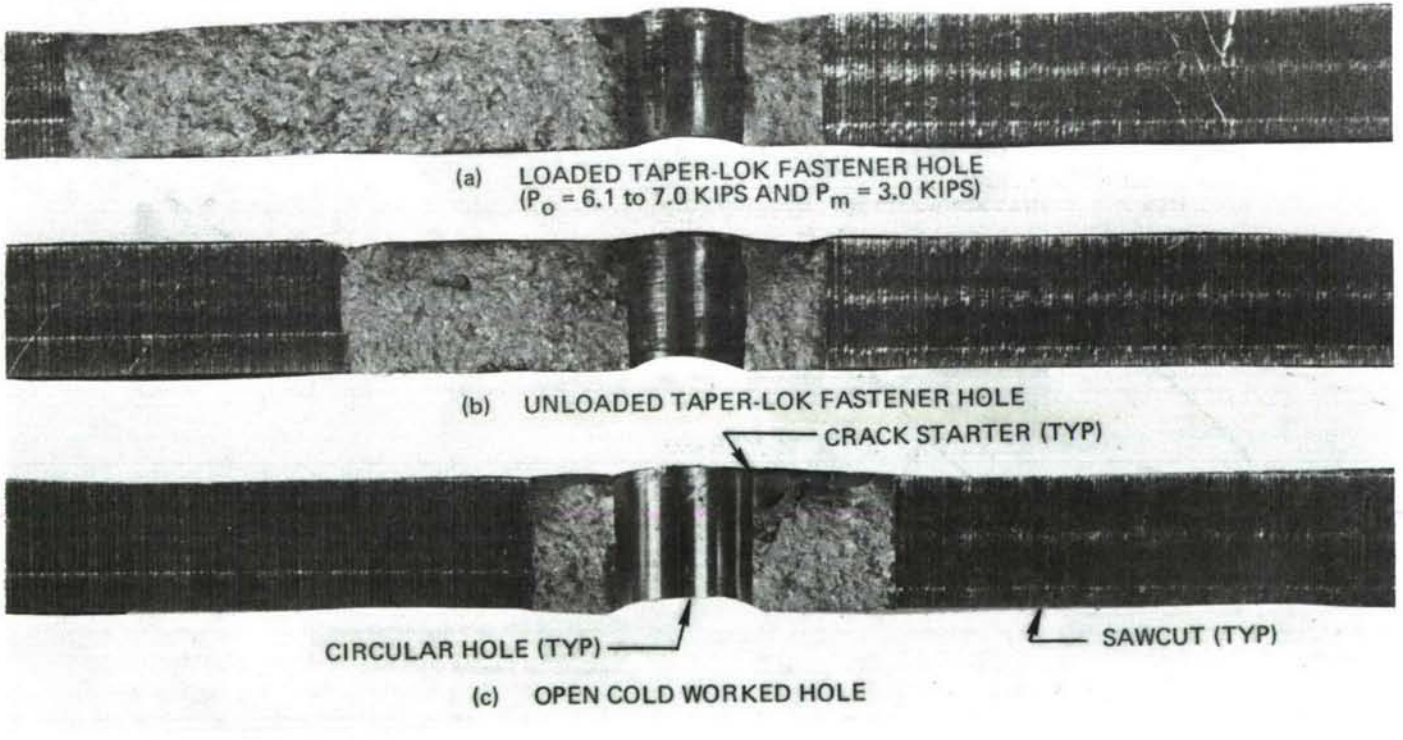


Figure 161: Typical Fracture Surfaces For 6A1-4V Beta Annealed Titanium Alloy Taper-Lok Fastener Specimens Tested Under Periodic Overload Loading Profiles

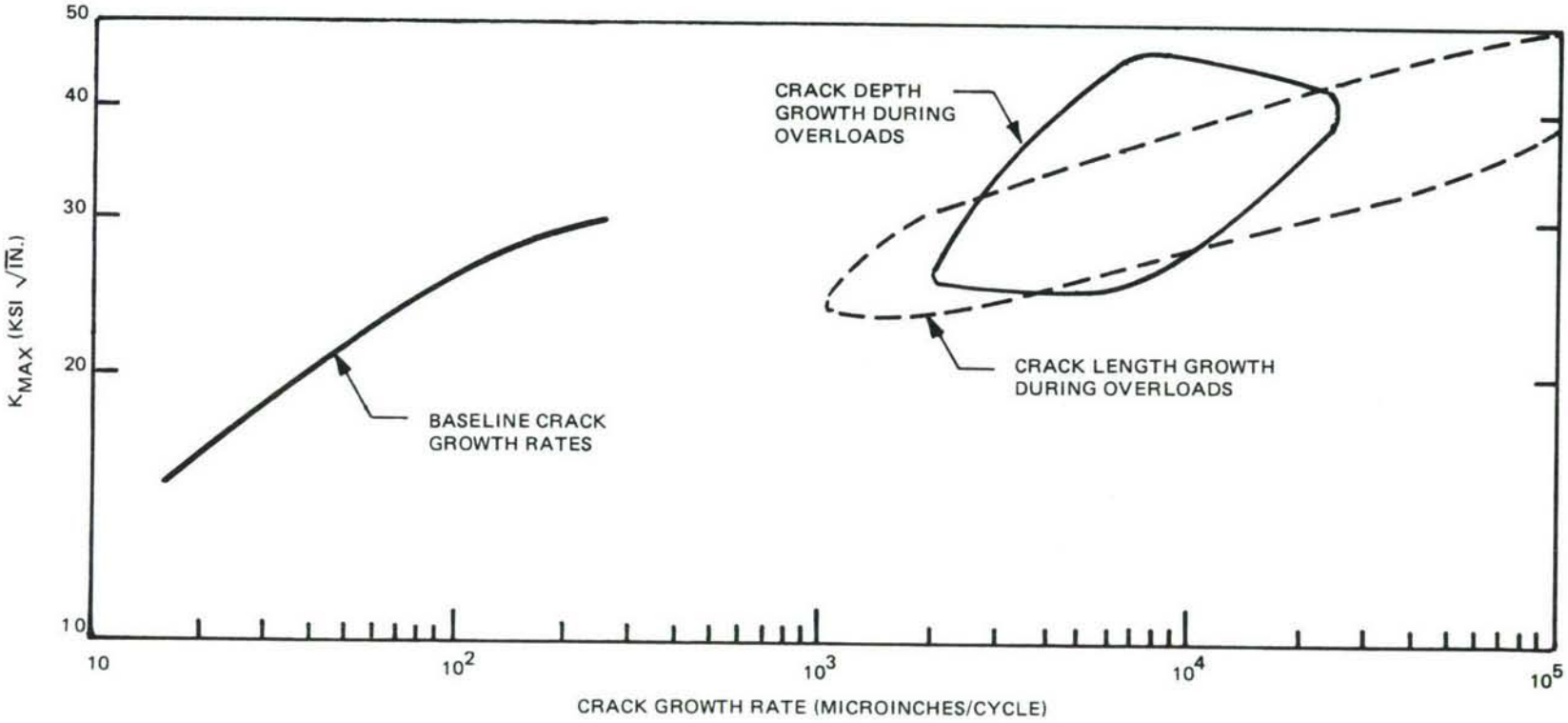


Figure 162: Comparison of Baseline and Overload Crack Growth Rates for 2219-T851 Aluminum Alloy Overload Tests (Open Holes, Filled Holes, Loaded Close Tolerance Holes)

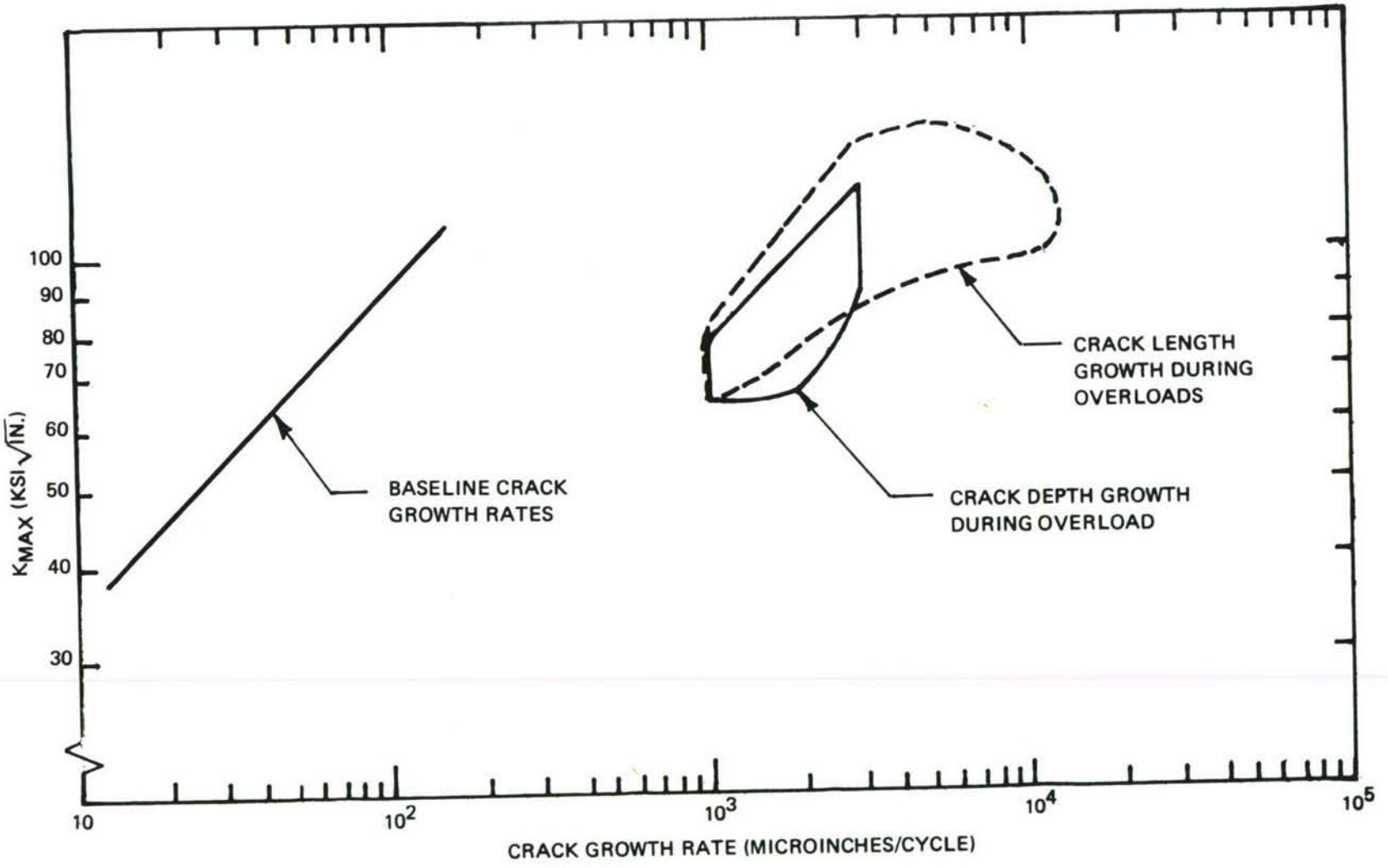


Figure 163: Comparison of Baseline and Overload Crack Growth Rates for 9Ni-4Co-0.2C Steel Alloy Overload Tests (Open Holes, Filled Holes, Loaded Close Tolerance Holes)

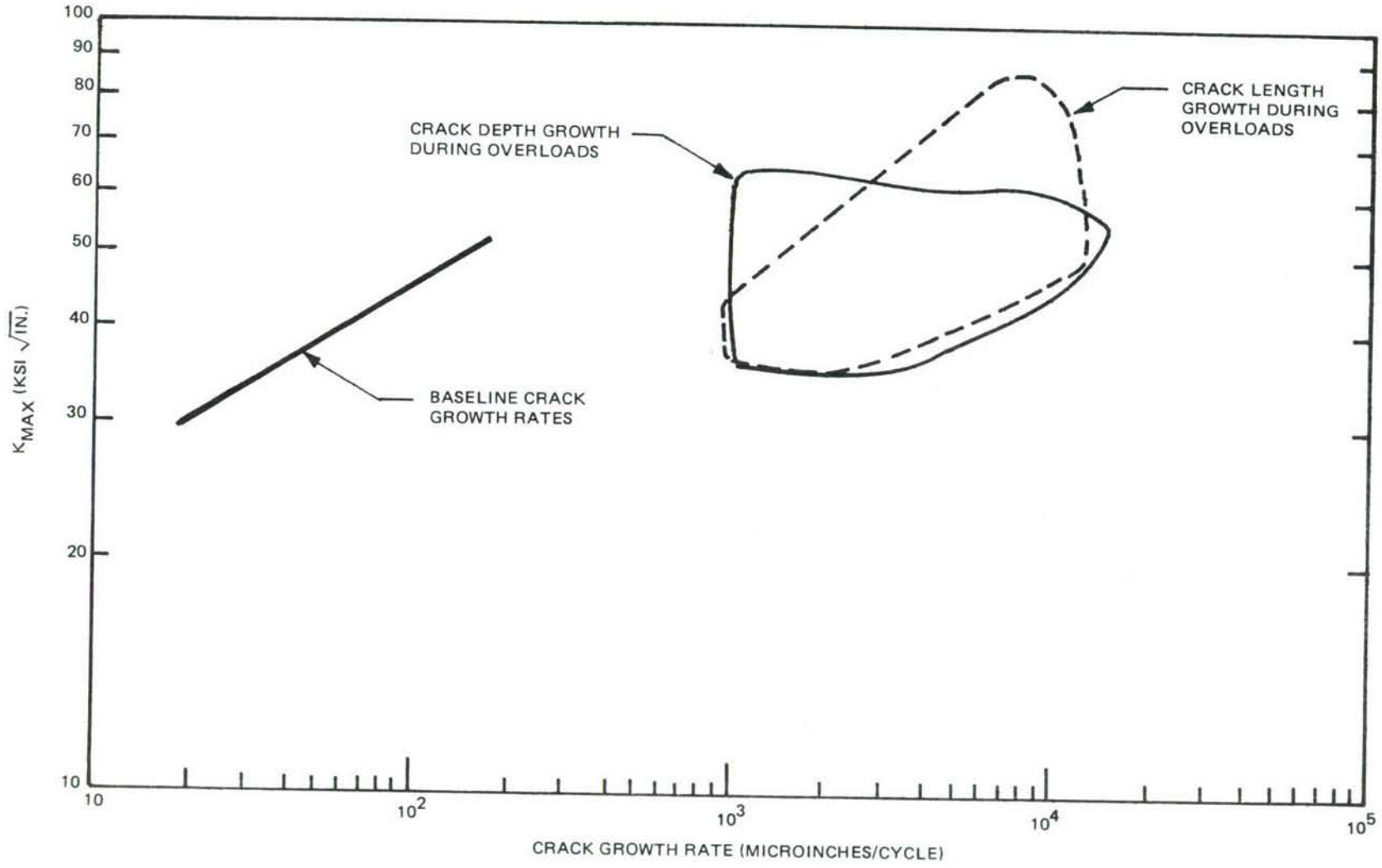
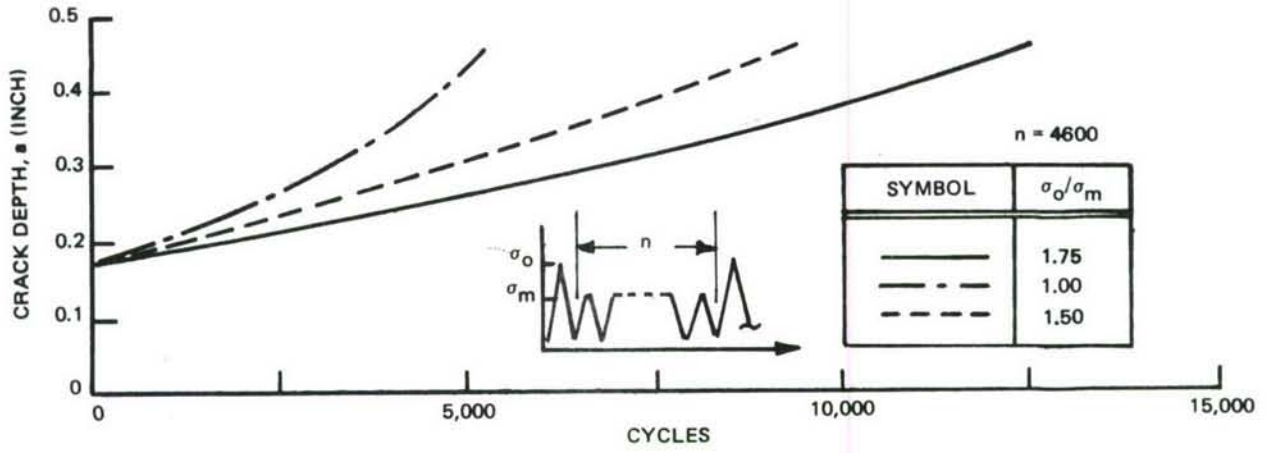
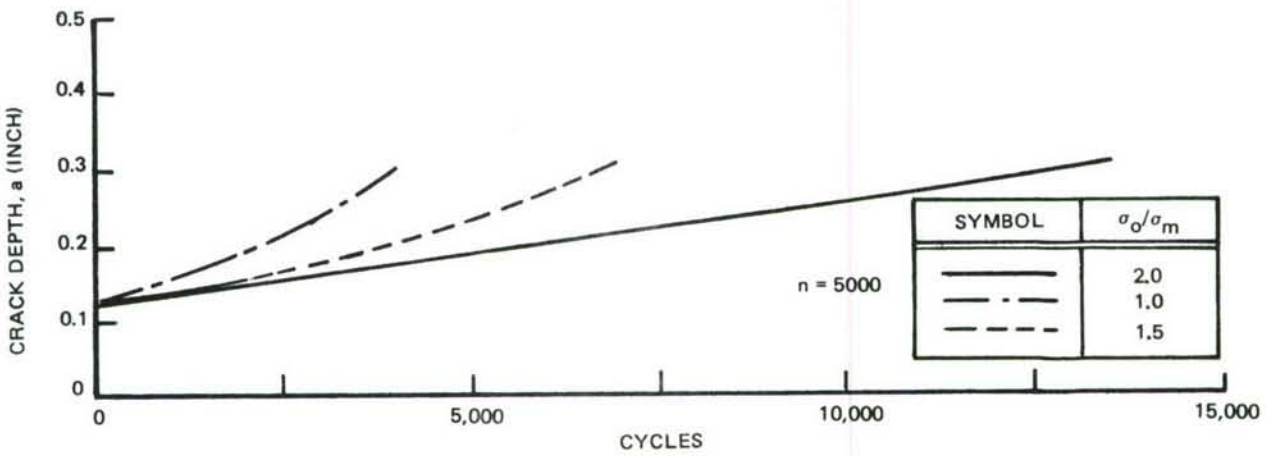


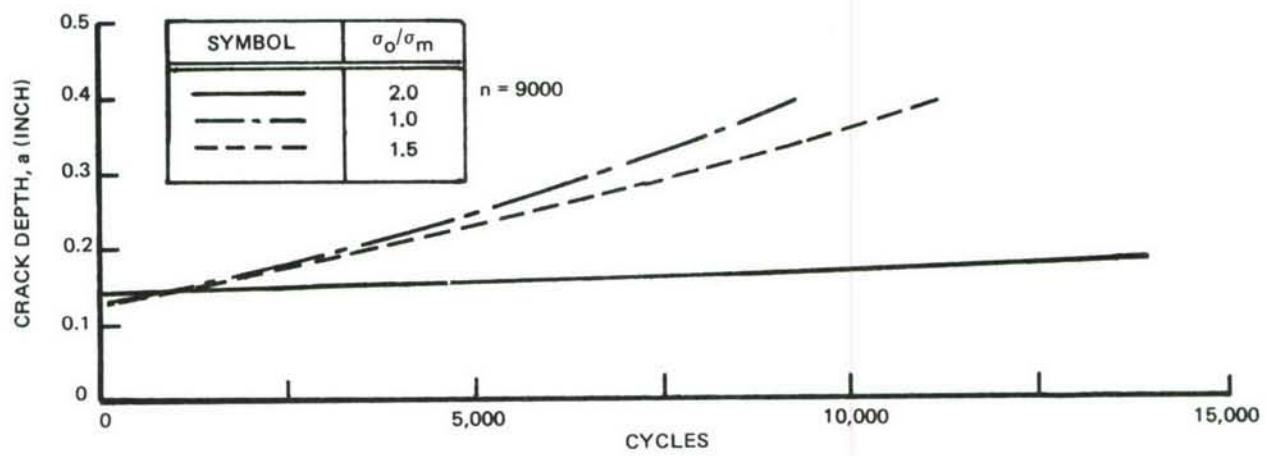
Figure 164: Comparison of Baseline and Overload Crack Growth Rates for 6A1-4V Beta Annealed Titanium Alloy Overload Tests (Open Holes, Filled Holes, Loaded Close Tolerance Holes)



(a) 2219-T851 ALUMINUM



(b) 9Ni-4Co-0.2C STEEL



(c) 6Al-4VβA TITANIUM

Figure 165: Effect of Overload Ratio on Growth of Part-Thru Cracks Originating at Loaded Close Tolerance Fastener Holes

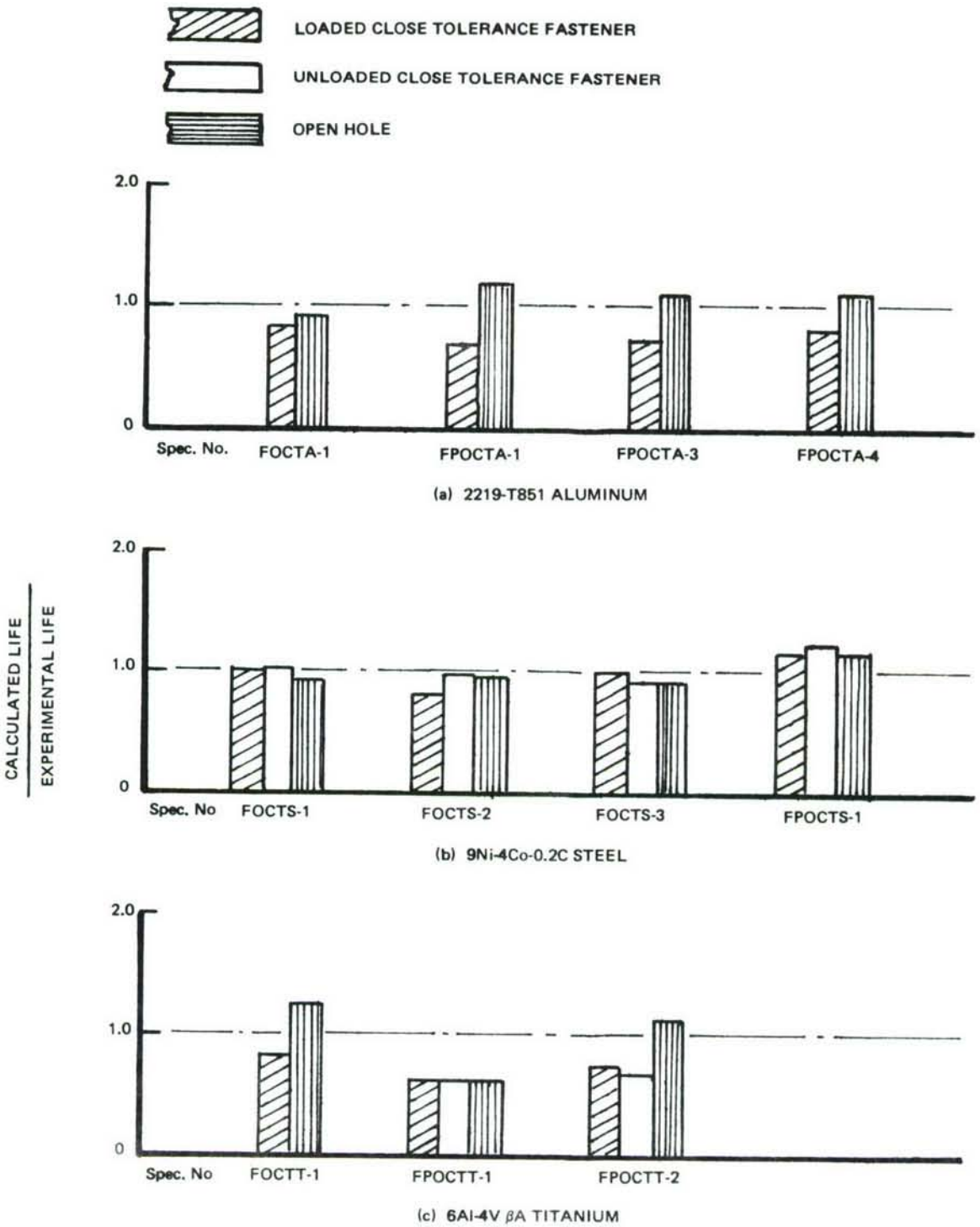


Figure 166: Comparison of Calculated and Experimental Lives for Part–Thru Cracks Originating at Loaded and Unloaded Close Tolerance Fasteners and Open Holes

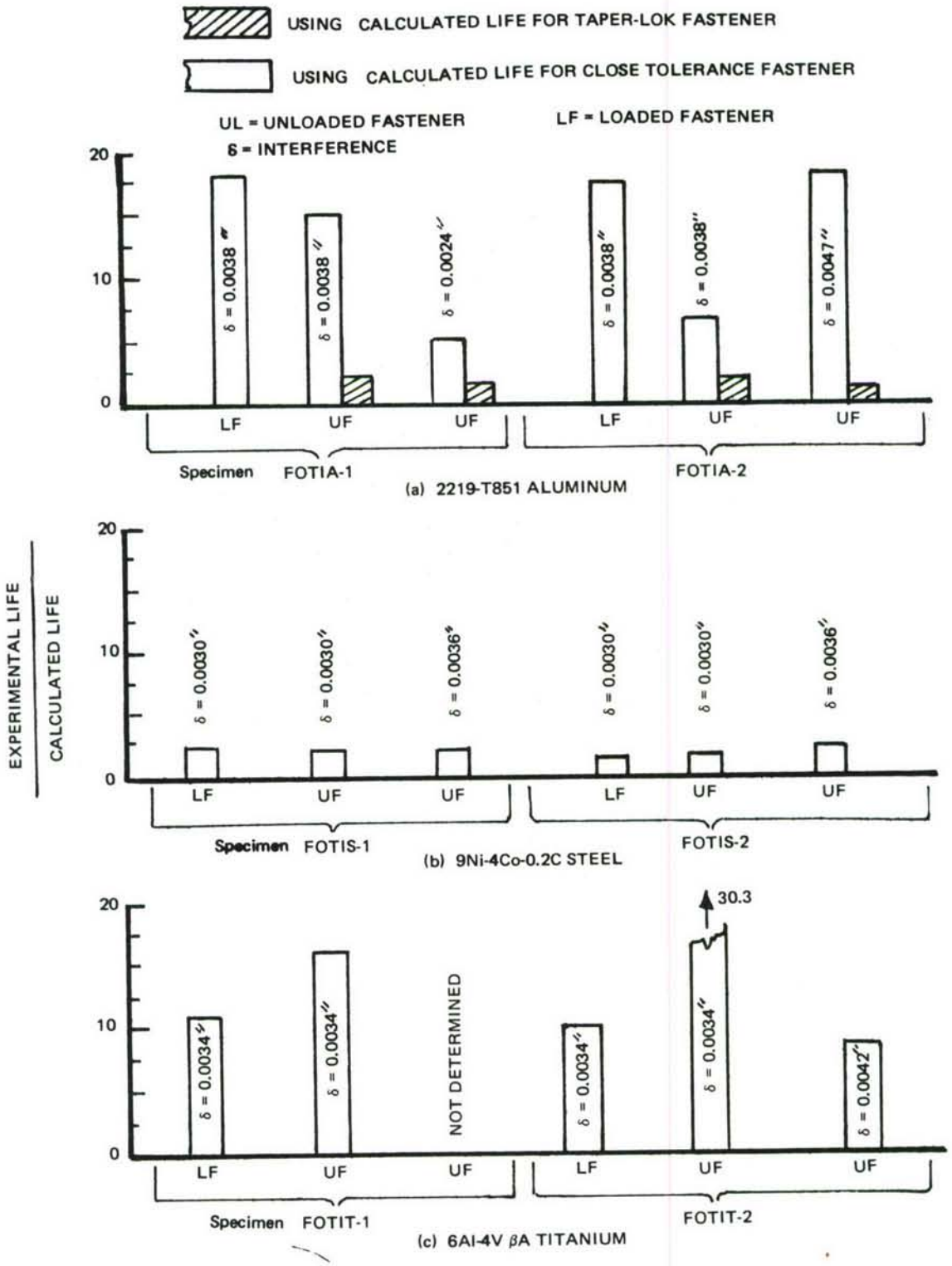


Figure 167: Comparison of Calculated and Experimental Lives for Thru Cracks Originating at Taper-Lok Filled Fastener Holes

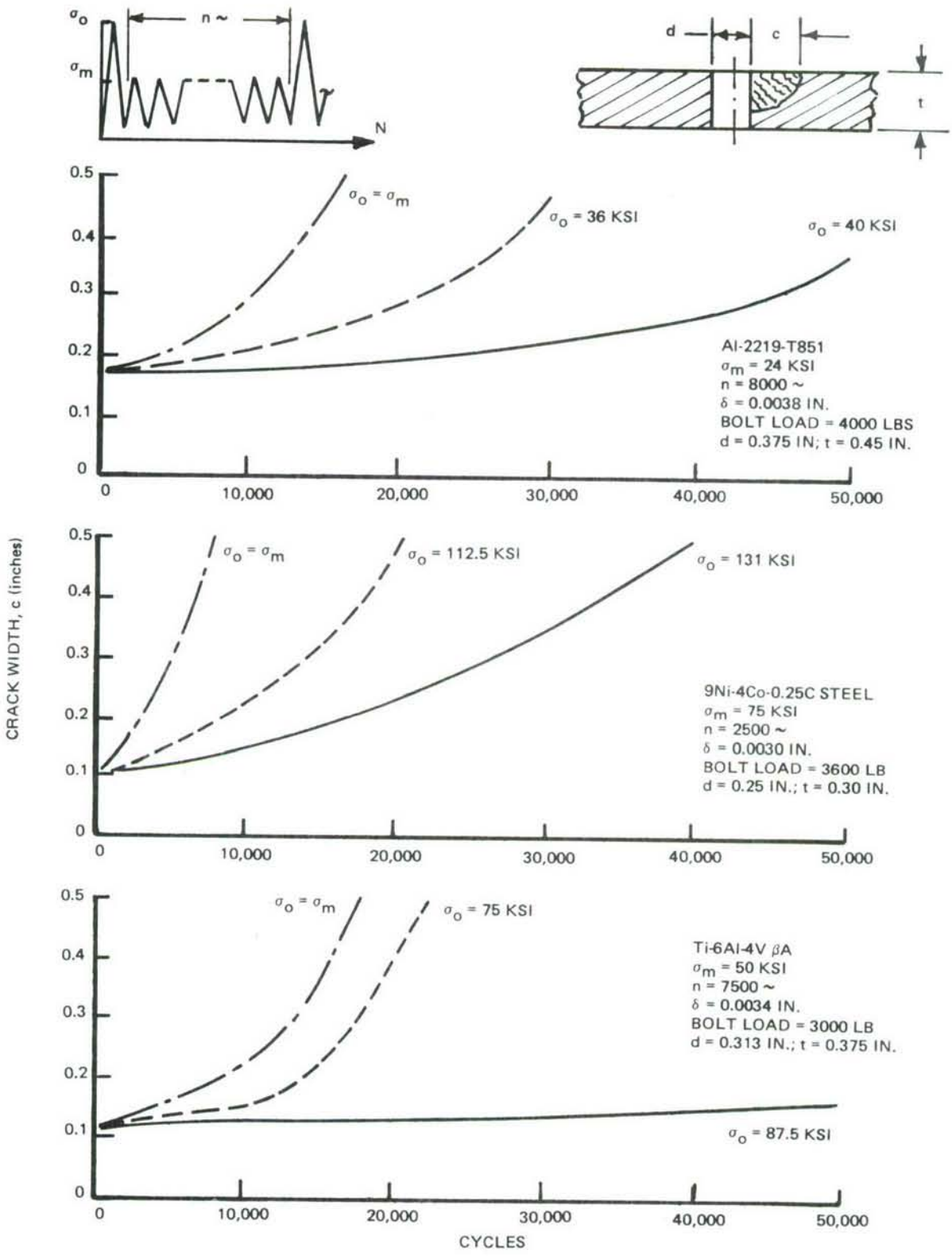


Figure 168: Effect of Overload Magnitude on Fatigue Growth of Part–Thru Cracks Originating at Loaded Taper-Lok Fastener Holes

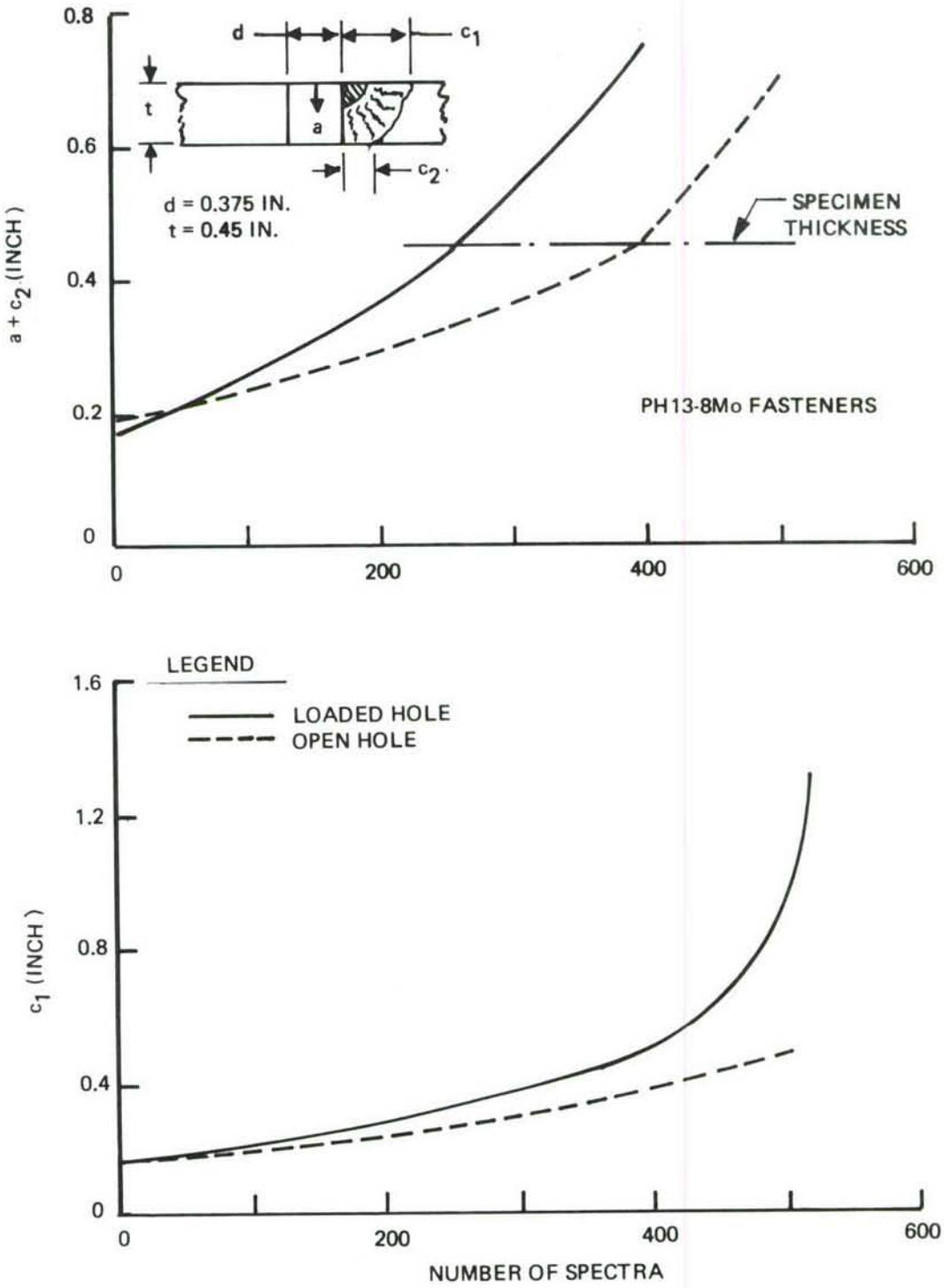


Figure 169: Crack Growth Behavior for Loaded and Open Close Tolerance Holes in 2219-T851 Aluminum Alloy Subjected to Bomber Spectrum

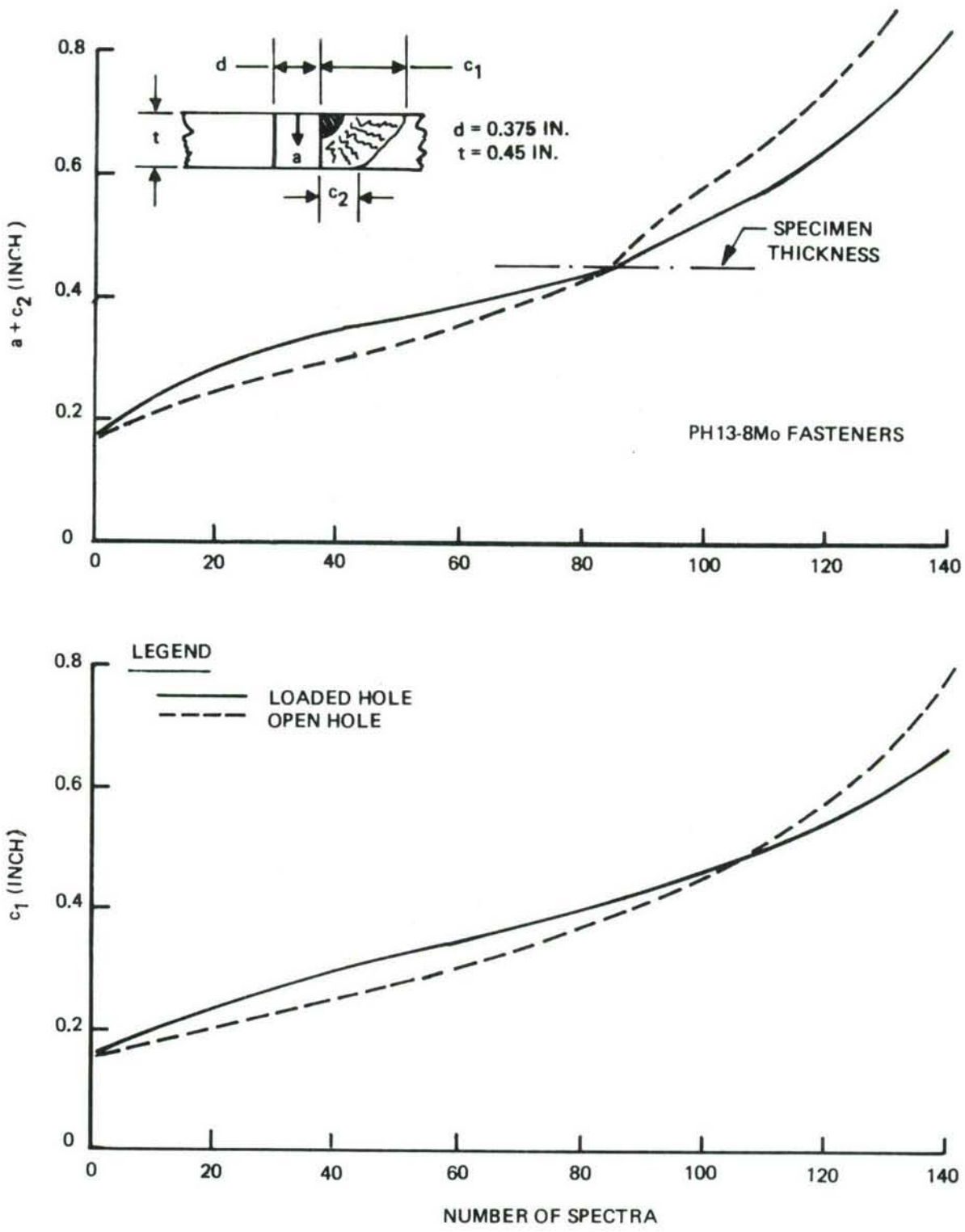


Figure 170: Crack Growth Behavior for Loaded and Open Close Tolerance Holes in 2219-T851 Aluminum Alloy Subjected to Fighter Spectrum

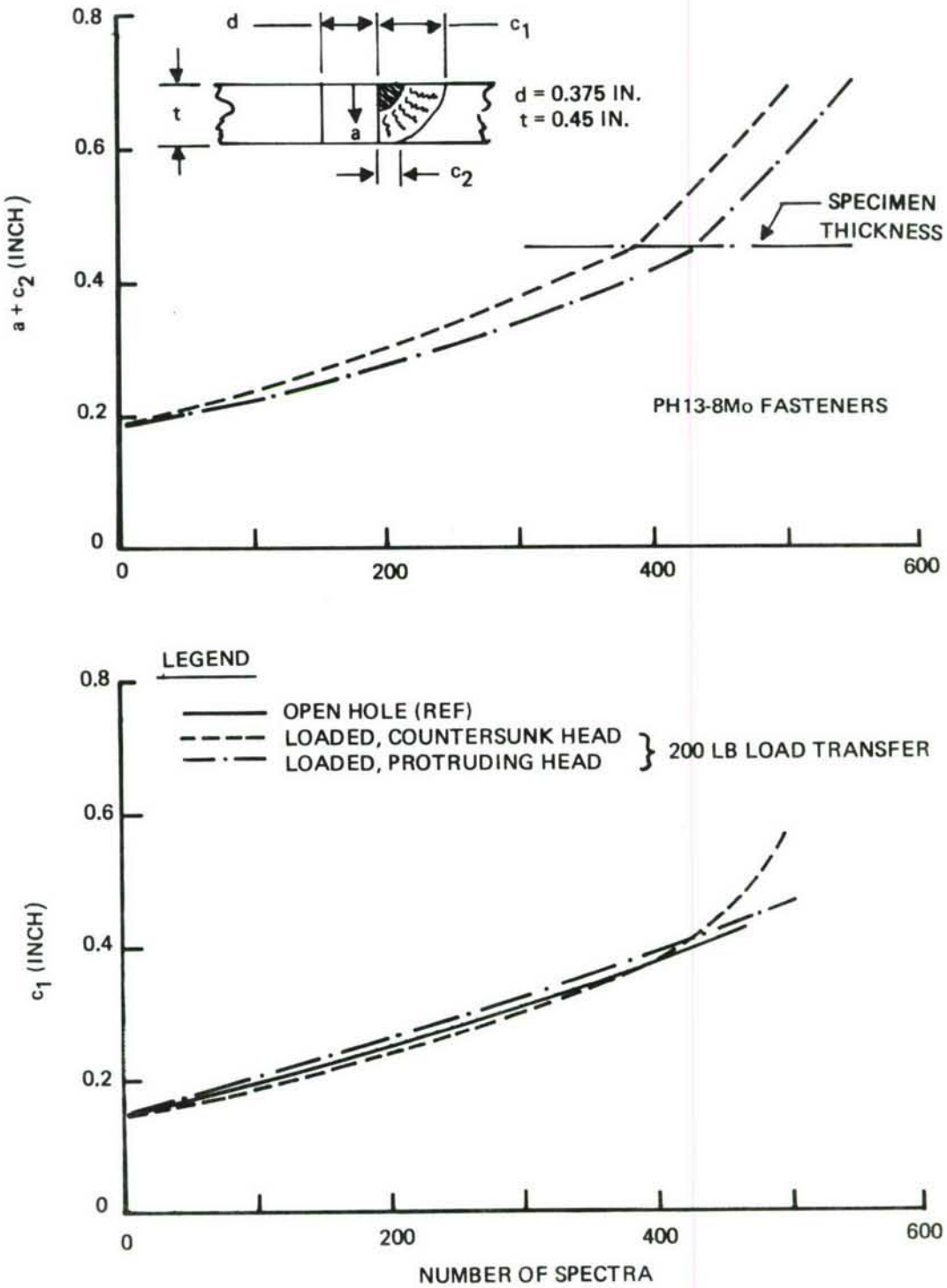


Figure 171: Crack Growth Behavior for 2219-T851 Close Tolerance Fastener Hole Flaws Subjected to Bomber Spectrum

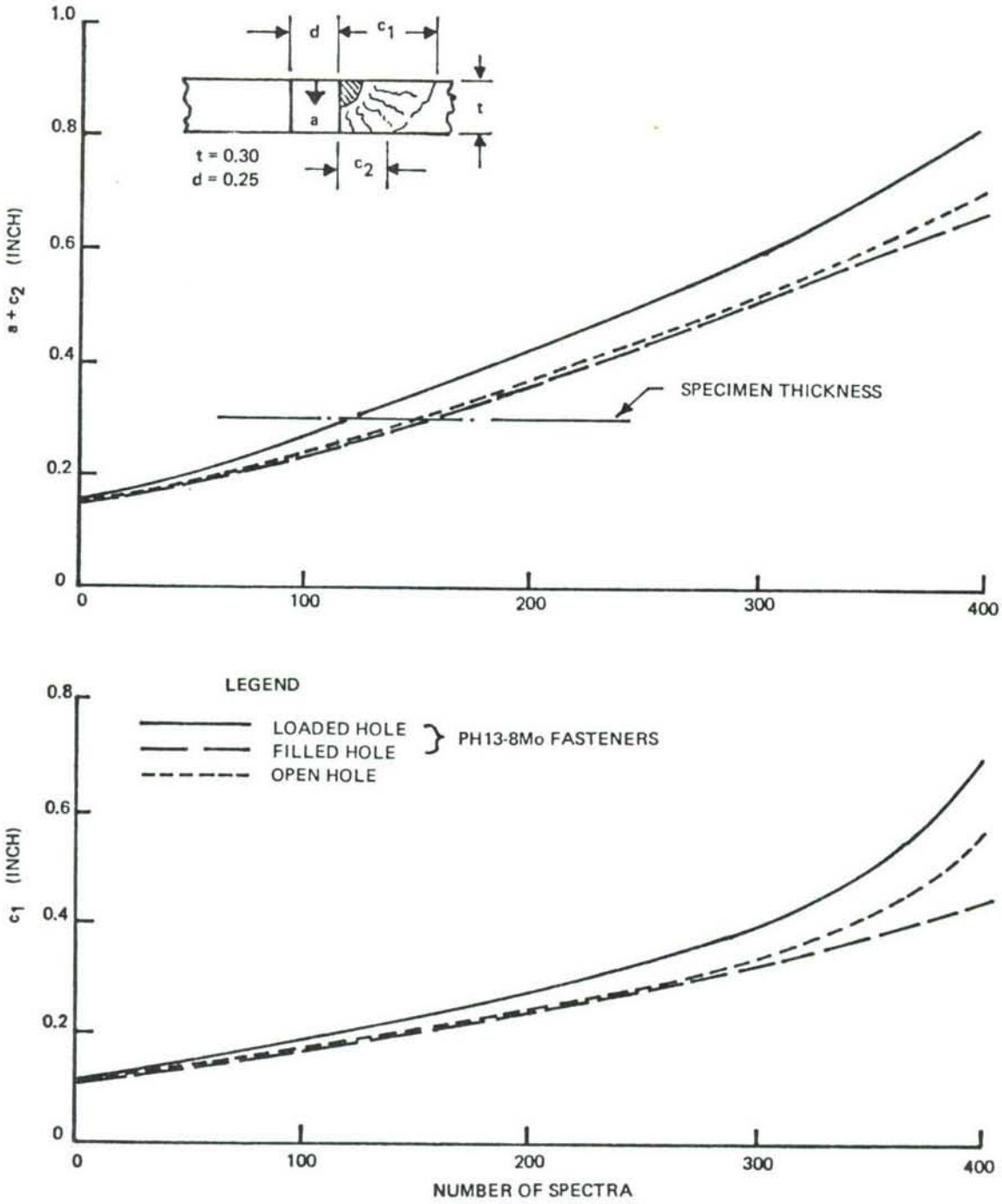


Figure 172: Crack Growth Behavior for Loaded, Filled and Open Close Tolerance Holes in 9Ni-4Co-0.2C Steel Alloy Subjected to Bomber Spectrum

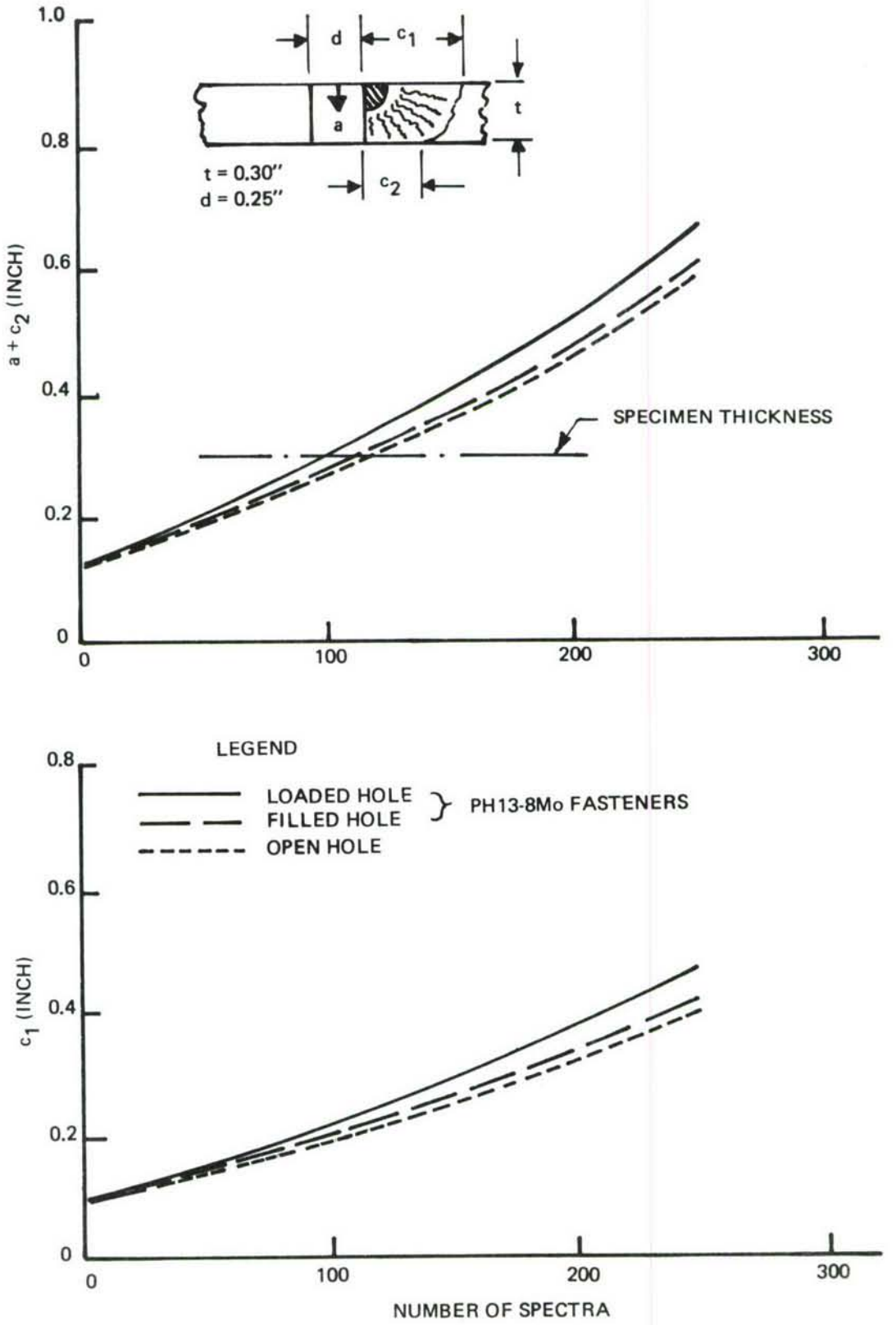


Figure 173: Crack Growth Behavior for Loaded and Open Close Tolerance Holes in 9Ni-4Co-0.2C Steel Alloy Subjected to Fighter Spectrum

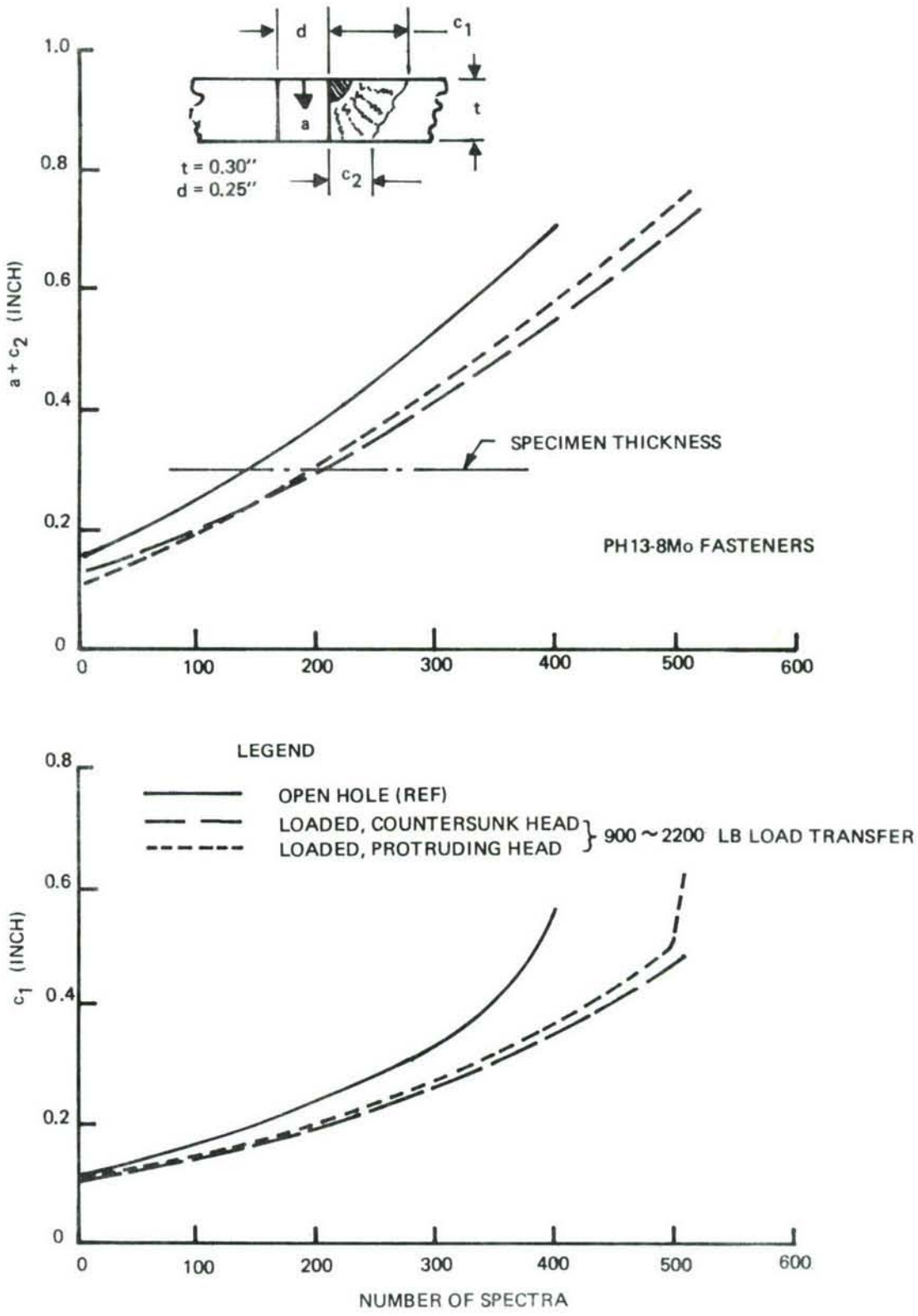


Figure 174: Crack Growth Behavior for 9Ni-4Co-0.2 Steel Close Tolerance Fastener Hole Flaws Subjected to Bomber Spectrum

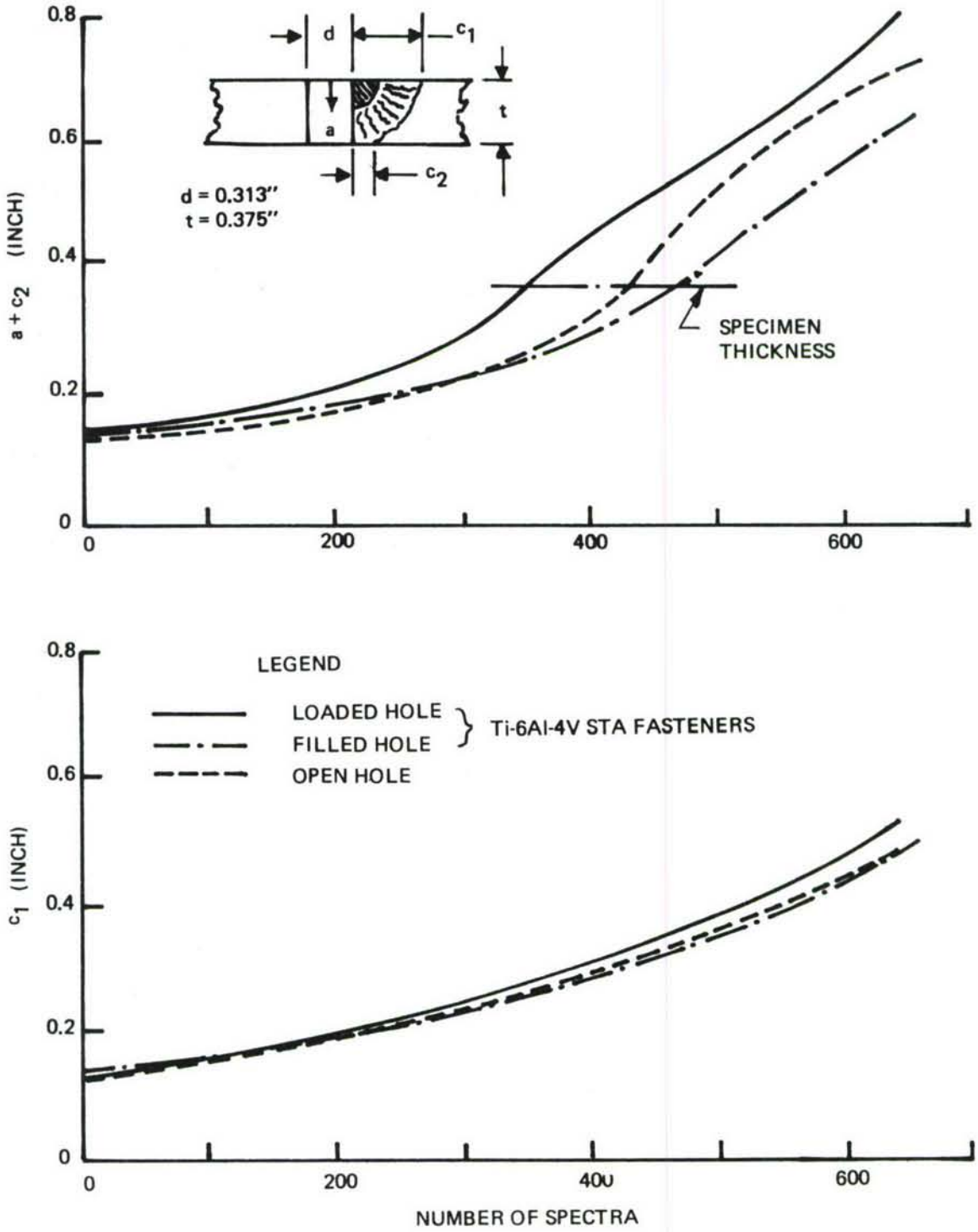


Figure 175: Crack Growth Behavior of Loaded, Filled, and Open Close Tolerance Holes in Ti-6Al-4V βA Alloy Subjected to Bomber Spectrum

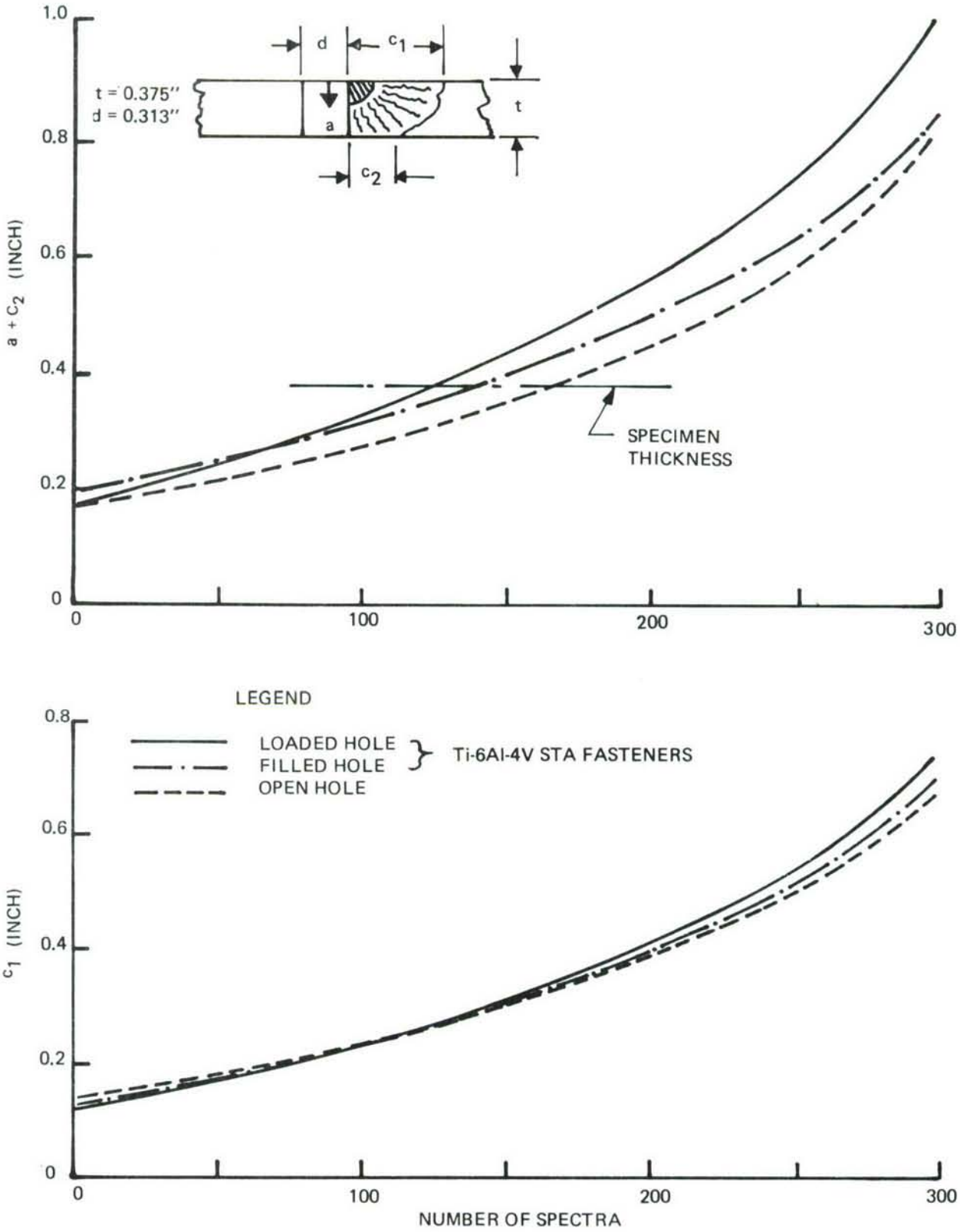


Figure 176: Crack Growth Behavior of Loaded, Filled, and Open Close Tolerance Holes in Ti-6Al-4V βA Alloy Subjected to Fighter Spectrum

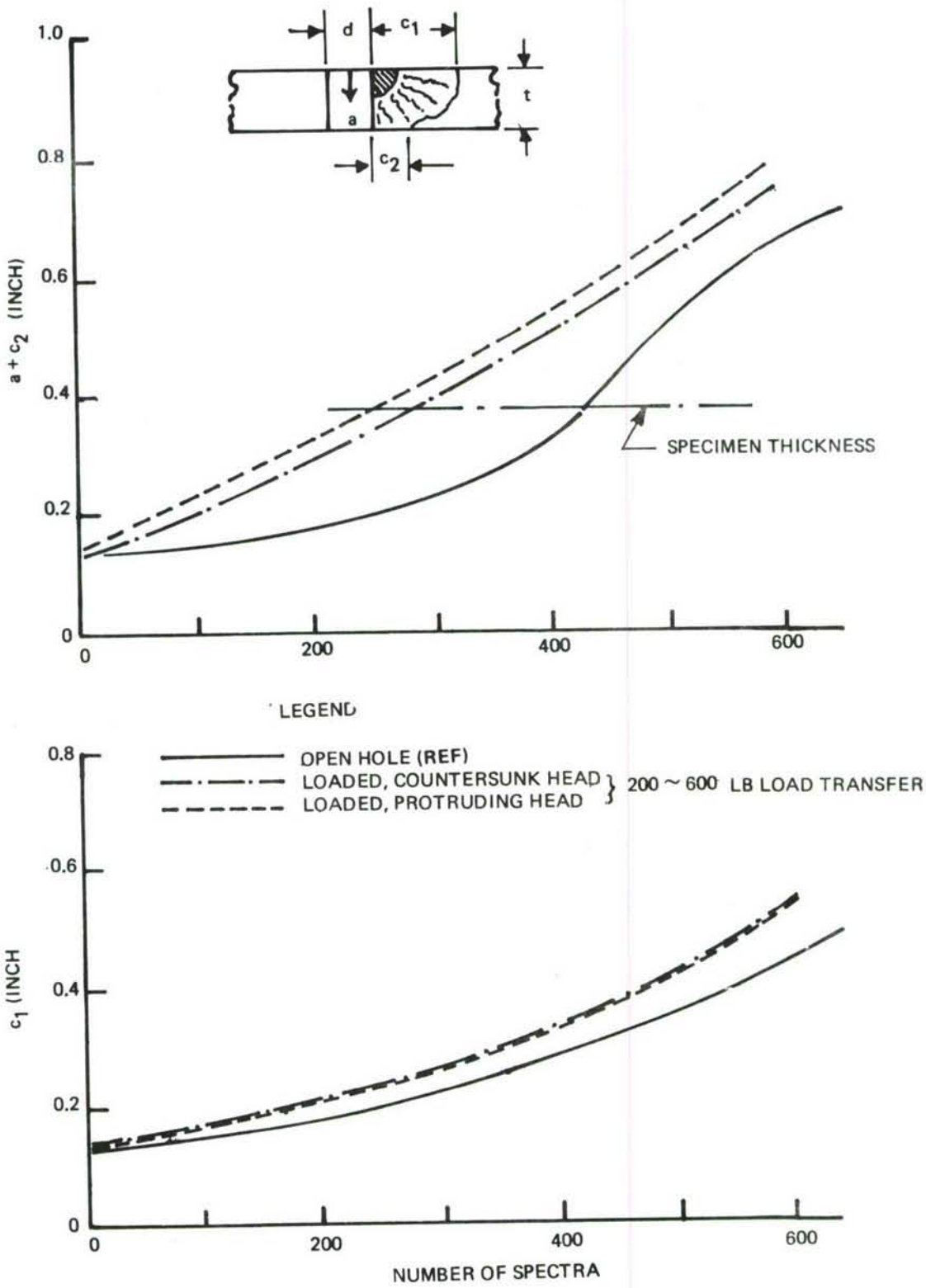


Figure 177: Crack Growth Behavior for Ti-6Al-4V β A Close Tolerance Fastener Hole Flaws Subjected to Bomber Spectrum

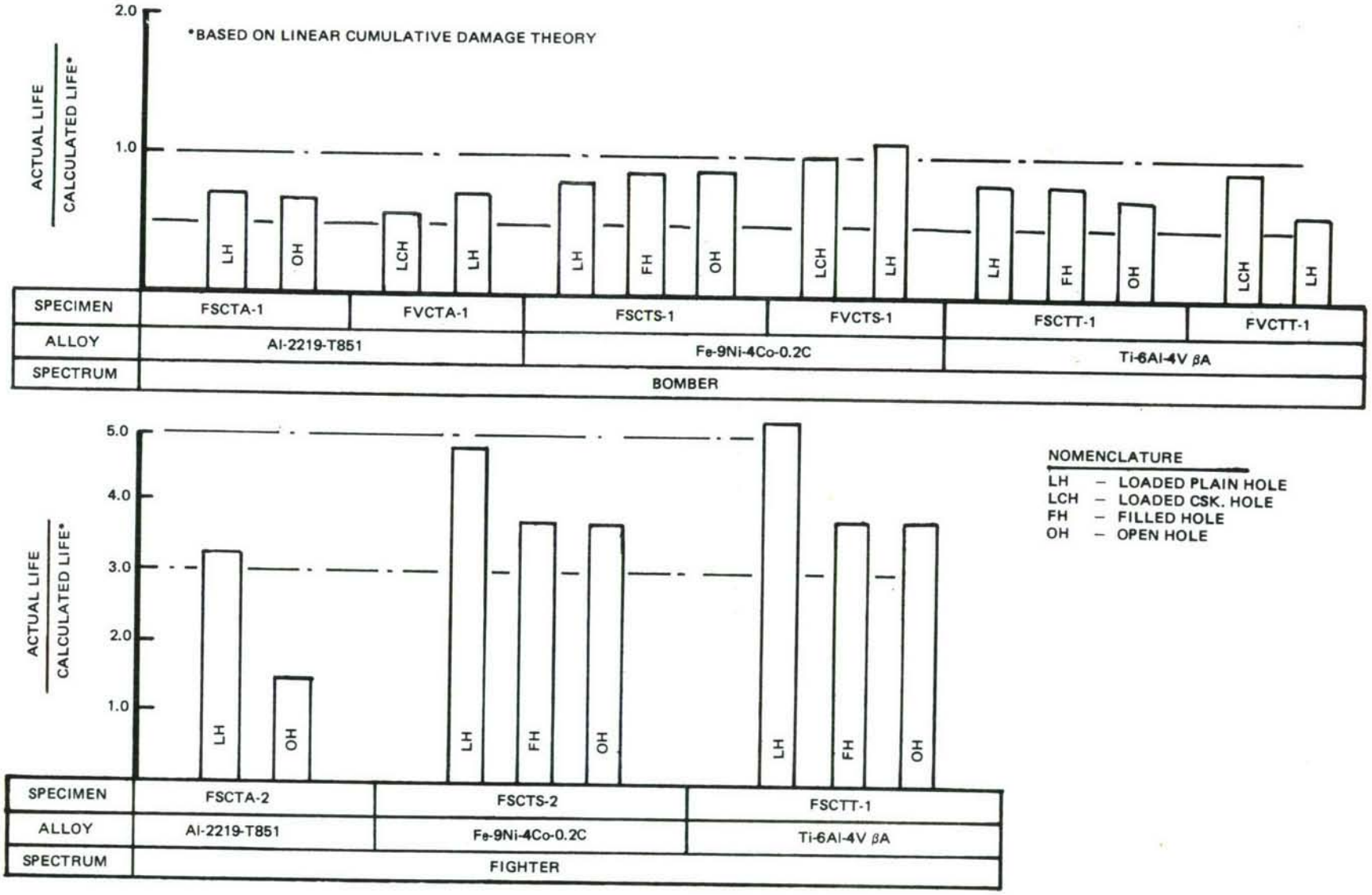


Figure 178: Comparison of Actual and Calculated Lives for Part–Thru Cracks Originating at Open and Close Tolerance Fastener Filled Holes Subjected to Spectrum Loadings

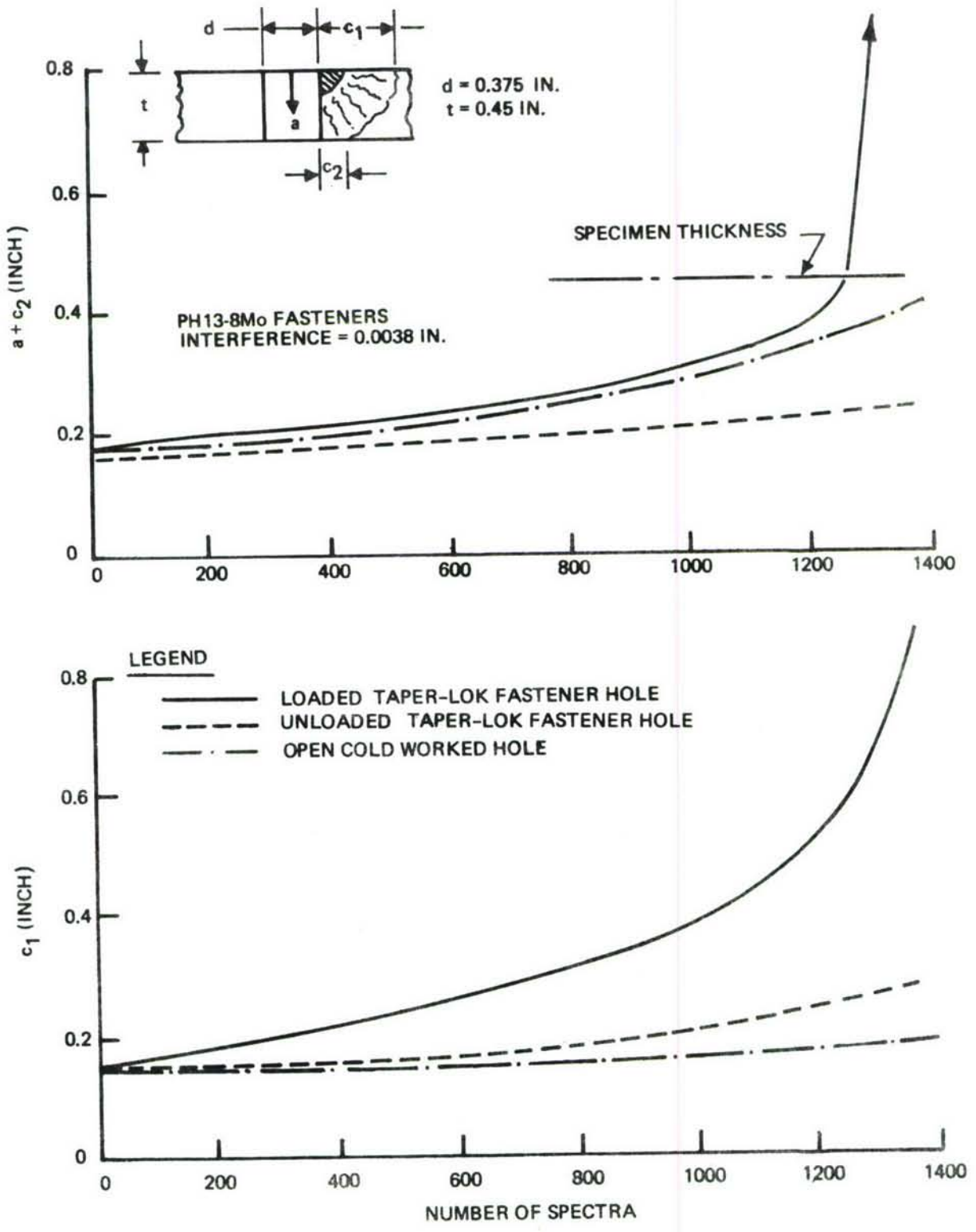


Figure 179: Crack Growth Behavior for Loaded Taper-Lok, Unloaded Taper-Lok and Open Cold Worked Fastener Holes in 2219–T851 Aluminum Alloy Subjected to Bomber Spectrum

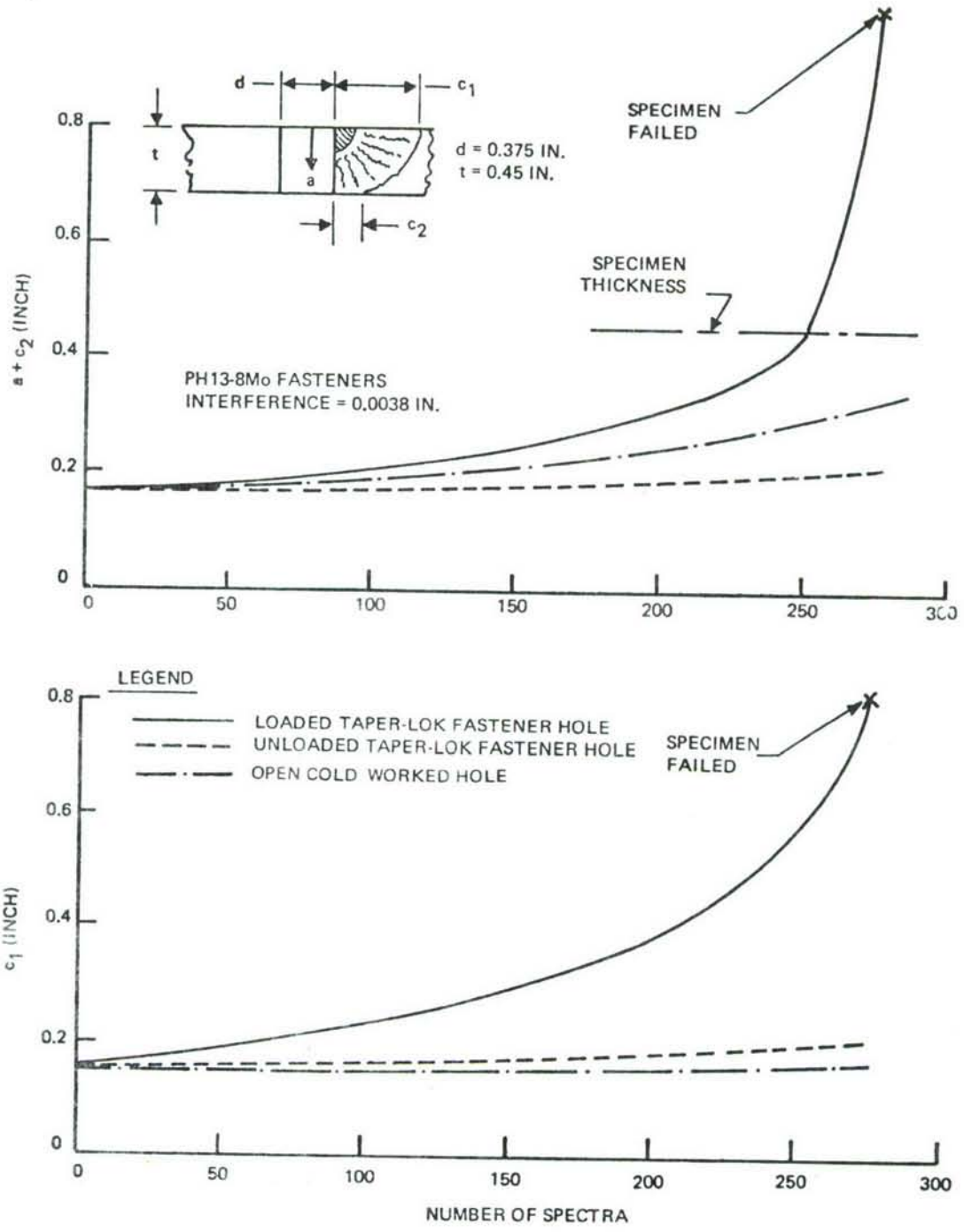


Figure 180: Crack Growth Behavior for Loaded Taper-Lok, Unloaded Taper-Lok, and Open Cold Worked Fastener Holes in 2219–T851 Aluminum Alloy Subjected to Fighter Spectrum

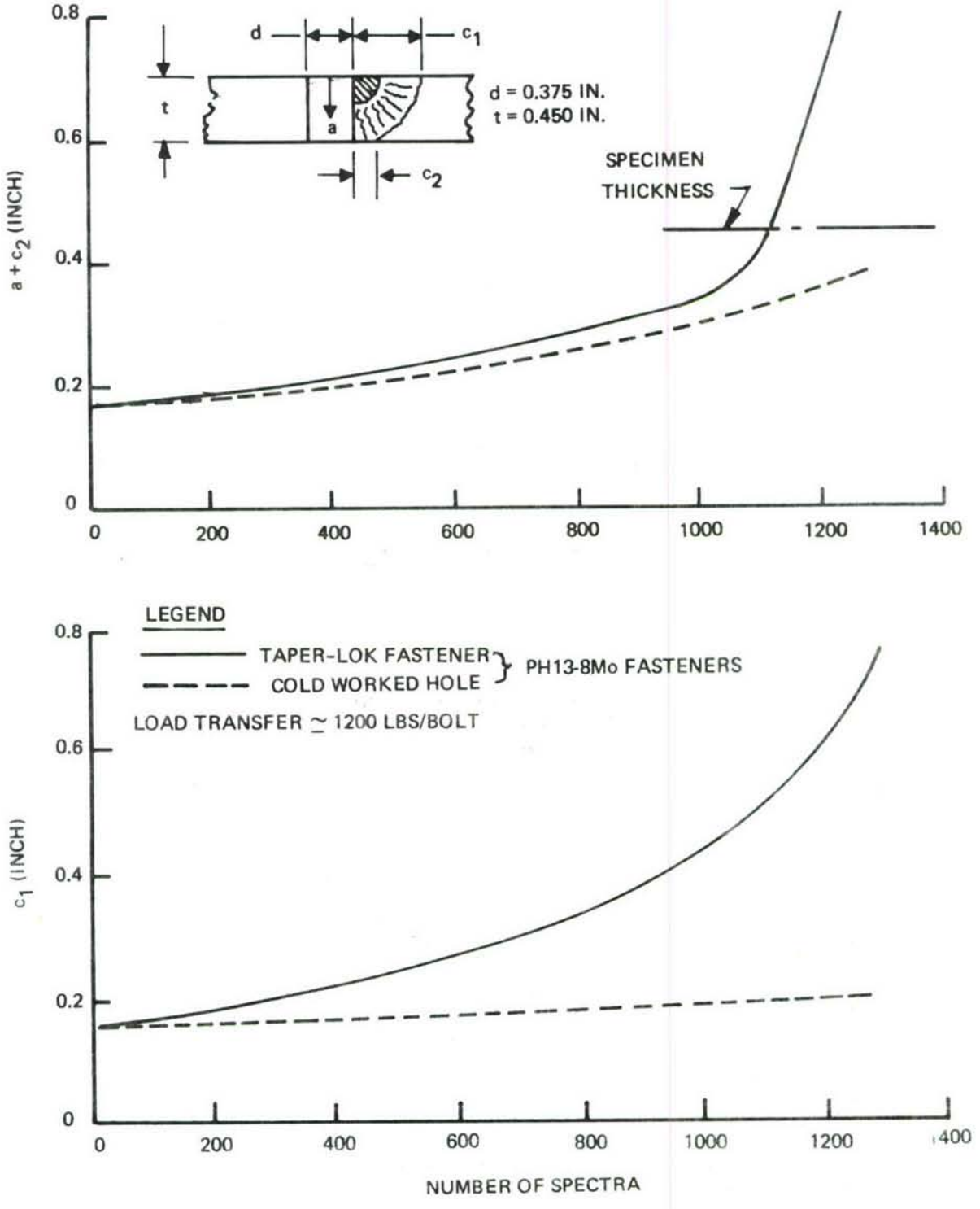


Figure 181: Crack Growth Behavior for 2219-T851 Aluminum Alloy Taper-Lok/Cold Worked Fastener Hole Verification Specimen (Bomber Spectrum)

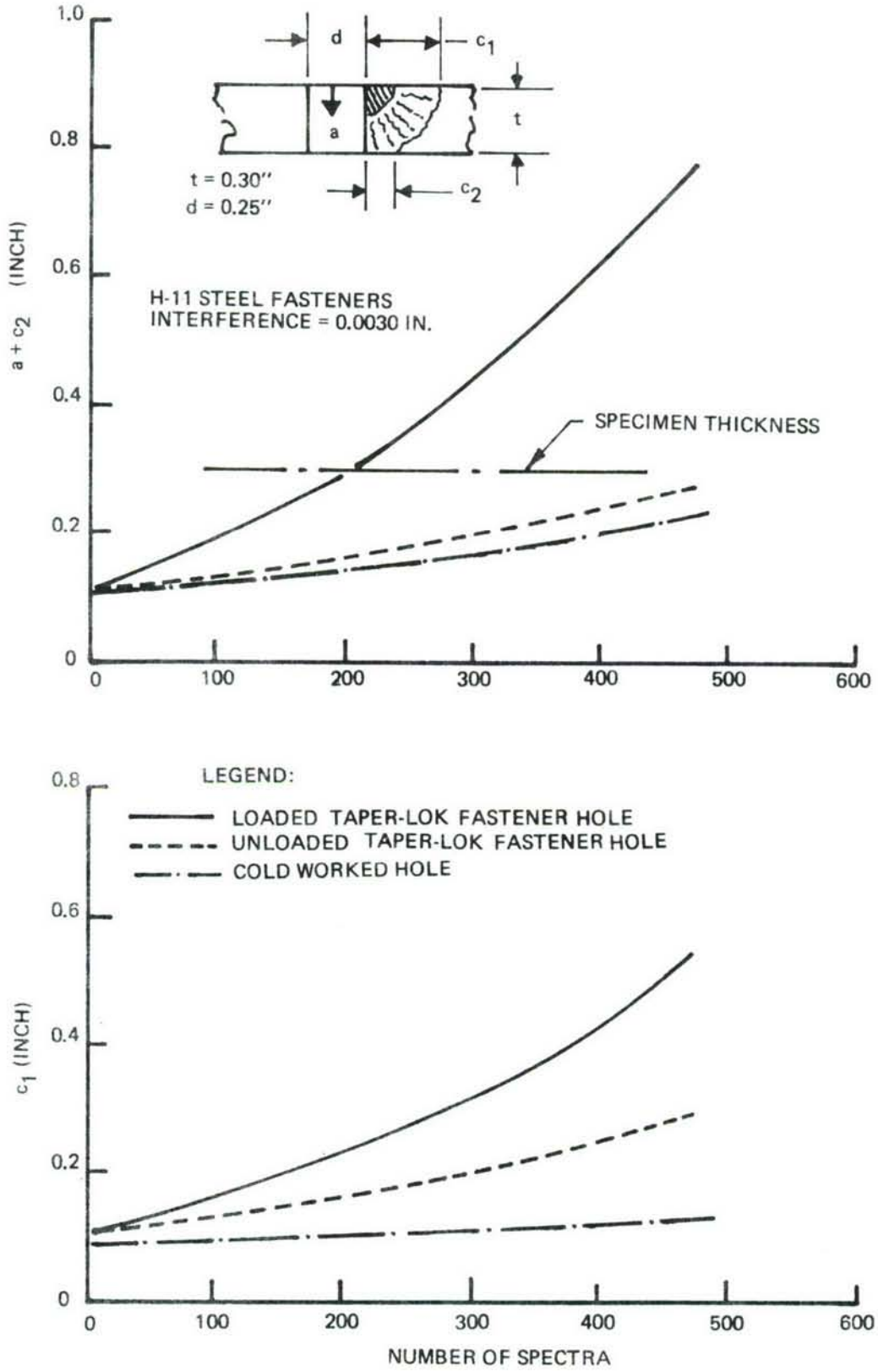


Figure 182: Crack Growth Behavior for Loaded and Unloaded Taper-Lok Fastener Holes in 9Ni-4Co-0.2C Steel Alloy Subjected to Bomber Spectrum

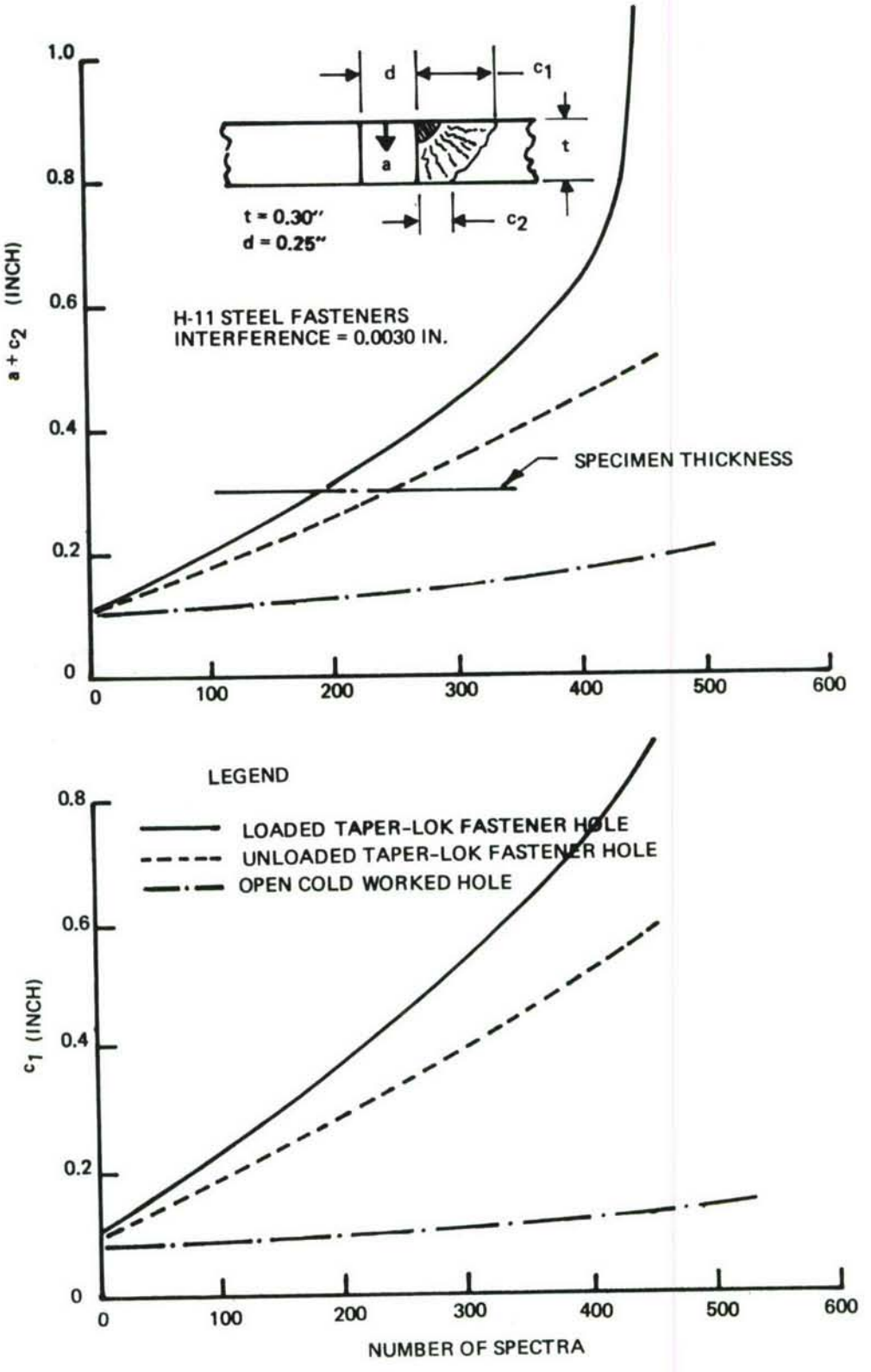


Figure 183: Crack Growth Behavior for Loaded and Unloaded Taper-Lok Fastener Holes in 9Ni-4Co-0.2C Steel Alloy Subjected to Fighter Spectrum

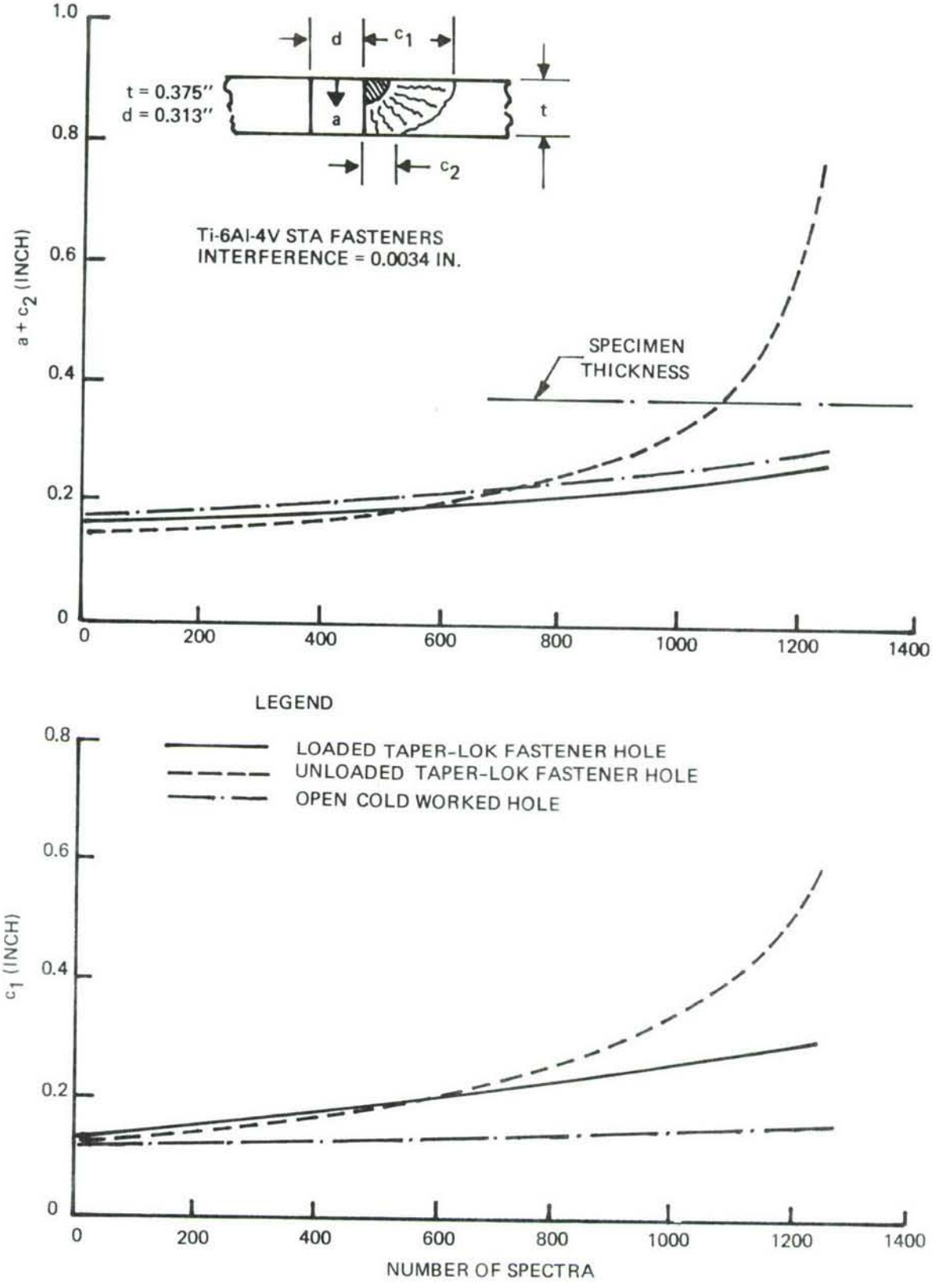


Figure 184: Crack Growth Behavior for Loaded and Unloaded Taper-Lok Fastener Holes in 6Al-4V βA Titanium Alloy Subjected to Bomber Spectrum (Specimen FSCIT-1)

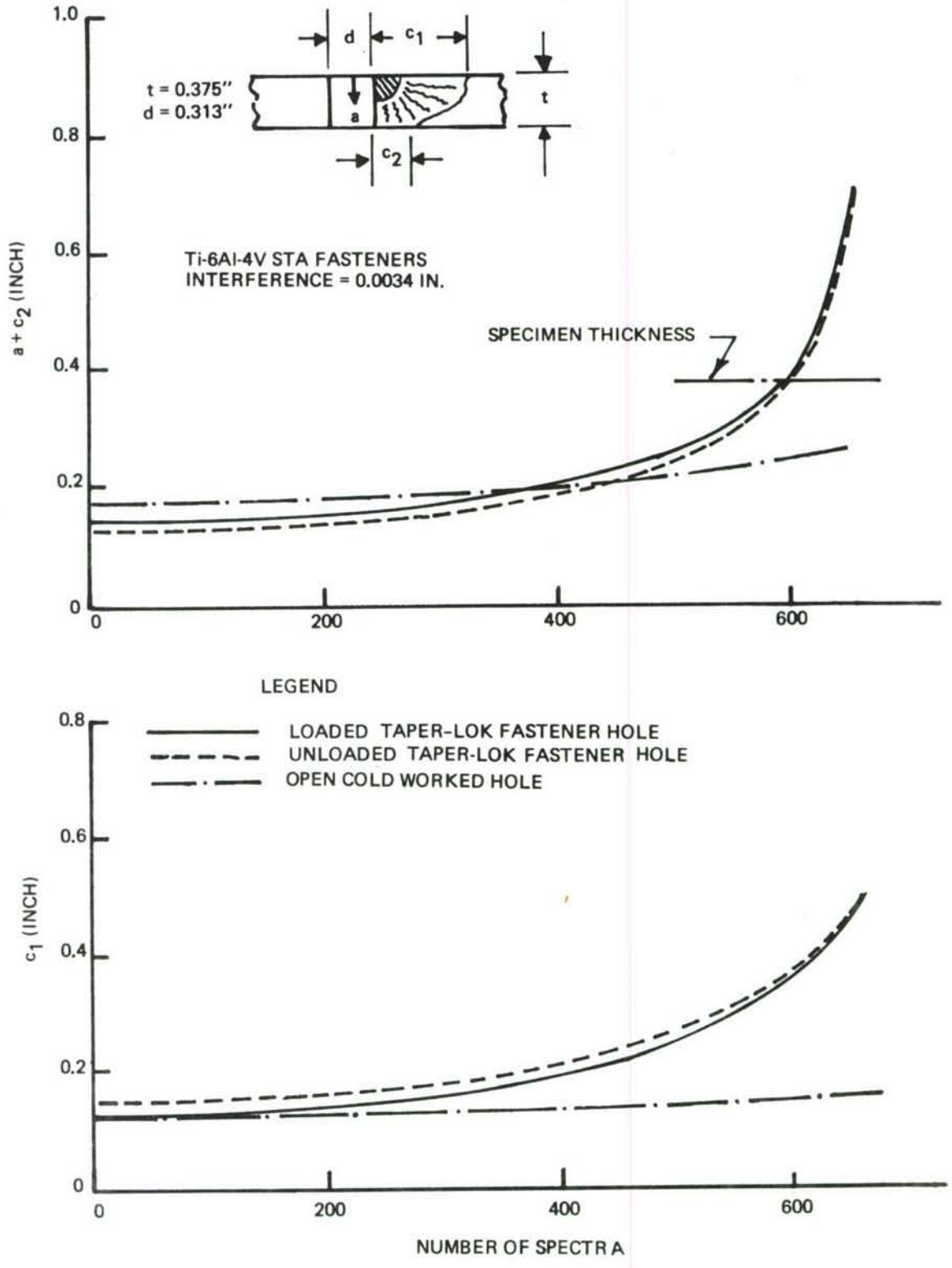


Figure 185: Crack Growth Behavior for Loaded Taper-Lok, Unloaded Taper-Lok, and Open Cold Worked Fastener Holes in 6A1–4VβA Titanium Alloy Subjected to Bomber Spectrum (Specimen FSCIT -2)

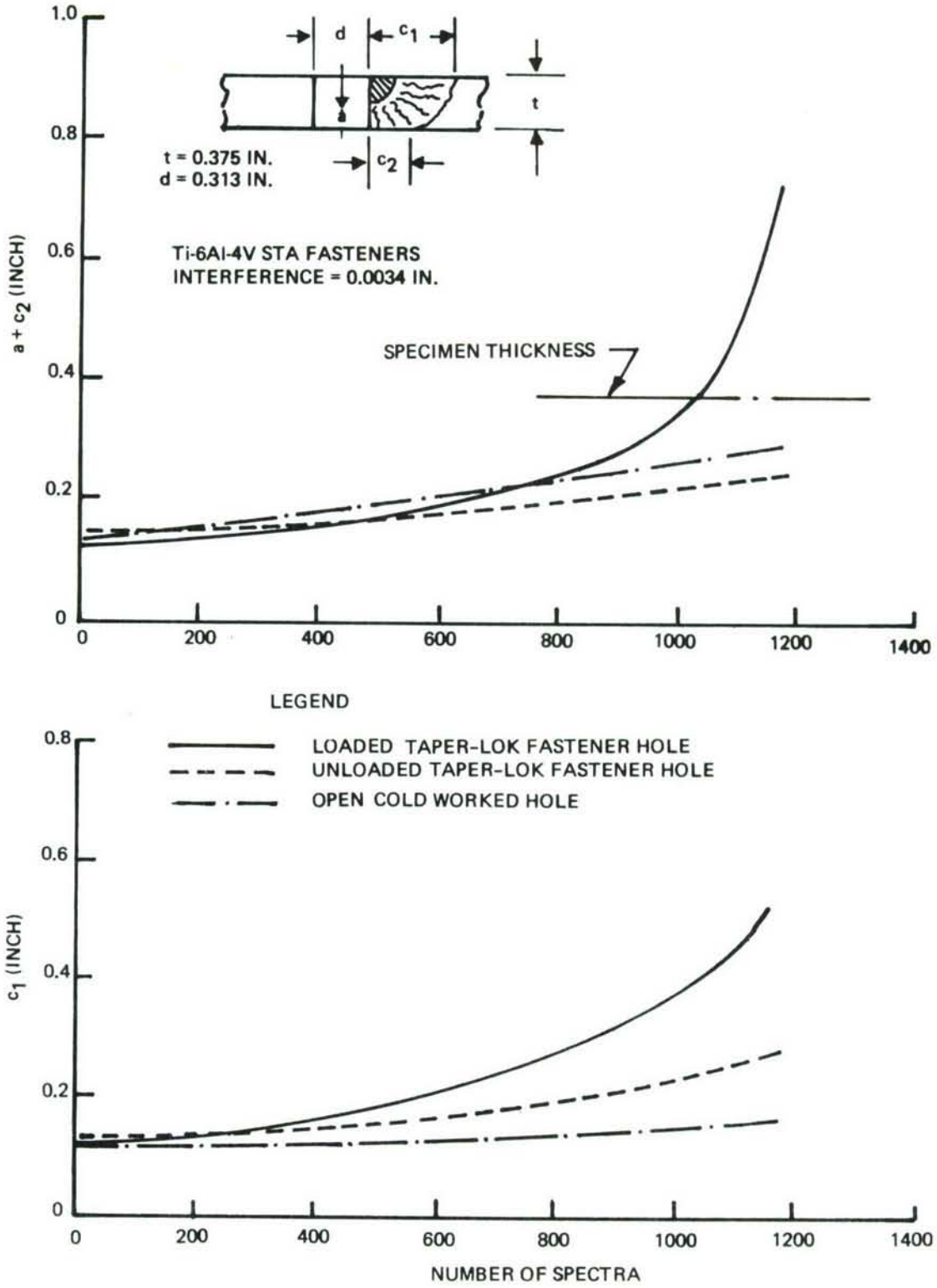


Figure 186. Crack Growth Behavior for Loaded Taper-Lok, Unloaded Taper-Lok, and Open Cold Worked Fastener Holes in 6A1-4VβA Titanium Alloy Subjected to Fighter Spectrum (Specimen FSCIT-3)

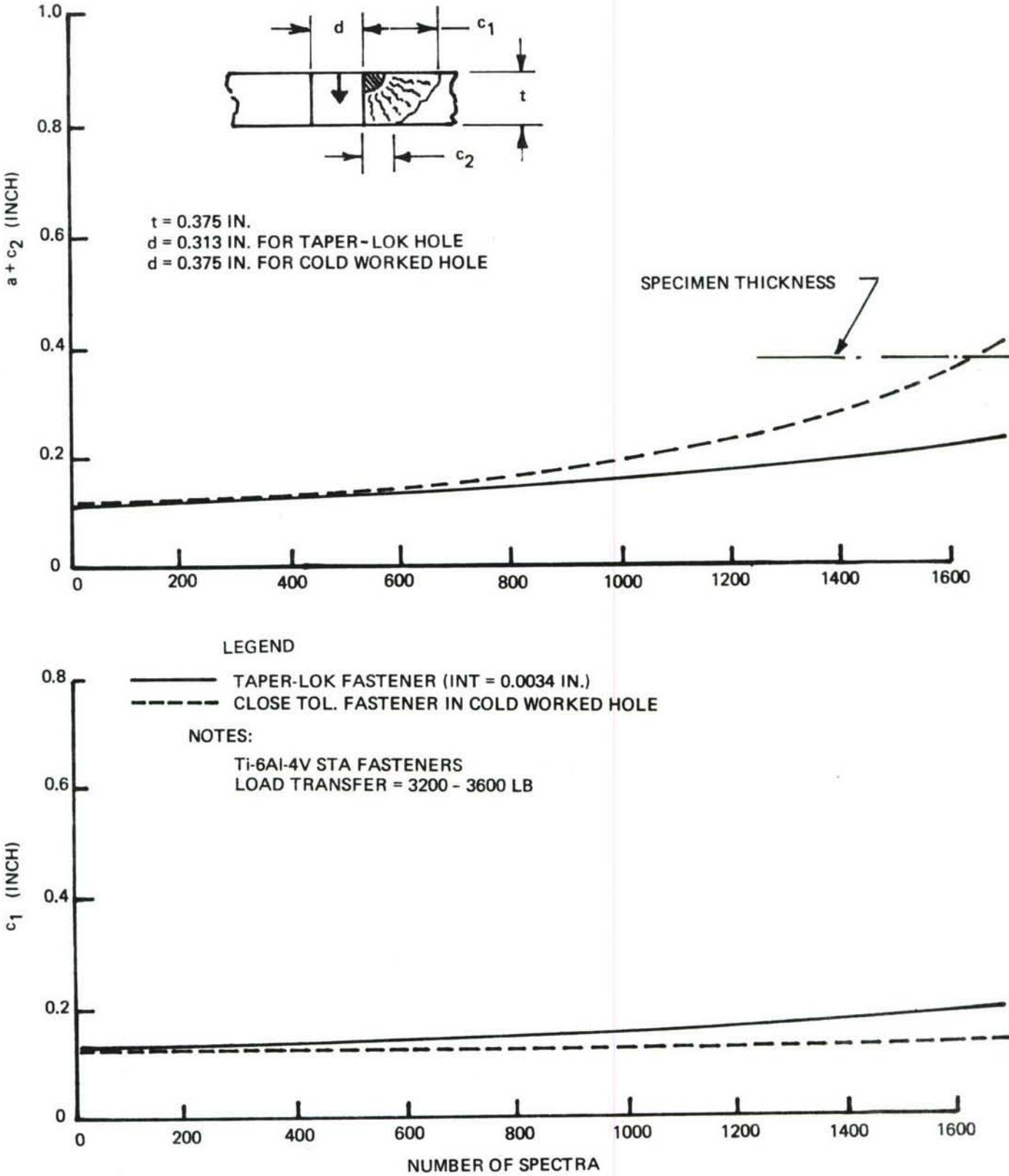


Figure 187: Crack Growth Behavior for 6Al-4V βA Titanium Alloy Taper-Lok Fastener/Cold Worked Hole Verification Specimen (Bomber Spectrum)

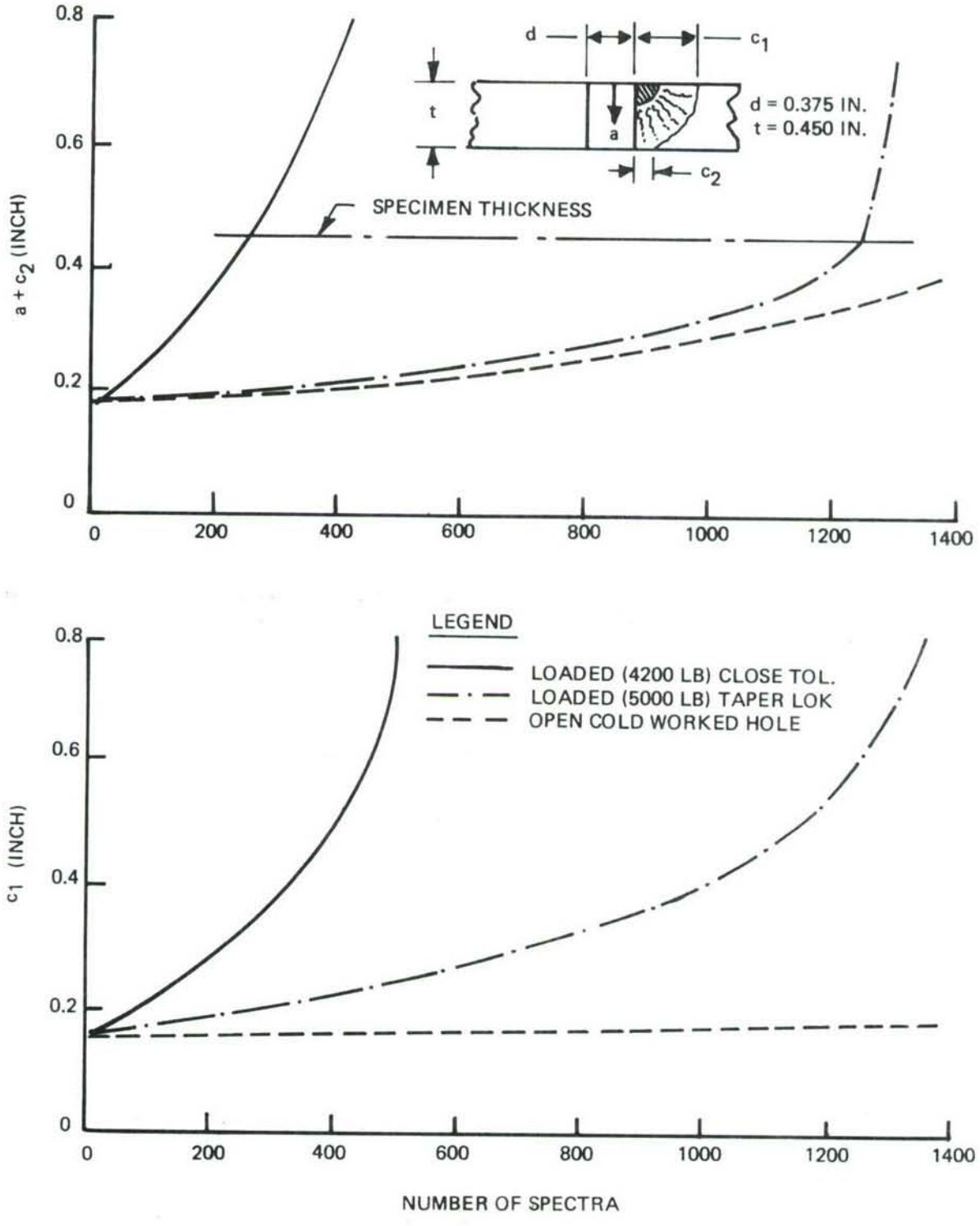


Figure 188: Comparison of Crack Growth Behavior for Loaded Close Tolerance, Loaded Taper-Lok, and Open Cold Worked Holes in 2219-T851 Aluminum Alloy Subjected to Bomber Spectrum

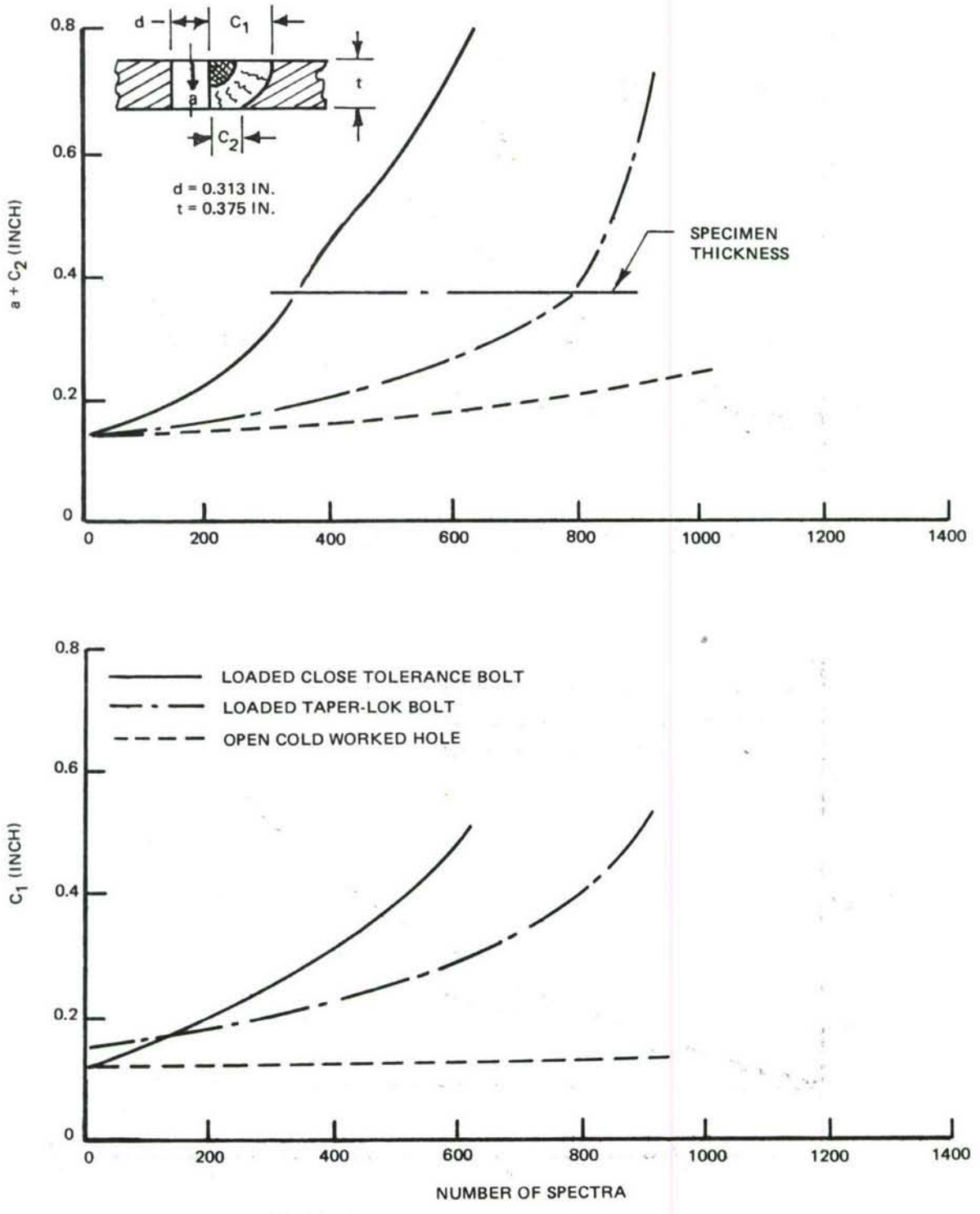


Figure 189: Comparison of Crack Growth Behavior for Part–Thru Cracks Originating at Loaded Close Tolerance, Loaded Taper-Lok, and Open Cold Worked Holes in 6A1-4V βA Titanium Alloy Specimens Subjected to Bomber Spectrum

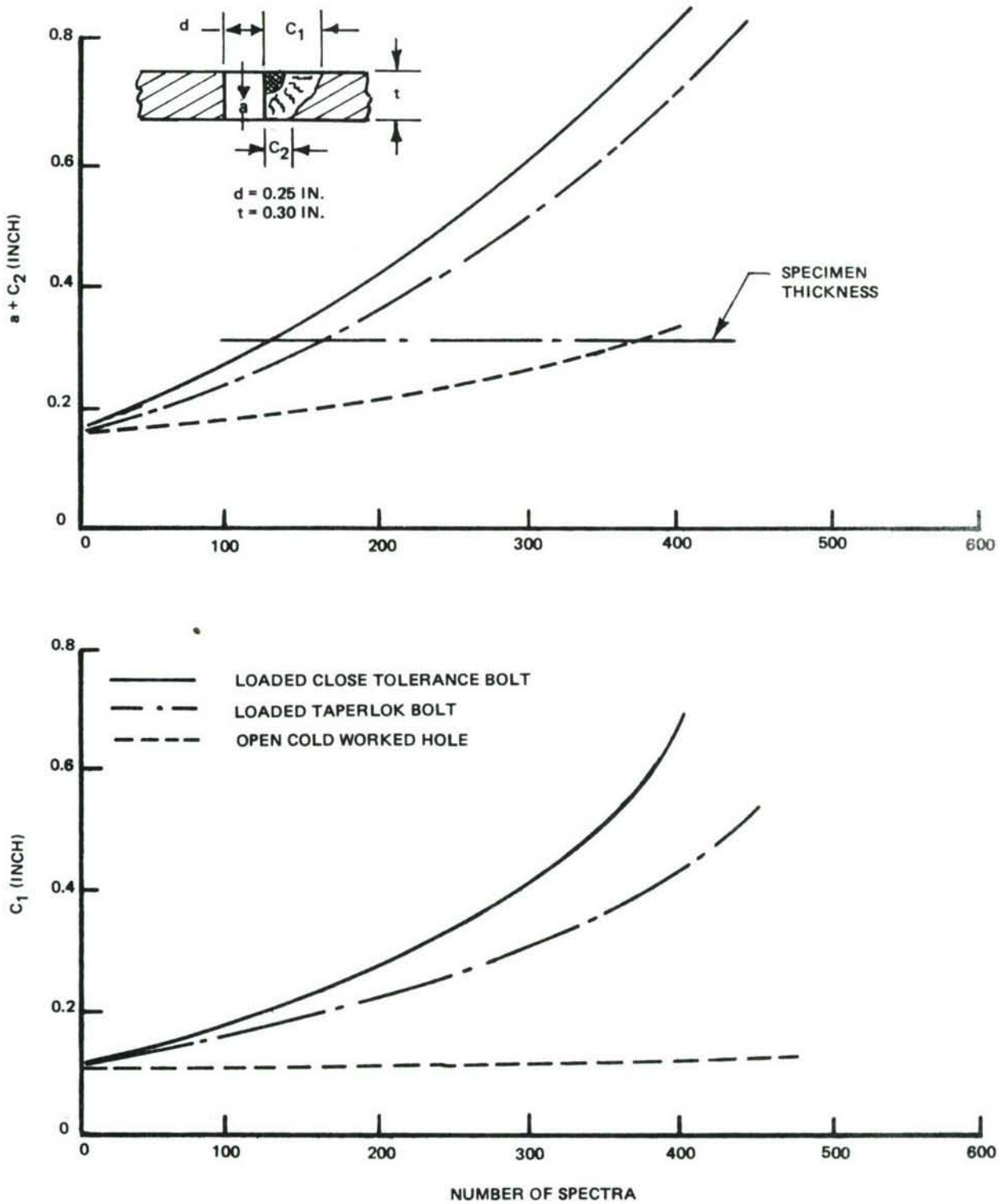


Figure 190: Comparison of Crack Growth Behavior of Part–Thru Cracks Originating at Loaded Close Tolerance, Loaded Taperlok, and Open Cold Worked Holes in 9Ni-4Co-0.2C Steel Alloy Specimens Subjected to Bomber Spectrum

Table 1: Chemical Composition of Materials

ELEMENT (% BY WEIGHT EXCEPT AS NOTED)	2219–T851 ALUMINUM PLATE (SPEC. LIMITS)		Ti-6Al-4V βA PLATE (SPEC. LIMITS)		9Ni-4Co-0.2C STEEL PLATE	4340 STEEL PLATE
	MAX.	MIN.	MAX.	MIN.		
COPPER	5.80	6.80	—	—	0.15	0.16
SILICON	—	0.20	—	—	0.07	0.32
MANGANESE	0.20	0.40	—	—	0.24	0.72
MAGNESIUM	—	0.02	—	—	—	—
IRON	—	0.30	0.25	—	BAL	BAL.
CARBON	—	—	0.08	—	0.19	0.41
COBALT	—	—	—	—	4.58	—
NICKEL	—	—	—	—	9.32	1.80
CHROMIUM	—	—	—	—	0.78	0.78
MOLYBDENUM	—	—	—	—	0.96	0.23
PHOSPHORUS	—	—	—	—	0.007	0.010
SULPHUR	—	—	—	—	0.003	0.014
ZINC	—	—	—	—	—	—
VANADIUM	0.05	0.15	4.50	3.50	0.09	—
NITROGEN	—	—	0.03	—	—	—
OXYGEN	—	—	0.13	0.06	—	—
HYDROGEN	—	—	0.0125	—	—	—
ZIRCONIUM	0.10	0.25	—	—	—	—
TITANIUM	0.10	0.20	BAL.	BAL.	—	—
ALUMINUM	BAL.	BAL.	6.30	5.50	—	—

Table 2: Mechanical Properties Of Materials

ALLOY	SPECIMEN WIDTH × THICKNESS (IN)	GRAIN DIRECTION	ULTIMATE TENSILE STRENGTH (KSI)	0.2% OFFSET YIELD STRENGTH (KSI)	ELONGATION IN 1.0 IN. GAGE LENGTH (%)	ELONGATION IN 2.0 IN. GAGE LENGTH (%)	REDUCTION IN AREA (%)
2219-T851 ALUMINUM (1.0 INCH THICK PLATE)	0.50 X 0.25	LONG.	66.3 66.0 66.1	52.7 52.6 52.6	16 16 16	11 11 11	27 29 28 (AVG)
		TRANS.	66.2 66.5 66.3	51.2 51.5 51.3	15 15 15	11 11 11	26 24 25 (AVG)
Ti-6Al-4V BETA ANNEALED (0.60 INCH THICK PLATE)	0.50 X 0.25	LONG.	138.3 138.6 138.4	125.4 125.3 125.3	16 16 16	10 11 10	27 25 26 (AVG)
		TRANS.	138.5 138.7 138.6	128.5 127.5 128.0	17 16 16	12 11 11	26 24 25 (AVG.)
9Ni-4Co-0.2C STEEL (0.50 INCH THICK PLATE)	0.50 X 0.20	LONG.	203.4 202.9 203.2	186.3 184.2 185.3	24 23 23	13 14 13	56 57 56 (AVG)
		TRANS.	204.7 202.2 203.5	188.0 185.2 186.6	22 24 23	13 13 13	53 57 55 (AVG)
4340 STEEL (0.625 INCH THICK PLATE)	0.50 X 0.25	(LOT A) LONG.	253.4 253.2 250.6 252.4	227.8 227.0 225.7 226.8	13 13 13 13	9 9 9 9	50 47 45 47 (AVG)
		(LOT B) LONG.	233.9 227.8 231.4 231.0	229.7 227.8 231.4 229.6	— — —	1 1 1 1	— — — (AVG)

Table 3: Summary of Fasteners Used in Test Program

PLATE ALLOY	FASTENER DETAILS					
	TYPE	ALLOY	TENSILE STRENGTH (ksi)	HEAD CONFIGURATION	FINISH AND LUBRICATION	SUPPLIER
2219-T851 ALUMINUM	TAPER SHANK (3/8" DIA)	PH13-8Mo STEEL	220-240	PROTRUDING SHEAR 100° TENSION	PASSIVATED CETYL ALCOHOL	OMARK IND PBF
	CLOSE TOLERANCE (3/8" DIA)	PH 13-8Mo STEEL	220-240	12 POINT	PASSIVATED CETYL ALCOHOL	OMARK INDUSTRIES
Ti-6Al-4V BETA ANN.	TAPER SHANK (5/16" DIA)	Ti-6Al-4VSTA	160	PROTRUDING SHEAR 100° SHEAR	UNPLATED PHOS. FLOURIDE CETYL ALCOHOL	OMARK IND. PBF
	CLOSE TOLERANCE (5/16" DIA)	Ti-6Al-4V STA	160	12 POINT		DUMONT AV.
9Ni-4Co-0.2C AND 4340 STEELS	TAPER SHANK (1/4" DIA)	H-11 STEEL	260-290	PROTRUDING SHEAR 100° SHEAR	DIFFUSED Cd-Ni LUBECO # 2123	GD/FW
	CLOSE TOLERANCE (1/4" DIA)	PH13-18Mo STEEL	220-240	12 POINT	PASSIVATED CETYL ALCOHOL	OMARK IND.

Table 4: Bomber Spectrum

LOAD LAYER	LOAD (% LIMIT)		CYCLES/ MISSION	LOAD LAYER	LOAD (% LIMIT)		CYCLES/ MISSION
	MAX.	MIN.			MAX.	MIN.	
1	-3	-15	1	23	34	0	1
2	100	58	1 EVERY 100	24	24	13	4
3	90	58	1 EVERY 10	25	72	8	1
4	68	58	1	26	56	11	9
5	58	45	1	27	38	19	10
6	69	65	1	28	99	53	1 EVERY 100
7	70	40	1	29	88	-12	1 EVERY 10
8	56	49	3	30	75	53	1
9	51	24	1	31	-3	-15	1
10	63	51	2	32	85	56	1
11	51	43	1	33	88	51	1
12	69	36	1	34	53	33	1
13	36	13	1	35	62	53	2
14	48	36	6	36	53	46	1
15	36	30	1	37	81	48	1
16	76	31	1	38	69	58	1
17	53	32	1	39	70	32	1
18	71	55	1 EVERY 10	40	45	40	1
19	62	33	1	41	59	43	5
20	51	40	1	42	55	46	29
21	55	13	1	43	-3	-15	1
22	38	23	6	44	-4	-14	1

ALLOY	LIMIT STRESS (KSI)
Al-2219-T851	33.6
Ti-6Al-4Vβ A	70.0
Fe-9Ni-4Co-0.2C	130.0

Table 5: Fighter Spectrum

LOAD LAYER	LOAD (% LIMIT) MAX.	LOAD (% LIMIT) MIN.	CYCLES PER MISSION	STEP	LOAD (% LIMIT) MAX.	LOAD (% LIMIT) MIN.	CYCLES PER MISSION
1	63.2	17.5	10	34	103.1	5.8	1
2	55.3	17.5	9	35	70.8	3.4	5
3	70.8	3.4	1	36	47.0	16.4	4
4	28.9	13.2	13	37	46.5	-18.9	1
5	70.8	3.4	1	38	37.5	17.5	5
6	37.5	17.5	39	39	63.2	17.5	1
7	70.8	3.4	1	40	28.9	13.2	1
8	84.8	7.0	1	41	47.0	16.4	16
9	47.0	16.4	18	42	70.8	3.4	3
10	37.5	17.5	39	43	55.3	17.5	13
11	28.9	13.2	26	44	37.5	17.5	39
12	76.4	4.6	1	45	28.9	13.2	13
13	47.0	16.4	18	46	47.0	16.4	18
14	28.9	13.2	13	47	63.2	17.5	5
15	47.0	16.4	19	48	28.9	13.2	13
16	76.4	4.6	1	49	70.8	3.4	1
17	55.3	17.5	28	50	47.0	16.4	19
18	37.5	17.5	39	51	37.5	17.5	39
19	63.2	17.5	5	52	55.3	17.5	9
20	47.0	16.4	19	53	28.9	13.2	13
21	37.5	17.5	39	54	37.5	17.5	39
22	70.8	3.4	1	55	28.9	13.2	13
23	63.2	17.5	4	56	63.2	17.5	5
24	76.4	4.6	1	57	76.4	4.6	1
25	94.4	14.7	5	58	37.5	17.5	39
26	37.5	17.5	12	59	55.3	17.5	9
27	63.2	17.5	2	60	47.0	16.4	36
28	76.4	4.6	2	61	55.3	17.5	9
29	66.4	22.2	7	62	70.8	3.4	3
30	63.2	17.5	10	63	84.8	7.0	1
31	66.4	22.2	4	64	63.2	17.5	10
32	55.3	17.5	30	65	118.1	4.1	1 EVERY 6 STARTING WITH 1ST MISSION
33	47.0	16.4	7	66	120.4	-14.2	1 EVERY 18 STARTING WITH 18TH MISSION

ALLOY	LIMIT STRESS (KSI)
Al-2219-T851	30.9
Ti-6Al-4V β A	61.8
Fe-9Ni-4Co-0.2C	91.0

Table 6: Baseline Crack Growth Rate Test Program

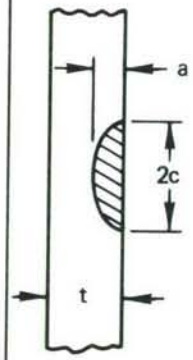
ALLOYS	SPECIMEN THICKNESS (IN)	INITIAL FLAW GEOMETRY	$(a/2c)_i$	RANGE OF (a/t)	STRESS STATES	STRESS RATIO	NUMBER OF SPECIMENS
2219-T851 ALUMINUM 6Al-4V βA TITANIUM 9Ni-4Co-0.2C STEEL	1.00 (Al) 0.60 (Ti) 0.50 (Fe)		0.30	0.2/0.6	TENSION	0.1 0.3 0.5	6 6 6
			0.15 0.40	0.2/0.5	BENDING	0.1 0.5	3 3
	0.45 (Al) 0.375 (Ti) 0.250 (Fe)		—	—	—	0.1 0.5	3 3

Table 7: Uniform Load Test Program For Surface Flaws

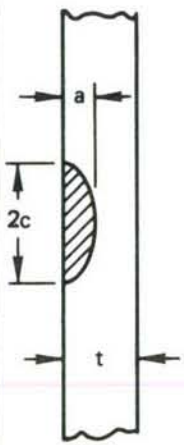
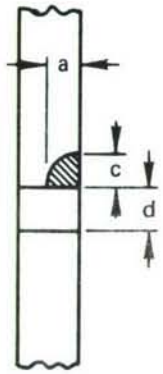
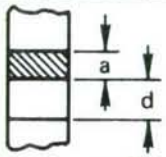
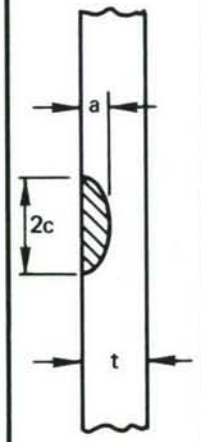
INITIAL FLAW GEOMETRY	ALLOYS/ THICKNESS (IN)	$(a/2c)_i$	$(a/t)_i$	STRESS STATE	STRESS RATIO	NUMBER OF SPECIMENS
	2219-T851 ALUMINUM/0.450 6Al-4V βA TITANIUM/0.375 9Ni-4Co-0.2C STEEL/0.300	0.15 0.30 0.45	< 0.5	TENSION	0.1	3
					0.5	3
		0.15 0.30 0.45	> 0.5	TENSION	0.1	3
					0.5	3
		0.30	< 0.5	TENSION + BENDING	0.1	3
					0.5	3

Table 8: Uniform Load Test Program For Cracked Fastener Holes

ALLOY	SPECIMEN THICKNESS (IN)	INITIAL FLAW GEOMETRY	INITIAL FLAW DEPTH, a (IN)	HOLE DIAMETER (IN)	STRESS STATE	FLAW ORIGINS	NUMBER OF SPECIMENS
2219-T851 ALUMINUM 6Al-4V βA TITANIUM 9Ni-4Co-0.2C STEEL	0.450 (Al) 0.375 (Ti) 0.300 (Fe)		0.150 (Al) 0.125 (Ti) 0.100 (Fe)	0.375 (Al) 0.313 (Ti) 0.250 (Fe)	TENSION	LIF UIFH UIFL	3
						LCT OH FH	3
					TENSION + BENDING	UIFH	3
				0.375	TENSION	LCW UCWH UCWL	3
			0.05	0.375 (Al) 0.313 (Ti) 0.250 (Fe)	TENSION	LIF UIFH UIFL	6

LIF = LOADED INTERFERENCE FIT FASTENER
UIFH = UNLOADED INT. FIT FASTENER–HIGH PROTRUSION
UIFL = UNLOADED INT. FIT FASTENER–LOW PROTRUSION
LCT = LOADED CLOSE TOLERANCE FASTENER
OH = OPEN HOLE
FH = FILLED HOLE
LCW = LOADED COLD WORKED HOLE
UCWH = UNLOADED COLD WORKED HOLE–HIGH EXPANSION
UCWL = UNLOADED COLD WORKED HOLE–LOW EXPANSION

Table 9: Periodic Overload Test Program For Surface Flaws

INITIAL FLAW GEOMETRY	ALLOYS/ THICKNESS (IN)	$(a/2c)_i$	$(a/t)_i$	STRESS STATE	LOADING SPECTRA		NUMBER OF SPECIMENS
					$\frac{\sigma_{ol}}{\sigma_{MAX}}$	τ	
	2219-T851 ALUMINUM/0.450 6Al-4V βA TITANIUM/0.375 9Ni-4Co-0.2C STEEL/0.300	0.15 0.30 0.45	< 0.5	TENSION	3 VALUES	VARIABLE	18
		0.15 0.30 0.45	> 0.5	TENSION	3 VALUES	VARIABLE	18
		0.30	< 0.5	TENSION + BENDING	2 VALUES	VARIABLE	9

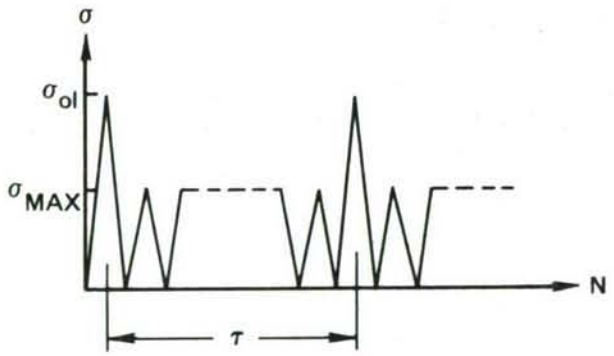
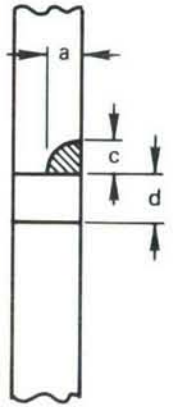
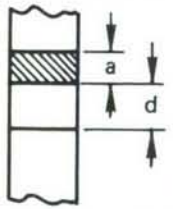


Table 10: Periodic Overload Test Program For Cracked Fastener Holes

ALLOY	SPECIMEN THICKNESS (IN)	INITIAL FLAW GEOMETRY	$\frac{\sigma_{OVERLOAD}}{\sigma_{CYCLIC}}$	INITIAL FLAW DEPTH, a (IN)	HOLE DIAMETERS d (IN)	FLAW [a] ORIGINS	NUMBER OF SPECIMENS
2219-T851 ALUMINUM 6Al-4V βA TITANIUM 9Ni-4Co-0.2C STEEL	0.450 (ALUMINUM) 0.375 (TITANIUM) 0.300 (STEEL)		3 VALUES	0.150 (ALUMINUM) 0.125 (TITANIUM) 0.100 (STEEL)	0.375 (Al and ALL CWH'S) 0.313 (Ti) 0.250 (Fe)	LIF UIFH UIFL	9
						LIF UIFH CWH	12
						LCT OH FH	6
					0.375	LCW UCWH UCHL	3
			1 VALUE	0.05	0.375 (Al) 0.313 (Ti) 0.250 (Fe)	LIF UIFH UIFL	3

(a) SEE TABLE 8 FOR DEFINITION OF ACRONYMS

Table 11: Spectrum Load Test Program For Surface Flaws

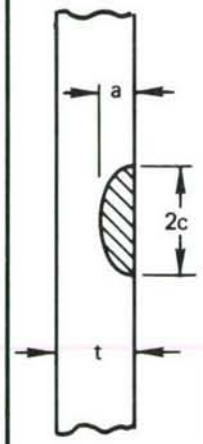
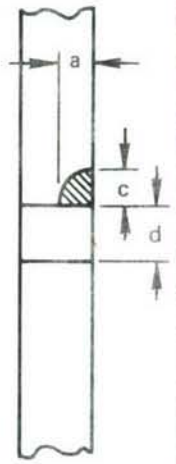
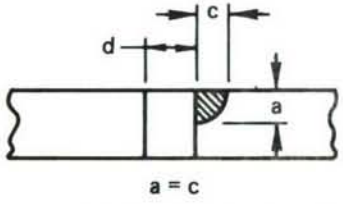
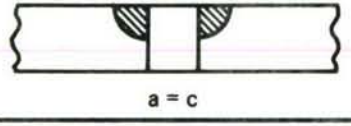
INITIAL FLAW GEOMETRY	ALLOYS/ THICKNESS (IN)	$(a/2c)_i$	$(a/t)_i$	STRESS STATE	SPECTRUM TYPE	NUMBER OF SPECIMENS
	2219-T851 ALUMINUM/0.450 6Al-4V βA TITANIUM/0.375 9Ni-4Co-0.2C STEEL/0.300	0.15 0.30 0.45	< 0.5	TENSION	BOMBER	3
					FIGHTER	3
			> 0.5	TENSION	BOMBER	3
					FIGHTER	3

Table 12: ***Spectrum Loading Test Program for Cracked Fastener Holes***

INITIAL FLAW GEOMETRY	ALLOYS	SPECIMEN THICKNESS (IN)	HOLE DIAMETER d (IN)	INITIAL FLAW DEPTH, a (IN)	FLAW ORIGINS	LOADING SPECTRUM	NUMBER OF SPECIMENS
	2219-T851 ALUMINUM 6Al-4V βA TITANIUM 9Ni-4Co-0.2C STEEL	0.450 (ALUMINUM) 0.375 (TITANIUM) 0.300 (STEEL)	0.375 (Al and ALL CWH'S) 0.313 (Ti) 0.250 (Fe)	0.150 (ALUMINUM) 0.125 (TITANIUM) 0.100 (STEEL)	LIF UIF CWH	BOMBER	3
						FIGHTER	3
					LCT FH OH	BOMBER	3
						FIGHTER	3
					LIF CWH	BOMBER	3
					PLCT CLCT	BOMBER	3

LIF = LOADED INTERFERENCE FIT
UIF = UNLOADED INTERFERENCE FIT
CWH = COLD WORKED HOLE
FH = FILLED CLOSE TOLERANCE HOLE
OH = OPEN HOLE
(P or C) LCT = (PLAIN OR CSK) LOADED CLOSE TOLERANCE

Table 13: Stress Intensity Factor Verification Program For Cracked Fastener Holes

ALLOYS	TEST SERIES	FLAW GEOMETRY	HOLE DIA (IN)	(a/t)	FLAW[a] ORIGINS	NUMBER OF TESTS
SPECIMEN: 4340 (220-240) FASTENER: H-11 (260-290)	1		$\begin{pmatrix} 0.250 \\ 0.375^{(b)} \end{pmatrix}$	0.4 0.6 0.8	OH UIFH UIFL LIF LCT	6 6 3 3 3
	2		$\begin{pmatrix} 0.250 \\ 0.375^{(b)} \end{pmatrix}$	0.4 0.6 0.8	OH UIFH UIFL LIF LCT	6 6 3 3 3

(a) SEE TABLE 8 FOR DEFINITION OF ACRONYMS

(b) FOR OH AND UIFH TESTS ONLY

Table 14: Comparison of Actual and Predicted Results for Uniform Load Cyclic Tests of Surface Flawed 2219-T851 Aluminum Alloy

STRESS STATE	SPECIMEN NO.	THICK (in)	STRESS RATIO	PEAK CYCLIC STRESS (ksi)	INITIAL FLAW DIMENSIONS		FINAL (a/t) ACTUAL & PREDICTED	FINAL a/2c		LOADING CYCLES	
					$(a/2c)_i$	$(a/t)_i$		ACTUAL	PRE-DICTED	ACTUAL	PRE-DICTED
Uniform Tension	SUTA1-1	0.448	0.1	18	0.191	0.286	0.791	0.347	0.405	19,500	24,200
					0.294	0.317	0.679	0.400	0.432	18,800	25,900
					0.428	0.483	1.000	0.385	0.505	16,000	23,200
Uniform Tension	SUTA1-2	0.449	0.1	10	0.163	0.548	1.000	0.264	0.287[e]	26,500	36,800[e]
					0.293	0.662	1.000	0.339	0.402	32,400	38,900
					0.422	0.813	1.000	0.419	0.472	19,000	24,100
Uniform Tension	SUTA5-1	0.449	0.5	30	0.171	0.254	0.688	0.318	0.375	15,600	16,500
					0.305	0.330	0.635	0.361	0.424	16,200	15,900
					0.437	0.468	0.784	0.359	0.473	14,100	14,000
Uniform Tension	SUTA5-2	0.447	0.5	18	0.142	0.476	1.000	0.251	0.285	28,200	27,300
					0.280	0.635	1.000	0.327	0.396	30,200	24,200
					0.442	0.805	0.972	0.394	0.482	18,400	14,400

e = extrapolated

Table 15: Comparison of Actual and Predicted Results for Uniform Load Cyclic Tests of Surface Flawed 9Ni-4Co-0.2C Steel Alloy

STRESS STATE	SPECIMEN NO.	THICK (in)	STRESS RATIO	PEAK CYCLIC STRESS (ksi)	INITIAL FLAW DIMENSIONS		FINAL (a/t) ACTUAL & PREDICTED	FINAL a/2c		LOADING CYCLES	
					$(a/2c)_i$	$(a/t)_i$		ACTUAL	PRE-DICTED	ACTUAL	PRE-DICTED
Uniform Tension	SUTS1-1	0.306	0.10	44	0.163 0.322 0.447	0.173 0.245 0.343	0.964 1.000 1.000	0.406 0.440 0.427	0.475 0.502 0.510	57,000 57,500 43,500	60,900 63,400 51,700
Uniform Tension	SUTS1-2	0.305	0.10	30	0.149 0.294 0.441	0.484 0.642 0.802	1.000 1.000 1.000	0.268 0.373 0.438	0.287 0.402 0.484	29,200 27,300 21,900	31,300 26,900 17,100
Uniform Tension	SUTS1-3	0.300	0.10	60	0.165 0.318 0.440	0.183 0.257 0.370	1.000 0.984 1.000	0.396 0.418 0.426	0.475 0.493 0.505	22,800 22,300 16,400	25,800 25,900 20,500
Uniform Tension	SUTS5-2	0.291	0.50	45	0.149 0.294 0.428	0.512 0.670 0.835	1.000 1.000 1.000	0.261 0.340 0.402	0.275 0.389 0.466	23,700 22,500 15,500	26,800 22,300 12,100

Table 16: Comparison of Actual and Predicted Results For Uniform Load Cyclic Tests of Surface Flawed 6Al-4V βA Titanium Alloy

STRESS STATE	SPECIMEN NO.	THICK. (IN.)	STRESS RATIO	PEAK CYCLIC STRESS (KSI)	INITIAL FLAW DIMENSIONS		FINAL (a/t) ACTUAL & PREDICTED	FINAL a/2c		LOADING CYCLES	
					$(a/2c)_i$	$(a/t)_i$		ACTUAL	PREDICTED	ACTUAL	PREDICTED
UNIFORM TENSION	SUTT1-1	0.376	0.10	45	0.145	0.191	1.000	0.418	0.487	17,900	23,000
					0.285	0.268	1.000	0.448	0.511	19,700	25,200
					0.451	0.404	1.000	0.443	0.518	13,300	18,800
UNIFORM TENSION	SUTT1-2	0.370	0.10	27	0.138	0.470	1.000	0.261	0.287	13,800	22,700
					0.427	0.810	1.000	0.416	0.484	9,900	12,400
					—	—	—	—	—	—	—
UNIFORM TENSION	SUTT5-1	0.372	0.50	70	0.145	0.194	0.780	0.385	0.432	15,600	17,000
					0.297	0.285	0.815	0.429	0.471	15,500	18,400
					0.439	0.398	1.000	0.435	0.515	11,700	16,300
UNIFORM TENSION	SUTT5-2	0.382	0.50	42	0.157	0.519	1.000	0.265	0.292	12,800	16,100
					0.441	0.810	1.000	0.429	0.492	8,182	11,500
					—	—	—	—	—	—	—

Table 17: Summary of Test Parameters for 2219-T851 Aluminum Alloy Surface Flaw Tension Overload Tests

TEST TYPE	$(a/t)_i$	SPECIMEN ID	PEAK CYCLIC STRESS (ksi)	$\frac{\sigma_o}{\sigma_m}$	OVERLOAD PERIOD(S) (CYCLES)
SINGLE OVERLOAD	< 0.5	SOTA-1	18	2.0	19,400
		SOTA-2	18	1.5	9,600 6,465
		SOTA-3	18	- 0.1	7,880 5,850
	> 0.5	SOTA-4	10	2.0	—
		SOTA-5	10	1.5	—
		SOTA-6	10	- 0.1	—
PERIODIC OVERLOAD	< 0.5	SPOTA-1	18	2.0	9,000
		SPOTA-2	18	2.0	13,000
		SPOTA-3	18	1.5	3,000
	> 0.5	SPOTA-4	10	2.0	6,500
		SPOTA-5	10	2.0	5,945 13,000
		SPOTA-6	10	1.5	1,000

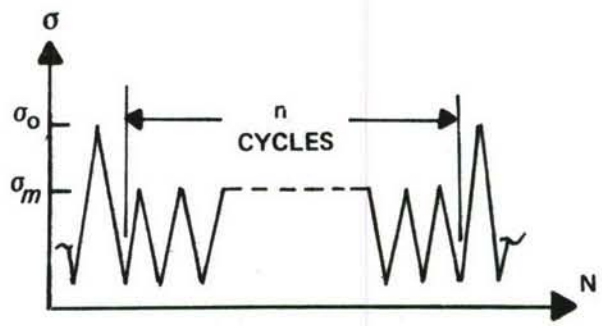


Table 18: Summary of Test Parameters for 9Ni-4Co-0.2C Steel Alloy Surface Flaw Tension Overload Tests

TEST TYPE	$(\frac{a}{t})_i$	SPECIMEN I.D.	PEAK CYCLIC STRESS (KSI)	$\frac{\sigma o}{\sigma m}$	OVERLOAD PERIOD (S) (CYCLES)
SINGLE OVERLOAD	<0.5	SOTS-1	60	2.0	15,000 12,350
		SOTS-2	60	1.5	7,140 5,096 4,283
		SOTS-3	60	− 0.1	10,900 3,500
	>0.5	SOTS-4	30	2.0	36,050 29,175
		SOTS-5	30	1.5	24,750 24,020
		SOTS-6	30	− 0.1	23,445 24,020
PERIODIC OVERLOAD	<0.5	SPOTS-1	60	2.0	7,500
		SPOTS-2	60	2.0	11,000
		SPOTS-3	60	1.5	1,500
	>0.5	SPOTS-4	30	2.0	7,500
		SPOTS-5	30	2.0	11,000
		SPOTS-6	30	1.5	1,500

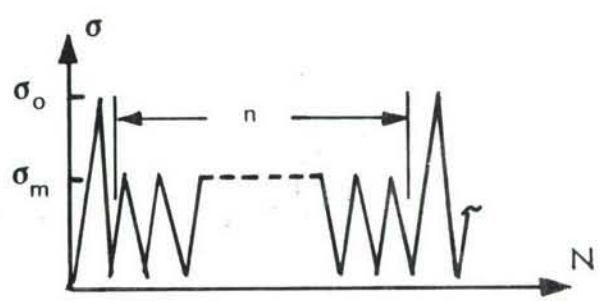


Table 19: Summary of Test Parameters for Ti-6Al-4V Beta Annealed Alloy Surface Flawed Tension Overload Tests

TEST TYPE	$(\frac{a}{t})_i$	SPECIMEN I.D.	PEAK CYCLIC STRESS (KSI)	$\frac{\sigma o}{\sigma m}$	OVERLOAD PERIOD(S) (CYCLES)
SINGLE OVERLOAD	<0.5	SOTT-1	45	2.0	21,394
		SOTT-2	45	1.5	7,350
		SOTT-3	45	-0.1	7,350
	>0.5	SOTT-4	27	2.0	19,578
		SOTT-5	27	1.5	—
		SOTT-6	27	(2.0 + -0.2)	—
PERIODIC OVERLOAD	<0.5	SPOTT-1	45	2.0	13,000
		SPOTT-2	45	(2.0 + -0.2)	13,000
		SPOTT-3	45	1.5	5,000
	>0.5	SPOTT-4	27	2.0	7,500
		SPOTT-5	27	(2.0 + -0.2)	7,500
		SPOTT-6	27	1.5	4,300

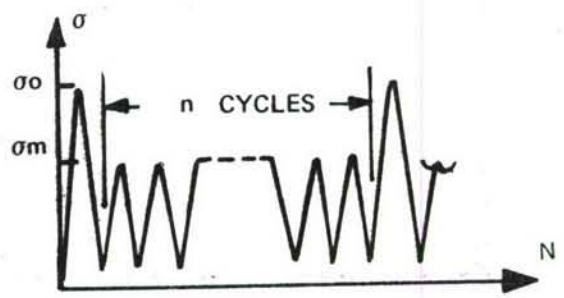


Table 20: Results of 2219-T851 Aluminum Alloy Single Overload Surface Flaw Specimens (Shallow Flaw Tests)

SPECIMEN I.D.	OVERLOAD RATIO	FLAW NO.	FLAW DIMENSIONS (t = 0.45 IN.)		OVERLOAD VARIABLES		RESULTS	
			a/2c	a/t	K_o $(KSI\sqrt{IN})$	$\frac{1}{3\pi}\left(\frac{K_o}{\sigma_{ys}}\right)$ (IN.)	Δa_p (IN)	N_d CYCLES
SOTA - 1	2.0	1	0.18	0.26	22.4	0.020	0.020	6,400
			0.31	0.50	26.4	0.028	0.030	5,700
		2	0.30	0.32	21.1	0.018	0.020	4,700
			0.55	0.40	24.5	0.024	0.030	5,400
		3	0.43	0.45	21.4	0.018	0.028	8,300
			0.43	0.69	28.4	0.032	0.028	6,000
SOTA-2	1.5	1	0.18	0.27	16.4	0.011	0.016	700
		2	0.32	0.34	15.6	0.010	0.016	1,900
		3	0.43	0.48	16.4	0.011	0.018	2,200
			0.42	0.65	20.3	0.017	0.023	900
SOTA-3	- 0.1	1	0.16	0.25	—	—	0	0
			0.28	0.43	—	—	0	0
		2	0.31	0.33	—	—	0	0
			0.38	0.48	—	—	0	0
		3	0.44	0.48	—	—	0	0
			0.43	0.66	—	—	0	0

Table 21: Results of 2219-T851 Aluminum Alloy Single Overload Surface Flaw Tests (Deep Flaw Specimens)

SPECIMEN	OVERLOAD RATIO	FLAW NO.	FLAW DIMENSIONS (t = 0.45 IN.)		OVERLOAD VARIABLES		RESULTS	
			a/2c	a/t	K_o (KSI $\sqrt{IN}$)	$\frac{1}{3\pi}\left(\frac{K_o}{\sigma_{ys}}\right)^2$ (IN.)	Δa_p (IN)	Nd (CYCLES)
SOTA-4	2.0	1	0.16	0.53	18.4	0.014	0.045	4700
		2	0.29	0.65	17.6	0.012	0.019	4400
		3	0.43	0.82	17.5	0.012	0.036	5800
SOTA-5	1.5	1	0.16	0.55	13.9	0.008	0.009	~400
		2	0.29	0.65	13.1	0.007	0	0
		3	0.43	0.80	12.9	0.007	0	0
SOTA-6	-0.1	1	0.16	0.52	—	—	0	0
		2	0.29	0.66	—	—	0	0
		3	0.45	0.83	—	—	0	0

Table 22: Results of 9Ni-4Co-02.C Steel Alloy Single Overload Surface Flaw Tests (Shallow Flaw Specimens)

SPECIMEN I.D.	OVER-LOAD RATIO	FLAW NO.	FLAW DIMENSIONS (t = 0.30 IN.)		OVERLOAD VARIABLES		RESULTS	
			a/2c	a/t	K_o (KSI $\sqrt{IN.}$)	$\frac{1}{3\pi}\left(\frac{K_o}{\sigma_{ys}}\right)^2$ (IN.)	Δa_p (IN.)	N_d (~)
SOTS-1	2.0	1	0.16	0.17	50.1	0.008	0.022	7400
			0.31	0.36	60.0	0.010	0.021	4900
		2	0.29	0.23	49.2	0.007	0.022	7800
			0.37	0.37	55.6	0.009	0.020	5400
		3	0.44	0.36	51.4	0.008	0.021	5200
			0.46	0.62	67.0	0.014	0.018	5000
SOTS-2	1.5	1	0.16	0.18	37.2	0.004	0.012	1500
			0.27	0.30	42.4	0.005	*a*	700
			0.33	0.42	46.4	0.007	*a*	800
			0.37	0.53	50.5	0.008	*a*	1300
		2	0.32	0.26	36.9	0.004	*a*	600
			0.38	0.38	41.7	0.005	*a*	300
			0.41	0.50	46.2	0.007	*a*	500
			0.42	0.61	52.3	0.008	*a*	600
		3	0.45	0.37	37.3	0.004	*a*	0
			0.47	0.50	43.5	0.006	*a*	300
			0.46	0.63	50.4	0.008	*a*	900
			0.45	0.76	58.8	0.011	*a*	500

a COULD NOT BE DETERMINED

Table 23: Results of 9Ni-4Co-0.2C Steel Alloy Single Overload Surface Flaw Tests (Deep Flaw Specimens)

SPECIMEN I.D.	OVER-LOAD RATIO	FLAW NO.	FLAW DIMENSIONS (t = 0.30 IN.)		OVERLOAD VARIABLES		RESULTS	
			a/2c	a/t	K_o (KSI $\sqrt{IN.}$)	$\frac{1}{3\pi}\left(\frac{K_o}{\sigma_{ys}}\right)^2$ (IN)	Δa_p (IN)	N_d ($\sim$)
SOTS-4	2.0	1	0.15	0.45	43.3	0.006	0.019	6700
		2	0.30	0.67	42.5	0.006	0.026	6600
		3	0.45	0.85	42.1	0.006	0.018	6000
SOTS-5	1.5	1	0.16	0.51	32.6	0.003	0.020	700
		2	0.29	0.65	31.7	0.003	0.009	400
		3	0.43	0.82	32.3	0.003	*a*	*a*
SOTS-6	-0.1	1	0.15	0.51	—	—	*a*	*a*
		2	0.30	0.67	—	—	*a*	*a*
		3	0.42	0.81	—	—	*a*	*a*

a TOO SMALL TO BE DETERMINED

Table 24: Results of 6Al-4V βA Titanium Alloy Single Overload Surface Flaw Tests (Shallow Flaw Specimens)

SPECIMEN I.D.	OVERLOAD RATIO	FLAW NO.	FLAW DIMENSIONS (t = 0.375 IN)		OVERLOAD VARIABLES		RESULTS	
			a/2c	a/t	K_o (KSI$\sqrt{\text{IN}}$)	$\frac{1}{3\pi}\left(\frac{K_o}{\sigma_{ys}}\right)^2$ (IN.)	Δa_p (IN.)	N_d (~)
SOTT-1	2.0	1	0.14	0.19	44.9	0.013	0.045	14,300
			0.31	0.42	54.1	0.019	0.019	8,000
		2	0.45	0.40	44.5	0.013	0.025	7,800
SOTT-2	1.5	1	0.15	0.20	33.9	0.007	≅0.04	≅ 3,000
			0.27	0.36	39.2	0.010	0.022	2,300
		2	0.44	0.39	32.8	0.007	0.011	700
			0.51	0.59	38.5	0.010	0.010	900
SOTT-3	-0.1	1	0.14	0.19	—	—	*a*	*a*
		2	0.44	0.39	—	—	*a*	*a*

a TOO SMALL TO BE DETERMINED

Table 25: Results of 6Al-4V βA Titanium Alloy Single Overload Surface Flaw Tests (Deep Flaw Specimens)

SPECIMEN I.D.	OVERLOAD RATIO	FLAW NO.	FLAW DIMENSIONS (t = 0.375 IN.)		OVERLOAD VARIABLES		RESULTS	
			a/2c	a/t	K_o (KSI$\sqrt{\text{IN}}$)	$\frac{1}{3\pi}\left(\frac{K_o}{\sigma_{ys}}\right)^2$ (IN.)	Δa_p (IN.)	N_d (~)
SOTT-4	2.0	1	0.15	0.50	44.3	0.013	0.018	5900
		2	0.43	0.81	43.1	0.012	0.022	9000
SOTT-5	1.5	1	0.26	0.53	34.0	0.007	0.006	400
		2	0.43	0.80	31.4	0.006	0.010	950
SOTT-6	$\left\{\begin{matrix}2.0\\+\\-0.1\end{matrix}\right\}$	1	0.15	0.57	48.1	0.015	0.013	3000
		2	0.43	0.80	42.1	0.011	0.017	4200

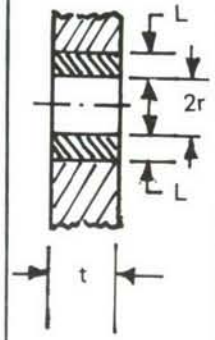
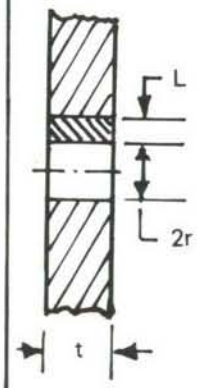
Table 26: Summary of Test Parameters for Surface Flaw Specimens Subjected to Tension/Bending Stresses

ALLOY	TEST TYPE	SPECIMEN CODE	PEAK CYCLIC STRESS (KSI)		OVERLOAD STRESS (KSI)		OVERLOAD PERIOD (cycles)
			Tension	Bending	Tension	Bending	
ALUMINUM 2219-T851	SINGLE OVERLOAD	SOBA-1	18	18	36	0	$n_1 = 3700$ $n_2 = \infty$
		SOBA-2	18	18	27	0	$n_1 = 3300$ $n_2 = 2250$ $n_3 = \infty$
	PERIODIC OVERLOAD	SPOBA-1	18	18	36	0	1650
STEEL 9Ni-4Co-0.2C	SINGLE OVERLOAD	SOBS-1	60	30	87	27	6400
	PERIODIC OVERLOAD	SPOBS-1	60	30	88	27	1600
		SPOBS-2	60	30	87	27	1000
TITANIUM 6Al-4VβA	SINGLE OVERLOAD	SOBT-1	45	22.5	63.5	20	4300
	PERIODIC OVERLOAD	SPOBT-1	45	22.5	63.5	20	2000
		SPOBT-2	45	22.5	63.5	20	1000

Table 27: Comparison of Actual and Predicted Lives for Spectrum Loaded Surface Flaw Specimens

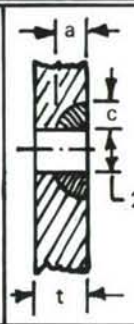
ALLOY	THICK (in)	SPECTRUM TYPE	INITIAL FLAW DIMENSIONS		ACTUAL & PREDICTED FINAL (a/t)	FINAL a/2c		LIFE (MISSIONS)	
			$(a/t)_i$	$(a/2c)_i$		ACTUAL	PRE DICTED	ACTUAL	PRE DICTED
2219-T851 Aluminum	0.45	BOMBER	0.246	0.166	0.612	0.335	0.349	714	696
			0.344	0.325	0.654	0.404	0.432	714	736
			0.483	0.448	1.000	0.386	0.512	714	761
			0.542	0.163	1.000	0.222	0.289	131	169
			0.647	0.287	0.820	0.311	0.345	131	116
			0.809	0.441	1.000	0.409	0.486	110	119
		FIGHTER	0.240	0.165	0.618	0.333	0.421	179	84
			0.342	0.318	0.660	0.400	0.431	179	92
			0.462	0.443	1.000	0.398	0.512	164	102
			0.489	0.148	0.889	0.230	0.259	24	24
			0.651	0.290	0.822	0.308	0.346	24	14
			0.793	0.432	1.000	0.364	0.481	19	16
9Ni-4Co-0.2C(190-210 ksi) Steel	0.30	BOMBER	0.178	0.158	0.577	0.378	0.375	543	363
			0.255	0.311	0.631	0.447	0.440	543	382
			0.362	0.450	1.000	0.459	0.508	543	446
			0.487	0.148	0.908	0.244	0.260	132	100
			0.643	0.294	1.000	0.361	0.397	132	96
			0.809	0.423	1.000	0.402	0.464	60	53
		FIGHTER	0.184	0.167	1.000	0.434	0.477	299	129
			0.267	0.327	1.000	0.468	0.500	274	127
			0.367	0.468	1.000	0.468	0.510	242	107
			0.488	0.147	1.000	0.266	0.271	67	24
			0.641	0.293	1.000	0.356	0.396	73	21
			0.818	0.434	1.000	0.431	0.472	40	11
Ti-6Al-4V Beta Annealed	0.375	BOMBER	0.215	0.157	0.585	0.377	0.366	845	950
			0.436	0.465	1.000	0.460	0.522	845	1051
			0.485	0.149	1.000	0.272	0.295	190	151
			0.775	0.423	1.000	0.421	0.483	141	112
		FIGHTER	0.223	0.163	1.000	0.407	0.489	393	216
			0.430	0.451	1.000	0.433	0.520	316	180
			0.493	0.149	1.000	0.261	0.292	84	25
			0.820	0.434	1.000	0.433	0.483	51	14

Table 28: Summary of Stress Intensity Factor Formulae for Thru-Cracked Fastener Holes

CASE	CRACK GEOMETRY	FASTENER TYPE	LOADING	STRESS INTENSITY FORMULAE	F
BOWIE SOLN.		OPEN HOLE	UNIFORM TENSION	$K_I = F_1 \cdot \sigma \sqrt{\pi L}$	FIG. 85
1a		CLOSE TOL	UNIFORM TENSION	SAME AS BOWIE SOLUTION	—
1b		CLOSE TOL	FASTENER LOAD	$K_I = F_3 \ \sigma_b \sqrt{\pi L}$	FIG. 96
1c		CLOSE TOL	UNIFORM TENSION + FASTENER LOAD	SUPERPOSE CASES 1a AND 1b	—
1d		TAPER-LOK	INTERFERENCE ONLY	NO GENERAL FORMULA: SEE SECTION 4.2.4	—
1e		TAPER-LOK	INTERFERENCE + UNIFORM TENSION	NO GENERAL FORMULA: SEE SECTION 4.2.4	—
BOWIE SOLN.		OPEN HOLE	UNIFORM TENSION	$K_I = F_2 \cdot \sigma \sqrt{\pi L}$	FIG. 85
2a		CLOSE TOL	UNIFORM TENSION	SAME AS BOWIE SOLUTION	—
2b		CLOSE TOL	FASTENER LOAD	$K_I = F_4 \cdot \sigma_b \sqrt{\pi L}$	FIG. 96
2c		CLOSE TOL	UNIFORM TENSION + FASTENER LOAD	SUPERPOSE CASES 2a AND 2b	—
2d		TAPER-LOK	INTERFERENCE ONLY	NO GENERAL FORMULA: SEE SECTION 4.2.4	—
2e		TAPER-LOK	INTERFERENCE + UNIFORM TENSION	NO GENERAL FORMULA: SEE SECTION 4.2.4	—

NOTE: σ_b = AVERAGE BEARING STRESS

Table 29: Summary of Stress Intensity Factor Formulae for Part-Thru-Cracked Fastener Holes

CASE NO.	CRACK GEOMETRY	FASTENER TYPE	LOADING	STRESS INTENSITY FORMULA	F	M_F	M_B
3a		OPEN HOLE	UNIFORM TENSION	$K_I = F_5 \cdot K_{Ie} \cdot M_F \cdot M_B$	FIG. 90	$M_F = 1.0 + 0.12\,(1-a/2c)^2$ FOR $\beta < 90^o$ $M_F = 1.11$ @ $\beta = 90^o$	FIG. 92
3b		CLOSE TOL	UNIFORM TENSION	SAME AS 3a	—		
3c		CLOSE TOL	FASTENER LOADING	$K_I = F_6 \cdot K_{Ieb} \cdot M_F \cdot M_B$	FIG. 97		
3d		CLOSE TOL	UNIFORM TENSION + FASTENER LOADING	SUPERPOSE 3b AND 3c	—		
4a		OPEN HOLE	UNIFORM TENSION	$K_I = F_5 \cdot K_{Ie} \cdot M_F \cdot M_B \sqrt{\frac{2r + \pi ac/4t}{2r + 2\pi ac/4t}}$	FIG. 90		
4b		CLOSE TOL	UNIFORM TENSION	SAME AS 4a	—		
4c		CLOSE TOL	FASTENER LOADING	$K_I = F_6 \cdot K_{Ieb} \cdot M_F \cdot M_B \sqrt{\frac{2r + \pi ac/4t}{2r + 2\pi ac/4t}}$	FIG. 97		
4d		CLOSE TOL	UNIFORM TENSION + FASTENER LOADING	SUPERPOSE 4b AND 4c	—		

$K_{Ie} = \sigma \sqrt{\pi a/Q}\ (\cos^2\beta + a^2/c^2 \sin^2\beta)^{1/4}$ FOR $a/c < 1.0$

$K_{Ie} = \sigma \sqrt{\pi c/Q}\ (\sin^2\beta + c^2/a^2 \cos^2\beta)^{1/4}$ FOR $a/c > 1.0$

$K_{Ieb} = \sigma_b \sqrt{\pi a/Q}\ (\cos^2\beta + a^2/c^2 \sin^2\beta)^{1/4}$ FOR $a/c < 1.0$

$K_{Ieb} = \sigma_b \sqrt{\pi c/Q}\ (\sin^2\beta + c^2/a^2 \cos^2\beta)^{1/4}$ FOR $a/c > 1.0$

σ_b IS THE BEARING STRESS

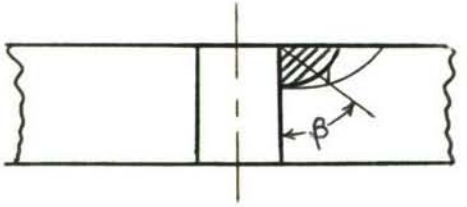


Table 30: Static Fracture Tests of Surface Flaws in 0.30 Thick 4340 Steel Alloy at Room Temperature

SPECIMEN NUMBER	THICKNESS, t (INCH)	WIDTH, W (INCH)	FLAW DEPTH, a (INCH)	FLAW LENGTH, 2c (INCH)	a/2c	a/t	σ AT FIRST "POP" (KSI)	σ FAILURE (KSI)	σ FAIL / σy [1]	STRESS INTENSITY @ a (KSI√IN)
SFT-1	0.3035	2.5082	0.144	0.554	0.260	0.474	116.7	116.7	0.51	71.5
SFT-2	0.3058	2.4910	0.152	0.566	0.269	0.497	117.2	120.8	0.53	75.5

Table 31: Static Fracture Tests of Through-Cracks in 0.30 Thick 4340 Steel Alloy at Room Temperature

SPECIMEN NUMBER	THICKNESS, t (INCH)	WIDTH, W (INCH)	FLAW LENGTH, 2c (INCH)	σ AT FIRST "POP" (KSI)	σ FAILURE (KSI)	σ FAIL / σy [1]	STRESS INTENSITY @ c (KSI√IN)
CCT-1	0.3040	2.4908	0.850	51.9	54.8	0.24	68.3
CCT-2	0.3066	2.5048	0.853	52.7	56.5	0.25	70.9

[1] σy = 228.2 KSI

Table 32: Static Fracture Tests of 0.30 Thick 4340 Steel With Corner Flaws Emanating From Close Tolerance Holes

HOLE CONDITION	HOLE DIA., d (INCH)	SPECIMEN NUMBER	THICKNESS, t (INCH)	WIDTH w (INCH)	FLAW DEPTH, a (INCH)	FLAW LENGTH, c (INCH)	a/c	c/r	a/t	σ @ FIRST "POP" (KSI)	σ FAILURE (KSI)	$\sigma_{FAIL}/\sigma_{ys}$ [1]	STRESS INTENSITY @$\beta = 25^{o}$ (KSI$\sqrt{IN}$)	STRESS INTENSITY @$\beta = 90^{o}$ (KSI$\sqrt{IN}$)
OPEN HOLE, CORNER FLAW ON ONE SIDE	0.250	V120-1	0.2983	1.7576	0.134	0.120	1.117	0.960	0.449	93.5	109.9	0.48	75.3	69.8
		V120-2	0.3037	2.0006	0.216	0.171	1.263	1.368	0.711	92.2	92.2	0.40	66.0	64.3
		V120-3	0.3055	2.4898	0.243	0.243	1.000	1.944	0.795	87.4	87.4	0.38	68.2	58.5
OPEN HOLE, CORNER FLAW ON ONE SIDE	0.375	V130-1	0.3055	2.4870	0.148	0.122	1.213	0.651	0.485	76.9	76.9	0.34	59.8	58.0
		V130-2	0.3065	3.0008	0.186	0.184	1.011	0.981	0.607	77.4	77.4	0.34	65.4	56.6
		V130-3	0.3032	3.0058	0.228	0.240	0.950	1.280	0.752	74.6	81.6	0.36	74.0	60.2
OPEN HOLE, TWO CORNER FLAWS	0.250	V220-1	0.3032	2.4977	0.132	0.122	1.082	0.976	0.435	94.4	100.4	0.44	73.9	67.3
					0.132	0.121	1.091	0.968	0.435					
		V220-2	0.3050	2.9943	0.187	0.180	1.039	1.440	0.613	84.9	87.8	0.38	72.0	63.3
					0.189	0.188	1.005	1.504	0.620					
		V220-3	0.3085	3.5000	0.235	0.236	0.996	1.888	0.762	71.6	75.0	0.33	68.3	57.6
					0.235	0.246	0.955	1.968	0.762					
OPEN HOLE, TWO CORNER FLAWS	0.375	V230-1	0.3038	3.0005	0.129	0.127	1.016	0.677	0.425	84.8	87.3	0.38	72.3	67.3
					0.142	0.127	1.118	0.677	0.467					
		V230-2	0.2997	3.5004	0.168	0.178	0.944	0.949	0.561	78.2	85.3	0.37	80.6	63.9
					0.172	0.194	0.887	1.035	0.574					
		V230-3	0.3030	4.2525	0.231	0.237	0.975	1.264	0.762	59.4	64.8	0.28	65.9	61.5
					0.229	0.243	0.942	1.296	0.756					

[1] σ_{ys} = 228.2 KSI

Table 33: Static Fracture Tests of 0.30 Thick 4340 Steel with Corner Flaws Emanating from Loaded Close Tolerance Holes

HOLE CONDITION	HOLE DIA, d (INCH)	SPECIMEN NUMBER	THICKNESS, t (INCH)	WIDTH, w (INCH)	FLAW DEPTH a (INCH)	FLAW LENGTH c (INCH)	a/c	c/r	a/t	$P_{FAILURE}$ AT HOLE (KIPS)	$\sigma_{FAILURE}$ (KSI)	% OF LOAD THROUGH BOLT	σ_{FAIL}/σ_y [1]	STRESS INTENSITY $\beta = 25°$ (KSI $\sqrt{IN.}$)	STRESS INTENSITY $\beta = 90°$ (KSI $\sqrt{IN.}$)
LOADED HOLE. CORNER FLAW ON ONE SIDE	0.25	V12LT-1	0.3071	2.4962	0.123	0.112	1.10	0.90	0.40	3.5	104.1	4%	0.46	78.3	70.9
		V12LT-2	0.2959	2.4916	0.182	0.188	0.97	1.50	0.62	2.6	82.7	4%	0.36	66.1	55.8
		V12LT-3	0.2995	2.4912	0.222	0.238	0.93	1.90	0.74	4.0	89.8	6%	0.39	78.4	63.4
LOADED HOLE, TWO CORNER FLAWS	0.25	V22LT-1	0.3056	2.4970	0.130	0.120	1.08	0.96	0.43	3.3	85.8	5%	0.38	70.2	63.0
					0.130	0.112	1.16	0.90	0.43						
		V22LT-2	0.3064	3.0045	0.180	0.186	0.98	1.49	0.59	3.7	85.8	5%	0.38	78.0	67.3
					0.182	0.180	1.01	1.44	0.59						
		V22LT-3	0.3042	3.5012	0.240	0.244	0.98	1.95	0.79	5.3	78.1	6%	0.34	85.8	70.5
					0.234	0.240	0.97	1.92	0.77						

[1] σ_y = 228.2 KSI

Table 34: Static Fracture Tests of 0.30 Thick 4340 Steel with One Corner Flaw Emanating from Taper-Lok Holes

HOLE CONDITION	HOLE DIA, d (INCH)	SPECIMEN NUMBER	THICK-NESS, t (INCH)	WIDTH, w (INCH)	FLAW DEPTH a (INCH)	FLAW LENGTH c (INCH)	a/c	c/r	a/t	σ @ FIRST "POP" (KSI)	σ FAIL-URE (KSI)	σ_{FAIL}/σ_y [1]	STRESS INTENSITY @ $\beta = 25^o$ (KSI $\sqrt{IN.}$)	STRESS INTENSITY @ $\beta = 90^o$ (KSI $\sqrt{IN.}$)
FILLED HOLE, INTERFERENCE LEVEL = 0.0018 IN., CORNER FLAW ON ONE SIDE	0.250	V12UL-1	0.3012	1.7575	0.123	0.116	1.06	0.93	0.41	106.7	106.7	0.47	NA	NA
		V12UL-2	0.2995	1.9980	0.174	0.182	0.96	1.46	0.58	92.7	97.8	0.43	NA	NA
		V12UL-3	0.3035	2.4965	0.236	0.241	0.98	1.93	0.78	88.4	88.4	0.39	NA	NA
FILLED HOLE, INTERFERENCE LEVEL = 0.0042 IN., CORNER FLAW ON ONE SIDE	0.250	V12UH-1	0.3025	1.7568	0.140	0.138	1.01	1.10	0.46	100.3	109.5	0.48	NA	NA
		V12UH-2	0.3020	1.9962	0.184	0.180	1.02	1.44	0.61	90.6	102.9	0.45	NA	NA
		V12UH-3	0.3027	2.4970	0.246	0.249	0.99	1.99	0.81	83.4	88.6	0.39	NA	NA
FILLED HOLE, INTERFERENCE LEVEL = 0.0054 IN., CORNER FLAW ON ONE SIDE	0.375	V13UH-1	0.2985	2.4890	0.134	0.135	1.00	0.72	0.45	108.1	109.0	0.48	NA	NA
		V13UH-2	0.3075	2.9923	0.182	0.182	1.00	0.97	0.59	75.5	80.4	0.35	NA	NA
		V13UH-3	0.3038	3.0038	0.244	0.236	1.04	1.26	0.80	78.5	83.7	0.37	NA	NA

NA = NOT AVAILABLE

[1] σ_y = 228.2 KSI

Table 35: Static Fracture Tests of 0.30 Thick 4340 Steel With Two Corner Flaws Emanating From Taperlok Holes

HOLE CONDITION	HOLE DIA., d (INCH)	SPECIMEN NUMBER	THICKNESS, t (INCH)	WIDTH, w (INCH)	FLAW DEPTH, a (INCH)	FLAW LENGTH, c (INCH)	a/c	c/r	a/t	σ @ FIRST "POP" (KSI)	$\sigma_{FAILURE}$ (KSI)	$\sigma_{FAIL}/\sigma_{ys}$ [1]	STRESS INTENSITY @ $\beta = 25^{o}$ (KSI $\sqrt{IN}$)	STRESS INTENSITY @ $\beta = 90^{o}$ (KSI $\sqrt{IN}$)
FILLED HOLE, INTERFERENCE LEVEL = 0.0018", TWO CORNER FLAWS	0.250	V22UL-1	0.3080	2.5063	0.126	0.110	1.14	0.88	0.41	107.8	107.8	0.47	NA	NA
					0.116	0.111	1.04	0.89	0.38					
		V22UL-2	0.3050	3.0013	0.186	0.180	1.03	1.44	0.61	94.5	94.5	0.41	NA	NA
					0.190	0.180	1.06	1.44	0.62					
		V22 UL-3	0.3025	3.5005	0.234	0.241	0.97	1.93	0.77	75.6	75.6	0.33	NA	NA
					0.236	0.249	0.94	1.99	0.78					
FILLED HOLE, INTERFERENCE LEVEL= 0.0042", TWO CORNER FLAWS	0.250	V22 UH-1	0.2985	2.5045	0.126	0.126	1.00	1.01	0.42	100.3	109.4	0.48	NA	NA
					0.125	0.122	1.02	0.98	0.42					
		V22 UH-2	0.3071	2.9930	0.179	0.180	0.99	1.44	0.58	85.8	91.4	0.40	NA	NA
					0.174	0.179	0.97	1.43	0.57					
		V22 UH-3	0.3093	3.5030	0.228	0.249	0.92	1.99	0.74	78.4	78.4	0.34	NA	NA
					0.231	0.246	0.94	1.97	0.75					
FILLED HOLE, INTERFERENCE LEVEL = 0.0054", TWO CORNER FLAWS	0.375	V23 UH-1	0.3028	3.0036	0.130	0.136	0.96	0.73	0.43	121.0	121.0	0.53	NA	NA
					0.139	0.136	1.02	0.73	0.46					
		V23 UH-2	0.3065	3.5000	0.179	0.186	0.96	0.99	0.58	80.5	87.6	0.38	NA	NA
					0.178	0.179	1.00	0.95	0.58					
		V23 UH-3	0.2995	4.2508	0.234	0.242	0.97	1.29	0.78	51.8	62.2	0.27	NA	NA
					0.234	0.246	0.95	1.31	0.78					

NA = NOT AVAILABLE

[1] σ_{ys} = 228.2 KSI

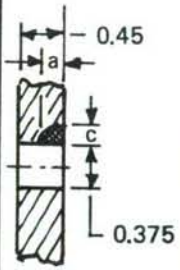
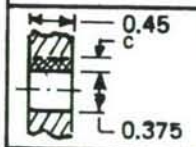
Table 36: Static Fracture Tests of 0.30 Thick 4340 Steel with Corner Flaws Emanating from Loaded Taper-lok Holes

HOLE CONDITION	HOLE DIA, d (INCH)	SPECIMEN NUMBER	THICKNESS, t (INCH)	WIDTH, w (INCH)	FLAW DEPTH, a (INCH)	FLAW LENGTH c (INCH)	a/c	c/r	a/t	$P_{FAILURE}$ AT HOLE (KIPS)	$\sigma_{FAILURE}$ (KSI)	% OF LOAD THROUGH BOLT	σ_{FAIL}/σ_y [1]	STRESS INTENSITY @ $\beta = 25°$ KSI $\sqrt{IN.}$	STRESS INTENSITY @ $\beta = 90°$ KSI $\sqrt{IN.}$
LOADED HOLE, INTERFERENCE LEVEL = 0.0042 IN., CORNER FLAW ON ONE SIDE	0.25	V12LF-1	0.3064	2.4892	0.130	0.142	0.92	1.14	0.42	10.2	101.0	13%	0.44	NA	NA
		V12LF-2	0.3052	2.5082	0.174	0.175	0.99	1.40	0.57	7.7	96.9	10%	0.42	NA	NA
		V12LF-3	0.3068	2.5005	0.240	0.240	1.00	1.92	0.78	6.3	88.0	9%	0.39	NA	NA
LOADED HOLE, INTERFERENCE LEVEL = 0.0042 IN., TWO CORNER FLAWS	0.25	V22LF-1	0.3041	2.4924	0.135	0.125	1.08	1.00	0.44	10.1	94.2	14%	0.41	NA	NA
					0.130	0.116	1.12	0.93	0.43						
		V22LF-2	0.3030	3.0010	0.180	0.167	1.08	1.34	0.59	8.6	77.4	12%	0.34	NA	NA
					0.179	0.178	1.00	1.42	0.59						
		V22LF-3	0.2991	3.4958	0.240	0.251	0.96	2.01	0.80	6.4	71.7	9%	0.31	NA	NA
					0.241	0.246	0.99	1.97	0.81					NA	NA

NA = NOT AVAILABLE

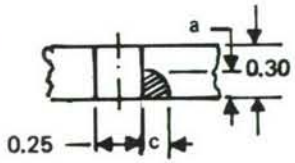
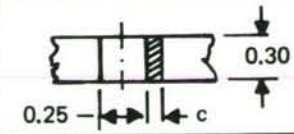
[1] σ_y = 228.2 KSI

Table 37: Summary of Test Parameters For 2219-T851 Aluminum Alloy Uniform Cyclic Load Tests of Cracks Originating At Fastener Holes

FLAW TYPE	SPECIMEN CODE	HOLE		FASTENER			FLAW		PEAK [a] CYCLIC STRESS (KSI)
		NUMBER	CONDITION	TYPE	INTERFERENCE IN)	LOAD (LBS)	a_i (IN)	$2c_i$ (IN)	
	FUCTA-1	1 2	AS-REAMED	CLOSE TOL.	NONE	4000 0	0.174 0.168	0.144 0.146	21
	TIA-1	1 2	AS-REAMED	TAPER-LOK	0.0060	0 0	0.140 0.162	0.154 0.150	21 18
	TIA-2	1	AS-REAMED	TAPER-LOK	0.0060	0	0.175	0.144	49
	FUCIA-1	1 2 3	AS-REAMED	TAPER-LOK	0.0024 0.0060 0.0024	4000 0 0	0.160 0.151 0.156	0.138 0.140 0.145	24
	FUCIA-2	1 2 3	AS-REAMED	TAPER-LOK	0.0038 0.0038 0.0024	4000 0 0	0.160 0.144 0.136	0.139 0.130 0.144	24
	FUCCA-1	1 2	COLD WORKED	CLOSE TOL.	NONE	4000 0	0.178 0.176	0.150 0.150	28
	FUCTA-1	1 2 3	AS-REAMED	TAPER-LOK	0.0038 0.0038 0.0024	4000 0 0	– – –	0.060 0.078 0.090	24

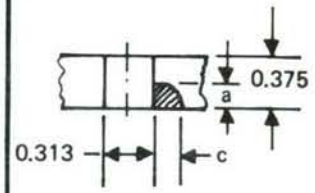
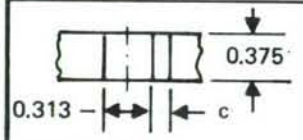
[a] STRESS RATIO = 0.1 FOR ALL TESTS

Table 38: Summary of Test Parameters for 9Ni-4Co-0.2C Steel Alloy Uniform Cyclic Load Tests of Cracks Originating at Fastener Holes

FLAW TYPE	SPECIMEN CODE	HOLE		FASTENER			FLAW		PEAK [a] CYCLIC STRESS (KSI)
		NUMBER	CONDITION	TYPE	INTERFERENCE (IN)	LOAD (LBS)	a_i (IN)	$2c_i$ (IN)	
	FUCTS-1	1 2 3	AS-REAMED	CLOSE TOL. CLOSE TOL. OPEN HOLE	NONE	3600 0 0	0.127 0.125 0.127	0.113 0.103 0.106	70
	TIS-1	1	AS-REAMED	TAPER-LOK	0.0030	0	0.125	0.105	80
	FUCIS-1	1 2 3	AS-REAMED	TAPER-LOK	0.0030 0.0030 0.0036	3600 0 0	0.109 0.106 0.106	0.105 0.106 0.094	75
	FUCCS-1	1 2 3	COLD WORKED	CLOSE TOL. CLOSE TOL. OPEN HOLE	NONE	3600 0 0	0.125 0.140 0.122	0.104 0.103 0.090	90
	FUTIS-1	1 2 3	AS-REAMED	TAPER-LOK	0.0030 0.0030 0.0036	3600 0 0	— — —	0.116 0.064 0.062	75

[a] STRESS RATIO = 0.1 FOR ALL TESTS

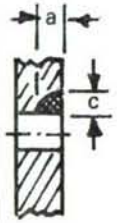
Table 39: Summary of Test Parameters for 6Al-4V Beta Annealed Titanium Alloy Uniform Cyclic Load Tests of Cracks Originating at Fastener Holes

FLAW TYPE	SPECIMEN CODE	HOLE		FASTENER			FLAW		PEAK [a] CYCLIC STRESS (KSI)
		NUMBER	CONDITION	TYPE	INTERFERENCE (IN)	LOAD (LBS)	a_i (IN)	$2c_i$ (IN)	
	FUCTT-1	1 2 3	AS-REAMED	CLOSE TOL. CLOSE TOL. OPEN HOLE	NONE	3000 0 0	0.128 0.114 0.114	0.138 0.136 0.124	35
	TIT-1	1	AS-REAMED	TAPERLOK	0.0034	0	0.131	0.126	35
	FUCIT-2	1 2 3	AS-REAMED	TAPERLOK	0.0034 0.0034 0.0042	3000 0 0	0.141 0.129 0.120	0.128 0.124 0.115	50
	FUCCT-1	1 2 3	COLD WORKED	CLOSE TOL. CLOSE TOL. OPEN HOLE	NONE	3000 0 0	0.130 0.128 b	0.112 0.123 b	55
	FUTIT-1	1 2 3	AS-REAMED	TAPERLOK	0.0034 0.0034 0.0042	3000 0 0	– – –	0.075 0.082 0.090	50

a STRESS RATIO = 0.1 FOR ALL TESTS

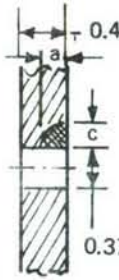
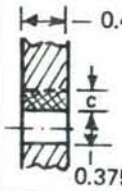
b COULD NOT BE DETERMINED

Table 40: Summary of Test Parameters For Uniform Load Combined Bending and Tension Tests of Cracks Originating At Taper-Lok Fastener Holes

FLAW TYPE	ALLOY	SPECIMEN CODE	FASTENER		FLAW		PEAK CYCLIC STRESS [a]	
			TYPE	INTERFERENCE (IN)	a_i (IN)	$2c_i$ (IN)	TENSION (KSI)	BENDING (KSI)
	2219-T851 ALUMINUM	FBCIA-1	TAPERLOK	0.0038	0.154	0.156	18	18
	9Ni-4Co-0.2C STEEL	FBCIS-1	TAPERLOK	0.0030	0.108	0.100	40	40
	6Al-4V βA TITANIUM	FBCIT-1	TAPERLOK	0.0034	0.122	0.125	30	30

[a] STRESS RATIO = 0.1 FOR ALL TESTS

Table 41: Summary of Test Details for 2219-T851 Aluminum Alloy Overload Tests of Cracks Originating at Fastener Holes

FLAW TYPE	SPECIMEN CODE	HOLE		FASTENER				FLAW		LOADING PROFILE (SEE FIG 16)	STRESSES			OVERLOAD PERIOD (CYCLES)
		NO.	CONDITION	TYPE	INTER-FERENCE (IN.)	OVER-LOAD (LBS)	PEAK CYCLIC LOAD (LBS)	a_i (IN.)	c_i (IN.)		σ_o (KSI)	σ_m (KSI)	σ_c (KSI)	
	FOCTA-1	1 2 a	REAMED	CLOSE TOL. OPEN HOLE –	NONE – –	8000 – –	4000 – –	0.170 0.162 0.147	0.156 0.156 0.156	A	36.8	21.0	0	9,200
	FPOCTA-1	1 2 a	REAMED	CLOSE TOL. OPEN HOLE –	NONE – –	8000 – –	4000 – –	0.176 0.178 0.148	0.162 0.161 0.153	A	36.8	21.0	0	4,600
	FPOCTA-2	1 2 a	REAMED	CLOSE TOL. OPEN HOLE –	NONE – –	8000 – –	4000 – –	0.164 0.164 0.146	0.154 0.159 0.156	C	36.8	21.0	-4.2	4,600
	FPOCTA-3	1 2 a	REAMED	CLOSE TOL. OPEN HOLE –	NONE – –	7000 – –	4000 – –	0.170 0.168 0.156	0.152 0.153 0.153	A	31.5	21.0	0	4,600
	FPOCTA-4	1 2 a	REAMED	CLOSE TOL. OPEN HOLE –	NONE – –	7000 – –	4000 – –	0.168 0.164 0.151	0.149 0.150 0.156	A	31.5	21.0	0	6,600
	FOTIA-1	1 2 3	REAMED	TAPER-LOK	0.0038 0.0038 0.0024	7600 0 0	4000 0 0	– – –	0.096 0.094 0.095	A	36.0	24.0	0	∞
	FOTIA-2	1 2 3	REAMED	TAPER-LOK	0.0038 0.0038 0.0024	7800 0 0	4000 0 0	– – –	0.109 0.089 0.098	A	36.0	24.0	0	31,000

a SURFACE FLAW

Table 41: Summary of Test Details for 2219-T851 Aluminum Alloy Overload Tests of Cracks Originating at Fastener Holes (Continued)

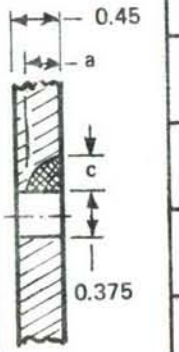
FLAW TYPE	SPECIMEN CODE	HOLE		FASTENER				FLAW		LOADING PROFILE (SEE FIG 16)	STRESSES			OVERLOAD PERIOD (CYCLES)
		NO.	CONDITION	TYPE	INTER-FERENCE (IN.)	OVER-LOAD (LBS)	PEAK CYCLIC LOAD (LBS)	a_i (IN.)	c_i (IN.)		σ_o (KSI)	σ_m (KSI)	σ_c (KSI)	
	FOCIA-1	1 2 3	REAMED	TAPERLOK	0.0038 0.0038 0.0024	7500 0 0	4000 0 0	0.150 0.150 0.145	0.118 0.117 0.111	A	36	24	0	21,480
	FOCIA-2	1 2 3	REAMED	TAPERLOK	0.0038 0.0038 0.0024	7000 0 0	4000 0 0	0.198 0.183 0.195	0.162 0.151 0.162	C	36	24	-4.2	∞
	FOCIA-3	1 2 3	REAMED	TAPERLOK	0.0038 0.0038 0.0024	7500 0 0	4000 0 0	0.158 0.153 0.160	0.152 0.144 0.150	A	40	24	0	16,000
	FPOCIA-1	1 2 3	REAMED REAMED COLD WORK	TAPERLOK TAPERLOK OPEN HOLE	0.0038 0.0038 –	9700 0 0	4000 0 0	0.160 0.154 0.143	0.150 0.148 0.144	A	40	24	0	8,000
	FPOCIA-2	1 2 3	REAMED	TAPERLOK TAPERLOK OPEN HOLE	0.0038 0.0038 –	8400 0 0	4000 0 0	0.162 0.152 0.163	0.148 0.148 0.150	A	36	24	0	8,000
	FOCCA-1	1 2 3	COLD WORKED	CLOSE TOL. CLOSE TOL. OPEN HOLE	– – –	8700 0 0	4000 0 0	0.176 0.144 0.177	0.152 0.138 0.144	A	39.2	28	0	∞

Table 42: Summary of Test Details for 9Ni-4Co-0.2C Steel Alloy Overload Tests of Cracks Originating at Fastener Holes

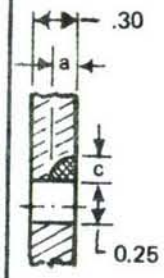
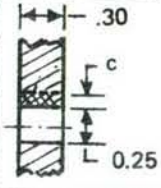
FLAW TYPE	SPECIMEN CODE	HOLE		FASTENER				FLAW		LOADING PROFILE (SEE FIG 16)	STRESSES			OVERLOAD PERIOD (CYCLES)
		NO.	CONDITION	TYPE	INTER-FERENCE (IN.)	OVER-LOAD (LBS)	PEAK CYCLIC LOAD (LBS)	a_i (IN.)	c_i (IN.)		σ_o (KSI)	σ_m (KSI)	σ_c (KSI)	
	FOCTS-1	1 2 3	REAMED	CLOSE TOL. CLOSE TOL. OPEN HOLE	– – –	6800 0 0	3600 0 0	0.120 0.114 0.118	0.104 0.100 0.108	A	140	70	0	n_1 = 10,830 n_2 = 9,230 n_3 = 8,500
	FOCTS-2	1 2 3	REAMED	CLOSE TOL. CLOSE TOL. OPEN HOLE	– – –	5800 0 0	3600 0 0	0.111 0.112 0.119	0.095 0.103 0.117	A	105	70	0	5400
	FOCTS-3	1 2 3	REAMED	CLOSE TOL. CLOSE TOL. OPEN HOLE	– – –	5800 0 0	3600 0 0	0.126 0.120 0.122	0.108 0.104 0.103	A	105	70	0	2500
	FPOCTS-1	1 2 3	REAMED	CLOSE TOL. CLOSE TOL. OPEN HOLE	– – –	6500 0 0	3600 0 0	0.123 0.120 0.118	0.110 0.113 0.106	A	140	70	0	5000
	FOTIS-1	1 2 3	REAMED	TAPERLOK	0.0030 0.0030 0.0036	6200 0 0	3600 0 0	– – –	0.055 0.054 0.053	A	112.5	75	0	8000
	FOTIS-2	1 2 3	REAMED	TAPERLOK	0.0030 0.0030 0.0036	8700 0 0	3600 0 0	– – –	0.050 0.055 0.050	A	131.3	75	0	8000

Table 42: Summary of Test Details for 9Ni-4Co-0.2C Steel Alloy Overload Tests of Cracks Originating at Fastener Holes (Continued)

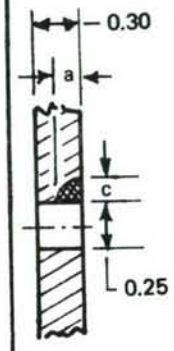
FLAW TYPE	SPECIMEN CODE	HOLE		FASTENER				FLAW		LOADING PROFILE (SEE FIG 16)	STRESSES			OVERLOAD PERIOD (CYCLES)
		NO.	CONDITION	TYPE	INTER-FERENCE (IN.)	OVER-LOAD (LBS)	PEAK CYCLIC LOAD (LBS)	a_i (IN.)	c_i (IN.)		σ_o (KSI)	σ_m (KSI)	σ_c (KSI)	
	FOCIS-1	1 2 3	REAMED	TAPERLOK	0.0030 0.0030 0.0036	7000 0 0	3600 0 0	0.105 0.112 0.110	0.101 0.092 0.104	A	112.5	75	0	5450
	FOCIS-2	1 2 3	REAMED	TAPERLOK	0.0030 0.0030 0.0036	8600 0 0	3600 0 0	0.114 0.104 0.104	0.110 0.100 0.109	A	131.3	75	0	8850
	FOCIS-3	1 2 3	REAMED	TAPERLOK	0.0030 0.0030 0.0036	7100 0 0	3600 0 0	0.108 0.106 0.112	0.103 0.106 0.108	A	112.5	75	0	2500
	FPOCIS-1	1 2 3	REAMED REAMED COLD WORK	TAPERLOK TAPERLOK OPEN HOLE	0.0030 0.0030 –	7600 0 0	3600 0 0	0.108 0.110 0.140	0.103 0.103 0.095	A	131.3	75	0	4900
	FPOCIS-2	1 2 3	REAMED REAMED COLD WORK	TAPERLOK TAPERLOK OPEN HOLE	0.0030 0.0030 –	8100 0 0	3600 0 0	0.111 0.112 0.140	0.111 0.108 0.091	C	131.3	75	-15	5450
	FPOCIS-3	1 2 3	REAMED REAMED COLD WORK	TAPERLOK TAPERLOK OPEN HOLE	0.0030 0.0030 –	7900 0 0	3600 0 0	0.103 0.110 0.120	0.096 0.099 0.084	A	131.3	75	0	2500
	FOCCS-1	1 2 3	COLD WORKED	CLOSE TOL. CLOSE TOL. OPEN HOLE	– – –	13,000 0 0	4000 0 0	0.110 0.114 0.113	0.082 0.082 0.084	A	135	90	0	∞

Table 43: Summary of Test Details for 6Al-4V Beta Annealed Titanium Alloy Overload Tests of Cracks Originating at Fastener Holes

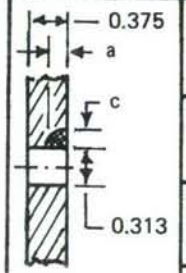
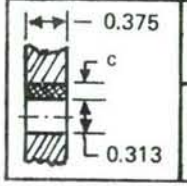
FLAW TYPE	SPECIMEN CODE	HOLE		FASTENER				FLAW		LOADING PROFILE (SEE FIG16)	STRESSES			OVERLOAD PERIOD (CYCLES)
		NO.	CONDITION	TYPE	INTER-FERENCE (IN.)	OVER-LOAD (LBS)	PEAK CYCLIC LOAD (LBS)	a_i (IN.)	c_i (IN.)		σ_o (KSI)	σ_m (KSI)	σ_c (KSI)	
	FOCTT-1	1 2 3	REAMED	CLOSE TOL. CLOSE TOL. OPEN HOLE	– – –	7300 0 0	3000 0 0	0.132 0.132 0.149	0.132 0.132 0.130	A	70	35	0	12,687
	FPOCTT-1	1 2 3	REAMED	CLOSE TOL. CLOSE TOL. OPEN HOLE	– – –	8000 0 0	3000 0 0	0.149 0.152 0.145	0.135 0.140 0.134	A	70	35	0	9,000
	FPOCTT-2	1 2 3	REAMED	CLOSE TOL. CLOSE TOL. OPEN HOLE	– – –	5200 0 0	3000 0 0	0.133 0.140 0.136	0.133 0.130 0.122	A	52.5	35	0	9,000
	FPOCTT-3	1 2 3	REAMED	CLOSE TOL. CLOSE TOL. CLOSE TOL.	– – –	6800 0 0	3000 0 0	0.158 0.165 0.180	0.126 0.118 0.130	C	70	35	-7	9,000
	FOTIT-1	1 2 3	REAMED	TAPERLOK	0.0034 0.0034 0.0042	8000 0 0	3000 0 0	– – –	0.085 0.079 0.085	A	75	50	0	33,000
	FOTIT-2	1 2 3	REAMED	TAPERLOK	0.0034 0.0034 0.0042	6200 0 0	3000 0 0	– – –	0.102 0.086 0.096	A	75	50	0	22,000

Table 43: Summary of Test Details for 6Al-4V Beta Annealed Titanium Alloy Overload Tests of Cracks Originating at Fastener Holes (Continued)

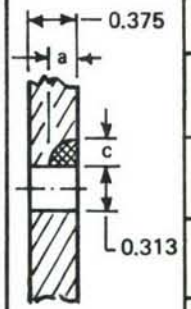
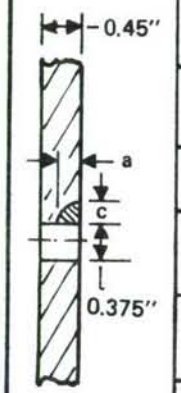
FLAW TYPE	SPECIMEN CODE	HOLE		FASTENER				FLAW		LOADING PROFILE (SEE FIG 16)	STRESSES			OVERLOAD PERIOD (CYCLES)
		NO.	CONDITION	TYPE	INTER-FERENCE (IN.)	OVER-LOAD (LBS)	PEAK CYCLIC LOAD (LBS)	a_i (IN.)	c_i (IN.)		σ_o (KSI)	σ_m (KSI)	σ_c (KSI)	
	FOCIT-1	1 2 3	REAMED	TAPERLOK	0.0034 0.0034 0.0021	6500 0 0	3000 0 0	0.126 0.132 0.128	0.128 0.121 0.124	A	87.5	50	0	n_1 = 19,900 n_2 = 7,400 n_3 = ∞
	FOCIT-2	1 2 3	REAMED	TAPERLOK	0.0034 0.0034 0.0042	6600 0 0	3000 0 0	0.140 0.150 0.148	0.118 0.124 0.123	A	75	50	0	15,000
	FOCIT-3	1 2 3	REAMED	TAPERLOK	0.0034 0.0034 0.0042	6000 0 0	3000 0 0	0.154 0.146 0.148	0.130 0.125 0.133	A	75	50	0	7,500
	FOCIT-4	1 2 3	REAMED	TAPERLOK	0.0034 0.0034 0.0042	8400 0 0	3000 0 0	0.176 0.154 0.128	0.136 0.136 0.136	C	75	50	-10	7,500
	FPOCIT-1	1 2 3	REAMED REAMED COLD WORK	TAPERLOK TAPERLOK OPEN HOLE	0.0034 0.0034 –	7000 0 0	3000 0 0	0.124 0.126 0.126	0.116 0.123 0.117	A	75	50	0	7,500
	FPOCIT-2	1 2 3	REAMED REAMED COLD WORK	TAPERLOK TAPERLOK OPEN HOLE	0.0034 0.0034 –	7100 0 0	3000 0 0	0.135 0.150 0.130	0.136 0.127 0.122	A	87.5	50	0	15,000
	FOCCT-1	1 2 3	COLD WORKED	CLOSE TOL. CLOSE TOL. OPEN HOLE	– – –	4600 0 0	3000 0 0	0.158 0.146 0.140	0.140 0.132 0.120	A	82.5	55	0	∞

Table 44: Summary of Test Details for 2219-T851 Aluminum Alloy Spectrum Load Tests of Cracks Originating at Fastener Hole

FLAW TYPE	SPECIMEN CODE	HOLE		FASTENER				FLAW		SPECTRUM	
		NO.	CONDITION	TYPE	HEAD DESIGN	INTER-FERENCE (IN.)	LIMIT LOAD (LBS)	a_i (IN.)	c_i (IN.)	TYPE	LIMIT STRESS (KSI)
	FSCTA-1	1 2 a	CONVENTIONAL REAM – –	CLOSE TOL. OPEN HOLE –	12 PT. – –	0 0 0	4800 – –	0.166 0.184 0.154	0.150 0.153 0.153	BOMBER	33.6
	FSCTA-2	1 2 a	CONVENTIONAL REAM – –	CLOSE TOL. OPEN HOLE –	12 PT – –	0 0 0	4800 – –	0.170 0.162 –	0.156 0.147 –	FIGHTER	30.9
	FVCTA-1	1 2	CONVENTIONAL REAM	CLOSE TOL. CLOSE TOL.	12 PT. 100° CSK	0 0	300 300	0.172 0.174	0.150 0.150	BOMBER	33.6
	FSCIA-1	1 2 3	TAPER REAM COLD WORKED	TAPERLOK OPEN HOLE	PROTRUDING –	0.0038 0.0038 0	5900 0 –	0.175 0.160 0.174	0.154 0.150 0.151	BOMBER	33.6
	FSCIA-2	1 2 3	TAPER REAM COLD WORKED	TAPERLOK OPEN HOLE	PROTRUDING –	0.0038 0.0038 0	4600 – –	0.166 0.166 0.169	0.154 0.152 0.148	FIGHTER	30.9
	FVCIA-1	1 2	TAPER REAM COLD WORKED	TAPERLOK CLOSE TOL.	PROTRUDING 12 PT.	0.0038 0	1300 1300	0.167 0.176	0.150 0.158	BOMBER	33.6

a SURFACE FLAW

Table 45: Summary of Test Details for 9Ni-4Co-0.2C Steel Alloy Spectrum Load Tests of Cracks Originating at Fastener Holes

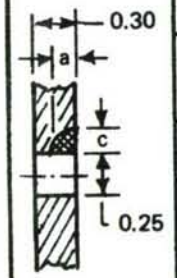
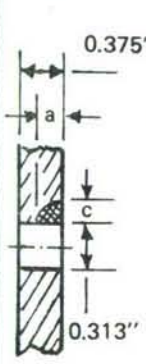
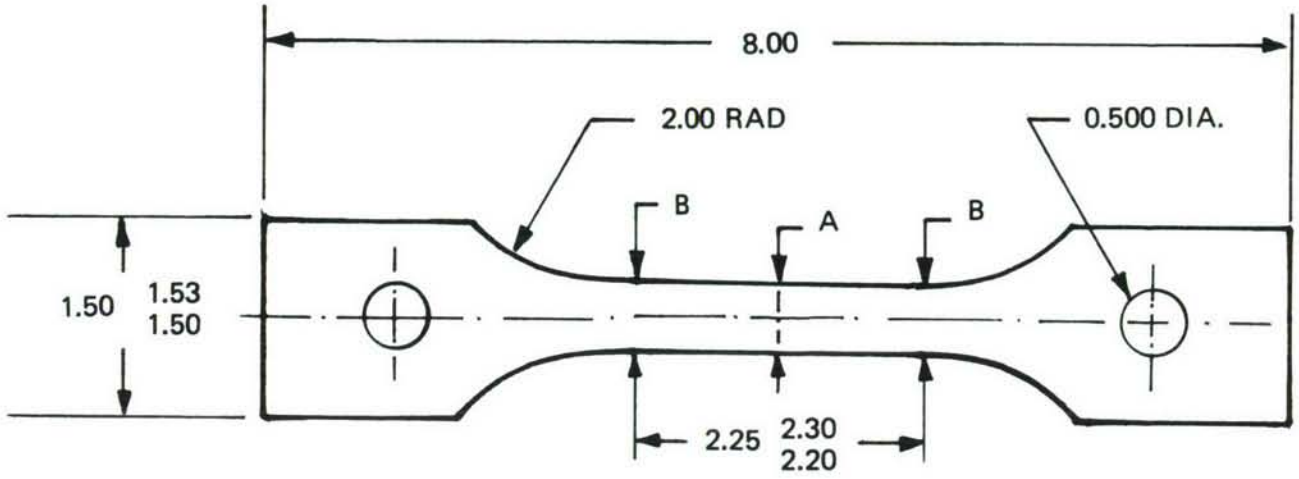
FLAW TYPE	SPECIMEN CODE	HOLE		FASTENER				FLAW		SPECTRUM	
		NO.	CONDITION	TYPE	HEAD DESIGN	INTER-FERENCE (IN.)	LIMIT LOAD (LBS)	a_i (IN.)	c_i (IN.)	TYPE	LIMIT STRESS (KSI)
	FSCTS-1	1	CONVENTIONAL REAM	CLOSE TOL.	12 PT.	0	5600	0.150	0.109	BOMBER	130
		2		CLOSE TOL.	12 PT.	0	0	0.149	0.110		
		3		OPEN HOLE	–	0	–	0.154	0.110		
	FSCTS-2	1	CONVENTIONAL REAM	CLOSE TOL.	12 PT.	0	5230	0.122	0.103	FIGHTER	91
		2		CLOSE TOL.	12 PT.	0	0	0.122	0.103		
		3		OPEN HOLE	–	0	–	0.121	0.101		
	FVCTS-1	1	CONVENTIONAL REAM	CLOSE TOL.	12 PT.	0	2200	0.122	0.102	BOMBER	130
		2		CLOSE TOL.	100° CSK	0	2200	0.124	0.104		
	FSCIS-1	1	TAPER REAM COLD WORKED	TAPERLOK	PROTRUDING	0.0030	4900	0.110	0.107	BOMBER	130
		2		TAPERLOK	PROTRUDING	0.0030	0	0.106	0.104		
		3		OPEN HOLE	–	–	–	0.110	0.097		
	FSCIS-2	1	TAPER REAM COLD WORKED	TAPERLOK	PROTRUDING	0.0030	4170	0.106	0.099	FIGHTER	91
		2		TAPERLOK	PROTRUDING	0.0030	0	0.106	0.096		
		3		OPEN HOLE	–	–	–	0.110	0.087		

Table 46: Summary of Test Details for 6Al-4V Beta Annealed Titanium Alloy Spectrum Load Tests of Cracks Originating at Fastener Holes

FLAW TYPE	SPECIMEN CODE	HOLE		FASTENER				FLAW		SPECTRUM	
		NO.	CONDITION	TYPE	HEAD DESIGN	INTER-FERENCE (IN.)	LIMIT LOAD (LBS)	a_i (IN.)	c_i (IN.)	TYPE	LIMIT STRESS (KSI)
	FSCTT-1	1 2 3	CONVENTIONAL REAM	CLOSE TOL. CLOSE TOL. OPEN HOLE	12 PT. 12 PT. –	0 0 0	4400 0 –	0.138 0.149 0.124	0.120 0.128 0.127	BOMBER	70.0
	FSCTT-2	1 2 3	CONVENTIONAL REAM	CLOSE TOL. CLOSE TOL. OPEN HOLE	12 PT. 12 PT. –	0 0 0	4750 0 –	0.168 0.196 0.166	0.127 0.134 0.142	FIGHTER	61.8
	FVCTT-1	1 2	CONVENTIONAL REAM	CLOSE TOL. CLOSE TOL.	12 PT. 100° CSK	0 0	600 600	0.128 0.150	0.130 0.130	BOMBER	70.0
	FSCIT-1	1 2 3	TAPER REAM COLD WORKED	TAPERLOK TAPERLOK OPEN HOLE	PROTRUDING PROTRUDING –	0.0034 0.0034 –	6100 0 –	0.160 0.144 0.166	0.132 0.122 0.120	BOMBER	70.0
	FSCIT-2	1 2 3	TAPER REAM COLD WORKED	TAPERLOK TAPERLOK OPEN HOLE	PROTRUDING PROTRUDING –	0.0034 0.0034 –	5625 0 –	0.142 0.122 0.170	0.129 0.152 0.125	FIGHTER	61.8
	FSCIT-3	1 2 3	TAPER REAM COLD WORKED	TAPERLOK TAPERLOK OPEN HOLE	PROTRUDING PROTRUDING –	0.0034 0.0034 –	6000 0 –	0.122 0.148 0.138	0.122 0.138 0.120	BOMBER	70.0
	FVCIT-1	1 2	TAPER REAM COLD WORKED	TAPERLOK CLOSE TOL.	PROTRUDING 12 PT.	0.0034 0	3500 3500	0.122 0.120	0.123 0.123	BOMBER	70.0

APPENDIX A --- TEST SPECIMENS

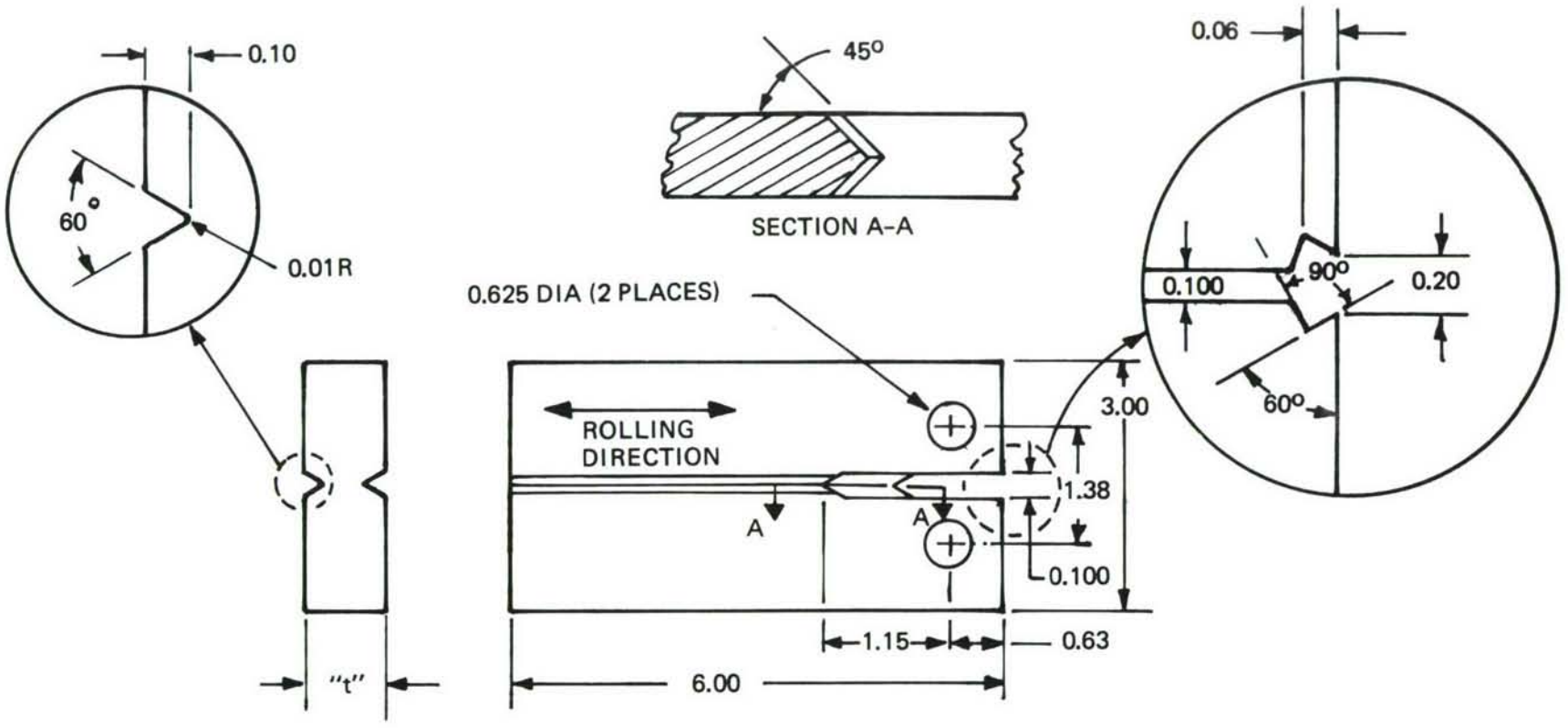
Nine different specimen configurations were used to conduct the tests described in the body of this report. Each configuration is detailed in Figures A1 through A9 and a summary identifying specimen configurations used for each alloy and test type is included in Table A1.



MATERIAL	THICKNESS
A1 2219-T851	0.25
Fe 9Ni-4Co-0.2C	0.20
Ti 6Al-4VβA	0.25
Fe 4340	0.25

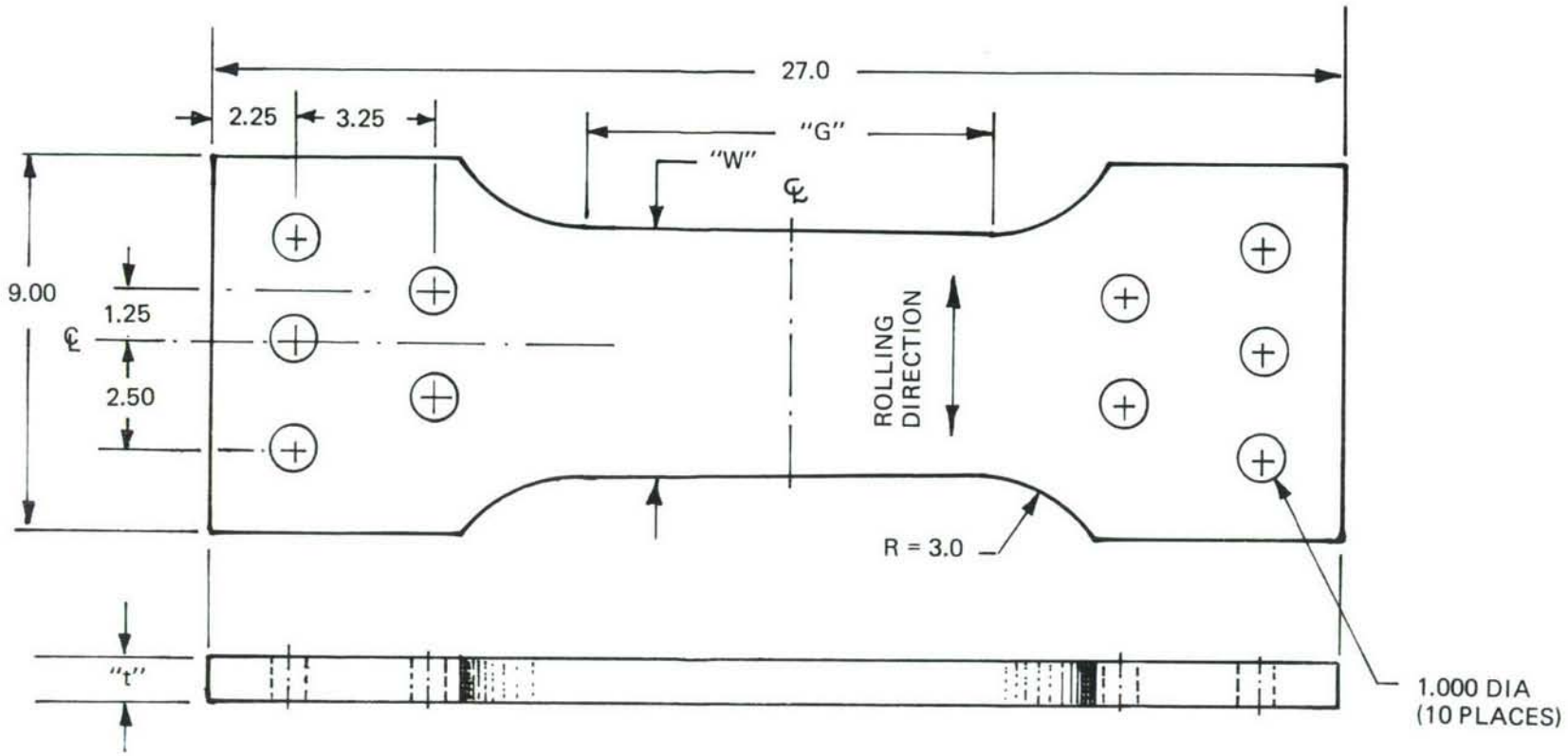
A	0.505 MAX 0.495 MIN
B	A + 0.003 TO A + 0.005

Figure A1: Mechanical Properties Specimen



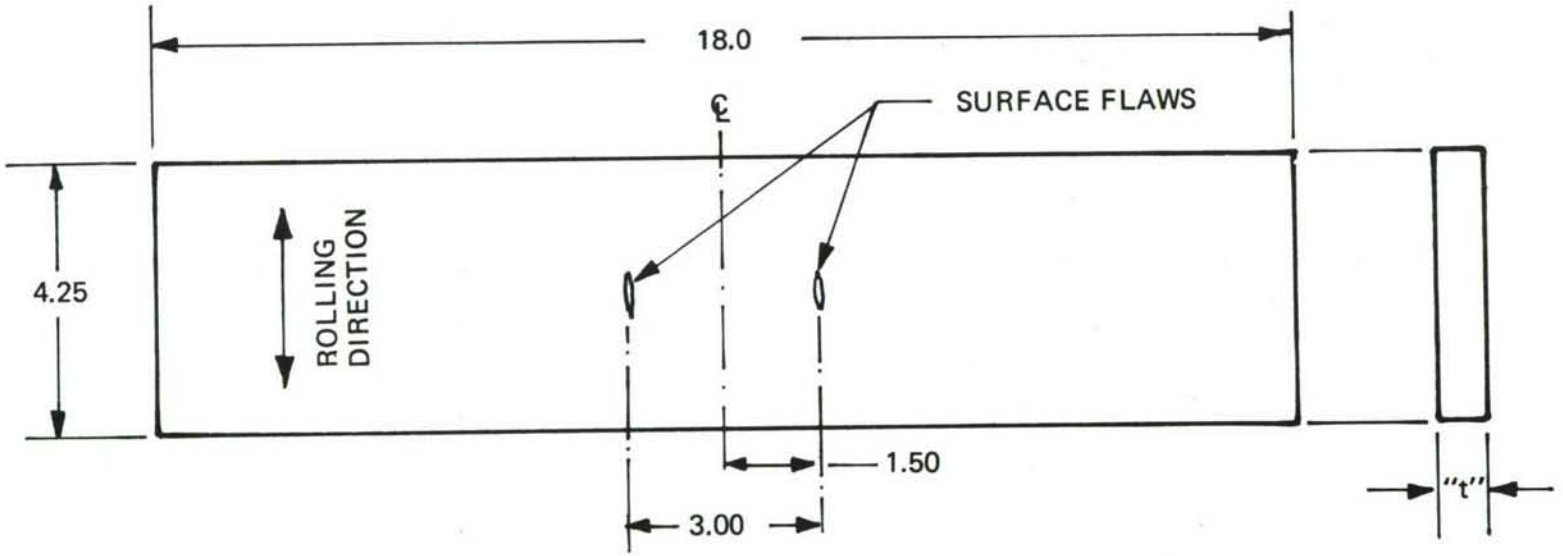
MATERIAL	THICKNESS, "t"
A1 2219-T851 Fe 9Ni-4Co-0.2C Ti 6Al-4V	0.45 0.50 0.60

Figure A2: Baseline Double Cantilever Beam Specimen



MATERIAL	THICKNESS, "t"	LENGTH, "G"	WIDTH, "W"
A1 2219-T851	0.95	10.00	6.00
Fe 9Ni-4Co-0.2C	0.48	10.00 OR 8.00	6.00, 4.25 OR 4.00
Ti 6Al-4Vβ A	0.60	10.00 OR 8.00	6.00 OR 4.25

Figure A3: Baseline Tension Specimens



MATERIAL	THICKNESS, "t"
A1 2219-T851 Fe 9Ni-4Co-0.2C Ti 6AI-4VβA	0.95 0.48 0.60

Figure A4: Baseline Bend Specimens

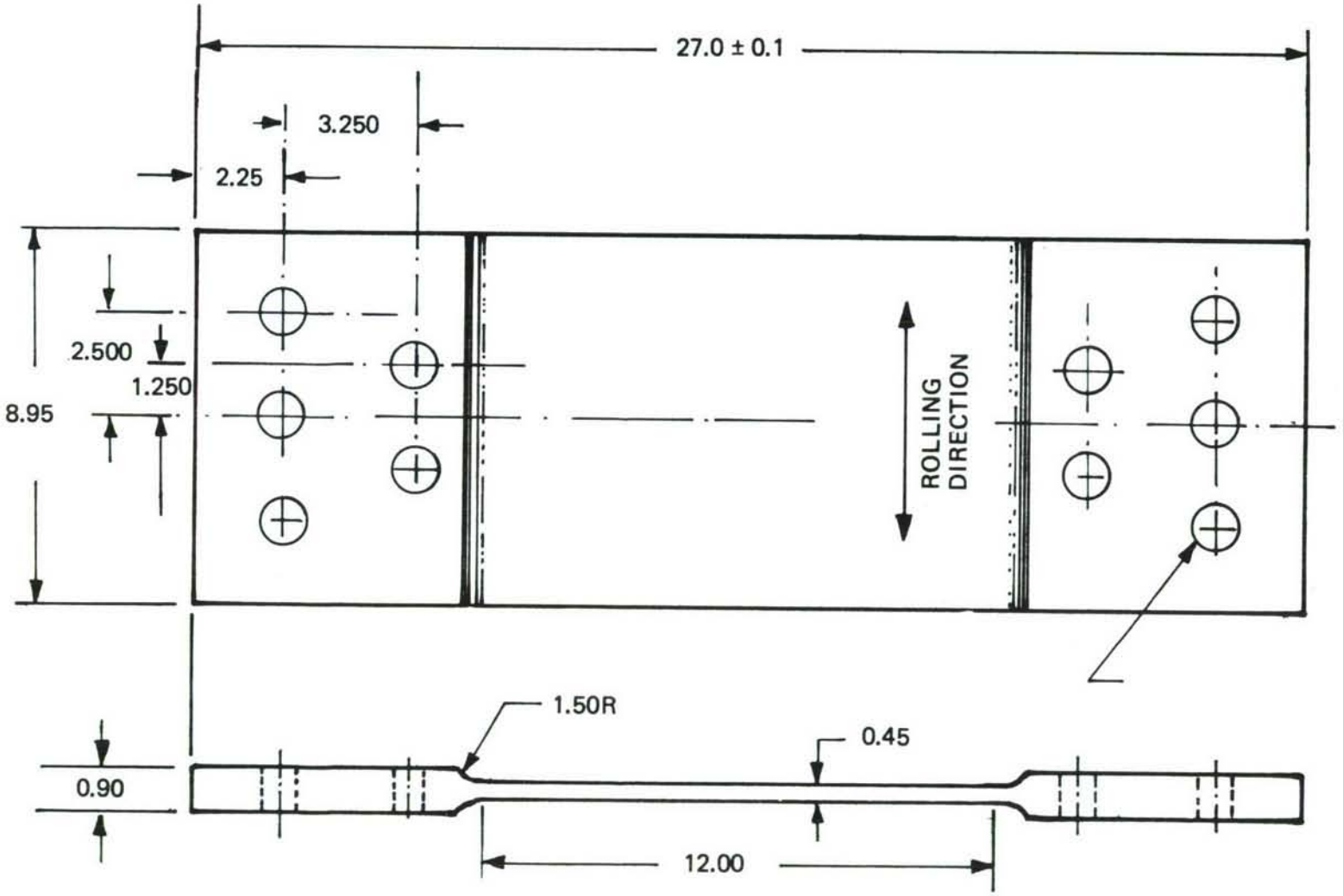
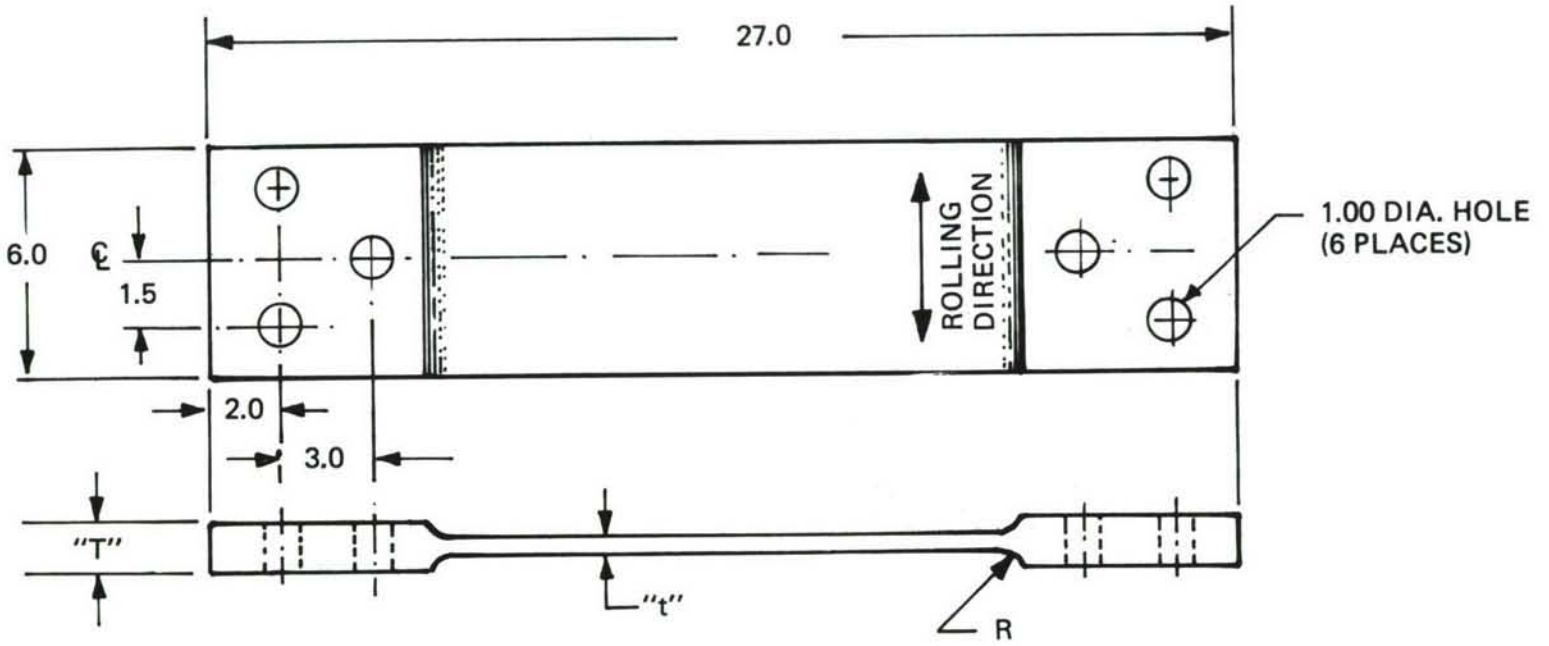
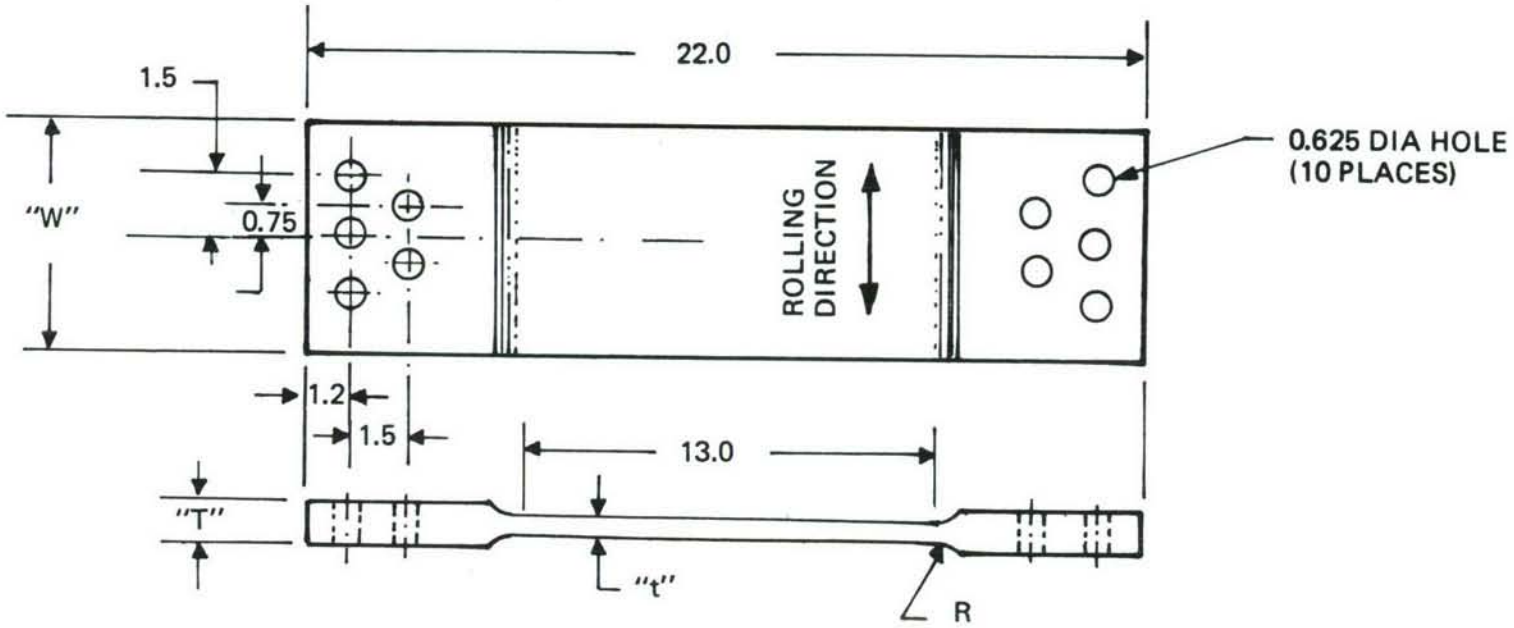


Figure A5: 2219-T851 Aluminum Alloy Surface Flaw Tension Specimen Used For Uniform Load, Overload, and Spectrum Load Tests



TYPE OF TEST	MATERIAL	THICKNESS, "t"	THICKNESS, "T"
FAH	Al 2219-T851	0.450	1.00
SF, FAH	Fe 9Ni-4Co-0.2C	0.300	0.50
SF, FAH	Ti 6Al-4VβA	0.375	0.63

Figure A6: Surface Flaw and Flaw at Hole Tension Specimen Used For Uniform Load, Overload, and Spectrum Load Tests



MATERIAL	WIDTH, "W"	THICKNESS, "t"	THICKNESS, "T"
A1 2219-T851	6.00	0.450	1.00
Fe 9Ni-4Co-0.2C	5.50	0.300	0.50
Ti 6Al-4VβA	6.00	0.375	0.63

Figure A7: Surface Flaw and Flaw at Hole Tension/Bending Specimen Used For Uniform Load and Overload Tests

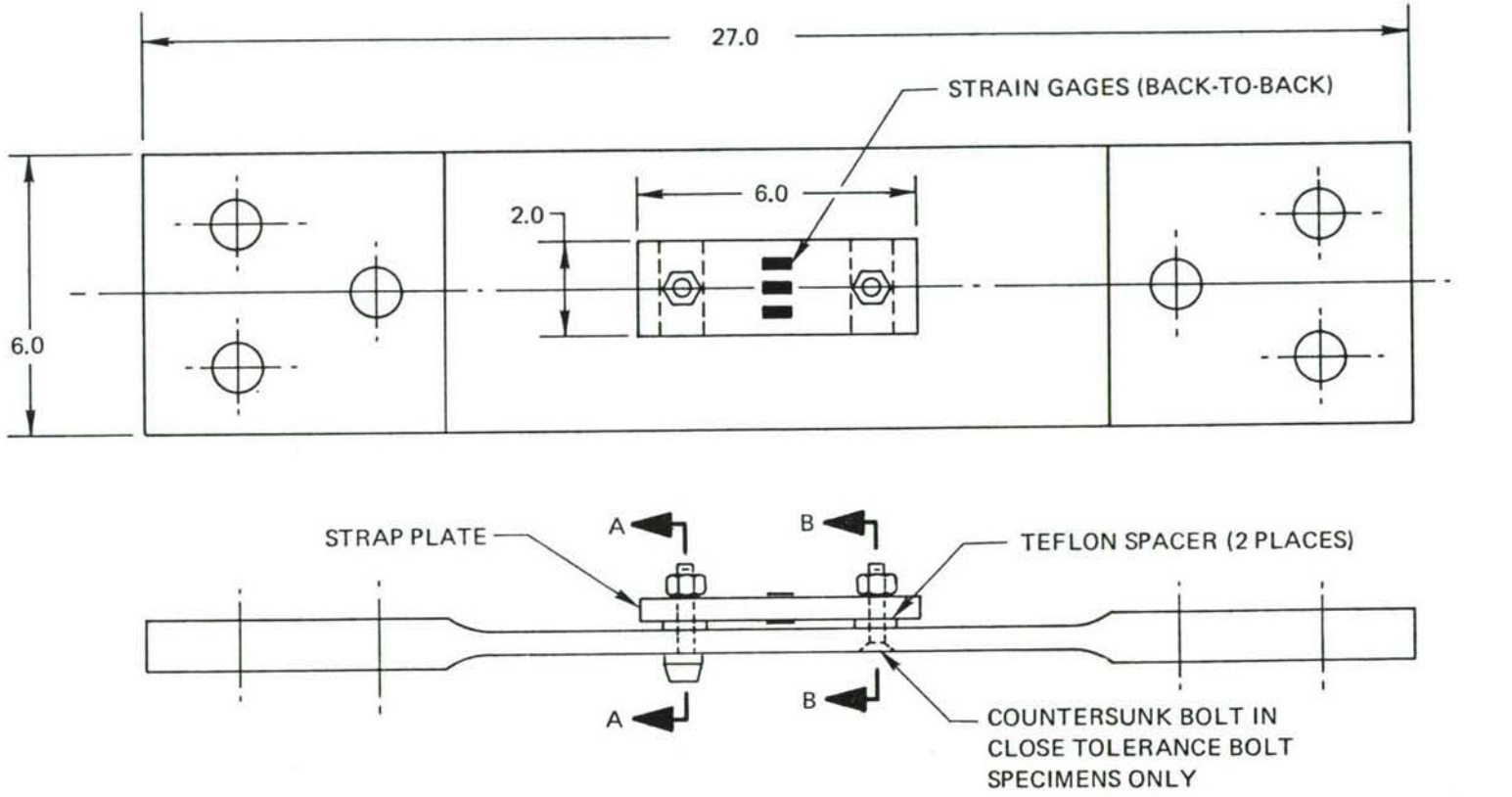


Figure A8: ***Specimen Configuration For Spectrum Loaded Verification Tests***

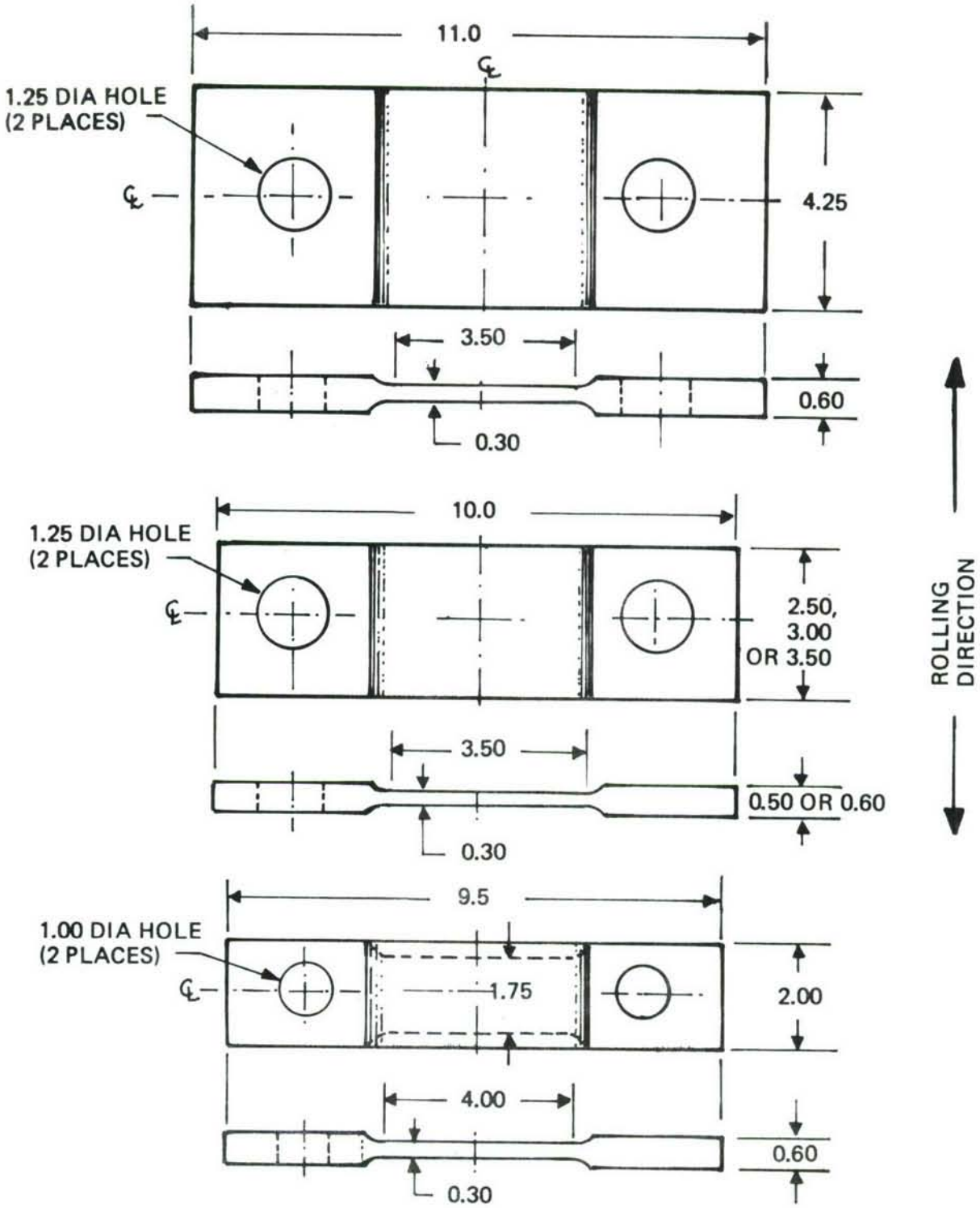


Figure A9: 4340 Steel Verification Test Specimen Configurations

Table A1: Summary of Specimen Configuration Used in Experimental Program

FLAW TYPE	TEST SERIES	ALLOY	STRESS STATE	SPECIMEN CONFIGURATION (FIG. NO.)
NONE	MECHANICAL PROPERTY	ALL ALLOYS	TENSION	A1
THRU CRACK	BASELINE DCB	Al 2219-T851 Fe 9Ni-4Co-0.2C Ti 6Al-4V βA	TENSION	A2
SURFACE FLAW	BASELINE	Al 2219-T851 Fe 9Ni-4Co-0.2C Ti 6Al-4V βA	TENSION BENDING	A3 A4
	UNIFORM LOAD OVERLOAD SPECTRUM LOAD	Al-2219-T851 Fe-9Ni-4Co-0.2C Ti-6Al-4V βA	TENSION	A5 A6 A6
			TENSION/BENDING	A7
FASTENER HOLE FLAW	UNIFORM LOAD OVERLOAD SPECTRUM LOAD	Al-2219-T851 Fe-9Ni-4Co-0.2C Ti-6Al-4V βA	TENSION TENSION/BENDING	A6 A7
	VERIFICATION	Al-2219-T851 Fe-9Ni-4Co-0.2C Ti-6Al-4V βA	TENSION	A8
	ANALYSIS VERIFICATION	Fe-4340	TENSION	A9

☆U.S.Government Printing Office: 1974 — 657-015/199

RECEIVED
11 DEC 1974
AFFDL